Title	Piezoelectric scaffolds: Mediating tendon regeneration by activation of piezosensitive receptors
Author(s)	Fernandez, Marc
Publication Date	2019-09-15
Publisher	NUI Galway
Item record	http://hdl.handle.net/10379/15514

Piezoelectric scaffolds: Mediating Tendon Regeneration by Activation of Piezosensitive Receptors.

A thesis submitted to the National University of Ireland for the Degree of Doctor of Philosophy

Marc Fernandez

June 2019

CURAM, Research Centre for Medical Devices
National University of Ireland, Galway

Research Supervisors: Dr Manus J.P Biggs and Professor Abhay Pandit

Table of contents

List of Figures

Chapter Two

Chapter Three

Chapter Four

TGF and BMP signalling respectively) stimulation at day 10. Expression of genes were differentially regulated in tenocytes cultured under mechancial and piezoelectric stimulation. Red = Up-regulated, green = down-regulated, grey = no change, colourless = not tested. 326

Figure 5-6. Histological images of intact tendon a) H&E staining showing cell organisation and collagen fibre bundles (in blue the cell nuclei, and in pink the extracellular matrix /cytoplasm). b) Herovici staining showing the distribution of collagen III and I. (in blue the young collagen and in red the mature collagen red) c)

Chapter Six

Appendices

Acknowledgements

Abstract

Tendon disease caused by trauma, illness or age-related degeneration constitutes an unmet clinical need. Tendon repair using different pharmacological and engineering strategies based on both synthetic and biological grafts has failed to restore native tendon function. Advancement in regenerative medicine and integrative physicomechanical approaches has enabled the development of electrically and mechanically active scaffolds that can recapitulate closer the native tendon tissue physical properties. In particular, electromechanical coupling (piezoelectricity) is present in all living beings and provides a basis for sense, thoughts and the mechanisms of tissue regeneration. Critically, the piezoelectric properties of musculoskeletal tissue have been recently measured at the molecular, fibrillar and tissue level and are mainly attributed to collagen type I - a fibrous protein abundant in mammals. This thesis is concerned with the study of the effect of piezoelectricity on biological processes such as cellular differentiation, cell growth, and cytoskeleton rearrangement to improve the functionality of tendon engineered substitutes.

Initially, piezoelectric nanocomposites were fabricated and displayed superior piezoelectric performance while enhancing tendon cell adhesion. Following the identification of optimal mechanical stimulation conditions, piezoelectric scaffolds showed the ability to negate the phenotypic drift and dedifferentiation of tendon cells in vitro. This system was assessed in vivo in clinically relevant full-thickness rat Achilles tendon injury model undergoing treadmill running. The effect of treadmill running was first evaluated and showed to enhance tendon regeneration. Piezoelectric scaffolds, in combination with treadmill running, proved to be able to speed the functional recovery of injured tendons through the activation of piezosensitive receptors at both 4 and 8 weeks. Analysis of the tissue with custom-made protein microarrays revealed that in addition to the modulation of tenogenic TGF-β/BMP signalling pathways, there was also activation of piezosensitive receptors TRP and Piezo family members. While changes in organisation and maturation of collagen I were not significant between piezoelectric and non-piezoelectric systems, changes in the ectopic bone formation were observed. Piezoelectric scaffolds were able to promote bone formation while maintaining also enhanced tenogenic potential indicative of the strong regenerative potential of piezoelectric scaffolds. Overall, the system shows promise for the treatment of tendon injuries in which regeneration of tendon is required.

Chapter One

Literature Review

Sections of this chapter have been previously published in:

Marc A. Fernandez-Yague, Sunny Akogwu Abbah, Laoise McNamara, Dimitrios I. Zeugolis, Abhay Pandit, Manus J. Biggs, Biomimetic approaches in bone tissue engineering: Integrating biological and physicomechanical strategies, Advanced Drug Delivery Reviews, **2015** 84,1-29

Marc A. Fernandez-Yague, Abhay Pandit, Manus J. Biggs, Piezoelectric control of tendon regeneration, JPhys Materials, **2019**, (under preparation)

1.1 Introduction

Tendon disease constitutes an unmet clinical need and remains a critical challenge in the field of orthopaedic surgery[1–3]. Harvesting tendon from autologous or allograft donor sites is an expensive and painful procedure, which is linked with added health risks associated with additional surgical procedures in elderly patients or disease transmission arising from allogeneic sources [4–7]. Innovative solutions are required to overcome the limitations of current tendon grafting approaches and *in vitro* strategies, through tissue engineering or regenerative medicine approaches, are showing promise for treating tendon diseases and for reconstructing tendon defects[8–10]. Tissue engineering approaches involve the combination of cells, biomaterial scaffolds and specific culture conditions incorporating biochemical and physical stimuli including mechanical[11,12] and electrical[13–15] stimulation to encourage *in vitro* tendon tissue formation. The next sections will describe in detail biomaterial-based strategies that have been reported to enhance tendon regeneration.

1 in 4 Adults

30 Million Procedures

€145 Billion per Year
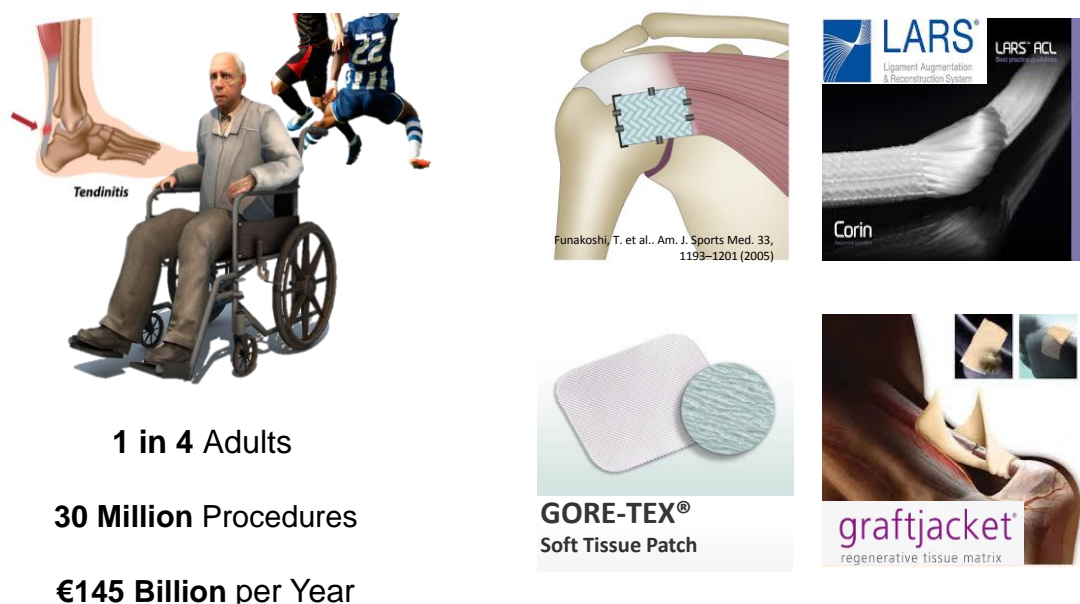
Figure 1-1**.** Traumatic injuries and various pathological diseases can impair normal tendon functions and lead to immobility, severe pain and deformity. Grafts commercially available for tendon repair include both synthetic LARS (carbon-based polymers), Gore-tex, fluoropolymer as well biological graft jacket, porcine dermis.[16]

Table 1-1.The most popular FDA approved and commercially available tendon-specific scaffolds [11].

Product	Company	Source	Cross-linking	Regulatory approval
Artelonw and SportmeshTM	Artimplant AB, Sweden and Biomet Sports Medicine (IN, USA)	Polyurethane urea polymer	Not applicable	Canada, Europe, FDA; Artimplant AB, Sweden
Bio-Blanketw	Kensey Nash Corporation (PA, USA)	Bovine dermis	Yes	FDA
CuffPatchw	Arthrotek (IN, USA)	Porcine SIS	Yes	FDA
Gore-Texw patch WL	Gore and Associates, Flagstaff (AZ, USA)	ePTFE	Not applicable	FDA
GraftJacketw	Wright Medical (TN, USA)	Human cadaver dermis	No	FDA
LARS	Dijon (France)	Terephthalic polyethene polyester	Not applicable	Canada, Europe
Leeds-Keiow or Poly-tapew	Xiros plc, Neoligaments (Leeds, UK); Yufu Itonaga Co., Ltd (Tokyo, Japan)	Polyester ethylene terephthalate	Not applicable	Canada, Europe, FDA
OrthADAPTw	Pegasus Biologic, Inc. (CA, USA)	Equine pericardium	Yes	FDA
PermacolTM	Zimmer (IN, USA)	Porcine dermis	Yes	FDA
RestoreTM	DePuy Orthopedics (IN, The USA)	Porcine SIS	No	US FDA
Shelhigh No-Reactw Encuff Patch	Shelhigh Inc. (NJ, USA)	Bovine or porcine pericardium	Yes	FDA
BioFibreTM scaffold	Wright	P4HB	No	FDA

Table 1-2. A table illustrating the clinical electrical stimulation devices used today with FDA approval [12]

Company	Device Name	Electrical Type	Description of Product
Orthofix	Physio-Stim Lite	PEMF	Tendon to bone healing in acute rotator cuff repair
Orthofix	Cervical and Spinal-Stim	PEMF	Noninvasive device for spinal fusion
Biomet	EBI bone healing system	PEMF	Noninvasive device for nonunion fractures, failed fusions and congenital pseudarthrosis
Biomet	OrthoPak 2 bone growth stimulator	CC	Noninvasive device for nonunion fractures
Biomet	SpinalPak bone growth stimulator	CC	Noninvasive device for spinal fusion for one to two levels
Biomet	OsteoGen and OsteoGen-D	DC	Surgically implanted device for nonunion and may also be used as an adjunct to internal/external fixation and autografts
Biomet	SpF implantable spine fusion stimulator	DC	The SpF-2T and SpF-4T are indicated for the spinal fusion of one or two levels, while the SpF-XL and SpF-XL IIb are indicated for the fusion of three or more levels

*DC indicates direct current; CC, capacitive coupling; FDA, Food and Drug Administration; PEMF, pulsed electromagnetic field

1.2 The development of smart biomaterials

The development of smart biomaterials capable of demonstrating modulated functionality in response to the dynamic physiological and mechanical environments that exist *in vivo* remains an essential challenge in tendon tissue engineering[17–21]. There is a need for a paradigm shift to achieve long-term repair and excellent clinical outcomes using biologically responsive approaches that focus on repair and reconstitution of tissue structure and function[22–25]. Despite considerable progress in the understanding of the biological and physicomechanical properties of organ and tissue homeostasis, relatively few orthopaedic biomaterials designed with biomimetic and bioresponsive properties have been translated into clinical solutions to date[26]. Nevertheless, according to the EU-Report on Nanotechnology, the global market for 'smart biomaterials' reached $47 billion in 2009 and will rise to $113 billion by 2025[27].

Most current orthopaedic technologies draw on simple or composite building blocks, yet next-generation tissue-engineering strategies must combine multiple functions such as drug release, receptor recognition, environmental responsiveness and tuned biodegradability, characteristics envisioned to play a vital role in next-generation biomedicine. Furthermore, traditional medical devices lack biomimicry, and mismatches in tissue morphology, or chemical and mechanical properties ultimately accelerate implant failure.

In particular current scaffold and implant, designs are characterised by a lack of responsiveness and long-term or permanent implants are not ideal for many applications, due to risks of stress shielding and implant loosening. Biomimetic approaches to biomaterial design enable molecular, structural and biological compatibility similar to that of the tissue being replaced to facilitate the regeneration of complex tissues. Multiple stimuli have been proposed as principal contributors or mediators of cell activity and tendon tissue formation, including physical factors (substrate topography, stiffness, shear stress and electrical forces) and biochemical (such as growth factors, genes or proteins). However, next-generation scaffolds and tissue-engineered constructs need to integrate a range of biological and physical properties for optimal tendon regeneration.

1.3   The tendon electroactive environment.

Tendon is a unique connective tissue that primarily transmits loads from muscle to bone, generating locomotion with high stability and efficiency[28]. In order to bear the continuous mechanical loading of movement under Earth's gravity, tendon structural and cellular components are highly dynamic and organised to ensure optimal tensile strength[29]. The tendon extracellular matrix (ECM) is mainly composed of parallel fibrils of collagen type I which interestingly, is a piezoelectric material, that is, capable of producing an electrical impulse in response to a mechanical stimulus[30–33].

a)   b)
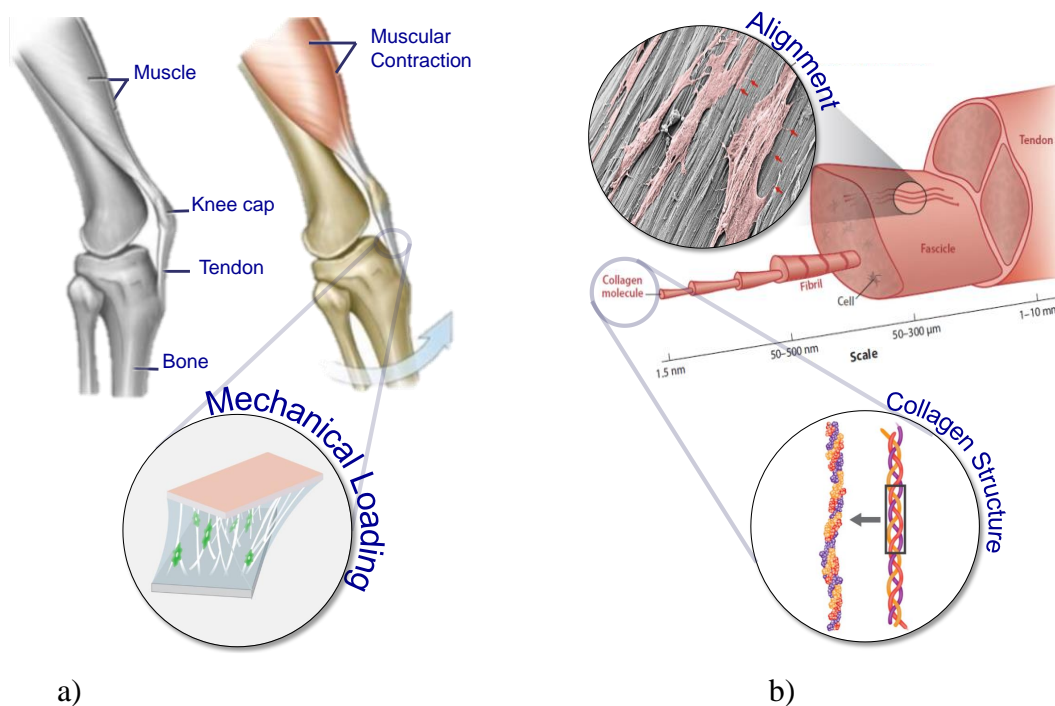
Figure 1-2. Tendon function at different scales architectures. a) At the macroscale, tendon functions as a purely load-bearing element to maximise the efficiency of locomotion, and it is up to store 40% of deformation energy. A high microscale organised ECM made up of collagen type parallelly oriented to the axis of maximum loading bears this mechanical energy b) At the molecular level, collagen is formed by small, oriented upon its backbone; electric dipoles originated from the asymmetric electronegative difference between carbonyl and amine groups

Most biopolymers are piezoelectric[32–34], due to differing degrees of polar bonds, which upon loading results in an asymmetric shift of charges in their molecular structure, inducing a change in electric polarisation. In the case of collagen, the electronegative difference between the carboxyl and amine functional groups arranged along the

backbone of the triple helix form an inherent electric dipole moment[30,32]. The tensile forces generated during locomotion are transferred through the collagenous structural components, generating dynamic electrical charges. The electrical signals generated by collagen piezoelectricity are likely to serve as a primary stimulus in tendon homeostasis [35–37]. At the cellular level, the electromechanical coupling represents an intricate layer of information that is transduced into intracellular biochemical responses through piezosensitive structures [38–40].

1.4 Physical properties of tendon: electromechanical coupling

As with most complex adaptive biological systems, tendon function is highly dependent on its structural cellular and extracellular components to respond to physiological loading. The extracellular components being mainly collagens, elastin, glycosaminoglycans (GAGs) and proteoglycans (PGs), with slight variations in their concentration between tendons found in different parts of the body.

Amongst all of the ECM constituents, collagen type I represents 80-90% of the tendon dry mass and perform essential functions, including maintenance of tissue architecture, transmission and absorption of loads and triggering of tissue regeneration[41–43]. Other collagens present in tendon include collagen types III, V, XII, and XIV[28,43]. In particular, Collagens XII and XIV act to prevent tissue injuries by acting act as plasticisers in response to large tendon deformations, helping collagen I bundle to glide over each other [44–46]. Further, during the ageing process, the amount of collagen type III in tendon becomes higher, resulting in tendon stiffness [47,48]. Conversely, collagen V plays a central role in fibril development and diameter growth [49–51]. When a tendon is developing, the formation of intermolecular covalent cross-links with neighbouring molecules happens via the enzyme lysyl oxidase, allowing the formation of a flexible structure with a high degree of alignment along the axis, enhancing tissue integrity.
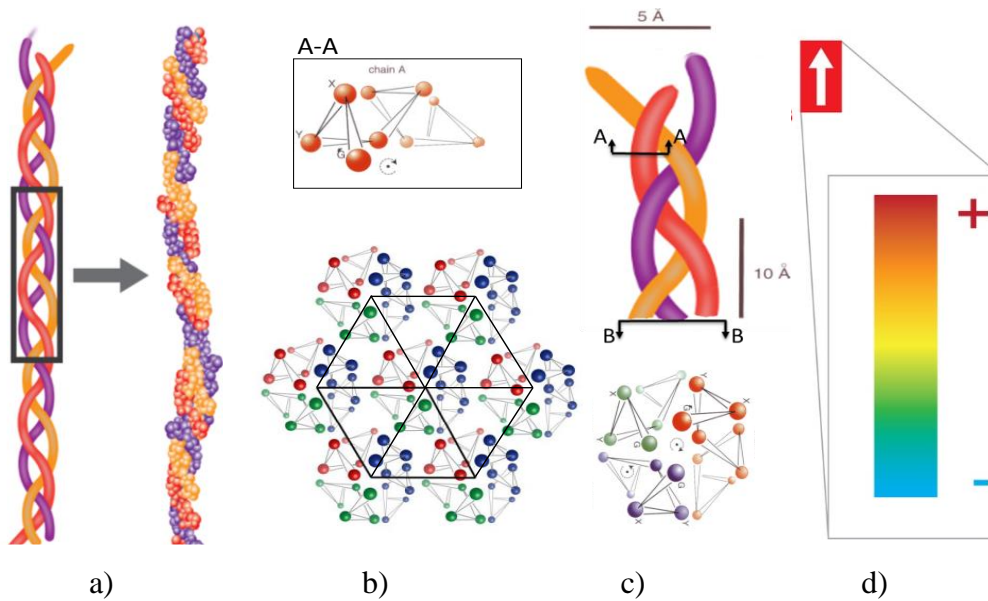
Figure 1-3. a) Schematic representation of the crystal structure of triple helix consisting of three polypeptides chains Note the cross-section of individual chain showing the triple Gly-X-Y where dotted lines indicated the prominent hydrophobic interactions. b) Cross-section of multiple individual collagen fibres resulting in a non-centrosymmetric hexagonal structure. C) Cross-section of the three chains. Note Glycine residues form the core of the triple-helix. D) Representation of individual electric dipole. Polar bonds between carbonyl and amine groups along the backbone of collagen results in a dipole moment or electrical polarisation.

The collagen base unit is a large protein (300 nm) that consists of three coiled polypeptide strands wound into a triple helix (two α1 chains and one α2 chain) and is arranged in a hierarchical architecture which ranges from the nano to the macro scale with varying physical properties. Each polypeptide is made up of the repeating amino acid sequence, Glycine (Gly) – Proline (X) –Hydroxyproline (Y) (Figure 1-3). Hydrogen bonds between the glycine domains (carbonyl groups) and the hydroxyl groups of hydroxyproline residues (amine group) stabilise the triple helix structure. As shown in Figure 1-3d, the dipoles created after stabilisation aligns with the central axis of the triple helix resulting in a remanent polarisation. Alternatively, if the positioning of these molecules is incorrect, or the molecules are not present, the collagen will degrade rapidly and will not show piezoelectric properties. Various studies have demonstrated that irregular molecular changes or structural defects in collagen result in tendon disorder [52–54].

Despite the extensive literature regarding the ultrastructural analysis of collagen and the effects of effector domains on biological functions, the contribution and nature of the electromechanical properties of twisted collagen at the molecular level, and how these properties affect tissue homeostasis remains unclear. Atomic simulations of collagen have revealed that collagen exhibits uniaxial polarisation along the long axis, possessing a piezoelectric coefficient of 2-3 pC/N and have verified that the origin of collagen piezoelectricity originates from the molecular reorientation upon deformation of the polar (charged) residues.

The first reports on biological tissue piezoelectricity appeared in 1954 by Yasuda and Fukada[55] who observed a piezoelectric effect in boiled bone and dried tendon which they attributed to collagen shearing). More recently, piezoelectricity in single collagen fibrils isolated from tendon or bone has been studied [56,57], taking advantage of the atomic force microscopy techniques - AFM and PFM, (Figure 1-4a). The study revealed that collagen fibrils possess unidirectional polarisation along their longitudinal axis but not vertically or radially. For many years, the relationship between bone piezoelectricity and bone growth or resorption has been investigated, and in particular, Bassett was one of the pioneers in understanding the effects of piezoelectricity on biological function (Figure 1-4b)[58]. During his studies on embryonic development of chick tibiae, he observed that cyclically loaded tibias produced significantly highe[58]r cartilaginous mass that unloaded tubas. From his observations, Basset concluded that electrical signals produced by strain gradients going from less to higher collagen-dense areas were acting as master regulator signals to initiate bone remodelling. However, recent evidence suggests that bone hydroxyapatite (HA)-mediated flexoelectricity and not collagen piezoelectricity is the primary source of bending induced polarisation in the bone[59]. However, to better understand the effects of piezoelectricity on tissue regeneration, it is first necessary to understand the effects of low amplitude electrical stimulation at the cellular level.

a)   b)
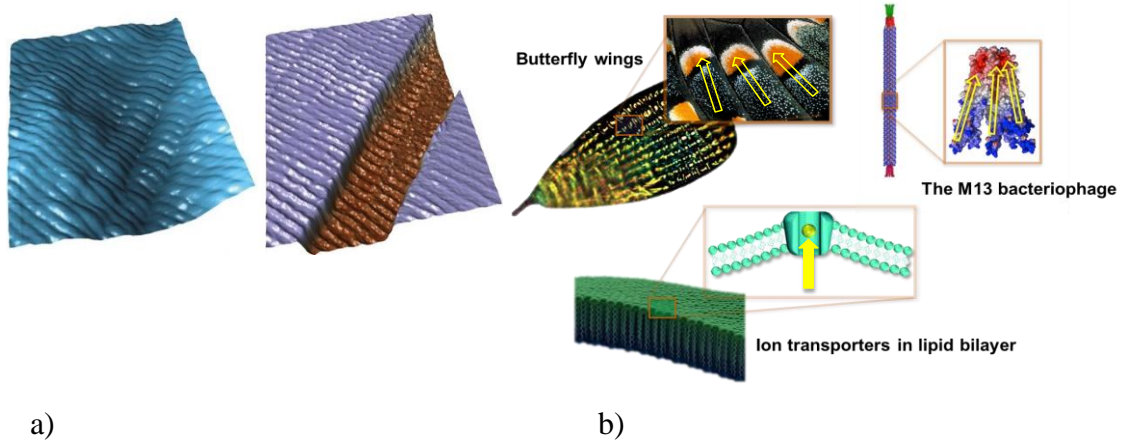
Figure 1-4**.** a) Topographic (left) and PFM phase (right) images of collagen fibres, 1.4 μm scan. Imaged with the MFP-3D AFM. b) Electromechanical coupling regulates various biological functions, including blood flow regulation, hearing, and pain sensation.

1.5   Tendon Cellular Components

The healthy tendon is both hypovascular and hypocellular, making its natural healing very difficult and slow. About 10% of the tendon dry mass is cellular component and around 90-95 % of the cells present are terminally differentiated fibroblastic-type cells termed tenocytes (TC) and their precursor's cells, tenoblasts. Significant differences have been found between young and adult's tenocytes, morphologically, mature tenocytes are much more flattened and less in number compared to embryonic or young tenocytes. In general, however, tenocytes possess long intracellular protrusions forming a linear cellular network of elongated (up to 300 μm) tenocytes with an increased ability to withstand mechanical loading.

Conversely, tenoblasts possess a rounded, spindle star-like or cuboid morphology and vary in size considerably (from 20 to 70 μm). The conversion from a tenoblast to tenocyte phenotype is considered a significant mediator of tendon tissue remodelling and can occur in response to mechanical stimuli or trauma[60]. Tenocytes can also be identified by the expression of specific protein and glycoproteins markers including collagen type I, collagen type III, decorin, scleraxis, tenascin C, tenomodulin and thrombospondin 4[61–64]. Interestingly, during embryonic development, scleraxis is highly specific for tenocytes and tenoblasts, as demonstrated by the development of severe tendon defects in scx-null mouse models[65,66]. However, there are currently no specific

biomarkers to distinguish tenoblasts from tenocytes. Other cell types present in tendon tissues include progenitor cells (tendon stem cells, TSCs), chondrocytes localised to musculoskeletal pressure and insertion sites, synovial cells (present in the tendon sheath), vascular cells and smooth muscle cells [67,68].

TSCs were first discovered by Bi *et al.* [69] and showed many similarities with mesenchymal stem cells such as the capacity to differentiate into bone, cartilage or adipose tissue. The existence of TSCs has been confirmed in human, equine, rabbit, rat and mouse tendon and represent a heterogeneous population with different stem subpopulations, raising many questions about the identity of subpopulations participating in tenogenesis [70]. A recent study using high throughput single-cell analysis to characterise the gene expression profile of isolated individual tendon cells identified a Nestin-expressing subpopulation of tendon cells that offered enhanced tenogenic potential [71]. Knockdown of Nestin expression in TSCs suppressed their clonogenic capacity and reduced their tenogenic potential significantly both *in vitro* and *in vivo*. The study concluded that TSCs expressed a significantly higher level of Nestin than tenocytes/tenoblasts. Despite the incomplete understanding of the role of TSC in tenogenesis, these findings indicate that Nestin is a specific marker for TSCs with strong tenogenic and regenerative potential. Therefore, precise identification and isolation of TSC subpopulations will facilitate their therapeutic application for treating injured tendons. Moreover, how to modulate the tenogenic potential of these TSCs for tendon repair is a prospective aim of this thesis.

1.6 Tendon stem cell differentiation mediated by signal transduction.

The fact that cells respond to their physicochemical environment is well established in tissue engineering[72,73]. Stem cells and their niche represent a complex adaptive system where the physicomechanical and biochemical properties of the niche provide cells with the specific information to regulate their function. The cell response includes homeostasis regulation, migration, positional information, and self-renewal and differentiation process into functional tissues [74,75]. The highly conserved instructive biochemical components of the environment comprises secreted glycoproteins and collagens that constitute a three-dimensional network, termed as ECM components. Cellular interaction within this matrix is mediated by biochemical compounds (i.e. growth factors, integrin's, metal ions) that define tissue identity as well as through

electromechanical gradients determined by the variation and density of the constituent collagens and ionic species. Critically, these variables, among others, have been shown to regulate cell adhesion and signal transduction-mediated cellular differentiation [76]. To further understand the role of these instructive physical features in tendon repair, the use of responsive systems to recapitulate in vitro the dynamic interactions between cellular components and its adaptive environment is of particular interest. In particular, the process of stem cell differentiation in tenogenesis can be induced by different physicomechanical strategies (signal transduction) including oxygen tension[77,78], hydrostatic pressure [79], mechanical stimulation[80,81], topography [82,83], bioelectric signals [84–86], rigidity [87–92] and growth factor concentrations[93–95].

1.6.1 Signal transduction through electrical cues.

Stimulation of tissue regeneration through electrical cues is a unique way of interacting with living cells that have been used in clinical applications for a long time. Several molecular components of cells are particularly sensitive to electrical cues, In particular, Voltage-operated calcium channels (VOCCs) allows the influx of extracellular calcium in response to changes in membrane potential and represents the basis of bioelectrical signalling.

Electricity is ubiquitous in living thing and electromechanical (EM) coupling (piezoelectricity) is present in all living beings (including humans) and provides the basis for perception, thoughts movement, cardiac activity, and mechanisms of musculoskeletal tissue regeneration[96].

 Studies of formation, restoration and remodelling of bone[97–99] and tendon[100,101] tissues by electrical stimulation arose following the discovery that bone and tendon are piezoelectric substances, indicating that electric fields induced in bone or tendon by cyclic loading could play a role in tissue remodelling. Critical studies by Fukada and Yasuda [102] have demonstrated that the electrical potentials induced by stress could modulate both cell activity and the orientation of ECM deposition. Furthermore, frequency rate, direction and magnitude of deformation determines the amplitude and direction of the electrical signals. For example, in articular cartilage, it has been reported that endogenous electrical signals control different physiological processes. This finding promotes the application of electrical stimulation for *in vivo* cartilage repair or *in vitro* chondrogenesis. For instance, *in vivo* studies have shown an increased cell

proliferation, glycosaminoglycan production and chondrogenesis-related gene expression[103–106] Recently, studies have also demonstrated *in vitro* MSC differentiation using electrical stimulation (ES) in the absence of exogenous growth factors via $Ca^{2+/}ATP$ oscillations[107].

In a musculoskeletal paradigm, it could be suggested that Wolff law and cell mechanotransduction are also explainable in terms of bioelectrical currents generated by deformation of the tissue. At the cellular level, electrical fields can guide the migration of different cells. Wound healing represents a good example; during wound healing, an electrical field generates as a consequence of the disruption of tissue barriers and an ion flux creates which disrupts regeneration and guides cell migration. Mounting evidence is emerging on the role of electrical fields on tissue formation and identity during embryogenesis[86,108–113]. These studies hypothesise that total cell resting membrane potential dictates tissue identity and endogenous electrical signals regulated by ion channels play an instructive role and can control cell fate during tissue healing [109,110].

1.6.2 Signal transduction through mechanical cues.

Ion channels are transmembrane pores that can act as sensitive biological mechanosensors (MS) in musculoskeletal cells. Cell membrane deformation, by stretch or shear stress, results in the mechanical opening of these pores, leading to downstream signalling events, qualifying these structures as MS, cellular structures which transduce mechanical signals into electrical or biochemical intracellular signals. In particular, MS have been extensively studied due to their implications in cardiac muscle pathologies and function[116]. Most notably, proteins in the Transient Receptor Potential (TRP) families among others (see Table 1-3) have been identified to be involved in the complex mechanosensitive process, including modulation of osteoclast differentiation or as urothelial MS that controls normal voiding [117–119]. To date, seven different subfamilies of these TRP channels have been identified from which TRPV1[120,121] and TRPV4[122–124] have shown to be highly mechanosensitive affecting tissue homeostasis and repair processes. More recently, two other ion channel proteins, Piezo 1 and Piezo 2, have been identified as (non-selective) mechanically activated cation channels whose expressions are vital for mechanotransduction processes during cartilage or vascular structures formation among others (see Figure 1-5). Piezo 1 and 2, transduce a broad range of mechanical signals throughout the body and also in the musculoskeletal system, for example, under compression of articular cartilage, Piezo 1 and 2 are

activated. Piezo 1 and piezo 2 are also very sensitive to repetitive mechanical signals as shown by knockout studies, which indicate repetitive shear-stress detection deficiencies in vasodilation[125] and deficiencies in the detection of mechanical vibrations in mice and humans[126–128] .A recent study demonstrates that mechanical stress regulates MSCs differentiation by stretch-activated ion channel piezo on drosophilia[129]. More importantly, in this study, Piezo mutant and overexpression phenotype was rescued by manipulating cytosolic Ca2+ levels, supporting again the hypothesis that calcium signalling or total resting membrane potential is more determinant than specific ion channel activation.

Table 1-3. Diversity of ion channels involved in mechanosensory transduction. ECM (extracellular matrix)

MS ion channel	Gating mechanism	Voltage sensitivity	g (pS)	Ionic selectivity	Oligomer	Block	Refs
TRPC1	Lipid bilayer Amphipaths*	Voltage independent	20	Ca2+ permeable Non-selective	Tetramer	La3+,Gd3+ ,	[78,103,112,99,134–
TRPC6	Amphipaths (lipid bilayer?)	Inward/outward rectification	31	Non-selective PCa/PNa =5	Tetramer	GsMTx-4, Gd3+	[78,103,94,137,99,134,1
TRPV1	ECM	Voltage independent	1.3–2.2	Non-selective PCa/PNa =3.8 (heat), 9.6 (vanilloids)	Tetramer	Neomycin, A-ruth. red	[103,78,138,135]
TRPV2	ECM?	Inward rectification	~60	Non-selective PCa/PNa =	Tetramer	Ruth. red, La3+	[78,103,139,135]
TRPV4	ECM Amphipaths (lipid bilayer?)	Voltage independent	~90	Cation-selective PCa/PNa =6	Tetramer	Ruth. red	[78,105,140,141,134,135
TRPM3	Membrane tension, Sphingolipids	Voltage independent	65–133	Non-selective PCa/PNa =1.6, Mn2+	Tetramer	La3+,Gd3+,2-APB	[78,109,107,135,142]
TRPM4	Membrane tension	Voltage dependent	25	Monovalent cations	Tetramer	ATP	[78,143,144,142]
TRPM7	Membrane tension	Outward rectification	105	Cation-selective PCa/PNa =3	Tetramer	Gd3+, ruth. red, sphingosine FTY720	[78,108,135,145,146]
TRPP1 TRPP2	CSK	Voltage independent	~2–3× 103 (−100 mV) 3–4× 103 (+100 mV)	Cation-selective Na+,K+,Ca2+	Tetramer, di-trimer	Gd3+,GsMTx-4	[78,147–149,135]
TRPA1	CSK, lipid bilayer	Depolarization re-opening	~100	PCa/PNa =0.8	Tetramer	Gd3+,ruth.red	[78,135,142]
TREK1 2P-type K+	Membrane tension Amphipaths (lipid bilayer?)	Outward rectification	84–116	K+ selective	Dimer	Gd3+,Mg2+ , amlodipine, amiloride	[78,114,150,151]
TREK2 2P-type K+	Membrane tension Amphipaths (lipid bilayer?)	Inward rectification	65–179	K+ selective	Dimer	Mg2+,Ba2+	[78,152,153]
TRAAK 2P-type K+	Membrane tension Amphipaths (lipid bilayer?)	Inward rectification	66–110	K+ selective	Dimer	Gd3+,amiloride	[78,114,154,155,151]
NMDA receptor	Lipid bilayer Amphipaths ECM	Voltage dependent Mg2+	45–60	Cation selective Ca2+ permeable Divalent cation block	Tetramer	Mg2+	[78,156,20,157]
Piezo 1	Lipid bilayer (?)	Voltage independent		Cation selective Na+,K+,Ca2+ and Mg2+	Tetramer	GsMTx-4, Gd3+,ruth.red	[124,121,120,122,158]
Piezo 2	Lipid bilayer (?)	Voltage independent		Cation selective	Tetramer	Gd3+,ruth.red	[120,121,158]

CSK (cytoskeleton) *Amphipaths (GsMTx4, PUFA's, membrane phospholipids), APB (2-aminoethoxydiphenyl borate). g = conductance, pS = 10−12 A. Modified from [78]; with permission.
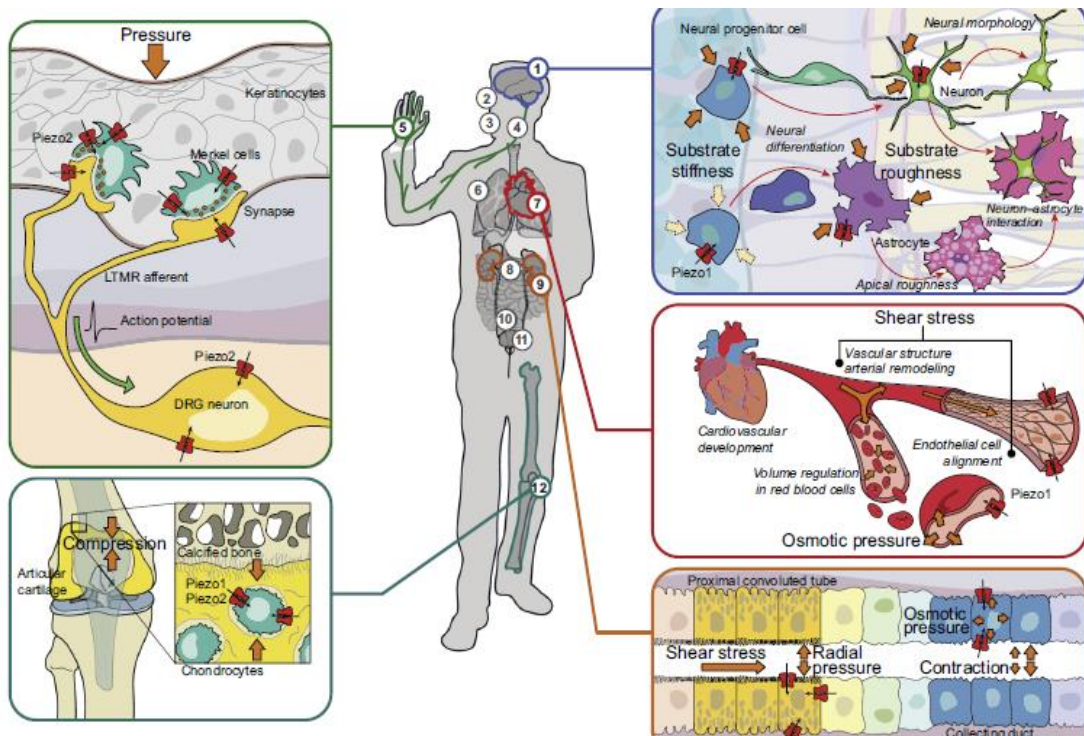
Figure 1-5. Schematic of the different roles of Piezo 1 and 2 within the human body. Tissues were piezo 1 and 2 have been observed include: 1, brain; 2, optic nerve head; 3, periodontal ligament; 4, trigeminal ganglion; 5, dorsal root ganglion and skin; 6, lungs; 7, cardiovascular system and red blood cells; 8, gastrointestinal system; 9, kidney; 10, colon; 11, bladder; and 12, articular cartilage. The function of Piezo in the neural, vascular, kidney, skin and cartilage tissues are shown in detail in call-out boxes. Top left, Merkel cells expression of Piezo 2 dysregulated) response to light touch (Loe Threshold Mechano Receptor, LTMR) and modulates dorsal root ganglion membrane depolarisation. Bottom left, under compression chondrocytes express both Piezo 1 and 2. Top right, neural progenitor cells sense the mechanical properties of the environment via Piezo 1 to initiate differentiation. Middle right, activation of Piezo 1 in endothelial cells leads to alignment in the direction of shear stress forces. Bottom right, a similar role of Piezo 1 in sensing fluid flow direction has been observed throughout the nephron of the kidney.

1.6.3 Signal transduction mediated by adhesion

Cells continuously adjust their function to maintain tissue homeostasis by integrating various biophysical cues and can interact with their surrounding via adhesion receptors

termed integrins. Since tendon cells adhere to collagen fibres, it is hypothesised that collagen fibre tension will govern many integrin-mediated signalling pathways to maintain tendon homeostasis. It has been shown, that loss of collagen fibre tension triggers downstream consequences including tendon cell apoptosis, collagenase secretion and TGFb1 overexpression *in vitro* [130–133]. In addition to tension, well known physical parameters that induce focal adhesion mediated differential cell function are: ligand density, spacing, substrate rigidity, fibre orientation and geometry (diameter) [134]. However, the exact mechanism of adhesion-mediated sensing remains still unclear. Nevertheless, there is a significant advantage of supramolecular cell-matrix adhesions over specific membrane receptors. For instance, a large number of specific proteins for mechanical sensation can manage different functional roles and therefore increase sensitivity, specificity and initiate more accurately precise intracellular biochemical signalling cascades (see Figure 1-6). Moreover, mechanotransductive processes through supramolecular adhesions occur via changes in the conformation of proteins (acting as ON-OFF switches or molecular clutch [133,135,136]) and leading to phosphorylation or coupling with other components. While focal adhesion signalling is directly related to cell migration, proliferation and differentiation (see Table 1-4) the role of intern mediated signalling in tendon homeostasis remains unclear. Furthermore, it is hypothesised that collagen tension-induced electrical signals (as results of piezoelectricity or electro-mechanotransduction) also plays an essential role in tendon homeostasis and function. Hence, the design of synthetic scaffolds capable of offering a modulated response to the dynamic environment and can recapitulate tissue-specific physicomechanical cues (including piezoelectricity) is of vital importance for tissue engineering applications [137]
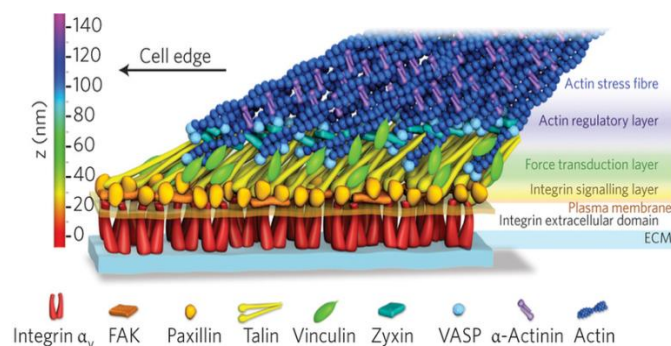
Figure 1-6 Molecular structure and connectivity of focal adhesions. Different nanoscale structured layers of molecules have different functional roles: 1) integrin/ECM binding domain 2) integrin signalling layer 3) force transduction layer 4) actin regulatory layer.

Table 1-4. Molecules at focal adhesions regulate various cell behaviours

Integrin avidity		FA turnover	Cell migration	Mechano-sensing	Proliferation	References
FAK	+/ _	+	+	+	+	[34,153,154,186]
Src	+/ _	+	+	+	+	[38,151,152]
p130Cas	+/ _		+		+	[62,71,187]
Crk	+/ _		+			[62,72,81]
Paxillin			+/_			[73,79,81,188]
Talin	+	?		+		[45,92,97]
Vinculin		?	+	+		[133,166]
Calpain	?	+	+			[124,125]
H-Ras	_	+	+		+	[189 –191]
R-Ras	+	_	+/_			[27,70,113]
Cdc42		+	+		+	[7,192,193]
Rac		+	+		+	[7,120,192,194,195]
Rho		_	+/_	+	+	[9,15,140,141,155,157,196]

Shown here is a table of focal adhesion proteins (top panel) or small GTPases (bottom panel) and their roles in focal adhesion dynamics and different cell behaviours. Legend: + a molecule has known positive role. - a molecule has known negative regulation; +/_, molecule has positive or negative role; role is implicated.

1.7 Mechanotransduction in the tendon.

That mechanical stimulation enhances tendon tissue regeneration *in vitro* is a well-accepted tenet of tendon tissue engineering, with a large number of studies concluding that mechanical forces enhance tenospecific differentiation and phenotypic maintenance. *In vivo*, cells in the tendon, are mechanosensitive (i.e., able to sense and respond to biophysical factors in the environment). This ability to detect and respond to mechanical forces is preserved in the different types of cells of tendon cells (tenoblasts, tenocytes and tendon stem cells. Their physicomechanical environment is a dynamic milieu of biophysical stimuli applied at different frequencies and magnitudes that includes strain, stress, shear, pressure, fluid flow, streaming potentials and acceleration [138–141].

Even though it is not possible to separate specific effects of each of these factors, it becomes clear that independently each of them can regulate cellular responses and influence remodelling events within the tendon. Furthermore, components of these specific factors – such as magnitude and frequency – also affect and regulate the cellular response. During locomotion, collagen fibres and adhered tendon cells are stretched mechanically resulting in intracellular changes (nuclear deformation and cytoskeleton reorganisation) that stimulate tenogenesis via activation of mechanotransductive pathway including ROCK/RhoA and focal adhesion kinase (FAK)[142]. It becomes clear that epigenetic factors such as mechanical loading play an essential role in defining cellular fate. For instance, mechanical clustering of focal adhesions initiates signalling pathways that can cause upregulations in transcription factors responsible for self-renewal, migration, differentiation or tenogenesis. It is recently demonstrated, that this complex mechanotransductive process influences gene transcription by altering chromosomes mechanically through linkers of nucleoskeleton deformations. On the other hand, rapid mechanically adaptive changes of receptor-proteins kinetics can likely transduce into pathways including integrin, G-protein, RTK and MAPK to initiate both anabolic (ECM synthesis) or catabolic processes (matrix metalloproteinases expression and ECM degradation).

To date, there is a need for further studies into the phenotypic, functional and molecular responses of tendon-derived cells to mechanical stress. In particular, different studies have investigated transcriptome changes as a function of mechanical loading in both mouse and rat tendon cells using microarray technologies [143,144]. As a result of these

studies, the adaptor protein paxillin and transforming growth factors were suggested as essential players in tendon repair. In a proteomics analysis study, human tenocytes were cultured on aligned polyglycolic acid (PGA) scaffolds and mechanically stimulated at different rates. The results showed that 195 proteins were upregulated and 189 proteins were downregulated significantly[145], indicating the high complexity of the mechanotransduction process. Mechanosensitive receptors, including focal adhesion and ion channels, are essential for mechanotransductive processes. This is clearly illustrated when both are inhibited, as tenogenesis and osteogenesis MSCs differentiation-related pathways become impaired[142,146,147]. Altogether, these studies indicate that the role of different biophysical cues in tendon mechanotransductive processes remains still unclear. It also highlights the importance of developing new techniques to study and target more accurately specific molecular pathways. Therefore, it is an objective of this thesis to enlarge the body of research in tendon biomechanics and develop novel *in vitro* tools to study the role of piezoelectricity on tendon cell mechanotransductive processes through activation of specific receptors.

1.7.1 The role of mechanical stimulation parameters (magnitude and frequency) in tendon cell function

Thanks to intermolecular collagen cross-linking, loading on tendon generates relatively large elastic deformations. During the daily physiological activity, the strain experienced in tendons fall within a range of 2-4% at relatively low-frequencies (0.5–3 Hz) and only for a very few cycles per day. However, in extreme conditions, the tendon can withstand up to 10% deformations with minimal collagen fibrils and cross-links ruptures.
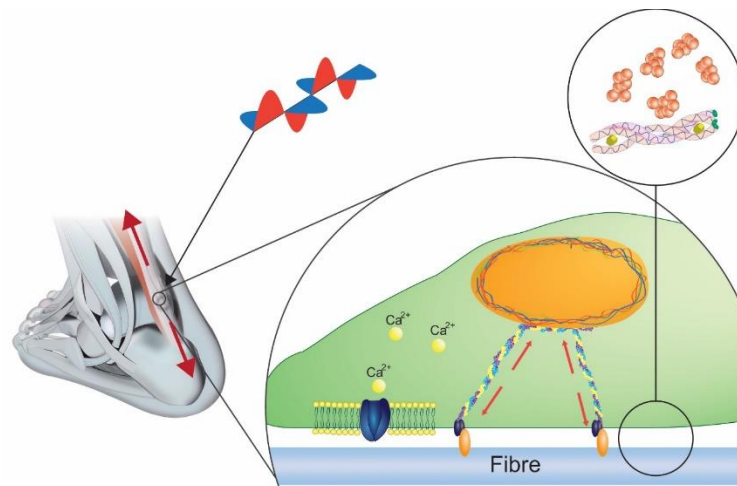
Figure 1-7. Mechanical stress and strain alter tendon healing processes. The physical environment is critical in modulating the number of tenoblasts and tenocytes as well as TSC differentiation. Fluid shear induces Ca^2 uptake via voltage-sensitive channel leading to both mechanotransduction and resulting in protein transcription, thus releasing growth factors such as TGF-β or IGF. However, it remains unclear how mechanical forces generated by the muscle are sensed and transduced through TGF-β signalling to modulate tendon homeostasis.

It has been hypothesised that strain in the tendon is the primary regulator for tenogenesis. Studies have shown that when tendon-derived stem cells are subjected to a low level of strain (<4%) they undergo tenogenic differentiation via TGF-β signalling and adopt an elongated phenotype; however, when the strain becomes too large (>8), tendon stem cells might differentiate into osteogenic lineages via Wnt and BMP signalling activation. Such contradictory results have led to use complex bioreactors combining mechanical loading with other physical approaches including biochemical, oxygen tension, electrical or topographical functionalization to obtain more reliable and sustain tenogenic phenotype maintenance *in vitro*.

Bioreactors are commonly utilised to support cell growth by enhancing cell distribution, ensuring transport of gases and nutrients in the medium, modulating temperature, oxygen concentration, pH, nutrient concentration, and biochemical and mechanical stimuli. Multiple tendon tissue bioreactors have been designed, including spinner flask, perfusion, rotating wall bioreactors and stretching being the mechanical stimulation the main active component of the bioreactor. Perfusion bioreactors are widely used and provide a constant, pulsating or oscillating fluid flow through a scaffold through the use of a peristaltic pump. The fluid flow allows for a homogeneous distribution of cell culture media but also applies mechanical stimulation to cells within the construct. The precise mechanisms by which mechanical stimulation can enhance regeneration are not yet fully understood. Computational modelling approaches have been applied to understand the influence of scaffold properties and external physical stimuli and predict the mechanical stimulation experienced by cells seeded within tissue-engineered scaffolds. These modelling approaches have been extended to include adaptive mechanoregulation algorithms that predict cell proliferation and bone tissue differentiation based on the magnitudes of mechanical stimulation (e.g. octahedral shear strain or fluid velocity). However, to produce competent predictions, it is indispensable

to understand first the effect of different mechanical stimuli in the relevant biological process, including cell differentiation and migration.

New emerging bioreactor technologies have emerged to offer greater control over the modulation of mechanotransductive pathways, thus providing a new route to engineering tendon-like environments. Over the last decade, extensive research has been performed on the structural and mechanical properties of the tendon to obtain the constitutive equations and predict tendon behaviour. In the past, vibrational analysis has been used to measure the elastic properties of tendons by determining its first resonance frequency. In more recent studies [148], bio-robotic systems have been developed to demonstrate that limb mechanical resonance (2.5 Hz) governs the spring-like behaviour of muscle-tendon interaction without the need for feedback from the neural network. However, during physical activity, repeated impacts are transferred, generating mechanical vibrations on flexor tendon (i.e. Achilles tendon) at much higher frequencies (25-50 Hz). Various studies have aimed to investigate the effect of low magnitude high frequency (LMHF) on MSC differentiation using different bioreactors. Recently, Lau et al. have proved MSC differentiation into osteoblasts in as little as 14 days using LMHF stimulation[149]. Curtis et al. demonstrated that even nanoscale vibrations (using piezoelectric actuators) at 50 Hz are sensitive enough to induce changes in the adhesion of endothelial cells by activation of endothelin-1 and kruppel-like factor 2[150].

Nanoscale high-frequency vibrational stimulation has been used recently in a study to promote osteoblastogenesis mediated by the MAPK pathway. This work identified that mechanical stimulation of 1000 Hz frequency with nanoscale displacements of 30 nm promotes significantly induced MSC differentiation without the use of any biochemical additives. The process was shown to be RhoA kinase (ROCK) dependent consistent with the osteogenesis process in 2D cultures via increased cytoskeleton tension (integrin-mediated pathway). While 1000 Hz seems high compared to traditional low magnitude high-frequency stimulation (up to 100 Hz), this frequency is in the same range at which hydrated bone becomes piezo active (972 Hz). Previous studies have shown that when cultured on 2D systems, nanovibrations induce MSC differentiation via cell adhesion mechanisms[151]. However, when high-frequency nanovibrations are employed, to 3D ECM hydrogels, MSC differentiation occurs via stretching-activated

ion channel including TREK, TRAAK, TRP and KCNK, and two recently discovered cation channels Piezo 1&2 that affect cytoskeletal organisation upon vibration.
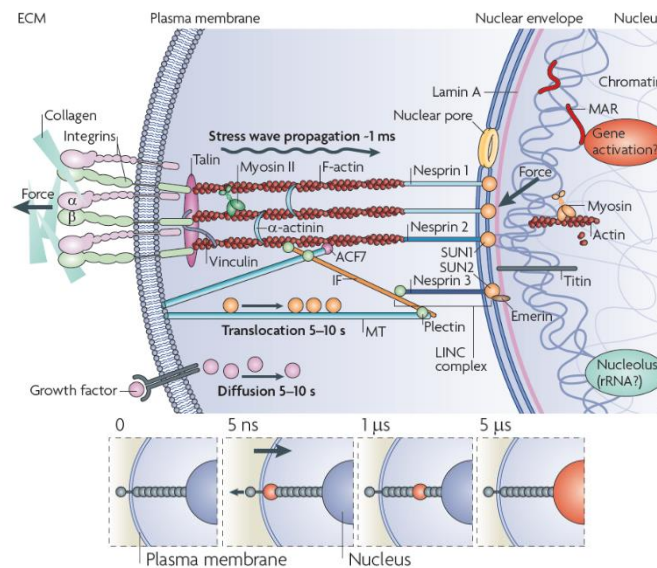
Figure 1-8. Molecules involved in ECM-Nucleus mechanotransduction: Proposed mechanism for forces propagated from the ECM to the nucleus over the discrete molecular network might initiate physiochemical and genetic changes. Forces applied to the cytoskeleton propagates into the nucleus in less than 5 µs highlighting the high capacity of cells to detect a wide range of mechanical vibration at frequencies up to 200 kHz.

Interestingly, in human adult tendon cells, two classes of ion channels have been identified, mechanosensitive and voltage-operated calcium channels which are thought to orchestrate physiological responses in tendon through mechanical loading

Table 1-5. Mechanical regulation of tendon cell cultures using bioreactors.

Mechanical regulation	Parameters of mechanical stimulation	Scaffold material (dimensions)	Results	Ref.
Custom-made step motor bioreactor with an environmental chamber	Cyclic stretching 2-mm, 90°rotation, 0.0167 Hz, 21 days	Collagen type I gels, *Bombyx mori*silkworm silk fibre matrices (length:30 mm)	Elongation of hBMSCs, cross-section cell density↑	76
Custom-made pneumatic cylinder bioreactor with LVDT for displacement monitoring	Cyclic stretching 2.4% strain, 0.0033 Hz, 8 h/day for 2 weeks	Type I collagen sponge (23±0.8 mm×9±0.8 mm ×3±0.1 mm)	Maximum force↑, linear stiffness↑, maximum stress↑, linear modulus↑	19
Custom-made step motor bioreactor	Cyclic stretching 10% strain, 0.25 Hz, 8 h/day for 7 days	Polyurethane construct (20×10×2 mm)	Type I collagen↑, TGFβ-1↑, CTGF, Elastin↑, alpha I↑, Procollagen↑, Fibronectin↑, MMP-1↑, elastic modulus↑	42
Custom-made bioreactor with load- displacement measure system	Cyclic stretching 9% strain, twice daily for 30 min each period separated by 8-h rest for 2 weeks	Small-intestine submucosa (3×5×95 μm)	Cell density↑, stiffness↑	35
Custom-made pneumatic cylinder bioreactor	Cyclic stretching 2.4% and 1.2% strain, 1 Hz, stimulation period: 8 h/day, 100 and 3000 cycles/day for 12 days	Type I collagen sponge	The stimulation pattern of 2.4% strain, 3000 cycles/day, 1 Hz has the best effect on increasing stiffness.	21
Custom-made pneumatic cylinder bioreactor	Cyclic stretching 2.4% strain, 0.0033 Hz, 8 h/day for 12 days	Type I purified bovine collagen gel, type I collagen sponges (length: 11 and 51 mm)	Stiffness↑	20
Custom-made linear actuator bioreactor with load cell for force measurement	Preloaded with 0.05 N, cyclic stretching 10%, 0.5 Hz, 2 h stimulation—2 h rest—2 h stimulation—18 h rest for 5 days	Porcine small intestine submucosa (length: 2 cm and width: 1 cm)	Improved fibre orientation, fibre angular dispersion↓, better organized collagen fibre, elongated cell morphology,	22
Custom-made linear actuator bioreactor with medium circulation system	Cyclic stretching 2% strain, 1 h/day, 0.0167 Hz for 1 and 2 weeks.	Human umbilical veins (wall thickness: 0.75 mm, outer diameter: 6.75±0.25 mm, length: 8.5 cm)	better cell distribution, more elongated cell morphology, cell proliferation↑, ultimate stress↑, elastic modulus↑	23

Custom-made pneumatic cylinder bioreactor with LVDT for displacement monitoring	Cyclic stretching 2.4% strain, 0.0033 Hz, 8 h/day for 2 weeks	Type I collagen sponge (94% pore volume; 62-mm mean pore diameter)	Type I collagen↑, linear stiffness↑	83
Custom-made step motor bioreactor	Cyclic stretching 10% strain, 2 h/day, 1 Hz for 14 days	Knitted silk-collagen sponge scaffold (5×0.5×0.2 cm)	Collagen I↑, Collagen III↑, Epha4↑, Scx↑, Sox9↓, Myosin↑, Integrin α1↑, Integrin α2↑, Integrin β1↑, Collagen content↑, Collagen diameter↑, better cell alignment	2
Custom-made linear motor bioreactor	Cyclic stretching 10% strain (5% offset, 5% amplitude), 1 Hz, 3 h/day, 1. 7, 14, and 21 days	Poly(ethylene glycol)-based hydrogel material oligo(poly(ethylene glycol) fumarate) (12.5×9.5×1.6 mm)	Collagen I↑, Collagen III↑, TNC↑, Tenascin-C↑	27
Ligagen L30-4C (Tissue Growth Technologies)	Cyclic stretching 1.25 N, 1 cycle/min, 1 h/day for 5 days	Acellular rabbit hindpaw tendon (length: 5 cm)	Ultimate tensile stress↑ (closed to fleshly harvested tendon), elastic modulus↑	36
Custom-made bioreactor	Cyclic stretching 2% strain, 1 h/day, 0.0167 Hz for 1 and 2 weeks.	Human umbilical veins (wall thickness: 0.41 mm) with Wharton's jelly matrix as central portion (total thickness: 0.75 mm)	Cell proliferation↑, tensile strength↑	28

1.7.2   The role of electrical cues in cell function.

In the words of the pioneer of developmental bioelectricity Michael Levin*: "The process of embryonic development is a remarkable one. A cell by self-assembly process can form an embryo, and each embryo develops different body parts. Recent studies have proposed that the three-dimensional structure and identity information is encoded in the environment available to every single cell. Many different cell types are created during embryonic development such as nerve, skin and, muscle. Moreover, all of them become arranged with the appropriate three-dimensional architecture, and this is a fundamental aspect of regenerative medicine. This ability of living tissues to assemble into complex forms is fundamental to most of the regenerative medicine applications. Then if we imagine that we could control the generation of any 3D complex architecture, we will have the key to address most of the degenerative diseases and even able to replace lost tissue."*

Electrical signals cooperate with all the other physical signals, including biochemical, and physicomechanical. In 1952; an exciting experiment demonstrated that the formation of a primitive form of amino acid is triggered by electrical energy. In this experiment, Dr Miller[152] filled a jar with methane, ammonia, hydrogen and water and using sparkling he demonstrated the generation of primitive forms of amino acids. The evolutionary theories that this experiment tried to validate are beyond the topic of this thesis; however, this experiment also aligns with the idea that electrical inputs trigger protein synthesis or post-translational modifications. In more relevant experiments, Levin *et al.*, exerted control upon the activity of transmembrane protein ion channels to regulate the levels of ionic exchange between the cell and its extracellular surroundings and therefore manipulate the membrane resting potential. It was observed that in a narrow range of voltages, specific tissue formation processes such as eye formation could be initiated even in ectopic regions such as the gut. **This study together with others** [84–86,108,110,111,153] **demonstrated that the ability of differentiation into another lineage (induced by physical regulators alone without any gene master regulator) is not restricted to stem cells and any cell regardless their differentiation stage can potentially transdifferentiate**.

Studies on rabbits have shown that electrical stimulation (direct current, DC) after full-thickness defect of the patellar tendon was enough to recover the functionality of the tendon in a short time compared to control conditions[154]. Electrically healed tendons

26

showed significantly higher tensile strength and decreased the relative proportion of collagen type III present. This study concluded that electrical stimulation could not change the collagen content; however, ES can modulate the ratio of collagen types.

In orthopaedic applications, electrical stimulation by pulsing electromagnetic fields (PEMFs), capacitive coupled electric field (CCEF) and electromagnetic stimulation (EMS) have been shown to enhance tissue regeneration *in vivo*. Recently, clinical trials on human have been conducted to assess the effects of low-voltage micro amperage stimulation (LVMAS) on wound healing. The results indicated that electric currents with intensities between 50 and 1000 μA facilitated healing in skin ulcers. These findings suggest that ES could also be beneficial for soft tissue healing such as tendons and ligaments, despite the healing mechanism remaining elusive. However, the need for implanted electrodes and a voltage generator which may elicit an adverse tissue reaction or inflammatory response limits the possible use of implantable stimulations in clinical applications. In this context, biomaterials that can produce bioelectric patterns similar to those of present in tendon and minimise foreign body reaction represents a key asset for tendon repair applications.

Several authors have studied the use of electrically conducting polymers for tissue engineering and recent studies using electrical stimulation through an electrically conductive scaffold of PPy/HE/PLLA suggest that these can provide specific cues by introducing electrical fields to modulate cell behaviour. Here, an optimal potential gradient of 200mV/mm and exposure time between 2 and 8h, was optimum for the upregulation of proliferation and the expression of specific markers. Also, composite conducting polymers reinforced with nanotubes offer enhanced mechanical, electrical and thermal properties that accelerate new tissue formation as previously shown. Recently, electrical stimulation through conductive fibres of PEDOT showed high expression of collagen I, collagen III, decorin, biglycan and aggrecan genes on tendon cells. However, further investigation is needed in the development of materials for a controlled biological response without the requirement for an external power supply.

Table 1-6**.** Electrical stimulation studies on musculoskeletal cells using external stimulators.

Electrical stimulation	Parameters	Cell source	Results
Microamperage low voltage	0.5 -6 uA	Tendon-derived cells	Below 1 uA, suppressed proliferation of synovial cells. Tenocytes proliferation was increased and promotes collagen production. Prevents adhesion
Microamaeprage low voltage	0.05-1.5 mA for 1,2 and 3 days	Equine tenocytes	Accelerated cell proliferation and DNA content. Differential behaviour in apoptosis depending on the rate per day.
Transcutaneous electrical nerve stimulation	0.05 -1.5 mA; 5-70 mA;1-2h	Tenocytes	More satisfactory results at higher frequencies. Proliferation increased. Production and maturation of collagen fibres were enhanced.
Extremely low frequency electromagnetic field	3 mT, 60 Hz	Mouse osteoblast-like cells (MC3T3-E1)	ALP (ERK1/2; PD98059) " Sirius red (Collagen detection) "
AC electric field	Interdigitated electrodes (1 Vcm, 1 Hz, 4 h/day for 14 days)	Human adipose-derived stem cells (hASCs)	Calcium deposition " 100 V/cm damage, 1000 V/cm dead. Gene expression " (ALP, Collagen I)
AC electric field	Parallel electrodes, carbon rods (20 mV cm,60 kHz, 40 min day21 for 28 days)	Human adipose-derived stem cells (hASCs)	Hsp27, 70 mRNA " (Heat shock protein)
Single electric field	Parallel electrodes, square wave electric pulses (1 V mm , 1 or 90s) after 4 days (10 V cm for 5 ms at 1 Hz)	Human embryonic stem cells (hESCs)	Reactive oxygen species (ROS)
DC electrical stimulation	Parallel electrodes (15 V, current density : 4.2 A m, 1 h day21 for 3 weeks)	Osteoblasts (CEL-11372, ATTC)	ALP, Calcium deposition " (3 week)
Pulsed electromagnetic fields (PEMFs)	Single quasi-rectangular pulses (300 ms, 7.5 Hz); electric fields (2 mV cm 21, 0.13 mT)	Human mesenchymal stem cells (hMSCs)	ALP " (early), Collagen GAPDH #
Multiple electrical stimulation	2V cm21, 6 h/day for four weeks	Saos-2 cells (ATCC)	ALP, Calcium deposition " Gene expression " (ALP, BMP2, Runx2, OC)
Pulsed electromagnetic fields (PEMFs)	75 6 2 Hz, 5 6 1 mV, 2 6 0.2 mT. 24 h day 21 for 22 days	Saos-2 cells (ATCC)	Gene expression " (Decorin, OC, OP, Collagen I, III)
Biphasic electric current stimulates (BEC)	1.5 mAcm22 at 3000 pulses/ s, 6 and 24 h day21 for 4 days	Rat calvarial osteoblasts	Cell proliferation "(31%)
Biphasic electric current stimulates (BEC)	250 ms, 1.5 mAcm22 at 100 pulses/s 25 ms, 15 mA cm 22 at 100 pulses/s	Human mesenchymal stem cells (hMSCs)	Cell proliferation, ALP, Calcium deposition "
Electrical stimulation	DC : 0.1 V cm21,1 Vcm21 , 10 V cm,30 min day; AC : 1 V cm—1 Hz, 30 min day	Human mesenchymal stem cells (hMSCs)	Gene expression " (ALP, OC, Collagen I) cell density, ALP "

1.8 Physicomechanical strategies for tendon regeneration.

Over the years, the compendium of physical, chemical and biological events at the interface between the tendon and an implanted device has evolved as a critical frontier in determining the long-term functional success of an implant. A fundamental tenet of medical device design has evolved from the excellent ability of biological systems to respond to topographical features or chemical stimuli, a process that has led to the development of next-generation biomaterials. The material surfaces encountered by tendon cells following implantation usually possess physical features resulting from the fabrication processes, and experimental studies have established that implant features ranging from micro to nano-scale significantly modifies the functional activity of cells and accelerates the maturation of tendon tissue at the device/tissue interface.

Additionally, the response of tendon cells to regulatory agents such as the TGF-β, insulin and ascorbic acid is enhanced by physicomechanical strategies including nanopatterning of surfaces, mechanical and electrical stimulation. These findings continue to inspire the search for new strategies that will consistently enhance functional bonding between devices and host tendon tissue.

1.8.1 Topographical functionalization to modulate cell adhesion

Adherent cells are sophisticated, self-sustaining units that require extracellular matrix (ECM) anchorage to proliferate and undergo differential function. Cells actively probe the physical properties of the ECM; their contractile machinery facilitating the formation of fine nanoscale protrusions termed filopodia, structures which gather spatial, topographical, and chemical information from the ECM and material surface and act as precursors to cellular adhesion.

Cell-scaffold interactions are determined by adhesion receptors (integrins) that act as communication channels between environment and intracellular machinery. Integrins are transmembrane receptor composed of non-covalently linked α and β subunits which bind to specific amino acid sequences found in adhesive proteins such as fibronectin (i.e. RGD tripeptide). Integrins associates with intracellular supramolecular complexes (focal adhesions, FA) that contain structural adaptor proteins such as vinculin, focal adhesion kinase, talin and paxillin. During the process of cell adhesion to a surface, integrins together with focal adhesions are recruited and clustered varying in number

and size depending on the external force determined by the matrix rigidity or mechanical stimuli, thus acting as mechanosensors. When the forces reached the critical threshold value, the FA will grow, and the cell will elongate following the direction of the force.

Material topography and in particular micros and nano-scale features have shown in vitro that can affect cellular behaviour through integrin-mediated cell adhesion. While microscale topography aims to create and use structures with a dimension range, which covers the cellular, subcellular and macromolecular scale, nanotechnology covers the atomic and molecular scales. Although microtopographical modification is well documented as a potent modulator of tissue integration, the extent to which nanotopography influences cell behaviour *in vivo* remains unclear, and investigations are still ongoing into the relevance of nanoscale topography in orthopaedic device manufacture and whether implants can be reliably fabricated to include these topographical structures. The processes that mediate the cellular reaction to nanoscale surface structures, however, are not well understood and may be direct (a direct result of the influence of the surface topography) or indirect (where the surface structure has affected the composition, orientation, or conformation of the adsorbed ECM components).

Several studies have demonstrated that physical signals control not only cell differentiation but also cell self-organisation (tissue formation) exploiting material surfaces ability to change cell contractility through focal adhesion formation and growth. In a recent study, tenogenic differentiation of hMSCs was mediated by nanopatterning (300 nm and 700 ridges) of material aiming to control initial cell adhesivity and contractility. For tenogenesis to initiate, it was observed that large focal adhesions (> 10 um), well oriented and confined (around 700 nm) were determinant. Interestingly, in similar studies, Dalby et studied the effects of different nanopatterns on osteogenesis. Five patterns using 120 nm diameter and 100 nm depth nanopits were investigated (square, hexagonal, disordered, highly disordered and planar) and all had an average spacing of approx. 300 nm. The results showed that highly ordered patterns such as hexagonal arrays of pits offered negligible osteoblastic differentiation and reduced cell number compared to control biochemically (OSM) stimulated cells. However, on a random pattern, cells were observed to differentiate into osteoblasts and produce bone nodules. This emphasises the dominant role of nanoscale features on

tissue specification such as tenogenesis or osteogenesis. It is hypothesised that the order/symmetry and distance of the focal adhesion produced by the MSCs were able to modulate the cell differentiation process. As a result, cytoskeletal tension and mechanotransductive pathways have an effect on chromosome positioning during cell division and gene expression.

Although a large number of studies have reported on the effects of nanotopographical structures on enhanced tenospecific function *in vitro,* a limited number of studies have been conducted on the effects of nanoscale implant modification *in vivo.* Studies are emerging and shown that nanotopography increases implant-tissue integration and favours *de novo* tendon formation*,* indicating that observed *in vitro* effects can be translated into a clinical response.

A range of fabrication methods are available for the generation of topographical features, range from photolithography, laser irradiation, electrospinning or electron beam lithography (nanoscale), to name but a few. Electrospinning emerged over ten years ago as an enabling technology to produce micron and nanoscale fibres that can emulate the morphology and structure of the ECM for tissue engineering applications. Such fibre-based scaffolds with high porosity and specific surface area and nanotopography are demonstrably potent effectors of cellular behaviour, mainly when fabricated into formats presenting fibre dimensions incorporating the micro to the nanoscale. Three-dimensional scaffolds containing electrospun micro and nanoscale fibres have been studied extensively in the context of tendon regeneration, with an aim to fabricating hierarchical environments that mimic the ECM and promote cell adhesion, proliferation and differentiation. However, despite numerous studies of functional differentiation on electrospun scaffolds, relatively little is known about whether nanofibrous scaffolds accommodate continuous differentiation of MSCs into tenocytes in the absence of inductive agents or further biomimicry

1.8.2   Biochemical functionalization for endocrine/paracrine signalling

Growth factors can mediate biological processes that are necessary for tissue repair following trauma or injury via autocrine and paracrine signalling. Supplementation with single growth factor can control tendon resident cell phenotype, differentiate stem cells into an endogenic lineage *in vitro*, and stimulate the reparative process *in vivo*, with variable degrees of efficacy in preclinical and clinical settings.
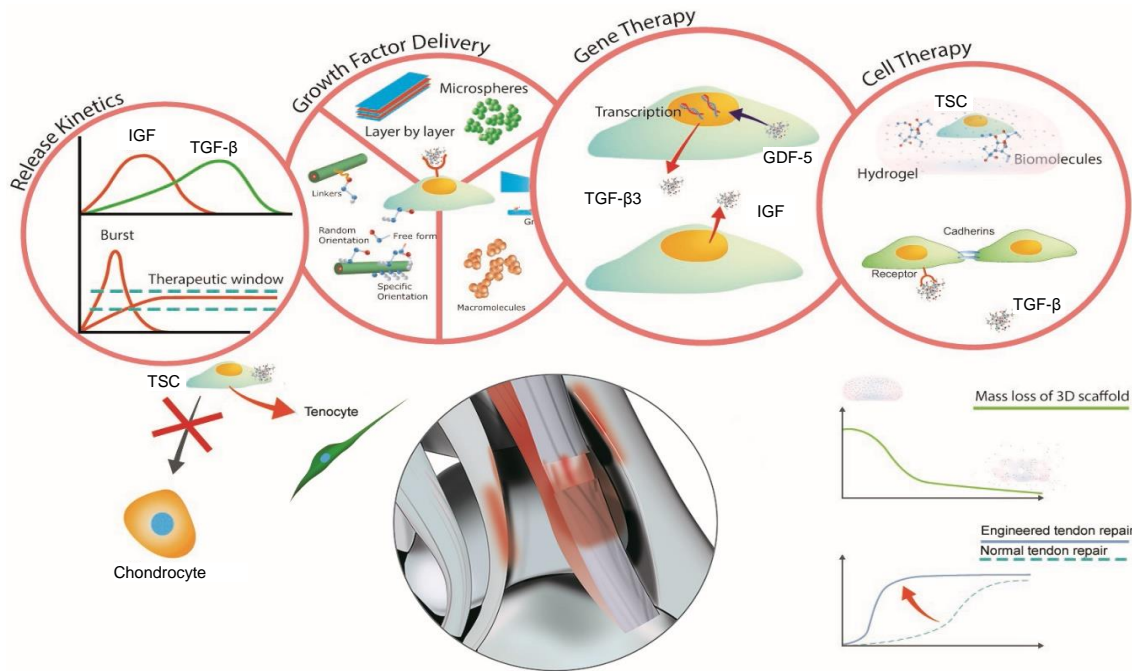
Figure 1-9. Tissue engineering and regenerative strategies. Application of biological agents such as WNT, BMP, and TSCs can accelerate tendon tissue repair. However, the delivery sequence of these biological agents is essential. For example, whereas both BMP and WNT are important for regeneration, the presence of BMP may downregulate WNT. Therefore, sequentially growth factor delivery may enhance the therapeutic efficacy of such biological agents. Gene Therapy has been used to generate populations of cells that constitutively express either growth factors to promote tissue regeneration. These strategies can be used alone to induce homing of endogenous MSCs or in combination with classical MSC based tissue engineering concepts (seeding of MSCs into scaffolds for implantation).

The strategy of concurrently modulating the chemical environments of tendon ruptures via controlled delivery/elution of potent pharmacological or biological agents from an implant represents an elegant method of targeted therapeutics. This strategy is peculiar in that it enables the higher local concentration of the bioactive agent at the site of need while the desirable bulk properties of the implant are unaltered. Such treatment is particularly useful in chronic tenosynovitis where high concentrations of antimicrobials are required over a prolonged period. It also offers the opportunity to maximise the local growth-inducing potentials of bioactive agents while minimising the local and systemic side effects that could be attributable to other routes of delivery such as systemic or

non-controllable local delivery. Besides, it prevents the implant from becoming a template for microbial growth.

Similarly, the delivery of an increasing number of growth factors inducing cytokines, peptides and proteins with significant roles in the tendon regeneration process has been investigated. Different growth factors are stimulated at multiple stages in the tendon repair leading to increased cellularity and tissue volume (figure). Among these, the bone morphogenetic proteins (BMP-12,-13, and -14 also known as GDF-7,-6 and-5)), transforming growth factor-beta (TGF-β), vascular growth factor (VEGF), fibroblast growth factor (FGF), platelet-derived growth factor (PDGF), insulin-like growth factor (IGF), and connective tissue growth factor (CTCG) continues to generate significant interest. Although controlled localised delivery of these agents represents a superior concept to bolus supraphysiological doses commonly employed in contemporary clinical applications, attainment of therapeutic efficacy remains challenging principally due to reduced loading efficacy. Besides, the protein conformation of many of these growth agents is sensitive to the local environment as well as the method of immobilisation.

Table 1-7. Signal transduction studies *in vitro* and *in vivo* using growth factors.

Biochemical regulation	In vitro study	Results	In vivo Study	Results	References
GDF-5	In vitro tenocyte augmentation with GDF-5 followed by in vivo midsubstance tenotomy and suture repair with or without 10 µg GDF-5 injections	Increased expression of aggrecan, Col.I, Col.III, scleraxis, tenomodulin, and MMP-9	Tendon insertion point resection and repair with dip-coated GDF-5 sutures	Increased stiffness, tensile strength, and cross-sectional area of lacerated tendons	[14]
GDF-5	Tenocytes augmented with varying GDF-5 concentrations	Increased tenocyte proliferation and ECM production. Increased expression of aggrecan, Col.I, Col.III, scleraxis, tenomodulin, and MMP-9	Tendon transection and repair with GDF-5 coated sutures	Increased stiffness, tensile strength, and cross-sectional area of lacerated tendons	[15]
GDF-5	ADMSCs augmented with varying GDF-5 concentrations	Increased proliferation and ECM production of ADSCs	Tendon transection and repair with GDF-5 coated sutures	Maximal load and collagen histology scores were higher for GDF-5 group than controls	[16]
GDF-7	Rat bone marrow-derived MSCs were cultured in monolayer and treated with GDF-7. These cells were then implanted in half-width defects of the calcaneal tendon	Administration of GDF-7 increased expression of scleraxis, tenomodulin, Col.I, and tenascin-c. When implanted in vivo, cells treated with GDF-7 increased cell number, matrix deposition, and alignment relative to untreated MSCs	Augmentation of double-row reattachment of the infraspinatus tendon with rhGDF-7 soaked Col.1/Col.III sponges	Tensile strength in rhGDF-7 collagen sponges was 2.1 times higher than in tendons augmented with untreated sponges	[24]
GDF-7 and BMP-13	Midsubstance tendon transections were left to heal unaided, or healing was enhanced by GDF-7 or BMP-13 injections	GDF-7 and BMP-13 both increased tissue volume and tenocyte infiltration. The rate of tendon repair as measured by tendon width overtime was enhanced in augmented rats	Quadricep ectopic implants of GDF-5, GDF-6, and GDF-7	Each GDF 5, 6, and 7 implant induced formation of organised Col.1 resembling neotendon	[26]
TFG-ß1		IGF-1 at 10 and 100 ng/mL maintained multipotency in tendon stem cells	TGF-b1 and IGF-1 were administered to patellar tendon defects via a fibrin sealant	Increased ultimate failure load, stress, and stiffness	
IGF-1	Tendon stem cell culture	GDF-5 increased Col.I expression at 10 and 100 ng/mL after 28 days	Collagenase-induced lesions of equine flexor digitorum superficialis tendon were treated with ten 2 µg rhIGF-1 injections	IGF-1 significantly reduced lesion size at all timepoints over the 8-week study but did not affect ultimate failure load, GAG content, or Col-I:Col-III ratios	[31]
TFG-ß1	Tenocytes cultured in Col.I hydrogels	Increased expression of Col.V, Col.XII, and	Achilles transsection repair by	Increased failure load and stiffness; dose-dependant increase in	[32]

	exposed to varying TGF-ß1 concentrations	scleraxis. No effect on Col.1 synthesis	Tsuge method with TGF-ß1 injection	procollagen I and III expression	
TFG-ß1	Cultured flexor tendon endotenon, epitenon, and sheath cells were exposed to 2 ng/mL TGF-ß1	Decreased expression of Col.I in endotenon cells; increased expression of Col.III in all three cell types	Patellar tendon transsection repair with TGF-ß1 injection	Improved tangent modulus and increased failure loads	[33]
IGF-1	Equine tendon and bone marrow derived cells were cultured in monolayer with or without IGF-1	IGF-1 enhanced cell number and collagen and GAG synthesis	Patellar	Nielsen et al. [40]	[36]
IGF-1 and FGF-2	Tendon cells were expanded in monolayer with or without FGF-2 augmentation. Other tendon cells were cultured in an acellular pulverized tendon matrix with or without IGF-1	FGF-2 significantly increased ECM and Col.III synthesis. IGF-1 increased and Col.I and Col.III expression	MSCs and MSCs cultured with IGF-1 were used to treat SDFT	MSC and MSC + IGF-1 improved histological scores but did not affect expression of Col-I or Col-III. There were no significant differences between the MSC and MSC + IGF-1 groups	[37]
IGF-1	Superficial digital flexor tendon explants were cultured with or without IGF-1	IGF-1 increased DNA content by 31 %, GAG content by 29 %, and collagen synthesis by 72 % relative to untreated controls	Racehorses with superficial digital flexor tendonitis were administered 4–5 intralesional IGF-1 injections	Treatments reduced echolucency in 23 of 26 subjects, and 63 % were able to return to racing	[38]
PDGF-BB	Tenocytes from rat intrasynovial tendons were cultured and treated with plasmids containing PDGF c-DNA	PDGF gene transfer increased expression of PDGF-BB and Col-I	Achilles tenotomy repair augmented by PDGF injections at 3 or 10 μg	The 3 μg injection caused a roughly 2-fold improvement in maximum load after 7 days. The 10 μg injection caused a twofold improvement in maximum load at 21 days	[67]

1.8.3 Piezoelectric materials for tendon tissue engineering:

One of the critical challenges in tendon tissue engineering is the development of new strategies that combine a scaffold with cellular elements and regulatory cues to provide enhanced tissue regeneration. The function and fate of the cells are regulated by multiples biofactors but also by variable extracellular and matrix-mediated signals such as strain, rigidity, electrical fields and topography, which have been described previously as promising strategies for the regulation both *in vitro* and *in vivo* of tendon regeneration. The physical properties of engineered scaffolds such as morphology/topography, porosity, and mechanical properties play an essential role in regulating cellular infiltration, following activity and healing. Also, the material composition and surface chemistry will mediate initial protein adsorption and subsequent cellular adhesion and differentiation *in vivo*.

The interaction between cellular components and engineered scaffolds are bidirectional; i.e., a cellular-induced response such as deformation of the scaffold changes material characteristics including pore size that in turn modulates cell infiltration behaviour. Consequently, stimuli-responsive or "smart" biomaterials offer significant possibilities for next-generation tendon regeneration strategies. The ideal strategy for regenerative tendon therapies is to use a "smart" biomaterial that can modulate the process of healing while providing mechanical support. In the search for materials capable of meeting both physicochemical and biological requirements for tissue regeneration, electroactive polymers have emerged as a field of interest. Interestingly, piezoelectric materials are well suited to tendon device design, exploiting the inherent large loading capacity of tendon tissues to produce stimulating current for tissue repair.

1.8.3.1 What is piezoelectricity*?*

Piezoelectric materials are dielectric materials with non-centrosymmetric crystallographic structure[155,156]. When a piezoelectric material is under an external force, the lattices are strained, changing the position of the electric charges barycenters. This polarisation is what we refer to as direct piezoelectricity. Conversely, when a voltage is applied to a piezoelectric material, a deformation of the lattices appears.
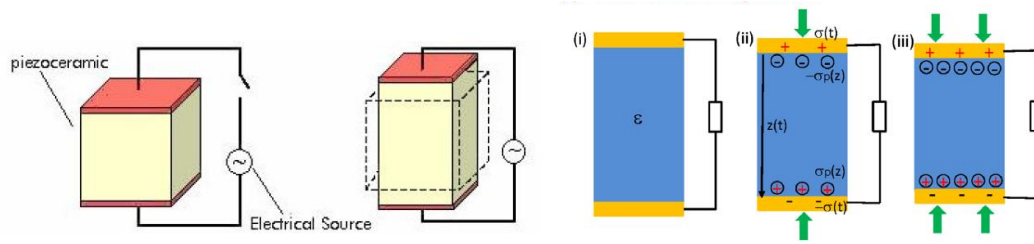
Figure 1-10. a) Direct or inverse piezoelectric effects b) Charge accumulation or polarisation is proportional to the applied pressure.

Fundamental physical principles: Constitutive equations

It is essential to understand the physics governing piezoelectricity to start by talking about one of the major discoveries in human history: **the unified theory of electromagnetism by Maxwell[157]**.

Maxwell in 1861 first postulated the term *displacement current* (J_D) [158,159] that unified two (in that time) independent theories: Ampere's law (magnetic field) and the continuity equation for electric charges (electric field). However, Maxwell introduced a radically new concept that its implications to today's technologies advancements are invaluable: *displacement current* is not the free flow of moving free charges (electric current) but the time-varying electric field (vacuum or media, $\varepsilon_0 \boldsymbol{E}$), plus a contribution from the motion of charges bound in atoms, dielectric polarization in materials (**P**).

$$\boldsymbol{D} = \varepsilon_0 \boldsymbol{E} + \boldsymbol{P}$$
Equation 1-1

Where the electric field **E,** displacement field **D**, polarisation field **P**, and permittivity in vacuum ε_0.

$$J_D = \frac{\partial D}{\partial t} = \varepsilon_0 \frac{\partial E}{\partial t} + \frac{\partial F}{\partial t}$$
Equation 1-2

. Briefly, this equation (the first component, $\varepsilon_0 \frac{\partial E}{\partial t}$) describes an electromagnetic wave behaviour and has been used to develop the wireless communication that we today use (TV, radio and internet).

Surprisingly, the second component ($\frac{\partial P}{\partial t}$), is still yet to be exploited for the development of new advanced technologies and piezoelectric materials can take full advantage of this

second term to produce displacement current as a response to physical stimuli such as stress/strain gradients or temperature changes.

$$P_i = (e)_{ijk}(s)_{jk}$$

<div align="right">Equation 1-3</div>

$$J_D = \frac{\partial P_i}{\partial t} = (e)_{ijk}\left(\frac{\partial s}{\partial t}\right)_{jk}$$

<div align="right">Equation 1-4</div>

Where $(s)_{jk}$ is the strain tensor and $(e)_{ijk}$ is a third order piezoelectric tensor

A piezoelectric material is usually anisotropic and is described mathematically within a piezoelectric constitutive equation. Unlike non-piezoelectric materials that show no relationship between electrical field and strain/stress field, piezoelectric materials main characteristic is the direct relationship between stress (T), strain (S), charge-density displacement (D) and an electric field (E). There a four possible forms of the piezoelectric constitutive equation: (1) strain-charge form, (2) stress-charge form, (3) strain-voltage form and (4) stress-voltage form. Briefly, four interconnected different piezoelectric constants s (e, g, h, d) define piezoelectric behaviour.

Piezoelectric constants
− d [C/N] = (Charge developed)/(applied stress)
− g [V-m/N] = (Electric field developed)/(applied stress)
− h [m/V]=(Strain developed)/(applied E-field)
− e [N/V-m] = (Stress developed)/(applied E-field)

Finally, to completely define the physical behaviour of any piezoelectric material four additional constants are used, two mechanical constants (c - stiffness, s - compliance) and two dielectric constants (ε - dielectric constant, β - permeability constant).
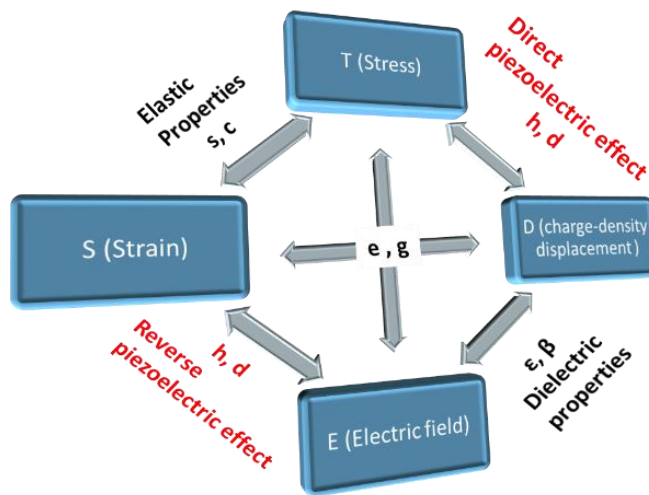
Figure 1-11. Relationship between the eight constants.

The following equations describe the electromechanical (stress-electrical field) coupling of a piezoelectric material:

$$T = c^E \cdot S - e \cdot E \; (E = const) \hspace{4cm} \text{Equation 1-5}$$

$$T = c^D \cdot S - h \cdot D \; (D = const) \hspace{4cm} \text{Equation 1-6}$$

Where E is an electric field, T stress, D displacement field S strain and, c^E and c^D are stiffness coefficients under constant E and D, e and h are piezoelectric coefficients.

Precise control of the mechanical (stiffness), electrical (dielectric constant) and piezoelectric coupling (piezoelectric coefficient) properties describe the performance of piezoelectric systems. The integration of piezoelectric materials in new technologies requires a full understanding of piezoelectric behaviour and in particular, the different conduction modes of electrical energy. Unlike current electromagnetic systems, the conduction mechanism mode in piezoelectric systems is capacitive, in which the electrical transport is transmitted not via the free flow of charges across the electrodes of the capacitor, but via electromagnetic wave and induction.

Based on a capacitor model, the output current of a piezoelectric can be represented by:

$$I = \frac{\partial Q}{\partial t} = C\frac{dV}{dt} + V\frac{dC}{dt} \hspace{4cm} \text{Equation 1-7}$$

Where **Q** is the stored charges in the capacitor, the first term $C\frac{dV}{\partial t}$ is the current introduced by a change in the applied voltage; the second term $V\frac{dC}{\partial t}$ is the current introduced by the variation in capacitance.

Since the variation in capacitance is rather small (changes in crystal size/thickness are minimal), the equation can be simplified to the contribution of just the first term:

$$I \approx C\frac{dV}{\partial t} = A\frac{dc}{dt}$$
Equation 1-8

Where **A** is the area of the electrode. Under short circuit condition, $\sigma = \sigma(z,t)$ and the result:

$$I = A\frac{d\sigma_p}{dt}\frac{dz}{dt}$$
Equation 1-9

It is fundamental for the use of piezoelectric systems in any biomedical engineering application to understand the physical implications of these equations. Importantly, two main distinct physical behaviours arose from these constitutive equations:

1) The electrical current is proportional to the charge density on the surface: Meaning that the surface charge, current and voltage are directly proportional to the force magnitude used to activate the system.

2) The velocity or changing rate (frequency) is not proportional to the charge density on the surface: Meaning that frequency of applied force has no effect on energy production, and any frequency can be used (upper operating limit is the resonant frequency). Friction and internal losses should be considered when choosing an operating frequency. Also, there is a low-frequency limit for measuring purposes since piezoelectric materials unsuitable for generating static electrical forces.

Piezoelectric modes: d_{31} and d_{33}

Piezoelectric materials are anisotropic materials due to their particular crystallographic structure, so their properties are dependent on the crystal orientation. Generally, the crystal orientation can be described using the three-dimensional axis system, placing axis 3 along with the thickness of the film and axis 1 along its longest side. All the physical parameters describing a piezoelectric material are described using tensors of different orders. The piezoelectric coefficients are presented in matrix form and denoted

by d*ij*, where index i refers to the direction of generated voltage, and index j refers to the direction of applied stress.

As already introduced, to precisely control or model a piezoelectric system, all the physical parameters need to be measured and are 63 in total: 36 flexibility coefficients **s**, 18 piezoelectric coefficients **d** and nine permittivity coefficients **ε**. Fortunately, there is still enough symmetry in a piezoelectric material (even in non- centrosymmetric systems) to reduce this number. As shown in Figure 1-12, the matrices for s, d and ε are reduced when taking into consideration this symmetry.

However, for this work and in general practice, only two piezoelectric coefficients are used: d33 and d31. Therefore, we usually refer to or speak respectively of a "3-3 mode" or "3-1 mode" of operation.

$$s = \begin{bmatrix} s_{11} & s_{12} & s_{13} & 0 & 0 & 0 \\ s_{12} & s_{22} & s_{13} & 0 & 0 & 0 \\ s_{13} & s_{13} & s_{33} & 0 & 0 & 0 \\ 0 & 0 & 0 & s_{44} & 0 & 0 \\ 0 & 0 & 0 & 0 & s_{44} & 0 \\ 0 & 0 & 0 & 0 & 0 & 2(s_{11}-s_{12}) \end{bmatrix}$$

$$d = \begin{bmatrix} 0 & 0 & 0 & 0 & d_{15} & 0 \\ 0 & 0 & 0 & d_{15} & 0 & 0 \\ d_{31} & d_{32} & d_{33} & 0 & 0 & 0 \end{bmatrix} \qquad \varepsilon = \begin{bmatrix} \varepsilon_{11} & 0 & 0 \\ 0 & \varepsilon_{22} & 0 \\ 0 & 0 & \varepsilon_{33} \end{bmatrix}$$

Figure 1-12. Coefficient matrices for piezoelectric materials.

A short introduction to PVDF polymers, including their properties and applications is presented in continuation.

1.8.3.2 Piezoelectric systems for biomedical applications based on PVDF and its copolymers

PVDF can produce electrical charges as a response to minute mechanical stress or strain changes. PVDF is a semi-crystalline polymer that can present five distinct crystalline phases: α, β, γ, δ and ε. Different phases are related to different chain conformations: TTT (all-trans) planar zigzag for the β-phase, TGTG' (trans-gauche-trans-gauche) for the α and δ phases and T3GT3G' for γ and ε phases (see Figure 1-13). Polyvinylidene difluoride (PVDF) and its copolymer PVDF-TrFE are a chemically stable thermoplastic fluoropolymer discovered in 1969 by Kawai[160]. The piezoelectric effect of PVDF is one order of magnitude higher than those of other piezoelectric polymers, including PLA and PHB. Since then, PVDF and its copolymers have been studied for their use of piezoelectric technologies.

Piezoelectric systems (PS) based on PVDF-based materials have the advantage of low power consumption, high sensitivity and ultrafast response. However, a common disadvantage is that achieving an excellent piezoelectric performance requires multiple processing processes. For PVDF, this is obtained by using the d_{33} mode; thus, aligning the internal dipoles in the same principal direction of the mechanical stretching/loading field. Various strategies have been studied to manipulate internal dipoles orientation on PVDF and its copolymers[161–165]. PVDF can be processed into four differing crystalline phases, known as the α, β, δ, and β-phase with all-trans planar zig-zag conformation (TTT) offers the best electroactive performance. The piezoelectric properties of PVDF derive from the strong dipole moment due to the electronegativity difference between Fluor and Hydrogen atoms ($5-8.10^{-30}$ C/m)[166]. Each polymeric chain has a dipole moment perpendicular to the polymer chain and, when the polymer chains are packed into crystals, the dipoles align parallel and a net dipole moment appears as it is the case in polar β, γ and δ (polar α) phases. In antiparallel chain dipoles, the net dipole moment is zero as the dipoles cancel each other as it is the case in non-polar α and ε (non-polar γ) phases. Besides, β-phase has attracted particular interest owing to its unique piezoelectric performance (net dipolar moment per unit cell is 8.10^{-30} C/m). The use of different procedures, including electric poling, mechanical stretching or incorporation of steric effect, can induce polar phase formation from the non-polar phase (see Figure 1-13). Mechanical stretching is the most common one, where the applied stress results in the alignment of polymer chains into the crystals and allows the dipoles to align perpendicularly to the applied stress direction. Another practical way to obtain β-phase is to use PVDF-based copolymers. The addition of another bigger monomer (TrFE) induces the by steric effect crystallisation into β-phase (almost 90%). One typically used PVDF copolymer is poly(vinylidene fluoride-co-trifluoroethylene), P(VDF-TrFE), which has a piezoelectric coefficient up to -38 pC/N (twice as much as PVDF). Unlike ceramic piezoelectrics where the piezoelectric mechanism is governed by dipole reorientation, piezoelectricity in PVDF is governed by volume electrostriction; as a result, the d_{33} and d_{31} piezoelectric coefficient are negative in PVDF.

a)   b)
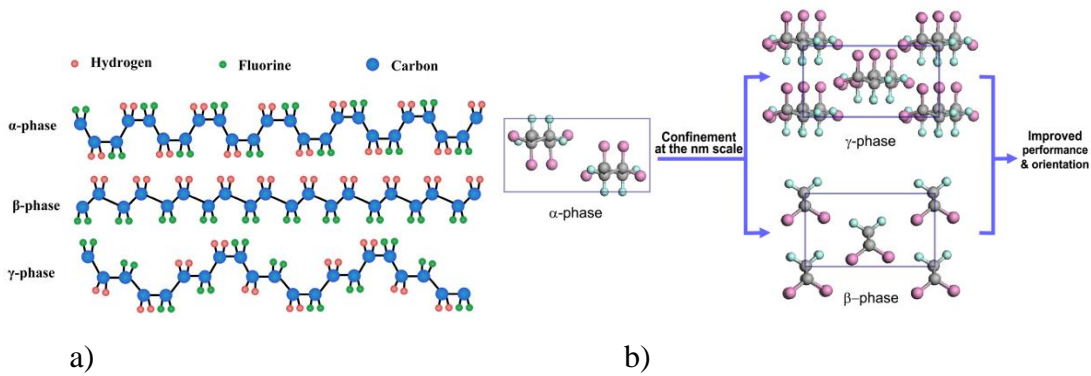
Figure 1-13. a) Nanostructures of the three most studied phases of PVDF-based materials b) Confinement effects in polymer nanostructures: (1) molecular packing density and counterbalance of the molecular interactions (2) reduction in dimension cause change in the long and short-range ordering of molecular dipoles, which in turn leads to size-dependent electrical performance change.

Owing to their flexibility, biocompatibility, transparency, mechanical adaptability, and chemical inertness, PVDF and its copolymer P(VDF-TrFE) present many advantages over other biomaterials used in biomedical applications as diagnostic tools (biosensors) or for *in vitro* tissue engineering applications[165,167–169]. For example, Cheng et al. developed a thin-film based on PVDF for implantable and self-powered to monitor blood pressure[170]. The system proved to be extraordinary sensitive (173mV/mm Hg), and stable (>50.000 cycles) compared to commonly used systems and showed a linear relationship between the output voltage of the device and the pressure. As an implantable device, these studies showed that PVDF is an excellent candidate and can be easily used to monitor various real-time biosignals to assess cardiac function or disease progression. As demonstrated by Persano et al. processing of PVDF into fine fibres by electrospinning can improve the sensitivity and detect up to 0.1 Pa differences in pressure[171]. A study by Chang et al. found that PVDF fibres sensitivity was increased by more than 20 % compared to PVDF films[172]. Also, changing the structure of the fibre influences piezoelectric performance. Pan et al.[173] compared the electrical output of solid and hollow fibres and demonstrated that hollow fibres produced up to 200% more energy. This study indicates that controlling the stiffness and mechanics of the fibres might be as relevant as to the processing methods to achieve excellent performance. Altogether, these results demonstrate the unique potential PVDF as a piezoelectric flexible biomaterial, and similar results can be obtained only using cytotoxic ceramic piezoelectric materials such as PZT. New research in

microfabrication technique and advanced materials have enabled the development of new sensors based on highly conformable PZT array. This system showed detection limits up to 0.005 Pa and high mechanical stability. Dagdeviren et al. demonstrated that the system could measure rapid changes (<0.1 ms) in viscoelastic properties of soft tissues such as the skin among other organs and established the clinical significance of piezoelectric devices for sensing applications[174].

Nevertheless, biological tissues might dynamically respond to the device sensing electrical activity, and little is know on how this might impact biological function or tissue repair processes. This question has attracted considerable attention in the tissue engineering field, and several studies have now demonstrated the modulated functional response of different cell types under both static and dynamic regime of electromechanical signals. Cell adhesion to PVDF has been first studied to understand the biological importance of the electrical surface charge using different cell types, including chondrocytes[175], osteoblasts [176,177], neurons [178,179] and MSCs [180]. Parssinen et al.[181] have recently used poled and non-poled films of PVDF to prove that surface polarisation significantly influences cell adhesión. The study showed that polarisation significantly increased FA density and promoted osteogenic MSC differentiation processes (only using osteogenic media). The study concluded that the surface charge might change specific protein adsorption kinetics and conformation and indirectly affect focal adhesion formation, which ultimately promotes adhesion-mediated MSC osteogenic differentiation.

Biomimetic approaches, replicating the native ECM fibrous structure of collagenous tissues using electrospun PVDF meshes have also attracted considerable attention. Recently, studies with PVDF and its derivative Polyvinylidene fluoride trifluoroethylene [PVDF (TrFE)] have detailed the generation of piezoelectric meshes via an electrospinning process with the of 100–200 nm in fibre diameter and increased β-phase compared to thicker fibres. MSCs that were cultured on highly piezoelectric meshes resulted in better cell attachment and earlier mineralisation than those of in non-piezoelectric meshes. In this study, scaffold piezoelectricity levels were modulated by material processing to obtain low and high voltage producing scaffolds. The results indicated that the use of meshes with lower piezoelectric activity-induced chondrogenic MSC differentiation demonstrated by high Collagen type II to I ratio protein expression. The authors discussed that differences in piezoelectric activity affected cell growth and in turn, alter differentiation. Interestingly, the effect of mechanical stimulus alone did

not have a pronounced effect on MSC chondrogenic or osteogenic differentiation. This finding supports that electrical activity might be more potent regulators than mechanical forces to promote desired cell function for MSC based applications. Although the cellular mechanisms of piezoelectric induced stem cell differentiation remain unclear.

Due to high PVDF viscoelastic properties, a mixture with more elastic components or composite approaches is generally required for *in vivo* applications where mechanical support is vital such as bone. For instance, J. Pereira et al. demonstrated that PVDF blend with natural rubber (corn) showed no *in vivo* adverse response in *a* study with rats for 42 days[182]. The composites were tolerated by cancellous bone with cell aggregates present outside the implanted region, suggesting bone healing. PVDF composites modified with carbon nanotubes are of particular interest nowadays. Research done by Stodolack *et al.* reported improved mechanical properties, increases in surface energy and composite roughness using PVDF/carbon nanotubes blends. The findings indicated the promotion of osteoblast attachment and proliferation. However, more studies are required to unravel the exact role of electrical activity induced by piezoelectric systems.

1.8.3.3 PVDF-TrFE Nanocomposites.

To obtain the electroactive phase of PVDF different strategies have been developed that focus on the development of specific processing procedures and the inclusion of particular fillers (i.e. nanoparticles, hydrated ionic salts or $BaTiO_3$)[183]. Piezoelectric nanoparticles embedded into the polymer (nanocomposites) including boron nitride nanotubes and barium titanate nanoparticles have been used to demonstrate enhanced cell function under ultrasound (US) stimulation[184,185]. Piezoelectric polymers, e.g. PVDF and its copolymers, have also been successfully used in this context. The suitability of polymer/ceramic piezoelectric composite films under US for neuronal stimulation through direct piezoelectric effect was demonstrated by Genchi et al. using P(VDF-TrFE) and BaTiO3[184]. Besides, recent work from Lanceros-Mendez group demonstrated wireless stimulation of cells using P(VDF-TrFE)/Terfenol-D composite film through magnetoelectric coupling effect[186,187].

To enhance the output performance PVDF films with well-controlled nanostructures is desired. Nanoporous PVDF was developed to address this issue. Cha et al. presented a porous PVDF-based system which was fabricated by a ZnO nanoparticle-assisted preparation method[188]. Recently, Cho et al. reported a high-performance P(VDF-TrFE)-

based system through a surface morphology engineering using solvent annealing method for simple and cost-effective fabrication. This surface morphology engineered presented eight times enhanced output voltage and current because of well-aligned electrical dipoles[189].

Various electric stimulation technologies were also applied in cell manipulation, which provided an exciting route for tissue engineering, and many of them have been proved useful in research and clinical settings. Guo et al. combined a highly electrically conductive rGO−PEDOT hybrid scaffold and the piezoelectric system as the electrical stimulation power source to build a self-powered neural differentiation system[190]. The rGO−PEDOT hybrid microfibre cannot only enhance the proliferation of MSCs but also function as a medium for step-driven pulse electrical stimulation signals, which can induce MSCs to differentiate into neural cells. The study realised an enhancement of MSC neural differentiation on the rGO−PEDOT hybrid microfibre under piezoelectrical pulse stimulation. Zheng et al. reported a biodegradable stimulator for short-term stimulation of neural cells *in vivo*[191]. This DC-pulsed EF oriented the growth direction of nerve cells cultured on the micro grating electrode successfully, which was crucial for neural repair.

1.9 Project Hypotheses and objectives

The above sections have detailed and discussed biomaterials-based strategies for tendon tissue engineering and regeneration. Scaffold-based therapies for tissue repair has been thriving since the discovery of bio tolerable materials including metals, polymers and ceramics. While these materials can provide functional and structural support, they remain relatively inert. Advances in manufacturing processes combined with a better understanding of molecular regulatory pathways have resulted in the rapidly emerging field of smart biomaterials. Next-generation biomaterials should be adaptive scaffold-based system specially designed to improve the biological function of a cell by actively responding to dynamic stimuli. Over the last decade, different smart materials have been developed including 1) augmented drug release systems (e.g., liposome, nanomaterials and polymeric controlled released upon pH, light temperature or light changes) 2) cell instructive materials to control cell fate (migration, proliferation and differentiation) and 3) regenerative cell-based systems (e.g. embedding stem cells into bioactive microgels); however, regulatory pathways of advance therapeutic medical products systems (e.g. systems containing a mixture of drug or cells) can hamper the progression into clinical trials. Therefore, it is anticipated that research on cell instructive biomaterials has a pivotal role in the continued progress in the field of tissue engineering and orthopaedics design.
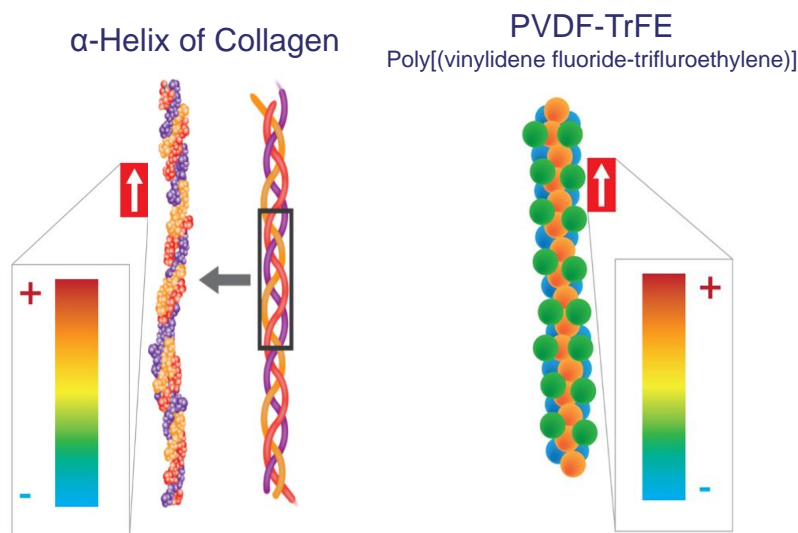
Figure 1-14 . Comparison of the origin for the inherent dipole or electrical polarisation of collagen type I triple helix and PVDF-TrFE molecule

This thesis supports the idea that piezoelectricity is a biologically functional property of collagen and plays a role in the repair of the musculoskeletal system (see Figure 1-14). Under large deformations or stress fields, collagens produce electrical signals that might initiate tissue remodelling through intracellular signalling to synthesise higher amount of ECM to return the tissue to its homeostatic strain level (i.e. higher produced ECM area will decrease the total strain/stress field.) In this thesis, it has been hypothesized that mechanically loaded electrospun PVDF-TrFE scaffolds can produce electrical charges in response to mechanical stimuli, and stimulate cell functional response via electromechanically activated transmembrane receptors. To prove this hypothesis the following objectives have been proposed :

- The development and fabrication of piezoelectric and non-piezoelectric materials with identical chemical properties.

- Investigate the effect of piezoelectricity on the maintenance of tenocytes phenotype and function in *vitro* conditions

- Investigate the effect of piezoelectricity on different biological functions such as cell adhesion and differentiation in human tendon-derived cells and assessed potential correlations with ion channel activation.

- Investigate the tissue regenerative capabilities of piezoelectric scaffolds in a clinically relevant animal model (Rat Achilles full-thickness model)

The development of such piezoelectric systems occurred in two parts: first, a suitable tissue-engineered platform was developed, and secondly, it was investigated the molecular changes induced by the piezoelectric properties of the proposed therapeutic strategy. To assess the proposed overall objectives and the development of such piezoelectric systems four phases were proposed.

1.9.1 Phase one: The fabrication and physical characterisation of 2D piezoelectric PVDF-TrFE and PVDF-TrFE/BNNT nanocomposite.

Main objective: To fabricate and characterise PVDF-TrFE based formulations to obtain highly piezoelectric systems.

Hypothesis: Addition of a second phase composed of piezoelectric Boron Nitride Nanotubes (BNNT) will enhance the β-phase formation during recrystallisation and enhance the piezoelectrical performance of PVDF-TrFE.

Specific Objectives:

- To optimise the dispersion of BNNT on PVDF-TrFE and annealing temperatures to fabricate PVDF-TrFE/BNNT nanocomposites.

- To optimise the poling conditions for PVDF-TrFE and nanocomposites to produce highly piezoelectric and non-piezoelectric films.

- To assess the effect of the addition of BNNT on the overall crystallinity level of nanocomposite relative to pristine films and assess the effect during the recrystallisation process using MDSC.

1.9.2 Phase two: The development of an *in vitro* platform for High frequency, Low-amplitude electromechanical stimulation of tendon-derived cells to promote the maintenance of tenogenic protein expression (protenogenic) signatures.

Main objective: To design and characterise an *in vitro* High frequency, Low-amplitude electromechanical system and assess its ability to maintain tendon specific function.

Hypothesis: Electromechanical stimulation through a bioadhesive piezoelectric system will promote the expression of tendon-specific markers.

Specific Objectives:

- To simulate using COMSOL Multiphysics simulation (structural, electrical and acoustic) the expected electrical output as a function of mechanical input (vibrations).

- To develop a suitable surface biofunctionalisation method for PVDF-TrFE surface to increase cellular attachment and sustained proliferation.

- To assess the effect of surface polarisation on the expression of tendon specific markers, cell adhesion and differentiation processes.

- To assess the effect of mechanical stimulation on the expression of tendon specific markers, cell adhesion and differentiation processes.

- To assess the effect electromechanical stimulation on the expression of tendon specific markers, cell adhesion and differentiation processes

1.9.3 Phase three: The fabrication and physical characterisation of highly anisotropic fibrous 3D piezoelectric scaffold and assess the effects of High Magnitude, Low-Frequency electromechanical stimulation on the genomic and proteomic response of human tendon cells.

Main objective: To assess the genomic changes that occur during cell differentiation as a function of High Magnitude, Low-Frequency electromechanical stimulation through an electrospun PVDF(TrFE) nano-scaffold.

Hypothesis: Electromechanical cues delivered through a low-frequency tensional loading of a nanofibrous scaffold will modulate genomic and proteomic function in tenocytes.

Specific Objectives:

- To fabricate piezoelectric and non-piezoelectric electrospun scaffolds that recreate the topographical features of native tendon structure and characterise electrical outputs under different low frequency, high magnitude physiologically relevant mechanical loading conditions.

- To optimise the loading conditions parameters to obtain a functional response of tendon-derived cells.

- To assess the influence of different levels of piezoelectricity on the expression of tendon specific markers, cell adhesion and differentiation processes.

1.9.4 Phase four: To assess the effect of electrospun piezoelectric scaffolds on the proteomic response during tendon repair in a rat full-thickness Achilles tendon transection model.

Main objective: To investigate piezoelectric scaffold-induced functional response and proteomic changes during the repair of a fully transected Achilles tendon on exercising

(and non-exercising) rats and compared to the gold standard for tendon repair (sutures and immobilisation).

Hypothesis: 1) The use of a highly aligned fibrous scaffold will promote recovery in comparison to the gold standard (sutures alone). 2) Achilles Tendon repair is enhanced by early mechanical loading such as moderate physical treadmill running (MTR) regimen. 3) The use of piezoelectric fibrous scaffolds will offer a distinct proteomic response compared to non-piezoelectric scaffolds

Specific Objectives:

- To fabricate electrospun piezoelectric and non-piezoelectric and characterise their electrical outputs under physiologically relevant mechanical loading conditions.

- To develop a protocol for moderate treadmill running of rats and for functional response assessment.

- To assess the effect of mechanical loading on the anabolic changes during tendon repair

- To assess the impact of an electrospun PVDF(TrFE) scaffold on tendon regeneration and investigated proteomic changes as a function of piezoelectric stimulation.

1.9.5 References

1.   Snedeker, J. G. & Foolen, J. Tendon injury and repair – A perspective on the basic mechanisms of tendon disease and future clinical therapy. *Acta Biomaterialia* **63**, 18–36 (2017).

2.   Walden, G. *et al.* A Clinical, Biological, and Biomaterials Perspective into Tendon Injuries and Regeneration. *Tissue Eng. Part B Rev.* (2017). doi:10.1089/ten.teb.2016.0181

3.   Docheva, D., Müller, S. A., Majewski, M. & Evans, C. H. Biologics for tendon repair. *Advanced Drug Delivery Reviews* (2015). doi:10.1016/j.addr.2014.11.015

4.   Kartus, J., Movin, T. & Karlsson, J. Donor-site morbidity and anterior knee problems after anterior cruciate ligament reconstruction using autografts. *Arthroscopy* (2001). doi:10.1053/jars.2001.28979

5.   Yasuda, K., Tsujino, J., Ohkoshi, Y., Tanabe, Y. & Kaneda, K. Graft Site Morbidity with Autogenous Semitendinosus and Gracilis Tendons. *Am. J. Sports Med.* (1995). doi:10.1177/036354659502300613

6.   Kartus, J., Movin, T. & Karlsson, J. Donor-site morbidity after anterior cruciate ligament reconstruction using autografts clinical, radiographic, histological, and ultrastructural aspects. in *Anterior Knee Pain and Patellar Instability* (2006). doi:10.1007/1-84628-143-1_19

7.   Seo, J. G. *et al.* Ankle morbidity after autogenous Achilles tendon harvesting for anterior cruciate ligament reconstruction. *Knee Surgery, Sport. Traumatol. Arthrosc.* (2009). doi:10.1007/s00167-009-0729-9

8.   Kuo, C. K., Marturano, J. E. & Tuan, R. S. Novel strategies in tendon and ligament tissue engineering: Advanced biomaterials and regeneration motifs. *BMC Sports Sci. Med. Rehabil.* **2**, 20 (2010).

9.   Lomas, A. J. *et al.* The past, present and future in scaffold-based tendon treatments. *Advanced Drug Delivery Reviews* **84**, 257–277 (2015).

10.   Liu, Y., Ramanath, H. S. & Wang, D. A. Tendon tissue engineering using scaffold enhancing strategies. *Trends in Biotechnology* **26**, 201–209 (2008).

11.   Mammoto, T. & Ingber, D. E. Mechanical control of tissue and organ development. *Development* (2010). doi:10.1242/dev.024166

12.   Obregón, R., Ramón-Azcón, J. & Ahadian, S. Bioreactors in Tissue Engineering.

in *Tissue Engineering for Artificial Organs: Regenerative Medicine, Smart Diagnostics and Personalized Medicine* (2016). doi:10.1002/9783527689934.ch6

13.   Plonsey, R., Barr, R. C., Plonsey, R. & Barr, R. C. Electrical Stimulation of Excitable Tissue. in *Bioelectricity* (2000). doi:10.1007/978-1-4757-3152-1_7

14.   Rajabi, A. H., Jaffe, M. & Arinzeh, T. L. Piezoelectric materials for tissue regeneration: A review. *Acta Biomater.* **24**, 12–23 (2015).

15.   Tandon, N. *et al.* Electrical stimulation systems for cardiac tissue engineering. *Nat. Protoc.* (2009). doi:10.1038/nprot.2008.183

16.   Chen, J., Xu, J., Wang, A. & Zheng, M. Scaffolds for tendon and ligament repair: Review of the efficacy of commercial products. *Expert Review of Medical Devices* **6**, 61–73 (2009).

17.   Longo, U. G., Lamberti, A., Maffulli, N. & Denaro, V. Tendon augmentation grafts: A systematic review. *Br. Med. Bull.* (2010). doi:10.1093/bmb/ldp051

18.   Yin, Z. *et al.* The regulation of tendon stem cell differentiation by the alignment of nanofibers. *Biomaterials* **31**, 2163–2175 (2010).

19.   Kew, S. J. *et al.* Regeneration and repair of tendon and ligament tissue using collagen fibre biomaterials. *Acta Biomaterialia* (2011). doi:10.1016/j.actbio.2011.06.002

20.   Font Tellado, S., Balmayor, E. R. & Van Griensven, M. Strategies to engineer tendon/ligament-to-bone interface: Biomaterials, cells and growth factors. *Advanced Drug Delivery Reviews* (2015). doi:10.1016/j.addr.2015.03.004

21.   Cross, L. M., Thakur, A., Jalili, N. A., Detamore, M. & Gaharwar, A. K. Nanoengineered biomaterials for repair and regeneration of orthopedic tissue interfaces. *Acta Biomaterialia* (2016). doi:10.1016/j.actbio.2016.06.023

22.   Pesqueira, T. *et al.* Engineering magnetically responsive tropoelastin spongy-like hydrogels for soft tissue regeneration. *J. Mater. Chem. B* (2018). doi:10.1039/c7tb02035j

23.   Pesqueira, T., Costa-Almeida, R. & Gomes, M. E. Magnetotherapy: The quest for tendon regeneration. *J. Cell. Physiol.* (2018). doi:10.1002/jcp.26637

24.   Silva, E. D. *et al.* Multifunctional magnetic-responsive hydrogels to engineer tendon-to-bone interface. *Nanomedicine Nanotechnology, Biol. Med.* (2018). doi:10.1016/j.nano.2017.06.002

25.   Gonçalves, A. I., Rodrigues, M. T. & Gomes, M. E. Tissue-engineered magnetic cell sheet patches for advanced strategies in tendon regeneration. *Acta Biomater.*

(2017). doi:10.1016/j.actbio.2017.09.014

26. Holzapfel, B. M. *et al.* How smart do biomaterials need to be? A translational science and clinical point of view. *Advanced Drug Delivery Reviews* (2013). doi:10.1016/j.addr.2012.07.009

27. J.E. Commission, ETN nanomedicine: roadmaps in nanomedicine towards 2020, Expert Report 2009, 2009, p. 56.

28. Schneider, M., Angele, P., Järvinen, T. A. H. & Docheva, D. Rescue plan for Achilles : Therapeutics steering the fate and functions of stem cells in tendon wound healing. *Adv. Drug Deliv. Rev.* **129**, 352–375 (2018).

29. Yin, W. *et al.* Biomaterials Functional replication of the tendon tissue microenvironment by a bioimprinted substrate and the support of tenocytic differentiation of mesenchymal stem cells. **33**, 7686–7698 (2012).

30. Brian, J. *et al.* The piezoelectric tensor of collagen fibrils determined at the nanoscale. (2017).

31. Manuscript, A. LAW ": A CRITICAL REVIEW. **31**, 733–741 (2010).

32. Manuscript, A. Nanoscale. (2018). doi:10.1039/C8NR01634H

33. Jacob, J., More, N., Kalia, K. & Kapusetti, G. Piezoelectric smart biomaterials for bone and cartilage tissue engineering. *Inflamm. Regen.* **38**, 2 (2018).

34. Vivekananthan, V. *et al.* Energy , Environmental , and Catalysis Applications Biocompatible collagen-nanofibrils : An approach for sustainable energy harvesting and battery-free humidity sensor applications Biocompatible collagen-nanofibrils : An approach for sustainable energy ha. (2018). doi:10.1021/acsami.8b02915

35. Michlovitz, S. L. Is there a role for ultrasound and electrical stimulation following injury to tendon and nerve? *J. Hand Ther.* (2005). doi:10.1197/j.jht.2005.02.013

36. Khan, S. I. & Burne, J. A. Inhibitory mechanisms following electrical stimulation of tendon and cutaneous afferents in the lower limb. *Brain Res.* (2010). doi:10.1016/j.brainres.2009.10.020

37. Williams, W. S. & Breger, L. Piezoelectricity in tendon and bone. *J. Biomech.* (1975). doi:10.1016/0021-9290(75)90076-7

38. Long, S. B., Campbell, E. B. & MacKinnon, R. Voltage sensor of Kv1.2: Structural basis of electromechanical coupling. *Science (80-.).* (2005). doi:10.1126/science.1116270

39. Pfeiffer, E. R., Tangney, J. R., Omens, J. H. & McCulloch, A. D. Biomechanics of Cardiac Electromechanical Coupling and Mechanoelectric Feedback. *J. Biomech. Eng.* (2014). doi:10.1115/1.4026221

40. Alcaino, C., Farrugia, G. & Beyder, A. Mechanosensitive Piezo Channels in the Gastrointestinal Tract. *Curr. Top. Membr.* **79**, 219–244 (2017).

41. Michael Lavagnino1, Michelle E. Wall2, Dianne Little3, Albert J. Banes2,4, Farshid Guilak3,4,5, and S. P. A. Tendon Mechanobiology: Current Knowledge and Future Research Opportunities. *J Orthop Res.* **33**, 813–822 (2015).

42. Yoshimoto, Y., Takimoto, A., Watanabe, H., Hiraki, Y. & Kondoh, G. Scleraxis is required for maturation of tissue domains for proper integration of the musculoskeletal system. *Nat. Publ. Gr.* 1–16 (2017). doi:10.1038/srep45010

43. Chen, X. *et al.* promote the commitment of human ES cells derived MSCs to tenocytes. 1–9 (2012). doi:10.1038/srep00977

44. Wu, F. & Nerlich, M. Tendons basic biology Tendon injuries: basic science and new repair proposals. *Efort Open Rev.* (2017). doi:10.1302/2058-5241.2.160075

45. Bayer, M. L. *et al.* The initiation of embryonic-like collagen fibrillogenesis by adult human tendon fibroblasts when cultured under tension. *Biomaterials* (2010). doi:10.1016/j.biomaterials.2010.02.062

46. Zhang, G. *et al.* Development of tendon structure and function: regulation of collagen fibrillogenesis. *J. Musculoskelet. Neuronal Interact.* (2005).

47. Kostrominova, T. Y. & Brooks, S. V. Age-related changes in structure and extracellular matrix protein expression levels in rat tendons. *Age (Omaha).* (2013). doi:10.1007/s11357-013-9514-2

48. Brumitt, J. & Cuddeford, T. CURRENT CONCEPTS OF MUSCLE AND TENDON ADAPTATION TO STRENGTH AND CONDITIONING. *Int. J. Sports Phys. Ther.* (2015).

49. Robinson, K. A. *et al.* Decorin and biglycan are necessary for maintaining collagen fibril structure, fiber realignment, and mechanical properties of mature tendons. *Matrix Biol.* (2017). doi:10.1016/j.matbio.2017.08.004

50. Shetye, S. S. *et al.* Collagen V haploinsufficiency results in deficient mechanical and structural recovery of injured mouse patellar tendons. *J. Orthop. Res.* (2017).

51. Spiess, K. & Zorn, T. M. T. Collagen types I, III, and V constitute the thick collagen fibrils of the mouse decidua. *Microsc. Res. Tech.* (2007). doi:10.1002/jemt.20381

52. Hulmes, D. J., Wess, T. J., Prockop, D. J. & Fratzl, P. Radial packing, order, and disorder in collagen fibrils. *Biophys. J.* (1995). doi:10.1016/S0006-3495(95)80391-7

53. Ireland, D. *et al.* Multiple changes in gene expression in chronic human Achilles tendinopathy. *Matrix Biol.* (2001). doi:10.1016/S0945-053X(01)00128-7

54. Deshmukh, S., Dive, A., Moharil, R. & Munde, P. Enigmatic insight into collagen. *J. Oral Maxillofac. Pathol.* (2016). doi:10.4103/0973-029x.185932

55. Anderson, J. C. & Eriksson, C. Piezoelectric properties of dry and wet bone. *Nature* **227**, 491–492 (1970).

56. Denning, D. *et al.* Electromechanical properties of dried tendon and isoelectrically focused collagen hydrogels. *Acta Biomater.* **8**, 3073–3079 (2012).

57. Denning, D., Paukshto, M. V., Habelitz, S. & Rodriguez, B. J. Piezoelectric properties of aligned collagen membranes. *J. Biomed. Mater. Res. - Part B Appl. Biomater.* **102**, 284–292 (2014).

58. Bassett, C. A. L. Biologic significance of piezoelectricity. *Calcif. Tissue Res.* **1**, 252–272 (1967).

59. Vasquez-Sancho, F., Abdollahi, A., Damjanovic, D. & Catalan, G. Flexoelectricity in Bones. *Adv. Mater.* **30**, 1–5 (2018).

60. Yao, L., Bestwick, C. S., Bestwick, L. A., Maffulli, N. & Aspden, R. M. Phenotypic Drift in Human Tenocyte Culture. *Tissue Eng.* (2006). doi:10.1089/ten.2006.12.ft-90

61. Zhu, J. *et al.* The regulation of phenotype of cultured tenocytes by microgrooved surface structure. *Biomaterials* **31**, 6952–6958 (2010).

62. Shukunami, C. *et al.* Scleraxis is a transcriptional activator that regulates the expression of Tenomodulin, a marker of mature tenocytes and ligamentocytes. *Sci. Rep.* (2018). doi:10.1038/s41598-018-21194-3

63. Berthet, E. *et al.* Smad3 binds Scleraxis and Mohawk and regulates tendon matrix organisation. *J. Orthop. Res.* (2013). doi:10.1002/jor.22382

64. Tan, S. L. *et al.* The effect of growth differentiation factor-5 (GDF-5) on the proliferation and tenogenic differentiation potential of human mesenchymal stem cells in vitro. *J. Univ. Malaya Med. Cent.* (2013).

65. Killian, M. L. & Thomopoulos, S. Scleraxis is required for the development of a functional tendon enthesis. *FASEB J.* (2016). doi:10.1096/fj.14-258236

66. Brown, D., Wagner, D., Li, X., Richardson, J. A. & Olson, E. N. Dual role of the

basic helix-loop-helix transcription factor scleraxis in mesoderm formation and chondrogenesis during mouse embryogenesis. *Development* (1999).

67. Sharma, P. & Maffulli, N. Biology of tendon injury: Healing, modeling and remodeling. *Journal of Musculoskeletal Neuronal Interactions* (2006).

68. Nourissat, G., Berenbaum, F. & Duprez, D. Tendon injury: from biology to tendon repair. *Nat. Rev. Rheumatol.* **11**, 223–233 (2015).

69. Bi, Y. *et al.* Identification of tendon stem/progenitor cells and the role of the extracellular matrix in their niche. *Nat. Med.* **13**, 1219–1227 (2007).

70. Lui, P. P. Y. Identity of tendon stem cells - how much do we know? *Journal of Cellular and Molecular Medicine* (2013). doi:10.1111/jcmm.12007

71. Yin, Z. *et al.* Single-cell analysis reveals a nestin+ tendon stem/progenitor cell population with strong tenogenic potentiality. *Sci. Adv.* **2**, 1–15 (2016).

72. Ruprecht, V. *et al.* How cells respond to environmental cues – insights from bio-functionalized substrates. *J. Cell Sci.* (2017). doi:10.1242/jcs.196162

73. Gupta, M. *et al.* Micropillar substrates: A tool for studying cell mechanobiology. *Methods Cell Biol.* (2015). doi:10.1016/bs.mcb.2014.10.009

74. Kshitiz *et al.* Control of stem cell fate and function by engineering physical microenvironments. *Integrative Biology (United Kingdom)* (2012). doi:10.1039/c2ib20080e

75. Guilak, F. *et al.* Control of Stem Cell Fate by Physical Interactions with the Extracellular Matrix. *Cell Stem Cell* (2009). doi:10.1016/j.stem.2009.06.016

76. Frantz, C., Stewart, K. M. & Weaver, V. M. The extracellular matrix at a glance. *J. Cell Sci.* (2010). doi:10.1242/jcs.023820

77. Fehrer, C. *et al.* Reduced oxygen tension attenuates differentiation capacity of human mesenchymal stem cells and prolongs their lifespan. *Aging Cell* (2007). doi:10.1111/j.1474-9726.2007.00336.x

78. Li, P. *et al.* Role of the ERK1/2 signaling pathway in osteogenesis of rat tendon-derived stem cells in normoxic and hypoxic cultures. *Int. J. Med. Sci.* (2016). doi:10.7150/ijms.16045

79. Reinwald, Y. & El Haj, A. J. Hydrostatic pressure in combination with topographical cues affects the fate of bone marrow-derived human mesenchymal stem cells for bone tissue regeneration. *J. Biomed. Mater. Res. - Part A* (2018). doi:10.1002/jbm.a.36267

80. Docheva, D., Müller, S. A., Majewski, M. & Evans, C. H. Biologics for tendon

repair. *Adv. Drug Deliv. Rev.* **84**, 222–239 (2015).

81.   Khan, K. M. & Scott, A. Mechanotherapy: How physical therapists' prescription of exercise promotes tissue repair. *British Journal of Sports Medicine* (2009). doi:10.1136/bjsm.2008.054239

82.   Wang, Z. *et al.* Functional regeneration of tendons using scaffolds with physical anisotropy engineered via microarchitectural manipulation. *Sci. Adv.* (2018). doi:10.1126/sciadv.aat4537

83.   Biggs, M. J. P. *et al.* Interactions with nanoscale topography: Adhesion quantification and signal transduction in cells of osteogenic and multipotent lineage. *J. Biomed. Mater. Res. - Part A* (2009). doi:10.1002/jbm.a.32196

84.   Levin, M. Bioelectric mechanisms in regeneration: Unique aspects and future perspectives. *Semin. Cell Dev. Biol.* (2009). doi:10.1016/j.semcdb.2009.04.013

85.   Tseng, A. S. & Levin, M. Transducing Bioelectric Signals into Epigenetic Pathways During Tadpole Tail Regeneration. *Anatomical Record* (2012). doi:10.1002/ar.22495

86.   Sundelacruz, S., Li, C., Choi, Y. J., Levin, M. & Kaplan, D. L. Bioelectric modulation of wound healing in a 3D invitro model of tissue-engineered bone. *Biomaterials* (2013). doi:10.1016/j.biomaterials.2013.05.040

87.   Engler, A. J., Sen, S., Sweeney, H. L. & Discher, D. E. Matrix elasticity directs stem cell lineage specification. *Cell* (2006). doi:10.1016/j.cell.2006.06.044

88.   Mamidi, A. *et al.* Mechanosignalling via integrins directs fate decisions of pancreatic progenitors. *Nature* (2018). doi:10.1038/s41586-018-0762-2

89.   Biggs, M. J. P. *et al.* The Functional Response of Mesenchymal Stem Cells to Electron-Beam Patterned Elastomeric Surfaces Presenting Micrometer to Nanoscale Heterogeneous Rigidity. *Adv. Mater.* **29**, 1702119 (2017).

90.   Wang, N., Tytell, J. D. & Ingber, D. E. Mechanotransduction at a distance: Mechanically coupling the extracellular matrix with the nucleus. *Nat. Rev. Mol. Cell Biol.* **10**, 75–82 (2009).

91.   Lin, X., Shi, Y., Cao, Y. & Liu, W. Recent progress in stem cell differentiation directed by material and mechanical cues. *Biomed. Mater.* (2016). doi:10.1088/1748-6041/11/1/014109

92.   Hao, J. *et al.* Mechanobiology of mesenchymal stem cells: Perspective into mechanical induction of MSC fate. *Acta Biomaterialia* (2015). doi:10.1016/j.actbio.2015.04.008

93. Molloy, T., Wang, Y. & Murrell, G. A. C. The roles of growth factors in tendon and ligament healing. *Sports Medicine* (2003). doi:10.2165/00007256-200333050-00004

94. Caliari, S. R. & Harley, B. A. C. The effect of anisotropic collagen-GAG scaffolds and growth factor supplementation on tendon cell recruitment, alignment, and metabolic activity. *Biomaterials* (2011). doi:10.1016/j.biomaterials.2011.04.021

95. Kjær, M. *et al.* From mechanical loading to collagen synthesis, structural changes and function in human tendon. *Scandinavian Journal of Medicine and Science in Sports* (2009). doi:10.1111/j.1600-0838.2009.00986.x

96. Zhao, M. *et al.* Electrical signals control wound healing through phosphatidylinositol-3-OH kinase-γ and PTEN. *Nature* (2006). doi:10.1038/nature04925

97. Ciombor, D. M. & Aaron, R. K. The role of electrical stimulation in bone repair. *Foot and Ankle Clinics* (2005). doi:10.1016/j.fcl.2005.06.006

98. Tandon, B., Blaker, J. J. & Cartmell, S. H. Piezoelectric materials as stimulatory biomedical materials and scaffolds for bone repair. *Acta Biomaterialia* (2018). doi:10.1016/j.actbio.2018.04.026

99. Mollon, B., Da Silva, V., Busse, J. W., Einhorn, T. A. & Bhandari, M. Electrical stimulation for long-bone fracture-healing: A meta-analysis of randomized controlled trials. *Journal of Bone and Joint Surgery - Series A* (2008). doi:10.2106/JBJS.H.00111

100. Yuan, X., Arkonac, D. E., Chao, P. H. G. & Vunjak-Novakovic, G. Electrical stimulation enhances cell migration and integrative repair in the meniscus. *Sci. Rep.* (2015). doi:10.1038/srep03674

101. Kloth, L. C. Electrical stimulation for wound healing: A review of evidence from in vitro studies, animal experiments, and clinical trials. *International Journal of Lower Extremity Wounds* (2005). doi:10.1177/1534734605275733

102. Fukada, E. & Yasuda, I. On the Piezoelectric Effect of Bone. *J. Phys. Soc. Japan* (1957). doi:10.1143/JPSJ.12.1158

103. Brighton, C. T., Jensen, L., Pollack, S. R., Tolin, B. S. & Clark, C. C. Proliferative and synthetic response of bovine growth plate chondrocytes to various capacitively coupled electrical fields. *J. Orthop. Res.* (1989). doi:10.1002/jor.1100070519

104. Armstrong, P. F., Brighton, C. T. & Star, A. M. Capacitively coupled electrical stimulation of bovine growth plate chondrocytes grown in pellet form. *J. Orthop. Res.* (1988). doi:10.1002/jor.1100060214

105. Wang, W., Wang, Z., Zhang, G., Clark, C. C. & Brighton, C. T. Up-regulation of chondrocyte matrix genes and products by electric fields. in *Clinical Orthopaedics and Related Research* (2004). doi:10.1097/01.blo.0000143837.53434.5c

106. Walther, M., Mayer, F., Kafka, W. & Schütze, N. Effects of weak, low-frequency pulsed electromagnetic fields (BEMER type) on gene expression of human mesenchymal stem cells and chondrocytes: An in vitro study. *Electromagn. Biol. Med.* (2007). doi:10.1080/15368370701580814

107. Kwon, H. J., Lee, G. S. & Chun, H. Electrical stimulation drives chondrogenesis of mesenchymal stem cells in the absence of exogenous growth factors. *Sci. Rep.* **6**, 1–13 (2016).

108. Mathews, J. & Levin, M. The body electric 2.0: recent advances in developmental bioelectricity for regenerative and synthetic bioengineering. *Current Opinion in Biotechnology* (2018). doi:10.1016/j.copbio.2018.03.008

109. McLaughlin, K. A. & Levin, M. Bioelectric signaling in regeneration: Mechanisms of ionic controls of growth and form. *Dev. Biol.* **433**, 177–189 (2018).

110. Tseng, A. & Levin, M. Cracking the bioelectric code: Probing endogenous ionic controls of pattern formation. *Commun. Integr. Biol.* (2013). doi:10.4161/cib.22595

111. Pai, V. P. *et al.* HCN2 Rescues brain defects by enforcing endogenous voltage pre-patterns. *Nat. Commun.* **9**, 998 (2018).

112. Levin, M. Molecular bioelectricity: how endogenous voltage potentials control cell behavior and instruct pattern regulation in vivo. *Mol. Biol. Cell* **25**, 3835–50 (2014).

113. Pietak, A. & Levin, M. Exploring Instructive Physiological Signaling with the Bioelectric Tissue Simulation Engine. *Front. Bioeng. Biotechnol.* **4**, (2016).

114. Zhao, M. Electrical fields in wound healing-An overriding signal that directs cell migration. *Seminars in Cell and Developmental Biology* (2009). doi:10.1016/j.semcdb.2008.12.009

115. Huang, Y., Li, Y., Chen, J., Zhou, H. & Tan, S. Electrical Stimulation Elicits

Neural Stem Cells Activation: New Perspectives in CNS Repair. *Front. Hum. Neurosci.* (2015). doi:10.3389/fnhum.2015.00586

116. Martinac, B. The ion channels to cytoskeleton connection as potential mechanism of mechanosensitivity. *Biochim. Biophys. Acta - Biomembr.* **1838**, 682–691 (2014).

117. Everaerts, W., Nilius, B. & Owsianik, G. The vanilloid transient receptor potential channel TRPV4: From structure to disease. *Progress in Biophysics and Molecular Biology* (2010). doi:10.1016/j.pbiomolbio.2009.10.002

118. Moran, M. M., McAlexander, M. A., Bíró, T. & Szallasi, A. Transient receptor potential channels as therapeutic targets. *Nature Reviews Drug Discovery* (2011). doi:10.1038/nrd3456

119. Earley, S. & Brayden, J. E. Transient Receptor Potential Channels in the Vasculature. *Physiol. Rev.* (2015). doi:10.1152/physrev.00026.2014

120. Liedtke, W. B. *TRPV Channels' Function in Osmo- and Mechanotransduction. TRP Ion Channel Function in Sensory Transduction and Cellular SignalingCascades* (2007).

121. Okumura, R. *et al.* The odontoblast as a sensory receptor cell? The expression of TRPV1 (VR-1) channels. *Arch. Histol. Cytol.* (2006). doi:10.1679/aohc.68.251

122. Qi, Y. *et al.* Uniaxial cyclic stretch stimulates TRPV4 to induce realignment of human embryonic stem cell-derived cardiomyocytes. *J. Mol. Cell. Cardiol.* (2015). doi:10.1016/j.yjmcc.2015.08.005

123. Goswami, R. *et al.* TRPV4 calcium-permeable channel is a novel regulator of oxidized LDL-induced macrophage foam cell formation. *Free Radic. Biol. Med.* (2017). doi:10.1016/j.freeradbiomed.2017.06.004

124. Suzuki, T. *et al.* TRPV4 (transient receptor potential vanilloid 4), a mechanosensor for bone is required for the maintenance of bone mineral density of mandible exposed to occlusal force. *J. Bone Miner. Res.* (2010).

125. Saotome, K. *et al.* Structure of the mechanically activated ion channel Piezo1. *Nature* (2018). doi:10.1038/nature25453

126. etem, ebru *et al.* The increased expression of Piezo1 and Piezo2 ion channels in human and mouse bladder carcinoma. *Adv. Clin. Exp. Med.* (2018). doi:10.17219/acem/71080

127. Gao, Q., Cooper, P. R., Walmsley, A. D. & Scheven, B. A. Role of Piezo Channels in Ultrasound-stimulated Dental Stem Cells. *J. Endod.* (2017).

doi:10.1016/j.joen.2017.02.022

128. Song, Y. *et al.* The Mechanosensitive Ion Channel Piezo Inhibits Axon Regeneration. *Neuron* (2019). doi:10.1016/j.neuron.2019.01.050

129. He, L., Si, G., Huang, J., Samuel, A. D. T. & Perrimon, N. Mechanical regulation of stem-cell differentiation by the stretch-activated Piezo channel. *Nature* **555**, 103–106 (2018).

130. Lavagnino, M., Arnoczky, S. P., Egerbacher, M., Gardner, K. L. & Burns, M. E. Isolated fibrillar damage in tendons stimulates local collagenase mRNA expression and protein synthesis. *J. Biomech.* (2006). doi:10.1016/j.jbiomech.2005.08.008

131. Maeda, T. *et al.* Conversion of mechanical force into TGF-β-mediated biochemical signals. *Curr. Biol.* (2011). doi:10.1016/j.cub.2011.04.007

132. Chen, Y., Ju, L., Rushdi, M., Ge, C. & Zhu, C. Receptor-mediated cell mechanosensing. *Mol. Biol. Cell* (2017). doi:10.1091/mbc.e17-04-0228

133. Elosegui-Artola, A., Trepat, X. & Roca-Cusachs, P. Control of Mechanotransduction by Molecular Clutch Dynamics. *Trends Cell Biol.* (2018). doi:10.1016/j.tcb.2018.01.008

134. Massia, S. P. & Hubbell, J. A. An RGD spacing of 440 nm is sufficient for integrin αvβ3-mediated fibroblast spreading and 140 nm for focal contact and stress fiber formation. *J. Cell Biol.* (1991). doi:10.1083/jcb.114.5.1089

135. Oria, R. *et al.* Force loading explains spatial sensing of ligands by cells. *Nature* (2017). doi:10.1038/nature24662

136. Salmeron-Sanchez, M. *et al.* Molecular clutch drives cell response to surface viscosity. *Proc. Natl. Acad. Sci.* (2018). doi:10.1073/pnas.1710653115

137. Fernandez-Yague, M. A. *et al.* Biomimetic approaches in bone tissue engineering: Integrating biological and physicomechanical strategies. *Advanced Drug Delivery Reviews* **84**, 1–29 (2015).

138. Galloway, M. T., Lalley, A. L. & Shearn, J. T. The role of mechanical loading in tendon development, maintenance, injury, and repair. *Journal of Bone and Joint Surgery - Series A* (2013). doi:10.2106/JBJS.L.01004

139. Wang, T. *et al.* Bioreactor Design for Tendon/Ligament Engineering. *Tissue Eng. Part B Rev.* **19**, 133–146 (2013).

140. Thomopoulos, S., Parks, W. C., Rifkin, D. B. & Derwin, K. A. Mechanisms of tendon injury and repair. in *Journal of Orthopaedic Research* (2015).

doi:10.1002/jor.22806

141. Screen, H. R. C., Berk, D. E., Kadler, K. E., Ramirez, F. & Young, M. F. Tendon functional extracellular matrix. in *Journal of Orthopaedic Research* (2015). doi:10.1002/jor.22818

142. Xu, B. *et al.* RhoA/ROCK, cytoskeletal dynamics, and focal adhesion kinase are required for mechanical stretch-induced tenogenic differentiation of human mesenchymal stem cells. *J. Cell. Physiol.* **227**, 2722–2729 (2012).

143. Mackley, J. R., Ando, J., Herzyk, P. & Winder, S. J. Phenotypic responses to mechanical stress in fibroblasts from tendon, cornea and skin. *Biochem. J.* (2006). doi:10.1042/bj20060057

144. Fong, K. D. *et al.* Microarray analysis of mechanical shear effects on flexor tendon cells. *Plast. Reconstr. Surg.* (2005). doi:10.1097/01.prs.0000182345.86453.4f

145. Deng, D. *et al.* Engineering human neo-tendon tissue in vitro with human dermal fibroblasts under static mechanical strain. *Biomaterials* (2009). doi:10.1016/j.biomaterials.2009.08.054

146. Maharam, E. *et al.* Rho/Rock signal transduction pathway is required for MSC tenogenic differentiation. *Bone Res.* **3**, (2015).

147. Lin, J. *et al.* Acta Biomaterialia Cell-material interactions in tendon tissue engineering. *Acta Biomater.* 1–11 (2018). doi:10.1016/j.actbio.2018.01.012

148. Robertson, B. D. & Sawicki, G. S. Unconstrained muscle-tendon workloops indicate resonance tuning as a mechanism for elastic limb behavior during terrestrial locomotion. *Proc. Natl. Acad. Sci.* (2015). doi:10.1073/pnas.1500702112

149. Lau, E. *et al.* Effect of low-magnitude, high-frequency vibration on osteogenic differentiation of rat mesenchymal stromal cells. *J. Orthop. Res.* (2011). doi:10.1002/jor.21334

150. Curtis, A. S. G. *et al.* Cell interactions at the nanoscale: Piezoelectric stimulation. *IEEE Trans. Nanobioscience* (2013). doi:10.1109/TNB.2013.2257837

151. Tsimbouri, P. M. *et al.* Stimulation of 3D osteogenesis by mesenchymal stem cells using a nanovibrational bioreactor. *Nat. Biomed. Eng.* (2017). doi:10.1038/s41551-017-0127-4

152. Miller, S. L. The mechanism of synthesis of amino acids by electric discharges. *BBA - Biochim. Biophys. Acta* (1957). doi:10.1016/0006-3002(57)90366-9

153. Pietak, A. & Levin, M. Bioelectrical control of positional information in development and regeneration: A review of conceptual and computational advances. *Progress in Biophysics and Molecular Biology* (2018). doi:10.1016/j.pbiomolbio.2018.03.008

154. Akai, M., Oda, H., Shirasaki, Y. & Tateishi, T. Electrical stimulation of ligament healing. An experimental study of the patellar ligament of rabbits. *Clin.Orthop.Relat Res.* (1988).

155. Sirohi, J. & Chopra, I. Fundamental understanding of piezoelectric strain sensors. *J. Intell. Mater. Syst. Struct.* (2000). doi:10.1106/8BFB-GC8P-XQ47-YCQ0

156. Ramadan, K. S., Sameoto, D. & Evoy, S. A review of piezoelectric polymers as functional materials for electromechanical transducers. *Smart Mater. Struct.* **23**, 033001 (2014).

157. Maxwell, J. C. A treatise on electricity and magnetism, Vol. II. *Journal of the Franklin Institute* (1954). doi:10.1017/CBO9780511709333

158. Wang, Z. L. On Maxwell's displacement current for energy and sensors: the origin of nanogenerators. *Mater. Today* **20**, 74–82 (2017).

159. Roche, J. The present status of Maxwell's displacement current. *Eur. J. Phys.* (1998). doi:10.1088/0143-0807/19/2/009

160. Kawai, H. The Piezoelectricity of Poly (vinylidene Fluoride). *Jpn. J. Appl. Phys.* **8**, 975–976 (1969).

161. Motamedi, A. S., Mirzadeh, H., Hajiesmaeilbaigi, F., Bagheri-Khoulenjani, S. & Shokrgozar, M. A. Piezoelectric electrospun nanocomposite comprising Au NPs/PVDF for nerve tissue engineering. *J. Biomed. Mater. Res. Part A* **105**, 1984–1993 (2017).

162. Yu, Y. *et al.* Biocompatibility and in vivo operation of implantable mesoporous PVDF-based nanogenerators. *Nano energy* **27**, 275–281 (2016).

163. Sobreiro-Almeida, R. *et al.* Human Mesenchymal Stem Cells Growth and Osteogenic Differentiation on Piezoelectric Poly(vinylidene fluoride) Microsphere Substrates. *Int. J. Mol. Sci.* **18**, 2391 (2017).

164. Lee, Y.-S., Wu, S., Arinzeh, T. L. & Bunge, M. B. Transplantation of Schwann Cells Inside PVDF-TrFE Conduits to Bridge Transected Rat Spinal Cord Stumps to Promote Axon Regeneration Across the Gap. *J. Vis. Exp.* (2017). doi:10.3791/56077

165. Sharma, T., Aroom, K., Naik, S., Gill, B. & Zhang, J. X. J. Flexible thin-film

PVDF-TrFE based pressure sensor for smart catheter applications. *Ann. Biomed. Eng.* **41**, 744–51 (2013).

166. Martins, P., Lopes, A. C. & Lanceros-Mendez, S. Electroactive phases of poly(vinylidene fluoride): Determination, processing and applications. *Prog. Polym. Sci.* **39**, 683–706 (2014).

167. Weber, N., Lee, Y.-S., Shanmugasundaram, S., Jaffe, M. & Arinzeh, T. L. Characterisation and in vitro cytocompatibility of piezoelectric electrospun scaffolds. *Acta Biomater.* **6**, 3550–3556 (2010).

168. Tseng, H. J., Tian, W. C. & Wu, W. J. P(VDF-TrFE) polymer-based thin films deposited on stainless steel substrates treated using water dissociation for flexible tactile sensor development. *Sensors (Switzerland)* **13**, 14777–14796 (2013).

169. Hitscherich, P. *et al.* The effect of PVDF-TrFE scaffolds on stem cell derived cardiovascular cells. *Biotechnol. Bioeng.* **113**, 1577–85 (2016).

170. Cheng, X. *et al.* Implantable and self-powered blood pressure monitoring based on a piezoelectric thinfilm: Simulated, in vitro and in vivo studies. *Nano Energy* **22**, 453–460 (2016).

171. Persano, L. *et al.* High performance piezoelectric devices based on aligned arrays of nanofibers of poly(vinylidenefluoride-co-trifluoroethylene). *Nat. Commun.* **4**, 1633 (2013).

172. Chang, C., Tran, V. H., Wang, J., Fuh, Y. K. & Lin, L. Direct-write piezoelectric polymeric nanogenerator with high energy conversion efficiency. *Nano Lett.* (2010). doi:10.1021/nl9040719

173. Pan, C. T. *et al.* Significant piezoelectric and energy harvesting enhancement of poly(vinylidene fluoride)/polypeptide fiber composites prepared through near-field electrospinning. *J. Mater. Chem. A* (2015). doi:10.1039/c5ta00147a

174. Dagdeviren, C. *et al.* Conformal piezoelectric systems for clinical and experimental characterisation of soft tissue biomechanics. *Nat. Mater.* **14**, 728–736 (2015).

175. Dadsetan, M. *et al.* The effects of fixed electrical charge on chondrocyte behavior. *Acta Biomater.* (2011). doi:10.1016/j.actbio.2011.01.012

176. Kitsara, M. *et al.* Permanently hydrophilic, piezoelectric PVDF nanofibrous scaffolds promoting unaided electromechanical stimulation on osteoblasts. *Nanoscale* (2019). doi:10.1039/c8nr10384d

177. Klee, D. *et al.* Surface modification of poly(vinylidenefluoride) to improve the

osteoblast adhesion. *Biomaterials* **24**, 3663–3670 (2003).

178. Defteralı, Ç. *et al.* In Vitro Evaluation of Biocompatibility of Uncoated Thermally Reduced Graphene and Carbon Nanotube-Loaded PVDF Membranes with Adult Neural Stem Cell-Derived Neurons and Glia. *Front. Bioeng. Biotechnol.* (2016). doi:10.3389/fbioe.2016.00094

179. Lee, Y.-S., Collins, G. & Livingston Arinzeh, T. Neurite extension of primary neurons on electrospun piezoelectric scaffolds. *Acta Biomater.* **7**, 3877–3886 (2011).

180. Ribeiro, C. *et al.* Dynamic piezoelectric stimulation enhances osteogenic differentiation of human adipose stem cells. *J. Biomed. Mater. Res. Part A* n/a-n/a (2014). doi:10.1002/jbm.a.35368

181. Parssinen, J. *et al.* Enhancement of adhesion and promotion of osteogenic differentiation of human adipose stem cells by poled electroactive poly(vinylidene fluoride). *J. Biomed. Mater. Res. - Part A* (2015). doi:10.1002/jbm.a.35234

182. Pereira, J. D. A. S. *et al.* Biomaterials from blends of fluoropolymers and corn starch - Implant and structural aspects. *Mater. Sci. Eng. C* (2014). doi:10.1016/j.msec.2013.12.008

183. Ribeiro, C. *et al.* Electroactive poly(vinylidene fluoride)-based structures for advanced applications. *Nat. Protoc.* **13**, 681–704 (2018).

184. Genchi, G. G. *et al.* P(VDF-TrFE)/BaTiO3 Nanoparticle Composite Films Mediate Piezoelectric Stimulation and Promote Differentiation of SH-SY5Y Neuroblastoma Cells. *Adv. Healthc. Mater.* **5**, 1808–20 (2016).

185. Genchi, G. G. *et al.* Ultrasound-activated piezoelectric P(VDF-TrFE)/boron nitride nanotube composite films promote differentiation of human SaOS-2 osteoblast-like cells. *Nanomedicine* **14**, 2421–2432 (2018).

186. Fang, F., Shan, S. C. & Yang, W. Magnetoelectric coupling of Terfenol-D/P(VDF-TrFe)/Terfenol-D laminates mediated by crystallite size of electroactive polymer. *Acta Mech.* **224**, 1169–1174 (2013).

187. Brito-Pereira, R., Ribeiro, C., Lanceros-Mendez, S. & Martins, P. Magnetoelectric response on Terfenol-D/ P(VDF-TrFE) two-phase composites. *Compos. Part B Eng.* **120**, 97–102 (2017).

188. Cha, S. *et al.* Porous PVDF as effective sonic wave driven nanogenerators. *Nano Lett.* (2011). doi:10.1021/nl202208n

189. Cho, K. Y. *et al.* Enhanced Electrical Properties of PVDF-TrFE Nanocomposite for Actuator Application. *Key Eng. Mater.* (2014). doi:10.4028/www.scientific.net/KEM.605.335

190. Guo, W. *et al.* Self-Powered Electrical Stimulation for Enhancing Neural Differentiation of Mesenchymal Stem Cells on Graphene-Poly(3,4-ethylenedioxythiophene) Hybrid Microfibers. *ACS Nano* (2016). doi:10.1021/acsnano.6b00200

191. Zheng, Q. *et al.* Biodegradable triboelectric nanogenerator as a life-time designed implantable power source. *Sci. Adv.* **2**, e1501478 (2016).

192. Nuccitelli, R. A Role for Endogenous Electric Fields in Wound Healing. *Current Topics in Developmental Biology* (2003). doi:10.1016/S0070-2153(03)58001-2

193. Ladoux, B. & Mège, R.-M. Mechanobiology of collective cell behaviours. *Nat. Rev. Mol. Cell Biol.* **18**, 743–757 (2017).

194. Iskratsch, T., Wolfenson, H. & Sheetz, M. P. Appreciating force and shape — the rise of mechanotransduction in cell biology. *Nat. Rev. Mol. Cell Biol.* **15**, 825–833 (2014).

195. Xia, S. & Kanchanawong, P. Nanoscale mechanobiology of cell adhesions. *Semin. Cell Dev. Biol.* **71**, 53–67 (2017).

196. Turner, C. H. *et al.* Mechanobiology of the skeleton. *Sci. Signal.* **2**, pt3 (2009).

197. Li, Q. *et al.* Structural mechanism of voltage-dependent gating in an isolated voltage-sensing domain. *Nat. Struct. Mol. Biol.* (2014). doi:10.1038/nsmb.2768

198. Wang, J., Tian, L., Chen, N., Ramakrishna, S. & Mo, X. The cellular response of nerve cells on poly-l-lysine coated PLGA-MWCNTs aligned nanofibers under electrical stimulation. *Mater. Sci. Eng. C. Mater. Biol. Appl.* **91**, 715–726 (2018).

199. Mario Cheong, G. L. *et al.* Conductive hydrogels with tailored bioactivity for implantable electrode coatings. *Acta Biomater.* **10**, 1216–26 (2014).

200. Cui, H. *et al.* In vitro studies on regulation of osteogenic activities by electrical stimulus on biodegradable electroactive polyelectrolyte multilayers. *Biomacromolecules* **15**, 3146–57 (2014).

201. Gilmore, K. J. *et al.* Skeletal muscle cell proliferation and differentiation on polypyrrole substrates doped with extracellular matrix components. *Biomaterials* **30**, 5292–304 (2009).

202. Chen, Q.-Q. *et al.* Electrical field stimulation induces cardiac fibroblast proliferation through the calcineurin-NFAT pathway. *Can. J. Physiol.*

Pharmacol. **90**, 1611–22 (2012).

203. Seo, G. Y. *et al.* A Novel Synthetic Material, BMM, Accelerates Wound Repair by Stimulating Re-Epithelialization and Fibroblast Activation. *Int. J. Mol. Sci.* **19**, 1164 (2018).

204. Head, B. P., Patel, H. H. & Insel, P. A. Interaction of membrane/lipid rafts with the cytoskeleton: impact on signaling and function: membrane/lipid rafts, mediators of cytoskeletal arrangement and cell signaling. *Biochim. Biophys. Acta* **1838**, 532–45 (2014).

205. Yang, G. *et al.* Regulation of adipose-tissue-derived stromal cell orientation and motility in 2D- and 3D-cultures by direct-current electrical field. *Dev. Growth Differ.* **59**, 70–82 (2017).

206. Greco, F. *et al.* Microwrinkled conducting polymer interface for anisotropic multicellular alignment. *ACS Appl. Mater. Interfaces* **5**, 573–84 (2013).

207. Serena, E. *et al.* Electrical stimulation of human embryonic stem cells: Cardiac differentiation and the generation of reactive oxygen species. *Exp. Cell Res.* **315**, 3611–3619 (2009).

208. Das, S. R. *et al.* Electrical Differentiation of Mesenchymal Stem Cells into Schwann-Cell-Like Phenotypes Using Inkjet-Printed Graphene Circuits. *Adv. Healthc. Mater.* **6**, 1601087 (2017).

209. Wu, Z. *et al.* Mechanosensory hair cells express two molecularly distinct mechanotransduction channels. *Nat. Neurosci.* **20**, 24–33 (2017).

210. Cox, C. D., Wann, K. T. & Martinac, B. Selectivity mechanisms in MscS-like channels. *Channels* **8**, 5–12 (2014).

211. Lacroix, J. J., Botello-Smith, W. M. & Luo, Y. Probing the gating mechanism of the mechanosensitive channel Piezo1 with the small molecule Yoda1. *Nat. Commun.* **9**, 2029 (2018).

212. Zilly, F. E. *et al.* Ca 2+ induces clustering of membrane proteins in the plasma membrane via electrostatic interactions. *EMBO J.* (2011). doi:10.1038/emboj.2011.53

213. Yang, W. P., Onuma, E. K. & Hui, S. W. Response of C3H/10T1/2 fibroblasts to an external steady electric field stimulation. Reorientation, shape change, ConA receptor and intramembranous particle distribution and cytoskeleton reorganisation. *Exp. Cell Res.* **155**, 92–104 (1984).

214. Vacek, T. P. *et al.* Electrical stimulation of cardiomyocytes activates

mitochondrial matrix metalloproteinase causing electrical remodeling. *Biochem. Biophys. Res. Commun.* **404**, 762–6 (2011).

215. Titushkin, I. & Cho, M. Regulation of cell cytoskeleton and membrane mechanics by electric field: role of linker proteins. *Biophys. J.* **96**, 717–28 (2009).

216. Liu, L. *et al.* Mechanoresponsive stem cells to target cancer metastases through biophysical cues. *Sci. Transl. Med.* (2017). doi:10.1126/scitranslmed.aan2966

217. Isaksson, H., Wilson, W., van Donkelaar, C. C., Huiskes, R. & Ito, K. Comparison of biophysical stimuli for mechano-regulation of tissue differentiation during fracture healing. *J. Biomech.* (2006). doi:10.1016/j.jbiomech.2005.01.037

218. Pruitt, B. L., Dunn, A. R., Weis, W. I. & Nelson, W. J. Mechano-Transduction: From Molecules to Tissues. *PLoS Biol.* (2014). doi:10.1371/journal.pbio.1001996

219. Sauer, H. *et al.* DC electrical field-induced c-fos expression and growth stimulation in multicellular prostate cancer spheroids. *Br. J. Cancer* **75**, 1481–8 (1997).

220. Ruffini, G. *et al.* Transcranial current brain stimulation (tCS): models and technologies. *IEEE Trans. Neural Syst. Rehabil. Eng.* **21**, 333–45 (2013).

221. Zhao, H., Steiger, A., Nohner, M. & Ye, H. Specific Intensity Direct Current (DC) Electric Field Improves Neural Stem Cell Migration and Enhances Differentiation towards βIII-Tubulin+ Neurons. *PLoS One* **10**, e0129625 (2015).

222. Wartenberg, M., Hescheler, J. & Sauer, H. Electrical fields enhance growth of cancer spheroids by reactive oxygen species and intracellular Ca2+. *Am. J. Physiol.* **272**, R1677-83 (1997).

223. Yamada, M. *et al.* Electrical Stimulation Modulates Fate Determination of Differentiating Embryonic Stem Cells. *Stem Cells* (2006). doi:10.1634/stemcells.2006-0011

224. Feng, J. F. *et al.* Electrical Guidance of Human Stem Cells in the Rat Brain. *Stem Cell Reports* (2017). doi:10.1016/j.stemcr.2017.05.035

225. Patel, Y. A. & Butera, R. J. Differential fiber-specific block of nerve conduction in mammalian peripheral nerves using kilohertz electrical stimulation. *J. Neurophysiol.* (2015). doi:10.1152/jn.00529.2014

226. Ackermann, D. M., Foldes, E. L., Bhadra, N. & Kilgore, K. L. Nerve conduction

block using combined thermoelectric cooling and high frequency electrical stimulation. *J. Neurosci. Methods* (2010). doi:10.1016/j.jneumeth.2010.07.043

227. Kadow-Romacker, A., Hoffmann, J. E., Duda, G., Wildemann, B. & Schmidmaier, G. Effect of mechanical stimulation on osteoblast- and osteoclast-like cells in vitro. *Cells Tissues Organs* (2009). doi:10.1159/000178022

228. Yao, R. & Wong, J. Y. The Effects of Mechanical Stimulation on Controlling and Maintaining Marrow Stromal Cell Differentiation Into Vascular Smooth Muscle Cells. *J. Biomech. Eng.* (2015). doi:10.1115/1.4029255

229. Zhang, C. *et al.* Effects of mechanical vibration on proliferation and osteogenic differentiation of human periodontal ligament stem cells. *Arch. Oral Biol.* (2012). doi:10.1016/j.archoralbio.2012.04.010

230. Tsimbouri, P. M. *et al.* Publisher Correction: Stimulation of 3D osteogenesis by mesenchymal stem cells using a nanovibrational bioreactor. *Nat. Biomed. Eng.* **1**, 1004–1004 (2017).

231. Karode, N., Fitzhenry, L., Matthews, S., Walsh, P. & Coffey, A. Enhancement of the Mechanical Properties of PEBAX Graphene Nanocomposite Using Supercritical Fluid Assisted Extrusion Polymer Processing Technique. *Mater. Sci. Forum* (2017). doi:10.4028/www.scientific.net/MSF.883.75

232. Avrami, M. Kinetics of phase change. I: General theory. *J. Chem. Phys.* (1939). doi:10.1063/1.1750380

233. Avrami, M. Kinetics of phase change. II Transformation-time relations for random distribution of nuclei. *J. Chem. Phys.* (1940). doi:10.1063/1.1750631

234. Avrami, M. Kinetics of Phase Change. *J. Chem. Phys.* (1939). doi:10.1590/S1516-14392000000300002

235. Avrami, M. Granulation, phase change, and microstructure kinetics of phase change. III. *J. Chem. Phys.* (1941). doi:10.1063/1.1750872

236. Jeziorny, A. Parameters characterizing the kinetics of the non-isothermal crystallization of poly(ethylene terephthalate) determined by d.s.c. *Polymer (Guildf).* (1978). doi:10.1016/0032-3861(78)90060-5

237. Ozawa, T. Kinetics of non-isothermal crystallization. *Polymer (Guildf).* (1971). doi:10.1016/0032-3861(71)90041-3

238. Liu, F. & Yang, G. Effects of anisotropic growth on the deviations from Johnson-Mehl-Avrami kinetics. *Acta Mater.* (2007). doi:10.1016/j.actamat.2006.10.022

239. Lanceros-Méndez, S., Mano, J. F., Costa, A. M. & Schmidt, V. H. FTIR and

DSC studies of mechanically deformed β-PVDF films. *J. Macromol. Sci. - Phys.* (2001). doi:10.1081/MB-100106174

240. Fialka, J. & Benes, P. Comparison of Methods for the Measurement of Piezoelectric Coefficients. *IEEE Trans. Instrum. Meas.* **62**, 1047–1057 (2013).

241. Binning, G., Rohrer, H., Gerber, C. & Weibel, E. Surface studies by scanning tunneling microscopy. *Phys. Rev. Lett.* (1982). doi:10.1103/PhysRevLett.49.57

242. Huang, H., Gu, L. & Ozaki, Y. Non-isothermal crystallization and thermal transitions of a biodegradable, partially hydrolyzed poly(vinyl alcohol). *Polymer (Guildf).* (2006). doi:10.1016/j.polymer.2006.03.089

243. Liu, Y., Wang, L., He, Y., Fan, Z. & Li, S. Non-isothermal crystallization kinetics of poly(L-lactide). *Polym. Int.* (2010). doi:10.1002/pi.2894

244. Furukawa, T. Ferroelectric properties of vinylidene fluoride copolymers. *Phase Transitions* (1989). doi:10.1080/01411598908206863

245. Vinogradov, A. & Holloway, F. Electro-mechanical properties of the piezoelectric polymer PVDF. *Ferroelectrics* (1999). doi:10.1080/00150199908230298

246. Martins, P. *et al.* Role of nanoparticle surface charge on the nucleation of the electroactive β-poly(vinylidene fluoride) nanocomposites for sensor and actuator applications. *J. Phys. Chem. C* (2012). doi:10.1021/jp3038768

247. Wang, Y. J. & Kim, D. Crystallinity, morphology, mechanical properties and conductivity study of in situ formed PVdF/LiClO4/TiO2nanocomposite polymer electrolytes. *Electrochim. Acta* (2007). doi:10.1016/j.electacta.2006.09.070

248. Steinhart, M., Senz, S., Wehrspohn, R. B., Gösele, U. & Wendorff, J. H. Curvature-directed crystallization of poly(vinylidene difluoride) in nanotube walls. *Macromolecules* (2003). doi:10.1021/ma0260039

249. Cao, Y. *et al.* Bridging tendon defects using autologous tenocyte engineered tendon in a hen model. *Plast. Reconstr. Surg.* (2002). doi:10.1097/00006534-200210000-00011

250. Chen, J. M., Willers, C., Xu, J., Wang, A. & Zheng, M.-H. Autologous Tenocyte Therapy Using Porcine-Derived Bioscaffolds for Massive Rotator Cuff Defect in Rabbits. *Tissue Eng.* (2007). doi:10.1089/ten.2006.0266

251. Spanoudes, K., Gaspar, D., Pandit, A. & Zeugolis, D. I. The biophysical, biochemical, and biological toolbox for tenogenic phenotype maintenance in vitro. *Trends Biotechnol.* **32**, 474–482 (2014).

252. Stoll, C. *et al.* Extracellular matrix expression of human tenocytes in three-dimensional air-liquid and PLGA cultures compared with tendon tissue: Implications for tendon tissue engineering. *J. Orthop. Res.* (2010). doi:10.1002/jor.21109

253. Juncosa-Melvin, N., Matlin, K. S., Holdcraft, R. W., Nirmalanandhan, V. S. & Butler, D. L. Mechanical Stimulation Increases Collagen Type I and Collagen Type III Gene Expression of Stem Cell–Collagen Sponge Constructs for Patellar Tendon Repair. *Tissue Eng.* (2007). doi:10.1089/ten.2006.0339

254. Jiang, C., Shao, L., Wang, Q. & Dong, Y. Repetitive mechanical stretching modulates transforming growth factor-β induced collagen synthesis and apoptosis in human patellar tendon fibroblasts. *Biochem. Cell Biol.* (2012). doi:10.1139/o2012-024

255. Kilian, K. A., Bugarija, B., Lahn, B. T. & Mrksich, M. Geometric cues for directing the differentiation of mesenchymal stem cells. *Proc. Natl. Acad. Sci. U. S. A.* **107**, 4872–7 (2010).

256. Nikukar, H. *et al.* Osteogenesis of mesenchymal stem cells by nanoscale mechanotransduction. *ACS Nano* (2013). doi:10.1021/nn400202j

257. Wang, J. H.-C. *et al.* Cyclic mechanical stretching of human tendon fibroblasts increases the production of prostaglandin E2 and levels of cyclooxygenase expression: a novel in vitro model study. *Connect. Tissue Res.* **44**, 128–33 (2003).

258. Zhang, J. & Wang, J. H. C. Production of PGE2 increases in tendons subjected to repetitive mechanical loading and induces differentiation of tendon stem cells into non-tenocytes. *J. Orthop. Res.* (2010). doi:10.1002/jor.20962

259. Love, M. R., Palee, S., Chattipakorn, S. C. & Chattipakorn, N. Effects of electrical stimulation on cell proliferation and apoptosis. *J. Cell. Physiol.* **233**, 1860–1876 (2018).

260. Balint, R., Cassidy, N. J. & Cartmell, S. H. Electrical Stimulation: A Novel Tool for Tissue Engineering. *Tissue Eng. Part B Rev.* **19**, 48–57 (2013).

261. Shao, S. *et al.* Osteoblast function on electrically conductive electrospun PLA/MWCNTs nanofibers. *Biomaterials* (2011). doi:10.1016/j.biomaterials.2011.01.051

262. Ning, C., Zhou, Z., Tan, G., Zhu, Y. & Mao, C. Electroactive polymers for tissue regeneration: Developments and perspectives. *Progress in Polymer Science*

(2018). doi:10.1016/j.progpolymsci.2018.01.001

263. Zhang, J., Li, M., Kang, E. T. & Neoh, K. G. Electrical stimulation of adipose-derived mesenchymal stem cells in conductive scaffolds and the roles of voltage-gated ion channels. *Acta Biomater.* **32**, 46–56 (2016).

264. Chiu, C. H., Lei, K. F. & Yeh, W. L. Development of a co-culture device for the study of human tenocytes in response to the combined stimulation of electric field and platelet rich plasma (PRP). *Biomed. Microdevices* (2017). doi:10.1007/s10544-017-0214-z

265. Basas, Á. *et al.* Effects of a strength protocol combined with electrical stimulation on patellar tendinopathy: 42 months retrospective follow-up on 6 high-level jumping athletes. *Phys. Ther. Sport* **34**, 105–112 (2018).

266. Yanase, K. *et al.* Electrical Stimulation to the Infraspinatus on Hypertrophy and Strength of the Shoulder. *Int. J. Sports Med.* **39**, 828–834 (2018).

267. Yan, Z. *et al.* [Effects of electrical stimulation on the differentiation of mesenchymal stem cells into cardiomyocyte-like cells]. *Sheng Wu Yi Xue Gong Cheng Xue Za Zhi* **30**, 556–61 (2013).

268. Pardo-Pastor, C. *et al.* Piezo2 channel regulates RhoA and actin cytoskeleton to promote cell mechanobiological responses. *Proc. Natl. Acad. Sci. U. S. A.* **115**, 1925–1930 (2018).

269. Islam, A., Mbimba, T., Younesi, M. & Akkus, O. Effects of substrate stiffness on the tenoinduction of human mesenchymal stem cells. *Acta Biomater.* **58**, 244–253 (2017).

270. Barsby, T., Bavin, E. P. & Guest, D. J. Three-Dimensional Culture and Transforming Growth Factor Beta3 Synergistically Promote Tenogenic Differentiation of Equine Embryo-Derived Stem Cells. *Tissue Eng. Part A* (2014). doi:10.1016/j.foreco.2016.02.006

271. Qi, J. *et al.* IL-1β decreases the elastic modulus of human tenocytes. *J. Appl. Physiol.* (2006). doi:10.1152/japplphysiol.01128.2005

272. Tsuzaki, M., Bynum, D., Almekinders, L., Faber, J. & Banes, A. J. Mechanical loading stimulates ecto-ATPase activity in human tendon cells. *J. Cell. Biochem.* (2005). doi:10.1002/jcb.20491

273. Archambault, J., Tsuzaki, M., Herzog, W. & Banes, A. J. Stretch and interleukin-1β induce matrix metalloproteinases in rabbit tendon cells in vitro. *J. Orthop. Res.* (2002). doi:10.1016/S0736-0266(01)00075-4

274. Tsuzaki, M. *et al.* IL-1β induces COX2, MMP-1, -3 and -13, ADAMTS-4, IL-1β and IL-6 in human tendon cells. *J. Orthop. Res.* (2003). doi:10.1016/S0736-0266(02)00141-9

275. Jelinsky, S. A., Archambault, J., Li, L. & Seeherman, H. Tendon-selective genes identified from rat and human musculoskeletal tissues. *J. Orthop. Res.* **28**, n/a-n/a (2009).

276. Delgado Caceres, M., Pfeifer, C. G. & Docheva, D. Understanding Tendons: Lessons from Transgenic Mouse Models. *Stem Cells Dev.* **27**, 1161–1174 (2018).

277. Inaba, S., Akaishi, K., Mori, T. & Hane, K. Analysis of the resonance characteristics of a cantilever vibrated photothermally in a liquid. *J. Appl. Phys.* (1993). doi:10.1063/1.353060

278. Kwak, M. K. & Kim, K. C. Axisymmetric vibration of circular plates in contact with fluid. *J. Sound Vib.* (1991). doi:10.1016/0022-460X(91)90696-H

279. Nikukar, H. *et al.* Osteogenesis of Mesenchymal Stem Cells by Nanoscale Mechanotransduction. *ACS Nano* **7**, 2758–2767 (2013).

280. Wang, T. *et al.* Programmable mechanical stimulation influences tendon homeostasis in a bioreactor system. *Biotechnol. Bioeng.* (2013). doi:10.1002/bit.24809

281. Zhang, J. & Wang, J. H. C. Mechanobiological response of tendon stem cells: Implications of tendon homeostasis and pathogenesis of tendinopathy. *J. Orthop. Res.* (2010). doi:10.1002/jor.21046

282. Aspenberg, P. Stimulation of tendon repair: Mechanical loading, GDFs and platelets. a mini-review. *International Orthopaedics* (2007). doi:10.1007/s00264-007-0398-6

283. Busch, T., Köttgen, M. & Hofherr, A. TRPP2 ion channels: Critical regulators of organ morphogenesis in health and disease. *Cell Calcium* (2017). doi:10.1016/j.ceca.2017.05.005

284. Chachisvilis, M., Zhang, Y.-L. & Frangos, J. A. G protein-coupled receptors sense fluid shear stress in endothelial cells. *Proc. Natl. Acad. Sci.* (2006). doi:10.1073/pnas.0607224103

285. Wu, J., Lewis, A. H. & Grandl, J. Touch, Tension, and Transduction – The Function and Regulation of Piezo Ion Channels. *Trends Biochem. Sci.* **42**, 57–71 (2017).

286. Popov, C. *et al.* Mechanical stimulation of human tendon stem/progenitor cells

results in upregulation of matrix proteins, integrins and MMPs, and activation of p38 and ERK1/2 kinases. *BMC Mol. Biol.* **16**, 1–11 (2015).

287. Maksimovic, S. *et al.* Epidermal Merkel cells are mechanosensory cells that tune mammalian touch receptors. *Nature* (2014). doi:10.1038/nature13250

288. Zhang, W., Yan, Z., Jan, L. Y. & Jan, Y. N. Sound response mediated by the TRP channels NOMPC, NANCHUNG, and INACTIVE in chordotonal organs of Drosophila larvae. *Proc. Natl. Acad. Sci.* (2013). doi:10.1073/pnas.1312477110

289. Kim, J. *et al.* A TRPV family ion channel required for hearing in Drosophila. *Nature* (2003). doi:10.1038/nature01733

290. Rayleigh, J. W. S. *The Theory of Sound Vol. II. Macmillan* (1896). doi:10.1017/CBO9781107415324.004

291. Sroka, J., Zimolag, E., Lasota, S. & Korohoda, W. Electrotaxis : Cell Directional Movement in Electric Fields. **1749**, 325–340

292. Banks, T. A., Luckman, P. S. B., Frith, J. E. & Cooper-White, J. J. Effects of electric fields on human mesenchymal stem cell behaviour and morphology using a novel multichannel device. *Integr. Biol. (Camb).* **7**, 693–712 (2015).

293. Guerin, S. *et al.* Control of piezoelectricity in amino acids by supramolecular packing. *Nat. Mater.* (2018). doi:10.1038/NMAT5045

294. Boriek, A. M. & Kumar, A. Regulation of Intracellular Signal Transduction Pathways by Mechanosensitive Ion Channels. in *Mechanosensitive Ion Channels* (2007). doi:10.1007/978-1-4020-6426-5_14

295. Coste, B. *et al.* Piezo1 and Piezo2 are essential components of distinct mechanically activated cation channels. *Science (80-.).* (2010). doi:10.1126/science.1193270

296. Goodier, H. C. J. *et al.* Comparison of transforming growth factor beta expression in healthy and diseased human tendon. *Arthritis Res. Ther.* (2016). doi:10.1186/s13075-016-0947-8

297. Zhuang, H. *et al.* Electrical stimulation induces the level of TGF-β1 mRNA in osteoblastic cells by a mechanism involving calcium/calmodulin pathway. *Biochem. Biophys. Res. Commun.* (1997). doi:10.1006/bbrc.1997.7118

298. Hirata, H., Tatsumi, H., Hayakawa, K. & Sokabe, M. Non-channel mechanosensors working at focal adhesion-stress fiber complex. *Pflügers Arch. - Eur. J. Physiol.* **467**, 141–155 (2015).

299. Prindle, A. *et al.* Ion channels enable electrical communication in bacterial

communities. *Nature* (2015). doi:10.1038/nature15709

300. Brohawn, S. G., Campbell, E. B. & MacKinnon, R. Physical mechanism for gating and mechanosensitivity of the human TRAAK K+ channel. *Nature* (2014). doi:10.1038/nature14013

301. Lin, Y. Lo, Moolenaar, H., van Weeren, P. R. & van de Lest, C. H. A. Effect of microcurrent electrical tissue stimulation on equine tenocytes in culture. *Am. J. Vet. Res.* (2006). doi:10.2460/ajvr.67.2.271

302. STROYAN, J. J. PROCESSING AND CHARACTERISATION OF PVDF, PVDF-TrFE, AND PVDF-TrFE-PZT COMPOSITES. *J. Chem. Inf. Model.* (2013). doi:10.1017/CBO9781107415324.004

303. Dodds, J. S., Meyers, F. N. & Loh, K. J. Piezoelectric characterisation of PVDF-TrFE thin films enhanced with ZnO nanoparticles. *IEEE Sens. J.* (2012). doi:10.1109/JSEN.2011.2182043

304. Chen, H. J. *et al.* Investigation of PVDF-TrFE composite with nanofillers for sensitivity improvement. *Sensors Actuators, A Phys.* (2016). doi:10.1016/j.sna.2016.04.056

305. Simoes, R. D., Rodriguez-Perez, M. A., De Saja, J. A. & Constantino, C. J. L. Thermomechanical characterisation of PVDF and P(VDF-TrFE) blends containing corn starch and natural rubber. *J. Therm. Anal. Calorim.* (2010). doi:10.1007/s10973-009-0285-z

306. Seminara, L., Capurro, M., Cirillo, P., Cannata, G. & Valle, M. Electromechanical characterisation of piezoelectric PVDF polymer films for tactile sensors in robotics applications. *Sensors Actuators, A Phys.* (2011). doi:10.1016/j.sna.2011.05.004

307. Mohamad Hafiz, M. W. *et al.* Effect of Annealing Temperature on the Crystallinity, Morphology and Ferroelectric of Polyvinylidenefluoride-Trifluoroethylene (PVDF-TrFE) Thin Film. *Adv. Mater. Res.* (2013). doi:10.4028/www.scientific.net/AMR.812.60

308. Lu, X., Qu, H. & Skorobogatiy, M. Piezoelectric microstructured fibers via drawing of multimaterial preforms. *Sci. Rep.* (2017). doi:10.1038/s41598-017-01738-9

309. Wong, S. C., Baji, A. & Leng, S. Effect of fiber diameter on tensile properties of electrospun poly(ε-caprolactone). *Polymer (Guildf).* (2008). doi:10.1016/j.polymer.2008.08.022

310. Chen, F. *et al.* Mechanical characterisation of single high-strength electrospun polyimide nanofibres. *J. Phys. D. Appl. Phys.* (2008). doi:10.1088/0022-3727/41/2/025308

311. Baji, A., Mai, Y. W. & Wong, S. C. Effect of fiber size on structural and tensile properties of electrospun polyvinylidene fluoride fibers. *Polym. Eng. Sci.* (2015). doi:10.1002/pen.24020

312. Ico, G. *et al.* Size-dependent piezoelectric and mechanical properties of electrospun P(VDF-TrFE) nanofibers for enhanced energy harvesting. *J. Mater. Chem. A* (2016). doi:10.1039/c5ta10423h

313. O'Hagan, D. Understanding organofluorine chemistry. An introduction to the C-F bond. *Chem. Soc. Rev.* (2008). doi:10.1039/b711844a

314. Wang, J. H.-C. Mechanobiology of tendon. *J. Biomech.* (2006). doi:10.1016/j.jbiomech.2005.05.011

315. Lin, T. W., Cardenas, L. & Soslowsky, L. J. Biomechanics of tendon injury and repair. *J. Biomech.* (2004). doi:10.1016/j.jbiomech.2003.11.005

316. James, R., Kesturu, G., Balian, G. & Chhabra, A. B. Tendon: Biology, Biomechanics, Repair, Growth Factors, and Evolving Treatment Options. *Journal of Hand Surgery* (2008). doi:10.1016/j.jhsa.2007.09.007

317. Wang, J. H. C., Guo, Q. & Li, B. Tendon Biomechanics and Mechanobiology—A Minireview of Basic Concepts and Recent Advancements. *J. Hand Ther.* **25**, 133–141 (2012).

318. Rees, J. D., Wilson, A. M. & Wolman, R. L. Current concepts in the management of tendon disorders. *Rheumatology* (2006). doi:10.1093/rheumatology/kel046

319. Yang, G., Crawford, R. C. & Wang, J. H. C. Proliferation and collagen production of human patellar tendon fibroblasts in response to cyclic uniaxial stretching in serum-free conditions. *J. Biomech.* (2004). doi:10.1016/j.jbiomech.2004.01.005

320. Skutek, M., Van Griensven, M., Zeichen, J., Brauer, N. & Bosch, U. Cyclic mechanical stretching modulates secretion pattern of growth factors in human tendon fibroblasts. *Eur. J. Appl. Physiol.* (2001). doi:10.1007/s004210100502

321. Zeichen, J., Van Griensven, M. & Bosch, U. The proliferative response of isolated human tendon fibroblasts to cyclic biaxial mechanical strain. *Am. J. Sports Med.* (2000). doi:10.1177/03635465000280061901

322. Jagodzinski, M. *et al.* Influence of cyclic mechanical strain and heat of human

tendon fibroblasts on HSP-72. *Eur. J. Appl. Physiol.* (2006). doi:10.1007/s00421-005-0071-y

323. Skutek, M., Van Griensven, M., Zeichen, J., Brauer, N. & Bosch, U. Cyclic mechanical stretching of human patellar tendon fibroblasts: Activation of JNK and modulation of apoptosis. *Knee Surgery, Sport. Traumatol. Arthrosc.* (2003). doi:10.1007/s00167-002-0322-y

324. Youngstrom, D. W., Rajpar, I., Kaplan, D. L. & Barrett, J. G. A bioreactor system for in vitro tendon differentiation and tendon tissue engineering. *J. Orthop. Res.* **33**, 911–918 (2015).

325. Bayer, M. L. *et al.* Release of tensile strain on engineered human tendon tissue disturbs cell adhesions, changes matrix architecture, and induces an inflammatory phenotype. *PLoS One* (2014). doi:10.1371/journal.pone.0086078

326. Moffat, K. L. *et al.* Novel Nanofiber-Based Scaffold for Rotator Cuff Repair and Augmentation. *Tissue Eng. Part A* (2008). doi:10.1089/ten.tea.2008.0014

327. Dabiri, B. E., Lee, H. & Parker, K. K. A potential role for integrin signaling in mechanoelectrical feedback. *Progress in Biophysics and Molecular Biology* (2012). doi:10.1016/j.pbiomolbio.2012.07.002

328. Butler, D. L. *et al.* The use of mesenchymal stem cells in collagen-based scaffolds for tissue-engineered repair of tendons. *Nat. Protoc.* (2010). doi:10.1038/nprot.2010.14

329. Schwartz, A. & Thomopoulos, S. The role of mechanobiology in the attachment of tendon to bone. in *Structural Interfaces and Attachments in Biology* (2013). doi:10.1007/978-1-4614-3317-0_11

330. Durant, T. J. S. *et al.* Mesenchymal stem cell response to growth factor treatment and low oxygen tension in 3-dimensional construct environment. *Muscle Ligaments Tendons J.* (2019). doi:10.32098/mltj.01.2014.09

331. Bagnaninchi, P. O. *et al.* Chitosan Microchannel Scaffolds for Tendon Tissue Engineering Characterised Using Optical Coherence Tomography. *Tissue Eng.* (2007). doi:10.1089/ten.2006.0168

332. Bagnaninchi, P. & Yang, Y. Tissue engineering for tendon repair. *Br. J. Sport. ...* (2007). doi:10.1136/bjsm.2006.030643

333. Stanton, A. E., Tong, X., Lee, S. & Yang, F. Biochemical Ligand Density Regulates Yes-Associated Protein Translocation in Stem Cells through Cytoskeletal Tension and Integrins. *ACS Appl. Mater. Interfaces* (2019).

doi:10.1021/acsami.8b21270

334. Driscoll, T. P., Cosgrove, B. D., Heo, S. J., Shurden, Z. E. & Mauck, R. L. Cytoskeletal to Nuclear Strain Transfer Regulates YAP Signaling in Mesenchymal Stem Cells. *Biophys. J.* (2015). doi:10.1016/j.bpj.2015.05.010

335. Méjat, A. & Misteli, T. LINC complexes in health and disease. *Nucleus* (2010). doi:10.4161/nucl.1.1.10530

336. Crisp, M. *et al.* Coupling of the nucleus and cytoplasm: Role of the LINC complex. *J. Cell Biol.* (2006). doi:10.1083/jcb.200509124

337. Isermann, P. & Lammerding, J. Nuclear mechanics and mechanotransduction in health and disease. *Current Biology* (2013). doi:10.1016/j.cub.2013.11.009

338. Watkins-Castillo, S. & Andersson, G. United States Bone and Joint Initiative: The Burden of Musculoskeletal Diseases in the United States (BMUS). *The Burden of Musculoskeletal diseases int he United States* (2014).

339. Biewener, A. A. Muscle-tendon stresses and elastic energy storage during locomotion in the horse. *Comp. Biochem. Physiol. - B Biochem. Mol. Biol.* (1998). doi:10.1016/S0305-0491(98)00024-8

340. Yang, G., Rothrauff, B. B. & Tuan, R. S. Tendon and ligament regeneration and repair: Clinical relevance and developmental paradigm. *Birth Defects Research Part C - Embryo Today: Reviews* (2013). doi:10.1002/bdrc.21041

341. Foolen, J., Wunderli, S. L., Loerakker, S. & Snedeker, J. G. Tissue alignment enhances remodeling potential of tendon-derived cells - Lessons from a novel microtissue model of tendon scarring. *Matrix Biol.* (2018). doi:10.1016/j.matbio.2017.06.002

342. Kimura, A., Aoki, M., Fukushima, S., Ishii, S. & Yamakoshi, K. Reconstruction of a defect of the rotator cuff with polytetrafluoroethylene felt graft. Recovery of tensile strength and histocompatibility in an animal model. *J. Bone Joint Surg. Br.* (2003).

343. Rowe, R. W. D. The structure of rat tail tendon. *Connect. Tissue Res.* (1985). doi:10.3109/03008208509089839

344. Chan, H. K. F., Fung, D. T. C. & Ng, G. Y. F. Effects of Low-Voltage Microamperage Stimulation on Tendon Healing in Rats. *J. Orthop. Sport. Phys. Ther.* **37**, 399–403 (2007).

345. West, C. R. & Bowden, A. E. Using tendon inherent electric properties to consistently track induced mechanical strain. *Ann. Biomed. Eng.* (2012).

doi:10.1007/s10439-011-0504-1

346. Liu, Z. & Kim, J. Effect of Strain Rate and Loading on the Piezoelectric Properties of Tendon. **8**, 3193 (2006).

347. Subramanian, A., Kanzaki, L. F., Galloway, J. L. & Schilling, T. F. Mechanical force regulates tendon extracellular matrix organisation and tenocyte morphogenesis through TGFbeta signaling. *Elife* **7**, 1–24 (2018).

348. Kannus, P., Józsa, L., Natri, A. & Järvinen, M. Effects of training, immobilization and remobilization on tendons. *Scand. J. Med. Sci. Sports* (2010). doi:10.1111/j.1600-0838.1997.tb00121.x

349. Matsumoto, F., Trudel, G., Uhthoff, H. K. & Backman, D. S. Mechanical effects of immobilization on the Achilles' tendon. *Arch. Phys. Med. Rehabil.* (2003). doi:10.1016/S0003-9993(02)04834-7

350. Kim, B. S. *et al.* The effect of dry needling and treadmill running on inducing pathological changes in rat Achilles tendon. *Connect. Tissue Res.* **8207**, 1–17 (2015).

351. De Castro Pochini, A. *et al.* Overuse of training increases mechanoreceptors in supraspinatus tendon of rats SHR. *J. Orthop. Res.* (2011). doi:10.1002/jor.21320

352. Yuan, T. *et al.* Creating an animal model of tendinopathy by inducing chondrogenic differentiation with kartogenin. *PLoS One* (2016). doi:10.1371/journal.pone.0148557

353. Wada, S. *et al.* Post-operative Tendon Loading with Treadmill Running Delays Tendon-to-Bone Healing: Immunohistochemical Evaluation in a Murine Rotator Cuff Repair Model. *J. Orthop. Res.* (2019). doi:10.1002/jor.24300

354. Zhang, J. & Wang, J. H.-C. The Effects of Mechanical Loading on Tendons - An In Vivo and In Vitro Model Study. *PLoS One* (2013). doi:10.1371/journal.pone.0071740

355. Zhang, J., Pan, T., Liu, Y. & Wang, J. H. C. Mouse treadmill running enhances tendons by expanding the pool of Tendon Stem Cells (TSCs) and TSC-related cellular production of collagen. *J. Orthop. Res.* (2010). doi:10.1002/jor.21123

356. Glazebrook, M. A., Wright, J. R., Langman, M., Stanish, W. D. & Lee, J. M. Histological analysis of Achilles tendons in an overuse rat model. *J. Orthop. Res.* (2008). doi:10.1002/jor.20546

357. Houghton, L., Dawson, B. & Rubenson, J. Achilles tendon mechanical properties after both prolonged continuous running and prolonged intermittent shuttle

running in cricket batting. *J. Appl. Biomech.* (2013). doi:10.1123/jab.29.4.453

358. Eliasson, P., Andersson, T. & Aspenberg, P. Achilles tendon healing in rats is improved by intermittent mechanical loading during the inflammatory phase. *J. Orthop. Res.* (2012). doi:10.1002/jor.21511

359. Xu, S. Y. *et al.* Response of Decorin to different intensity treadmill running. *Mol. Med. Rep.* (2018). doi:10.3892/mmr.2018.8802

360. Xu, S. Y. *et al.* Intensity-dependent effect of treadmill running on rat Achilles tendon. *Exp. Ther. Med.* (2018). doi:10.3892/etm.2018.6084

361. Kuo, C. K. & Tuan, R. S. Mechanoactive Tenogenic Differentiation of Human Mesenchymal Stem Cells. *Tissue Eng. Part A* (2008). doi:10.1089/ten.tea.2006.0415

362. Scott, A. *et al.* Mechanical force modulates scleraxis expression in bioartificial tendons. *J. Musculoskelet. Neuronal Interact.* (2011).

363. Lohberger, B. *et al.* Impact of cyclic mechanical stimulation on the expression of extracellular matrix proteins in human primary rotator cuff fibroblasts. *Knee Surgery, Sport. Traumatol. Arthrosc.* (2016). doi:10.1007/s00167-015-3790-6

364. Sawaguchi, N. *et al.* Effect of cyclic three-dimensional strain on cell proliferation and collagen synthesis of fibroblast-seeded chitosan-hyaluronan hybrid polymer fiber. *J. Orthop. Sci.* (2010). doi:10.1007/s00776-010-1488-7

365. D., D. Running far and fast: An emerging role of tenomodulin. *J. Orthop. Res.* (2017).

366. Zhang, J., Yuan, T. & Wang, J. H.-C. Moderate treadmill running exercise prior to tendon injury enhances wound healing in aging rats. *Oncotarget* (2016). doi:10.18632/oncotarget.7381

367. Cushman, D. & Rho, M. E. Conservative Treatment of Subacute Proximal Hamstring Tendinopathy Using Eccentric Exercises Performed With a Treadmill: A Case Report. *J. Orthop. Sport. Phys. Ther.* (2015). doi:10.2519/jospt.2015.5762

368. Heinemeier, K. M. *et al.* Uphill running improves rat Achilles tendon tissue mechanical properties and alters gene expression without inducing pathological changes. *J. Appl. Physiol.* (2012). doi:10.1152/japplphysiol.00401.2012

369. Abraham, T., Fong, G. & Scott, A. Second harmonic generation analysis of early Achilles tendinosis in response to in vivo mechanical loading. *BMC Musculoskelet. Disord.* (2011). doi:10.1186/1471-2474-12-26

370. Jafari, L., Vachon, P., Beaudry, F. & Langelier, E. Histopathological, biomechanical, and behavioral pain findings of achilles tendinopathy using an animal model of overuse injury. *Physiol. Rep.* (2015). doi:10.14814/phy2.12265

371. Ng, G. Y. F., Chung, P. Y. M., Wang, J. S. & Cheung, R. T. H. Enforced bipedal downhill running induces Achilles tendinosis in rats. *Connect. Tissue Res.* (2011). doi:10.3109/03008207.2011.562334

372. Mendias, C. L., Gumucio, J. P., Bakhurin, K. I., Lynch, E. B. & Brooks, S. V. Physiological loading of tendons induces scleraxis expression in epitenon fibroblasts. *J. Orthop. Res.* (2012). doi:10.1002/jor.21550

373. Esteves de Lima, J. *et al.* TGFβ and FGF promote tendon progenitor fate and act downstream of muscle contraction to regulate tendon differentiation during chick limb development. *Development* (2016). doi:10.1242/dev.136242

374. Brent, A. E. FGF acts directly on the somitic tendon progenitors through the Ets transcription factors Pea3 and Erm to regulate scleraxis expression. *Development* (2004). doi:10.1242/dev.01275

375. Shukunami, C., Takimoto, A., Oro, M. & Hiraki, Y. Scleraxis positively regulates the expression of tenomodulin, a differentiation marker of tenocytes. *Dev. Biol.* (2006). doi:10.1016/j.ydbio.2006.06.036

376. Hammerman, M., Aspenberg, P. & Eliasson, P. Microtrauma stimulates rat Achilles tendon healing via an early gene expression pattern similar to mechanical loading. *J. Appl. Physiol.* (2013). doi:10.1152/japplphysiol.00741.2013

377. Cheng, N., Hoof, V. A. N. & Hoogmartens, M. J. Generation , Protein Synthesis , and Membrane Transport in Rat Skin. *Clin. Orthop. Relat. Researc* (1982).

378. Meng, X. *et al.* PI3K mediated electrotaxis of embryonic and adult neural progenitor cells in the presence of growth factors. *Exp. Neurol.* (2011). doi:10.1016/j.expneurol.2010.11.002

379. Sung, K. M. *et al.* Control of neonatal human dermal fibroblast migration on poly(lactic-co-glycolic acid)-coated surfaces by electrotaxis. *J. Tissue Eng. Regen. Med.* (2015). doi:10.1002/term.1986

380. Li, S. *et al.* Electrical Stimulation Activates Fibroblasts through the Elevation of Intracellular Free Ca 2+ : Potential Mechanism of Pelvic Electrical Stimulation Therapy . *Biomed Res. Int.* (2019). doi:10.1155/2019/7387803

381. Lee, G. S., Kim, M. G. & Kwon, H. J. Electrical stimulation induces direct

reprogramming of human dermal fibroblasts into hyaline chondrogenic cells. *Biochem. Biophys. Res. Commun.* (2019). doi:10.1016/j.bbrc.2019.04.027

382. Ni, M. *et al.* Engineered scaffold-free tendon tissue produced by tendon-derived stem cells. *Biomaterials* **34**, 2024–2037 (2013).

383. Xu, S.-Y., Li, S.-F. & Ni, G.-X. Strenuous Treadmill Running Induces a Chondrocyte Phenotype in Rat Achilles Tendons. *Med. Sci. Monit.* (2016). doi:10.12659/msm.897726

384. Carpenter, J. E., Flanagan, C. L., Thomopoulos, S., Yian, E. H. & Soslowsky, L. J. The effects of overuse combined with intrinsic or extrinsic alterations in an animal model of rotator cuff tendinosis. *Am. J. Sports Med.* (1998). doi:10.1177/03635465980260061101

385. Szomor, Z. L., Appleyard, R. C. & Murrell, G. A. C. Overexpression of nitric oxide synthases in tendon overuse. *J. Orthop. Res.* (2006). doi:10.1002/jor.20009

386. Thampatty, B. P. & Wang, J. H. C. Mechanobiology of young and aging tendons: In vivo studies with treadmill running. *J. Orthop. Res.* (2017). doi:10.1002/jor.23761

387. Heinemeier, K. M. *et al.* Effect of unloading followed by reloading on expression of collagen and related growth factors in rat tendon and muscle. *J. Appl. Physiol.* (2009). doi:10.1152/japplphysiol.91092.2008

388. Zhang, J. & Wang, J. H. C. Moderate exercise mitigates the detrimental effects of aging on tendon stem cells. *PLoS One* (2015). doi:10.1371/journal.pone.0130454

389. Dey, D. *et al.* Two tissue-resident progenitor lineages drive distinct phenotypes of heterotopic ossification. *Sci. Transl. Med.* (2016). doi:10.1126/scitranslmed.aaf1090

390. Wood, L. K. & Brooks, S. V. Ten weeks of treadmill running decreases stiffness and increases collagen turnover in tendons of old mice. *J. Orthop. Res.* (2016). doi:10.1002/jor.22824

391. Gimbel, J. A. Long Durations of Immobilization in the Rat Result in Enhanced Mechanical Properties of the Healing Supraspinatus Tendon Insertion Site. *J. Biomech. Eng.* (2007). doi:10.1115/1.2721075

392. Wolfman, N. M. *et al.* Ectopic induction of tendon and ligament in rats by growth and differentiation factors 5, 6, and 7, members of the TGF-β gene family. *J. Clin. Invest.* (1997). doi:10.1172/JCI119537

393. Kishimoto, Y. *et al.* Wnt/β-catenin signaling suppresses expressions of Scx,

Mkx, and Tnmd in tendon-derived cells. *PLoS One* (2017). doi:10.1371/journal.pone.0182051

394. Zhou, S., Eid, K. & Glowacki, J. Cooperation between TGF-β and Wnt pathways during chondrocyte and adipocyte differentiation of human marrow stromal cells. *J. Bone Miner. Res.* (2004). doi:10.1359/JBMR.0301239

395. Chen, Y. *et al.* β-Catenin signaling pathway is crucial for bone morphogenetic protein 2 to induce new bone formation. *J. Biol. Chem.* (2007). doi:10.1074/jbc.M602700200

396. Zhang, R. *et al.* Wnt/β-catenin signaling activates bone morphogenetic protein 2 expression in osteoblasts. *Bone* (2013). doi:10.1016/j.bone.2012.09.029

397. Gaur, T. *et al.* Canonical WNT signaling promotes osteogenesis by directly stimulating Runx2 gene expression. *J. Biol. Chem.* (2005). doi:10.1074/jbc.M500608200

398. Kim, J. B. *et al.* Bone regeneration is regulated by Wnt signaling. *J. Bone Miner. Res.* (2007). doi:10.1359/jbmr.070802

399. Minear, S. *et al.* Wnt proteins promote bone regeneration. *Sci. Transl. Med.* (2010). doi:10.1126/scitranslmed.3000231

400. Krishnan, V., Bryant, H. U. & MacDougald, O. A. Regulation of bone mass by Wnt signaling. *Journal of Clinical Investigation* (2006). doi:10.1172/JCI28551

401. Robling, A. G. *et al.* Mechanical stimulation of bone in vivo reduces osteocyte expression of Sost/sclerostin. *J. Biol. Chem.* (2008). doi:10.1074/jbc.M705092200

402. Majidinia, M., Sadeghpour, A. & Yousefi, B. The roles of signaling pathways in bone repair and regeneration. *Journal of cellular physiology* (2018). doi:10.1002/jcp.26042

403. Tu, X. *et al.* Sost downregulation and local Wnt signaling are required for the osteogenic response to mechanical loading. *Bone* (2012). doi:10.1016/j.bone.2011.10.025

404. Brighton, C. T., Wang, W., Seldes, R., Zhang, G. & Pollack, S. R. Signal transduction in electrically stimulated bone cells. *J. Bone Jt. Surg. - Ser. A* (2001). doi:10.2106/00004623-200110000-00009

405. Ashrafi, M., Alonso-Rasgado, T., Baguneid, M. & Bayat, A. The efficacy of electrical stimulation in experimentally induced cutaneous wounds in animals. *Veterinary dermatology* (2016). doi:10.1111/vde.12328

406. Kim, T. H., Cho, H. & Lee, S. M. High-Voltage Pulsed Current Stimulation Enhances Wound Healing in Diabetic Rats by Restoring the Expression of Collagen, α-Smooth Muscle Actin, and TGF-β1. *Tohoku J. Exp. Med.* (2014). doi:10.1620/tjem.234.1

407. Wang, Y., Rouabhia, M., Lavertu, D. & Zhang, Z. Pulsed electrical stimulation modulates fibroblasts' behaviour through the Smad signalling pathway. *J. Tissue Eng. Regen. Med.* (2017). doi:10.1002/term.2014

408. Wang, H., Liu, J., Zeng, J., Zeng, C. & Zhou, Y. Expression of TβR-2, Smad3 and Smad7 in the vaginal anterior wall of postpartum rats with stress urinary incontinence. *Arch. Gynecol. Obstet.* (2015). doi:10.1007/s00404-014-3495-y

409. Li, Y. *et al.* Effect of integrin β1 in the treatment of stress urinary incontinence by electrical stimulation. *Mol. Med. Rep.* 4727–4734 (2019). doi:10.3892/mmr.2019.10145

410. Hamadi, A. Regulation of focal adhesion dynamics and disassembly by phosphorylation of FAK at tyrosine 397. *J. Cell Sci.* (2005). doi:10.1242/jcs.02565

411. Park, M. S., Kim, Y. H. & Lee, J. W. FAK mediates signal crosstalk between type II collagen and TGF-beta 1 cascades in chondrocytic cells. *Matrix Biol.* (2010). doi:10.1016/j.matbio.2009.10.001

412. Jing, D. *et al.* Pulsed electromagnetic fields partially preserve bone mass, microarchitecture, and strength by promoting bone formation in hindlimb-suspended rats. *J. Bone Miner. Res.* (2014). doi:10.1002/jbmr.2260

413. Jing, D. *et al.* Moderate-intensity rotating magnetic fields do not affect bone quality and bone remodeling in hindlimb suspended rats. *PLoS One* (2014). doi:10.1371/journal.pone.0102956

414. Jing, D. *et al.* Pulsed electromagnetic fields improve bone microstructure and strength in ovariectomized rats through a Wnt/Lrp5/β-catenin signaling-associated mechanism. *PLoS One* (2013). doi:10.1371/journal.pone.0079377

415. Lei, T. *et al.* Pulsed electromagnetic fields (PEMF) attenuate changes in vertebral bone mass, architecture and strength in ovariectomized mice. *Bone* (2018). doi:10.1016/j.bone.2017.12.008

416. Kim, M. O., Jung, H., Kim, S. C., Park, J. K. & Seo, Y. K. Electromagnetic fields and nanomagnetic particles increase the osteogenic differentiation of human bone marrow-derived mesenchymal stem cells. *Int. J. Mol. Med.* (2015).

doi:10.3892/ijmm.2014.1978

417. Petecchia, L. *et al.* Electro-magnetic field promotes osteogenic differentiation of BM-hMSCs through a selective action on Ca^{2+} -related mechanisms. *Sci. Rep.* (2015). doi:10.1038/srep13856

418. Rouabhia, M., Park, H., Meng, S., Derbali, H. & Zhang, Z. Electrical stimulation promotes wound healing by enhancing dermal fibroblast activity and promoting myofibroblast transdifferentiation. *PLoS One* (2013). doi:10.1371/journal.pone.0071660

419. Cheng, G. *et al.* Sinusoidal electromagnetic field stimulates rat osteoblast differentiation and maturation via activation of NO-cGMP-PKG pathway. *Nitric Oxide - Biol. Chem.* (2011). doi:10.1016/j.niox.2011.05.009

420. Diniz, P., Soejima, K. & Ito, G. Nitric oxide mediates the effects of pulsed electromagnetic field stimulation on the osteoblast proliferation and differentiation. *Nitric Oxide - Biol. Chem.* (2002). doi:10.1016/S1089-8603(02)00004-6

421. Pilla, A. *et al.* Electromagnetic fields as first messenger in biological signaling: Application to calmodulin-dependent signaling in tissue repair. *Biochim. Biophys. Acta - Gen. Subj.* (2011). doi:10.1016/j.bbagen.2011.10.001

422. Hong, J. M., Kang, K. S., Yi, H. G., Kim, S. Y. & Cho, D. W. Electromagnetically controllable osteoclast activity. *Bone* (2014). doi:10.1016/j.bone.2014.02.005

423. Yuan, J., Xin, F. & Jiang, W. Underlying Signaling Pathways and Therapeutic Applications of Pulsed Electromagnetic Fields in Bone Repair. *Cellular Physiology and Biochemistry* (2018). doi:10.1159/000489206

424. Pall, M. L. Electromagnetic fields act via activation of voltage-gated calcium channels to produce beneficial or adverse effects. *J. Cell. Mol. Med.* **17**, 958–965 (2013).

Chapter Two

Fabrication and physical characterisation of 2D piezoelectric PVDF-TrFE/BNNT nanocomposite

2.1   Introduction.

During wound healing and tissue development, endogenous electric fields (EF's) appear to play an important role in regulating different biological processes[86,96,192]. Even though this phenomenon has been known for more than 100 years, how cells sense and respond to EFs and the mechanisms underlying EF-cell interactions remains unclear, limiting the therapeutic use of ES in a clinical setting. It is mostly reported that cells interact with their surrounding microenvironment through receptors and ion channels, which can transduce chemical, mechanical and electrical signals outside-in and inside-out the cells[193–196]. Transmembrane proteins, including ion channels and receptors, have been proposed as sensing elements in therapeutic electrical stimulation of tissues as they have been shown to respond to EF[84,110,197].

The modulatory effect of EFs has been investigated in different cell types including neurons[198,199], osteoblasts[200], myoblasts[201], fibroblasts[202,203], endothelial cells[204], muscle cell[201] and epithelial cells[96,114,192] and there is large body of gathering evidence that stimulation via EF can regulate multiple cell functions, including cell growth[205], adhesion[198,200,204], proliferation[202,203,206] and differentiation[201,207,208] It is thought that EF mediated modulation of cellular function can occur through two distinct pathways: (1) indirect stimulation, via EF charging of transmembrane proteins, which modulates intracellular flow of ions (i.e calcium, potassium)[209–212] or induces a redistribution of membrane receptors (2) direct stimulation, via EF-cytoplasm charged elements inside the cell[213–215]. To produce the above-mentioned effects native EFs can be manipulated in the charged extracellular microenvironment or across the cell membrane using chemical or physical approaches. Generally, scientists have utilised biochemical agents such as growth factors, small molecule inhibitors or antibodies to manipulate endogenous EFs and therefore cell behavior[108,153]. However, associated toxicity, biochemical synthesis complexity and bioactivity-dependence on multiple factors (i.e. specificity, pharmacokinetics, and clearance rates) have limited the therapeutic use of these biochemical agents. Conversely, employing physical stimuli based approaches such as ES to manipulate EFs to alter the cell membrane potential and subsequently affect ion flux across the membrane, represent a much safer and controllable therapeutic system[216–218].

Correctly, it has been shown that direct current ES (DS, between 100–400 V/m) induces electrostatic responses of different cell types (i.e. neural cells, adipose-derived stem cells and osteoblasts)[219–221]. Furthermore, it has been shown to indirectly affect intracellular

calcium dynamics[222], epithelial cell proliferation, stem cell migration and differentiation[223,224]. While electrostatic responses of excitable cells have been explored extensively to develop therapeutic strategies, recently, electrodynamic stimulation has attracted attention as a therapeutic approach. Recent studies on the effect of alternating currents (AC) on excitable cells have observed a strong frequency-dependence on the cellular responses such as axonal elongation and neurite outgrowth on neurons under high-frequency ES (1kHz)[225,226]. Interestingly, this frequency dependence response is also extended to non-excitable cells. For instance, in bone cells and stem cells, it has been shown that low-frequency electrical signals (<60 Hz)[227–229] promote cell proliferation whereas high-frequency signals (> 1kHz) induce cell differentiation[230].

Unfortunately, the use of different stimulation frequencies to probe physiological responses have not been mainly studied, and only a few studies have been performed. Besides, to date the most common stimulators types fall into two categories: (1) cell chambers directly connected to a stimulating conductor element (electrode) or (2) isolated cell chamber indirectly connected through salt bridges to the electrode. In this chapter, we have developed a novel PVDF-TrFE/BNNT nanocomposite that is suitable for tendon cell culture and displays a superior piezoelectric performance relative to pristine films.

2.2   Materials and Methods

2.2.1   2D film processing.

2.2.1.1 Spin coating

To process uniform thin films ranging from tens of nanometers to several micron spin coating process has been used in this work. Briefly, a low concentrated solution is applied to the centre of a substrate. Subsequently, the substrate starts spinning at a desired speed and acceleration rate. As a result of the speed, a centrifugal force acts on the fluid and spreads it homogenously across the substrate forcing the evaporation of the solvent. The excess of solution is then ejected off the substrate the edge. To control the thickness and uniformity it is important to control the following parameters: solution viscosity, spinning speed, acceleration and spinning duration. Finally, once the film is obtained and additional baking step to evaporate remaining solvent is used. In this work, dimethylformamide (DMF) and Acetone (6:4 ratio) were used as co-solvent system to generate solutions of P(VDF-TrFE) polymer and nanocomposites with different concentrations.

2.2.1.2 Solvent casting

The solvent casting method was used in this work to produce thick films around 20 to 40 um. This system represents a very simple method as it involves dropping a volume of the solution onto a substrate and letting the solvent evaporate. In order to control the evaporation rate, temperature and vacuum were used. Due to the lack of uniformity in thin films, this method was only used for processing thick films (>25 um). However, the main limitations are the fluctuations or changes in the thickness throughout the sample. To decrease this problem, small areas (1 cm^2) were used to reduce differences in thickness.

2.2.1.3 Metallization by Magnetron Sputtering

To deposit metallic electrodes to measure the electrical properties of the samples, sputtering was used. Sputtering is a physical vapour deposition technique, it uses high energy ion bombardment to remove atoms from a solid target (gold or platinum) and deposit them on a substrate in a vacuum chamber. Briefly, its operation mode is straightforward as it just has two electrodes: (1) cathode, where the target is and (2) anode, where the substrate is held. During its operation, then is filled with an inert gas (Argon) and after an electric field is applied between the two electrodes. A normal glow discharge (plasma) occurs as consequence of the collision of electrons with the gas generating ions. Finally, these ions are accelerated towards the target, and thin coating is deposited on top of the sample.

2.2.1.4 Nanoparticle dispersion.

BNNTs were purchased from BNNT, LLC, USA) and synthesised using a high temperature/pressure (HTP) method, also called the pressurized vapour/condenser method (PVC). The BNNT produced possess several walls between 1 to 5, a high aspect ratio (300 m2 /g) and high crystallinity. The purity is reportedly approximately 50% by mass containing residual impurities as micro-droplets of elemental boron and the material is used as-synthesized, without any purification or modification. In a typical experiment, 0,5 to 10 mg of BNNT was weighed out in a sample vial. Next, 10 to 20 mL of the co-solvent mixture (DMA:Acetone 6:4) was added to the sample vial for a final concentration of 0.05 to 1 mg per mL. The sample was left under magnetically stirring for at least 4 days (96 hours) to allow for sufficient interaction between the nanotubes and the solvent. Subsequently, these mixtures were then sonicated for 3 h (pulse 10s ON, 2s OFF) with an

output power of 17 W. Subsequently, the homogenized dispersion was centrifuged at 5000 rpm.

2.2.1.5 Thermal Annealing

All samples underwent post-fabrication thermal annealing to tailor films microstructural, electronic, phase, crystalline and charge transport properties. Specifically, an annealing process after film fabrication resulted in crystallisation of amorphous regions and also increased the crystallinity level of a phase in a preferred orientation. The annealing process was carried out at annealing temperature of 132ºC (between T_{fusion} and T_{curie}) in a rapid thermal process chamber for two hours. The film properties were functions of the annealing profile, including annealing and cooling rate. For both pristine P(VDF-TrFE) and nanocomposites, vacuum annealing for 2 hours and then cooled to room temperature in the oven after the oven was switched off (slow cooling rate) was used to facilitate the piezoelectric β-phase formation within the film

2.2.1.6 Thermoelectrical Poling

In this work, thermal poling was carried out in order to align the dipoles from the β-phase of the film. Thermal poling was carried out at controlled temperature (70ºC) to facilitate the rotation of the dipoles. The samples were subjected to compressive stress between two electrodes to counterbalance the changes in volume as a consequence of crystal rotations and. Then, the sample was exposed to high electrical field (> 50 MV/m, the coercive electrical field for PVDF-TrFE) for 1 hour.

2.2.2 Physical Characterisation

The following section describes the different techniques utilised to characterise the electrical properties of the piezoelectric films for cellular electric stimulation. Since the material is well known since its discovery in 1969, a large number of studies have been already performed and published. A brief description of the most popular techniques to study PVDF-TrFE electrical output will be presented. The described characterisations further include the development of a secure and cost-effective method of charge and open-voltage measurements, d_{33} direct measurements and PFM measurements.

2.2.2.1 Structural characterisation

2.2.2.2 X-ray diffraction (XRD)

XRD is a powerful technique to help to identify the crystalline structure of PVDF-trFE films. X-ray diffraction patterns from films were collected by using a Philips X'pert PRO automatic diffractometer operating at 40 kV and 40 mA, in theta-theta configuration, secondary monochromator with Cu-Kα radiation (λ = 1.5418 Å) and a PIXcel solid-state detector (active length in 2θ 3.347º). Data were collected from 5 to 70° 2θ (step size 0.026 and time per step = 347 s) at RT. A fixed divergence and antiscattering slit giving a constant volume of sample illumination were used. The signal deconvolution was evaluated using the peak-fit option of the WinPLOTR program. The profile fitting procedure (XRFIT calculation) uses pseudo-Voigt functions with a global FWHM (Full width at half maximum and a global eta (proportion of Lorentzian), and a linear background. Each peak is characterised by its position, intensity, FWHM and eta shifts with respect to the global parents. The average size of the crystalline domains β (coherently diffracting domains) of the samples was extracted from the broadening of the signal using the Scherrer equation:

$$\beta_{hkl} = k \cdot \lambda / L_{hkl} \cdot \cos\theta$$

Equation 2-1

where β_{hkl} is the broadening of the diffraction line measured at half the line maximum intensity (FWHM) taking into account instrumental contribution (β_{Inst}=0.1°), λ is the X-ray wavelength, L_{hkl} is the crystal size and θ is the diffraction angle. K is the Scherrer shape factor (k=0.9 was used for the calculations).

2.2.2.3 Differential scanning calorimetry (DSC)

The thermal transitions of the PVDF-TrFE scaffolds were determined on a DSC Q200 (TA Instruments). Samples of 8-10 mg were heated from -10ºC to 200ºC at 10ºC min-1. This first scan was used to determine the melting temperature (T_m) and the melting enthalpy (ΔH_m), as well as the Curie temperature (Tc) and the Curie enthalpy (ΔH_c). After this first scan, the samples were quenched in the DSC, and a second scan was collected from -10 to 200ºC at 10ºC min-1. For the non-isothermal crystallisation studies, the films were heated at a constant heating rate (30°C /min) from room temperature to 260°C and held there for 2 min to eliminate the residual crystals and memory effects due to thermal history, and then cooled to crystallize at the same cooling rate under nitrogen environment to room temperature. For isothermal crystallisation kinetics, the films were heated at a constant

heating rate of 30°C/ min from room temperature to 260°C and held there for 2 min to eliminate the thermal history, then the melt was cooled at the same rate up to 148°C and kept constant at 148°C for 10 min until the sample completely crystallized.

2.2.2.4 Modulated Differential Scanning calorimetry (MDSC)

MDSC experiments were carried out using TA instrument 2000 MDSC. An oscillation period of 60 seconds and amplitude of ±0.47 °C were used during the heating and cooling cycle. Samples were purged with the liquid nitrogen of 50ml/min for cooling. About 8mg of samples were encapsulated and sealed in Tzero pans. For all experiments, samples were isothermally kept for 3 minutes at the beginning and end of heating and cooling run and subjected to (a) quenching of samples from room temperature to -75 and kept isothermally for 3 min followed by heating at 3 °C/min to and (b) cooling to 3 °C/min from to 0 °C. A similar method was previously implemented for microphase studies and molecular movement in different copolymers[231].

2.2.2.5 Non-isothermal Crystallisation Kinetics

The characteristic behaviour of semi-crystalline polymers or its composites such as crystallinity and homogeneity can be determined not only by their chemical structure, chain conformation and molecular weight distribution but also by the mechanism and kinetics of crystallisation. It is well known that the properties of semi-crystalline block copolymer depend strongly on the crystallisation mechanism of different phases. These behavioural changes (degree and rate of crystallisation) to the effect of processing conditions can be observed by understanding the crystallisation kinetics.

The famous Avrami analysis was articulated to understand the phase change process, nucleation and growth of a given material and has been most commonly been used to determine the isothermal polymer crystallisation kinetics[232–235]; however, the same can also be used for non-isothermal conditions. The degree of phase conversion is given by:

$$X(t) = 1 - e^{-kt^n} \hspace{4cm} \text{Equation 2-2}$$

Where k is the Avrami constant describing the nucleation rate and the growth rate. n is the Avrami exponent which is dependent on the process dimensionalities. These Avrami parameters can be determined by using the double logarithmic form of the Avrami equation:

$$\mathrm{Log}\big[-\ln\big(1 - X(t)\big)\big] = \mathrm{Log}\,k + n\,\mathrm{Log}\,t \hspace{3cm} \text{Equation 2-3}$$

The parameters n and k are obtained from the slope and the intercept of the straight line by the plot of Log [-ln (1-X (t)) vs. Log t. The Avrami model has been modified by Jeziorny[236] to describe the non-isothermal crystallisation processes. Jeziorny's analysis describes that the kinetic constants can be determined by using Avrami equation; however, under non-isothermal conditions, crystallinity/phase change is the function of temperature X(T).

The relative crystallinity was calculated as a function of temperature and transformed to a time scale by using the relationship t = (T_{con} - T)/ ϕ, where, Tcon is the crystallisation onset temperature at crystallisation time t = 0, T and the temperature at the crystallisation time t and ϕ is the cooling rate. The reaction half-time (t1/2) can be calculated from the corrected kinetic constant (k') from the following equation:

$$t_{\frac{1}{2}} = \left(\frac{\ln 2}{k'}\right)^{1/n}$$
Equation 2-4

In most polymer non-isothermal studies, the modified Avrami model fails to provide actual information on the phase transition and the structure, therefore the classical Ozawa model or Avrami-Ozawa is most applicable to non-isothermal conditions[237]. The Ozawa model assumes extends the mathematical derivation proposed by Evans to non-isothermal crystallisation at constant cooling rate with infinite isothermal steps as follows:

$$1 - X(T) = e^{\frac{-k^*}{\phi^m}}$$
Equation 2-5

Where constant m is the Ozawa exponent, which is independent of temperature and k* is a heating/cooling function. The plot of ln [-ln (1-X (T)) vs. ln ϕ gives a linear fit, where the slope and intercept give the kinetic parameters m and k*. The Ozawa exponent m provides qualitative information on the nature of the nucleation and growth process, whereas k* includes information related to the overall crystallisation rate and indicates how fast crystallisation occurs.

Liu and coworkers[238] further combined Avrami and Ozawa equation for non-isothermal polymer crystallisation analysis given by the equation:

$$\ln \phi = \ln F(T) - b \ln t \quad (5)$$
Equation 2-6

Where, F (T) = [K*(T)/k]1/m, which defines the cooling rate required to reach specific degree of crystallinity in a given crystallisation time and b is the ratio between Avrami and Ozawa exponents. A plot of ln ϕ vs. ln t at specific degree of crystallinity gives a straight line, where the intercept and the slope gives the values of F (T) and b. The value of b is given by n/m.

2.2.2.6 Fourier transform infrared (FTIR)

Infrared spectra of PVDF-TrFE scaffolds were recorded on a Nicolet AVATAR370 Fourier transform infrared spectrophotometer (FTIR) operating in the Attenuated Total Reflectance (ATR-FTIR) mode. Spectra were taken with a resolution of 2 cm^{-1} and were averaged over 64 scans. Using the absorption band of α and β phases at 532 cm−1 and 846 cm−1, the fraction of β phases were calculated using the following equation The β-phase content F(β) was calculated by the following equation [239]:

$$F(\beta) = \frac{X_\beta}{X_\alpha + X_\beta} = \frac{A_\beta}{1.26 A_\alpha + A_\beta}$$

Equation 2-7

where A_{EA} is the absorbance value at 841 cm^{-1}, A_α is the absorbance at 764 cm^{-1}, and the factor 1.3 is the ratio of absorption coefficients at 841 cm-1 ($K_{841} = 7.7$ x 10^4 cm^2 mol^{-1}) to 764 cm^{-1} ($K_{764} = 6.1$ x 10^4 cm^2 mol^{-1}) at the respective wavenumber.

2.2.3 Dielectric properties

Dielectric characterisation of flat samples of thickness 30um was carried out using 2 electrode configurations using PARSTAT 2273 Advance electrochemical System. Two sides of the samples were sputter-coated with a 20 mm diameter gold electrode. The AC electrical signal of 1 V rms from 0.1Hz to 1 MHz. Components of Dielectric permittivity and tangent loss were extracted from the impedance phase and amplitude graphs.

2.2.4 Mechanical properties

Tensile analysis of thin films was performed using Zwick/Roell Z010 with 1 kN load cell with a crosshead speed of 500 mm/min and maximum extension of 500%. Thin films were cut per ASTM D 882 type specimen. Results are presented as average values of n = 5 replicate experiments with standard deviation.

2.2.5 Piezoelectric coefficient measurement techniques.

The design of sensors or stimulators using piezoelectric systems requires the use of specific techniques for their precise characterisation. The different methods of measuring piezoelectricity fall into three main categories and are the based on [240]:

- Dynamic methods: resonance analysis
- Converse piezoelectric effect : Laser interferometry and piezoresponse microscopy
- Direct piezoelectric effect: Berlincourt method

All those methods have different advantages and limitations and are preferred due to their accuracy. The main limitation associated to all these method is the requirements of highly specialized and complex measurement devices. Herein, a brief description of the different techniques is exposed and a discussion is presented about whether or not a particular technique is adequate for their use in this application.

2.2.5.1 Resonance analysis

This method is very popular mainly due to its ability to describe fully the piezoelectrical tensor of a material. However, this method was developed for the analysis of ceramic materials which could be easily shaped into various forms. The method requires samples of very specific size and shapes. In particular, a disc, cylinder and plate shapes are essential to describe the piezoelectric coefficients of the material tested. This method is not suitable since thin films cannot be easily shaped into those forms.

2.2.5.2 Laser interferometry

This method is employed in many published studies. It is based on the direct measurement of the displacement deflection of a piezoelectric element under an applied voltage. High resolution, within the nanoscale range, can be achieved with this method. The main drawback is that it requires an interferometric laser for the measurement of the displacements and the system must be protected from any parasitic background vibrations. This method is based on the converse piezoelectric effect and needs a highly reflective surface. Since PVDF-TrFE present different performances when it is used in the direct or converse method, it is recommended to use a direct method instead since it would describe more accurately the real performance of the device.

2.2.5.3 Quasi-static method

Finally, the last technique is described as a quasi-static approach. This method does not involve very complex machinery and complete set of measured internal controls to validate the measurements. The direct piezoelectric effect has to be taken into account in this method. The electric charge of a piezoelectric material can be obtained using a charge amplifier or a voltmeter with high input impedance such as Keithley 6217. In addition, dedicated devices named d33 meters using this method are commercially available from different companies.

This method is employed in this thesis since it allows the characterisation of both the d33 charge coefficient and the direct measurement of generated voltage per unit area, i.e. the

direct piezoelectric effect. For this purpose, an oscillatory force (10Hz-1kHz) was applied to the piezoelectric surface to induces a charge across the sample. The signal was then amplified, and the piezoelectric coefficient calculated using the following expression:

$$D = d\sigma + kE$$
<div align="right">Equation 2-8</div>

Since these measurements are performed with no electric field applied (E=0), we can obtain the piezoelectric coefficient using the simplified equation:

$$d = \left[\frac{\delta D}{\delta \sigma}\right]_E = \frac{Q}{A} / \frac{F}{A} = \frac{Q}{F}$$
<div align="right">Equation 2-9</div>

In order to further simplify the method, the electrode area was the same as the area of applied pressure. This makes the Berlincourt system very reliable and fast. However, it is not exempt from limitations. There are many variables that can alter the accuracy or stability of the system with compliance being one of the most sensitive parameters. The Berlincourt method works well with very stiff materials, generally ceramics, however, with more compliant materials such as polymers the system starts to lose accuracy and the d33 of very soft materials such as hydrogels or nanostructured systems such as electrospun scaffolds become problematic to analyse. Other parameters that can affect the accuracy of the method are sample geometry, pre-load force magnitude and frequency and atmospheric conditions (humidity and temperature). Finally, this is a comparative method so the measurement is highly dependent on the correct calibration using the reference material. In this work, we have used a commercially available d33 piezometer based on the Berlincourt method for the measurement of the d33 coefficient of the films.

Figure 2-1. d_{33} piezometer (PIEZOTEST PM3000)

2.2.5.4 Piezoresponse Force Microscopy (PFM)

Another very powerful technique used in this thesis is Atomic Force Microscopy (AFM) and its derivative, Piezoresponse Force Microscopy (PFM). Invented just 40 years ago

(1981)[241], AFM allows the generation of an atomic-level resolution topographical image by scanning a sample with an ultra-sharp (few atoms) tips. The principle of operation consists on the following steps: (1) tip deflects ($\Delta z = -F/k$) according to its spring constant (k) when the surface is contacted and (2) a feedback loop is sent to the system to keep the Force (F) constant between sample and tip. The vertical and lateral deflection is measured using a laser reflecting onto the tip apex and captured by a photodiode. Therefore, the vertical deflection represents the topography of the samples and the lateral deflection is associated with the frictional forces involved. There are generally two modes of scanning: contact and semi-contact (tapping). Contact mode offers higher resolution however; it also degrades the tip much faster. Instead, tapping is generally the preferred choice as it is gentler on the tip as it contacts the sample vibrating at its resonant frequency. PFM, is a modified AFM technique that facilitates the generation of both topographical and piezoelectric information from a sample.
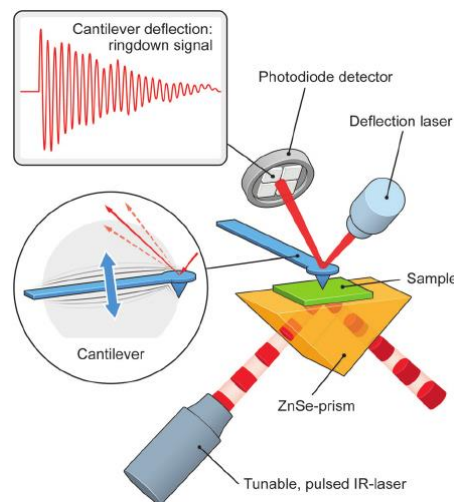
Figure 2-2. Main principle of operation of AFM. The AFM probe interacts with the sample through a raster scanning motion. The up/down and side to side motion of the AFM tip as it scans along the surface is monitored through a laser beam reflected off the cantilever. This reflected laser beam is tracked by a position-sensitive photo-detector (PSPD) that picks up the vertical and lateral motion of the probe.

PFM uses a conductive scanning probe that is comprised of a titanium nitride coating that unfortunately reduces considerably the resolution of the topographical measurements (radius of the tip is increased). To perform the measurements, a voltage is applied through the tip (V_{tip}) containing an AC and DC component :

$$V_{tip} = V_{DC+} V_{AC} \cos(wt) \hspace{3cm} \text{Equation 2-10}$$

The AC component is responsible for inducing deformation in the film that is detected at the tip. Since the signals generated are minimal, the system takes advantage of a lock-in amplifier that multiplies the signal.

Finally, in order to measure the piezoelectric coefficient of a particular material, the PFM system needs to be calibrated with a known sample or using the inverse-optical sensitivity coefficient (IOS). This coefficient describes the relationship between deformations recorded in Volts and deformations in meters and is dependant of the tip. This coefficient is obtained from the force-curve of the tip in a hard substrate.

2.2.5.5 Quantitative AFM Nanomechanical Mapping

In PeakForce™ QNM™, Young's modulus is calculated using a DMT model (see equation 1) that is applied to the unloading portion of the force-separation curve (see Figure 1). The DMT model can be viewed as a modified Hertzian model, which takes into account the adhesive forces between the tip and the surface. According to this approach, the reduced Young's modulus, Er , is given by:

$$E_r = \frac{3(F_{tip} - F_{adh})}{4\sqrt{Rd^3}}$$
 Equation 2-11

In equation 1, Ftip is the force on the AFM tip, Fadh is the adhesive force between the AFM tip and sample, R is the AFM tip radius, and d is the deformation depth.

The reduced Young's modulus E_r is related to the sample Young's modulus, Es, by

$$\frac{1}{E_r} = \frac{(1 - v_s^2)}{E_s} + \frac{(1 - v_I^2)}{E_I}$$
 Equation 2-12

Where EI is the indenter Young's modulus, vs is the Poisson's ratio of the indenter and v_s is the Poisson's ratio of the sample. In the present work, $E_I \gg E_s$, and so the second term on the right-hand side of equation 2 is negligible. The tip radius can be measured directly using a Scanning Electron Microscope or a tip calibration grating. Alternatively, the value of the radius can be derived from a reference sample (in the present work, polystyrene) using equation 1 and taking the modulus value to be that determined using IIT. In this study Poisson's ratio was assumed to be of 0.49.

AFM experiments were performed using a Bruker Dimension Icon AFM and two different probes: Bruker AFM Probes supplied PFTUNA and SCM-PIT probes and were selected based on the recommendations of for the range of polymer Young's moduli to be investigated (10 to 500 MPa). The experiments were carried out using an oscillation frequency of 2kHz, and the amplitude was set a constant value of 150 nm corresponding to an indentation rate of 0.6 mm/s. Before each experiment, the probes were calibrated,

determining each time the tip radius and spring constant. Each set of Young's modulus measurements correspond to 640 x 640 force-separation curves obtained over an area of 15 x 15 µm.

2.3 Results

2.3.1 2D films processing
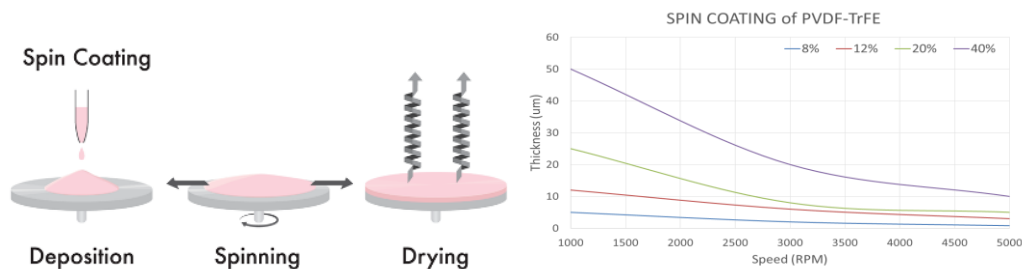
Figure 2-3. Deposition of thin films: Spincoating. First, a drop of polymeric solution at a specific concentration is deposited onto the substrate (cover glass). Then, the substrate accelerates and reaches a high rotational speed, and the majority of the solution is ejected from the side. Finally, the airflow dries the out the solvent leaving a thin film. The centripetal forces combined wh the surface tension of the solution enables a homogenous coating.

The optimal conditions to produce 5-10 um films were: 30 sec at 1000 rpm with 1-sec acceleration (see Figure 2-3), 50ºC to evaporate the solvent and 132ºC 100 min for annealing (max. crystallinity). The spin coating process was repeated 3 times in order to obtain thicker films. Immediately after each time, annealing was used to ensure dense film formation. After three times the film was annealed at a higher temperature for at least 100 min to provide excellent performance and maximise crystallinity level.

To produce thicker samples between 25 and 50 um, solvent casting technique was preferred. To obtain thick samples a highly concentrated solution of PVDF-TrFE (30% v/v) was poured into a petri dish and directly heated to 132ºC.
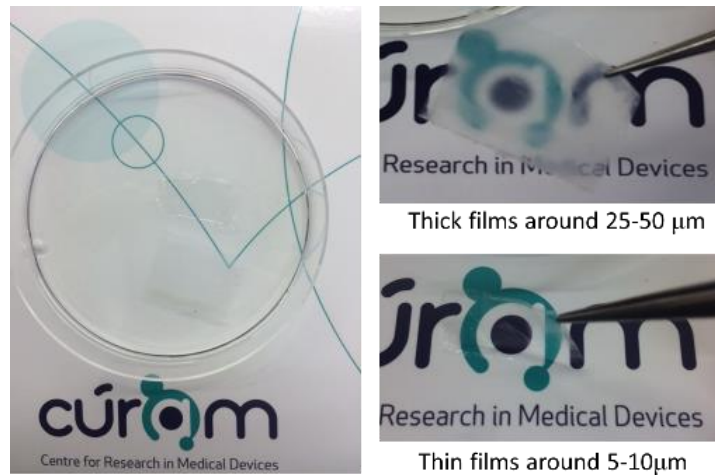
Figure 2-4. 2D Films of different thicknesses (5 and 50 um). The thinner films (5 um) show good transparency, unlike the thicker films (50um) that are more opaque due to different crystal structure.

2.3.2 Nanotubes incorporation: Nanocomposite fabrication

To fabricate nanocomposites solutions of stable and dispersed BNNT were needed. The optimal conditions were found using DMAc instead of DMF since it matches better the Hansen parameters of the tubes.

The Hansen solubility parameters for dispersion (δd), polar (δp), and hydrogen (δh) bonding represent the intermolecular interactions contributing to the solubility of a solute in a given solvent. Together the Hansen solubility parameters represent the Hildebrand parameter (δt), a numerical representation of the interaction between materials.

A graphical approach to Hansen solubility theory involves plotting the solvents and solutes in three-dimensional (3D) "Hansen space" with coordinates given by (δd, δp, δh) with the dispersion state or quality of the solute.
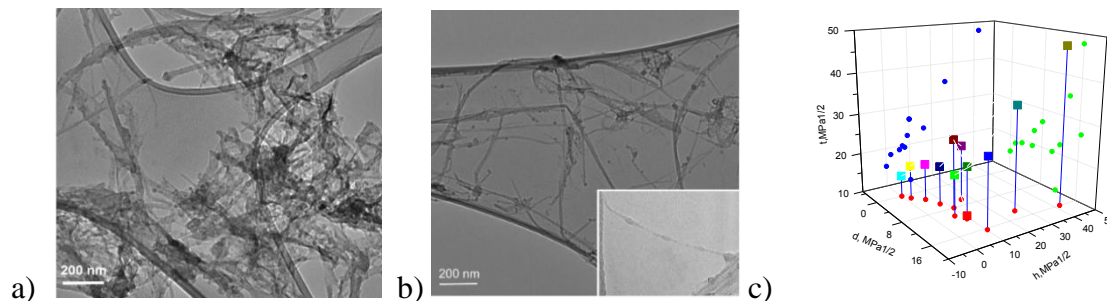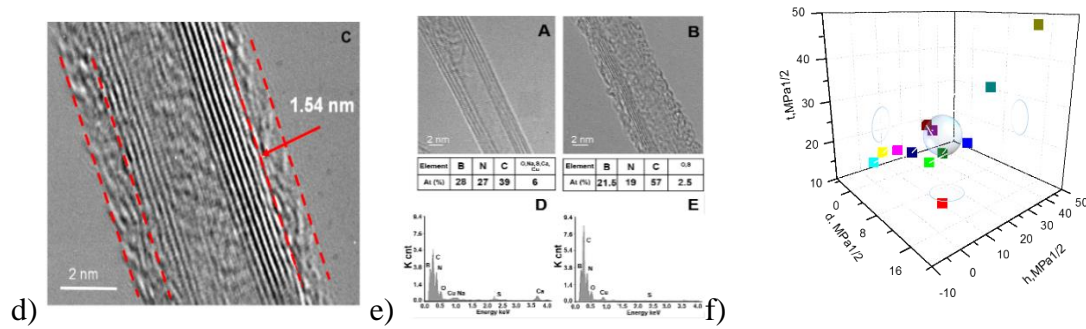
Figure 2-5. Organic Coating as a Route to Nanotubes Suspension stabilisation a) Strong aggregation in BNNT as a consequence of the polarity of B-N bond, which leads to more complicated intertube interactions b) Disaggregated nanotubes after functionalization c) Hansen parameters for different solvent and co-solvent systems. d) organic coating surrounding a BNNT e) chemical changes after coating f) Hansen parameters for BNNT.

Chemical approaches originally developed for BNNTS inspired initial attempts to functionalise and purify the BNNTs. For instance, we incorporate hydroxyl groups on BNNT by reaction with hydrogen peroxide or nitric acid at high temperature and pressures. But, such harsh conditions often lead to noticeable changes in the morphology and electronic properties. With the use of co-solvent systems and organic coating dispersible nanotubes could be obtained allowing the calculation of the Hansen parameters of BNNT. However, in most cases coated BNNT presented incomplete coating. Coated single BNNT coexisted with coated aggregates. This limit their applications in nano-biomedicine.

The polarity of the B-N bond offers access to precisely functionalization chemistries Amine interact with boron atoms of the BNNT sidewall via charge transfer. Moreover, the aromatic ring can interact via pi-pi interaction. By surveying a variety of solvents/co-solvents, surfactants, and polymers (A), a_solubility region for BNNTs was established (B) using Hansen solubility theory (see Figure 2-5).

2.3.3 Effect of Thermal annealing

As β-phase fraction has been described previously as being responsible for the piezoelectric effect in PVDF, the β phase fraction was studied using FTIR for different processing temperatures. It was observed that the annealing temperature has a direct impact on the β phase formation during the thin-film production process. The highest β phase fraction was observed in films of pristine PVDF-TrFE annealed at approx.. 122 ˚C, just above the Tc Curie temperature, which was verified using both DSC and MDSC

techniques. Similarly, for PVDF-TrFE/BNNT processed under 132˚C show F(β) equal to 0.79, similar to that of PVDF-TrFE annealed at 120 ˚C.

a)

BNNT Concentration	Beta Phase Fraction
1%	0.79
0 %	0.79

b)
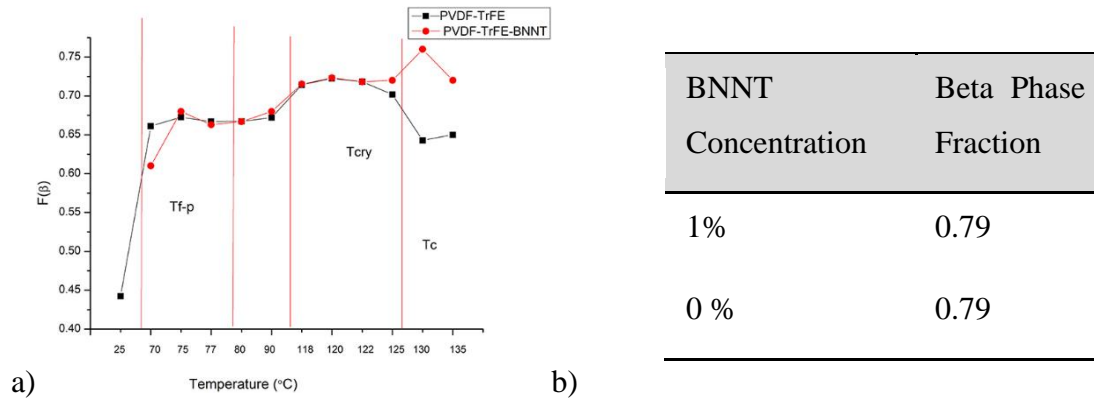
Figure 2-6. a) PVDF-TRFE annealed under different temperature conditions b) Annealed samples at 122 ℃
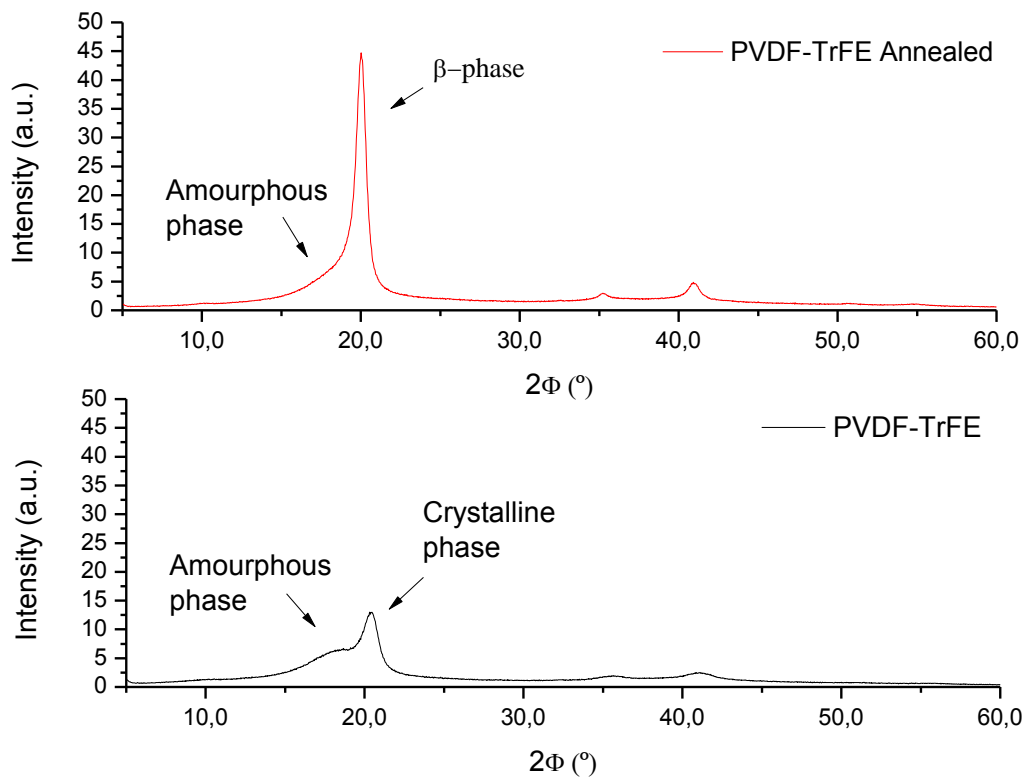
Figure 2-7. Effect of the annealing temperature.on the crystalline structure of pristine PVDF-TrFE films

Table 2-1. Structural parameters of the PVDF-TrFE crystals formed at room temperature or through annealing at 132ºC.

Sample	The crystallite size (nm)	Crystallinity (%)
PVDF-TrFE	8,34	57
Annealed PVDF-TrFE	17,39	63

At room temperatures (or below 70 ◦C), a diffraction peak from (110)/(200) of low intensity of P(VDF/TrFE) appeared, indicating the moderate presence of the crystalline phase of the P(VDF/TrFE) polymer. Conversely, at the annealing temperature of 132 ºC, the intensity of the diffraction peak is increased considerably. Also, the amorphous phase has been almost entirely converted into a crystalline phase. Despite an increase in the intensity of the (110)/(200) peak with higher annealing temperature, the full width at half maximum (FWHM) and the lattice constant remain independent of the annealing temperature.

Modulated DSC

Figure 2-8 shows typical DSC curves (heating and cooling of 5 ˚C/min) of PVDF -TrFE (as received), PVDF-TrFE solvent-cast and annealed at 120 ˚C, and PVDF-TrFE/BNNT 1 wt.% solvent-cast and annealed at 120˚C respectively.

For pristine samples, 2 distinct peaks (120ºC and 73ºC) can be observed that correspond to different crystal types. The peak at 120ºC corresponds to melting temperature (T_m). After annealing for 2 hours at 120ºC, the peak narrows down as a result of rearrangement of all polymer chains (all-trans). Interestingly, the incorporation of BNNT increased Tc (128ºC).

a)   b)
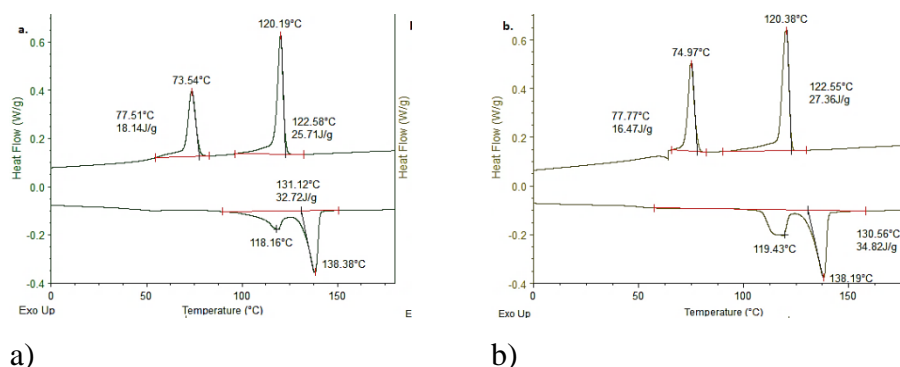
Figure 2-8. Typical DSC curve of PVDF-TrFE (a) as received, (b) and annealed at 120ºC

As observed in Figure 2-8 enthalpies of the melting heat in total heat flow (ΔH=32 J/g) , remains highest for annealed compared to pristine (ΔH=32 J/g).

The second peak is termed Curie temperature (Tc), where the paraelectric phase transits to the ferroelectric phase. Since it is well known that PVDF-TrFE will be crystallised into the ferroelectric phase when annealed between Tc and Tm, therefore, the ideal annealing temperature would be in between 110-150ºC.

Non-isothermal crystallisation
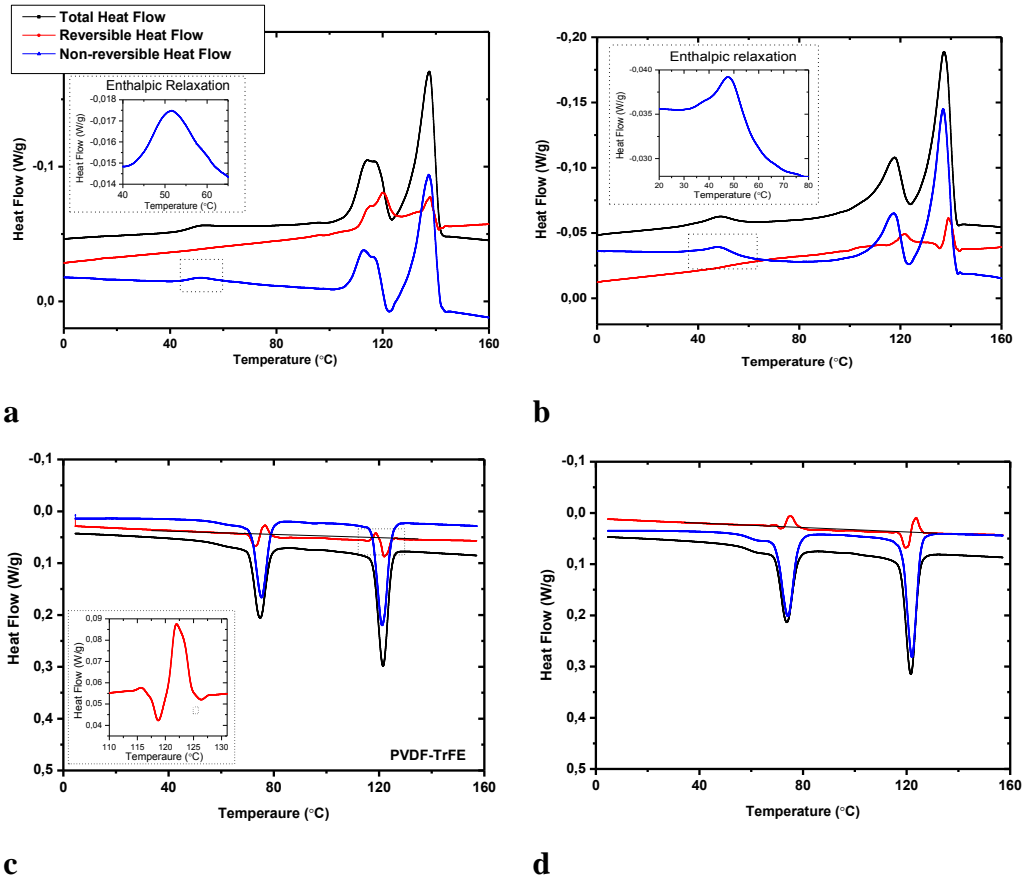
Figure 2-9. MDSC of PVDF-TrFE (a) as received and (b) annealed at 120 ˚C heating curves and (c) as received and (d) annealed at 120 ˚C cooling curves.

Figure 2-10 shows the Avrami plot resultant of primary as well as secondary crystallisation of PVDF-TrFE pristine and annealed for the first type of crystals formed at the higher temperature. The corresponding R^2 obtained from all plots were smaller than 1.

Table 2-9 shows the corresponding Avrami (kinetic) parameters n and k obtained from the slope and intercept of the plot obtained by fitting 3-35% Avrami curve. Also, $t_{1/2}$ (calculated from equation 3) and corresponding R^2 are also tabulated in Avrami parameters for second crystals.

a)

b)

c)
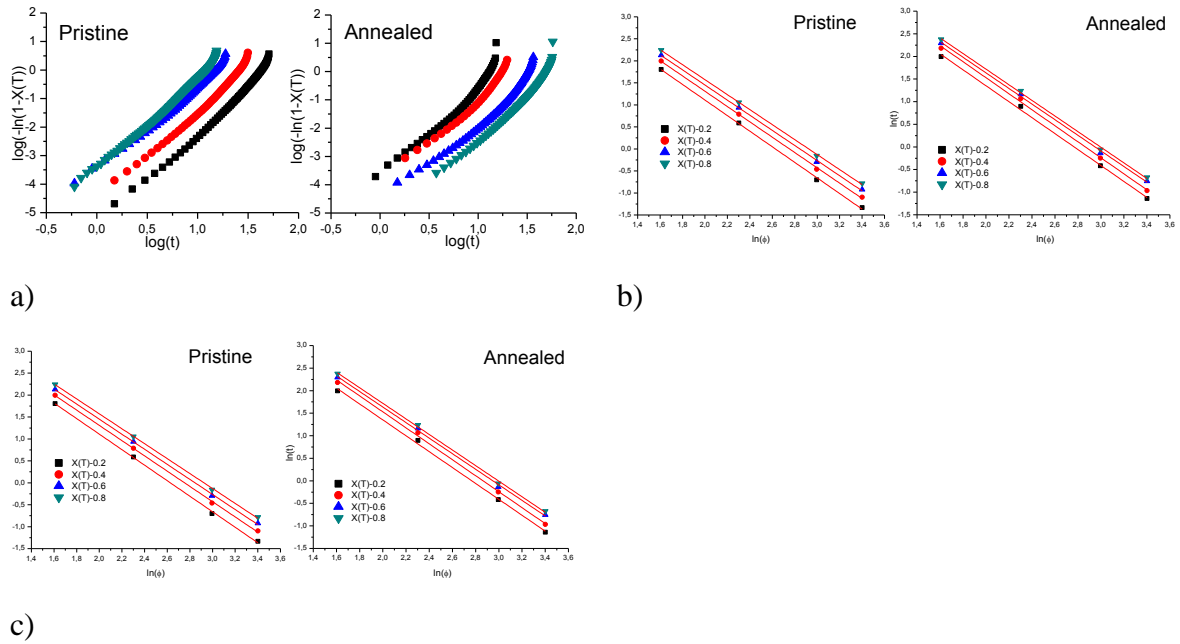
Figure 2-10. a) Avrami plot, b)1st and c) 2nd peak of PVDF TrFE pristine and annealed

In this work, the non-isothermal crystallisation analysis is mainly based on the primary crystallisation stage. As shown in Figure 2-10, at the early stage of crystallisation, ln[-ln(1 - Xt)] is in good linear relation with ln (R^2 close to 1). Therefore the modified Avrami equation is suitable for these systems. The Avrami exponent n of neat PVDF-TrFE decreases with increasing cooling rate and is mainly associated with crystallisation growth. The n values of PVDF-TrFE (n=3,55 ± 0,19) indicates that crystal growth of pristine and annealed PVDF-TrFE should be a spherical three-dimensional process. The highest values are obtained for PVDF-TrFE annealed (n= 4,00 ± 0,19) forming a more significant number of crystals. This suggests that annealing results in more nucleation sites, whereas pristine offers larger crystallisation growth. Similarly, the value $t_{1/2}$ also is associated with the crystallisation rate, the smaller this value, the faster the crystallisation process. Although higher n values are generally associated with the formation of smaller crystals (heterogeneous crystallisation), crystal formation in annealed PVDF-TrFE showed a slightly higher growth time ($t_{1/2}$) suggesting a slower crystallisation rate and bigger crystals compared to pristine PVDF-TrFE. This was observed in XRD analysis were the crystallite size was increased after annealing.

Table 2-2. Avrami 1st peak parameters of PVDF TrFE pristine and annealed. First crystals (Higher temperature crystals).

Sample Type	ϕ (˚C/min)	n	Log k	k'	$t_{1/2}$ (Sec.)	R^2
Pristine	5	3.75	-6.3	5.0119E-07	43.40	0.998
	10	3.67	-5.2	6.3096E-06	23.63	0.999
	20	3.41	-4.0	8.7096E-05	13.92	0.999
	30	3.37	-3.4	0.00039811	9.15	0.999
Annealed	5	3.71	-6.4	3.9811E-07	48.10	0.998
	10	4.11	-6.2	5.8884E-07	29.99	0.995
	20	3.99	-5.2	6.3096E-06	18.33	0.995
	30	4.00	-4.7	1.9498E-05	12.64	0.995

Figure 2-10 shows the Avrami plot of PVDF-TrFE pristine and annealed second types of crystals formed at a lower temperature.

Table 2-3 shows the corresponding Avrami parameters for the second crystals formations at lower temperatures. The n values PVDF-TrFE (n= 2.87 ± 0.11) indicates plate-like crystal aggregates. There is no significant difference in nucleation sites number in annealed PVDF-TrFE (n=2,83 ± 0,11). Similarly, there was no significant difference in t $_{1/2}$.

Table 2-3. Avrami 2nd peak parameters of PVDF TrFE pristine and annealed. Second crystals (Lower temperature crystals)

Sample Type	ϕ (˚C/min)	n	Log k	k'	$t_{1/2}$ (sec)	R^2
Pristine	5	2.75	-4.6	1.5849E-06	49.42	0.998
	10	2.83	-4.3	6.3096E-07	42.91	0.996
	20	2.90	-3.4	7.9433E-06	25.09	0.996
	30	3.01	-3.6	6.3096E-05	13.25	0.994
Annealed	5	2.67	-4.7	2.0417E-05	44.41	0.998
	10	2.89	-4.4	4.5709E-05	30.01	0.995
	20	2.83	-3.5	0.00039811	13.10	0.995
	30	2.94	-3.3	0.00022909	14.33	0.995

Avrami analysis can describe only the primary stage of the non-isothermal crystallisation process of pristine and annealed PVDF-TrFE. As non-isothermal crystallisation is a rate-dependent crystallisation process, Ozawa extended the Avrami theory to describe the non-isothermal crystallisation for a sample cooled at a constant rate from the molten state Avrami-Ozawa analysis for non-isothermal conditions provides a good insight on the nature of nucleation and growth process. The values a and K (T) can be obtained from the slope

and intercept of the plot. It becomes clear that the value of b decreases with increasing X(T) for all the sample types. Huang and Gu[242] et al reported that the value of X(T) indicates the rate of crystallisation, where lower values suggest higher crystallisation rate and vice versa. It also suggests that X(T) increases with higher crystallinity levels. However, the Ozawa approach is unsuitable for the description of the non-isothermal crystallisation of PVDF-TrFE. Rather, Liu et al.[243] proposed a different kinetic model by combining the Ozawa and Avrami equations, as follows:

$$\log K(T) - m \log \varphi = \log k + n \log t \qquad \text{Equation 2-13}$$

$$\log \varphi = \log F(T) - a \log t \qquad \text{Equation 2-14}$$

Table 2-4. Avrami-Ozawa plot of 1st peak of PVDF-TrFE processed under different processing conditions

Crystallinity	ln F(T)	a(=n/m)	Mean 'n'	Mean 'm'	Adj. R-Square
Pristine					
X(T)-0.2	4.7	1.76	3.55	2.06	0.999
X(T)-0.4	4.8	1.73			0.999
X(T)-0.6	4.9	1.71			0.999
X(T)-0.8	5.0	1.70			0.999
Annealed					
X(T)-0.2	4.8	1.76	4.0	2.29	0.998
X(T)-0.4	5.0	1.77			0.998
X(T)-0.6	5.0	1.72			0.998
X(T)-0.8	5.1	1.72			0.998

From

Table 2-4, the F(T) for annealed PVDF(TrFE) (ln F(T) = 4,98 ± 0,13) is higher than for pristine PVDF(TrFE) (ln F(T)=4,85 ± 0,13) and indicates that the crystallisation of PVDF-TrFE is restricted. The mean value of m (crystallisation rate) is calculated from the Avrami coefficient n and the value of a. The average value of m is lower than 3, implying that PVDF-TrFE crystallises through plate-like three-dimensional growth. The values of a are almost constant for both pristine and annealed samples, indicating the same three-dimensional growth kinetics.

Error! Not a valid bookmark self-reference. shows the Avrami plot of 2nd peak of pristine and annealed PVDF-TrFE thin-films. No significant differences were observed.

Table 2-5 Avrami-Osama plot of 2nd peak of PVDF-TrFE processed under different conditions.

Crystallinity	ln F(T)	b	Mean'n'	Mean 'm'	Adj. R-Square
Pristine					
X(T)-0.2	4.69	1.80	2.87	1.59	0.997
X(T)-0.4	4.97	1.80			0.997
X(T)-0.6	5.11	1.81			0.997
X(T)-0.8	5.22	1.82			0.998
Annealed					
X(T)-0.2	4.84	1.80	2.83	1.57	0.999
X(T)-0.4	5.10	1.81			0.999
X(T)-0.6	5.25	1.81			0.999
X(T)-0.8	5.38	1.80			0.999

2.3.4 Effect of Thermal Poling and BNNT incorporation
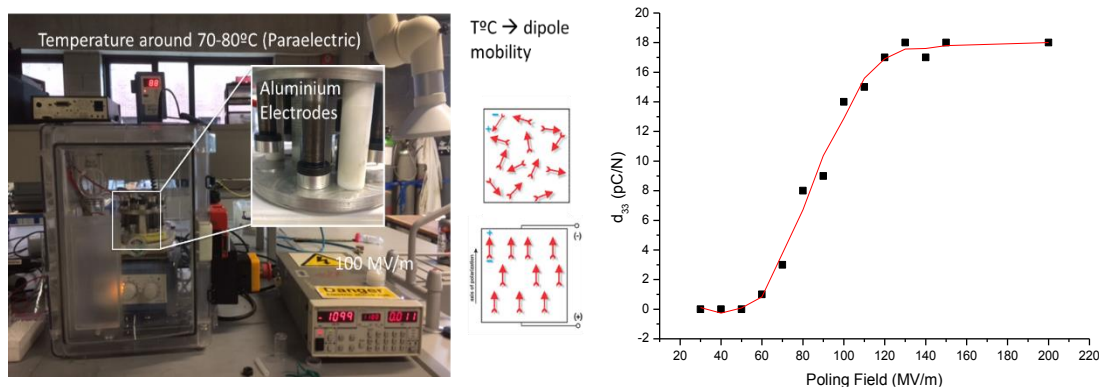
Figure 2-11. a) Dipole alignment using a custom made thermal electrical poling rig b) Increase of the d_{33} coefficient as function of the poling field in PVDF-TrFE films.
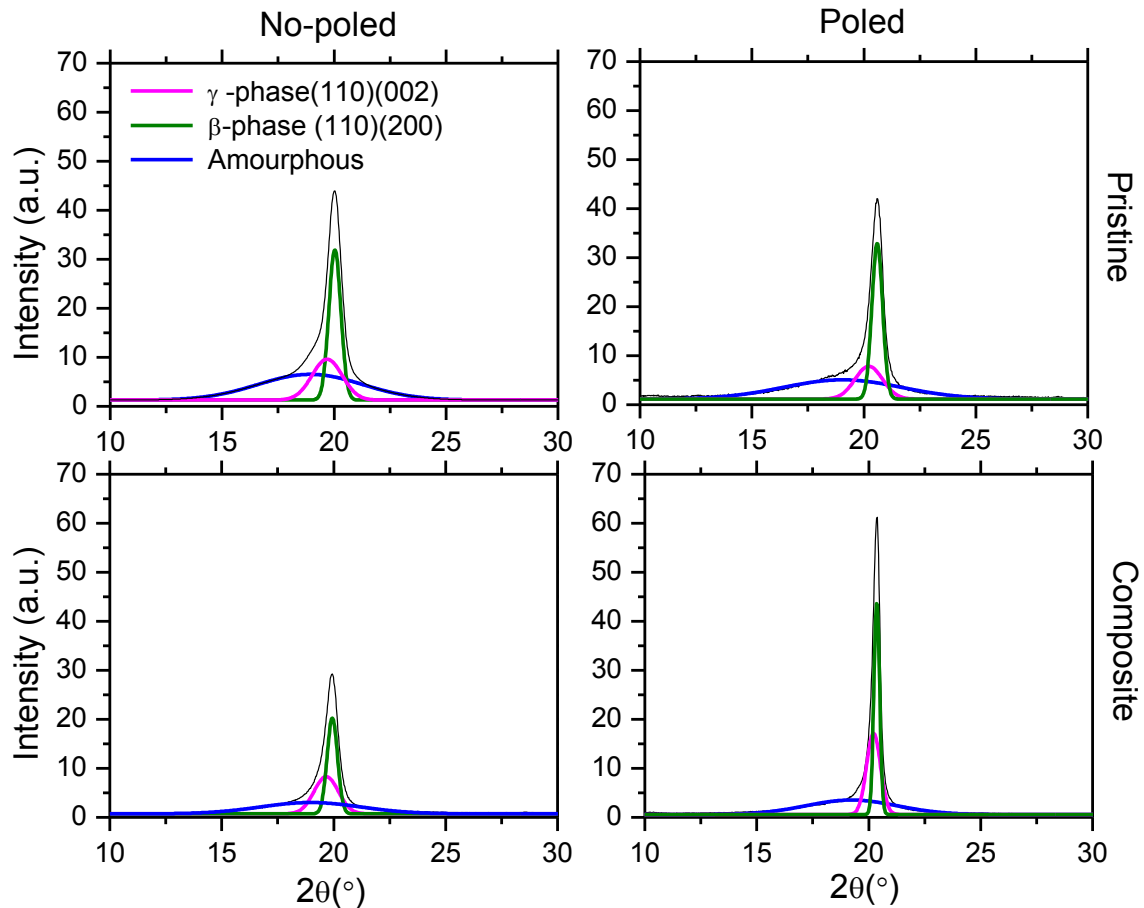
Figure 2-12. Effect of poling on the microstructure of annealed (left) and annealed and electrically poled (right) PVDF-TrFE and PVDF-TrFE/BNNT nanocomposite films.

Annealed PVDF-TrFE samples were polarized by applying up to 2000 volts in five cumulative steps of 400 volts across the sample. Each step involved the application of voltage for 10 minutes followed by a 5 minutes short circuit period to neutralize any access charge. A multi-step poling process like this, though time-consuming, reduces the chances of electric breakdown and results in higher polarisation.

Figure 2-12, it is observed the diffraction patterns for PVDF-TrFE and composite films where the sharp peak at 20.4° is the characteristic peak of β-phase P(VDF-TrFE) with (110/200) orientation planes. Before poling, it was obtained that the peak intensity of the (110/200) plane of P(VDF-TrFE) at $2\theta=20,4°$ decreased with the increase in volume fraction. In contrast, after poling the intensity of the peak increased considerably suggesting an increase of β-phase.

a

b

c
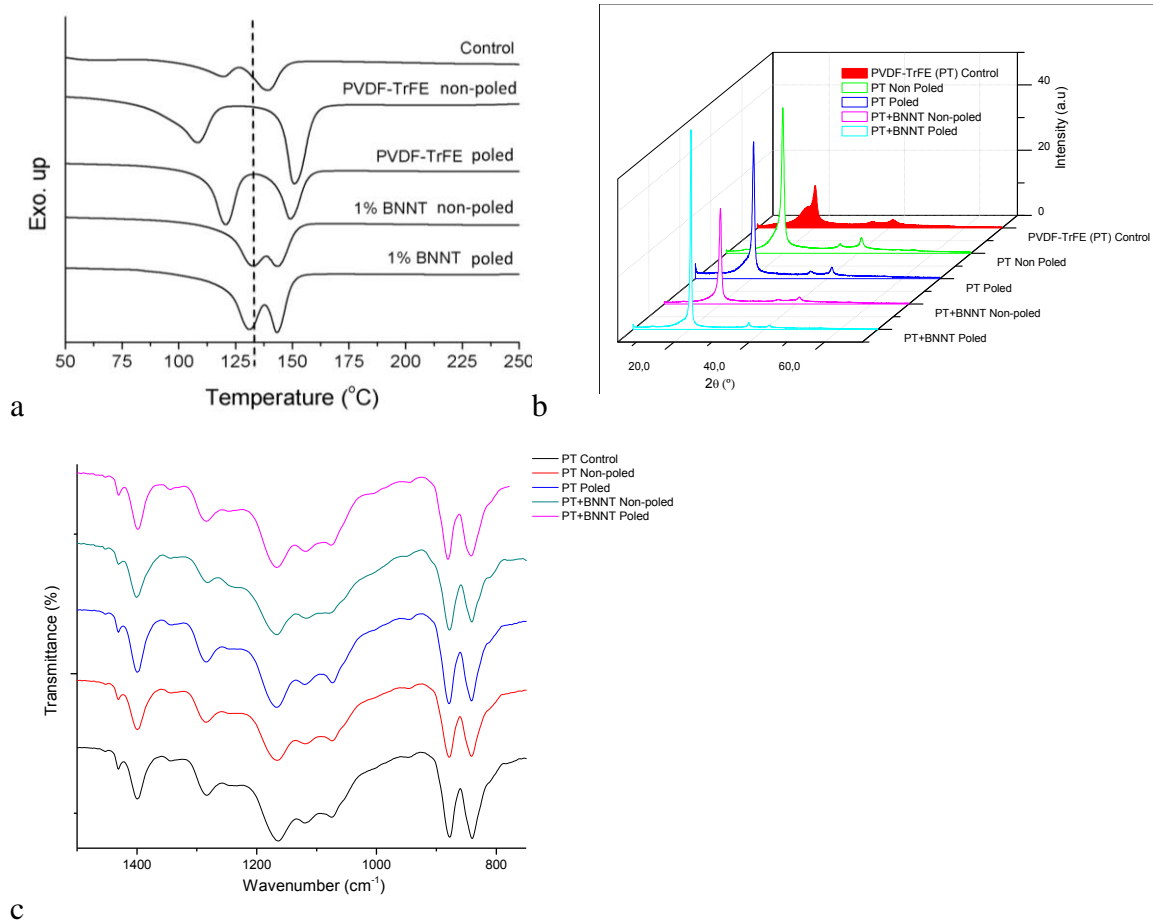
Figure 2-13. a) DSC, b) XRD and c) FTIR measurements of the different samples.

The quantification of the non-polar γ-phase has been more difficult, as exclusive FTIR bands corresponding to the γ-phase appear as shoulders (see Figure 2-14). This makes them very useful for qualitative identification of the corresponding phase but difficult for quantification.

Table 2-6. Structural crystals parameters obtained by XRD of PVDF-TrFE and PVDF-TrFE/BNNT nanocomposite formed at room temperature (RT) or annealed at 132ºC.

Sample	Total Crystallinity (%)	β-phase (polar)		γ-phase (non-polar)	
		Crystallinity (%)	Crystallite size (nm)	Crystallinity (%)	Crystallite size (nm)
PVDF-TrFE (RT)	32	32	8,34	0	-
PVDF-TrFE non-poled	62	23	17,29	39	12.40
PVDF-TrFE poled	55	35	24,39	20	15,31
PVDF-TrFE/BNNT non-poled	69	32	19,13	37	13,14
PVDF-TrFE/BNNT poled	69	36	33,02	33	13,82
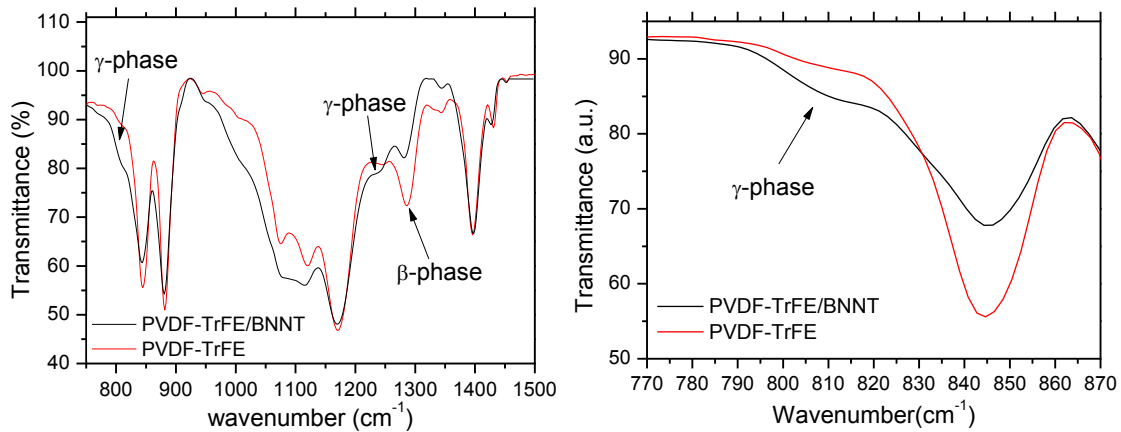
Figure 2-14. FTIR showing the different phases α, β, and γ of PVDF-TrFE annealed and poled.

Modulated DSC

Figure 2-15 shows typical DSC curves (heating and cooling of 5 ˚C/min) of PVDF-TrFE/BNNT 1 wt.% cast and annealed at 132˚C.
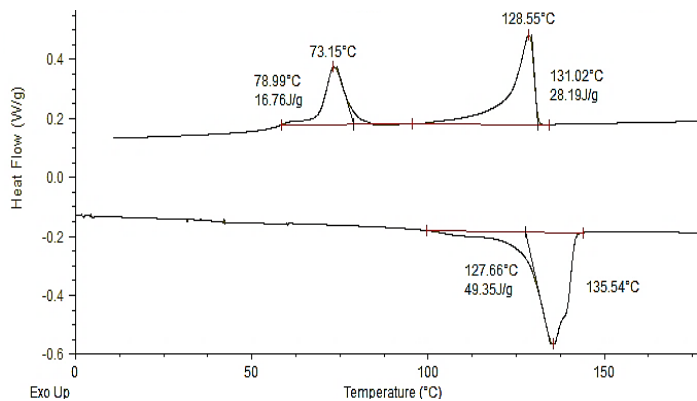
Figure 2-15. Typical DSC curve of a PVDF-TrFE thin-film with 1% v/v BNNT incorporated.

As observed in Figure 2-15enthalpy of the melting heat in total heat flow (ΔH=49.35 J/g), remains highest for BNNT composites compared to pristine (ΔH=32 J/g).

Figure (a) and (b) show the MDSC curve of pristine PVDF-TrFE and annealed PVDF-TrFE, respectively.

In particular, around Tc (120ºC), the peak intensity in the kinetic component curve disappears after annealing, this is results of crystal polymorphism restriction.
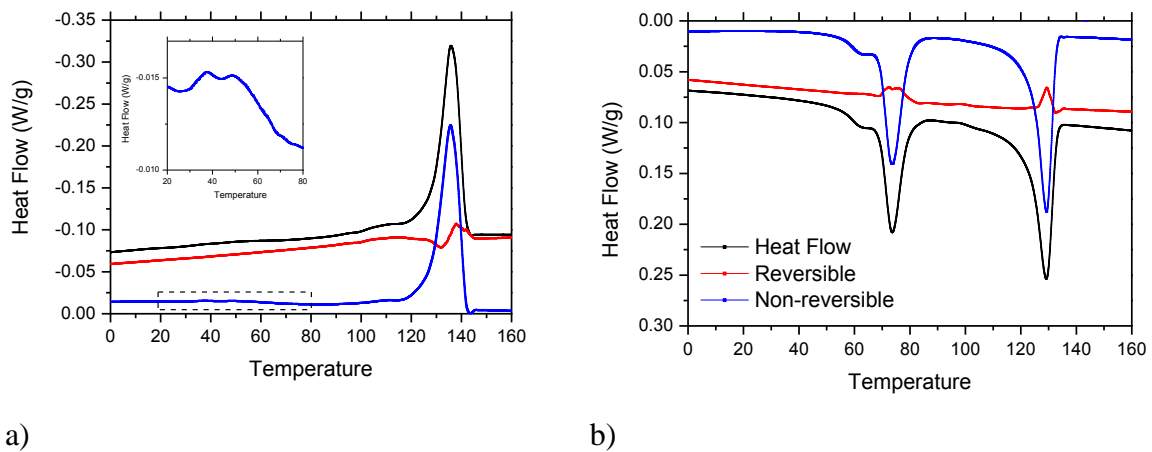
Figure 2-16. MDSC curve of PVDF-TrFE/BNNT (a) heating cycle and (b) cooling cycle.

During the cooling cycle, as shown in Figure 2-16, a low molecular movement is observed in both PVDF-TrFE processed types, however, crystals were formed mainly due to kinetics processes as observed in the non-reversible curve and a slight high molecular movement can be observed during the crystal formation process. This low molecular movement during the melting temperature as well as during the crystal formation process results in high viscoelastic properties of the materials.

Interpretation of different thermal events and crystal formation processes is described using MDSC, whereas, crystallisation kinetics is described as continuation.

Non-isothermal Crystallisation Kinetics

Table 2-7 shows the percentage of crystallinity in PVDF, PVDF-TrFE and PVDF-TrFE-BNNT 1% nanocomposite. An increase in crystallinity was observed following annealing of PVDF-TRFE. Similarly, an increase in crystallinity in semi crystalline PVDF-TRFE was evident with the addition of 1 wt|% of BNNT into the polymeric matrix as presented in Table 2-7. The increase in crystallinity in PVDF-TrFE with the addition of BNNT is attributed to change in crystal kinetics with associated crystallisation mechanism changes which was further verified using crystal kinetic studies.

Table 2-7. Crystallinity of different PVDF and PVDF-TrFE processed under different conditions

Materials	% Crystallinity
PVDF as received	55.40 ± 1.2
PVDF-TrFE as received	57.01 ± 0.56
PVDF-TrFE thin films (annealed)	64.07 ± 0.36
PVDF-BNNT 1 % (annealed)	69.23 ± 1.01

Figure 2-17 shows the Avrami plot of the PVDF-TRFE-BNNT nanocomposite. The corresponding R^2 obtained from all plots were smaller than unity. Also shown are the corresponding Avrami parameters n and k obtained from the slope and intercept of the plot obtained by fitting the Avrami curve. In addition, $t_{1/2}$ (calculated from the equation) and corresponding R^2 are tabulated in

Table 2-8 for all the curve types.

a)   b)   c)
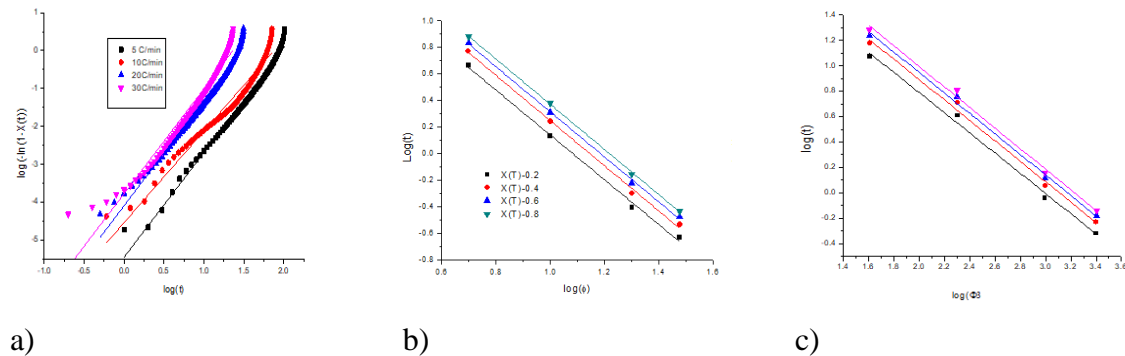
Figure 2-17   a) Avrami plot b) 1st peak and c) 2nd peak of PVDF TrFE -BNNT 1% composites

Table 2-8. Avrami parameters for a PVDF TrFE /BNNT nanocomposite.

	ϕ ($^\circ$C/min)	n	Log k	k'	$t_{1/2}$ (Sec.)	R^2
First crystals	5	3.01	-4.66	2.16E-05	31.4	0.990
(Higher temperature	10	3.01	-3.98	0.000104	18.62	0.985
crystals)	20	3.18	-3.44	0.000363	10.75	0.995
	30	3.01	-3.09	0.000813	9.41	0.975
Second crystals	5	2.75	-5.44	3.55E-06	83.91	0.987
(lower temperature	10	2.42	-4.53	2.88E-05	64.59	0.958
crystals)	20	2.79	-4.09	8.08E-05	25.69	0.979
	30	2.77	-3.77	0.000168	20.19	0.969

When compared to the pristine PVDF-TrFE, the Avrami exponent of PVDF TrFE /BNNT nanocomposites remains constant for the first as well as for the second crystal dynamics formed with increasing temperature. However, the structure formed was also due to a spherical three-dimensional process. In addition, lower n values obtained for PVDF-

TrFE/BNNT composites suggests a slower crystallisation and crystal formed at lower temperatures were associated with a decreased n value, suggesting that the crystal growth at lower temperature is a two-dimensional process. These observations suggest that the crystal growth is confined with the addition of BNNT at lower as well as at higher temperatures. Interestingly, as the value of $t_{1/2}$ decreased with the addition of BNNT for crystal formed at high temperature, this suggests that crystallisation occurs more rapidly. Conversely, the higher $t_{1/2}$ value at low temperatures suggests the formation of large and fewer crystals. It can be inferred then that the addition of 1.0 wt% BNNT can act as nucleating agent, leading to a higher crystallisation rate than that of pristine PVDF-TrFE.

An Ozawa plot of PVDF-TrFE/BNNT showed a non-linear behaviour, Similar to PVDF-TrFE. Therefore, the Avrami-Ozawa model was used. From

Table 2-9, it can be observed that for PVDF-TrFE/BNNT nanocomposites, each value of Xt, and the value of F(T) was lower under all cooling temperature compared to pristine PVDF-TrFE. These results suggest a higher crystallisation rate. The value of a remains relatively constant to one decimal place over different percentage of crystallinity for all samples.

Table 2-9 Avrami-Osawa parameters of 1st and 2nd peak of PVDF-TrFE/BNNT composites.

Equation Crystallinity	ln F(T)	a	Mean'n'	Mean 'm'	R^2
PVDF-TrFE- BNNT Second crystals (at higher temperature)					
X(T)-0.2	1.82	1.69			0.995
X(T)-0.4	1.94	1.70			0.996
X(T)-0.8	2.07	1.70			0.999
X(T)-0.8	2.07	1.70			0.999
PVDF-TrFE- BNNT Second crystals (at lower temperature)					
X(T)-0.2	2.37	0.80			0.994
X(T)-0.4	2.49	0.80			0.994
X(T)-0.6	2.61	0.80			0.994
X(T)-0.8	2.37	0.81			0.994

Electrical characterisation of PVDF-TrFE and PVDF-TrFE-BNNT

Figure 2-18a shows the electrical properties of PVDF-TrFE. The dielectric permittivity of solvent-cast films was observed between 11.5 - 8 over the range of alternating current frequencies measured. The dielectric permittivity as a result of the dipole movement and the dielectric loss of the heating effect was found to be lower at higher frequencies (ca. 0.1 at 1 kHz). The conductivity and imaginary dielectric modulus showed no DC conductance and no pure Maxwell-sillar Relaxation (MWS relaxation) due to lack of charge carriers within a polymer matrix.

a)

b)
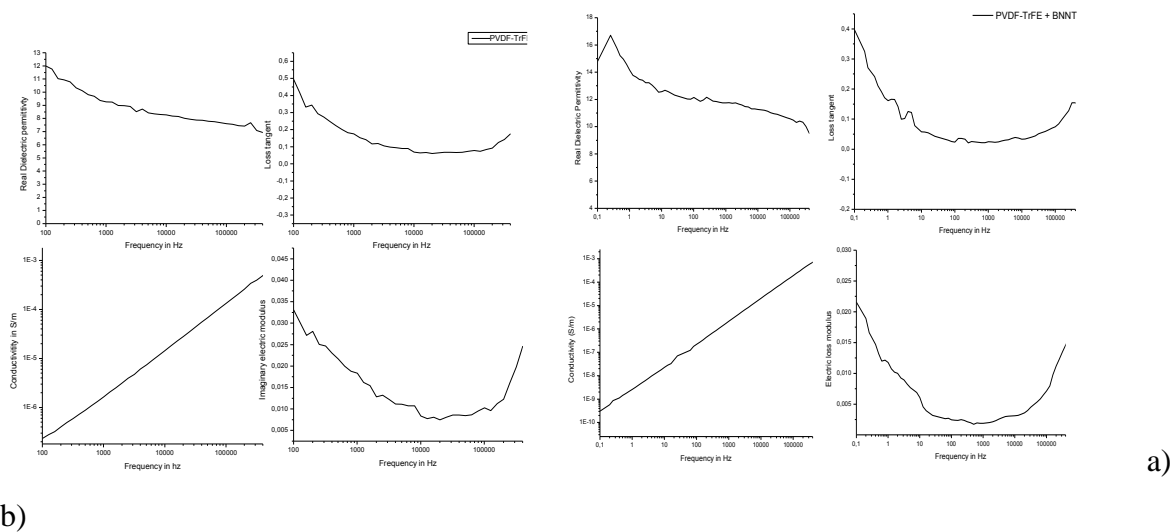
Figure 2-18. Electrical properties of a) PVDF-TrFE pristine and b) PVDF-TrFE/BNNT composite thin-film. There was no significant difference in permittivity as well as dielectric loss. However, a sharp drop of dielectric loss, as well as dielectric permittivity, was observed at very low frequencies.

A higher dielectric permittivity in BNNT at low frequencies was attributed to an accumulation of high charge carriers (due to BNNT nanotubes) in the polymer matrix. Similarly, a slight increase in dielectric permittivity was also observed due to the high interfacial polarization between the polymer and BNNTs relative to the pristine polymer films. As with pristine PVDF-TrFE films, no pure DC conductance or MWS polarisation was observed with PVDF-TrFE -BNNT composites.

The magnitude of the electric field and sample temperature are essential parameters in the poling process. Generally, the higher the induced polarisation provided the by poling field,

the larger the coercive field of the material. The coercive field for PVDF and its copolymers is typically between 50 and 120 MV/m (120 V/µm)[244]. Although the poling may be done at room temperature, an elevated temperature improves dipole mobility and consequently increases the material polarizability. Another issue to consider is warping of the films during the poling process due to the change in volume during orientation of the dipoles. Poling at elevated temperatures can help minimize warping due to relaxation of the polymer film and help it conform to the 'new' poled volume, especially at the boundary between the poled and non-poled areas. Unlike the poling field for which larger values will produce larger polarization, there is an optimum poling temperature that results in maximum polarization and piezoelectric properties[245]. Typical optimum poling temperatures are in the range 65 °C to 100 °C.

Mechanical properties.
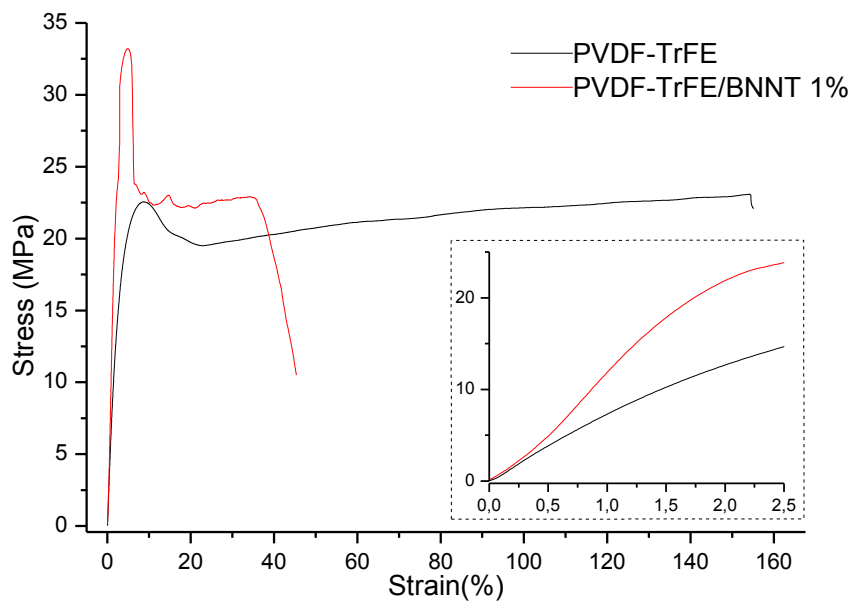
Figure 2-19. Tensile tests of PVDF-TrFE and PVDF-TrFE-BNNT 1 wt. % composites at room temperature

Table 2-10. Mechanical properties of PVDF-TrFE and PVDF-TrFE/BNNT composites

Materials	Young's Modulus (MPa)	Modulus of Resilience (MPa)	Modulus of Toughness (MPa)
PVDF-TrFE annealed	801.2 ± 32.8	65.7 ± 6.6	3307.1±252.3
PVDF-TrFE/BNNT 1wt % annealed	1009.1 ± 56.2	112.3 ±12.06	988.2±102.3

Piezoresponse Force Microscopy (PFM)

Local heterogeneities characteristic of nanocomposite materials can significantly affect the macroscopic piezoelectric performance. Therefore, is vital to probe electrical and mechanical properties using piezoresponse force microscopy (PFM) with resolution comparable to the size of the interfaces in the composites.

Figure 2-20 shows the topography and PFM images of a composite PVDF-TrFE/BNNT film in the as-prepared state and after poling with ± 20 V. The topography images demonstrates that irrespective of the addition of BNNT to the polymer matrix, the surface structure is maintained.

a)   b)   c)
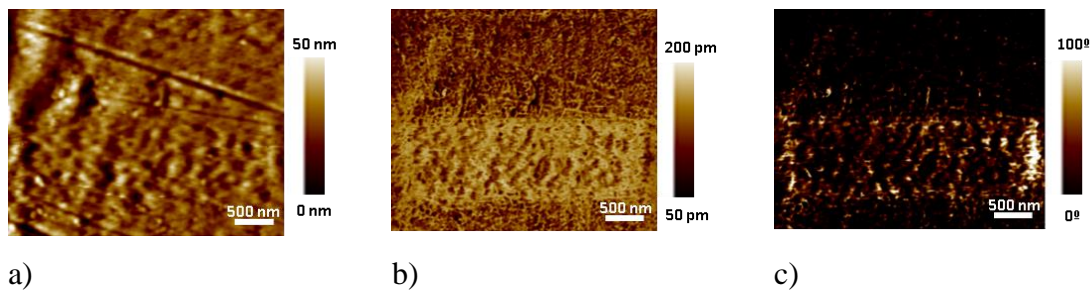
Figure 2-20. AFM Images of a pristine PVDF-TrFE after poling by +/−2 0V a specific region (rectangle) a) Topography b) Piezoresponse Amplitude c) Piezoresponse Phase

The poling was done by scanning an area under a bias voltage applied to the tip. It was possible to observe two distinct domains with oppositely oriented polarisation (phase, figure c). Briefly, the dark and bright contrast corresponds to the orientation of polarization (90 and -90º). The poled domains did not decrease nor decay remaining stable for at least 48 hours after poling.
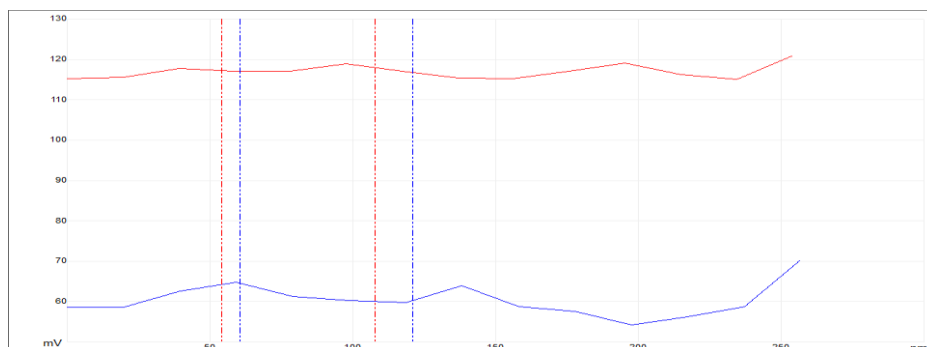
Figure 2-21. a) Piezoresponse amplitude profile inside (in red) or outside (in blue) the poled area (rectangle 1x 3 um) showing uniform polarization.

In the Figure 2-22 , representative image of composite samples are shown.

a)   b)
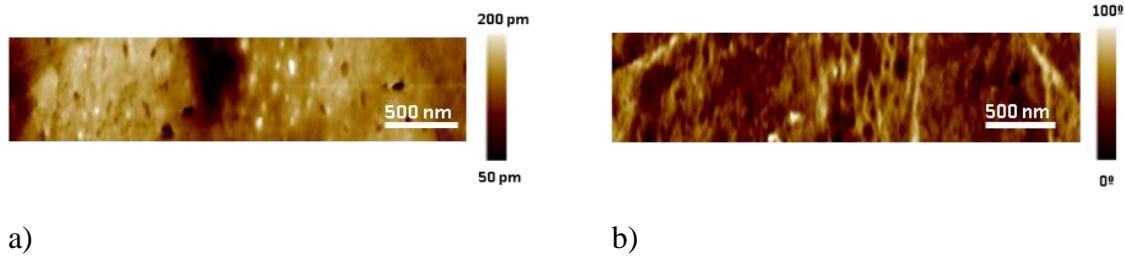
Figure 2-22. a)PFM amplitude and b)PFM Phase channels of PVDF-TrFE/BNNT composite samples.

As observed with MDSC and tensile analysis, atomic force microscopy also demonstrated a significant improvement in the mechanical dissipation of PVDF-TrFE on the addition of BNNT 1 wt.%. The ratio of elastic component to viscous component of the material is illustrated by dissipation and one of the significant factors for evaluation of viscoelastic properties of polymer-based blends and composites. The decrease in the relative scale of dissipation indicates that PVDF-TrFE reinforcement with BNNT results in the formulation of more resilient material (higher spring constant) relative to pristine PVDF-TrFE.

a)   b)
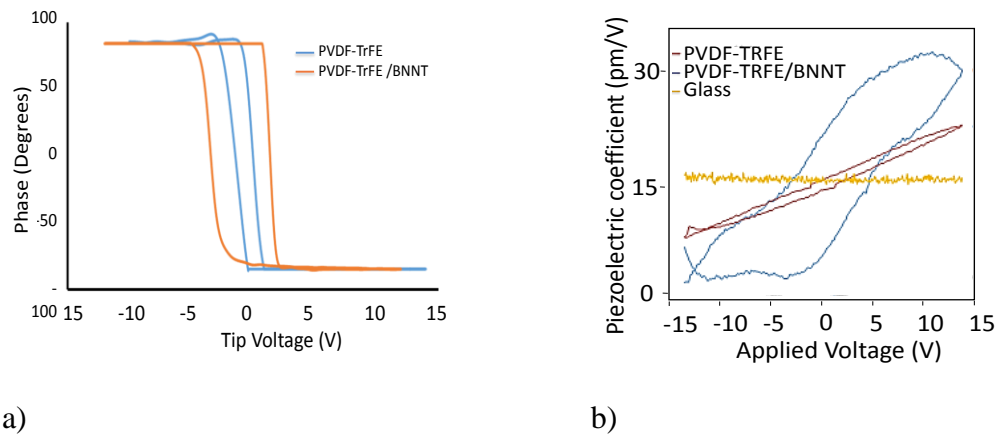
Figure 2-23. Switching spectroscopy PFM (SS-PFM) for the a) phase and b) amplitude

Figure 2-23 shows representative hysteresis loops that were measured at the same positions in three different samples. Loops presented different forms; however, non-continuous loops were obtained for control samples in contrast to PVDF-TrFE samples. Specifically, the effect of BNNT addition on the aligned polarization of PVDF-TrFE/BNNT nanocomposite films was investigated. It was confirmed that the degree of polarization alignment to the surface normal increased for the nanocomposite. The higher coercive

119

indicates that the pristine sample has a molecular structure with more stable conformation and requires less energy for an applied electric field compared to the nanocomposite. Molecular motions involved in the process of this flipping process can be hindered by the incorporation of BNNT. This behaviour could be reproduced at several locations.

2.4 Discussion

Recent advances in tissue engineering are based on developing tissue-analogue structures by exploiting the intrinsic ability of cells to synthesise tissue-specific extracellular matrices. Understanding how biochemical and biophysical cues interplay to recreate functional tissues in vitro have advanced the field; however, none of the current approaches can successfully maintain tenocyte function and avoid the phenotypical drift to extend the time of cells in culture. In recent years, mechanically adaptive and responsive materials have generated significant interest for regulating cellular functions. Herein, we developed and characterised a system to stimulate cells with electromechanical cues based on a nanovibrational waves activated PVDF-TrFE piezoelectric membrane.

PVDF possesses excellent electromechanical properties including ease of processability, excellent electroactivity and low acoustic/mechanical impedance in liquid environments. PVDF can exhibit five distinct crystalline phases ($\alpha_{non-polar}$, β_{polar}, $\gamma_{non-polar}$, α_{polar} and γ_{polar}) depending on processing conditions. The α-phase is the most thermodynamically stable while β-phase presents the highest electroactive performance. Different methods have been applied to preferentially induce β-phase formation including mechanical stretching and thermal treatments[166,183]. In this study, we used a copolymer PVDF-TrFE (75/25) which crystallizes predominantly in the β-phase upon the addition of a third fluoride in the TrFE monomer unit with a large steric hindrance, which favors the all-trans conformation, and therefore induces the β phase regardless of the processing method. Furthermore, it was demonstrateed that highly reproducible thin films of approx. 25 ± 1 µm could be fabricated using a spin-coating method (see Figure 2-3) employing a 20 % v/v solution of PVDF-TrFE in triple-step process at 1000 rpm for 30 sec as reported by [166]. However, one of the main disadvantages of thin-film formation using a spin-coating process is excessive film porosity and surface roughness. To avoid this problem solvent baking under vacuum (under 20 mTorr) was used for solvent-cast films or an annealing process used after spin coating. To ensure dense film formation and low surface roughness prompt thermal annealing at 50ºC after spin-coating using a hot plate was employed. This technique allows

high uniformity in terms of both the crystalline phase and thickness throughout the film. Also, thermal annealing allows high transparency (~95%) film formulation, in contrast to films obtained at room temperature (~70%). The addition of BNNT fillers also affected the spin-coating film thickness, especially for lower spin rates (1,000 rpm), and the higher the BNNT concentration, the thicker the film. Besides, transparency was reduced with increased BNNT concentration (see Figure 2-4).

Following the spin-coating process, PVDF-TrFE was melt-wetted at 200 °C to eliminate thermal history. Wetted templates were then annealed for 2 h at 132 °C, which is between the observed Curie point (Tc) and melting point (Tm), to modify the β-phase crystallisation according to previous studies.Figure 2-13 shows the XRD analysis of the 20 wt % PVDF-TrFE films under room temperature and annealing temperatures of 132ºC for 2 h. The crystallisation of PVDF-TrFE was mainly β-phase ($2\theta = 20,4°$) for annealed samples and a combination with γ phase ($2\theta = 19.2°$) for non-annealed samples, indicating that the major phase is a mixture of non-polar γ phase and polar phase β. From the XRD analysis (Figure 2-12), it was possible to observe a significant peak at $2\theta = 20.4°$ (the β-phase crystallisation) with 1 wt% BNNT-doping, while the pristine PVDF-TrFE presented a lower amplitude, wider peak. The formation of γ -phase in PVDF-TrFE/BNNT nanocomposite film can be confirmed by the presence of specific transmittance bands in the FTIR spectra (812 and 1234 cm^{-1}). Figure 2-14 shows the FTIR spectra of BNNT-doped PVDF-TrFE. It was possible to observe that BNNT incorporation changed the crystallinity of PVDF-TrFE since the peak intensity of the β-phase (840 cm−1) changed slightly after incorporation of BNNT. The XRD results showed an increase in the overall crystallinity (from 62 to 69%) and in particular the β-phase crystallinity increased from 28 to 36 %. The formation of β-phase in PVDF-TrFE/BNNT nanocomposites can be attributed to the specific interaction between the B-N polar groups found in BNNT and the CF2 segments of the PVDF-TrFE polymer[246,247]. A higher crystallinity level and crystal size were achieved for poled BNNT nanocomposite materials. FTIR was used to confirm the presence of the different crystalline phases. The peaks at the wavenumbers 812, 831, 882 and 1234 cm−1 corresponded to the γ -phase while those of 1400, 1280 and 840 cm^{-1} corresponded to the β-phase[166]. The peak at 840 cm^{-1} has the highest absorbance in the β-phase while the peak at 812 cm^{-1} has the highest absorbance in the γ -phase. In summary, annealing results in an increase of the β-phase crystallisation, which is adopted in the subsequent process of BNNT-doping using annealing between Tc and Tm.

It was observed that BNNT incorporation resulted in an increased presence of γ –phase as also indicated by XRD results. Wide-angle XRD in reflection mode (Figure 2-12) was performed on bulk PVDF-TrFE and nanocomposites before and after annealing and poling. XRD spectra (Figure 2-13) confirmed the peaks at 18.5°, 19.2°, 20.4° characteristic of the non-polar γ phase and the peak at 2θ = 20.4° and 35.8º and 40.9º is related to the diffraction of polar β phase at (110) and (200). Closer inspection of the (200,110) region (Figure 2-12) indicated the presence of both non-ferroelectric (19.2°) and ferroelectric (20.4°) phases in bulk PVDF-TrFE, where the intensity of the ferroelectric β-phase (20.4) peak was roughly twice that of the non-ferroelectric peak. Films after annealing without poling show much more crystallinity as a peak at 20.4 becomes very narrow, and the broad peak at 18.3 disappears (amorphous region). Results compare favourably to prior reports. Additionally, the intensity of the non-ferroelectric phase peak increased relative to the β peak for the composite. XRD and FTIR measurements also confirmed an increase in the overall crystallinity as a result of annealing and BNNT-doping. This can be explained since, in crowded volumes, crystallisation to the β phase is preferred because the β phase is denser than the non-ferroelectric, and chains are more efficiently packed in the β phase.

DSC was also used to calculate the crystalline percentage, but could not distinguish the different crystalline polar and non-polar phases. However, DSC results complement the results obtained by XRD and FTIR. DSC thermograms measured during the heating of PVDF-TrFE films annealed (poled and non-poled) are shown in Figure 2-8. Upon heating, non-poled and poled PVDF-TrFE underwent a Curie transition (~118 °C) and melting (~138 °C); upon cooling, the polymer crystallised (~120 °C) and then underwent Curie transition at 73 °C. Significant hysteresis of the Curie transition (~55°) was present upon heating and cooling. The thermal responses of composite films were distinctly different from those of pristine PVDF-TrFE. Upon heating, the total heat flow showed a single broad peak at 127 and 135°C.

In contrast, bulk PVDF-TrFE showed multiple first-order transitions (Melting, Curie). For composites, the melting temperature was depressed so that it coincided with the Curie transition. Upon cooling, two peaks with maxima were detected at 128 and 73°C. The sharp crystallisation peak observed for the bulk polymer was also observed for composite films. The influence of BNNT-doping on the melting temperature signifies a transition from homogenous to heterogeneous nucleation, as discussed by Steinhart[248]

In the case of homopolymer PVDF in confinement, heterogeneous nucleation is typified by a sharp crystallisation peak upon cooling in DSC, which was observed for bulk and PVDF-

TrFE composites. A crystallisation transition, such as noted in the composite, is indicative of heterogenous nucleation where more defects to initiate crystal growth were present. When BNNT was added, crystallisation was increased by ~10 °C relative to pristine PVDF-TrFE. It was clear that the addition of BNNT influenced the crystalline structure by creating more ordered crystallites. The observation of first-order transitions (Curie and melting) in the non-reversing curve was somewhat unusual because both are generally indicated by changes in heat capacity (captured by the reversing curve). However, this particular behaviour is possible for materials of high crystallinity. The increase of crystallinity can be attributed to the increase in crystallite size along the molecular chain direction in combination with changes in the crystal lattice structure.

Generally, two endothermic peaks were observed for all investigated films. The first event, around 120°C, partially overlapped with an exothermic peak. This exothermic event corresponds to a crystallisation process typical of solvent cast PVDF-TrFE, controlled by the solvent evaporation rate and resulting biphase crystalline structure. As the separation of overlapping phenomena (i.e. melting, crystallisation, and Curie phase transitions) using conventional DSC is difficult; the thermal properties of PVDF-TrFE and composites were then probed using Modulated DSC (MDSC).

Figure 2-9 shows the MDSC curve of pristine PVDF-TrFE and annealed PVDF-TrFE, respectively. In MDSC, the total heat flow is divided into two main events (a) Heating capacity component (reversing curve) and (b) Kinetic component (Non-reversing curve). The reversing curve is a direct measure of specific heat capacity, which in turn is a measure of the change in molecular movement within a polymer, occurring on a time scale shorter than a modulation period. Similarly, the non-reversing curve shows the kinetics phenomena, which occurs due to events more extended than a modulation period. The main differences observed as a result of the annealing process was the restriction of the molecular moment depicted by a decrease in peak intensities of the "kinetic" component (non-reversing curve).

Further, endothermic and exothermic peaks (at around 120°C and 138°C) were observed. Endothermic and exothermic activity near 120°C (Tc) express the fusion of the metastable phase continuing transitions to stable crystals, and the endothermic peak at 138°C is considered as a fusion of stable crystals. In particular, around Tc (120ºC), the peak intensity in the kinetic component curve disappeared after annealing, this was a result of crystal polymorphism restriction. It is expected that stable β-phase crystals are predominant in annealed samples and therefore, no transition from metastable phases to

stable phases will occur (i.e. γ to β phase transition). In non-annealed samples, an endothermic peak at 120ºC due to the molecular movement for crystal formation was observed. However, for annealed samples, the creation of crystals is restricted and is denoted by an exothermic peak (see Figure 2-9). Therefore, it is suggested that annealed samples provide more homogenous crystals associated with a higher molecular movement (higher crystallinity) and temperature phase separation. It is important to note that the most significant physical changes due to annealing were observed in the molecular movement, indicating that annealing at any temperature between Tc and Tm might not always prove to be the optimum for enhancing polymer crystallinity. These results suggest that stable and homogenous crystals formation occurred with annealing at near-Tc, where β-phase transformation occurs from the tightly packed crystals resulting in films of high crystallinity. The FTIR and XRD analyses also confirmed these results.

The incorporation of BNNT presented similar results where no enthalpy relaxation was observed. In contrast to pristine samples, composite materials exhibited a large increase in the Tc, and the melting temperature was depressed so that it coincided with the Curie transition. During the cooling cycle, as shown in Figure 2-16, the reversing curve demonstrated very low molecular movement compared to pristine PVDF-TrFE; however, crystals were formed mainly due to kinetics process as observed in the non-reversible curve and a little molecular movement could be observed during the crystal formation process. Little molecular movement during the melting temperature as well as during the crystal formation process is associated with higher viscoelastic properties of the material. The sharp crystallisation peak observed for pristine and annealed samples was not observed for composite specimens, which suggests that the broad exothermic peaks observed in cooling are overlapping crystallisation and Curie transition events. In other words, crystallisation from the melt is suppressed at lower temperatures. Curie transition peaks appeared to narrow and shift to higher temperatures. The observed influence of BNNT on polymer melting and crystallisation results in a homogeneous to heterogeneous transition nucleation, as observed in MDSC and tensile graphs (increased elasticity and toughness), atomic force microscopy also indicated a significant improvement in mechanical properties of PVDF-TrFE on the addition of BNNT 1 wt.% as shown in Figure 2-21.

A careful examination of the reversing and non-reversing curves indicates the relative dynamics of the Curie (Tc) and melting/crystallisation transitions (see Figure 2-16). For all groups, the amplitude of each transition (in the non-reversing curve) was larger than that of

the reversing curve. This indicates that the time-scales of melting, crystallisation, and the Curie transition are longer than the period of modulation, 60 s. Also, the appearance of Curie and melting transition (first-order transitions) in the non-reversing curve is unusual, since both usually are observed just in the reversing curve (due to heat capacity changes). However, this is a clear indication of highly crystalline materials. In addition, the hysteresis observed for the Curie transition can be explained by this longer time-scale where a significant degree of cooling is needed to start the transition. It is known that changes in available volume during transitions results in thermal hysteresis. The decreased response in the reversing curve is due to the rapid conversion of smaller and fewer unstable crystals.

Interpretation of different thermal events and crystal processes was described using MDSC, whereas, crystallisation kinetics was described as a continuation. The increase in crystallinity of PVDF-TrFE with the addition of BNNT was attributed to a change in crystal kinetics, which was verified using crystal kinetic studies. The Avrami model (characterised by Avrami constant n and exponent k) is commonly used to describe changes in the volume of the crystals as a function of time during crystallisation. Compared to pristine PVDF-TrFE, the Avrami exponent k for composites remained fairly constant with a heating rate for first as well as for secondary crystallisation formed with increasing temperature. However, the formed crystals were still complex three-dimensional and spherical. In addition, the lower Avrami constant "n" obtained for PVDF-TrFE/BNNT composites suggests reduced reaction dynamics. At a constant growth dimension, n is decreased by 1 when nucleation is heterogeneous rather than homogeneous. For the same nucleation mechanism, n increases with the growth dimension, e.g. from 1 for rods, to 2 for discs and finally to 3 for spheres in the case of heterogeneous nucleation. It has been proposed that spherulites start to grow as rods, which indeed happens in the case of PVDF. Also, for crystals formed at a lower temperature, the "n value" was slightly decreased with the addition of BNNT. The growth of crystal formed at a lower temperature was two-dimensional with a constant nucleation rate. These observations suggest that the crystal growth is confined with the addition of BNNT at lower as well as at higher temperatures. As the value of $t_{1/2}$ decreased with the addition of BNNT for crystals formed at a higher temperature, it suggests that the crystals were formed more rapidly; however, the higher value of $t_{1/2}$ at lower temperature suggests the formation of larger crystals.

As observed with PVDF-TrFE, the Ozawa plot of PVDF-TrFE-BNNT showed a non-linear behaviour, therefore the Avrami-Ozawa model, characterised by F(T), was used to

describe non-isothermal crystallisation kinetics. Huang and Gu et al. reported that the value of F(T) could be considered to indicate the polymer crystallisation rate, where lower values suggest higher crystallisation rate and higher values suggest lower crystallisation rate[242]. It also suggests that F(T) increases with higher values of crystallinity. From Table 2-9 Avrami-Osawa parameters of 1st and 2nd peak of PVDF-TrFE/BNNT composites., for all PVDF-TrFE-BNNT composites, the lower value of F(T) under all cooling temperatures suggest a higher crystallisation rate than pristine PVDF-TrFE. The value of b remained almost constant to one decimal place over a different percentage of crystallinity for all samples. The mean value of m was calculated from Avrami coefficient n and the value of b.

 Figure 2-18 shows the electrical properties of PVDF-TrFE and PVDF-TrFE-BNNT composites. The dielectric permittivity of pristine and composite films was measured to be 8 and 11.5 respectively over the range of frequencies measured. The dielectric permittivity resulting from dipole movement and the dielectric loss resulting from heating effect was found to be lower at higher frequencies (ca. 0.1 at 1 kHz) for both PVDF-TrFE and PVDF-TrFE-BNNT composite film types. The conductivity and imaginary dielectric modulus showed no DC conductance and no pure Maxwell-sillar relaxation (MWS relaxation) due to lack of charge carriers within the polymer matrix. For composites, a sharp drop in a dielectric loss, as well as higher dielectric permittivity, was observed at very low frequencies. Higher dielectric permittivity in composite films at low frequency was attributed to the accumulation of high charge carriers (due to BNNT nanotubes) in the polymer matrix. Similarly, a slight increase in the dielectric permittivity was also observed due to the high interfacial polarization between the polymer and BNNT nanotubes compared to the pristine polymer.

Local heterogeneities, characteristic of nanocomposite materials, can significantly affect the macroscopic piezoelectric performance. Figure 2-22 shows the topography and PFM images of a composite PVDF-TrFE/BNNT film in the as-prepared state and after poling with ± 20 V. The topography images demonstrated that irrespective of the addition of BNNT, the polymer surface maintained its original structure. In contrast, PFM spectroscopy showed an increased in the coercive voltage, indicating a higher number of dipoles present in the composite films. These results are in good agreement with the above-explained crystallisation studies where the addition of BNNT resulted in the formation of a different crystal structure.

2.5   Conclusions

Here, for the first time, evidence has been presented on the increased β-phase formation and total crystallinity in PVDF-TrFE by incorporating BNNT as a second phase using modulated differential scanning calorimetry (MDSC). The surface morphology, crystallisation, mechanical, electrical and ferroelectric properties of pristine and composite films of P(VDF-TrFE) and effect of annealing were assessed. Thermal analysis showed that composite films had a ferroelectric Curie transition at around 130ºC (10ºC more than for pristine films) and melting temperature for both film types at around 140ºC. A significant increase in crystallinity and mechanical, dielectric and ferroelectric properties was observed for composite films. Briefly, crystallisation studies showed that BNNT-doping significantly benefits the β-phase crystallisation of PVDF-TrFE films. XRD and FTIR measurements also confirmed an increase in the overall crystallinity as a result of BNNT doping. This can be explained since, in crowded volumes, crystallisation to the β phase is preferred because the β phase is denser than the non-ferroelectric γ-phase, in which chains are more efficiently packed. These observations suggest that crystal growth is confined with the addition of BNNT. PFM spectroscopy showed an increased in the coercive voltage that indicates a higher number of dipoles present in the composite films due to a different crystal structure. These results were ascribed to crystallisation enhancement due to depression of molecular mobility and increased kinetic selection mechanism for crystal growth and orientation in the confined space of composite films besides of interaction between PVDF-TrFE segments CF2 and BNNT polar groups BN.

Also, crystallisation studies have shown that the most significant changes due to annealing are observed in the restriction of molecular movement. These results suggest that the most optimal temperature to obtain highly stable and homogenous crystals is the temperature just around Tc, where β-phase transformation occurs from the tightly packed crystals resulting in high crystallinity. In summary, incorporation of BNNT resulted in increased mechanical properties, melting and crystallisation temperatures, and crystallinity via restriction of molecular movement. Importantly, annealing temperature appears to be critical for maximising the β-phase formation.

The cellular viability of tendon cells (up to 10 days) was examined on unmodified and modified PVDF-TrFE films using Tissue culture plastic (TCP) as control. It was observed that cell death was not induced in any of the experimental or control groups. However, cell proliferation assays confirmed that the immobilisation of fibronectin resulted in a more

sustained and enhanced proliferation of cells. A polyacrylic acid/fibronectin functionalization approach was employed to promote cell adhesion, and PVDF-TRFE/BNNT nanocomposites were shown to induce increased cell attachment and sustained proliferation relative to pristine PVDF-TrFE. Furthermore, nanocomposite PVDF-TrFE/BNNT showed a higher cell attachment and proliferation rate compared to pristine samples. It was concluded that the inclusion of BNNTs negates the anti-adhesive effects of negatively charged PVDF-TrFE surfaces. This study shows that PVDF-TrFE/BNNT nanocomposite hold great potential for tissue engineering applications.

2.6 References

1. Snedeker, J. G. & Foolen, J. Tendon injury and repair – A perspective on the basic mechanisms of tendon disease and future clinical therapy. *Acta Biomaterialia* **63**, 18–36 (2017).

2. Walden, G. *et al.* A Clinical, Biological, and Biomaterials Perspective into Tendon Injuries and Regeneration. *Tissue Eng. Part B Rev.* (2017). doi:10.1089/ten.teb.2016.0181

3. Docheva, D., Müller, S. A., Majewski, M. & Evans, C. H. Biologics for tendon repair. *Advanced Drug Delivery Reviews* (2015). doi:10.1016/j.addr.2014.11.015

4. Kartus, J., Movin, T. & Karlsson, J. Donor-site morbidity and anterior knee problems after anterior cruciate ligament reconstruction using autografts. *Arthroscopy* (2001). doi:10.1053/jars.2001.28979

5. Yasuda, K., Tsujino, J., Ohkoshi, Y., Tanabe, Y. & Kaneda, K. Graft Site Morbidity with Autogenous Semitendinosus and Gracilis Tendons. *Am. J. Sports Med.* (1995). doi:10.1177/036354659502300613

6. Kartus, J., Movin, T. & Karlsson, J. Donor-site morbidity after anterior cruciate ligament reconstruction using autografts clinical, radiographic, histological, and ultrastructural aspects. in *Anterior Knee Pain and Patellar Instability* (2006). doi:10.1007/1-84628-143-1_19

7. Seo, J. G. *et al.* Ankle morbidity after autogenous Achilles tendon harvesting for anterior cruciate ligament reconstruction. *Knee Surgery, Sport. Traumatol. Arthrosc.* (2009). doi:10.1007/s00167-009-0729-9

8. Kuo, C. K., Marturano, J. E. & Tuan, R. S. Novel strategies in tendon and ligament tissue engineering: Advanced biomaterials and regeneration motifs. *BMC Sports Sci. Med. Rehabil.* **2**, 20 (2010).

9. Lomas, A. J. *et al.* The past, present and future in scaffold-based tendon treatments. *Advanced Drug Delivery Reviews* **84**, 257–277 (2015).

10. Liu, Y., Ramanath, H. S. & Wang, D. A. Tendon tissue engineering using scaffold enhancing strategies. *Trends in Biotechnology* **26**, 201–209 (2008).

11. Mammoto, T. & Ingber, D. E. Mechanical control of tissue and organ development. *Development* (2010). doi:10.1242/dev.024166

12. Obregón, R., Ramón-Azcón, J. & Ahadian, S. Bioreactors in Tissue Engineering. in *Tissue Engineering for Artificial Organs: Regenerative Medicine, Smart*

Diagnostics and Personalized Medicine (2016). doi:10.1002/9783527689934.ch6

13. Plonsey, R., Barr, R. C., Plonsey, R. & Barr, R. C. Electrical Stimulation of Excitable Tissue. in *Bioelectricity* (2000). doi:10.1007/978-1-4757-3152-1_7

14. Rajabi, A. H., Jaffe, M. & Arinzeh, T. L. Piezoelectric materials for tissue regeneration: A review. *Acta Biomater.* **24**, 12–23 (2015).

15. Tandon, N. *et al.* Electrical stimulation systems for cardiac tissue engineering. *Nat. Protoc.* (2009). doi:10.1038/nprot.2008.183

16. Chen, J., Xu, J., Wang, A. & Zheng, M. Scaffolds for tendon and ligament repair: Review of the efficacy of commercial products. *Expert Review of Medical Devices* **6**, 61–73 (2009).

17. Longo, U. G., Lamberti, A., Maffulli, N. & Denaro, V. Tendon augmentation grafts: A systematic review. *Br. Med. Bull.* (2010). doi:10.1093/bmb/ldp051

18. Yin, Z. *et al.* The regulation of tendon stem cell differentiation by the alignment of nanofibers. *Biomaterials* **31**, 2163–2175 (2010).

19. Kew, S. J. *et al.* Regeneration and repair of tendon and ligament tissue using collagen fibre biomaterials. *Acta Biomaterialia* (2011). doi:10.1016/j.actbio.2011.06.002

20. Font Tellado, S., Balmayor, E. R. & Van Griensven, M. Strategies to engineer tendon/ligament-to-bone interface: Biomaterials, cells and growth factors. *Advanced Drug Delivery Reviews* (2015). doi:10.1016/j.addr.2015.03.004

21. Cross, L. M., Thakur, A., Jalili, N. A., Detamore, M. & Gaharwar, A. K. Nanoengineered biomaterials for repair and regeneration of orthopedic tissue interfaces. *Acta Biomaterialia* (2016). doi:10.1016/j.actbio.2016.06.023

22. Pesqueira, T. *et al.* Engineering magnetically responsive tropoelastin spongy-like hydrogels for soft tissue regeneration. *J. Mater. Chem. B* (2018). doi:10.1039/c7tb02035j

23. Pesqueira, T., Costa-Almeida, R. & Gomes, M. E. Magnetotherapy: The quest for tendon regeneration. *J. Cell. Physiol.* (2018). doi:10.1002/jcp.26637

24. Silva, E. D. *et al.* Multifunctional magnetic-responsive hydrogels to engineer tendon-to-bone interface. *Nanomedicine Nanotechnology, Biol. Med.* (2018). doi:10.1016/j.nano.2017.06.002

25. Gonçalves, A. I., Rodrigues, M. T. & Gomes, M. E. Tissue-engineered magnetic cell sheet patches for advanced strategies in tendon regeneration. *Acta Biomater.* (2017). doi:10.1016/j.actbio.2017.09.014

26. Holzapfel, B. M. *et al.* How smart do biomaterials need to be? A translational science and clinical point of view. *Advanced Drug Delivery Reviews* (2013). doi:10.1016/j.addr.2012.07.009

27. J.E. Commission, ETN nanomedicine: roadmaps in nanomedicine towards 2020, Expert Report 2009, 2009, p. 56.

28. Schneider, M., Angele, P., Järvinen, T. A. H. & Docheva, D. Rescue plan for Achilles : Therapeutics steering the fate and functions of stem cells in tendon wound healing. *Adv. Drug Deliv. Rev.* **129**, 352–375 (2018).

29. Yin, W. *et al.* Biomaterials Functional replication of the tendon tissue microenvironment by a bioimprinted substrate and the support of tenocytic differentiation of mesenchymal stem cells. **33**, 7686–7698 (2012).

30. Brian, J. *et al.* The piezoelectric tensor of collagen fibrils determined at the nanoscale. (2017).

31. Manuscript, A. LAW ": A CRITICAL REVIEW. **31**, 733–741 (2010).

32. Manuscript, A. Nanoscale. (2018). doi:10.1039/C8NR01634H

33. Jacob, J., More, N., Kalia, K. & Kapusetti, G. Piezoelectric smart biomaterials for bone and cartilage tissue engineering. *Inflamm. Regen.* **38**, 2 (2018).

34. Vivekananthan, V. *et al.* Energy , Environmental , and Catalysis Applications Biocompatible collagen-nanofibrils : An approach for sustainable energy harvesting and battery-free humidity sensor applications Biocompatible collagen-nanofibrils : An approach for sustainable energy ha. (2018). doi:10.1021/acsami.8b02915

35. Michlovitz, S. L. Is there a role for ultrasound and electrical stimulation following injury to tendon and nerve? *J. Hand Ther.* (2005). doi:10.1197/j.jht.2005.02.013

36. Khan, S. I. & Burne, J. A. Inhibitory mechanisms following electrical stimulation of tendon and cutaneous afferents in the lower limb. *Brain Res.* (2010). doi:10.1016/j.brainres.2009.10.020

37. Williams, W. S. & Breger, L. Piezoelectricity in tendon and bone. *J. Biomech.* (1975). doi:10.1016/0021-9290(75)90076-7

38. Long, S. B., Campbell, E. B. & MacKinnon, R. Voltage sensor of Kv1.2: Structural basis of electromechanical coupling. *Science (80-.).* (2005). doi:10.1126/science.1116270

39. Pfeiffer, E. R., Tangney, J. R., Omens, J. H. & McCulloch, A. D. Biomechanics of Cardiac Electromechanical Coupling and Mechanoelectric Feedback. *J. Biomech. Eng.* (2014). doi:10.1115/1.4026221

40.	Alcaino, C., Farrugia, G. & Beyder, A. Mechanosensitive Piezo Channels in the Gastrointestinal Tract. *Curr. Top. Membr.* **79**, 219–244 (2017).

41.	Michael Lavagnino1, Michelle E. Wall2, Dianne Little3, Albert J. Banes2,4, Farshid Guilak3,4,5, and S. P. A. Tendon Mechanobiology: Current Knowledge and Future Research Opportunities. *J Orthop Res.* **33**, 813–822 (2015).

42.	Yoshimoto, Y., Takimoto, A., Watanabe, H., Hiraki, Y. & Kondoh, G. Scleraxis is required for maturation of tissue domains for proper integration of the musculoskeletal system. *Nat. Publ. Gr.* 1–16 (2017). doi:10.1038/srep45010

43.	Chen, X. *et al.* promote the commitment of human ES cells derived MSCs to tenocytes. 1–9 (2012). doi:10.1038/srep00977

44.	Wu, F. & Nerlich, M. Tendons basic biology Tendon injuries: basic science and new repair proposals. *Efort Open Rev.* (2017). doi:10.1302/2058-5241.2.160075

45.	Bayer, M. L. *et al.* The initiation of embryonic-like collagen fibrillogenesis by adult human tendon fibroblasts when cultured under tension. *Biomaterials* (2010). doi:10.1016/j.biomaterials.2010.02.062

46.	Zhang, G. *et al.* Development of tendon structure and function: regulation of collagen fibrillogenesis. *J. Musculoskelet. Neuronal Interact.* (2005).

47.	Kostrominova, T. Y. & Brooks, S. V. Age-related changes in structure and extracellular matrix protein expression levels in rat tendons. *Age (Omaha).* (2013). doi:10.1007/s11357-013-9514-2

48.	Brumitt, J. & Cuddeford, T. CURRENT CONCEPTS OF MUSCLE AND TENDON ADAPTATION TO STRENGTH AND CONDITIONING. *Int. J. Sports Phys. Ther.* (2015).

49.	Robinson, K. A. *et al.* Decorin and biglycan are necessary for maintaining collagen fibril structure, fiber realignment, and mechanical properties of mature tendons. *Matrix Biol.* (2017). doi:10.1016/j.matbio.2017.08.004

50.	Shetye, S. S. *et al.* Collagen V haploinsufficiency results in deficient mechanical and structural recovery of injured mouse patellar tendons. *J. Orthop. Res.* (2017).

51.	Spiess, K. & Zorn, T. M. T. Collagen types I, III, and V constitute the thick collagen fibrils of the mouse decidua. *Microsc. Res. Tech.* (2007). doi:10.1002/jemt.20381

52.	Hulmes, D. J., Wess, T. J., Prockop, D. J. & Fratzl, P. Radial packing, order, and disorder in collagen fibrils. *Biophys. J.* (1995). doi:10.1016/S0006-3495(95)80391-7

53.	Ireland, D. *et al.* Multiple changes in gene expression in chronic human Achilles tendinopathy. *Matrix Biol.* (2001). doi:10.1016/S0945-053X(01)00128-7

54. Deshmukh, S., Dive, A., Moharil, R. & Munde, P. Enigmatic insight into collagen. *J. Oral Maxillofac. Pathol.* (2016). doi:10.4103/0973-029x.185932

55. Anderson, J. C. & Eriksson, C. Piezoelectric properties of dry and wet bone. *Nature* **227**, 491–492 (1970).

56. Denning, D. *et al.* Electromechanical properties of dried tendon and isoelectrically focused collagen hydrogels. *Acta Biomater.* **8**, 3073–3079 (2012).

57. Denning, D., Paukshto, M. V., Habelitz, S. & Rodriguez, B. J. Piezoelectric properties of aligned collagen membranes. *J. Biomed. Mater. Res. - Part B Appl. Biomater.* **102**, 284–292 (2014).

58. Bassett, C. A. L. Biologic significance of piezoelectricity. *Calcif. Tissue Res.* **1**, 252–272 (1967).

59. Vasquez-Sancho, F., Abdollahi, A., Damjanovic, D. & Catalan, G. Flexoelectricity in Bones. *Adv. Mater.* **30**, 1–5 (2018).

60. Yao, L., Bestwick, C. S., Bestwick, L. A., Maffulli, N. & Aspden, R. M. Phenotypic Drift in Human Tenocyte Culture. *Tissue Eng.* (2006). doi:10.1089/ten.2006.12.ft-90

61. Zhu, J. *et al.* The regulation of phenotype of cultured tenocytes by microgrooved surface structure. *Biomaterials* **31**, 6952–6958 (2010).

62. Shukunami, C. *et al.* Scleraxis is a transcriptional activator that regulates the expression of Tenomodulin, a marker of mature tenocytes and ligamentocytes. *Sci. Rep.* (2018). doi:10.1038/s41598-018-21194-3

63. Berthet, E. *et al.* Smad3 binds Scleraxis and Mohawk and regulates tendon matrix organisation. *J. Orthop. Res.* (2013). doi:10.1002/jor.22382

64. Tan, S. L. *et al.* The effect of growth differentiation factor-5 (GDF-5) on the proliferation and tenogenic differentiation potential of human mesenchymal stem cells in vitro. *J. Univ. Malaya Med. Cent.* (2013).

65. Killian, M. L. & Thomopoulos, S. Scleraxis is required for the development of a functional tendon enthesis. *FASEB J.* (2016). doi:10.1096/fj.14-258236

66. Brown, D., Wagner, D., Li, X., Richardson, J. A. & Olson, E. N. Dual role of the basic helix-loop-helix transcription factor scleraxis in mesoderm formation and chondrogenesis during mouse embryogenesis. *Development* (1999).

67. Sharma, P. & Maffulli, N. Biology of tendon injury: Healing, modeling and remodeling. *Journal of Musculoskeletal Neuronal Interactions* (2006).

68. Nourissat, G., Berenbaum, F. & Duprez, D. Tendon injury: from biology to tendon

repair. *Nat. Rev. Rheumatol.* **11**, 223–233 (2015).

69. Bi, Y. *et al.* Identification of tendon stem/progenitor cells and the role of the extracellular matrix in their niche. *Nat. Med.* **13**, 1219–1227 (2007).

70. Lui, P. P. Y. Identity of tendon stem cells - how much do we know? *Journal of Cellular and Molecular Medicine* (2013). doi:10.1111/jcmm.12007

71. Yin, Z. *et al.* Single-cell analysis reveals a nestin+ tendon stem/progenitor cell population with strong tenogenic potentiality. *Sci. Adv.* **2**, 1–15 (2016).

72. Ruprecht, V. *et al.* How cells respond to environmental cues – insights from bio-functionalized substrates. *J. Cell Sci.* (2017). doi:10.1242/jcs.196162

73. Gupta, M. *et al.* Micropillar substrates: A tool for studying cell mechanobiology. *Methods Cell Biol.* (2015). doi:10.1016/bs.mcb.2014.10.009

74. Kshitiz *et al.* Control of stem cell fate and function by engineering physical microenvironments. *Integrative Biology (United Kingdom)* (2012). doi:10.1039/c2ib20080e

75. Guilak, F. *et al.* Control of Stem Cell Fate by Physical Interactions with the Extracellular Matrix. *Cell Stem Cell* (2009). doi:10.1016/j.stem.2009.06.016

76. Frantz, C., Stewart, K. M. & Weaver, V. M. The extracellular matrix at a glance. *J. Cell Sci.* (2010). doi:10.1242/jcs.023820

77. Fehrer, C. *et al.* Reduced oxygen tension attenuates differentiation capacity of human mesenchymal stem cells and prolongs their lifespan. *Aging Cell* (2007). doi:10.1111/j.1474-9726.2007.00336.x

78. Li, P. *et al.* Role of the ERK1/2 signaling pathway in osteogenesis of rat tendon-derived stem cells in normoxic and hypoxic cultures. *Int. J. Med. Sci.* (2016). doi:10.7150/ijms.16045

79. Reinwald, Y. & El Haj, A. J. Hydrostatic pressure in combination with topographical cues affects the fate of bone marrow-derived human mesenchymal stem cells for bone tissue regeneration. *J. Biomed. Mater. Res. - Part A* (2018). doi:10.1002/jbm.a.36267

80. Docheva, D., Müller, S. A., Majewski, M. & Evans, C. H. Biologics for tendon repair. *Adv. Drug Deliv. Rev.* **84**, 222–239 (2015).

81. Khan, K. M. & Scott, A. Mechanotherapy: How physical therapists' prescription of exercise promotes tissue repair. *British Journal of Sports Medicine* (2009). doi:10.1136/bjsm.2008.054239

82. Wang, Z. *et al.* Functional regeneration of tendons using scaffolds with physical

anisotropy engineered via microarchitectural manipulation. *Sci. Adv.* (2018). doi:10.1126/sciadv.aat4537

83. Biggs, M. J. P. *et al.* Interactions with nanoscale topography: Adhesion quantification and signal transduction in cells of osteogenic and multipotent lineage. *J. Biomed. Mater. Res. - Part A* (2009). doi:10.1002/jbm.a.32196

84. Levin, M. Bioelectric mechanisms in regeneration: Unique aspects and future perspectives. *Semin. Cell Dev. Biol.* (2009). doi:10.1016/j.semcdb.2009.04.013

85. Tseng, A. S. & Levin, M. Transducing Bioelectric Signals into Epigenetic Pathways During Tadpole Tail Regeneration. *Anatomical Record* (2012). doi:10.1002/ar.22495

86. Sundelacruz, S., Li, C., Choi, Y. J., Levin, M. & Kaplan, D. L. Bioelectric modulation of wound healing in a 3D invitro model of tissue-engineered bone. *Biomaterials* (2013). doi:10.1016/j.biomaterials.2013.05.040

87. Engler, A. J., Sen, S., Sweeney, H. L. & Discher, D. E. Matrix elasticity directs stem cell lineage specification. *Cell* (2006). doi:10.1016/j.cell.2006.06.044

88. Mamidi, A. *et al.* Mechanosignalling via integrins directs fate decisions of pancreatic progenitors. *Nature* (2018). doi:10.1038/s41586-018-0762-2

89. Biggs, M. J. P. *et al.* The Functional Response of Mesenchymal Stem Cells to Electron-Beam Patterned Elastomeric Surfaces Presenting Micrometer to Nanoscale Heterogeneous Rigidity. *Adv. Mater.* **29**, 1702119 (2017).

90. Wang, N., Tytell, J. D. & Ingber, D. E. Mechanotransduction at a distance: Mechanically coupling the extracellular matrix with the nucleus. *Nat. Rev. Mol. Cell Biol.* **10**, 75–82 (2009).

91. Lin, X., Shi, Y., Cao, Y. & Liu, W. Recent progress in stem cell differentiation directed by material and mechanical cues. *Biomed. Mater.* (2016). doi:10.1088/1748-6041/11/1/014109

92. Hao, J. *et al.* Mechanobiology of mesenchymal stem cells: Perspective into mechanical induction of MSC fate. *Acta Biomaterialia* (2015). doi:10.1016/j.actbio.2015.04.008

93. Molloy, T., Wang, Y. & Murrell, G. A. C. The roles of growth factors in tendon and ligament healing. *Sports Medicine* (2003). doi:10.2165/00007256-200333050-00004

94. Caliari, S. R. & Harley, B. A. C. The effect of anisotropic collagen-GAG scaffolds and growth factor supplementation on tendon cell recruitment, alignment, and metabolic activity. *Biomaterials* (2011). doi:10.1016/j.biomaterials.2011.04.021

95. Kjær, M. *et al.* From mechanical loading to collagen synthesis, structural changes and function in human tendon. *Scandinavian Journal of Medicine and Science in Sports* (2009). doi:10.1111/j.1600-0838.2009.00986.x

96. Zhao, M. *et al.* Electrical signals control wound healing through phosphatidylinositol-3-OH kinase-γ and PTEN. *Nature* (2006). doi:10.1038/nature04925

97. Ciombor, D. M. & Aaron, R. K. The role of electrical stimulation in bone repair. *Foot and Ankle Clinics* (2005). doi:10.1016/j.fcl.2005.06.006

98. Tandon, B., Blaker, J. J. & Cartmell, S. H. Piezoelectric materials as stimulatory biomedical materials and scaffolds for bone repair. *Acta Biomaterialia* (2018). doi:10.1016/j.actbio.2018.04.026

99. Mollon, B., Da Silva, V., Busse, J. W., Einhorn, T. A. & Bhandari, M. Electrical stimulation for long-bone fracture-healing: A meta-analysis of randomized controlled trials. *Journal of Bone and Joint Surgery - Series A* (2008). doi:10.2106/JBJS.H.00111

100. Yuan, X., Arkonac, D. E., Chao, P. H. G. & Vunjak-Novakovic, G. Electrical stimulation enhances cell migration and integrative repair in the meniscus. *Sci. Rep.* (2015). doi:10.1038/srep03674

101. Kloth, L. C. Electrical stimulation for wound healing: A review of evidence from in vitro studies, animal experiments, and clinical trials. *International Journal of Lower Extremity Wounds* (2005). doi:10.1177/1534734605275733

102. Fukada, E. & Yasuda, I. On the Piezoelectric Effect of Bone. *J. Phys. Soc. Japan* (1957). doi:10.1143/JPSJ.12.1158

103. Brighton, C. T., Jensen, L., Pollack, S. R., Tolin, B. S. & Clark, C. C. Proliferative and synthetic response of bovine growth plate chondrocytes to various capacitively coupled electrical fields. *J. Orthop. Res.* (1989). doi:10.1002/jor.1100070519

104. Armstrong, P. F., Brighton, C. T. & Star, A. M. Capacitively coupled electrical stimulation of bovine growth plate chondrocytes grown in pellet form. *J. Orthop. Res.* (1988). doi:10.1002/jor.1100060214

105. Wang, W., Wang, Z., Zhang, G., Clark, C. C. & Brighton, C. T. Up-regulation of chondrocyte matrix genes and products by electric fields. in *Clinical Orthopaedics and Related Research* (2004). doi:10.1097/01.blo.0000143837.53434.5c

106. Walther, M., Mayer, F., Kafka, W. & Schütze, N. Effects of weak, low-frequency pulsed electromagnetic fields (BEMER type) on gene expression of human

mesenchymal stem cells and chondrocytes: An in vitro study. *Electromagn. Biol. Med.* (2007). doi:10.1080/15368370701580814

107. Kwon, H. J., Lee, G. S. & Chun, H. Electrical stimulation drives chondrogenesis of mesenchymal stem cells in the absence of exogenous growth factors. *Sci. Rep.* **6**, 1–13 (2016).

108. Mathews, J. & Levin, M. The body electric 2.0: recent advances in developmental bioelectricity for regenerative and synthetic bioengineering. *Current Opinion in Biotechnology* (2018). doi:10.1016/j.copbio.2018.03.008

109. McLaughlin, K. A. & Levin, M. Bioelectric signaling in regeneration: Mechanisms of ionic controls of growth and form. *Dev. Biol.* **433**, 177–189 (2018).

110. Tseng, A. & Levin, M. Cracking the bioelectric code: Probing endogenous ionic controls of pattern formation. *Commun. Integr. Biol.* (2013). doi:10.4161/cib.22595

111. Pai, V. P. *et al.* HCN2 Rescues brain defects by enforcing endogenous voltage pre-patterns. *Nat. Commun.* **9**, 998 (2018).

112. Levin, M. Molecular bioelectricity: how endogenous voltage potentials control cell behavior and instruct pattern regulation in vivo. *Mol. Biol. Cell* **25**, 3835–50 (2014).

113. Pietak, A. & Levin, M. Exploring Instructive Physiological Signaling with the Bioelectric Tissue Simulation Engine. *Front. Bioeng. Biotechnol.* **4**, (2016).

114. Zhao, M. Electrical fields in wound healing-An overriding signal that directs cell migration. *Seminars in Cell and Developmental Biology* (2009). doi:10.1016/j.semcdb.2008.12.009

115. Huang, Y., Li, Y., Chen, J., Zhou, H. & Tan, S. Electrical Stimulation Elicits Neural Stem Cells Activation: New Perspectives in CNS Repair. *Front. Hum. Neurosci.* (2015). doi:10.3389/fnhum.2015.00586

116. Martinac, B. The ion channels to cytoskeleton connection as potential mechanism of mechanosensitivity. *Biochim. Biophys. Acta - Biomembr.* **1838**, 682–691 (2014).

117. Everaerts, W., Nilius, B. & Owsianik, G. The vanilloid transient receptor potential channel TRPV4: From structure to disease. *Progress in Biophysics and Molecular Biology* (2010). doi:10.1016/j.pbiomolbio.2009.10.002

118. Moran, M. M., McAlexander, M. A., Bíró, T. & Szallasi, A. Transient receptor potential channels as therapeutic targets. *Nature Reviews Drug Discovery* (2011). doi:10.1038/nrd3456

119. Earley, S. & Brayden, J. E. Transient Receptor Potential Channels in the Vasculature. *Physiol. Rev.* (2015). doi:10.1152/physrev.00026.2014

120. Liedtke, W. B. *TRPV Channels' Function in Osmo- and Mechanotransduction. TRP Ion Channel Function in Sensory Transduction and Cellular SignalingCascades* (2007).

121. Okumura, R. *et al.* The odontoblast as a sensory receptor cell? The expression of TRPV1 (VR-1) channels. *Arch. Histol. Cytol.* (2006). doi:10.1679/aohc.68.251

122. Qi, Y. *et al.* Uniaxial cyclic stretch stimulates TRPV4 to induce realignment of human embryonic stem cell-derived cardiomyocytes. *J. Mol. Cell. Cardiol.* (2015). doi:10.1016/j.yjmcc.2015.08.005

123. Goswami, R. *et al.* TRPV4 calcium-permeable channel is a novel regulator of oxidized LDL-induced macrophage foam cell formation. *Free Radic. Biol. Med.* (2017). doi:10.1016/j.freeradbiomed.2017.06.004

124. Suzuki, T. *et al.* TRPV4 (transient receptor potential vanilloid 4), a mechanosensor for bone is required for the maintenance of bone mineral density of mandible exposed to occlusal force. *J. Bone Miner. Res.* (2010).

125. Saotome, K. *et al.* Structure of the mechanically activated ion channel Piezo1. *Nature* (2018). doi:10.1038/nature25453

126. etem, ebru *et al.* The increased expression of Piezo1 and Piezo2 ion channels in human and mouse bladder carcinoma. *Adv. Clin. Exp. Med.* (2018). doi:10.17219/acem/71080

127. Gao, Q., Cooper, P. R., Walmsley, A. D. & Scheven, B. A. Role of Piezo Channels in Ultrasound-stimulated Dental Stem Cells. *J. Endod.* (2017). doi:10.1016/j.joen.2017.02.022

128. Song, Y. *et al.* The Mechanosensitive Ion Channel Piezo Inhibits Axon Regeneration. *Neuron* (2019). doi:10.1016/j.neuron.2019.01.050

129. He, L., Si, G., Huang, J., Samuel, A. D. T. & Perrimon, N. Mechanical regulation of stem-cell differentiation by the stretch-activated Piezo channel. *Nature* **555**, 103–106 (2018).

130. Lavagnino, M., Arnoczky, S. P., Egerbacher, M., Gardner, K. L. & Burns, M. E. Isolated fibrillar damage in tendons stimulates local collagenase mRNA expression and protein synthesis. *J. Biomech.* (2006). doi:10.1016/j.jbiomech.2005.08.008

131. Maeda, T. *et al.* Conversion of mechanical force into TGF-β-mediated biochemical signals. *Curr. Biol.* (2011). doi:10.1016/j.cub.2011.04.007

132. Chen, Y., Ju, L., Rushdi, M., Ge, C. & Zhu, C. Receptor-mediated cell mechanosensing. *Mol. Biol. Cell* (2017). doi:10.1091/mbc.e17-04-0228

133. Elosegui-Artola, A., Trepat, X. & Roca-Cusachs, P. Control of Mechanotransduction by Molecular Clutch Dynamics. *Trends Cell Biol.* (2018). doi:10.1016/j.tcb.2018.01.008

134. Massia, S. P. & Hubbell, J. A. An RGD spacing of 440 nm is sufficient for integrin αvβ3-mediated fibroblast spreading and 140 nm for focal contact and stress fiber formation. *J. Cell Biol.* (1991). doi:10.1083/jcb.114.5.1089

135. Oria, R. *et al.* Force loading explains spatial sensing of ligands by cells. *Nature* (2017). doi:10.1038/nature24662

136. Salmeron-Sanchez, M. *et al.* Molecular clutch drives cell response to surface viscosity. *Proc. Natl. Acad. Sci.* (2018). doi:10.1073/pnas.1710653115

137. Fernandez-Yague, M. A. *et al.* Biomimetic approaches in bone tissue engineering: Integrating biological and physicomechanical strategies. *Advanced Drug Delivery Reviews* **84**, 1–29 (2015).

138. Galloway, M. T., Lalley, A. L. & Shearn, J. T. The role of mechanical loading in tendon development, maintenance, injury, and repair. *Journal of Bone and Joint Surgery - Series A* (2013). doi:10.2106/JBJS.L.01004

139. Wang, T. *et al.* Bioreactor Design for Tendon/Ligament Engineering. *Tissue Eng. Part B Rev.* **19**, 133–146 (2013).

140. Thomopoulos, S., Parks, W. C., Rifkin, D. B. & Derwin, K. A. Mechanisms of tendon injury and repair. in *Journal of Orthopaedic Research* (2015). doi:10.1002/jor.22806

141. Screen, H. R. C., Berk, D. E., Kadler, K. E., Ramirez, F. & Young, M. F. Tendon functional extracellular matrix. in *Journal of Orthopaedic Research* (2015). doi:10.1002/jor.22818

142. Xu, B. *et al.* RhoA/ROCK, cytoskeletal dynamics, and focal adhesion kinase are required for mechanical stretch-induced tenogenic differentiation of human mesenchymal stem cells. *J. Cell. Physiol.* **227**, 2722–2729 (2012).

143. Mackley, J. R., Ando, J., Herzyk, P. & Winder, S. J. Phenotypic responses to mechanical stress in fibroblasts from tendon, cornea and skin. *Biochem. J.* (2006). doi:10.1042/bj20060057

144. Fong, K. D. *et al.* Microarray analysis of mechanical shear effects on flexor tendon cells. *Plast. Reconstr. Surg.* (2005). doi:10.1097/01.prs.0000182345.86453.4f

145. Deng, D. *et al.* Engineering human neo-tendon tissue in vitro with human dermal fibroblasts under static mechanical strain. *Biomaterials* (2009).

doi:10.1016/j.biomaterials.2009.08.054

146. Maharam, E. *et al.* Rho/Rock signal transduction pathway is required for MSC tenogenic differentiation. *Bone Res.* **3**, (2015).

147. Lin, J. *et al.* Acta Biomaterialia Cell-material interactions in tendon tissue engineering. *Acta Biomater.* 1–11 (2018). doi:10.1016/j.actbio.2018.01.012

148. Robertson, B. D. & Sawicki, G. S. Unconstrained muscle-tendon workloops indicate resonance tuning as a mechanism for elastic limb behavior during terrestrial locomotion. *Proc. Natl. Acad. Sci.* (2015). doi:10.1073/pnas.1500702112

149. Lau, E. *et al.* Effect of low-magnitude, high-frequency vibration on osteogenic differentiation of rat mesenchymal stromal cells. *J. Orthop. Res.* (2011). doi:10.1002/jor.21334

150. Curtis, A. S. G. *et al.* Cell interactions at the nanoscale: Piezoelectric stimulation. *IEEE Trans. Nanobioscience* (2013). doi:10.1109/TNB.2013.2257837

151. Tsimbouri, P. M. *et al.* Stimulation of 3D osteogenesis by mesenchymal stem cells using a nanovibrational bioreactor. *Nat. Biomed. Eng.* (2017). doi:10.1038/s41551-017-0127-4

152. Miller, S. L. The mechanism of synthesis of amino acids by electric discharges. *BBA - Biochim. Biophys. Acta* (1957). doi:10.1016/0006-3002(57)90366-9

153. Pietak, A. & Levin, M. Bioelectrical control of positional information in development and regeneration: A review of conceptual and computational advances. *Progress in Biophysics and Molecular Biology* (2018). doi:10.1016/j.pbiomolbio.2018.03.008

154. Akai, M., Oda, H., Shirasaki, Y. & Tateishi, T. Electrical stimulation of ligament healing. An experimental study of the patellar ligament of rabbits. *Clin.Orthop.Relat Res.* (1988).

155. Sirohi, J. & Chopra, I. Fundamental understanding of piezoelectric strain sensors. *J. Intell. Mater. Syst. Struct.* (2000). doi:10.1106/8BFB-GC8P-XQ47-YCQ0

156. Ramadan, K. S., Sameoto, D. & Evoy, S. A review of piezoelectric polymers as functional materials for electromechanical transducers. *Smart Mater. Struct.* **23**, 033001 (2014).

157. Maxwell, J. C. A treatise on electricity and magnetism, Vol. II. *Journal of the Franklin Institute* (1954). doi:10.1017/CBO9780511709333

158. Wang, Z. L. On Maxwell's displacement current for energy and sensors: the origin of nanogenerators. *Mater. Today* **20**, 74–82 (2017).

159. Roche, J. The present status of Maxwell's displacement current. *Eur. J. Phys.* (1998). doi:10.1088/0143-0807/19/2/009

160. Kawai, H. The Piezoelectricity of Poly (vinylidene Fluoride). *Jpn. J. Appl. Phys.* **8**, 975–976 (1969).

161. Motamedi, A. S., Mirzadeh, H., Hajiesmaeilbaigi, F., Bagheri-Khoulenjani, S. & Shokrgozar, M. A. Piezoelectric electrospun nanocomposite comprising Au NPs/PVDF for nerve tissue engineering. *J. Biomed. Mater. Res. Part A* **105**, 1984–1993 (2017).

162. Yu, Y. *et al.* Biocompatibility and in vivo operation of implantable mesoporous PVDF-based nanogenerators. *Nano energy* **27**, 275–281 (2016).

163. Sobreiro-Almeida, R. *et al.* Human Mesenchymal Stem Cells Growth and Osteogenic Differentiation on Piezoelectric Poly(vinylidene fluoride) Microsphere Substrates. *Int. J. Mol. Sci.* **18**, 2391 (2017).

164. Lee, Y.-S., Wu, S., Arinzeh, T. L. & Bunge, M. B. Transplantation of Schwann Cells Inside PVDF-TrFE Conduits to Bridge Transected Rat Spinal Cord Stumps to Promote Axon Regeneration Across the Gap. *J. Vis. Exp.* (2017). doi:10.3791/56077

165. Sharma, T., Aroom, K., Naik, S., Gill, B. & Zhang, J. X. J. Flexible thin-film PVDF-TrFE based pressure sensor for smart catheter applications. *Ann. Biomed. Eng.* **41**, 744–51 (2013).

166. Martins, P., Lopes, A. C. & Lanceros-Mendez, S. Electroactive phases of poly(vinylidene fluoride): Determination, processing and applications. *Prog. Polym. Sci.* **39**, 683–706 (2014).

167. Weber, N., Lee, Y.-S., Shanmugasundaram, S., Jaffe, M. & Arinzeh, T. L. Characterisation and in vitro cytocompatibility of piezoelectric electrospun scaffolds. *Acta Biomater.* **6**, 3550–3556 (2010).

168. Tseng, H. J., Tian, W. C. & Wu, W. J. P(VDF-TrFE) polymer-based thin films deposited on stainless steel substrates treated using water dissociation for flexible tactile sensor development. *Sensors (Switzerland)* **13**, 14777–14796 (2013).

169. Hitscherich, P. *et al.* The effect of PVDF-TrFE scaffolds on stem cell derived cardiovascular cells. *Biotechnol. Bioeng.* **113**, 1577–85 (2016).

170. Cheng, X. *et al.* Implantable and self-powered blood pressure monitoring based on a piezoelectric thinfilm: Simulated, in vitro and in vivo studies. *Nano Energy* **22**, 453–460 (2016).

171. Persano, L. *et al.* High performance piezoelectric devices based on aligned arrays of

nanofibers of poly(vinylidenefluoride-co-trifluoroethylene). *Nat. Commun.* **4**, 1633 (2013).

172. Chang, C., Tran, V. H., Wang, J., Fuh, Y. K. & Lin, L. Direct-write piezoelectric polymeric nanogenerator with high energy conversion efficiency. *Nano Lett.* (2010). doi:10.1021/nl9040719

173. Pan, C. T. *et al.* Significant piezoelectric and energy harvesting enhancement of poly(vinylidene fluoride)/polypeptide fiber composites prepared through near-field electrospinning. *J. Mater. Chem. A* (2015). doi:10.1039/c5ta00147a

174. Dagdeviren, C. *et al.* Conformal piezoelectric systems for clinical and experimental characterisation of soft tissue biomechanics. *Nat. Mater.* **14**, 728–736 (2015).

175. Dadsetan, M. *et al.* The effects of fixed electrical charge on chondrocyte behavior. *Acta Biomater.* (2011). doi:10.1016/j.actbio.2011.01.012

176. Kitsara, M. *et al.* Permanently hydrophilic, piezoelectric PVDF nanofibrous scaffolds promoting unaided electromechanical stimulation on osteoblasts. *Nanoscale* (2019). doi:10.1039/c8nr10384d

177. Klee, D. *et al.* Surface modification of poly(vinylidenefluoride) to improve the osteoblast adhesion. *Biomaterials* **24**, 3663–3670 (2003).

178. Defteralı, Ç. *et al.* In Vitro Evaluation of Biocompatibility of Uncoated Thermally Reduced Graphene and Carbon Nanotube-Loaded PVDF Membranes with Adult Neural Stem Cell-Derived Neurons and Glia. *Front. Bioeng. Biotechnol.* (2016). doi:10.3389/fbioe.2016.00094

179. Lee, Y.-S., Collins, G. & Livingston Arinzeh, T. Neurite extension of primary neurons on electrospun piezoelectric scaffolds. *Acta Biomater.* **7**, 3877–3886 (2011).

180. Ribeiro, C. *et al.* Dynamic piezoelectric stimulation enhances osteogenic differentiation of human adipose stem cells. *J. Biomed. Mater. Res. Part A* n/a-n/a (2014). doi:10.1002/jbm.a.35368

181. Parssinen, J. *et al.* Enhancement of adhesion and promotion of osteogenic differentiation of human adipose stem cells by poled electroactive poly(vinylidene fluoride). *J. Biomed. Mater. Res. - Part A* (2015). doi:10.1002/jbm.a.35234

182. Pereira, J. D. A. S. *et al.* Biomaterials from blends of fluoropolymers and corn starch - Implant and structural aspects. *Mater. Sci. Eng. C* (2014). doi:10.1016/j.msec.2013.12.008

183. Ribeiro, C. *et al.* Electroactive poly(vinylidene fluoride)-based structures for

advanced applications. *Nat. Protoc.* **13**, 681–704 (2018).

184. Genchi, G. G. *et al.* P(VDF-TrFE)/BaTiO3 Nanoparticle Composite Films Mediate Piezoelectric Stimulation and Promote Differentiation of SH-SY5Y Neuroblastoma Cells. *Adv. Healthc. Mater.* **5**, 1808–20 (2016).

185. Genchi, G. G. *et al.* Ultrasound-activated piezoelectric P(VDF-TrFE)/boron nitride nanotube composite films promote differentiation of human SaOS-2 osteoblast-like cells. *Nanomedicine* **14**, 2421–2432 (2018).

186. Fang, F., Shan, S. C. & Yang, W. Magnetoelectric coupling of Terfenol-D/P(VDF-TrFe)/Terfenol-D laminates mediated by crystallite size of electroactive polymer. *Acta Mech.* **224**, 1169–1174 (2013).

187. Brito-Pereira, R., Ribeiro, C., Lanceros-Mendez, S. & Martins, P. Magnetoelectric response on Terfenol-D/ P(VDF-TrFE) two-phase composites. *Compos. Part B Eng.* **120**, 97–102 (2017).

188. Cha, S. *et al.* Porous PVDF as effective sonic wave driven nanogenerators. *Nano Lett.* (2011). doi:10.1021/nl202208n

189. Cho, K. Y. *et al.* Enhanced Electrical Properties of PVDF-TrFE Nanocomposite for Actuator Application. *Key Eng. Mater.* (2014). doi:10.4028/www.scientific.net/KEM.605.335

190. Guo, W. *et al.* Self-Powered Electrical Stimulation for Enhancing Neural Differentiation of Mesenchymal Stem Cells on Graphene-Poly(3,4-ethylenedioxythiophene) Hybrid Microfibers. *ACS Nano* (2016). doi:10.1021/acsnano.6b00200

191. Zheng, Q. *et al.* Biodegradable triboelectric nanogenerator as a life-time designed implantable power source. *Sci. Adv.* **2**, e1501478 (2016).

192. Nuccitelli, R. A Role for Endogenous Electric Fields in Wound Healing. *Current Topics in Developmental Biology* (2003). doi:10.1016/S0070-2153(03)58001-2

193. Ladoux, B. & Mège, R.-M. Mechanobiology of collective cell behaviours. *Nat. Rev. Mol. Cell Biol.* **18**, 743–757 (2017).

194. Iskratsch, T., Wolfenson, H. & Sheetz, M. P. Appreciating force and shape — the rise of mechanotransduction in cell biology. *Nat. Rev. Mol. Cell Biol.* **15**, 825–833 (2014).

195. Xia, S. & Kanchanawong, P. Nanoscale mechanobiology of cell adhesions. *Semin. Cell Dev. Biol.* **71**, 53–67 (2017).

196. Turner, C. H. *et al.* Mechanobiology of the skeleton. *Sci. Signal.* **2**, pt3 (2009).

197. Li, Q. *et al.* Structural mechanism of voltage-dependent gating in an isolated voltage-sensing domain. *Nat. Struct. Mol. Biol.* (2014). doi:10.1038/nsmb.2768

198. Wang, J., Tian, L., Chen, N., Ramakrishna, S. & Mo, X. The cellular response of nerve cells on poly-l-lysine coated PLGA-MWCNTs aligned nanofibers under electrical stimulation. *Mater. Sci. Eng. C. Mater. Biol. Appl.* **91**, 715–726 (2018).

199. Mario Cheong, G. L. *et al.* Conductive hydrogels with tailored bioactivity for implantable electrode coatings. *Acta Biomater.* **10**, 1216–26 (2014).

200. Cui, H. *et al.* In vitro studies on regulation of osteogenic activities by electrical stimulus on biodegradable electroactive polyelectrolyte multilayers. *Biomacromolecules* **15**, 3146–57 (2014).

201. Gilmore, K. J. *et al.* Skeletal muscle cell proliferation and differentiation on polypyrrole substrates doped with extracellular matrix components. *Biomaterials* **30**, 5292–304 (2009).

202. Chen, Q.-Q. *et al.* Electrical field stimulation induces cardiac fibroblast proliferation through the calcineurin-NFAT pathway. *Can. J. Physiol. Pharmacol.* **90**, 1611–22 (2012).

203. Seo, G. Y. *et al.* A Novel Synthetic Material, BMM, Accelerates Wound Repair by Stimulating Re-Epithelialization and Fibroblast Activation. *Int. J. Mol. Sci.* **19**, 1164 (2018).

204. Head, B. P., Patel, H. H. & Insel, P. A. Interaction of membrane/lipid rafts with the cytoskeleton: impact on signaling and function: membrane/lipid rafts, mediators of cytoskeletal arrangement and cell signaling. *Biochim. Biophys. Acta* **1838**, 532–45 (2014).

205. Yang, G. *et al.* Regulation of adipose-tissue-derived stromal cell orientation and motility in 2D- and 3D-cultures by direct-current electrical field. *Dev. Growth Differ.* **59**, 70–82 (2017).

206. Greco, F. *et al.* Microwrinkled conducting polymer interface for anisotropic multicellular alignment. *ACS Appl. Mater. Interfaces* **5**, 573–84 (2013).

207. Serena, E. *et al.* Electrical stimulation of human embryonic stem cells: Cardiac differentiation and the generation of reactive oxygen species. *Exp. Cell Res.* **315**, 3611–3619 (2009).

208. Das, S. R. *et al.* Electrical Differentiation of Mesenchymal Stem Cells into Schwann-Cell-Like Phenotypes Using Inkjet-Printed Graphene Circuits. *Adv. Healthc. Mater.* **6**, 1601087 (2017).

209. Wu, Z. *et al.* Mechanosensory hair cells express two molecularly distinct mechanotransduction channels. *Nat. Neurosci.* **20**, 24–33 (2017).

210. Cox, C. D., Wann, K. T. & Martinac, B. Selectivity mechanisms in MscS-like channels. *Channels* **8**, 5–12 (2014).

211. Lacroix, J. J., Botello-Smith, W. M. & Luo, Y. Probing the gating mechanism of the mechanosensitive channel Piezo1 with the small molecule Yoda1. *Nat. Commun.* **9**, 2029 (2018).

212. Zilly, F. E. *et al.* Ca 2+ induces clustering of membrane proteins in the plasma membrane via electrostatic interactions. *EMBO J.* (2011). doi:10.1038/emboj.2011.53

213. Yang, W. P., Onuma, E. K. & Hui, S. W. Response of C3H/10T1/2 fibroblasts to an external steady electric field stimulation. Reorientation, shape change, ConA receptor and intramembranous particle distribution and cytoskeleton reorganisation. *Exp. Cell Res.* **155**, 92–104 (1984).

214. Vacek, T. P. *et al.* Electrical stimulation of cardiomyocytes activates mitochondrial matrix metalloproteinase causing electrical remodeling. *Biochem. Biophys. Res. Commun.* **404**, 762–6 (2011).

215. Titushkin, I. & Cho, M. Regulation of cell cytoskeleton and membrane mechanics by electric field: role of linker proteins. *Biophys. J.* **96**, 717–28 (2009).

216. Liu, L. *et al.* Mechanoresponsive stem cells to target cancer metastases through biophysical cues. *Sci. Transl. Med.* (2017). doi:10.1126/scitranslmed.aan2966

217. Isaksson, H., Wilson, W., van Donkelaar, C. C., Huiskes, R. & Ito, K. Comparison of biophysical stimuli for mechano-regulation of tissue differentiation during fracture healing. *J. Biomech.* (2006). doi:10.1016/j.jbiomech.2005.01.037

218. Pruitt, B. L., Dunn, A. R., Weis, W. I. & Nelson, W. J. Mechano-Transduction: From Molecules to Tissues. *PLoS Biol.* (2014). doi:10.1371/journal.pbio.1001996

219. Sauer, H. *et al.* DC electrical field-induced c-fos expression and growth stimulation in multicellular prostate cancer spheroids. *Br. J. Cancer* **75**, 1481–8 (1997).

220. Ruffini, G. *et al.* Transcranial current brain stimulation (tCS): models and technologies. *IEEE Trans. Neural Syst. Rehabil. Eng.* **21**, 333–45 (2013).

221. Zhao, H., Steiger, A., Nohner, M. & Ye, H. Specific Intensity Direct Current (DC) Electric Field Improves Neural Stem Cell Migration and Enhances Differentiation towards βIII-Tubulin+ Neurons. *PLoS One* **10**, e0129625 (2015).

222. Wartenberg, M., Hescheler, J. & Sauer, H. Electrical fields enhance growth of

cancer spheroids by reactive oxygen species and intracellular Ca2+. *Am. J. Physiol.* **272**, R1677-83 (1997).

223. Yamada, M. *et al.* Electrical Stimulation Modulates Fate Determination of Differentiating Embryonic Stem Cells. *Stem Cells* (2006). doi:10.1634/stemcells.2006-0011

224. Feng, J. F. *et al.* Electrical Guidance of Human Stem Cells in the Rat Brain. *Stem Cell Reports* (2017). doi:10.1016/j.stemcr.2017.05.035

225. Patel, Y. A. & Butera, R. J. Differential fiber-specific block of nerve conduction in mammalian peripheral nerves using kilohertz electrical stimulation. *J. Neurophysiol.* (2015). doi:10.1152/jn.00529.2014

226. Ackermann, D. M., Foldes, E. L., Bhadra, N. & Kilgore, K. L. Nerve conduction block using combined thermoelectric cooling and high frequency electrical stimulation. *J. Neurosci. Methods* (2010). doi:10.1016/j.jneumeth.2010.07.043

227. Kadow-Romacker, A., Hoffmann, J. E., Duda, G., Wildemann, B. & Schmidmaier, G. Effect of mechanical stimulation on osteoblast- and osteoclast-like cells in vitro. *Cells Tissues Organs* (2009). doi:10.1159/000178022

228. Yao, R. & Wong, J. Y. The Effects of Mechanical Stimulation on Controlling and Maintaining Marrow Stromal Cell Differentiation Into Vascular Smooth Muscle Cells. *J. Biomech. Eng.* (2015). doi:10.1115/1.4029255

229. Zhang, C. *et al.* Effects of mechanical vibration on proliferation and osteogenic differentiation of human periodontal ligament stem cells. *Arch. Oral Biol.* (2012). doi:10.1016/j.archoralbio.2012.04.010

230. Tsimbouri, P. M. *et al.* Publisher Correction: Stimulation of 3D osteogenesis by mesenchymal stem cells using a nanovibrational bioreactor. *Nat. Biomed. Eng.* **1**, 1004–1004 (2017).

231. Karode, N., Fitzhenry, L., Matthews, S., Walsh, P. & Coffey, A. Enhancement of the Mechanical Properties of PEBAX Graphene Nanocomposite Using Supercritical Fluid Assisted Extrusion Polymer Processing Technique. *Mater. Sci. Forum* (2017). doi:10.4028/www.scientific.net/MSF.883.75

232. Avrami, M. Kinetics of phase change. I: General theory. *J. Chem. Phys.* (1939). doi:10.1063/1.1750380

233. Avrami, M. Kinetics of phase change. II Transformation-time relations for random distribution of nuclei. *J. Chem. Phys.* (1940). doi:10.1063/1.1750631

234. Avrami, M. Kinetics of Phase Change. *J. Chem. Phys.* (1939). doi:10.1590/S1516-

14392000000300002

235. Avrami, M. Granulation, phase change, and microstructure kinetics of phase change. III. *J. Chem. Phys.* (1941). doi:10.1063/1.1750872

236. Jeziorny, A. Parameters characterizing the kinetics of the non-isothermal crystallization of poly(ethylene terephthalate) determined by d.s.c. *Polymer (Guildf).* (1978). doi:10.1016/0032-3861(78)90060-5

237. Ozawa, T. Kinetics of non-isothermal crystallization. *Polymer (Guildf).* (1971). doi:10.1016/0032-3861(71)90041-3

238. Liu, F. & Yang, G. Effects of anisotropic growth on the deviations from Johnson-Mehl-Avrami kinetics. *Acta Mater.* (2007). doi:10.1016/j.actamat.2006.10.022

239. Lanceros-Méndez, S., Mano, J. F., Costa, A. M. & Schmidt, V. H. FTIR and DSC studies of mechanically deformed β-PVDF films. *J. Macromol. Sci. - Phys.* (2001). doi:10.1081/MB-100106174

240. Fialka, J. & Benes, P. Comparison of Methods for the Measurement of Piezoelectric Coefficients. *IEEE Trans. Instrum. Meas.* **62**, 1047–1057 (2013).

241. Binning, G., Rohrer, H., Gerber, C. & Weibel, E. Surface studies by scanning tunneling microscopy. *Phys. Rev. Lett.* (1982). doi:10.1103/PhysRevLett.49.57

242. Huang, H., Gu, L. & Ozaki, Y. Non-isothermal crystallization and thermal transitions of a biodegradable, partially hydrolyzed poly(vinyl alcohol). *Polymer (Guildf).* (2006). doi:10.1016/j.polymer.2006.03.089

243. Liu, Y., Wang, L., He, Y., Fan, Z. & Li, S. Non-isothermal crystallization kinetics of poly(L-lactide). *Polym. Int.* (2010). doi:10.1002/pi.2894

244. Furukawa, T. Ferroelectric properties of vinylidene fluoride copolymers. *Phase Transitions* (1989). doi:10.1080/01411598908206863

245. Vinogradov, A. & Holloway, F. Electro-mechanical properties of the piezoelectric polymer PVDF. *Ferroelectrics* (1999). doi:10.1080/00150199908230298

246. Martins, P. *et al.* Role of nanoparticle surface charge on the nucleation of the electroactive β-poly(vinylidene fluoride) nanocomposites for sensor and actuator applications. *J. Phys. Chem. C* (2012). doi:10.1021/jp3038768

247. Wang, Y. J. & Kim, D. Crystallinity, morphology, mechanical properties and conductivity study of in situ formed PVdF/LiClO4/TiO2nanocomposite polymer electrolytes. *Electrochim. Acta* (2007). doi:10.1016/j.electacta.2006.09.070

248. Steinhart, M., Senz, S., Wehrspohn, R. B., Gösele, U. & Wendorff, J. H. Curvature-directed crystallization of poly(vinylidene difluoride) in nanotube walls.

Macromolecules (2003). doi:10.1021/ma0260039

249. Cao, Y. *et al.* Bridging tendon defects using autologous tenocyte engineered tendon in a hen model. *Plast. Reconstr. Surg.* (2002). doi:10.1097/00006534-200210000-00011

250. Chen, J. M., Willers, C., Xu, J., Wang, A. & Zheng, M.-H. Autologous Tenocyte Therapy Using Porcine-Derived Bioscaffolds for Massive Rotator Cuff Defect in Rabbits. *Tissue Eng.* (2007). doi:10.1089/ten.2006.0266

251. Spanoudes, K., Gaspar, D., Pandit, A. & Zeugolis, D. I. The biophysical, biochemical, and biological toolbox for tenogenic phenotype maintenance in vitro. *Trends Biotechnol.* **32**, 474–482 (2014).

252. Stoll, C. *et al.* Extracellular matrix expression of human tenocytes in three-dimensional air-liquid and PLGA cultures compared with tendon tissue: Implications for tendon tissue engineering. *J. Orthop. Res.* (2010). doi:10.1002/jor.21109

253. Juncosa-Melvin, N., Matlin, K. S., Holdcraft, R. W., Nirmalanandhan, V. S. & Butler, D. L. Mechanical Stimulation Increases Collagen Type I and Collagen Type III Gene Expression of Stem Cell–Collagen Sponge Constructs for Patellar Tendon Repair. *Tissue Eng.* (2007). doi:10.1089/ten.2006.0339

254. Jiang, C., Shao, L., Wang, Q. & Dong, Y. Repetitive mechanical stretching modulates transforming growth factor-β induced collagen synthesis and apoptosis in human patellar tendon fibroblasts. *Biochem. Cell Biol.* (2012). doi:10.1139/o2012-024

255. Kilian, K. A., Bugarija, B., Lahn, B. T. & Mrksich, M. Geometric cues for directing the differentiation of mesenchymal stem cells. *Proc. Natl. Acad. Sci. U. S. A.* **107**, 4872–7 (2010).

256. Nikukar, H. *et al.* Osteogenesis of mesenchymal stem cells by nanoscale mechanotransduction. *ACS Nano* (2013). doi:10.1021/nn400202j

257. Wang, J. H.-C. *et al.* Cyclic mechanical stretching of human tendon fibroblasts increases the production of prostaglandin E2 and levels of cyclooxygenase expression: a novel in vitro model study. *Connect. Tissue Res.* **44**, 128–33 (2003).

258. Zhang, J. & Wang, J. H. C. Production of PGE2 increases in tendons subjected to repetitive mechanical loading and induces differentiation of tendon stem cells into non-tenocytes. *J. Orthop. Res.* (2010). doi:10.1002/jor.20962

259. Love, M. R., Palee, S., Chattipakorn, S. C. & Chattipakorn, N. Effects of electrical

stimulation on cell proliferation and apoptosis. *J. Cell. Physiol.* **233**, 1860–1876 (2018).

260. Balint, R., Cassidy, N. J. & Cartmell, S. H. Electrical Stimulation: A Novel Tool for Tissue Engineering. *Tissue Eng. Part B Rev.* **19**, 48–57 (2013).

261. Shao, S. *et al.* Osteoblast function on electrically conductive electrospun PLA/MWCNTs nanofibers. *Biomaterials* (2011). doi:10.1016/j.biomaterials.2011.01.051

262. Ning, C., Zhou, Z., Tan, G., Zhu, Y. & Mao, C. Electroactive polymers for tissue regeneration: Developments and perspectives. *Progress in Polymer Science* (2018). doi:10.1016/j.progpolymsci.2018.01.001

263. Zhang, J., Li, M., Kang, E. T. & Neoh, K. G. Electrical stimulation of adipose-derived mesenchymal stem cells in conductive scaffolds and the roles of voltage-gated ion channels. *Acta Biomater.* **32**, 46–56 (2016).

264. Chiu, C. H., Lei, K. F. & Yeh, W. L. Development of a co-culture device for the study of human tenocytes in response to the combined stimulation of electric field and platelet rich plasma (PRP). *Biomed. Microdevices* (2017). doi:10.1007/s10544-017-0214-z

265. Basas, Á. *et al.* Effects of a strength protocol combined with electrical stimulation on patellar tendinopathy: 42 months retrospective follow-up on 6 high-level jumping athletes. *Phys. Ther. Sport* **34**, 105–112 (2018).

266. Yanase, K. *et al.* Electrical Stimulation to the Infraspinatus on Hypertrophy and Strength of the Shoulder. *Int. J. Sports Med.* **39**, 828–834 (2018).

267. Yan, Z. *et al.* [Effects of electrical stimulation on the differentiation of mesenchymal stem cells into cardiomyocyte-like cells]. *Sheng Wu Yi Xue Gong Cheng Xue Za Zhi* **30**, 556–61 (2013).

268. Pardo-Pastor, C. *et al.* Piezo2 channel regulates RhoA and actin cytoskeleton to promote cell mechanobiological responses. *Proc. Natl. Acad. Sci. U. S. A.* **115**, 1925–1930 (2018).

269. Islam, A., Mbimba, T., Younesi, M. & Akkus, O. Effects of substrate stiffness on the tenoinduction of human mesenchymal stem cells. *Acta Biomater.* **58**, 244–253 (2017).

270. Barsby, T., Bavin, E. P. & Guest, D. J. Three-Dimensional Culture and Transforming Growth Factor Beta3 Synergistically Promote Tenogenic Differentiation of Equine Embryo-Derived Stem Cells. *Tissue Eng. Part A* (2014).

doi:10.1016/j.foreco.2016.02.006

271. Qi, J. *et al.* IL-1β decreases the elastic modulus of human tenocytes. *J. Appl. Physiol.* (2006). doi:10.1152/japplphysiol.01128.2005

272. Tsuzaki, M., Bynum, D., Almekinders, L., Faber, J. & Banes, A. J. Mechanical loading stimulates ecto-ATPase activity in human tendon cells. *J. Cell. Biochem.* (2005). doi:10.1002/jcb.20491

273. Archambault, J., Tsuzaki, M., Herzog, W. & Banes, A. J. Stretch and interleukin-1β induce matrix metalloproteinases in rabbit tendon cells in vitro. *J. Orthop. Res.* (2002). doi:10.1016/S0736-0266(01)00075-4

274. Tsuzaki, M. *et al.* IL-1β induces COX2, MMP-1, -3 and -13, ADAMTS-4, IL-1β and IL-6 in human tendon cells. *J. Orthop. Res.* (2003). doi:10.1016/S0736-0266(02)00141-9

275. Jelinsky, S. A., Archambault, J., Li, L. & Seeherman, H. Tendon-selective genes identified from rat and human musculoskeletal tissues. *J. Orthop. Res.* **28**, n/a-n/a (2009).

276. Delgado Caceres, M., Pfeifer, C. G. & Docheva, D. Understanding Tendons: Lessons from Transgenic Mouse Models. *Stem Cells Dev.* **27**, 1161–1174 (2018).

277. Inaba, S., Akaishi, K., Mori, T. & Hane, K. Analysis of the resonance characteristics of a cantilever vibrated photothermally in a liquid. *J. Appl. Phys.* (1993). doi:10.1063/1.353060

278. Kwak, M. K. & Kim, K. C. Axisymmetric vibration of circular plates in contact with fluid. *J. Sound Vib.* (1991). doi:10.1016/0022-460X(91)90696-H

279. Nikukar, H. *et al.* Osteogenesis of Mesenchymal Stem Cells by Nanoscale Mechanotransduction. *ACS Nano* **7**, 2758–2767 (2013).

280. Wang, T. *et al.* Programmable mechanical stimulation influences tendon homeostasis in a bioreactor system. *Biotechnol. Bioeng.* (2013). doi:10.1002/bit.24809

281. Zhang, J. & Wang, J. H. C. Mechanobiological response of tendon stem cells: Implications of tendon homeostasis and pathogenesis of tendinopathy. *J. Orthop. Res.* (2010). doi:10.1002/jor.21046

282. Aspenberg, P. Stimulation of tendon repair: Mechanical loading, GDFs and platelets. a mini-review. *International Orthopaedics* (2007). doi:10.1007/s00264-007-0398-6

283. Busch, T., Köttgen, M. & Hofherr, A. TRPP2 ion channels: Critical regulators of

organ morphogenesis in health and disease. *Cell Calcium* (2017). doi:10.1016/j.ceca.2017.05.005

284. Chachisvilis, M., Zhang, Y.-L. & Frangos, J. A. G protein-coupled receptors sense fluid shear stress in endothelial cells. *Proc. Natl. Acad. Sci.* (2006). doi:10.1073/pnas.0607224103

285. Wu, J., Lewis, A. H. & Grandl, J. Touch, Tension, and Transduction – The Function and Regulation of Piezo Ion Channels. *Trends Biochem. Sci.* **42**, 57–71 (2017).

286. Popov, C. *et al.* Mechanical stimulation of human tendon stem/progenitor cells results in upregulation of matrix proteins, integrins and MMPs, and activation of p38 and ERK1/2 kinases. *BMC Mol. Biol.* **16**, 1–11 (2015).

287. Maksimovic, S. *et al.* Epidermal Merkel cells are mechanosensory cells that tune mammalian touch receptors. *Nature* (2014). doi:10.1038/nature13250

288. Zhang, W., Yan, Z., Jan, L. Y. & Jan, Y. N. Sound response mediated by the TRP channels NOMPC, NANCHUNG, and INACTIVE in chordotonal organs of Drosophila larvae. *Proc. Natl. Acad. Sci.* (2013). doi:10.1073/pnas.1312477110

289. Kim, J. *et al.* A TRPV family ion channel required for hearing in Drosophila. *Nature* (2003). doi:10.1038/nature01733

290. Rayleigh, J. W. S. *The Theory of Sound Vol. II*. *Macmillan* (1896). doi:10.1017/CBO9781107415324.004

291. Sroka, J., Zimolag, E., Lasota, S. & Korohoda, W. Electrotaxis : Cell Directional Movement in Electric Fields. **1749**, 325–340

292. Banks, T. A., Luckman, P. S. B., Frith, J. E. & Cooper-White, J. J. Effects of electric fields on human mesenchymal stem cell behaviour and morphology using a novel multichannel device. *Integr. Biol. (Camb).* **7**, 693–712 (2015).

293. Guerin, S. *et al.* Control of piezoelectricity in amino acids by supramolecular packing. *Nat. Mater.* (2018). doi:10.1038/NMAT5045

294. Boriek, A. M. & Kumar, A. Regulation of Intracellular Signal Transduction Pathways by Mechanosensitive Ion Channels. in *Mechanosensitive Ion Channels* (2007). doi:10.1007/978-1-4020-6426-5_14

295. Coste, B. *et al.* Piezo1 and Piezo2 are essential components of distinct mechanically activated cation channels. *Science (80-.).* (2010). doi:10.1126/science.1193270

296. Goodier, H. C. J. *et al.* Comparison of transforming growth factor beta expression in healthy and diseased human tendon. *Arthritis Res. Ther.* (2016). doi:10.1186/s13075-016-0947-8

297. Zhuang, H. *et al.* Electrical stimulation induces the level of TGF-β1 mRNA in osteoblastic cells by a mechanism involving calcium/calmodulin pathway. *Biochem. Biophys. Res. Commun.* (1997). doi:10.1006/bbrc.1997.7118

298. Hirata, H., Tatsumi, H., Hayakawa, K. & Sokabe, M. Non-channel mechanosensors working at focal adhesion-stress fiber complex. *Pflügers Arch. - Eur. J. Physiol.* **467**, 141–155 (2015).

299. Prindle, A. *et al.* Ion channels enable electrical communication in bacterial communities. *Nature* (2015). doi:10.1038/nature15709

300. Brohawn, S. G., Campbell, E. B. & MacKinnon, R. Physical mechanism for gating and mechanosensitivity of the human TRAAK K+ channel. *Nature* (2014). doi:10.1038/nature14013

301. Lin, Y. Lo, Moolenaar, H., van Weeren, P. R. & van de Lest, C. H. A. Effect of microcurrent electrical tissue stimulation on equine tenocytes in culture. *Am. J. Vet. Res.* (2006). doi:10.2460/ajvr.67.2.271

302. STROYAN, J. J. PROCESSING AND CHARACTERISATION OF PVDF, PVDF-TrFE, AND PVDF-TrFE-PZT COMPOSITES. *J. Chem. Inf. Model.* (2013). doi:10.1017/CBO9781107415324.004

303. Dodds, J. S., Meyers, F. N. & Loh, K. J. Piezoelectric characterisation of PVDF-TrFE thin films enhanced with ZnO nanoparticles. *IEEE Sens. J.* (2012). doi:10.1109/JSEN.2011.2182043

304. Chen, H. J. *et al.* Investigation of PVDF-TrFE composite with nanofillers for sensitivity improvement. *Sensors Actuators, A Phys.* (2016). doi:10.1016/j.sna.2016.04.056

305. Simoes, R. D., Rodriguez-Perez, M. A., De Saja, J. A. & Constantino, C. J. L. Thermomechanical characterisation of PVDF and P(VDF-TrFE) blends containing corn starch and natural rubber. *J. Therm. Anal. Calorim.* (2010). doi:10.1007/s10973-009-0285-z

306. Seminara, L., Capurro, M., Cirillo, P., Cannata, G. & Valle, M. Electromechanical characterisation of piezoelectric PVDF polymer films for tactile sensors in robotics applications. *Sensors Actuators, A Phys.* (2011). doi:10.1016/j.sna.2011.05.004

307. Mohamad Hafiz, M. W. *et al.* Effect of Annealing Temperature on the Crystallinity, Morphology and Ferroelectric of Polyvinylidenefluoride-Trifluoroethylene (PVDF-TrFE) Thin Film. *Adv. Mater. Res.* (2013). doi:10.4028/www.scientific.net/AMR.812.60

308. Lu, X., Qu, H. & Skorobogatiy, M. Piezoelectric microstructured fibers via drawing of multimaterial preforms. *Sci. Rep.* (2017). doi:10.1038/s41598-017-01738-9

309. Wong, S. C., Baji, A. & Leng, S. Effect of fiber diameter on tensile properties of electrospun poly(ε-caprolactone). *Polymer (Guildf).* (2008). doi:10.1016/j.polymer.2008.08.022

310. Chen, F. *et al.* Mechanical characterisation of single high-strength electrospun polyimide nanofibres. *J. Phys. D. Appl. Phys.* (2008). doi:10.1088/0022-3727/41/2/025308

311. Baji, A., Mai, Y. W. & Wong, S. C. Effect of fiber size on structural and tensile properties of electrospun polyvinylidene fluoride fibers. *Polym. Eng. Sci.* (2015). doi:10.1002/pen.24020

312. Ico, G. *et al.* Size-dependent piezoelectric and mechanical properties of electrospun P(VDF-TrFE) nanofibers for enhanced energy harvesting. *J. Mater. Chem. A* (2016). doi:10.1039/c5ta10423h

313. O'Hagan, D. Understanding organofluorine chemistry. An introduction to the C-F bond. *Chem. Soc. Rev.* (2008). doi:10.1039/b711844a

314. Wang, J. H.-C. Mechanobiology of tendon. *J. Biomech.* (2006). doi:10.1016/j.jbiomech.2005.05.011

315. Lin, T. W., Cardenas, L. & Soslowsky, L. J. Biomechanics of tendon injury and repair. *J. Biomech.* (2004). doi:10.1016/j.jbiomech.2003.11.005

316. James, R., Kesturu, G., Balian, G. & Chhabra, A. B. Tendon: Biology, Biomechanics, Repair, Growth Factors, and Evolving Treatment Options. *Journal of Hand Surgery* (2008). doi:10.1016/j.jhsa.2007.09.007

317. Wang, J. H. C., Guo, Q. & Li, B. Tendon Biomechanics and Mechanobiology—A Minireview of Basic Concepts and Recent Advancements. *J. Hand Ther.* **25**, 133–141 (2012).

318. Rees, J. D., Wilson, A. M. & Wolman, R. L. Current concepts in the management of tendon disorders. *Rheumatology* (2006). doi:10.1093/rheumatology/kel046

319. Yang, G., Crawford, R. C. & Wang, J. H. C. Proliferation and collagen production of human patellar tendon fibroblasts in response to cyclic uniaxial stretching in serum-free conditions. *J. Biomech.* (2004). doi:10.1016/j.jbiomech.2004.01.005

320. Skutek, M., Van Griensven, M., Zeichen, J., Brauer, N. & Bosch, U. Cyclic mechanical stretching modulates secretion pattern of growth factors in human tendon fibroblasts. *Eur. J. Appl. Physiol.* (2001). doi:10.1007/s004210100502

321. Zeichen, J., Van Griensven, M. & Bosch, U. The proliferative response of isolated human tendon fibroblasts to cyclic biaxial mechanical strain. *Am. J. Sports Med.* (2000). doi:10.1177/03635465000280061901

322. Jagodzinski, M. *et al.* Influence of cyclic mechanical strain and heat of human tendon fibroblasts on HSP-72. *Eur. J. Appl. Physiol.* (2006). doi:10.1007/s00421-005-0071-y

323. Skutek, M., Van Griensven, M., Zeichen, J., Brauer, N. & Bosch, U. Cyclic mechanical stretching of human patellar tendon fibroblasts: Activation of JNK and modulation of apoptosis. *Knee Surgery, Sport. Traumatol. Arthrosc.* (2003). doi:10.1007/s00167-002-0322-y

324. Youngstrom, D. W., Rajpar, I., Kaplan, D. L. & Barrett, J. G. A bioreactor system for in vitro tendon differentiation and tendon tissue engineering. *J. Orthop. Res.* **33**, 911–918 (2015).

325. Bayer, M. L. *et al.* Release of tensile strain on engineered human tendon tissue disturbs cell adhesions, changes matrix architecture, and induces an inflammatory phenotype. *PLoS One* (2014). doi:10.1371/journal.pone.0086078

326. Moffat, K. L. *et al.* Novel Nanofiber-Based Scaffold for Rotator Cuff Repair and Augmentation. *Tissue Eng. Part A* (2008). doi:10.1089/ten.tea.2008.0014

327. Dabiri, B. E., Lee, H. & Parker, K. K. A potential role for integrin signaling in mechanoelectrical feedback. *Progress in Biophysics and Molecular Biology* (2012). doi:10.1016/j.pbiomolbio.2012.07.002

328. Butler, D. L. *et al.* The use of mesenchymal stem cells in collagen-based scaffolds for tissue-engineered repair of tendons. *Nat. Protoc.* (2010). doi:10.1038/nprot.2010.14

329. Schwartz, A. & Thomopoulos, S. The role of mechanobiology in the attachment of tendon to bone. in *Structural Interfaces and Attachments in Biology* (2013). doi:10.1007/978-1-4614-3317-0_11

330. Durant, T. J. S. *et al.* Mesenchymal stem cell response to growth factor treatment and low oxygen tension in 3-dimensional construct environment. *Muscle Ligaments Tendons J.* (2019). doi:10.32098/mltj.01.2014.09

331. Bagnaninchi, P. O. *et al.* Chitosan Microchannel Scaffolds for Tendon Tissue Engineering Characterised Using Optical Coherence Tomography. *Tissue Eng.* (2007). doi:10.1089/ten.2006.0168

332. Bagnaninchi, P. & Yang, Y. Tissue engineering for tendon repair. *Br. J. Sport. ...*

(2007). doi:10.1136/bjsm.2006.030643

333. Stanton, A. E., Tong, X., Lee, S. & Yang, F. Biochemical Ligand Density Regulates Yes-Associated Protein Translocation in Stem Cells through Cytoskeletal Tension and Integrins. *ACS Appl. Mater. Interfaces* (2019). doi:10.1021/acsami.8b21270

334. Driscoll, T. P., Cosgrove, B. D., Heo, S. J., Shurden, Z. E. & Mauck, R. L. Cytoskeletal to Nuclear Strain Transfer Regulates YAP Signaling in Mesenchymal Stem Cells. *Biophys. J.* (2015). doi:10.1016/j.bpj.2015.05.010

335. Méjat, A. & Misteli, T. LINC complexes in health and disease. *Nucleus* (2010). doi:10.4161/nucl.1.1.10530

336. Crisp, M. *et al.* Coupling of the nucleus and cytoplasm: Role of the LINC complex. *J. Cell Biol.* (2006). doi:10.1083/jcb.200509124

337. Isermann, P. & Lammerding, J. Nuclear mechanics and mechanotransduction in health and disease. *Current Biology* (2013). doi:10.1016/j.cub.2013.11.009

338. Watkins-Castillo, S. & Andersson, G. United States Bone and Joint Initiative: The Burden of Musculoskeletal Diseases in the United States (BMUS). *The Burden of Musculoskeletal diseases int he United States* (2014).

339. Biewener, A. A. Muscle-tendon stresses and elastic energy storage during locomotion in the horse. *Comp. Biochem. Physiol. - B Biochem. Mol. Biol.* (1998). doi:10.1016/S0305-0491(98)00024-8

340. Yang, G., Rothrauff, B. B. & Tuan, R. S. Tendon and ligament regeneration and repair: Clinical relevance and developmental paradigm. *Birth Defects Research Part C - Embryo Today: Reviews* (2013). doi:10.1002/bdrc.21041

341. Foolen, J., Wunderli, S. L., Loerakker, S. & Snedeker, J. G. Tissue alignment enhances remodeling potential of tendon-derived cells - Lessons from a novel microtissue model of tendon scarring. *Matrix Biol.* (2018). doi:10.1016/j.matbio.2017.06.002

342. Kimura, A., Aoki, M., Fukushima, S., Ishii, S. & Yamakoshi, K. Reconstruction of a defect of the rotator cuff with polytetrafluoroethylene felt graft. Recovery of tensile strength and histocompatibility in an animal model. *J. Bone Joint Surg. Br.* (2003).

343. Rowe, R. W. D. The structure of rat tail tendon. *Connect. Tissue Res.* (1985). doi:10.3109/03008208509089839

344. Chan, H. K. F., Fung, D. T. C. & Ng, G. Y. F. Effects of Low-Voltage Microamperage Stimulation on Tendon Healing in Rats. *J. Orthop. Sport. Phys. Ther.* **37**, 399–403 (2007).

345. West, C. R. & Bowden, A. E. Using tendon inherent electric properties to consistently track induced mechanical strain. *Ann. Biomed. Eng.* (2012). doi:10.1007/s10439-011-0504-1

346. Liu, Z. & Kim, J. Effect of Strain Rate and Loading on the Piezoelectric Properties of Tendon. **8**, 3193 (2006).

347. Subramanian, A., Kanzaki, L. F., Galloway, J. L. & Schilling, T. F. Mechanical force regulates tendon extracellular matrix organisation and tenocyte morphogenesis through TGFbeta signaling. *Elife* **7**, 1–24 (2018).

348. Kannus, P., Józsa, L., Natri, A. & Järvinen, M. Effects of training, immobilization and remobilization on tendons. *Scand. J. Med. Sci. Sports* (2010). doi:10.1111/j.1600-0838.1997.tb00121.x

349. Matsumoto, F., Trudel, G., Uhthoff, H. K. & Backman, D. S. Mechanical effects of immobilization on the Achilles' tendon. *Arch. Phys. Med. Rehabil.* (2003). doi:10.1016/S0003-9993(02)04834-7

350. Kim, B. S. *et al.* The effect of dry needling and treadmill running on inducing pathological changes in rat Achilles tendon. *Connect. Tissue Res.* **8207**, 1–17 (2015).

351. De Castro Pochini, A. *et al.* Overuse of training increases mechanoreceptors in supraspinatus tendon of rats SHR. *J. Orthop. Res.* (2011). doi:10.1002/jor.21320

352. Yuan, T. *et al.* Creating an animal model of tendinopathy by inducing chondrogenic differentiation with kartogenin. *PLoS One* (2016). doi:10.1371/journal.pone.0148557

353. Wada, S. *et al.* Post-operative Tendon Loading with Treadmill Running Delays Tendon-to-Bone Healing: Immunohistochemical Evaluation in a Murine Rotator Cuff Repair Model. *J. Orthop. Res.* (2019). doi:10.1002/jor.24300

354. Zhang, J. & Wang, J. H.-C. The Effects of Mechanical Loading on Tendons - An In Vivo and In Vitro Model Study. *PLoS One* (2013). doi:10.1371/journal.pone.0071740

355. Zhang, J., Pan, T., Liu, Y. & Wang, J. H. C. Mouse treadmill running enhances tendons by expanding the pool of Tendon Stem Cells (TSCs) and TSC-related cellular production of collagen. *J. Orthop. Res.* (2010). doi:10.1002/jor.21123

356. Glazebrook, M. A., Wright, J. R., Langman, M., Stanish, W. D. & Lee, J. M. Histological analysis of Achilles tendons in an overuse rat model. *J. Orthop. Res.* (2008). doi:10.1002/jor.20546

357. Houghton, L., Dawson, B. & Rubenson, J. Achilles tendon mechanical properties after both prolonged continuous running and prolonged intermittent shuttle running in cricket batting. *J. Appl. Biomech.* (2013). doi:10.1123/jab.29.4.453

358. Eliasson, P., Andersson, T. & Aspenberg, P. Achilles tendon healing in rats is improved by intermittent mechanical loading during the inflammatory phase. *J. Orthop. Res.* (2012). doi:10.1002/jor.21511

359. Xu, S. Y. *et al.* Response of Decorin to different intensity treadmill running. *Mol. Med. Rep.* (2018). doi:10.3892/mmr.2018.8802

360. Xu, S. Y. *et al.* Intensity-dependent effect of treadmill running on rat Achilles tendon. *Exp. Ther. Med.* (2018). doi:10.3892/etm.2018.6084

361. Kuo, C. K. & Tuan, R. S. Mechanoactive Tenogenic Differentiation of Human Mesenchymal Stem Cells. *Tissue Eng. Part A* (2008). doi:10.1089/ten.tea.2006.0415

362. Scott, A. *et al.* Mechanical force modulates scleraxis expression in bioartificial tendons. *J. Musculoskelet. Neuronal Interact.* (2011).

363. Lohberger, B. *et al.* Impact of cyclic mechanical stimulation on the expression of extracellular matrix proteins in human primary rotator cuff fibroblasts. *Knee Surgery, Sport. Traumatol. Arthrosc.* (2016). doi:10.1007/s00167-015-3790-6

364. Sawaguchi, N. *et al.* Effect of cyclic three-dimensional strain on cell proliferation and collagen synthesis of fibroblast-seeded chitosan-hyaluronan hybrid polymer fiber. *J. Orthop. Sci.* (2010). doi:10.1007/s00776-010-1488-7

365. D., D. Running far and fast: An emerging role of tenomodulin. *J. Orthop. Res.* (2017).

366. Zhang, J., Yuan, T. & Wang, J. H.-C. Moderate treadmill running exercise prior to tendon injury enhances wound healing in aging rats. *Oncotarget* (2016). doi:10.18632/oncotarget.7381

367. Cushman, D. & Rho, M. E. Conservative Treatment of Subacute Proximal Hamstring Tendinopathy Using Eccentric Exercises Performed With a Treadmill: A Case Report. *J. Orthop. Sport. Phys. Ther.* (2015). doi:10.2519/jospt.2015.5762

368. Heinemeier, K. M. *et al.* Uphill running improves rat Achilles tendon tissue mechanical properties and alters gene expression without inducing pathological changes. *J. Appl. Physiol.* (2012). doi:10.1152/japplphysiol.00401.2012

369. Abraham, T., Fong, G. & Scott, A. Second harmonic generation analysis of early Achilles tendinosis in response to in vivo mechanical loading. *BMC Musculoskelet. Disord.* (2011). doi:10.1186/1471-2474-12-26

370. Jafari, L., Vachon, P., Beaudry, F. & Langelier, E. Histopathological, biomechanical, and behavioral pain findings of achilles tendinopathy using an animal model of overuse injury. *Physiol. Rep.* (2015). doi:10.14814/phy2.12265

371. Ng, G. Y. F., Chung, P. Y. M., Wang, J. S. & Cheung, R. T. H. Enforced bipedal downhill running induces Achilles tendinosis in rats. *Connect. Tissue Res.* (2011). doi:10.3109/03008207.2011.562334

372. Mendias, C. L., Gumucio, J. P., Bakhurin, K. I., Lynch, E. B. & Brooks, S. V. Physiological loading of tendons induces scleraxis expression in epitenon fibroblasts. *J. Orthop. Res.* (2012). doi:10.1002/jor.21550

373. Esteves de Lima, J. *et al.* TGFβ and FGF promote tendon progenitor fate and act downstream of muscle contraction to regulate tendon differentiation during chick limb development. *Development* (2016). doi:10.1242/dev.136242

374. Brent, A. E. FGF acts directly on the somitic tendon progenitors through the Ets transcription factors Pea3 and Erm to regulate scleraxis expression. *Development* (2004). doi:10.1242/dev.01275

375. Shukunami, C., Takimoto, A., Oro, M. & Hiraki, Y. Scleraxis positively regulates the expression of tenomodulin, a differentiation marker of tenocytes. *Dev. Biol.* (2006). doi:10.1016/j.ydbio.2006.06.036

376. Hammerman, M., Aspenberg, P. & Eliasson, P. Microtrauma stimulates rat Achilles tendon healing via an early gene expression pattern similar to mechanical loading. *J. Appl. Physiol.* (2013). doi:10.1152/japplphysiol.00741.2013

377. Cheng, N., Hoof, V. A. N. & Hoogmartens, M. J. Generation , Protein Synthesis , and Membrane Transport in Rat Skin. *Clin. Orthop. Relat. Researc* (1982).

378. Meng, X. *et al.* PI3K mediated electrotaxis of embryonic and adult neural progenitor cells in the presence of growth factors. *Exp. Neurol.* (2011). doi:10.1016/j.expneurol.2010.11.002

379. Sung, K. M. *et al.* Control of neonatal human dermal fibroblast migration on poly(lactic-co-glycolic acid)-coated surfaces by electrotaxis. *J. Tissue Eng. Regen. Med.* (2015). doi:10.1002/term.1986

380. Li, S. *et al.* Electrical Stimulation Activates Fibroblasts through the Elevation of Intracellular Free Ca 2+ : Potential Mechanism of Pelvic Electrical Stimulation Therapy . *Biomed Res. Int.* (2019). doi:10.1155/2019/7387803

381. Lee, G. S., Kim, M. G. & Kwon, H. J. Electrical stimulation induces direct reprogramming of human dermal fibroblasts into hyaline chondrogenic cells.

Biochem. Biophys. Res. Commun. (2019). doi:10.1016/j.bbrc.2019.04.027

382. Ni, M. *et al.* Engineered scaffold-free tendon tissue produced by tendon-derived stem cells. *Biomaterials* **34**, 2024–2037 (2013).

383. Xu, S.-Y., Li, S.-F. & Ni, G.-X. Strenuous Treadmill Running Induces a Chondrocyte Phenotype in Rat Achilles Tendons. *Med. Sci. Monit.* (2016). doi:10.12659/msm.897726

384. Carpenter, J. E., Flanagan, C. L., Thomopoulos, S., Yian, E. H. & Soslowsky, L. J. The effects of overuse combined with intrinsic or extrinsic alterations in an animal model of rotator cuff tendinosis. *Am. J. Sports Med.* (1998). doi:10.1177/03635465980260061101

385. Szomor, Z. L., Appleyard, R. C. & Murrell, G. A. C. Overexpression of nitric oxide synthases in tendon overuse. *J. Orthop. Res.* (2006). doi:10.1002/jor.20009

386. Thampatty, B. P. & Wang, J. H. C. Mechanobiology of young and aging tendons: In vivo studies with treadmill running. *J. Orthop. Res.* (2017). doi:10.1002/jor.23761

387. Heinemeier, K. M. *et al.* Effect of unloading followed by reloading on expression of collagen and related growth factors in rat tendon and muscle. *J. Appl. Physiol.* (2009). doi:10.1152/japplphysiol.91092.2008

388. Zhang, J. & Wang, J. H. C. Moderate exercise mitigates the detrimental effects of aging on tendon stem cells. *PLoS One* (2015). doi:10.1371/journal.pone.0130454

389. Dey, D. *et al.* Two tissue-resident progenitor lineages drive distinct phenotypes of heterotopic ossification. *Sci. Transl. Med.* (2016). doi:10.1126/scitranslmed.aaf1090

390. Wood, L. K. & Brooks, S. V. Ten weeks of treadmill running decreases stiffness and increases collagen turnover in tendons of old mice. *J. Orthop. Res.* (2016). doi:10.1002/jor.22824

391. Gimbel, J. A. Long Durations of Immobilization in the Rat Result in Enhanced Mechanical Properties of the Healing Supraspinatus Tendon Insertion Site. *J. Biomech. Eng.* (2007). doi:10.1115/1.2721075

392. Wolfman, N. M. *et al.* Ectopic induction of tendon and ligament in rats by growth and differentiation factors 5, 6, and 7, members of the TGF-β gene family. *J. Clin. Invest.* (1997). doi:10.1172/JCI119537

393. Kishimoto, Y. *et al.* Wnt/β-catenin signaling suppresses expressions of Scx, Mkx, and Tnmd in tendon-derived cells. *PLoS One* (2017). doi:10.1371/journal.pone.0182051

394. Zhou, S., Eid, K. & Glowacki, J. Cooperation between TGF-β and Wnt pathways

during chondrocyte and adipocyte differentiation of human marrow stromal cells. *J. Bone Miner. Res.* (2004). doi:10.1359/JBMR.0301239

395. Chen, Y. *et al.* β-Catenin signaling pathway is crucial for bone morphogenetic protein 2 to induce new bone formation. *J. Biol. Chem.* (2007). doi:10.1074/jbc.M602700200

396. Zhang, R. *et al.* Wnt/β-catenin signaling activates bone morphogenetic protein 2 expression in osteoblasts. *Bone* (2013). doi:10.1016/j.bone.2012.09.029

397. Gaur, T. *et al.* Canonical WNT signaling promotes osteogenesis by directly stimulating Runx2 gene expression. *J. Biol. Chem.* (2005). doi:10.1074/jbc.M500608200

398. Kim, J. B. *et al.* Bone regeneration is regulated by Wnt signaling. *J. Bone Miner. Res.* (2007). doi:10.1359/jbmr.070802

399. Minear, S. *et al.* Wnt proteins promote bone regeneration. *Sci. Transl. Med.* (2010). doi:10.1126/scitranslmed.3000231

400. Krishnan, V., Bryant, H. U. & MacDougald, O. A. Regulation of bone mass by Wnt signaling. *Journal of Clinical Investigation* (2006). doi:10.1172/JCI28551

401. Robling, A. G. *et al.* Mechanical stimulation of bone in vivo reduces osteocyte expression of Sost/sclerostin. *J. Biol. Chem.* (2008). doi:10.1074/jbc.M705092200

402. Majidinia, M., Sadeghpour, A. & Yousefi, B. The roles of signaling pathways in bone repair and regeneration. *Journal of cellular physiology* (2018). doi:10.1002/jcp.26042

403. Tu, X. *et al.* Sost downregulation and local Wnt signaling are required for the osteogenic response to mechanical loading. *Bone* (2012). doi:10.1016/j.bone.2011.10.025

404. Brighton, C. T., Wang, W., Seldes, R., Zhang, G. & Pollack, S. R. Signal transduction in electrically stimulated bone cells. *J. Bone Jt. Surg. - Ser. A* (2001). doi:10.2106/00004623-200110000-00009

405. Ashrafi, M., Alonso-Rasgado, T., Baguneid, M. & Bayat, A. The efficacy of electrical stimulation in experimentally induced cutaneous wounds in animals. *Veterinary dermatology* (2016). doi:10.1111/vde.12328

406. Kim, T. H., Cho, H. & Lee, S. M. High-Voltage Pulsed Current Stimulation Enhances Wound Healing in Diabetic Rats by Restoring the Expression of Collagen, α-Smooth Muscle Actin, and TGF-β1. *Tohoku J. Exp. Med.* (2014). doi:10.1620/tjem.234.1

407. Wang, Y., Rouabhia, M., Lavertu, D. & Zhang, Z. Pulsed electrical stimulation modulates fibroblasts' behaviour through the Smad signalling pathway. *J. Tissue Eng. Regen. Med.* (2017). doi:10.1002/term.2014

408. Wang, H., Liu, J., Zeng, J., Zeng, C. & Zhou, Y. Expression of TβR-2, Smad3 and Smad7 in the vaginal anterior wall of postpartum rats with stress urinary incontinence. *Arch. Gynecol. Obstet.* (2015). doi:10.1007/s00404-014-3495-y

409. Li, Y. *et al.* Effect of integrin β1 in the treatment of stress urinary incontinence by electrical stimulation. *Mol. Med. Rep.* 4727–4734 (2019). doi:10.3892/mmr.2019.10145

410. Hamadi, A. Regulation of focal adhesion dynamics and disassembly by phosphorylation of FAK at tyrosine 397. *J. Cell Sci.* (2005). doi:10.1242/jcs.02565

411. Park, M. S., Kim, Y. H. & Lee, J. W. FAK mediates signal crosstalk between type II collagen and TGF-beta 1 cascades in chondrocytic cells. *Matrix Biol.* (2010). doi:10.1016/j.matbio.2009.10.001

412. Jing, D. *et al.* Pulsed electromagnetic fields partially preserve bone mass, microarchitecture, and strength by promoting bone formation in hindlimb-suspended rats. *J. Bone Miner. Res.* (2014). doi:10.1002/jbmr.2260

413. Jing, D. *et al.* Moderate-intensity rotating magnetic fields do not affect bone quality and bone remodeling in hindlimb suspended rats. *PLoS One* (2014). doi:10.1371/journal.pone.0102956

414. Jing, D. *et al.* Pulsed electromagnetic fields improve bone microstructure and strength in ovariectomized rats through a Wnt/Lrp5/β-catenin signaling-associated mechanism. *PLoS One* (2013). doi:10.1371/journal.pone.0079377

415. Lei, T. *et al.* Pulsed electromagnetic fields (PEMF) attenuate changes in vertebral bone mass, architecture and strength in ovariectomized mice. *Bone* (2018). doi:10.1016/j.bone.2017.12.008

416. Kim, M. O., Jung, H., Kim, S. C., Park, J. K. & Seo, Y. K. Electromagnetic fields and nanomagnetic particles increase the osteogenic differentiation of human bone marrow-derived mesenchymal stem cells. *Int. J. Mol. Med.* (2015). doi:10.3892/ijmm.2014.1978

417. Petecchia, L. *et al.* Electro-magnetic field promotes osteogenic differentiation of BM-hMSCs through a selective action on Ca^{2+} -related mechanisms. *Sci. Rep.* (2015). doi:10.1038/srep13856

418. Rouabhia, M., Park, H., Meng, S., Derbali, H. & Zhang, Z. Electrical stimulation

promotes wound healing by enhancing dermal fibroblast activity and promoting myofibroblast transdifferentiation. *PLoS One* (2013). doi:10.1371/journal.pone.0071660

419. Cheng, G. *et al.* Sinusoidal electromagnetic field stimulates rat osteoblast differentiation and maturation via activation of NO-cGMP-PKG pathway. *Nitric Oxide - Biol. Chem.* (2011). doi:10.1016/j.niox.2011.05.009

420. Diniz, P., Soejima, K. & Ito, G. Nitric oxide mediates the effects of pulsed electromagnetic field stimulation on the osteoblast proliferation and differentiation. *Nitric Oxide - Biol. Chem.* (2002). doi:10.1016/S1089-8603(02)00004-6

421. Pilla, A. *et al.* Electromagnetic fields as first messenger in biological signaling: Application to calmodulin-dependent signaling in tissue repair. *Biochim. Biophys. Acta - Gen. Subj.* (2011). doi:10.1016/j.bbagen.2011.10.001

422. Hong, J. M., Kang, K. S., Yi, H. G., Kim, S. Y. & Cho, D. W. Electromagnetically controllable osteoclast activity. *Bone* (2014). doi:10.1016/j.bone.2014.02.005

423. Yuan, J., Xin, F. & Jiang, W. Underlying Signaling Pathways and Therapeutic Applications of Pulsed Electromagnetic Fields in Bone Repair. *Cellular Physiology and Biochemistry* (2018). doi:10.1159/000489206

424. Pall, M. L. Electromagnetic fields act via activation of voltage-gated calcium channels to produce beneficial or adverse effects. *J. Cell. Mol. Med.* **17**, 958–965 (2013).

Chapter Three

The development of a high frequency, low-amplitude electromechanical system for the maintenance of protenogenic signatures in tendon derived cell cultures

The main findings of this chapter have been published in:

Marc A. Fernandez-Yague, Anup Poudel, Tofail Syed A. M., Manus J. P. Biggs. Boron Nitride Nanotube Addition Enhances the Crystallinity and Cytocompatibility of PVDF-TrFE Frontiers in Chemistry; **2019**;7; 364.

Marc A. Fernandez-Yague, Anup Poudel, Aimee Stapleton, Tofail Syed A. M., Manus J. P. Biggs. The functional response of tendon cells cultured on vibrationally activated piezoelectric structures (in preparation).

3.1 Introduction

Tissue engineering represents a promising approach to tendon regeneration, a unique hypocellular connective tissue with low vascularisation and spontaneous regeneration capacity in vivo. In particular, tenocyte delivery strategies hold promise in tendon regeneration, and studies[249,250] indicate that these tendon-derived cells confer increased tenogenic potential over tissue engineering approaches employing fibroblast or mesenchymal stem cells. Unfortunately, the expansion of tenocytes in standard culture conditions is hampered by phenotypic drift due to an extreme sensitivity to the culture microenvironment. Several studies have reported detrimental changes to tenocyte morphology and associated downregulations in tenospecific biomarker expression (Collagen I, Decorin, Tenascin C, Tenomodulin and Scleraxis) after as few as four passages under conventional *in vitro* culture [60,251]. In their native microenvironment, tenocytes are exposed to a various and particular combination of biochemical (i.e. growth factors) and biophysical cues that control their function. Thus, a fundamental tenet of functional tendon tissue engineering is the biomimetic design of materials capable of closely imitating the physicochemical properties that tenocytes encounter their native environment.

Current approaches to tenocyte culture have focused on the development of 3D systems, topographical functionalization, mechanical loading, electrical stimulation, growth factor supplementation or oxygen tension conditions, which have demonstrated varying degrees of success. Stoll et al. showed a higher expression of tenospecific biomarkers in tenocytes cultured in a PLGA matrix at high density compared to conventional culture conditions[252]. Under physiological conditions tenocytes, in their native microenvironment, are primarily exposed to extracellular mechanical forces that are translated into intracellular signalling cascades, a process referred to as mechanotransduction. Critically, several studies have shown that mechanical loading supports the maintenance of a tendon phenotype and sustained tendon-related protein synthesis[253,254] through Rho-A/ROCK[255] and MAPK[151,256] regulated intracellular tension. However, excessive mechanical loading results in downregulation of these signalling cascades associated with early tendon repair and dedifferentiation towards an osteochondrogenic lineage [257,258].

Conversely, electrical stimulation (ES) is also a potent regulatory biophysical modulator of multiple cellular signalling pathways[259,260]. It has been shown that ES can affect proliferation and differentiation of stem cells and terminally differentiated cells, including osteoblasts[261–263]. Endogenous electrical signals have also been measured in the tendon during normal physiological conditions, prompting the exploration of electrical stimulation for tenocyte expansion *in vitro*[264] or tendon repair[265,266]. Indeed, ES is known to support the development and accelerate the regeneration of many tissues. However, the underlying mechanism remains elusive [267]. Furthermore, ES has been shown to induced MSC condensation and chondrogenesis by driving Ca^{2+}/ATP oscillation and to significantly increasing MSC TGF-beta expression [107].

Thus, electrical stimulation and mechanical loading are proven modulators of cell differentiation. Although it can be inferred that in tenocytes, mechanical loading induces the maintenance of an elongated tenocyte morphology, it can be hypothesised that electrical signals play a fundamental role in tenocyte differentiation and the dedifferentiation process. Thus, mechanical and electrical forces may be considered as primary biophysical cues for tenocyte phenotype and functional maintenance, and thanks to advancements in sensitive electroactive materials, bioreactor systems can be designed to provide electromechanical stimulation to cells in culture. In this chapter, a novel high-frequency, low-amplitude bioreactor system employing a PVDF TrFE diaphragm is described and evaluated experimentally and in silico. Furthermore, the role of high-frequency, low-amplitude electromechanical stimulation in cellular function and the ability of this bioreactor to maintain tendon cell function is explored in vitro.

3.1.1   Mechanotransductive signalling pathways for tendon tissue engineering

The modulation of cellular signalling pathways in response to extracellular cues has been extensively studied *in vitro*[18,89,268]. Mechanobiology of tendon cells is determinant for the maintenance of tissue homeostasis, and several studies have shown that endogenous and exogenous mechanical cues act as critical regulators of tendon-derived cells function. Physiological mechanical cues, including substrate rigidity and mechanical loading to maintain tendon function, have been identified. Anowarul et al.[269], studied the tenoinduction of MCS using Type I collagen substrates with elastic modulus in the range of

0.1 to 100 MPa and observed higher expression of tenogenic markers with increasing stiffness. However, upregulation of osteogenic-related markers was also upregulated at the same conditions because the signalling pathways for tenogenic and osteochondrogenic differentiation of MSC are both related to TGF-beta signalling (see Figure 3-1a).

Similarly, several studies have demonstrated that exogenous addition of transforming growth factor-beta 3 (TGF-β3) induces tendon differentiation of MSCs *in vitro* [270]. As investigations on the tendon mechanobiology continue to emerge, it becomes clear that there is no one unique mechanotransductive pathway involved in tendon repair but rather several interacting mechanisms with differing roles. For instance, other relevant signalling pathways that have been demonstrated to be related to changes in substrate rigidity include MAPK/ERK and PI3K/AKT, integrin-dependent downstream signalling pathways involved in stiffness-mediated osteogenic differentiation (see Figure 3-1b).
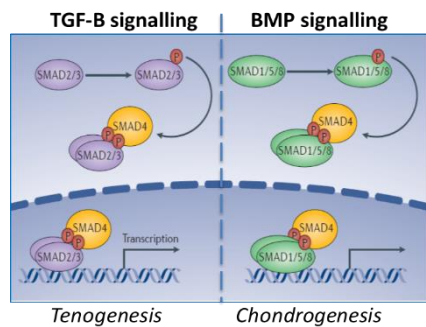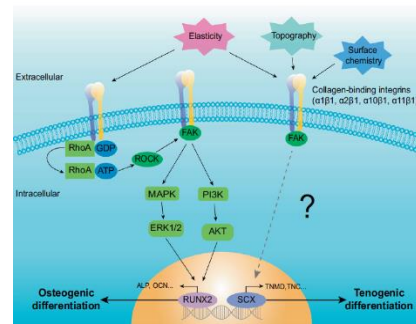
a)   b)

Figure 3-1. a) TGF-beta signalling pathways for tenogenesis or ostechondrogenesis. b) Schematic representation of the signalling pathways of integrin-mediated osteogenic/tenogenic differentiation. Abbreviation: AKT (also known as PKB), protein kinase B; ERK1/2: extracellular signal-regulated kinase 1/2; FAK: focal adhesion kinase; GDP: guanosine diphosphate; GTP: guanosine triphosphate; PI3K: phosphatidylinositol 3-kinase; MAPK, mitogen-activated protein kinase; ROCK: Rho-associated protein kinase

Tendon extracellular matrix act as a sensitive and "smart" sensor that dynamically responds to endogenous and exogenous mechanical signals. Exogenous mechanical forces are translated by tendon cells into biochemical signalling and affect biological functions of the

166

tendon, including cell differentiation and tissue repair. Main mechanotransductive mechanisms are continuously investigated, and studies suggest that might be related to activation of cell receptors and ion channels, intracellular calcium activity or changes in protein expression [41]. However, different environmental factors can change tenocytes mechanosensitivity. A mounting body of research studies suggests that biochemical agents can regulate mechanosensitivity and cell response to mechanical stimulation, including ATP and cytokines (IL-1β) [271,272]. Interestingly, ATP and IL-1β production increases under mechanical loading and promote the maintenance of tenocyte phenotype by modulating cytoskeleton rigidity. IL-1β Is a pro-inflammatory cytokine that stimulates MMP (1,2,3,9 and 13)[273,274] production to modulate ECM elastic properties to prevent possible rupture due to over rigidity. These studies suggest that tenocyte phenotype is susceptible to changes in its mechanoenvironment and special interestest has grown over the last decades to characterise and identify the biomarkers for tenocytes correctly.

3.1.2 Tendon-related biomarkers

Tenocytes have been extensively studied, and many markers have been proposed as positive markers including Collagen type I, collagen type III, tenascin C, scleraxis (Scx) and tenomodulin (Tnmd). Jelinsky et al. [275] compared mRNA expression levels across six human (tendon, muscle, cartilage, bone marrow, fat) and 13 rat (tendon, ligament, muscle, cartilage, bone, bone marrow, fat, bladder, heart, kidney, liver, lung, testis) tissues and concluded that Tnmd and Thbs4 are selectively expressed in tendon tissue. The use of gene silencing has proven to be extremely useful to define tenospecific signalling pathways and master regulators of tendon function, for instance, the application of siRNA to GSK-1 showed the specific regulation of TNMD via Wnt/β-catenin signalling in MSC's cultured in collagen gels [276]. Tenomodulin has been recognised as a biomarker for tendon differentiation, and its expression is regulated by transcription factors, including Scleraxis. Further studies using knock out technologies have shown that only loss of Scleraxis and TGF-β signalling leads to severe tendon developmental phenotypes, while mice deficient for various proteoglycans, Mohawk, EGR1 and 2, and Tenomodulin presented mild phenotypes.

Table 1. Native tenocyte cell (TC) characteristics

Morphology	Positive markers		Negative markers
Spindle and elongated shape	**Collagen I** **Collagen III** **Collagen V** **Decorin** **Biglycan** **Tenascin-C** **Scleraxis**	Sox9 Elastin Aggrecan Fibronectin **Tenomodulin** COMP	Upregulation of osteogenic (e.g., BMP signalling, alkaline phosphatase) and chondrogenic (collagen II) markers is indicative of unintended **trans-differentiation**

In this chapter, a novel high-frequency, low-amplitude bioreactor system employing a PVDF TrFE diaphragm is described and evaluated experimentally. A computational model was develop based on the contour conditions and validated experimentally. Furthermore, the role of high-frequency, low-amplitude electromechanical stimulation in cellular function and the ability of this bioreactor to maintain tendon cell function is explored *in vitro*. It is hypothesised that typical tenocyte phenotypic drift could be counteracted by cellular stimulation with electrical and mechanical cues under nano-vibrational conditions.

Thus, the objectives of the chapter are:

1. To develop a surface functionalization protocol to promote cell attachment and sustain the proliferation of cells on piezoelectric and non-piezoelectric membranes produced with PVDF-TrFE.

2. To assess the cytocompatibility of electroactive materials under dynamic and static conditions.

3. To evaluate the effect of piezoelectricity on tenocyte function using tendon-specific and non-specific biomarkers.

4. To determine main signalling pathways affected by high-frequency, low-amplitude piezoelectric stimulation in human tenocytes

3.2 Materials and methods

3.2.1 Vibration apparatus.

The bioreactor surface area was designed to hold two 6-well plates (Corning, NY) simultaneously with dimensions of 130×178 mm. The piezo actuators we used (PL088.30, Physik Instrumente, Karlsruhe, Germany) were low-profile actuators with a large attachment area. The top plate of the platform used the magnetic attachment to secure the 6-well plates. Standard 30 mm diameter, 3 mm thickness Fe2O3 ferrite magnets (Magnet Expert, Tuxford, UK) were bonded to the tissue culture plates. The quoted magnetic flux at the surface of these magnets is 700 gauss (0.07 T), which as a static magnetic field is not thought to be high enough to alter cellular function. However, these magnets, being Halbach arrays, are only magnetic on the side facing the bioreactor and away from the cell culture, therefore any stray magnetic fields would be far smaller. To power, the piezo array, a high-voltage piezo driver (Model ENV 150, Piezosystem Jena, Germany) was used, which is capable of providing 160 Vpk–pk. The sine wave modulation of the amplifier output was provided by a signal generator (Model 33210 A, Agilent, Santa Clara, CA)

3.2.2 Electromechanical actuation simulation

A piezoelectric stimulation can be modelled as a coupled mechanical and electrical system. Before the general estimation of piezoelectric performance, different physical properties of the materials such as permittivity or stiffness are required for the simulation.

3.2.2.1 Output voltage in static conditions

The equation using the piezoelectric coupling matrix that describes the behaviour of a piezoelectrical material is given by $T = c^D \cdot S - h \cdot D$ (D = const)

Equation 1-6. The boundary conditions and piezoelectric activation mode (loading conditions) will determine the output voltage. In the case of a voltage generating piezoelectric system (stimulator), the coupling matrix should in the form of the generated electric field [Volts] or charge [Coulomb] by applied stress [N] or strain [m].

In the case of a film excited by a vibrational wave, we consider the boundary conditions of stress (T) constant for the generated electric field, E. The equation is then rewritten in the following form:

$$E = -g_{ij}T + \beta^T D \qquad \text{Equation 3-1}$$

Where β^T is the permeability (under constant T) and g_{ij} is a transposed matrix of g.

Since the experimental conditions are under open circuit, the displacement current D is, therefore, zero, and the matrix simplifies to:

$$(E) = -g_{ij}(T) \qquad \text{Equation 3-2}$$

Therefore, it is possible to extract from the second expression of the equation (E) the output voltage that can be expressed as follows:

$$(V/t) = -g_{ij}.(YM.\varepsilon) \quad [\text{V/m}] \qquad \text{Equation 3-3}$$

Where t is the thickness of the piezoelectric film, YM the young modulus and ε the strain.

Furthermore, considering the stress applied homogenously, the output voltage becomes independent of the size (length) of the sample, and only the thickness is considered. It is also important to note that this equation is only valid in the elastic range of PVDF-TrFE, where the strain and stress are linearly proportional. A graphical representation of the output voltage for a 30 µm thick PVDF is shown in Figure 3-2.
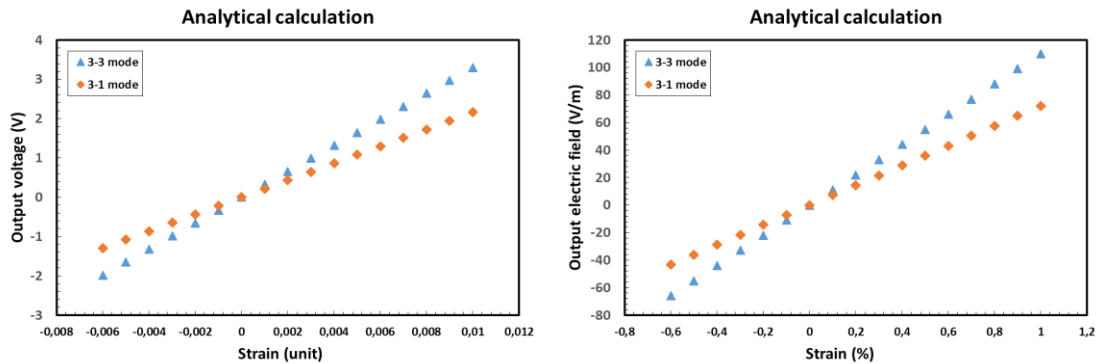
Figure 3-2. The theoretical absolute voltage output of 30 µm PVDF for 3-3 and 3-1 modes. g31 and g33 are 0.216 and 0.33 V.m / N, respectively.

This figure represents a distorted view of the problem since homogenous stress or strain is not applicable in the real system. Therefore COMSOL simulation can offer a more representative value of the output voltage in specified operational conditions

3.2.2.2 Output voltage in dynamic conditions (vibrations)

In dynamic conditions, the system is exposed to vibrations that generate stress-strain fields in the material. In turn, the stress-strain field is translated into electrical charges at the surface of the piezoelectric material. Therefore, the system can be electrically modelled as a current source that charges a "capacitor" (formed by the upper and bottom surfaces of the piezoelectric film). While the system is vibrating close to resonance model can be represented by a current source IP connected in parallel with a capacitor (C_P) and a resistor (R_P). As the vibration follow a sinusoidal wave, then the current source can be described by $I(t) = I0 \sin2\pi f0t$, where $f0$ is the excitation frequency. The theoretical electric power generated by a piezoelectric harvester is given as:

$$V(t) = I(t).Z_{INT}$$
                                                                   Equation 3-4

where I is the amplitude of the current source and $Zint$ is the equivalent internal impedance of the system.

Our system consists of a circular membrane clamped at the periphery and free to oscillate, also called a diaphragm. When observing the boundary conditions, we see a heterogeneous distribution of strain in the piezoelectric layer while vibrating, the volumetric strain is higher at the middle of the membrane and near the clamped end and very little in between this two areas (see Figure 3-3).
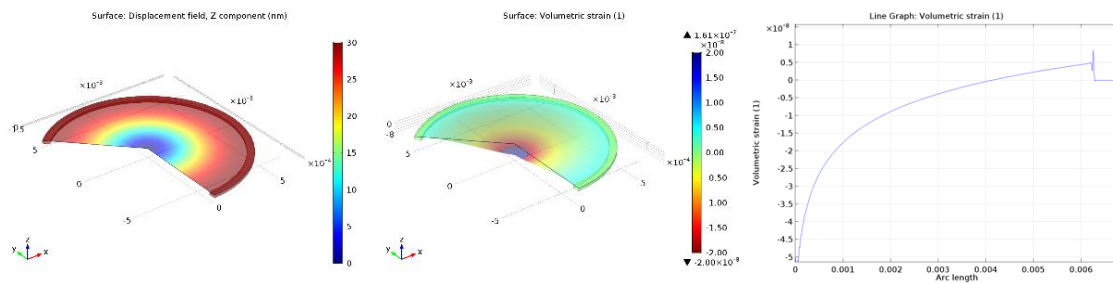
Figure 3-3. 3D Membrane displacement, 3D membrane volumetric strain and volumetric strain vs radius

3.2.2.3 Output Voltages under Pre-tension and natural frequencies

Our model is based on a pre-tensioned membrane clamped at the periphery (diaphragm, see Figure 3-4), and we use the 3D membrane interface to compute the natural frequencies on COMSOL.
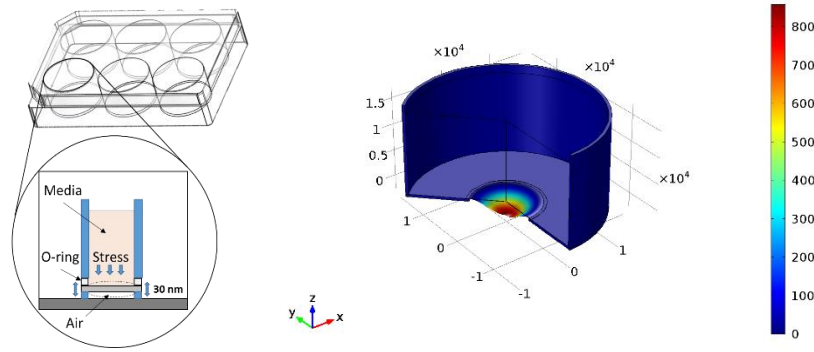
Figure 3-4. Set-up of the piezoelectric stimulator system. A 3D printed insert was developed to hold the piezoelectric membrane and keep it stressed.

A pre-tensioned system is a clear example of "stress-stiffening", where the transverse stiffness of a membrane is directly proportional to the tensile force. The analytical solution for the natural frequencies of the vibrating membrane given in Ref. 1 is:

$$f_{ij} = \frac{k_{ij}}{2\pi R} \sqrt{\frac{T_0}{h\rho}}$$

Equation 3-5

The values k_{ij} are derived from the roots of the Bessel functions of the first kind. In Table 3-1, the computed results are compared with the results of the theoretical value from equation 3-5.. The agreement obtained was excellent.

Table 3-1. Comparison between computed and theoretical values of resonant frequencies

Mode number	Factor	Analytical frequency (Hz)	COMSOL result (Hz)
1	$k10 = 2.4048$	172.8	172.8
2	$k11 = 3.8317$	275.3	275.3

3.2.3 Surface functionalisation for enhanced tendon cell proliferation.

For the prolonged culture of tendon cells on synthetic hydrophobic surfaces, chemical functionalization of the surface with relevant ligands is generally required. In this work, we used a standard protein such as fibronectin, widely used in for tissue engineering applications.

Surfaces were oxygen plasma treated for 45 seconds at 30 W and the flow rate of oxygen at 30 ml/min. Briefly, radicals formed and reacted with oxygen to form hydroperoxides on the polymeric surface. Subsequently, hydroperoxides decomposed due to thermal gradients and produced secondary radicals that initiate the polymerisation of acrylic acid (AAc). After oxygen plasma polymerisation, treated surfaces were immersed in a 20% v/v AAc aqueous solution at 90°C, which was previously purged with nitrogen using a reflux system to avoid changes in concentration. Next, the pAAc functionalised surfaces were rinsed with distilled H_2O for 18 hours to remove unreacted monomers. Finally, carboxyl groups were activated with 0.1 M EDC and 0.1 M NHS (1:1) for 1 hour immediately after films were immersed in a fibronectin solution (10 µg/ml) for 2 hours at room temperature.

3.2.4 Tenocytes and MSC cell culture

Human tendon derived cells were harvested from patellar tendon during tendon grafting operations after obtaining written informed consent in the University Hospital Galway. From these tissue specimens, primary human tenocytes were isolated and cultured. They were identified as tenocytes through their characteristic growth pattern and by detection of scleraxis (SCX) and tenomodulin (TNMD) expression. d. The studies were performed with cells at passage 2–3 and a total of at least 3 donors were used for all assays. Primary bone marrow MSCs were sourced from Promocell (Heidelberg, Germany) All cells were maintained in Dulbecco's Modified Eagle's Medium (DMEM/F-12 with Glutamax, Gibco-BRL) supplemented with penicillin (100 U ml−1), streptomycin (10µg ml−1) (both Sigma-Aldrich) and 10% fetal calf serum (Gibco-BRL). Cells were detached by incubation with 0.05% trypsin for 5 min at 37°C. l. All cell culture was performed in an incubator at 37 °C with 5% CO2. The basal culture media was removed and replenished every 2–3 days.

3.2.5 Cell proliferation assay

For cell proliferation analysis, tenocytes were seeded onto all experimental and control films in a modified 6-well plate (see Figure 3-4) at 4.5×10^4 cells/film (n=3). Cell metabolic activity and proliferation were assessed by Alamar Blue assay (Sigma-Aldrich). The cells were incubated in medium supplemented with 10% (v/v) Alamar Blue dye for 4 hours. A 100 μL sample of the medium with reduced Alamar blue was transferred and the absorbance at 570 and 590 nm measured in a 96-well plate using a Varioskan Flash Plate reader. Non-seeded biomaterial in the same medium was used as a negative control. The percentage of AlamarBlue reduction was calculated as follows:

Reduction of Alamar Blue (%) = ((O2 × A1) − (O1 × A2)/(R1 × N2) − (R2 × N1)) × 100

where O1 and O2 are the molar extinction coefficients of oxidized AlamarBlue at wavelengths 570 nm and 600 nm, respectively; R1 and R2 are the molar extinction coefficients of reduced AlamarBlue at wavelengths 570 nm and 600 nm, respectively; A1 and A2 are the observed absorbance readings for test wells at wavelengths 570 nm and 600 nm, respectively; and N1 and N2 are the observed absorbance readings for the negative control wells at wavelengths 570 nm and 600 nm, respectively.

3.2.6 Live/dead assay

Viable cells were seeded at a density of 5000/cm^2 (n = 5) on PVDF films for quantitative analysis using fluorescent microscopy. Tenocytes were cultured for 1, 3, or 7 days. Untreated live and dead cells were used as controls for quantitative analysis. Live/Dead Assay (Life Technologies) was used to visualise viable and necrotic cells. After each culture time, samples were washed with PBS and stained with calcein and ethidium bromide following the manufacturer recommendations. The samples were immediately analyzed (after incubation) with a Varioskan Flash plate reader. Samples were subsequently imaged on an Olympus IX81 inverted fluorescent microscopy with the 20× objective.

3.2.7 Protein expression.

Protein Antibody Microarray was custom made. Nexterion slide H microarray slides were purchased from Schott AG (Mainz, Germany). Alexa Fluor 555 carboxylic acid succinimidyl ester was obtained from Life Technologies (Carlsbad, CA, USA). Protein

samples were labeled with Alexa Fluor 555 carboxylic acid succinimidyl ester according to manufacturer's instructions. The excess label was removed, and the buffer was exchanged with PBS, pH 7.4, by centrifugation through 3 kDa molecular weight cutoff filters. Absorbance at 555 and 280 nm was measured for labelled samples and calculations were performed according to manufacturer's instructions using an arbitrary extinction coefficient of 100,000 and molecular mass of 100,000 to enable quantification of relative protein concentration and label substitution efficiency. All commercial antibodies (Table 1) were buffer exchanged into PBS and quantified by bicinchoninic acid (BCA) assay. Antibodies were diluted to print concentration in PBS and printed in six replicates on Nexterion H amine-reactive, hydrogel-coated glass slides using a SciFLEXARRAYER S3 piezoelectric printer (Scienion, Berlin, Germany) under constant humidity (62% +/− 2%) at 20 °C. Each feature was printed using ≈1 nL of diluted antibody using an uncoated 90 µm glass nozzle with eight replicated subarrays per microarray slide. After printing, slides were incubated in a humidity chamber overnight at room temperature to facilitate complete conjugation. The slides were then blocked in 100×10^{-3} m ethanolamine in 50×10^{-3} m sodium borate, pH 8.0, for 1 h at room temperature. Slides were washed in PBS with 0.05% Tween 20 (PBS-T) three times for 2 min each wash followed by one wash in PBS, dried by centrifugation ($470 \times$ g, 5 min), and then stored with a desiccant at 4 °C until use. Incubations were carried out in the dark. Microarray slides were incubated as previously described. Initially, one labelled sample was titrated (2.5–15 µg mL−1) for optimal signal to noise ratio and all samples were subsequently incubated for 1 h at 23 °C at 9 µg mL−1 in Tris-buffered saline (TBS; $20 \times 10−3$ m Tris-HCl, $100 \times 10−3$ m NaCl, $1 \times 10−3$ m CaCl2, $1 \times 10−3$ m MgCl2, pH 7.2) with 0.05% Tween 20 (TBS-T). All microarray experiments were carried out using three replicate slides. Alexa Fluor 555 labelled cells lysate (10 µg mL−1) were incubated in two separate subarrays on every slide to confirm retained antibody performance and printing, respectively (figure 1). After incubation, slides were washed three times in TBS-T for 2 min per wash, once in TBS and then centrifuged dry as above. Dried slides were scanned immediately on an Agilent G2505 microarray scanner using the Cy3 channel (532 nm excitation, 90% photomultiplier tubes (PMT), 5 µm resolution) and intensity data were saved as a .tif file. Antibody microarrays were verified to remain active for at least 2 weeks after printing and all incubations were carried out within that timeframe. Data extraction

from .tif files was performed mainly as previously described. Data were normalized to the mean of three replicate microarray slides (subarray-by-subarray using subarray total intensity, n = 4, 24 data points). Unsupervised hierarchical clustering of normalised data was performed using Hierarchical Clustering Explorer v3.0 (http://www.cs.umd.edu/hcil/hce/hce3.html) using the parameters no prefiltering, complete linkage, and Euclidean distance. All data presented here were confirmed using at least four replicates for each of the test groups and control group. The results are expressed as the mean of the values ± standard error of the mean.

Different types of arrays were fabricated to investigated tendon regeneration or phenotype maintenance (tenogenesis), intracellular molecular pathways (signalling) or membrane proteins (receptors).

Table 2. *Tenogenesis array.* Proteins associated with tendon regeneration or tenocyte function.

Proteins	Abbreviation	Purchased from
Scleraxis	SCX	Abcam
Tenomodulin	TNMD	Abcam
Byglican	BGN	Abcam
Decorin	DCN	Abcam
Thrombospondin 4	THBS-4	Abcam
Tenascin C	TNC	Abcam
Collagen I	COLI	Abcam
Collagen III	COLIII	Abcam
Collagen V	COLV	Abcam

Table 3. _Signalling array_. Proteins associate to different signalling pathways (MAPK, FAK, TGF-B, BMP and WNT).

Proteins	Abbreviation	Purchased from
Smad 1	SMAD1	Cell signalling
Smad 3	SMAD3	Cell signalling
Smad1/5/8	SMAD1/5/8	Cell signalling
Phosphorylated Smad 1/5/8	pSMAD158	Cell signalling
Focal adhesion kinase	FAK	Cell signalling
Phosphorylated FAK	pFAK	Cell signalling
MAPK	ERK1/2	Cell signalling
pMAPK	pERK1/2	Cell signalling
Wnt/ β-catenin	β -Catenin	Millipore
Active β-catenin	Active β-Catenin	Millipore

Table 4_. Receptors array_. Proteins associate to cell membrane receptors.

Proteins	Abbreviation	Purchased from
TRPV1	TRPV1	Abcam
Piezo1	Piezo1	Abcam
Piezo2	Piezo2	Abcam
TRPA1	TRPA1	Abcam
KCNK2	KCNK2	Abcam
KCNK4	KCNK4	Abcam
L-type Ca2+	L-type Ca2+	Abcam
BMPR1A	BMPR1A	Abcam
Integrin1	ITG1	Abcam
Integrin3	ITG3	Abcam
Integrin5	ITG5	Abcam

3.2.8 Inhibition studies: Cytoskeletal inhibition

TCs were seeded at 7.5x 10^3 cells/cm2 in stimulated and control culture conditions for 5 days in the presence or absence of inhibitors of ROCK (Y27632, Sigma) at 10 μ M and myosin II (blebbistatin, Sigma cat. B0560) at 5 uM. Inhibitors were added fresh with all medium changes for the duration of the experiment.

3.2.9 Statistical Analysis

Data are presented as means ± SD from three or more separate experiments, as indicated. Data were analyzed using Minitab 8. Student's -test (for single comparison) or one-way ANOVA (for multigroup comparisons) with Tukey post hoc test was used to denote statistical significance.

3.3   Results

3.3.1   Design of high-frequency, low magnitude stimulation system

Characteristics of a membrane, such as its thickness, width, stiffness and residual stress, determine the resonance frequency of the membrane. A piezoelectric membrane generates electrical output voltage in response to applied mechanical stress and strain and is directly proportional to the thickness of the material. It is known that with increasing thickness, resonance frequency decreases gradually; however, thicker samples produce higher levels of energy. In this work, we have found that an optimal thickness of 25 µm for the thermal poling process, effective operation (>200 Hz) and electrical output. The membrane vibrates with relatively large amplitude at its resonant frequencies (eigenmodes), thus generates more prodigious electrical signal output on the resonating position than those on non-resonating positions. The schematic with dimensions and the resonant frequencies are shown in Figure 3-5.
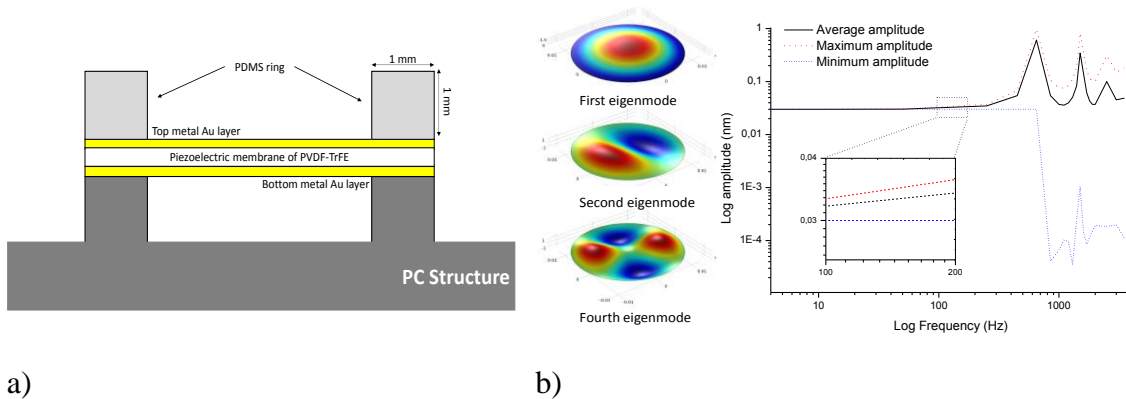
a)   b)

Figure 3-5.a) Thin-film PVDF-TrFE membrane structure and boundary conditions b) COMSOL harmonic response modelling of the membrane in the range of 0 to 2,000 Hz (30 nm amplitude). The response of membrane follows the input vibration reliably until reaching 700 Hz (magnified inset shows 100-200 Hz). Above this frequency, first, second and third resonant modes (700 Hz, 1500 Hz and 2500 Hz) cause significant amplification and deformations at the membrane, shown by the minimum and maximum amplitudes are taken from the modelled membrane.

Table 3-2. Values of the parameters used to create the model of the membrane. The outer edge of the membrane is supported in the transverse direction. Two points have constraints in the in-plane direction to avoid rigid body motions.

Model Parameters				
Geometry		Material		
Membrane radius, R	Membrane thickness, h	Young's modulus, E	Poisson's ratio, ν	Mass density, ρ
6,25 mm	25 um	1 GPa	0.33	1780 kg/m3

3.3.1.1 Optimisation of physical dimensions of the membrane

Membranes were operated at low-frequency stimulation (0,5 Hz) using a square function to ensure that the membrane shows its maximum electrical output. Since a square wave includes all the frequencies at once (see figure), it is expected that the maximum output voltage corresponds to the resonant frequency for the membrane. The function of a square wave is :

$$f(x) = \sum_{n=1,2,3,\cdots} \frac{1}{n}\sin(nx) \qquad\qquad \text{Equation 3-6}$$

a)   b)
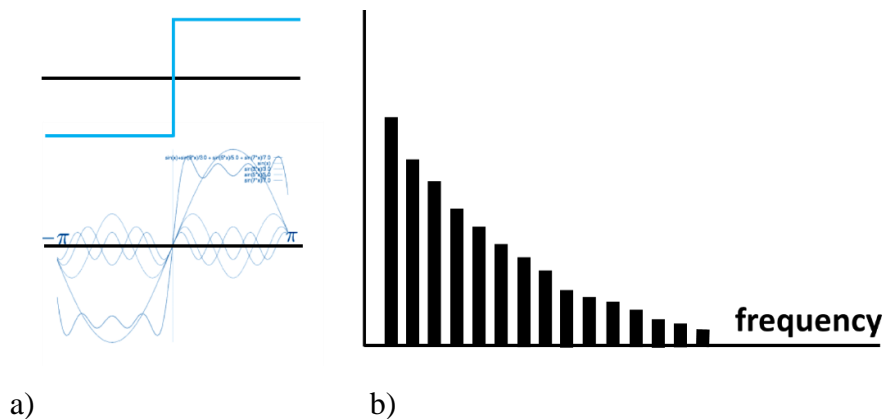
Figure 3-6 a) Spatial frequency analysis of a step edge (top) and Fourier series (bottom) b) Fourier decomposition of the step edge.

It is important to note that membranes with resonant frequencies closer to low values will be favoured by this method. Therefore, a frequency sweep at the same amplitude was also used to validate the obtained results.

Also, it is observed that at low frequencies, the high output impedance of the membrane results in a low pass filter and the signal becomes attenuated (see figure). Therefore, it is needed to use a data acquisition system that matches the input impedance with the output impedance of the membrane to perform a precise measurement of the electrical output.

a)   b)
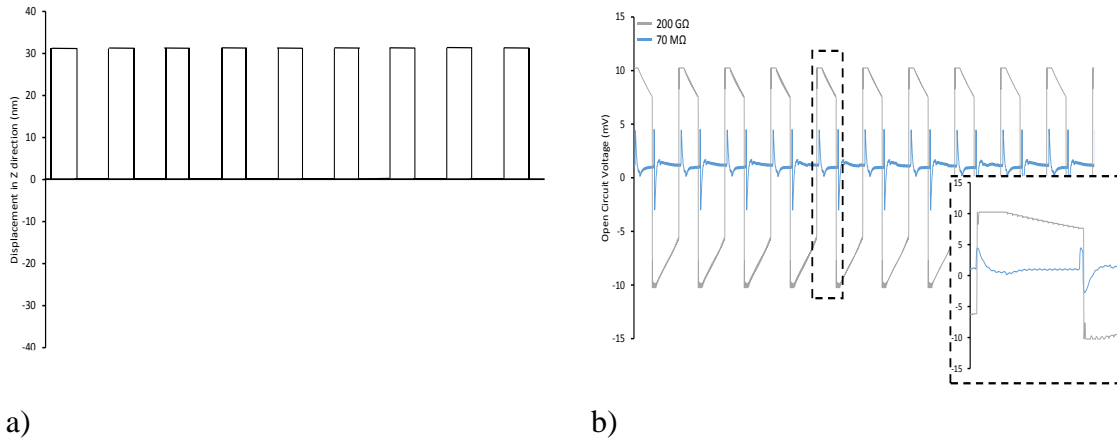
Figure 3-7 a) Generated square function to stimulate the membrane mechanically at low frequency (0,5 Hz) b) Output voltage measured using two types of equipment with different input impedance (70 MOhm and 200 MOhm).
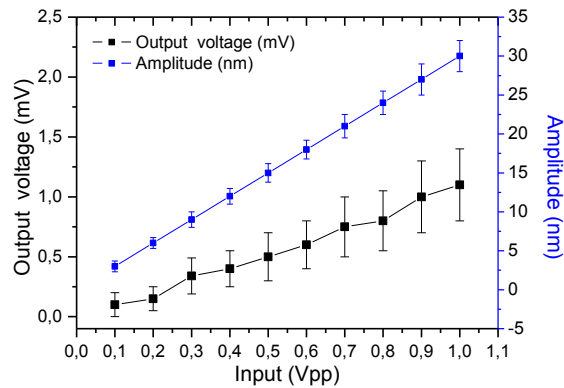
Figure 3-8 Interferometric calibration of the bioreactor for one frequency (200 Hz).Vibration amplitude and output voltage are linearly dependant on the input voltage (peak to peak) of the bioreactor

As observed in

Figure 3-8, the maximum output obtained was around 1 mV for 30 nm of displacement (0,033 mV/nm).

3.3.1.2 Vibrational membrane behaviours.

When the membrane is exposed to nano-vibrational waves (see figure), electrical signals are generated as shown in the figure. At the vibration wave frequency 1500 Hz, the membrane (PVDF-TrFE/BNNT) generated a periodic voltage output with a peak value as high as 3 mV. The electrical output is of a typical AC (alternating current).

To avoid false readings, background noise and interfering signals introduced by instruments and connecting cables, we used fast Fourier transform (FFT) technique to process the output signals (see Figure 3-7).
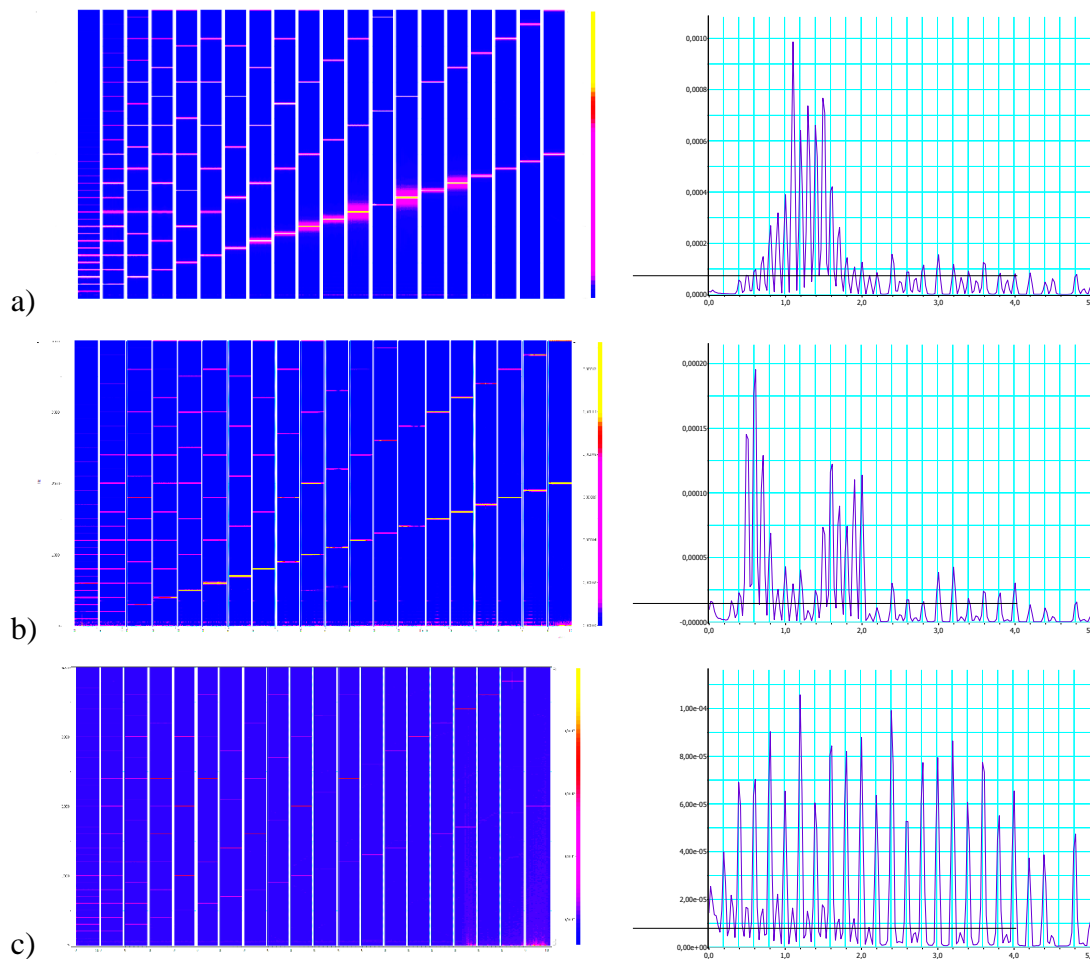
Figure 3-9. FFT decomposition of a) PVDF-TrFE/BNNT (poled) b) PVDF-TrFE (Poled) and c) PVDF-TrFE (non-poled).

After filtering with FFT using the nano vibration frequency, the output voltage was very similar to the raw data (see Figure 3-9). However, when FFT was used on the frequencies beyond the frequency of vibration were much smaller, and therefore, it was possible to obtain a more detailed profile and more accurate reading of the outputs. By maintaining constant the amplitude of vibration and varying the frequency, the effect of frequency on voltage output was examined. As shown in Figure 3-10, the voltage output changes with vibration frequency. It was observed that the maximum value was obtained at 1500 Hz, and after that value, the signal decreased. A fluctuation or drop of the voltage is observed at frequencies between 900-1300 Hz. The voltage output decreased to nearly zero when the frequency was over 5 kHz.

a)   b)
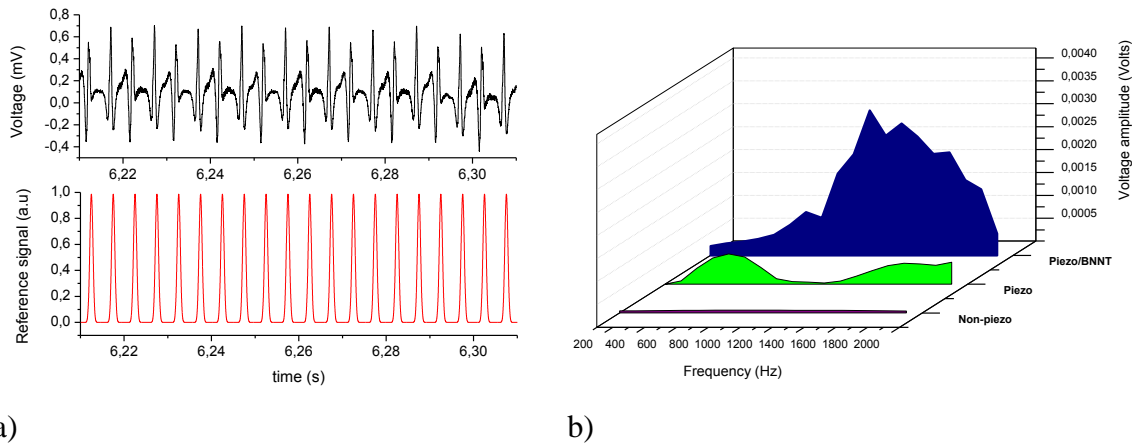
Figure 3-10. a) Representative image of electrical response (top) and input frequency used for FFT (bottom) b) FFT filtered data for the 3 samples.

The sensitivity of the membrane is an important parameter to cellular electrical stimulators (CES). The following equation can calculate the sensitivity (S) for the CES,

$$S = \frac{V}{D}$$

Equation 3-7

Where V is the voltage and D the displacement of the bioreactor. Based on the figure, the sensitivity of the membrane was as high as 0,18 mV/nm for nanocomposites. For comparison, a PVDF-TrFE (PT) film (the same dimension and thickness) was also subjected to the same test. As shown in the figure, at the same frequency (1500 Hz), the

outputs from the sample were significantly smaller for PT films. The maximum sensitivity achieved by the PT film was 0,033 mV/nm.

Effect of cellular electrical stimulator structure

It is noticeable that the size of the membrane (or hole size) plays an essential role in the final output voltage. If the membrane was not suspended across a hole, the device could generate less than 5% (3,33%) of the voltage.

The hole size (membrane diameter) affected the voltage output and therefore, the sensitivity. As observed in Figure 3-11, when the hole was smaller than 6 mm, the sensitivity was lower than 0,1 mV/nm. The sensitivity increases with hole-size up to 12.5 mm. Further increasing the diameter resulted in increasing the sensitivity.

a)   b)
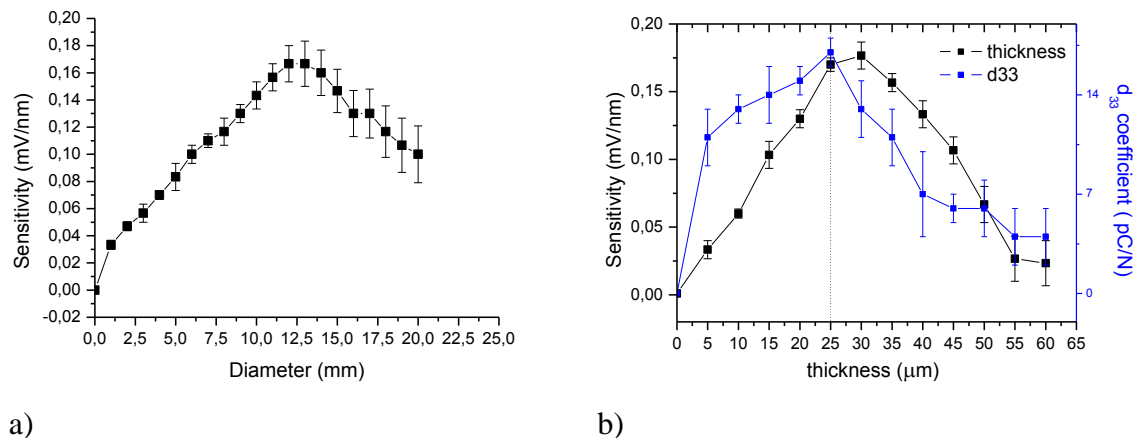
Figure 3-11 Sensitivity of the stimulator devices. Effect of (a) hole diameter (membrane thickness, 25 µm; sound wave frequency, 700 Hz; displacement 30 nm), the (b) thickness of the membrane (hole diameter, 12.5 mm; vibrational wave frequency, 700 Hz; 30 nm displacement).

Finally, the optimal membrane diameter and thickness were 12.5 mm and 25 µm, respectively.

Vibration characteristics: resonant frequencies (Eigenfrequencies)

A membrane is defined as an entirely flexible two-dimensional plane of zero thickness held in tension by force so significant that deflections cause no change in the membrane tension.

The vibration characteristics, and thus, resonant frequency, are almost entirely dependent upon geometry and material properties. Membrane geometry is specified by shape, size, thickness, and cross-section. The material properties influencing resonant frequency include the density, residual or internal stress, elastic modulus, and Poisson's ratio.
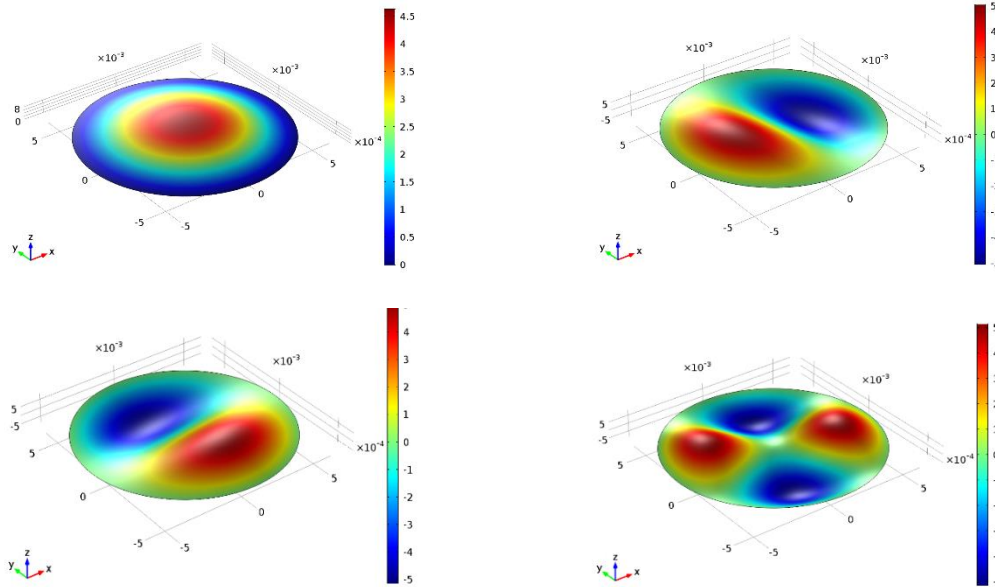
Figure 3-12. Membrane morphologies at the first 4 eigenfrequencies of a circular membrane with uniform pretension. The modes correspond to the indices (m,n) = (1,0); (1,1); (1,1) and (1,2); respectively. Note that modes 2 and 3 are duplicates with identical natural frequencies. Scales are not showing real displacements.
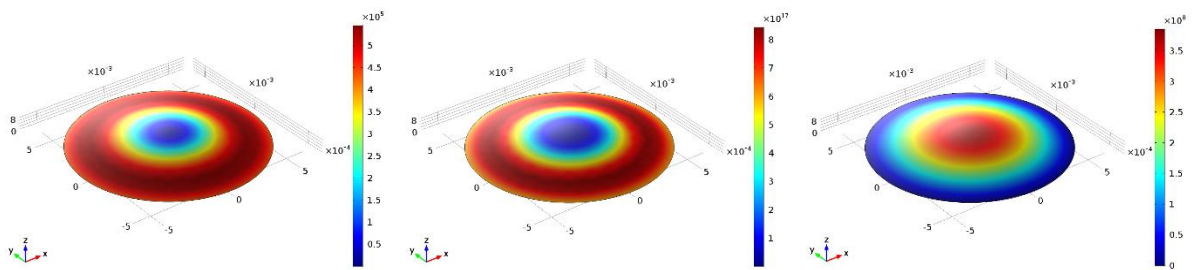
a) First principal strain   b) Von Mises stress (N/m^2)   c) Acceleration (m/s^2)

Figure 3-13. Different characteristics of a membrane under first natural frequency.

A finite element method (COMSOL Multiphysics 5.2) was used to analyze the resonant frequencies of the film. The modelling parameters such as pre-stress and fluid interaction

185

needed to be incorporated to obtain an excellent fidelity in the model. After defining a pre-stress and incorporating the fluid-membrane interaction, the model represented accurately the experimental observations (see).
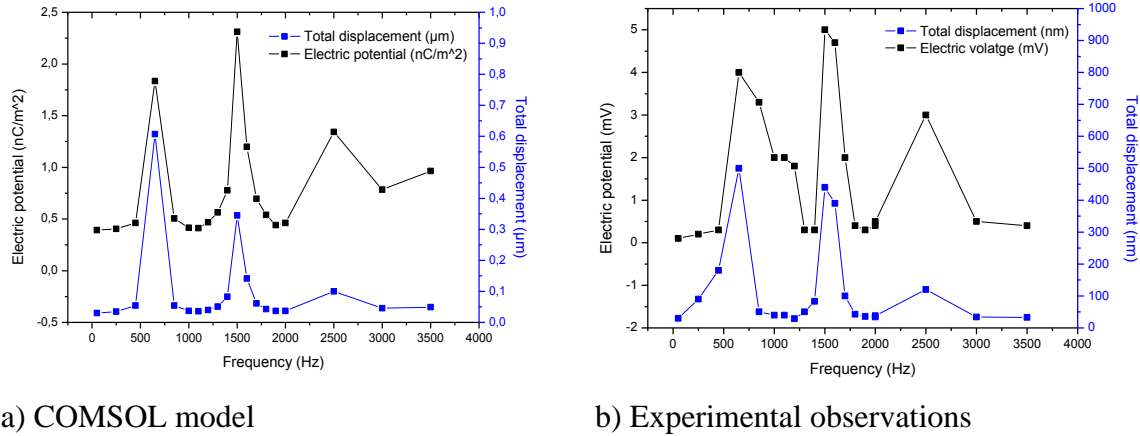
a) COMSOL model   b) Experimental observations

Figure 3-14. a) Displacement and electrical output obtained using the COMSOL model b) Experimental data obtained using LVD and data acquisition system.

It was observed that specific frequencies gave "peaks of voltage output" which seem to correspond with the "physical vibration amplitude peaks", however, the relationship between amplitude and voltage was not the same for all frequencies.

Effect of pre-stress

The membrane needs to undergo the transition from membrane behaviour to plate behaviour, which depends profoundly on the tension of the membrane. In this way, a membrane with small tension forces requires a thinner thickness to produce a plate-like response and vice versa.

An eigenfrequency simulation with a pre-stressed structure can be simulated in two ways. In a general case, the prestress is given by some external loading and is thus the result of a previous step in the solution. Such a study would consist of two steps: One stationary step for computing the prestressed state, and one step for the eigenfrequency. If stresses are known in advance, it is possible to use an initial stress condition. This is shown in this study.

The resonant frequencies of the 12,5 mm diameter and 25 µm thickness membrane in "pseudo"non-pre-tensioned condition (T_0= 5 N/m):

$$N_0 = \begin{bmatrix} 5 & 0 \\ 0 & 5 \end{bmatrix} N/m$$

The first natural frequency using equation 3-5 has been found at 649,13 Hz in a vacuum.

Table 3-3. Comparison between analytical and computed natural frequencies (in a vacuum)

Mode	Factor	Analytical frequency	COMSOL result (Hz)
1	k10 = 2.4048	649,13	649,1
2	k11 = 3.8317	1034,3	1034,2
3	k11 = 3.8317	1034,3	1034,2
4	k12 = 5.1356	1386,4	1386,2
5	k12 = 5.1356	1386,4	1386,2
6	k20 = 5.5201	1490,3	1490,0

In the computed results using COMSOL are compared with the analytical results. The agreement is excellent. The mode shapes for the first four modes are shown in Figure 3-12. Note that some of the modes have duplicate eigenvalues, which is a common property for structures with symmetries.

Pre-stress is here used to provide stiffness and maintain the shape (see Figure 3-15) of the membrane and ultimately control the resonant frequencies. It was observed that as the pre-stress was increased, the first resonant frequency was found at higher values. The results were compared to analytically obtained results, and the differences were less than 0.1%.

a)

187

b)
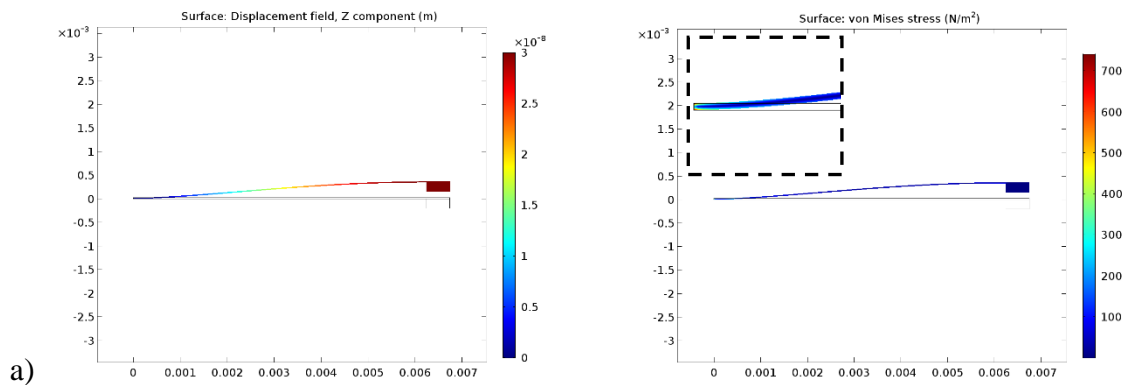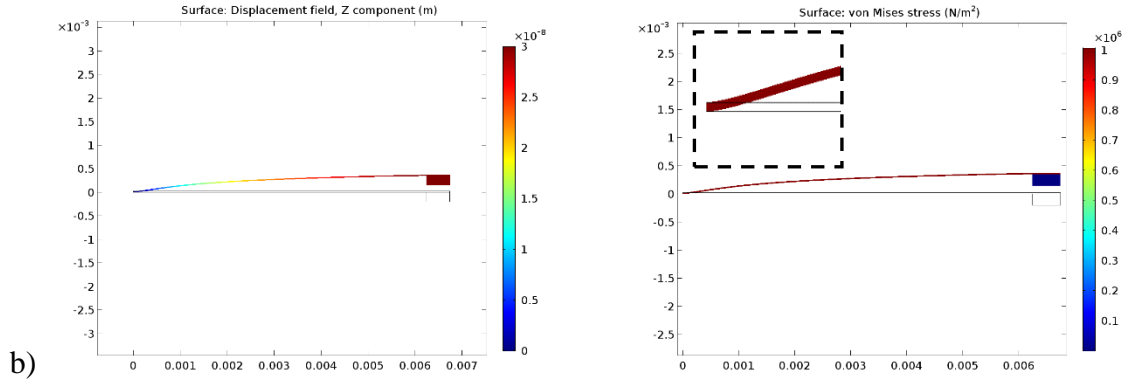
Figure 3-15. Displacement and stress generated in half of the membrane (6,25mm) under two conditions of pre-stress a) 1 N/m and b) 50 N/m.

If we apply a pre-stress of 2MPa (T_0 = 50 N/m) then the calculated and simulated first resonant frequency is 2052,7 Hz.

Table 3-4. Comparison between analytical and computed natural frequencies under pre-stress of 25 N /m.

Mode	Factor	Analytical frequency	COMSOL result (Hz)
1	k10 = 2.4048	2052,7	2052,7
2	k11 = 3.8317	3270,7	3270,8
3	k11 = 3.8317	3270,7	3270,8
4	k12 = 5.1356	4383,7	4384,2
5	k12 = 5.1356	4383,7	4384,2
6	k20 = 5.5201	4711,9	4619,7

For a membrane-based electrical stimulator, the tension of the membrane could be used to tune the resonant frequency of the vibrating membrane. According to equation 3-8, the frequencies of the un-stressed and pre-stressed membrane are proportional to the square root of the tension, which means that the square of the new effective frequency is proportional to the membrane tension (see Figure 3-16. Example of membrane resonance frequency as a function of change in applied tension.. The effective membrane frequency to the fundamental frequency is a function of the change in membrane tension. This relationship is shown in Figure 3-16. Example of membrane resonance frequency as a

function of change in applied tension., where the theoretical calculations agree well with the FEM simulation results in COMSOL. Therefore, tuning the membrane tension could significantly alter the resonant frequency of the device, which would be useful in the development of stimulator devices which can target specific frequencies.
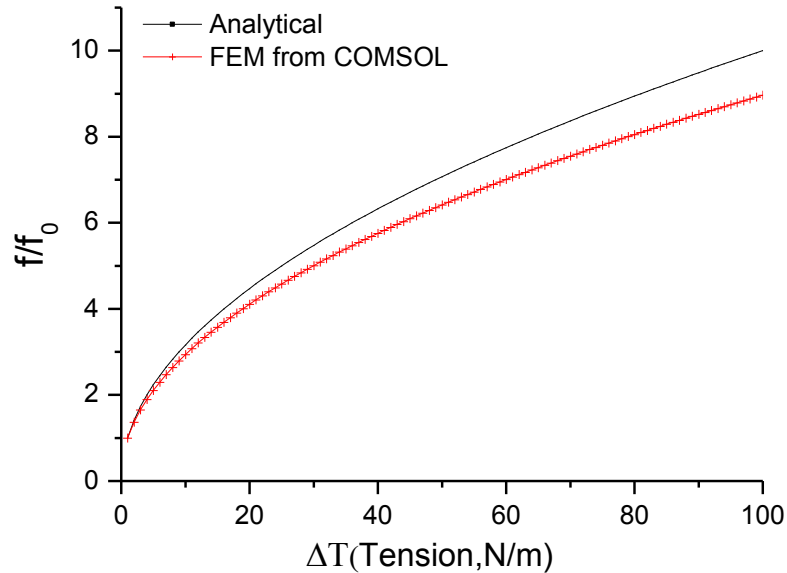
Figure 3-16. Example of membrane resonance frequency as a function of change in applied tension.

3.3.1.3 Effects of membrane-fluid interactions

The media surrounding a vibrating membrane having a dramatic impact on the structure, adding "virtually" mass and damping. Generally, it is known that the natural frequencies of structures interacting or fully immersed with water decrease significantly (compared to in air). The vibration of the membrane is transferred to the water movement and increases the total kinetic energy of the composite system. Assuming that the mode shapes do not change under the influence of water, the following approximate formula can be used to predict the natural frequency change when the circular membrane is in contact with water:

$$f_w = f_a / \sqrt{1 + \beta . \Gamma} \hspace{5cm} \text{Equation 3-8}$$

Where β is called a thickness correction factor and Γ is the non-dimensionalised added virtual mass incremental (NAVMI) factor.

The main properties of the liquid that may have an impact on the resonant frequency are the viscosity, density and pressure. Viscosity has a negligible impact on resonant frequency for fluids with viscosities less than 0.006 N·s/m2 (water viscosity is 0.001 N·s/m2 and air viscosity is 0.000018 N·s/m2). The viscosity dissipates system energy resulting in a faster decay in free vibration and reducing the resonant frequency amplitude at forced vibration. Inaba et al. showed that the resonant frequency decreased with higher viscosity. However, no shift was observed for the frequency of the resonance[277].

Physically, a shift in resonant frequency is attributed exclusively to an added mass effect. Briefly, the movement of the fluid in phase with the relative movement of the vibrating membrane results in a virtually added mass to the membrane. This effect was first described by Lamb who showed that membrane-fluid interactions could be described by the ratio between the kinetic energies of the membrane and fluid, a factor known as an added virtual mass incremental factor, or AVMI factor. The AVMI method can be used to predict the effect of fluid loading on vibrating structures. Kwak and Kim showed how the AVMI factor could be used to accurately predict the resonant frequency of a circular membrane under various clamping conditions[278]. They showed that the AVMI factor, β, could be solved merely as:

$$\beta . \Gamma = \frac{\rho_f}{\rho_p} . \frac{r_p}{t_p}$$ Equation 3-9

with: ρ_f: fluid density ρ_P: membrane density r_P: plate radius t_p: plate thickness Γ: non-dimensional added virtual mass incremental (AVMI) factor accounting for vibration mode and clamping.

Table 3-5 presents the values of NAVMI factors for a uniform thickness circular plate. In this table, 'n' represents the order of the mode number and 'N' denotes the number of terms used in the interpolation function to approximate the mode shape.

Table 3-5. Non-dimensional added virtual mass incremental factor Γ for a uniform thickness circular membrane.

Modes	n						
	0	1	2	3	4	5	6
	0,6669	0,2807	0,1671	0,1182	0,082	0,0651	0,0541

The solution becomes extremely difficult because although the membrane solution is two-dimensional, the fluid movement is three-dimensional, adding to its complexity. It is important to note that the first two orders modal NAVMI factors are far bigger than the NAVMI factors. That indicates that the first two vibration modes are more sensitive to water than the other modes.

Table 3-6. Parameters for calculating the thickness factor

Plate radius, r_p	Plate thickness, t_p	Membrane density, ρ_p	Water density, ρ_w
6,25 mm	25 µm	$1,78 \times 10^3$ kg/m^3	$1,0 \times 10^3$ kg/m^3

In this study, the following parameters for the uniform circular plate are found in table 3-6 and the value for β.Γ is 140,5. Taking the AVMI factor for the first natural frequency then we obtain the following:

$$f_w/f_a = 0,103 \text{ for } n=1 \text{ and } fw = 689,9 \ Hz$$

Table 3-7. Obtained and calculated results of the first resonant frequencies.

Modes	AIR			WATER		
	Analytical	COMSOL	Observation	Analytical	COMSOL	Observation
1	3270,8	2833,9	3800	689,94	696,1	700
2	4384,2	4250,9	-	1232,5	1500,2	1500
3	4619,7	6778,1	-	1325,3	2500,3	2500

It is also observed that the natural frequencies of the membrane exposed to water are smaller than those exposed to air, and the natural frequencies of the membrane exposed to

water with both sides are smaller than those of the circular plate exposed to water with one side.
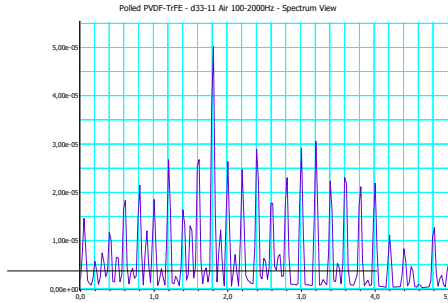
AIR   WATER
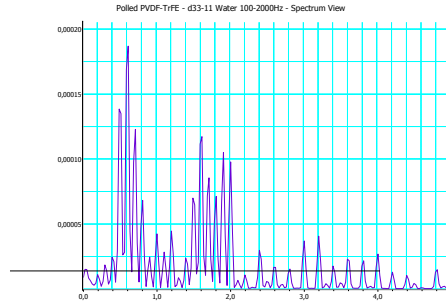
a)   PVDF-TrFE Poled (rms for air 0,01-0,03 mV and rms for water=0,1-0,3 mV)
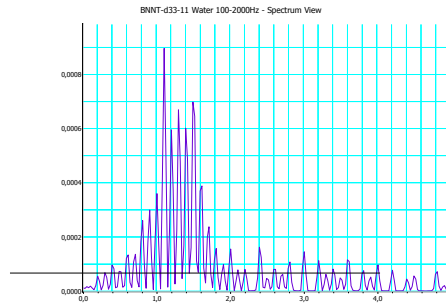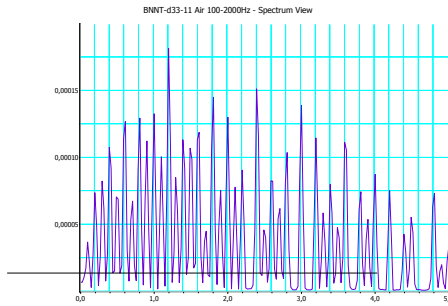
b)   Nanocomposite (rms for air =0,1-0,2 mV and rms for water=1-5 mV)
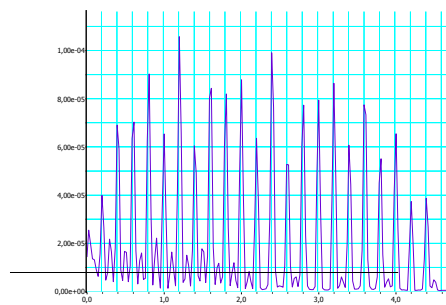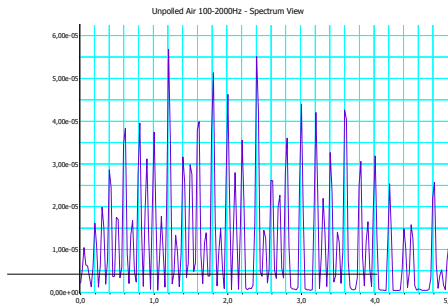
c)   PVDF_TrFE non-poled (rm for air =0,02–0,04 mV and rms for water =0,04-0,06 mV)

Figure 3-17. Effect of membrane-fluid interactions results in the shift of resonant frequency.

3.3.1.4 Effect of vibration frequency and modes on electrical outputs

The direct measurements of the output voltage from the films offer a total generated electrical field of 12 V/m. These results were also confirmed with the COMSOL model. As shown in the figure 3-18 when the membrane is under a single displacement of 30 nm, it can generate an entire field of 12 V /m. It is important to note that the model offers a greater understanding of how the distribution of the field is on the membrane, whereas in this was not possible to confirm it with the direct observations.
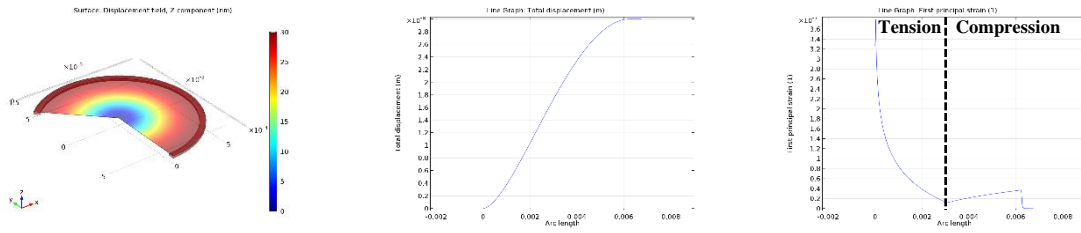
a) The first mode (displacement and strain)
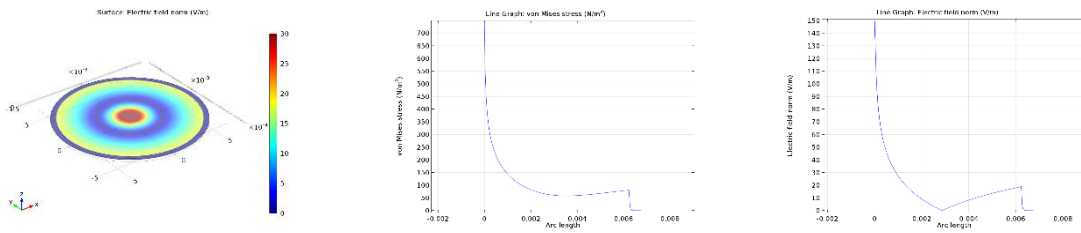
b) The first mode (stress and electric field)
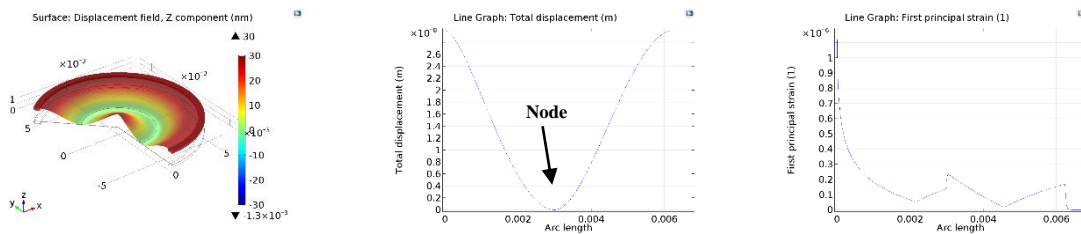
c) The second mode (displacement and strain)
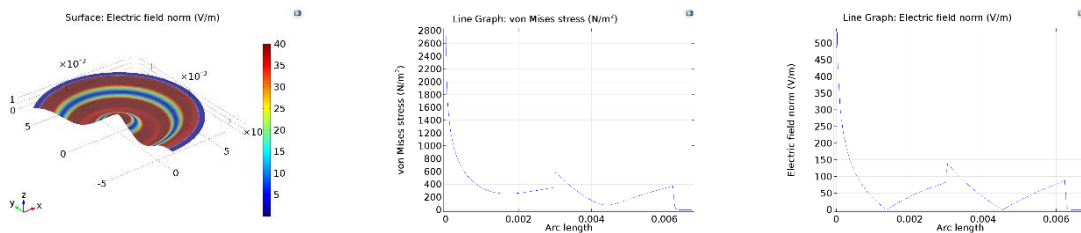
d) The second mode (stress and electric field)

Figure 3-18. Different modes associated to 700 Hz (a,b) and 1500Hz (c,d).

From a mechanical point of view, it is essential to note that the stresses/strains developed in the surface are heterogeneous and depend upon the mode of operation chosen. It is noticeable that the number of nodes (areas with displacement equal to 0) increases with mode number (n=1,2,…). The appearance of a node increases the number and level of electric field gradients over the entire membrane surface (see Figure 3-18). Therefore, at higher mode (higher resonant frequency) the level of localised voltage gradients is increased.

3.3.2 Tendon cell culture under static conditions

3.3.2.1 Cell viability on PVDF-TrFE composites. Addition of BNNT in PVDF-TrFE enhances cell adhesion.

In order to assess the ability of PVDF-TrFE materials to support tissue interfacing applications, formulations with significant electromechanical outputs (annealed PVDF-TrFE and PVDF-TrFE/BNNT nanocomposite films) were used to evaluate cell viability up to 10 days in culture. Tissue culture plastic (TCP) was a control substrate. It was observed that cell viability was maintained on all experimental and control substrates following functionalisation with fibronectin, and no cell death was observed (figure 7). However, cell proliferation assays confirmed that cells cultured on PVDF-TrFE/BNNT nanocomposites demonstrated a more sustained and enhanced proliferation for up to 10 days in culture (see Figure 3-19).
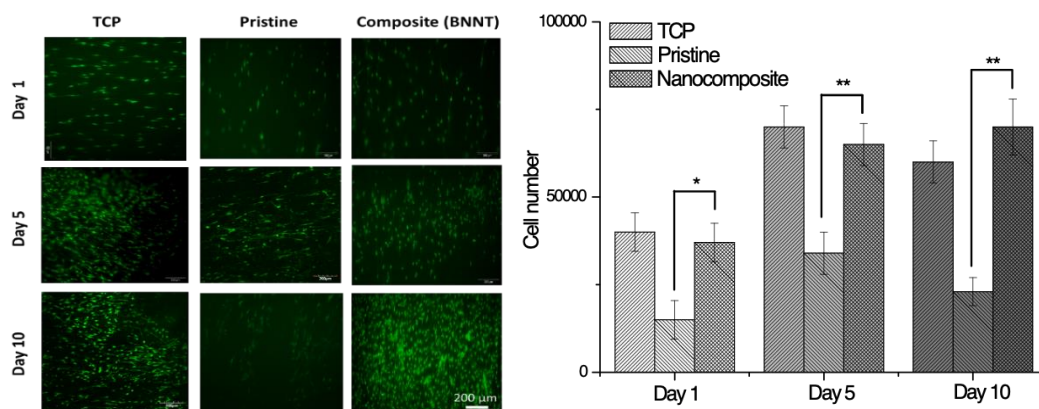
Figure 3-19. a) Live/dead assay on pristine PVDF-TrFE and nanocomposite PVDF-TrFE/BNNT substrates for 1, 5 and 10 days in vitro. b) Proliferation behaviour of human

194

tenocytes cells on pristine PVDF-TrFE and nanocomposite PVDF-TrFE/BNNT substrates for 1, 5 and 10 days in vitro. (**p<0.01 ; *p<0.05 to respect to pristine)

After one day in culture, differences in cellular behaviour were observed *in vitro*. It was observed, that the incorporation of BNNT increased cell adhesion. In particular, a 2-fold increase compared to pristine samples was observed for BNNT nanocomposites. This difference increased further after 5 and 10 days. This effect could be attributed to the superimposed nanotexture on the topography, the result of the incorporation of BNNT or to the electrically neutral surface of BNNTs that might act as an anchoring site for cells. As previously demonstrated by Biggs et al.[21], the cellular rigidity sensing machinery is capable of detecting discrete heterogeneous rigidity differences in their extracellular environment up to the nanometer level comparable to that of the nanotubes. Several authors have shown similar effects on cell behaviour; Giannini et al[22] have observed increased adhesion of fibroblasts cultured on surfaces characterised by protruding nanotubes. Furthermore, Zhang et al. [23] demonstrated that cell Rho A–mediated proliferation increases with increasing topography induced by nanotube incorporation. Finally, Genchi et al. [24] have demonstrated that incorporation of BNNT in PVDF-TrFE can promote the differentiation of human osteoblasts.

As proliferation, especially with pristine samples was not maintained for long periods of times (i.e. 10 days), a protocol of functionalization with fibronectin, a central protein component of the tendon, was used.

3.3.2.2 The effect of surface polarisation on tendon cell proliferation. Surface Biofunctionalization is required for sustained tendon cell proliferation

Many factors contribute to the creation and maintenance of an optimal microenvironment for cell growth in vitro, e.g. the consistency of the growth medium, the addition of supplements, and the surface on which the cells grow. The nature of the surface on which cells are cultured plays an essential role in their ability to attach, proliferate, migrate and function. Components of the extracellular matrix (ECM) are often used to coat glass or plastic surfaces to enhance cell attachment in vitro. As shown previously, one physical factor that is intrinsic to piezoelectric surfaces is the remnant polarisation after poling

(charging) the surfaces of the materials. This electrical polarisation can be either positive or negative and may affect cell attachment or proliferation.
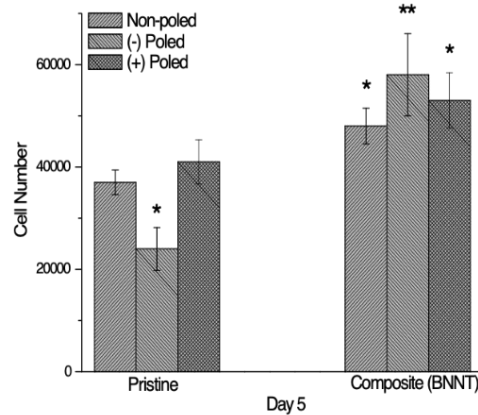
Figure 3-20.Proliferation rate at day 5 of tendon cell cultured on unpolarised and polarised pristine and composite samples. (**$p<0.01$; *$p<0.05$ to respect to non-poled)

Therefore, the difference in cell proliferation when cultured on polarised and non-polarised samples with and without the incorporation of BNNT was investigated.

Interestingly, it was observed that negatively charged annealed PVDF-TrFE films educed tenocyte adhesion and proliferation relative to unpoled and positively charged pristine annealed PVDF-TrFE films (Figure 3). This can be explained as an electrostatic response. Since the membrane of tendon cells is also charged negatively, it can be inferred that electrostatic repulsion can compete with integrin-mediated cell attachment. In a similar study performed by Ribero et al., changes in cell proliferation were also observed as a consequence of the state of polarisation of PVDF surfaces. Conversely, the anti-proliferative effect of negatively charged pristine annealed PVDF-TrFE films was not observed in negatively charged annealed PVDF-TrFE 1 wt. % of BNNT nanocomposite films. In addition, it was observed that cells attached and proliferate better on composite samples regardless of the polarisation state. Again, it can be inferred that this effect is attributed to the modified substrate topography as a result of the BNNT incorporation and also to the electrically neutral surface presented by BNNTs that might act as an anchoring site for cells adhesion. [25–27].

Finally, fibronectin was bound to the PVDF-TrFE surface using a non-covalent (adsorbed) or covalent method. Due to the lack of functional groups on the surface which would allow a covalent attachment of the protein, it was necessary to first generate available surface functional groups by plasma-induced hydroperoxide formation (see Figure 4). Subsequently, a thermally initiated copolymerization reaction with polyacrylic acid was performed. Finally, the carboxy groups were activated using 0.2 M EDC in 1 M NaH_2PO_4 (pH = 4.8) solution for 60 min at room temperature followed by coupling with fibronectin (10 ug/ml) in PBS for 2h.
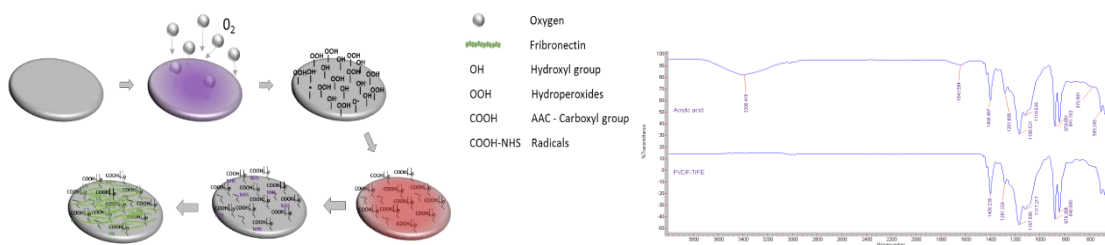
Figure 3-21. Surface modification method using oxygen (low temperature) plasma treatment of the PVDF-TrFE surface. The bombardment of the surface with oxygen ions results in the formation of hydroperoxides that can be used to graft polyacrylic acid the surface and maximise the surface energy to allow attachment of fibronectin through carbodiimide chemistry. FTIR shows functional groups after polyacrylic acid reaction on the PVDF-TrFE surface.
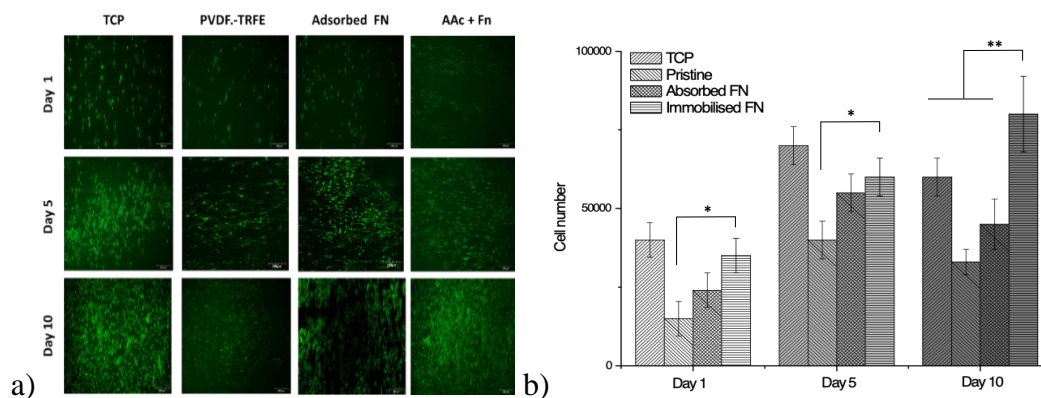
Figure 3-22.a) Live/dead images of cells and b) Proliferation rate at day 1,5 and 10 days of tendon cells cultured on TCP, pristine, pristine with adsorbed Fn and pristine samples with chemically bonded Fn (Immobilised). (**$p < 0.01$; *$p < 0.05$ to respect to -pristine)

197

Following tenocyte seeding, by day 1 it was possible to observe differences in cellular metabolic activity and proliferation. It is noticeable that the addition of fibronectin (either absorbed or immobilised) lead to an increase in cell attachment. However, a 2-fold increase with respect to pristine samples is observed for the surfaces demonstrating immobilised fibronectin. This result is similar to those obtained previously by Klee et al. on PVDF surfaces grafted with fibronectin using a similar process. Furthermore, it was not possible to observe a significant difference in cell proliferation on samples with adsorbed or covalently functionalized fibronectin at day 1 or 5. Conversely, after 10 days of culture proliferation was only sustained on PVDF-TrFE surfaces with immobilised fibronectin. It is possible to argue that the efficacy of this methodology lies in the exposure of previously hidden active sites of the fibronectin that become accessible for the cells. Salmeron *et al.* have obtained similar results on fibronectin covalently attached to PEA that results on the exposure of cell binding and growth factor binding domains[28].
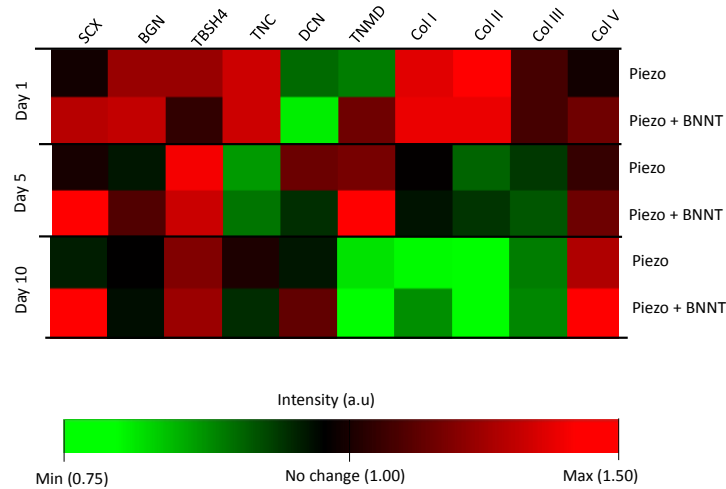
Figure 3-23. Microarray normalised (against non-piezoelectric control in static conditions) protein expression data of human tenocytes cultured following 1, 5 and 10 days in culture.

It is observed that the addition of BNNT into PVDF-TrFE enhances significantly further cell adhesion and promoted sustained expression of tenogenic transcription factor SCX relative to non-piezoeletric and pristine films. Although TNMD expression was also increased on PVDF-TrFE/BNNT composites at days 1 and 5, it decreased drastically after 10 days along with collagen I, II and III expression. These time points were chosen since

they reflect typical tendon culture growth and phenotypic drift progression model for TNMD and SCX[60].

3.3.2.3 Signalling pathways associated with surface polarization. Gene expression of tenocytes is modulated by the surface polarization

a)   b)
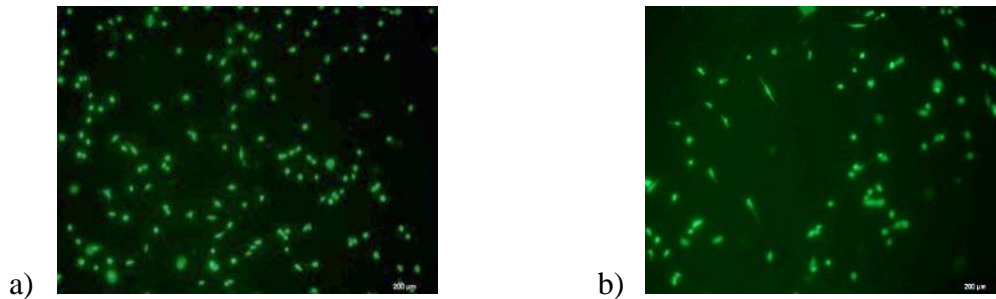
Figure 3-24. Live/dead of cells on a) non-piezoelectric and b) piezoelectric substrates after 24 hours.

An array (n=3) of different genes (96 genes) was used to evaluate the differences between cells cultured on piezoelectric or non-piezoelectric materials. In the following figure we can observe the gene network generated in IPA using predictive biochemical interactions that link gene changes to signalling pathways, such as ERK and the canonical TGF-β/BMP signalling pathway.
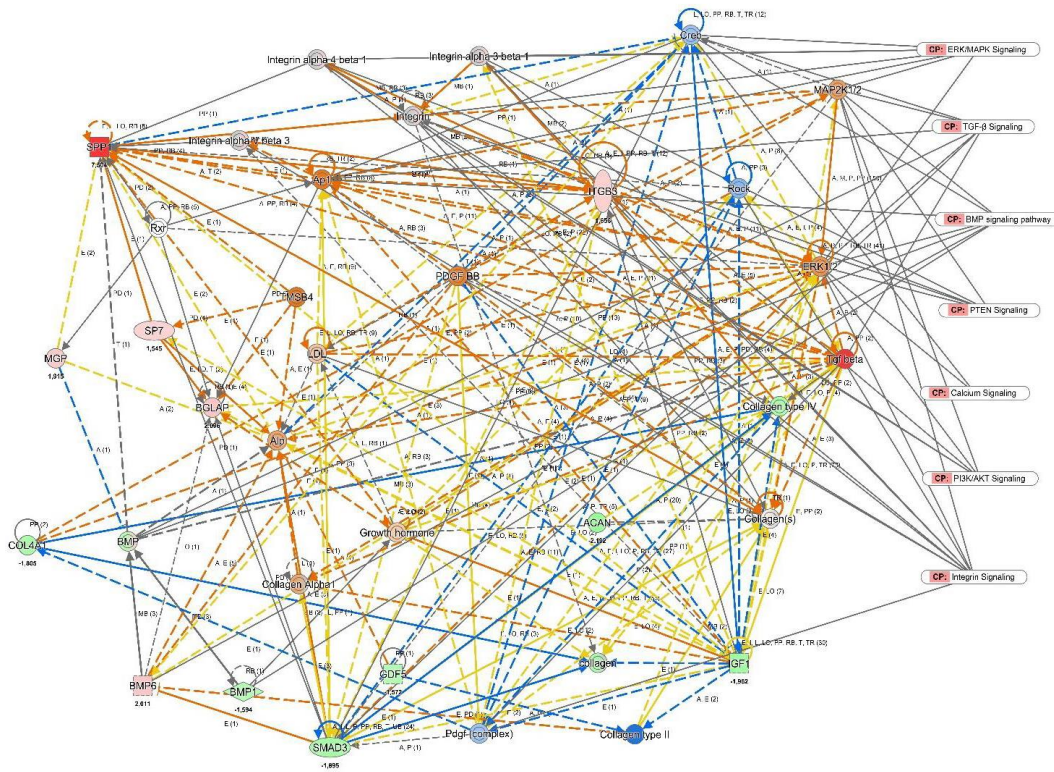
Figure 3-25. The network for tendon cells on piezoelectric surfaces, demonstrating the mainly predicted biochemical upregulation of these pathways. Data are mean relative to non-piezoelectric control (n=3).

From the analysis using IPA software, it was obtained that TGF-β (p-value=1.41x10^{-13}) was an upstream regulator. The canonical pathways activated were related to TGF-β /BMP signalling and adhesion signalling pathways including integrin, FAK and paxillin.

a)

b)
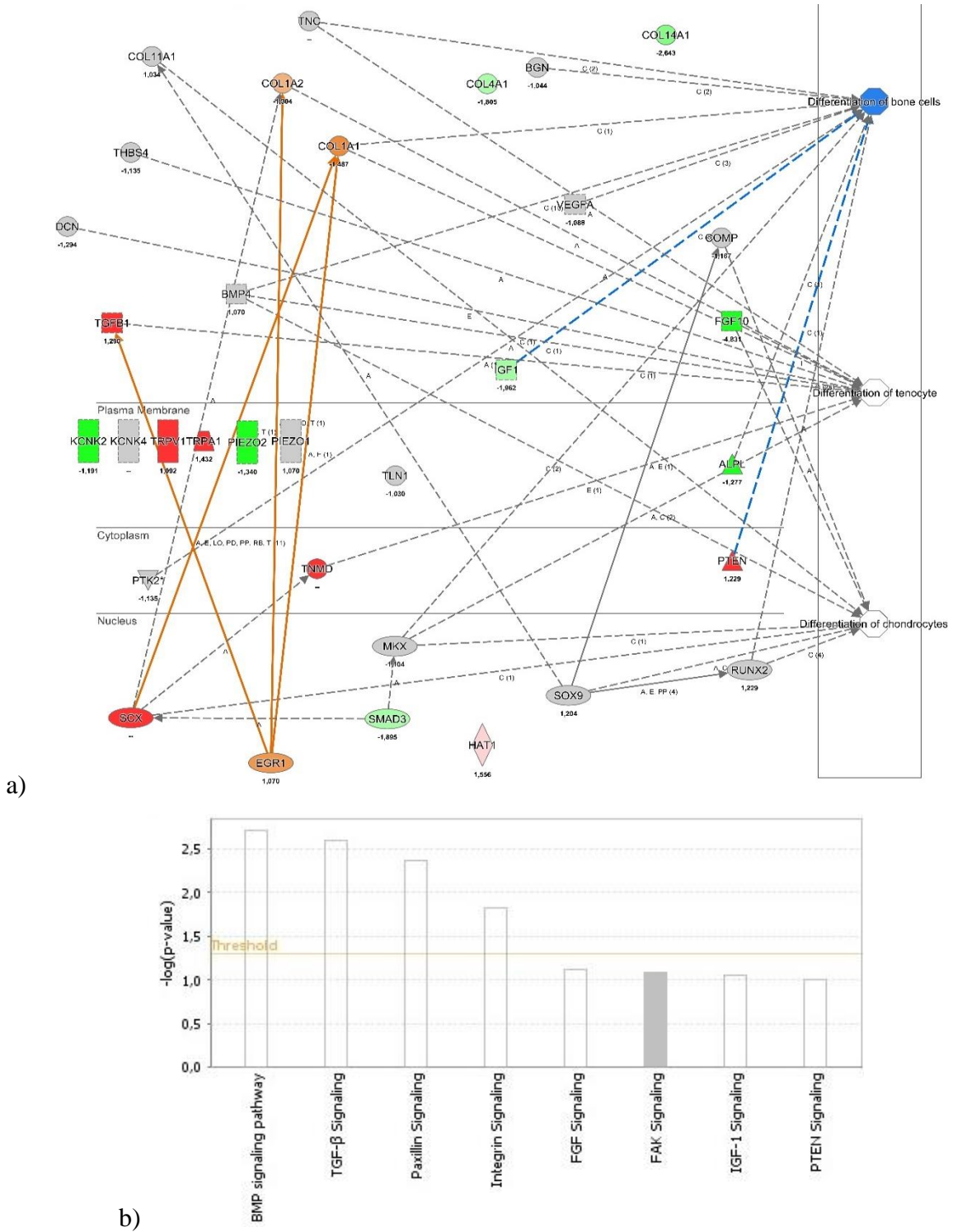
Figure 3-26. a) Signalling pathway associated with cellular differentiation processes towards bone, cartilage or tendon formation under electromechanical stimulation. b) Canonical pathways associated with electromechanical stimulation effect on tenocytes.
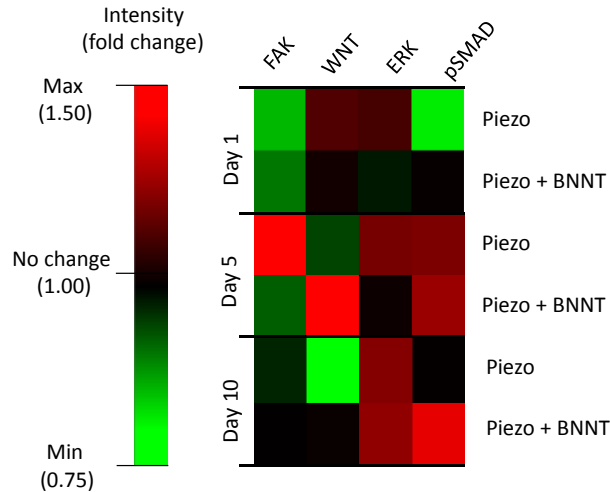
Figure 3-27. Expression of proteins related to different signalling pathways (MAPK, FAK, TGF-β and Wnt) of tendon cells cultured on piezoelectric systems for 1, 5 and 10 days. (normalised against non-piezoelectric films) (**p<0.01 ; *p<0.05 to respect to static control)

After 10 days, tendon cells (see Figure 3-27) activation of TGF-β/BMP signalling pathway was significantly stimulated by nanocomposites films at days 1, 5 and 10. Also, the MAPK/ERK pathway was upregulated at all times on both piezoelectric systems. These findings correlate with the genomic results obtained as well. Conversely, under static conditions, Wnt/β-catenin pathway was also consistently activated by the highly polarised surface of the nanocomposite.

3.3.2.4 Signal transduction mechanism by the surface polarisation
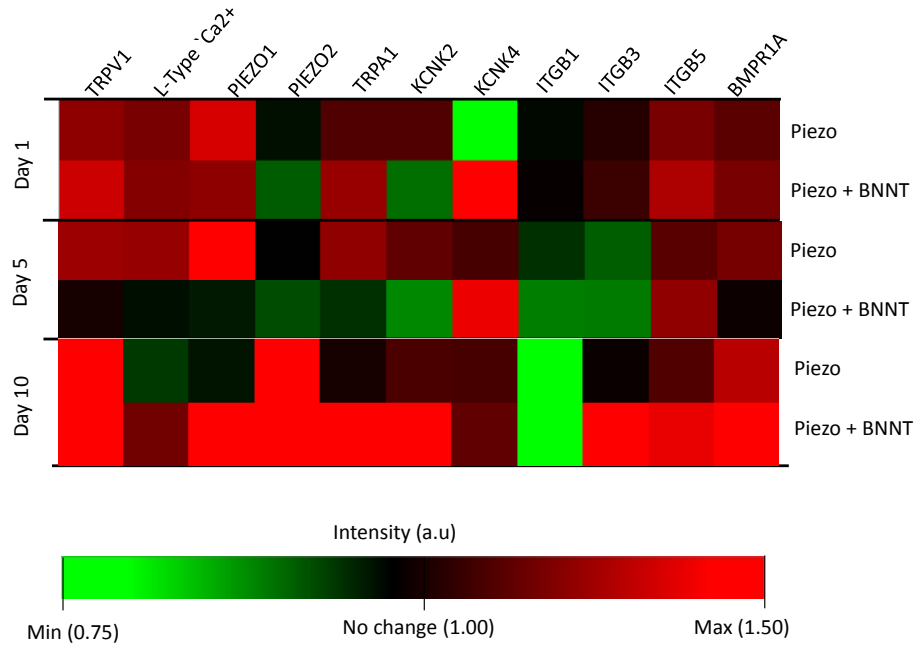
Figure 3-28. Expression of proteins related to signal transduction mechanisms of tendon cells cultured on piezoelectric systems for 1, 5 and 10 days. (normalised against non-piezoelectric films) (**$p<0.01$; *$p<0.05$ to respect to static control)

Figure 3-28 shows that surface polarisation results in increased expression of ion channels Piezo 2 and TRPV1 after 10 days of culture. Across all the time points, TRPV1 was highly expressed along with TRPA1 and Piezo1.

Genomic analysis indicated that the TGF-signalling pathway was upregulated in cells cultured on piezoelectric surfaces. It was observed that cells cultured on piezoelectric surfaces induced downregulation of the dedifferentiation process towards the bone. Besides, an upregulation in the expression of TRP-family ion channel proteins TRPA1 and TRPV-1 and downregulation of PIEZO2 was observed.

3.3.3 The functional response of Tendon and MSC cell culture under dynamic conditions

Here we assessed differential tenocyte and MSC functional response to high frequency, low amplitude mechanical and electromechanical stimulation.

3.3.3.1 Effect of mechanical stimulation on MSC culture. MSC underwent osteogenesis when nano vibrated at 1000 Hz

The ability of the system to promote osteogenic differentiation on stem cells (from bone marrow) was confirmed using previously reported protocols. It has been shown in the previous studies[151,279] that MSC commits towards osteoblastic lineage when cultured under acoustic stimulation of nanoscale amplitude (30 nm) and 1000 Hz frequency in a 2D or 3D environment. In this study, non-crosslinked collagen gels (2mg/ml and 100 Pa elastic modulus) were used as representative 3D fibrous structures. It should be noted that in these initial studies, piezoelectric materials were not employed, just mechanical stimulation was applied directly to cells in culture by a nano-vibrational bioreactor as described previously[151,279]
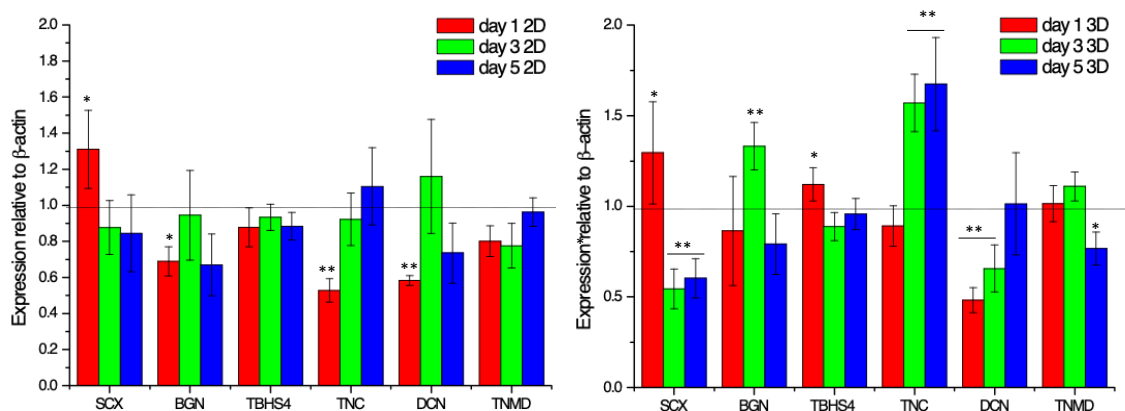
Figure 3-29. Protein expression of MSC nano stimulated at 1000 Hz on a) 2D (films) or b) 3D (collagen gels, 2mg/ml, 100 Pa) systems for 1, 3 and 5 days (n=4). (**p<0.01 ; *p<0.05 to respect to static control)

As shown in Figure 3-10, tenogenic markers were all downregulated on MSC's cultured on films. Effectively, at the same conditions of, tenogenic markers such as SCX, TNMD, BGN and THBS4 were downregulated on MSC's suggesting that at these conditions, osteogenic pathways are activated. Thus, this system offers an excellent possibility to study phenotypic drift in tenocytes cultures towards osteospecific lineage.
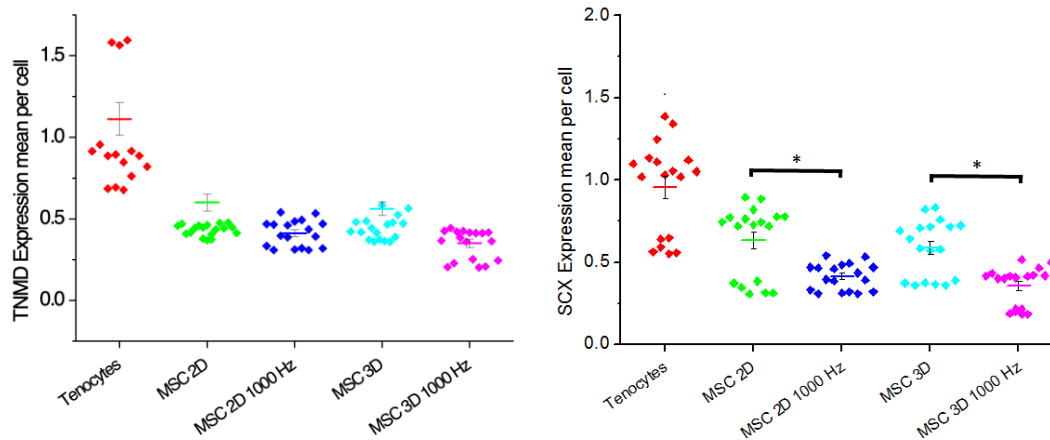
Figure 3-30. Expression of tendon-specific markers in MSCs stimulated at 1000 Hz (30 nm amplitude) for 5 days compared to non-stimulated MSCs and tenocytes.). (**p<0.01 ; *p<0.05 to respect to static control) (**p<0.01 ; *p<0.05 to respect to static control)

Unlike osteogenesis in MSCs, differentiation towards a tenogenic lineage might require a multifactorial approach. As shown by Figure 3-11, SCX was significantly downregulated after 5 days of continuous vibration, and MSCs commitment towards osteogenic lineage was observed [280–282]. Also, even though no significant differences were observed for the rest of tendon related proteins (BGN, DCN, THBSP4, TNC, TNMD and COLV), a similar trend was noted. Also, compared to tenocytes, expression levels of tendon markers SCX and TNMD were significantly lower except for TNC, THBS4 and Collagen V (see Figure 3-31).
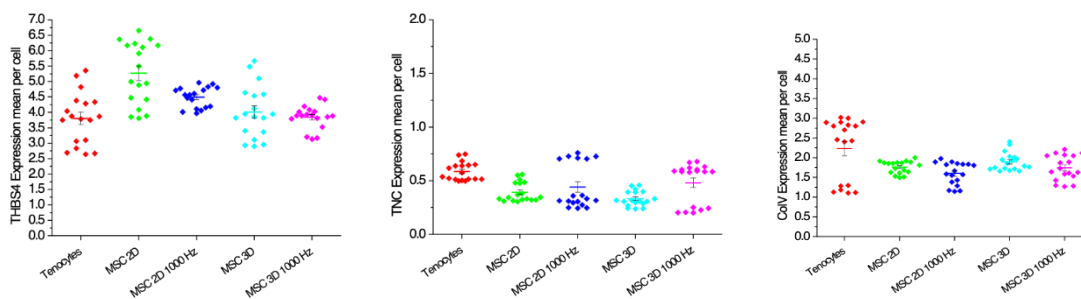
Figure 3-31. Comparison of the expression of tendon-specific markers in MSCs (stimulated for 5 days and non-stimulated) and in human tenocytes (non-stimulated). (**p<0.01 ; *p<0.05 to respect to static control)

3.3.3.2 Signalling pathways associated with MSC osteogenesis
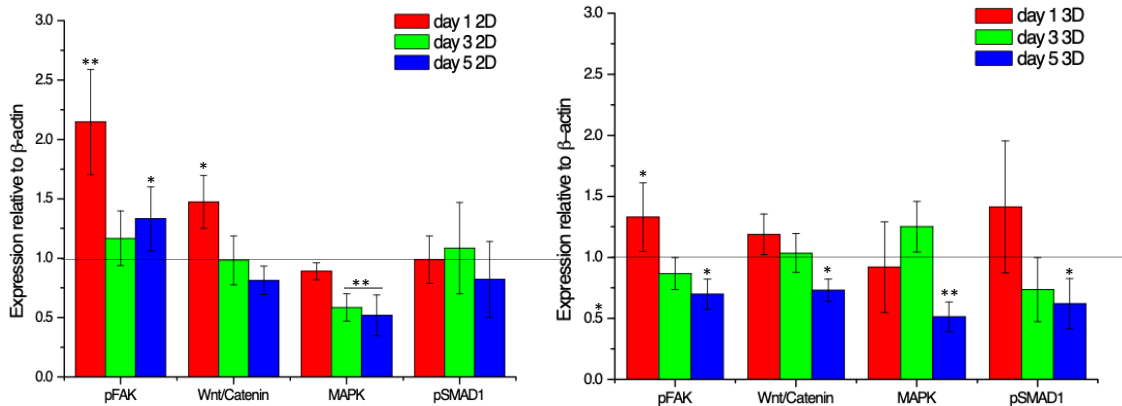
Figure 3-32. Expression of proteins related to different signalling pathways (MAPK, FAK, TGF-β and Wnt) from MSCs nano stimulated for 1, 3 or 5 days on a) 2D or b) 3D systems. (**p<0.01 ; *p<0.05 to respect to static control)

As shown in Figure 3-13, protein expression data showed that activation of the FAK signalling pathway is involved in MSC osteogenesis. FAK signalling was significantly activated (see Figure 3-14) in 2D surfaces but not in 3D structures just after 1 day of stimulation. Conversely, activation of MAPK was more pronounced in 3D (see Figure 3-15) compared than in 2D cultures. Finally, consistent Wnt signalling was observed for both 2D and 3D systems see (Figure 3-16), suggesting that Wnt signalling is required for MSC osteogenesis. Besides, TGF-β/ BMP signalling was also pronounced on both systems.
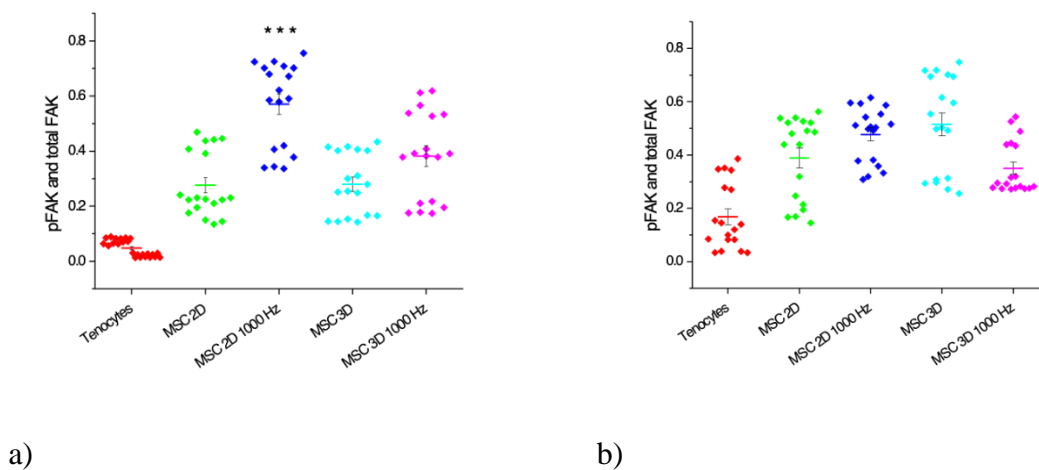
a)   b)

Figure 3-33. a) Day 1 and b) day 5 of adhesion-related protein in MSC compared to tenocytes non-stimulated. (**p<0.01 ; *p<0.05 to respect to static control)

a)

b)
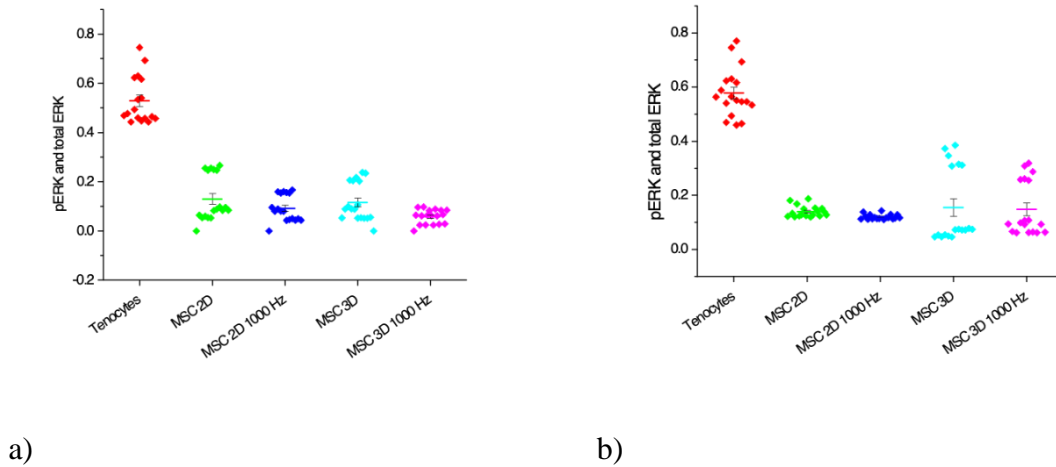
Figure 3-34. Day 1 and day 5 of MAPK related protein in MSC compared to non-stimulated tenocytes. (**p<0.01 ; *p<0.05 to respect to static control)

a)

b)
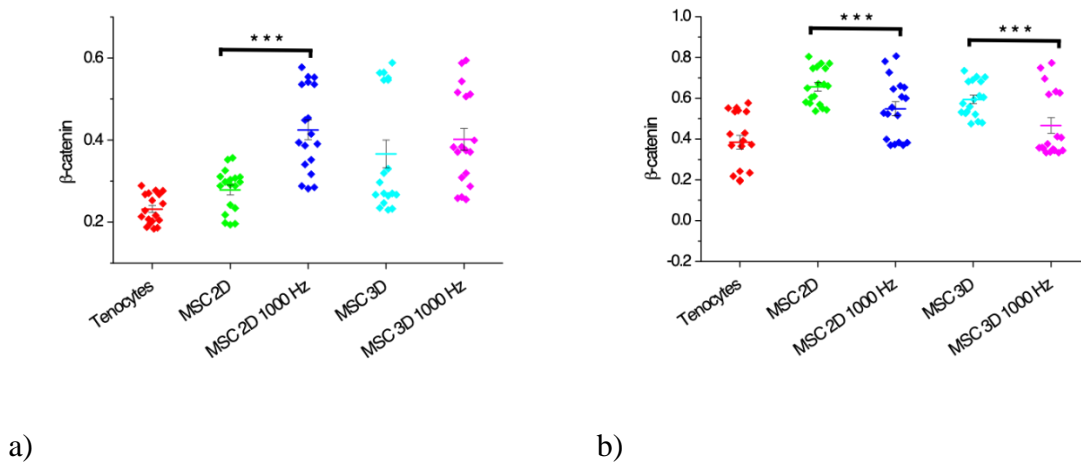
Figure 3-35. Day 1 and day 5 of Wnt/β-catenin related proteins for MSC compared to tenocytes non-stimulated. (**p<0.01 ; *p<0.05 to respect to static control)

a)   b)
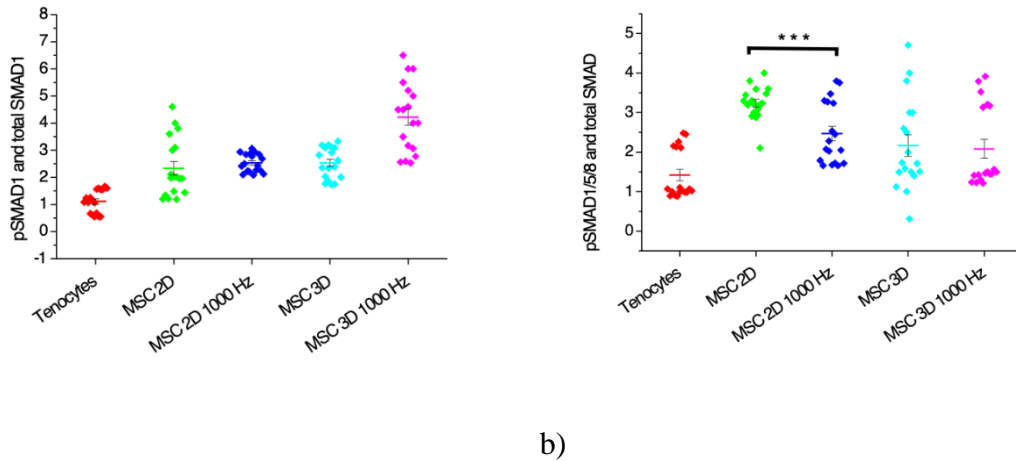
Figure 3-36. Day 1 and day 5 of SMADs related proteins for MSC compared to tenocytes non-stimulated. (***p<0.001, **p<0.01 ; *p<0.05 to respect to static control)

As previously reported [151], the 2D paradigm for MSC osteogenesis is via adhesion-mediated signalling ROCK. However, in 3D cultures, other vibration sensing mechanisms including cellular mechanoreceptors might play a central role in MSC differentiation processes.

3.3.3.3 Signal transduction mechanism by mechanical stimulation on MSC cells

Cellular response (i.e. intracellular tension) to mechanical stimulation generally include the activation of integrins and differing mechanoreceptors such as transient receptor potential (TRP) ion channels, cation channels (K^+ and Ca^{2+}) and piezo channels[283–286]. Therefore, the activation of these receptors was investigated.
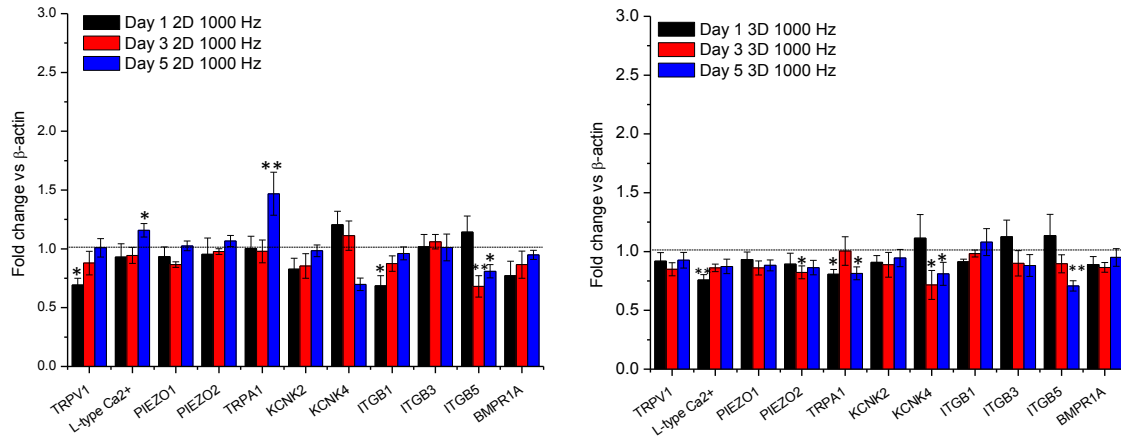
Figure 3-37. Ion channels (PIEZO, TRP, K$^+$ and Ca^{2+}), integrins (β1,3 and5) and BMP receptor expression of MSC under mechanical stimulation at 1000 Hz for 1,3 and 5 days of culture. (***p<0.001, **p<0.01 ; *p<0.05 to respect to static Hz)

After 10 days of MSC culture, no significant modulation of mechanoreceptors expression was observed. Interestingly, just the TRPA1 ion channel was significantly upregulated after 5 days of culture on 2D films that correlate with MSC differentiation towards osteogenic lineage.

3.3.3.4 Effect of mechanical stimulation on tendon cell cultures. Tenocyte function was maintained under low mechanical stimulation (700Hz).

As shown in the previous reports[9,37], the frequency of vibrations (and not the amplitude) can be used to activate osteogenic pathways. In previous studies, lower frequencies, including 500 Hz, did not have the same triggering effects. In this study, 700 Hz and 1500 Hz were used based on the hypothesis that osteogenic pathways are activated when using frequencies of 1000 Hz. To assess this hypothesis, human tendon-derived cells were cultured on non-piezoelectric materials to assess the effect of nanokicking alone (nano stimulation) on the expression of tenospecific proteins.
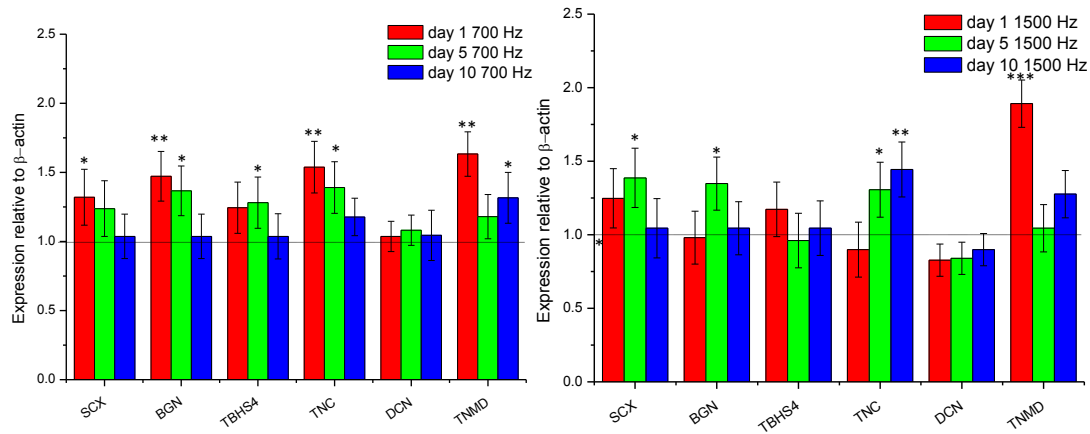
Figure 3-38. Expression of protein related to tendon function on tenocytes under mechanical stimulation at 700 Hz or 1500 Hz for 10 days. (***p<0.001, **p<0.01 ; *p<0.05 to respect to static control)
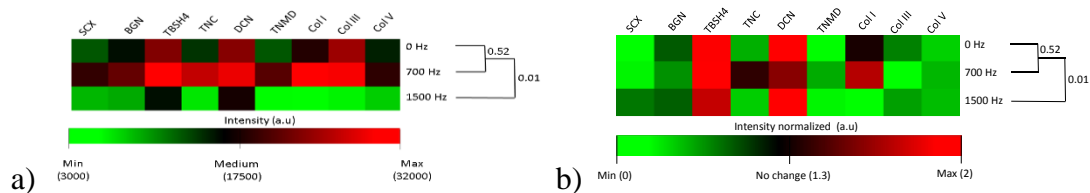
Figure 3-39. Microarray a) non-normalised and b) normalised (against static control) protein expression data of human tenocytes cultured with frequencies 1500Hz following 10 days in culture.

As shown in Figure 3-39, stimulation at 700 Hz had a positive effect on the expression of tendon-related proteins. Following 10 days in culture, cells exposed to 700 Hz vibrational stimulation demonstrated more significant expression of TNC, COLI and TNMD relative to tenocytes stimulated with a frequency of 1500 Hz. Also, the ratio of COLIII/I was increased at 1500 Hz, suggesting tenocyte de-differentiation or phenotypic drift. It was Furthermore, at day 10 an increase in the synthesis of Collagen III and Tenomodulin, was observed in tenocytes stimulated at 1500 Hz.

3.3.3.5 Signalling pathways associated with mechanical stimulation

As discussed in the introduction, the signalling pathway associated with tenogenic events during mechanical stimulation is TGF-β/BMP. Conversely, pathways associated with

osteogenic events during excessive mechanical stimulation is Wnt/β-catenin. MAPK/ERK and FAK signalling pathways are adhesion-related mechanosensitive pathways that have been shown to interact with the aforementioned canonical pathways Wnt and TGF-β/BMP.
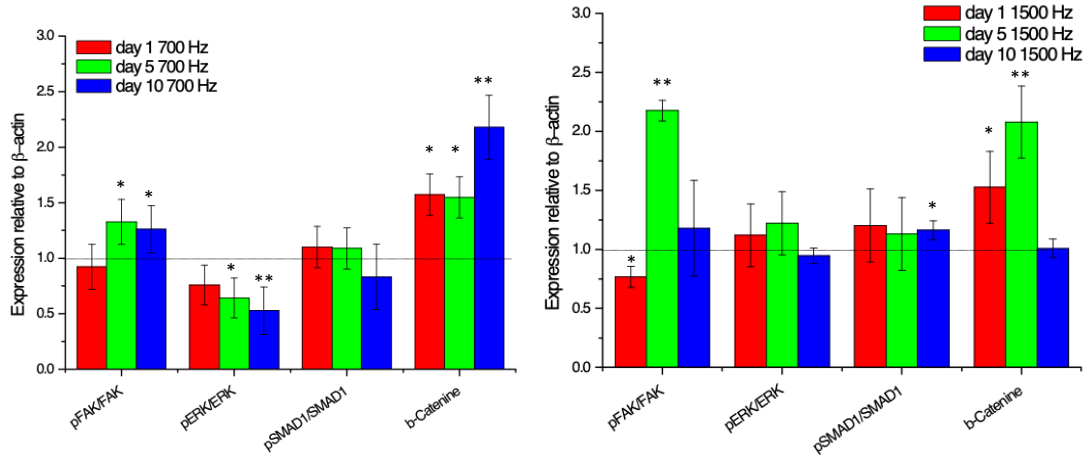
Figure 3-40. Expression of protein related to signalling pathways on tenocytes under nano stimulation (non-piezoelectric films) at 700 Hz or 1500 Hz for 1,5 and 10 days of continuous stimulation (***p<0.001, **p<0.01 ; *p<0.05 to respect to static control)

As shown in Figure 3-40, mechanical stimulation resulted in the activation of Wnt signalling for both system cultures (2D and ·3D).
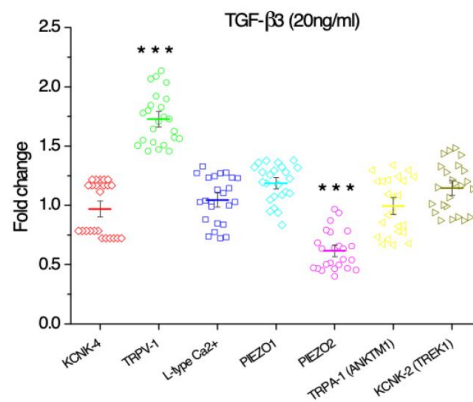
Figure 3-41. Comparison of the expression of tendon-specific markers in stimulated tenocytes mechanically, (stimulated for 5 days at 1500 Hz) with TGF-β3 (20 ng/ml) and non-stimulated tenocytes (static). (**p<0.01 ; *p<0.05 to respect to static control)

Next, we also tested the effect of TGF-β/BMP effect on the main tendon protein markers expression, and we compared to the effect of mechanical stimulation. The results showed that mechanical stimulation resulted in a more significant increase of early tendon marker SCX at day 5 but TGF-β activation increased late tendon markers TNMD and TNC (see Figure 3-41).

3.3.3.6 Signal transduction mechanism by mechanical stimulation on tendon cells
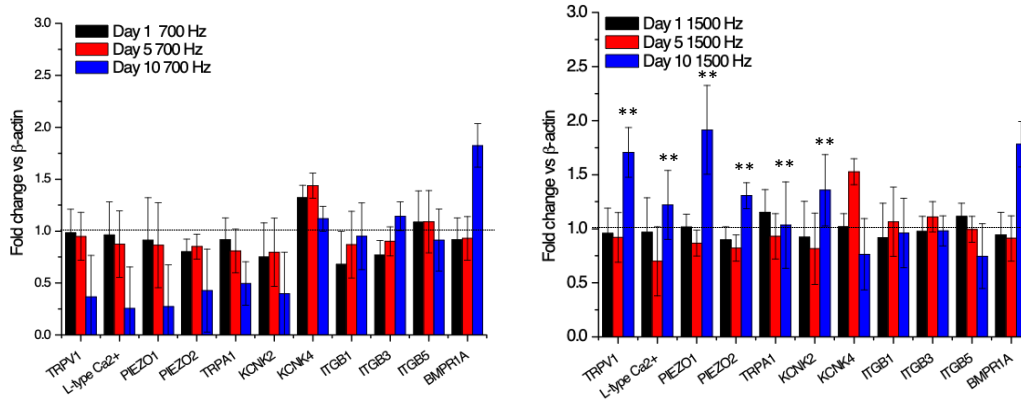
Figure 3-42. Ion channels (PIEZO, TRP, K$^+$ and Ca^{2+}), integrins (β1,3 and5) and BMP receptor expression of tenocytes under mechanical stimulation. at 700 Hz and 1500 for 1,5 and 10 days of culture. (***p<0.001, **p<0.01 ; *p<0.05 to respect to 700 Hz)

It was observed a significant modulation of PIEZO,TRP and cation ion channel activation at day 10 (see figure 3-42) between the low and high level of mechanical stimulation (700 Hz and 1500 Hz). These results suggest that the main mechanism for osteogenic differentiation or phenotypic drift of tendon cells involves the activation of mechanosensitive receptors that include ion channels.
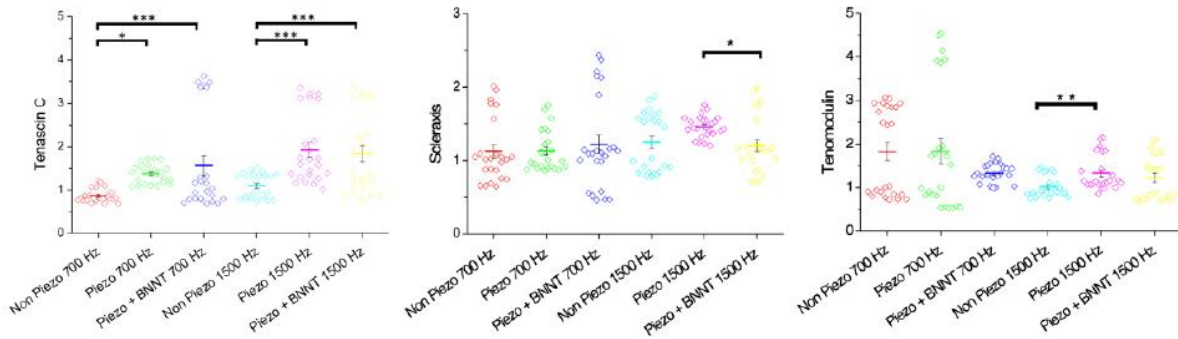
Figure 3-43. Receptors and tendon markers expression under nano stimulation at day 5 with or without the addition of TGF-β3 (20ng/ml) to induce phenotype maintenance

As shown in Figure 3-43, when Tenogenic TGF-β signalling pathway is activated, TRPV1 and PIEZO2 ion channels activation are significantly modulated. These results prove that cell differentiation processes are correlated with changes in ion channel activation. It is clear that TRP and Piezo channel is implicated in the transduction of vibrational forces. Studies have shown that TRP and Piezo channels in hair cells are sensitive to high-frequency vibration produced by fluid pressure changes during the hearing function[287–289].

3.3.3.7 Effect of electromechanical stimulation
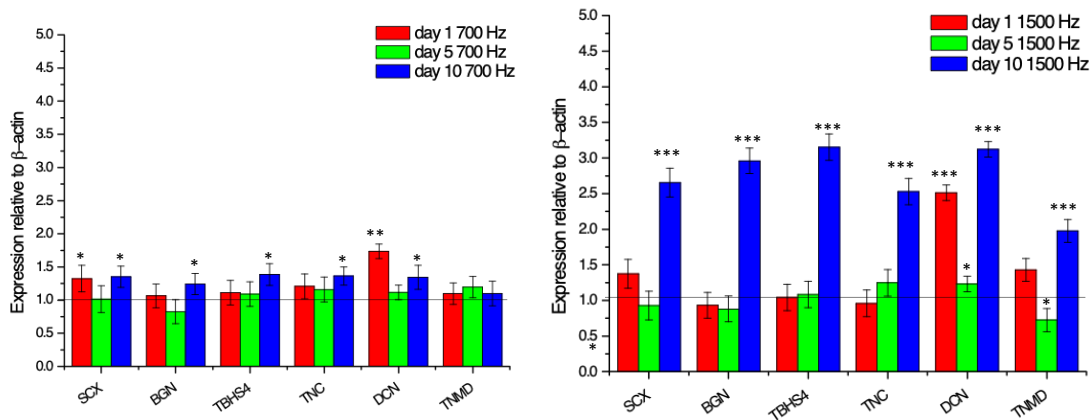
Figure 3-44. Expression of protein related to tendon function on tenocytes under high frequency, low-magnitude electromechanical stimulation(piezo+BNNT) at a 700 Hz or b 1500 Hz.). (***p<0.001, **p<0.01 ; *p<0.05 to respect to non-piezoelectric control)

213

Unlike with mechanical stimulation at 1500 Hz , electromechanical stimulation resulted in a significant increase of all tenogenic markers. These results suggest that piezoelectric stimulation might have a positive effect on maintaining tendon cell function.
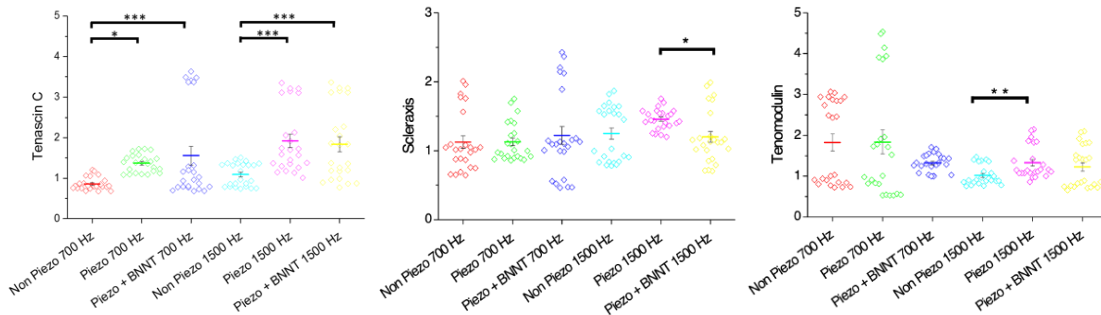
Figure 3-45. Expression of tenogenic markers at day 5 for piezoelectric and non-piezoelectric materials.). (***p<0.001, **p<0.01 ; *p<0.05 to respect to non-piezoelectric control)
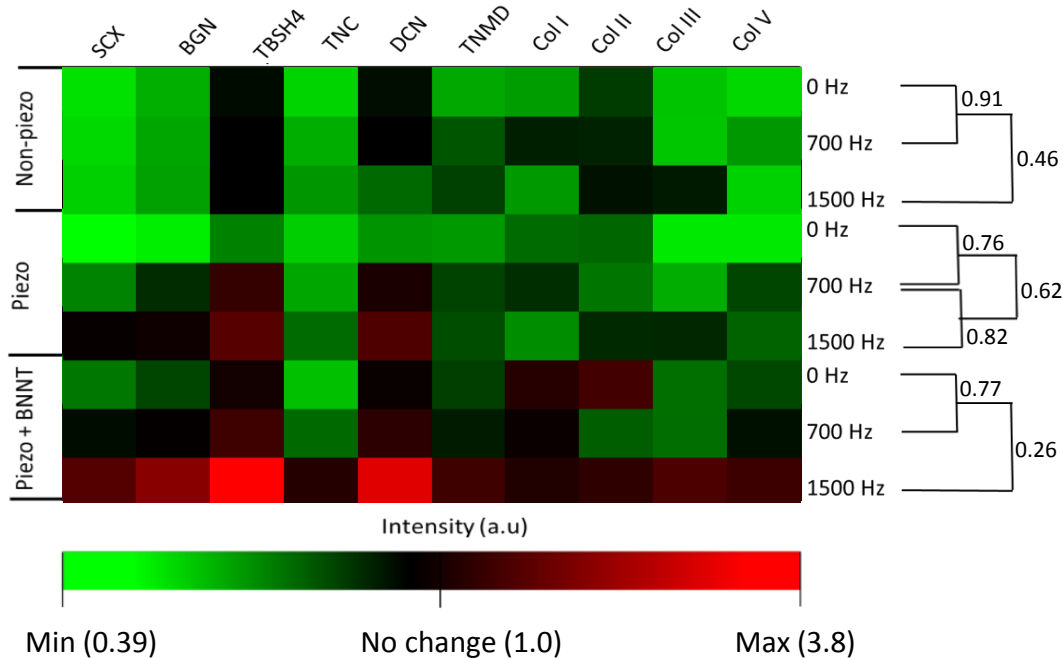
Figure 3-46. Tenogenesis and receptors array of the different frequencies of either mechanical or electromechanical stimulation (day 10)

Cellular responses to mechanical stimulation include activation of ion channel receptor and integrin and might be followed by cytoskeletal tension and rigidity. Besides, there is an

increasing body of research suggesting that intracellular tension increases during cell differentiation processes. Therefore, we hypothesised that piezoelectric stimulation promotes tendon function maintenance through the increase of cytoskeletal tension. To test this hypothesis, we evaluated the effect of cytoskeletal tension using tension inhibitors such as the ROCK inhibitor (Y27632) and the myosin II inhibitor (blebbistatin).

As shown in Figure 3-45, day 5 and 1500 Hz stimulation frequency was chosen as time point and stimulation condition where tendon related markers and signalling pathways were significantly upregulated for piezoelectric stimulation but downregulated under mechanical stimulation. Following the seeding protocol previously reported, which allows 1 h for cell attachment in 10% serum, cells were synchronised at G0 by serum starvation (1% serum) for 24 h. After synchronising, cells were released back into the cell cycle using 10% serum for 23 h before the addition of inhibitors. of ROCK inhibitor (Y27632) or the Myosin II inhibitor (blebbistatin, blebb).
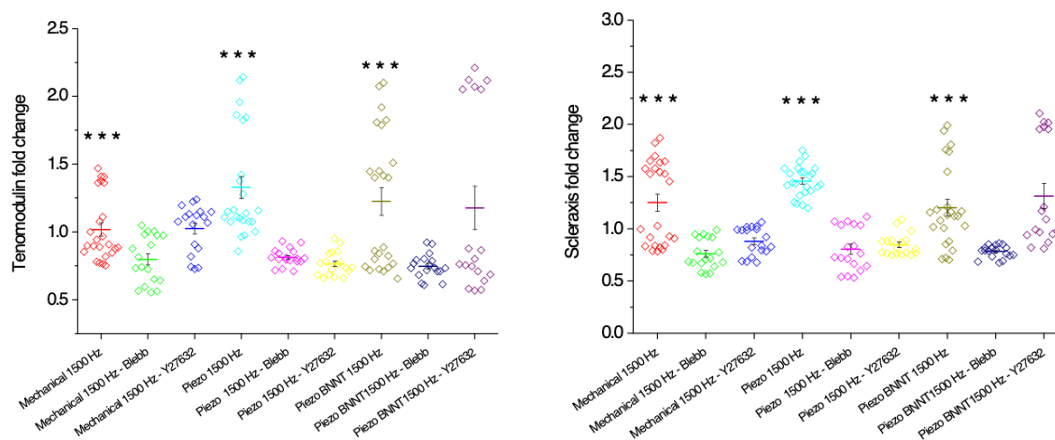
Figure 3-47. Receptors expression under mechanical stimulation and high frequency, low-magnitude electromechanical stimulation at day 5 with or without the addition of ROCK inhibitor (Y27632) or the Myosin II inhibitor (blebbistatin, blebb). (***p<0.001, **p<0.01 ; *p<0.05 to respect to non-piezoelectric control).

As shown in Figure 3-47, piezoelectrically induced SCX and TNMD upregulation were inhibited by a decrease in intracellular tension. Conversely, inhibition of intracellular tension did not have the same significant effect on TNMD for mechanical stimulation.

3.3.3.8 Signalling pathways associated with piezoelectricity

The signalling pathways identified in the gene arrays were MAPK/ERK, TGF/BMP, FAK and Wnt/Catenin . The preliminary results indicated that the surface polarisation of PVDF-TrFE differentially modulated these pathways. These findings suggest that piezoelectric stimulation might further modulate the activity of these pathways and their downstream events including gene and protein expression.

To test this hypothesis, day 5 was chosen since it is a representative time point where tenocytes underwent a significant increase of functional tendon response under piezoelectric stimulation. Briefly, tendon cells were culture on piezoelectric and non-piezoelectric films.. Actuation was via the Nanokicker bioreactor operating at both at 700 and 1500 Hz In order to assess the efficacy of piezoelectric materials in electromechanical stimulation. Both pristine PVDF TrFE and PVDF TrFE/BNNT nanocomposites were investigated in vitro and compared to non-piezoelectric control materials.
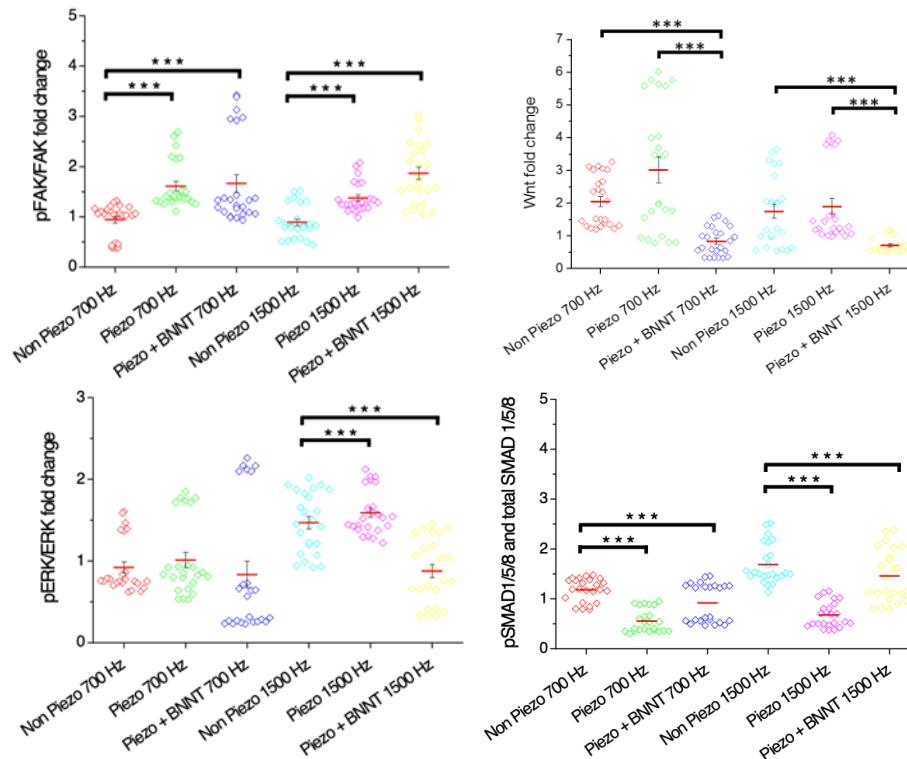
Figure 3-48. Signalling pathways-associated protein expression at day 5.). (***p<0.001, **p<0.01 ; *p<0.05 to respect to non-piezoelectric control)

The inhibition of intracellular tension using ROCK and Myosin II inhibitors was used to test the effect of cytoskeletal tension on the activation of the signalling pathways.
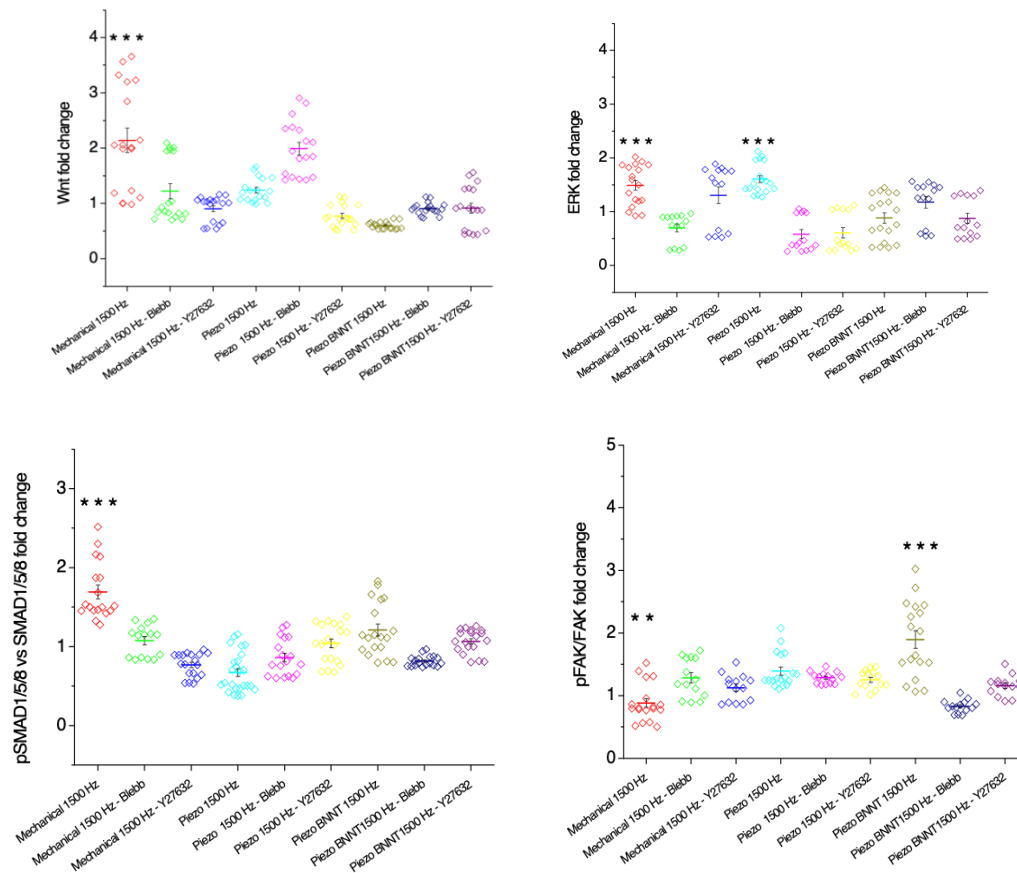
Figure 3-49. Key members of signalling pathways expression under mechanical stimulation and high frequency, low-magnitude electromechanical stimulation at day 5 with or without the addition of ROCK inhibitor (Y27632) or the Myosin II inhibitor (blebbistatin, blebb).). (***$p<0.001$, **$p<0.01$; *$p<0.05$ to respect to non-piezoelectric control)

As shown in Figure 3-49, mechanically induced osteogenic pathways Wnt activation was significantly modulated by intracellular tension. Inhibiting intracellular tension during piezoelectric stimulation, it significantly activated Wnt and BMP signalling. Also, piezoelectrically-induced FAK signalling activation was significantly decreased with the inhibition of intracellular tension. These findings suggest that piezoelectric induction of tendon function maintenance is mediated through FAK activation and Wnt deactivation.

3.3.3.9 Signal transduction mechanism by piezoelectrical stimulation
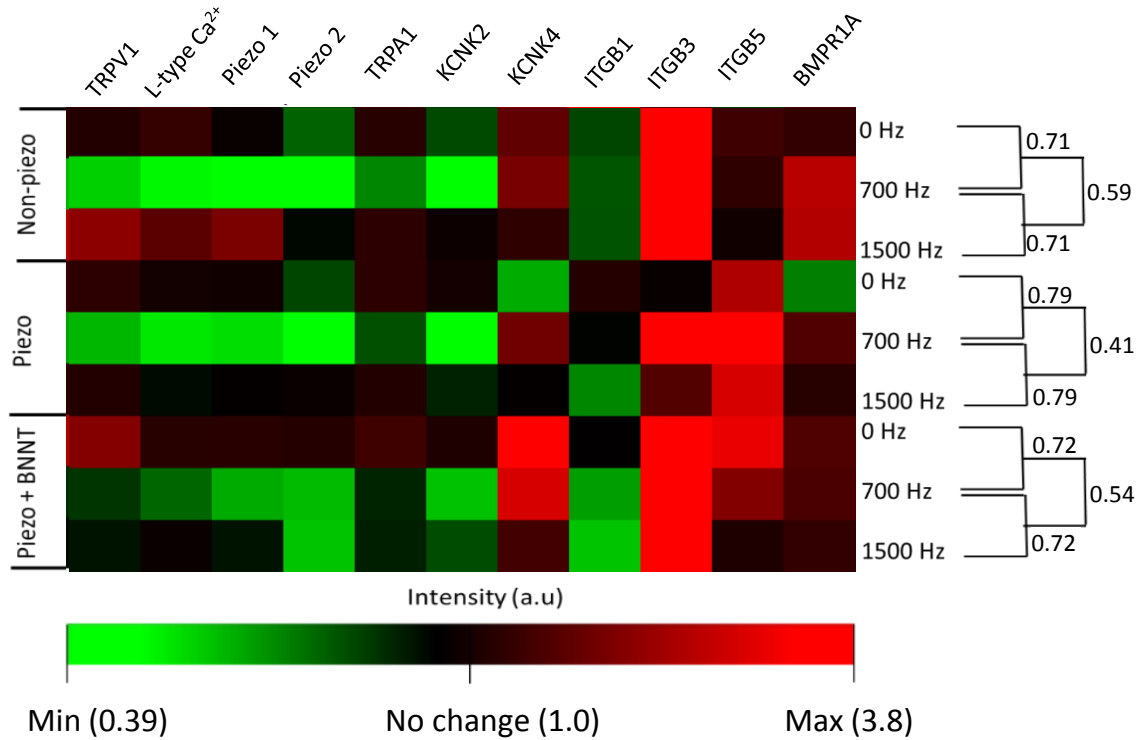
Figure 3-50. Tenogenesis and receptors array of the different frequencies of stimulation (day 10)
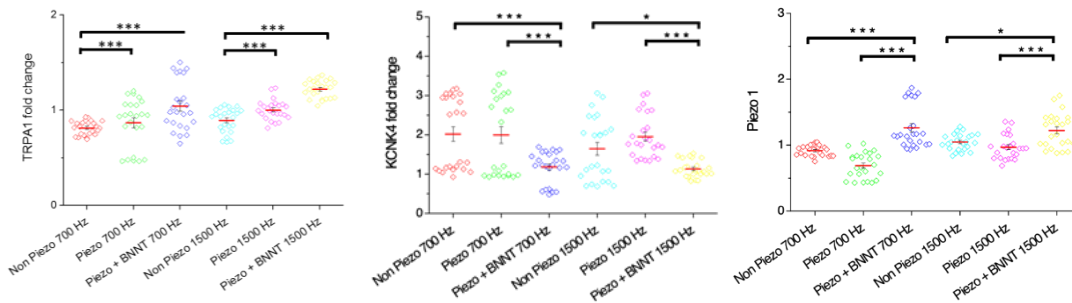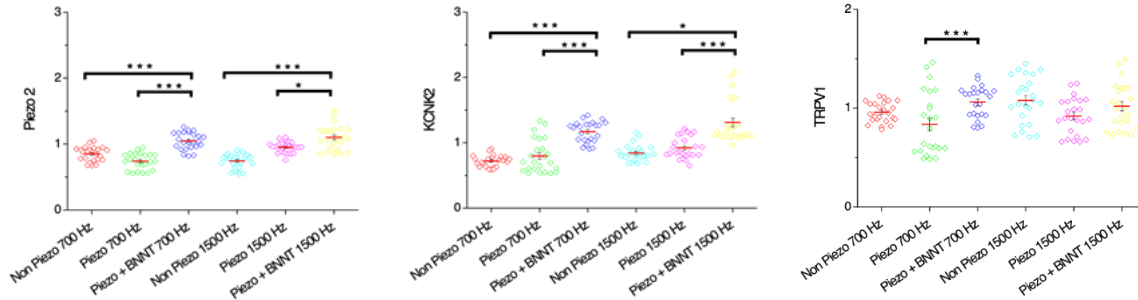
Figure 3-51. Receptors expression comparison between mechanical stimulation and high frequency, low-magnitude electromechanical stimulation day 5.

Cellular response (i.e. intracellular tension) to mechanical stimulation generally include the activation of differing cell receptors such as integrins, transient receptor potential (TRP) ion channels, cation channels (K^+ and Ca^{2+}) and piezo channels[283–286]. Therefore, the activation of these receptors was investigated.

Following the seeding protocol previously reported, which allows 1 h for cell attachment in 10% serum, cells were synchronised at G0 by serum starvation (1% serum) for 24 h. After synchronising, cells were released back into the cell cycle using 10% serum for 23 h before the addition of inhibitors. of ROCK inhibitor (Y27632) or the Myosin II inhibitor (blebbistatin, blebb).
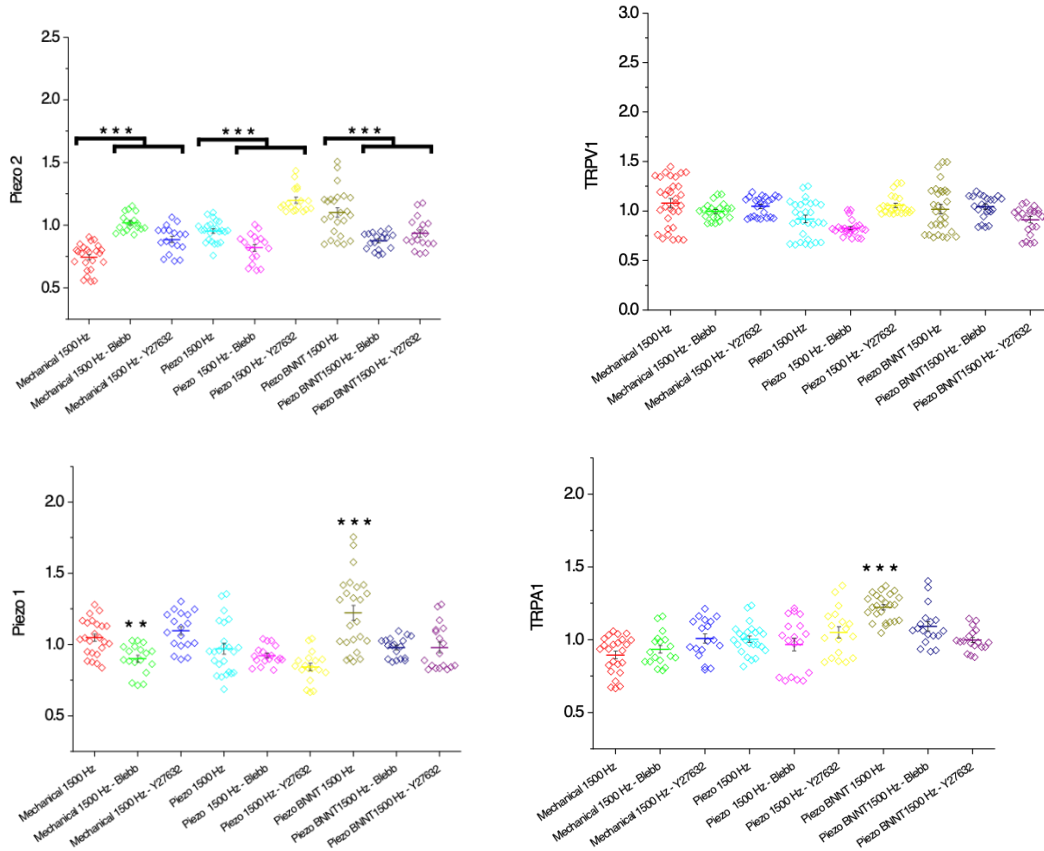
Figure 3-52. Receptors and tendon markers expression under mechanical stimulation at day 5 with or without the addition of TGF-β3 (20ng/ml) to induce phenotype maintenance
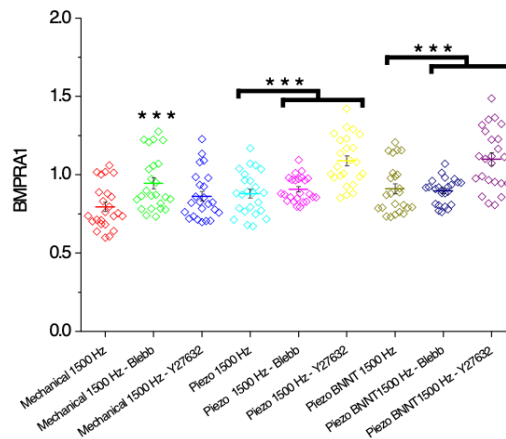
Figure 3-53. BMP receptor expression under mechanical stimulation and high frequency, low-magnitude electromechanical stimulation at day 5 with or without the addition of ROCK inhibitor (Y27632) or the Myosin II inhibitor (blebbistatin, blebb).

3.4   Discussion

3.4.1   High-Frequency Low Magnitude Electromechanical Bioreactor for tendon function maintenance

Finally, the sensitivity of the films was also evaluated, looking at the output voltage as a response to vibrational waves. A piezoelectric membrane generates electrical output voltage in response to applied mechanical stress and strain and is directly proportional to the thickness of the material. The sensitivity of the films is more significant when it achieves mechanical resonance at specific frequencies. The membrane vibrates with relatively large amplitude at its resonant frequencies (eigenmodes), thus generating more significant electrical signal outputs in the resonating position than those on non-resonating positions. The schematic with dimensions and the resonant frequencies are shown in figure 3. Characteristics of a membrane, such as its thickness, width, stiffness and residual stress, determine the resonance frequency of the membrane. It is known that with increasing thickness, resonance frequency decreases gradually; however, thicker samples produce higher levels of energy. In this work, we have found that an optimal thickness of 25 µm is necessary for the electrical poling process.   When the membrane was exposed to nanovibrational waves (see Figure 3-5.a) Thin-film PVDF-TrFE membrane structure and boundary conditions b) COMSOL harmonic response modelling of the membrane in the range of 0 to 2,000 Hz (30 nm amplitude). The response of membrane follows the input vibration reliably until reaching 700 Hz (magnified inset shows 100-200 Hz). Above this frequency, first, second and third resonant modes (700 Hz, 1500 Hz and 2500 Hz) cause significant amplification and deformations at the membrane, shown by the minimum and maximum amplitudes are taken from the modelled membrane.), electrical signals are generated as shown in Figure 3-9. By maintaining constant the amplitude of vibration and varying the frequency, the effect of frequency on voltage output was examined. As shown in Figure 3-9, the voltage output changed with vibration frequency. It was observed that the maximum value was obtained at 1500 Hz and after that value, the signal decreased. Resonant frequencies were found around 700 and 1500 Hz. At the vibration wave frequency 1500 Hz, the membrane (PVDF-TrFE/BNNT) generated a periodic voltage output with a peak value as high as 3 mV. The electrical output is of a typical AC

(alternating current). A fluctuation or drop in the voltage is observed at frequencies between 900-1300 Hz for pristine samples. The voltage output decreased to nearly zero when the frequency was over 5 kHz. The sensitivity of the membrane was as high as 0.18 mV/nm for nanocomposites and reduced to 0.03 mV/nm in pristine PVDF-TrFE films.

The aperture size (membrane diameter) affected the voltage output and therefore, the sensitivity. As observed in Figure 3-11, when the aperture was smaller than 6 mm, the sensitivity was lower than 0.1 mV/nm, yet increased with an aperture size up to 12.5 mm. Further increasing the diameter increased the sensitivity. A membrane can be considered as a "perfectly" flexible two-dimensional plane without thickness that deflections cause no apparent change in the membrane tension[290]. The vibration characteristics, including resonant frequency, are almost dependent upon membrane geometry and physical properties. Membrane geometry is defined by shape, size, thickness, and cross-section. A finite element method (COMSOL Multiphysics 5.2) was used to analyse the resonant frequencies of the film. The modelling parameters such as pre-stress and fluid interaction needed to be incorporated to obtain an excellent fidelity between the models and experimental work. After defining a pre-stress and incorporating the fluid-membrane interactions, the model represented the experimental observations accurately (see Figure 3-14). The membrane needs to undergo the transition from membrane behaviour to plate behaviour, which depends profoundly on the tension of the membrane. In this way, a membrane with small tension forces requires a thinner thickness to produce a plate-like response and vice versa. Pre-stress is here used to provide stiffness and maintain the shape of the membrane and ultimately control the system resonant frequencies (see Figure 3-15). It was observed that as the pre-stress was increased, the first resonant frequency was shifted to higher values. The modelled results were compared to experimentally obtained results, and the differences were less than 0.1%. If a pre-stress of 2MPa (T_0=50 N/m) was applied, then the calculated and COMSOL simulated first resonant frequency was found at 2052.7 Hz. For a membrane-based electrical stimulator, the tension of the membrane could be used to tune the resonant frequency of the vibrating membrane. The effective membrane frequency to the original frequency is a function of the change in membrane tension. This relationship is shown in Figure 3-16, where the theoretical calculations agree well with the FEM simulation results in COMSOL. Therefore, tuning the membrane tension could

significantly alter the resonant frequency of the device, which would be useful in the development of stimulator devices which can target specific frequencies.

The media surrounding a vibrating membrane has a dramatic effect on the structure, adding "virtual" mass and damping. Generally, it is known that the natural frequencies of structures interacting or fully immersed with water decrease significantly (compared to in air). The vibration of the membrane is transferred to the water movement and increases the total kinetic energy of the composite system. The main properties of the liquid that may have an impact on the resonant frequency are the viscosity, density and pressure. Viscosity has a negligible impact on resonant frequency for fluids with viscosities less than 0.006 N·s/m2 (water viscosity is 0.001 N·s/m2 and air viscosity is 0.000018 N·s/m2). The viscosity dissipates system energy resulting in a faster decay in free vibration and reducing the resonant frequency amplitude at forced vibration. Inaba et al.[277] showed that the resonant frequency decreased with higher viscosity; however, no shift was observed for the frequency of the resonance. Physically, a shift in resonant frequency is attributed exclusively to an added mass effect. Briefly, the movement of the fluid in phase with the relative movement of the vibrating membrane results in a virtually added mass to the membrane. This effect was first described by Lamb et al. who showed that membrane-fluid interactions could be described by the ratio between the kinetic energies of the membrane and fluid, a factor known as added virtual mass incremental (AVMI) factor. The AVMI method can be used to predict the effect of fluid loading on vibrating structures. Kwak and Kim[278] showed how the AVMI factor could be used to accurately predict the resonant frequency of a circular membrane under various clamping conditions. It is also observed that the natural frequencies of the membrane exposed to water are smaller than those exposed to air, and the natural frequencies of the membrane exposed to water with both sides are smaller than those of the circular plate exposed to water with one side.

The direct measurements of the output voltage from the films offer a total generated an electrical field of 12 V/m. These results were also confirmed with the COMSOL model. As shown in the figure when the membrane is under a single displacement of 30 nm, it can generate a total electrical field of 12 V /m. It is important to note that the model offers a greater understanding of how the electrical field is distributed across the membrane; however, it was not possible to confirm with direct observations. From a mechanical point

of view, it is essential to note that the stresses/strains developed in the surface are heterogeneous and depend upon the mode of operation chosen. It is noticeable that the number of nodes (areas with displacement equal to 0) increases with mode number (n=1,2..). The appearance of a node increases the number and level of electric field gradients over the entire membrane surface (see Figure 3-18). Therefore, at higher mode (higher resonant frequency) the level of localised voltage gradients is increased.

3.4.2 MSC tenogenic and osteogenic signalling pathways

MSCs can differentiate into bone or tendon cells through specific pathways based on selected physical and chemical cues, including soluble growth factors and mechanical stimuli. It has been shown in previous studies that MSC commit towards osteoblastic lineage when cultured under 1000 Hz frequency nano-vibrational stimulation (nano stimulation) in 2D or 3D environments through Wnt/β-catenin (3D) and RhoA/Rock pathways (2D)[7]. During nano stimulation-induced MSCs osteogenesis, key tendon master regulators such as SCX and tendon-related markers such as TNMD, BGN and THBS4 (see Figure 10) are being downregulated demonstrating that this system offers an excellent possibility to study phenotypic drift during tenocytes culture expansion. The results in this study showed that 1000 Hz nano stimulation-induced SCX downregulation via adhesion activated (phosphorylation of FAK) RhoA/Rock signalling pathway.

Several studies have shown that moderate uniaxial cyclic mechanical stimulations induce MSCs tenogenesis and can maintain tendon phenotype; however, intense mechanical stimulation lead to MSCs osteogenesis or tenocytes dedifferentiation through several concomitant osteogenic and tenogenic signalling pathways co-occurring [5,30]. Moreover, in a recent study, it has been shown that MSC's can differentiate into tenocytes through Rho/Rock signal transduction pathway using aligned scaffolds to force MSC's to elongate and increase the stress fibre formation[31]. These results suggest that independently of the approach adopted, activation of Rho/Rock pathway is necessary to induce MSCs tenogenesis but might require further control of co-occurring osteogenic pathways including BMP and Wnt signalling pathways. Is therefore suggested that unlike MSC osteogenesis, MSC differentiation towards tenogenic lineage[31] or tenocyte phenotype maintenance requires a multifactorial approach including mild mechanical loading, contact

guidance, durotaxis or electrotaxis to induce Rho/Rock while avoiding osteogenic pathways. In this study, we explore that combination of mechanical loading and electrotactic cues to maintain tenogenic differentiation.

3.4.3 Effect of electrical signals in gene expression

Electric signals (ES) are not instrumental just for electrically excitable cells such as neural or muscle cells. Instead, alteration of the cell membrane potential via ES can affect intracellular signalling pathways and modulate several biological functions including migration, apoptosis, proliferation, muscle regeneration, osteogenesis and tendon healing[32]. The importance of electrical stimuli is generally underrated in tissue engineering application, although electric cues (potential and currents) play a fundamental role in embryogenesis[207,223,291]. In previous studies, it has been demonstrated that the application of electrical fields to cell populations results in cytoskeletal rearrangements, the redistribution of membrane receptors and changes in calcium dynamics[96]. Also, it has been shown that electrical stimulation can guide cell differentiation by inducing a more elongated cell morphology (perpendicular to the electrical field vector) and enhance cell adhesion[292].

Furthermore, piezoelectricity is present on many biological structures, including bone[33,34] and tendon[35]. Most biopolymers, i.e. polysaccharides, amino acids and proteins, display piezoelectric behaviour[293] and are thought to regulate several physiological functions including pain sensation, hearing and blood pressure regulation[294,295].

For this reason, mimicking the intrinsic piezoelectric properties of the specific extracellular environment hold promising potential to control cell function. In this work, a custom-made gene microarray of 96 different genes was used to evaluate cellular differentiation, adhesion, cell receptor expression and extracellular matrix production in human tendon cells cultured on piezoelectric and non-piezoelectric surfaces to investigate the effect of surface polarisation.

The immobilisation of proteins onto a biomaterial surface has been proved to be a necessary approach to promote cells attachment to materials with low surface energy levels. In this work, PVDF-TrFE surface functionalization with physically absorbed fibronectin was compared to functionalization with covalently attached fibronectin. Immobilisation of

proteins represents a successful methodology to retain the activity and block the degradation of proteins compared to non-immobilizing methodologies. Here, Carboxyl groups were incorporated onto the surface of PVDF-TrFE through the grafting of acrylic acid, which was subsequently activated through carbodiimide chemistry to immobilise fibronectin to the fluorinated polymer surface covalently.

Modulation to specific gene networks was studied through Ingenuity Pathway Analysis using predictive biochemical interactions that link gene changes to signalling pathways. It was observed that tendon cells cultured on piezoelectric surfaces induced downregulation of dedifferentiation process (ALPL down-regulation) towards bone phenotype and upregulation of tendon-related markers such as SCX, SOX9, COMP or THBSP4. Further, upregulation of TRP-family ion channel proteins TRPA1 and TRPV-1 and downregulation of PIEZO2 was correlated. IPA analysis identified that TGF-β1 (p-value=1,41E-13) was an upstream regulator for tendon phenotype maintenance, activating TGF-β/BMP signalling and adhesion-related signalling proteins including multiple integrins, FAK and paxillin. TGF-β is a well-recognised factor that induces ECM synthesis and modulates several cellular processes, including cellular differentiation[296]. These findings suggest that surface polarisation modulates TGF-β secretion. Previous studies have already shown the clinical significance of ES in tissue regeneration and demonstrated that induces secretion of TGF-in osteoblasts via calcium pathways[297]. In a different study, ES enhanced the expression levels of chondrogenic markers (collagen II, Sox9 and Aggrecan) on MSCs without any use of exogenous growth factors via calcium/ATP oscillations. However, inhibition of TFG-β but not BMP signalling blocked the chondrogenesis of MSCs demonstrating the direct link between ES, TGF-β and differentiation processes.

3.4.4 Mechanical stimulation of tenocytes

For these experiments, we used human tendon-derived cells cultured on non-piezoelectric materials to assess the effect of "nanokicking" alone (nano stimulation) on select protein expression. It is observed that stimulation at different frequencies has a positive effect on the expression of tendon-related proteins at both frequencies used (700 and 1500 Hz). However, the tenospecific function was maintained to a higher level in cells cultured at lower frequencies, and regulations in TNC, COLI and DCN were noted in cells stimulated

at 700 Hz. Also, collagen production was increased at 1500 Hz, suggesting that de-differentiation or phenotypic drift was occurring. Pathways associated with the dedifferentiation process towards an osteogenic lineage included ERK/β-catenin (non-canonical) and SMAD1/5/8 (canonical) signalling pathways linked to BMP/TGF signalling. In a previous study by Tsimbouri et al., it was proposed that that nanokicking mediated modulation of the signalling pathway are dependent on cell membrane receptors including ion channels and BMP receptors[7]. Therefore, the sensitivity of the receptors in nano stimulated tendon cell was studied in this chapter, revealing a significant up-regulation in BMP receptor (BMPR1A) expression and overall ion channels expression, in particular, TRPV1 and Piezo1 when stimulated at 1500 Hz. This result aligns well with the proposed idea that TRP-family channels influence nano stimulation-induced MSC osteogenesis through the β-catenin/Wnt pathway activation of bone transcription factors [151]. In this pathway, ion influx through the TRPV channels causes the activation of protein kinase C (PKC) and ERK, mediating β-catenin activity. Despite the fact that an upregulation in TNMD expression was observed particularly at 1500 Hz, an increase in markers of dedifferentiation were also observed, including collagen II, the ratio of collagen III to collagen I, the activation of osteogenic signalling pathways β-catenin and Smad, and a decrease in tendon-related markers (BGN,TNC,TBHS4). To emulate the effects of increased of BMP signalling in tenocytes, we added TGF-β3 soluble growth factor to the culture media and a significant upregulation of TNMD, but downregulation of SCX was observed. These changes were associated with downregulation of Piezo2 and upregulation of TRPV1.

3.4.5 Dedifferentiated tenocytes regain their phenotype under high frequency, low-magnitude electromechanical stimulation (HFLMEMS).

Next, the combinatorial effect of mechanical loading in combination with electrical charges was evaluated *in vitro*. No dedifferentiation processes and enhanced expression of SCX and TNMD were shown when applying electrical stimulation together with vibrational stimulation through piezoelectric films. The most significant levels of SCX and tendon related markers TBHS4, DCN and BGN were observed on tenocytes undergoing continuous high frequency, low-magnitude electromechanical stimulation at 1500 Hz for 10

days (see Figure 23). The effect was proportionally more pronounced when a higher level of electrical stimulation was used. Significant down-regulation was observed in the expression of cell receptors and ion channels BMPR1A and Piezo and TRP, respectively, relative to tenocytes under mechanical stimulation alone. Specifically, high frequency, low-magnitude electromechanical stimulation-induced increased adhesion and the downregulation of pathways associated with osteogenesis (β-catenin and Smad signalling). It can be hypothesised that electrical signals interfere with BMP receptor signalling and, modulating functional pathways in tendon cells via Piezo 1/2 and TRPA1 ion channel changes in sensitivity

Different studies have demonstrated the link between mechanosensors activation, including ion channels and adhesion-proteins with ultimately increased intracellular tension and rigidity via specific signalling pathways[298–300]. In order to probe whether ion channel activation might play a central role in the de-differentiation process of tenocytes, cytoskeletal tension perturbation was subsequently performed.

3.4.6 Molecular mechanism and receptors sensitivity related to high frequency, low-magnitude electromechanical stimulation

Ion channel sensitivity to nano and high frequency, low-magnitude electromechanical stimulation was performed to relate ion channel expression to cytoskeletal tension. There is a common consensus in the biomechanics field that the expression and activation of different receptors are associated with intracellular tension, including KCNK[37], TRP[38] and Piezo[39,40] ion channels family. Protein expression at days 1, 5 and 10 of the channels Piezo1, Piezo2 (sensitive to vibrations and electrically polarized environments), TRPA1, TRPV1, L-type Ca^{2+}, (sensitive to calcium signalling through PKC), KCNK2 and KCNK4 (potassium channel subfamily K receptor 2 and 4, sensitive to membrane stretching) was evaluated in tenocytes in vitro under EMS.

EMS of tenocytes produced a similar trend of up-regulation concerning the expression of all of the ion channels tested. Notably, expression of the TRP and Piezo family of ion channels were downregulated on cells mechanically stimulated (EMS at 1500 Hz); On the other hand, this trend was completely reversed when stimulated at the same frequency under EMS. Interestingly, β-catenin and BMP signalling were also significantly

downregulated under EMS at 1500 Hz, meaning that EMS might regulate these pathways. This effect has been previously described in excitable cells, where the electrical activity of neural cells affects the phosphorylation status and nuclear level of activated Smads, the canonical components of BMP signalling. In the same study, it was shown that BMP signalling, in turn, decreased ion channel expression via ERK1/2[41]. These results suggest that electrical cues prevent de-differentiation through the modulation of ion channel expression.

In previous studies on MSC osteospecific differentiation, it was shown that mechanical stimulation results in an increase of intracellular tension to mediate osteogenesis. Therefore, it was hypothesised that if ion channels are involved in the dedifferentiation processes during the phenotypic drift of tenocytes, they should be sensitive to tension inhibitors, such as the ROCK inhibitor (Y27632) and the myosin II inhibitor (blebbistatin). To test this hypothesis tenocytes were stimulated in vitro at 1500 Hz for 5 days (300nm amplitude).

It was observed that the expression of on channels was modulated at day 5 using TGF-β3 stimulation, with Piezo 2 being significantly downregulated and TRPV1 significantly upregulated. This trend was noted also in tenocytes subjected to mechanical stimulation at 1500 Hz. The investigated tendon related markers were maintained at this frequency (SCX, TNMD); however, osteogenic pathways were observed to be activated (specifically Smad signalling and Wnt/β-catenin). Following the addition of Y27632 and blebbistatin, the expression of Piezo2 was reduced, indicating that a relationship exists between the expression of his receptor and cellular tension. Conversely, TRPV1 did not show a tension-dependant relationship and expression under mechanical stimulation or EMS was unchanged. Finally, BMPR was shown to be downregulated under EMS but upregulates under cytoskeletal inhibition. These findings suggest that mechanical stimulation at higher frequencies induces the upregulation of osteogenic transcription factors through activation of adhesion mediated and osteogenic pathways Wnt. Interestingly, these effects were reversed when tenocytes were under EMS.

Furthermore, SCX was downregulated with the addition of Rho/Rock inhibitors suggesting intracellular tension is a mediator of tenospecific function during both mechanical

stimulation and EMS. The effect of ROCK/RhoA inhibition on tenogenic markers was also investigated in mechanically and electromechanically stimulated tendon-derived cells. BMP2 receptor (BMPR1a) was differentially regulated in blebbistatin-inhibited tenocytes under high frequency, low-magnitude electromechanical stimulation but not under mechanical stimulation. Indicating that cells become less responsive to BMP2 (osteogenic dedifferentiation) when stimulated electromechanically. Similarly, regulation of BMPR expression resulted in modulation of BMP signalling pathway.

3.5   Conclusion

Genomic analysis was performed to investigate the effects of high frequency, low amplitude electromechanical stimulation on multiple functional signalling pathways in human tenocyte cells. Gene analysis showed that electromechanically stimulated tenocytes and control tenocytes had different gene expression profiles, indicative of different phenotypes. Ingenuity pathway analysis (IPA) was used to predict biochemical interactions and to identify mechanistic networks related to biological functions (i.e differentiation). The main signalling pathways modulated by electromechanical and mechanical stimulation were related to cellular adhesion, cytoskeletal tension, ERK1/2 signalling, BMP/TGF-β signalling and calcium/Wnt signalling.

Using protein microarray technology, we showed that dedifferentiation towards an osteogenic lineage occurred in tenocytes intense mechanically stimulated at 1500 Hz but not under moderate mechanical stimulation at 700 Hz. However, osteogenic de-differentiation was shown to be reversible when applying electromechanical stimulation through piezoelectric films. It was further observed that the highest levels of SCX and tendon related markers TBHS4, DCN and BGN were present as a result of continuous high frequency, low-magnitude electromechanical stimulation at 1500 Hz for 10 days. Interestingly, SCX was downregulated when using Rho/Rock inhibitors, suggesting that this is the main pathway involved to modulate its expression during EMS. These data support the hypothesis that de-differentiation towards an osteogenic lineage is produced by mechanical stimulation but inhibited under EMS. It has been described in previous studies that mechanical stimulation is a process that involves intracellular tension, coupled with the activation of mechanoreceptors, such as Piezo, TRP and KCNK. However, when cells are exposed to high frequency, low-magnitude mechanical stimulation ion channels Piezo 2 is down-regulated similarly to the effect of TGF-B3 stimulation.

We have presented a new class of electromechanical system and showed that tenocyte phenotypic drift could be avoided without the use of chemicals, growth factors, or bioactive scaffolds, sophisticated bioreactors. The use of piezoelectric films with BNNT in this study provided superior cell adhesion and enhanced piezoelectric response at the operating

frequencies. This resulted in a functional response of tendon cells and allowed to prevent phenotypic drift of cells by interfering with activation of osteogenic pathway Wnt/β-catenin via increased intracellular tension and modulation of piezosensitive receptors TRP and Piezo.

3.6   References

1.   Snedeker, J. G. & Foolen, J. Tendon injury and repair – A perspective on the basic mechanisms of tendon disease and future clinical therapy. *Acta Biomaterialia* **63**, 18–36 (2017).

2.   Walden, G. *et al.* A Clinical, Biological, and Biomaterials Perspective into Tendon Injuries and Regeneration. *Tissue Eng. Part B Rev.* (2017). doi:10.1089/ten.teb.2016.0181

3.   Docheva, D., Müller, S. A., Majewski, M. & Evans, C. H. Biologics for tendon repair. *Advanced Drug Delivery Reviews* (2015). doi:10.1016/j.addr.2014.11.015

4.   Kartus, J., Movin, T. & Karlsson, J. Donor-site morbidity and anterior knee problems after anterior cruciate ligament reconstruction using autografts. *Arthroscopy* (2001). doi:10.1053/jars.2001.28979

5.   Yasuda, K., Tsujino, J., Ohkoshi, Y., Tanabe, Y. & Kaneda, K. Graft Site Morbidity with Autogenous Semitendinosus and Gracilis Tendons. *Am. J. Sports Med.* (1995). doi:10.1177/036354659502300613

6.   Kartus, J., Movin, T. & Karlsson, J. Donor-site morbidity after anterior cruciate ligament reconstruction using autografts clinical, radiographic, histological, and ultrastructural aspects. in *Anterior Knee Pain and Patellar Instability* (2006). doi:10.1007/1-84628-143-1_19

7.   Seo, J. G. *et al.* Ankle morbidity after autogenous Achilles tendon harvesting for anterior cruciate ligament reconstruction. *Knee Surgery, Sport. Traumatol. Arthrosc.* (2009). doi:10.1007/s00167-009-0729-9

8.   Kuo, C. K., Marturano, J. E. & Tuan, R. S. Novel strategies in tendon and ligament tissue engineering: Advanced biomaterials and regeneration motifs. *BMC Sports Sci. Med. Rehabil.* **2**, 20 (2010).

9.   Lomas, A. J. *et al.* The past, present and future in scaffold-based tendon treatments.

Advanced Drug Delivery Reviews **84**, 257–277 (2015).

10. Liu, Y., Ramanath, H. S. & Wang, D. A. Tendon tissue engineering using scaffold enhancing strategies. *Trends in Biotechnology* **26**, 201–209 (2008).

11. Mammoto, T. & Ingber, D. E. Mechanical control of tissue and organ development. *Development* (2010). doi:10.1242/dev.024166

12. Obregón, R., Ramón-Azcón, J. & Ahadian, S. Bioreactors in Tissue Engineering. in *Tissue Engineering for Artificial Organs: Regenerative Medicine, Smart Diagnostics and Personalized Medicine* (2016). doi:10.1002/9783527689934.ch6

13. Plonsey, R., Barr, R. C., Plonsey, R. & Barr, R. C. Electrical Stimulation of Excitable Tissue. in *Bioelectricity* (2000). doi:10.1007/978-1-4757-3152-1_7

14. Rajabi, A. H., Jaffe, M. & Arinzeh, T. L. Piezoelectric materials for tissue regeneration: A review. *Acta Biomater.* **24**, 12–23 (2015).

15. Tandon, N. *et al.* Electrical stimulation systems for cardiac tissue engineering. *Nat. Protoc.* (2009). doi:10.1038/nprot.2008.183

16. Chen, J., Xu, J., Wang, A. & Zheng, M. Scaffolds for tendon and ligament repair: Review of the efficacy of commercial products. *Expert Review of Medical Devices* **6**, 61–73 (2009).

17. Longo, U. G., Lamberti, A., Maffulli, N. & Denaro, V. Tendon augmentation grafts: A systematic review. *Br. Med. Bull.* (2010). doi:10.1093/bmb/ldp051

18. Yin, Z. *et al.* The regulation of tendon stem cell differentiation by the alignment of nanofibers. *Biomaterials* **31**, 2163–2175 (2010).

19. Kew, S. J. *et al.* Regeneration and repair of tendon and ligament tissue using collagen fibre biomaterials. *Acta Biomaterialia* (2011). doi:10.1016/j.actbio.2011.06.002

20. Font Tellado, S., Balmayor, E. R. & Van Griensven, M. Strategies to engineer

tendon/ligament-to-bone interface: Biomaterials, cells and growth factors. *Advanced Drug Delivery Reviews* (2015). doi:10.1016/j.addr.2015.03.004

21.   Cross, L. M., Thakur, A., Jalili, N. A., Detamore, M. & Gaharwar, A. K. Nanoengineered biomaterials for repair and regeneration of orthopedic tissue interfaces. *Acta Biomaterialia* (2016). doi:10.1016/j.actbio.2016.06.023

22.   Pesqueira, T. *et al.* Engineering magnetically responsive tropoelastin spongy-like hydrogels for soft tissue regeneration. *J. Mater. Chem. B* (2018). doi:10.1039/c7tb02035j

23.   Pesqueira, T., Costa-Almeida, R. & Gomes, M. E. Magnetotherapy: The quest for tendon regeneration. *J. Cell. Physiol.* (2018). doi:10.1002/jcp.26637

24.   Silva, E. D. *et al.* Multifunctional magnetic-responsive hydrogels to engineer tendon-to-bone interface. *Nanomedicine Nanotechnology, Biol. Med.* (2018). doi:10.1016/j.nano.2017.06.002

25.   Gonçalves, A. I., Rodrigues, M. T. & Gomes, M. E. Tissue-engineered magnetic cell sheet patches for advanced strategies in tendon regeneration. *Acta Biomater.* (2017). doi:10.1016/j.actbio.2017.09.014

26.   Holzapfel, B. M. *et al.* How smart do biomaterials need to be? A translational science and clinical point of view. *Advanced Drug Delivery Reviews* (2013). doi:10.1016/j.addr.2012.07.009

27.   J.E. Commission, ETN nanomedicine: roadmaps in nanomedicine towards 2020, Expert Report 2009, 2009, p. 56.

28.   Schneider, M., Angele, P., Järvinen, T. A. H. & Docheva, D. Rescue plan for Achilles : Therapeutics steering the fate and functions of stem cells in tendon wound healing. *Adv. Drug Deliv. Rev.* **129**, 352–375 (2018).

29.   Yin, W. *et al.* Biomaterials Functional replication of the tendon tissue microenvironment by a bioimprinted substrate and the support of tenocytic

differentiation of mesenchymal stem cells. **33**, 7686–7698 (2012).

30. Brian, J. *et al.* The piezoelectric tensor of collagen fibrils determined at the nanoscale. (2017).

31. Manuscript, A. LAW ": A CRITICAL REVIEW. **31**, 733–741 (2010).

32. Manuscript, A. Nanoscale. (2018). doi:10.1039/C8NR01634H

33. Jacob, J., More, N., Kalia, K. & Kapusetti, G. Piezoelectric smart biomaterials for bone and cartilage tissue engineering. *Inflamm. Regen.* **38**, 2 (2018).

34. Vivekananthan, V. *et al.* Energy , Environmental , and Catalysis Applications Biocompatible collagen-nanofibrils : An approach for sustainable energy harvesting and battery-free humidity sensor applications Biocompatible collagen-nanofibrils : An approach for sustainable energy ha. (2018). doi:10.1021/acsami.8b02915

35. Michlovitz, S. L. Is there a role for ultrasound and electrical stimulation following injury to tendon and nerve? *J. Hand Ther.* (2005). doi:10.1197/j.jht.2005.02.013

36. Khan, S. I. & Burne, J. A. Inhibitory mechanisms following electrical stimulation of tendon and cutaneous afferents in the lower limb. *Brain Res.* (2010). doi:10.1016/j.brainres.2009.10.020

37. Williams, W. S. & Breger, L. Piezoelectricity in tendon and bone. *J. Biomech.* (1975). doi:10.1016/0021-9290(75)90076-7

38. Long, S. B., Campbell, E. B. & MacKinnon, R. Voltage sensor of Kv1.2: Structural basis of electromechanical coupling. *Science (80-.).* (2005). doi:10.1126/science.1116270

39. Pfeiffer, E. R., Tangney, J. R., Omens, J. H. & McCulloch, A. D. Biomechanics of Cardiac Electromechanical Coupling and Mechanoelectric Feedback. *J. Biomech. Eng.* (2014). doi:10.1115/1.4026221

40. Alcaino, C., Farrugia, G. & Beyder, A. Mechanosensitive Piezo Channels in the

Gastrointestinal Tract. *Curr. Top. Membr.* **79**, 219–244 (2017).

41. Michael Lavagnino1, Michelle E. Wall2, Dianne Little3, Albert J. Banes2,4, Farshid Guilak3,4,5, and S. P. A. Tendon Mechanobiology: Current Knowledge and Future Research Opportunities. *J Orthop Res.* **33**, 813–822 (2015).

42. Yoshimoto, Y., Takimoto, A., Watanabe, H., Hiraki, Y. & Kondoh, G. Scleraxis is required for maturation of tissue domains for proper integration of the musculoskeletal system. *Nat. Publ. Gr.* 1–16 (2017). doi:10.1038/srep45010

43. Chen, X. *et al.* promote the commitment of human ES cells derived MSCs to tenocytes. 1–9 (2012). doi:10.1038/srep00977

44. Wu, F. & Nerlich, M. Tendons basic biology Tendon injuries: basic science and new repair proposals. *Efort Open Rev.* (2017). doi:10.1302/2058-5241.2.160075

45. Bayer, M. L. *et al.* The initiation of embryonic-like collagen fibrillogenesis by adult human tendon fibroblasts when cultured under tension. *Biomaterials* (2010). doi:10.1016/j.biomaterials.2010.02.062

46. Zhang, G. *et al.* Development of tendon structure and function: regulation of collagen fibrillogenesis. *J. Musculoskelet. Neuronal Interact.* (2005).

47. Kostrominova, T. Y. & Brooks, S. V. Age-related changes in structure and extracellular matrix protein expression levels in rat tendons. *Age (Omaha).* (2013). doi:10.1007/s11357-013-9514-2

48. Brumitt, J. & Cuddeford, T. CURRENT CONCEPTS OF MUSCLE AND TENDON ADAPTATION TO STRENGTH AND CONDITIONING. *Int. J. Sports Phys. Ther.* (2015).

49. Robinson, K. A. *et al.* Decorin and biglycan are necessary for maintaining collagen fibril structure, fiber realignment, and mechanical properties of mature tendons. *Matrix Biol.* (2017). doi:10.1016/j.matbio.2017.08.004

50. Shetye, S. S. *et al.* Collagen V haploinsufficiency results in deficient mechanical and structural recovery of injured mouse patellar tendons. *J. Orthop. Res.* (2017).

51. Spiess, K. & Zorn, T. M. T. Collagen types I, III, and V constitute the thick collagen fibrils of the mouse decidua. *Microsc. Res. Tech.* (2007). doi:10.1002/jemt.20381

52. Hulmes, D. J., Wess, T. J., Prockop, D. J. & Fratzl, P. Radial packing, order, and disorder in collagen fibrils. *Biophys. J.* (1995). doi:10.1016/S0006-3495(95)80391-7

53. Ireland, D. *et al.* Multiple changes in gene expression in chronic human Achilles tendinopathy. *Matrix Biol.* (2001). doi:10.1016/S0945-053X(01)00128-7

54. Deshmukh, S., Dive, A., Moharil, R. & Munde, P. Enigmatic insight into collagen. *J. Oral Maxillofac. Pathol.* (2016). doi:10.4103/0973-029x.185932

55. Anderson, J. C. & Eriksson, C. Piezoelectric properties of dry and wet bone. *Nature* **227**, 491–492 (1970).

56. Denning, D. *et al.* Electromechanical properties of dried tendon and isoelectrically focused collagen hydrogels. *Acta Biomater.* **8**, 3073–3079 (2012).

57. Denning, D., Paukshto, M. V., Habelitz, S. & Rodriguez, B. J. Piezoelectric properties of aligned collagen membranes. *J. Biomed. Mater. Res. - Part B Appl. Biomater.* **102**, 284–292 (2014).

58. Bassett, C. A. L. Biologic significance of piezoelectricity. *Calcif. Tissue Res.* **1**, 252–272 (1967).

59. Vasquez-Sancho, F., Abdollahi, A., Damjanovic, D. & Catalan, G. Flexoelectricity in Bones. *Adv. Mater.* **30**, 1–5 (2018).

60. Yao, L., Bestwick, C. S., Bestwick, L. A., Maffulli, N. & Aspden, R. M. Phenotypic Drift in Human Tenocyte Culture. *Tissue Eng.* (2006). doi:10.1089/ten.2006.12.ft-90

61. Zhu, J. *et al.* The regulation of phenotype of cultured tenocytes by microgrooved surface structure. *Biomaterials* **31**, 6952–6958 (2010).

62. Shukunami, C. *et al.* Scleraxis is a transcriptional activator that regulates the expression of Tenomodulin, a marker of mature tenocytes and ligamentocytes. *Sci. Rep.* (2018). doi:10.1038/s41598-018-21194-3

63. Berthet, E. *et al.* Smad3 binds Scleraxis and Mohawk and regulates tendon matrix organisation. *J. Orthop. Res.* (2013). doi:10.1002/jor.22382

64. Tan, S. L. *et al.* The effect of growth differentiation factor-5 (GDF-5) on the proliferation and tenogenic differentiation potential of human mesenchymal stem cells in vitro. *J. Univ. Malaya Med. Cent.* (2013).

65. Killian, M. L. & Thomopoulos, S. Scleraxis is required for the development of a functional tendon enthesis. *FASEB J.* (2016). doi:10.1096/fj.14-258236

66. Brown, D., Wagner, D., Li, X., Richardson, J. A. & Olson, E. N. Dual role of the basic helix-loop-helix transcription factor scleraxis in mesoderm formation and chondrogenesis during mouse embryogenesis. *Development* (1999).

67. Sharma, P. & Maffulli, N. Biology of tendon injury: Healing, modeling and remodeling. *Journal of Musculoskeletal Neuronal Interactions* (2006).

68. Nourissat, G., Berenbaum, F. & Duprez, D. Tendon injury: from biology to tendon repair. *Nat. Rev. Rheumatol.* **11**, 223–233 (2015).

69. Bi, Y. *et al.* Identification of tendon stem/progenitor cells and the role of the extracellular matrix in their niche. *Nat. Med.* **13**, 1219–1227 (2007).

70. Lui, P. P. Y. Identity of tendon stem cells - how much do we know? *Journal of Cellular and Molecular Medicine* (2013). doi:10.1111/jcmm.12007

71. Yin, Z. *et al.* Single-cell analysis reveals a nestin+ tendon stem/progenitor cell population with strong tenogenic potentiality. *Sci. Adv.* **2**, 1–15 (2016).

72. Ruprecht, V. *et al.* How cells respond to environmental cues – insights from bio-functionalized substrates. *J. Cell Sci.* (2017). doi:10.1242/jcs.196162

73.   Gupta, M. *et al.* Micropillar substrates: A tool for studying cell mechanobiology. *Methods Cell Biol.* (2015). doi:10.1016/bs.mcb.2014.10.009

74.   Kshitiz *et al.* Control of stem cell fate and function by engineering physical microenvironments. *Integrative Biology (United Kingdom)* (2012). doi:10.1039/c2ib20080e

75.   Guilak, F. *et al.* Control of Stem Cell Fate by Physical Interactions with the Extracellular Matrix. *Cell Stem Cell* (2009). doi:10.1016/j.stem.2009.06.016

76.   Frantz, C., Stewart, K. M. & Weaver, V. M. The extracellular matrix at a glance. *J. Cell Sci.* (2010). doi:10.1242/jcs.023820

77.   Fehrer, C. *et al.* Reduced oxygen tension attenuates differentiation capacity of human mesenchymal stem cells and prolongs their lifespan. *Aging Cell* (2007). doi:10.1111/j.1474-9726.2007.00336.x

78.   Li, P. *et al.* Role of the ERK1/2 signaling pathway in osteogenesis of rat tendon-derived stem cells in normoxic and hypoxic cultures. *Int. J. Med. Sci.* (2016). doi:10.7150/ijms.16045

79.   Reinwald, Y. & El Haj, A. J. Hydrostatic pressure in combination with topographical cues affects the fate of bone marrow-derived human mesenchymal stem cells for bone tissue regeneration. *J. Biomed. Mater. Res. - Part A* (2018). doi:10.1002/jbm.a.36267

80.   Docheva, D., Müller, S. A., Majewski, M. & Evans, C. H. Biologics for tendon repair. *Adv. Drug Deliv. Rev.* **84**, 222–239 (2015).

81.   Khan, K. M. & Scott, A. Mechanotherapy: How physical therapists' prescription of exercise promotes tissue repair. *British Journal of Sports Medicine* (2009). doi:10.1136/bjsm.2008.054239

82.   Wang, Z. *et al.* Functional regeneration of tendons using scaffolds with physical anisotropy engineered via microarchitectural manipulation. *Sci. Adv.* (2018).

doi:10.1126/sciadv.aat4537

83. Biggs, M. J. P. *et al.* Interactions with nanoscale topography: Adhesion quantification and signal transduction in cells of osteogenic and multipotent lineage. *J. Biomed. Mater. Res. - Part A* (2009). doi:10.1002/jbm.a.32196

84. Levin, M. Bioelectric mechanisms in regeneration: Unique aspects and future perspectives. *Semin. Cell Dev. Biol.* (2009). doi:10.1016/j.semcdb.2009.04.013

85. Tseng, A. S. & Levin, M. Transducing Bioelectric Signals into Epigenetic Pathways During Tadpole Tail Regeneration. *Anatomical Record* (2012). doi:10.1002/ar.22495

86. Sundelacruz, S., Li, C., Choi, Y. J., Levin, M. & Kaplan, D. L. Bioelectric modulation of wound healing in a 3D invitro model of tissue-engineered bone. *Biomaterials* (2013). doi:10.1016/j.biomaterials.2013.05.040

87. Engler, A. J., Sen, S., Sweeney, H. L. & Discher, D. E. Matrix elasticity directs stem cell lineage specification. *Cell* (2006). doi:10.1016/j.cell.2006.06.044

88. Mamidi, A. *et al.* Mechanosignalling via integrins directs fate decisions of pancreatic progenitors. *Nature* (2018). doi:10.1038/s41586-018-0762-2

89. Biggs, M. J. P. *et al.* The Functional Response of Mesenchymal Stem Cells to Electron-Beam Patterned Elastomeric Surfaces Presenting Micrometer to Nanoscale Heterogeneous Rigidity. *Adv. Mater.* **29**, 1702119 (2017).

90. Wang, N., Tytell, J. D. & Ingber, D. E. Mechanotransduction at a distance: Mechanically coupling the extracellular matrix with the nucleus. *Nat. Rev. Mol. Cell Biol.* **10**, 75–82 (2009).

91. Lin, X., Shi, Y., Cao, Y. & Liu, W. Recent progress in stem cell differentiation directed by material and mechanical cues. *Biomed. Mater.* (2016). doi:10.1088/1748-6041/11/1/014109

92. Hao, J. *et al.* Mechanobiology of mesenchymal stem cells: Perspective into

mechanical induction of MSC fate. *Acta Biomaterialia* (2015).
doi:10.1016/j.actbio.2015.04.008

93.   Molloy, T., Wang, Y. & Murrell, G. A. C. The roles of growth factors in tendon and ligament healing. *Sports Medicine* (2003). doi:10.2165/00007256-200333050-00004

94.   Caliari, S. R. & Harley, B. A. C. The effect of anisotropic collagen-GAG scaffolds and growth factor supplementation on tendon cell recruitment, alignment, and metabolic activity. *Biomaterials* (2011). doi:10.1016/j.biomaterials.2011.04.021

95.   Kjær, M. *et al.* From mechanical loading to collagen synthesis, structural changes and function in human tendon. *Scandinavian Journal of Medicine and Science in Sports* (2009). doi:10.1111/j.1600-0838.2009.00986.x

96.   Zhao, M. *et al.* Electrical signals control wound healing through phosphatidylinositol-3-OH kinase-γ and PTEN. *Nature* (2006). doi:10.1038/nature04925

97.   Ciombor, D. M. & Aaron, R. K. The role of electrical stimulation in bone repair. *Foot and Ankle Clinics* (2005). doi:10.1016/j.fcl.2005.06.006

98.   Tandon, B., Blaker, J. J. & Cartmell, S. H. Piezoelectric materials as stimulatory biomedical materials and scaffolds for bone repair. *Acta Biomaterialia* (2018). doi:10.1016/j.actbio.2018.04.026

99.   Mollon, B., Da Silva, V., Busse, J. W., Einhorn, T. A. & Bhandari, M. Electrical stimulation for long-bone fracture-healing: A meta-analysis of randomized controlled trials. *Journal of Bone and Joint Surgery - Series A* (2008). doi:10.2106/JBJS.H.00111

100.   Yuan, X., Arkonac, D. E., Chao, P. H. G. & Vunjak-Novakovic, G. Electrical stimulation enhances cell migration and integrative repair in the meniscus. *Sci. Rep.* (2015). doi:10.1038/srep03674

101.   Kloth, L. C. Electrical stimulation for wound healing: A review of evidence from in

vitro studies, animal experiments, and clinical trials. *International Journal of Lower Extremity Wounds* (2005). doi:10.1177/1534734605275733

102.   Fukada, E. & Yasuda, I. On the Piezoelectric Effect of Bone. *J. Phys. Soc. Japan* (1957). doi:10.1143/JPSJ.12.1158

103.   Brighton, C. T., Jensen, L., Pollack, S. R., Tolin, B. S. & Clark, C. C. Proliferative and synthetic response of bovine growth plate chondrocytes to various capacitively coupled electrical fields. *J. Orthop. Res.* (1989). doi:10.1002/jor.1100070519

104.   Armstrong, P. F., Brighton, C. T. & Star, A. M. Capacitively coupled electrical stimulation of bovine growth plate chondrocytes grown in pellet form. *J. Orthop. Res.* (1988). doi:10.1002/jor.1100060214

105.   Wang, W., Wang, Z., Zhang, G., Clark, C. C. & Brighton, C. T. Up-regulation of chondrocyte matrix genes and products by electric fields. in *Clinical Orthopaedics and Related Research* (2004). doi:10.1097/01.blo.0000143837.53434.5c

106.   Walther, M., Mayer, F., Kafka, W. & Schütze, N. Effects of weak, low-frequency pulsed electromagnetic fields (BEMER type) on gene expression of human mesenchymal stem cells and chondrocytes: An in vitro study. *Electromagn. Biol. Med.* (2007). doi:10.1080/15368370701580814

107.   Kwon, H. J., Lee, G. S. & Chun, H. Electrical stimulation drives chondrogenesis of mesenchymal stem cells in the absence of exogenous growth factors. *Sci. Rep.* **6**, 1–13 (2016).

108.   Mathews, J. & Levin, M. The body electric 2.0: recent advances in developmental bioelectricity for regenerative and synthetic bioengineering. *Current Opinion in Biotechnology* (2018). doi:10.1016/j.copbio.2018.03.008

109.   McLaughlin, K. A. & Levin, M. Bioelectric signaling in regeneration: Mechanisms of ionic controls of growth and form. *Dev. Biol.* **433**, 177–189 (2018).

110.   Tseng, A. & Levin, M. Cracking the bioelectric code: Probing endogenous ionic

controls of pattern formation. *Commun. Integr. Biol.* (2013). doi:10.4161/cib.22595

111. Pai, V. P. *et al.* HCN2 Rescues brain defects by enforcing endogenous voltage pre-patterns. *Nat. Commun.* **9**, 998 (2018).

112. Levin, M. Molecular bioelectricity: how endogenous voltage potentials control cell behavior and instruct pattern regulation in vivo. *Mol. Biol. Cell* **25**, 3835–50 (2014).

113. Pietak, A. & Levin, M. Exploring Instructive Physiological Signaling with the Bioelectric Tissue Simulation Engine. *Front. Bioeng. Biotechnol.* **4**, (2016).

114. Zhao, M. Electrical fields in wound healing-An overriding signal that directs cell migration. *Seminars in Cell and Developmental Biology* (2009). doi:10.1016/j.semcdb.2008.12.009

115. Huang, Y., Li, Y., Chen, J., Zhou, H. & Tan, S. Electrical Stimulation Elicits Neural Stem Cells Activation: New Perspectives in CNS Repair. *Front. Hum. Neurosci.* (2015). doi:10.3389/fnhum.2015.00586

116. Martinac, B. The ion channels to cytoskeleton connection as potential mechanism of mechanosensitivity. *Biochim. Biophys. Acta - Biomembr.* **1838**, 682–691 (2014).

117. Everaerts, W., Nilius, B. & Owsianik, G. The vanilloid transient receptor potential channel TRPV4: From structure to disease. *Progress in Biophysics and Molecular Biology* (2010). doi:10.1016/j.pbiomolbio.2009.10.002

118. Moran, M. M., McAlexander, M. A., Bíró, T. & Szallasi, A. Transient receptor potential channels as therapeutic targets. *Nature Reviews Drug Discovery* (2011). doi:10.1038/nrd3456

119. Earley, S. & Brayden, J. E. Transient Receptor Potential Channels in the Vasculature. *Physiol. Rev.* (2015). doi:10.1152/physrev.00026.2014

120. Liedtke, W. B. *TRPV Channels' Function in Osmo- and Mechanotransduction. TRP Ion Channel Function in Sensory Transduction and Cellular SignalingCascades*

(2007).

121. Okumura, R. *et al.* The odontoblast as a sensory receptor cell? The expression of TRPV1 (VR-1) channels. *Arch. Histol. Cytol.* (2006). doi:10.1679/aohc.68.251

122. Qi, Y. *et al.* Uniaxial cyclic stretch stimulates TRPV4 to induce realignment of human embryonic stem cell-derived cardiomyocytes. *J. Mol. Cell. Cardiol.* (2015). doi:10.1016/j.yjmcc.2015.08.005

123. Goswami, R. *et al.* TRPV4 calcium-permeable channel is a novel regulator of oxidized LDL-induced macrophage foam cell formation. *Free Radic. Biol. Med.* (2017). doi:10.1016/j.freeradbiomed.2017.06.004

124. Suzuki, T. *et al.* TRPV4 (transient receptor potential vanilloid 4), a mechanosensor for bone is required for the maintenance of bone mineral density of mandible exposed to occlusal force. *J. Bone Miner. Res.* (2010).

125. Saotome, K. *et al.* Structure of the mechanically activated ion channel Piezo1. *Nature* (2018). doi:10.1038/nature25453

126. etem, ebru *et al.* The increased expression of Piezo1 and Piezo2 ion channels in human and mouse bladder carcinoma. *Adv. Clin. Exp. Med.* (2018). doi:10.17219/acem/71080

127. Gao, Q., Cooper, P. R., Walmsley, A. D. & Scheven, B. A. Role of Piezo Channels in Ultrasound-stimulated Dental Stem Cells. *J. Endod.* (2017). doi:10.1016/j.joen.2017.02.022

128. Song, Y. *et al.* The Mechanosensitive Ion Channel Piezo Inhibits Axon Regeneration. *Neuron* (2019). doi:10.1016/j.neuron.2019.01.050

129. He, L., Si, G., Huang, J., Samuel, A. D. T. & Perrimon, N. Mechanical regulation of stem-cell differentiation by the stretch-activated Piezo channel. *Nature* **555**, 103–106 (2018).

130. Lavagnino, M., Arnoczky, S. P., Egerbacher, M., Gardner, K. L. & Burns, M. E. Isolated fibrillar damage in tendons stimulates local collagenase mRNA expression and protein synthesis. *J. Biomech.* (2006). doi:10.1016/j.jbiomech.2005.08.008

131. Maeda, T. *et al.* Conversion of mechanical force into TGF-β-mediated biochemical signals. *Curr. Biol.* (2011). doi:10.1016/j.cub.2011.04.007

132. Chen, Y., Ju, L., Rushdi, M., Ge, C. & Zhu, C. Receptor-mediated cell mechanosensing. *Mol. Biol. Cell* (2017). doi:10.1091/mbc.e17-04-0228

133. Elosegui-Artola, A., Trepat, X. & Roca-Cusachs, P. Control of Mechanotransduction by Molecular Clutch Dynamics. *Trends Cell Biol.* (2018). doi:10.1016/j.tcb.2018.01.008

134. Massia, S. P. & Hubbell, J. A. An RGD spacing of 440 nm is sufficient for integrin αvβ3-mediated fibroblast spreading and 140 nm for focal contact and stress fiber formation. *J. Cell Biol.* (1991). doi:10.1083/jcb.114.5.1089

135. Oria, R. *et al.* Force loading explains spatial sensing of ligands by cells. *Nature* (2017). doi:10.1038/nature24662

136. Salmeron-Sanchez, M. *et al.* Molecular clutch drives cell response to surface viscosity. *Proc. Natl. Acad. Sci.* (2018). doi:10.1073/pnas.1710653115

137. Fernandez-Yague, M. A. *et al.* Biomimetic approaches in bone tissue engineering: Integrating biological and physicomechanical strategies. *Advanced Drug Delivery Reviews* **84**, 1–29 (2015).

138. Galloway, M. T., Lalley, A. L. & Shearn, J. T. The role of mechanical loading in tendon development, maintenance, injury, and repair. *Journal of Bone and Joint Surgery - Series A* (2013). doi:10.2106/JBJS.L.01004

139. Wang, T. *et al.* Bioreactor Design for Tendon/Ligament Engineering. *Tissue Eng. Part B Rev.* **19**, 133–146 (2013).

140. Thomopoulos, S., Parks, W. C., Rifkin, D. B. & Derwin, K. A. Mechanisms of tendon injury and repair. in *Journal of Orthopaedic Research* (2015). doi:10.1002/jor.22806

141. Screen, H. R. C., Berk, D. E., Kadler, K. E., Ramirez, F. & Young, M. F. Tendon functional extracellular matrix. in *Journal of Orthopaedic Research* (2015). doi:10.1002/jor.22818

142. Xu, B. *et al.* RhoA/ROCK, cytoskeletal dynamics, and focal adhesion kinase are required for mechanical stretch-induced tenogenic differentiation of human mesenchymal stem cells. *J. Cell. Physiol.* **227**, 2722–2729 (2012).

143. Mackley, J. R., Ando, J., Herzyk, P. & Winder, S. J. Phenotypic responses to mechanical stress in fibroblasts from tendon, cornea and skin. *Biochem. J.* (2006). doi:10.1042/bj20060057

144. Fong, K. D. *et al.* Microarray analysis of mechanical shear effects on flexor tendon cells. *Plast. Reconstr. Surg.* (2005). doi:10.1097/01.prs.0000182345.86453.4f

145. Deng, D. *et al.* Engineering human neo-tendon tissue in vitro with human dermal fibroblasts under static mechanical strain. *Biomaterials* (2009). doi:10.1016/j.biomaterials.2009.08.054

146. Maharam, E. *et al.* Rho/Rock signal transduction pathway is required for MSC tenogenic differentiation. *Bone Res.* **3**, (2015).

147. Lin, J. *et al.* Acta Biomaterialia Cell-material interactions in tendon tissue engineering. *Acta Biomater.* 1–11 (2018). doi:10.1016/j.actbio.2018.01.012

148. Robertson, B. D. & Sawicki, G. S. Unconstrained muscle-tendon workloops indicate resonance tuning as a mechanism for elastic limb behavior during terrestrial locomotion. *Proc. Natl. Acad. Sci.* (2015). doi:10.1073/pnas.1500702112

149. Lau, E. *et al.* Effect of low-magnitude, high-frequency vibration on osteogenic differentiation of rat mesenchymal stromal cells. *J. Orthop. Res.* (2011).

doi:10.1002/jor.21334

150. Curtis, A. S. G. *et al.* Cell interactions at the nanoscale: Piezoelectric stimulation. *IEEE Trans. Nanobioscience* (2013). doi:10.1109/TNB.2013.2257837

151. Tsimbouri, P. M. *et al.* Stimulation of 3D osteogenesis by mesenchymal stem cells using a nanovibrational bioreactor. *Nat. Biomed. Eng.* (2017). doi:10.1038/s41551-017-0127-4

152. Miller, S. L. The mechanism of synthesis of amino acids by electric discharges. *BBA - Biochim. Biophys. Acta* (1957). doi:10.1016/0006-3002(57)90366-9

153. Pietak, A. & Levin, M. Bioelectrical control of positional information in development and regeneration: A review of conceptual and computational advances. *Progress in Biophysics and Molecular Biology* (2018). doi:10.1016/j.pbiomolbio.2018.03.008

154. Akai, M., Oda, H., Shirasaki, Y. & Tateishi, T. Electrical stimulation of ligament healing. An experimental study of the patellar ligament of rabbits. *Clin.Orthop.Relat Res.* (1988).

155. Sirohi, J. & Chopra, I. Fundamental understanding of piezoelectric strain sensors. *J. Intell. Mater. Syst. Struct.* (2000). doi:10.1106/8BFB-GC8P-XQ47-YCQ0

156. Ramadan, K. S., Sameoto, D. & Evoy, S. A review of piezoelectric polymers as functional materials for electromechanical transducers. *Smart Mater. Struct.* **23**, 033001 (2014).

157. Maxwell, J. C. A treatise on electricity and magnetism, Vol. II. *Journal of the Franklin Institute* (1954). doi:10.1017/CBO9780511709333

158. Wang, Z. L. On Maxwell's displacement current for energy and sensors: the origin of nanogenerators. *Mater. Today* **20**, 74–82 (2017).

159. Roche, J. The present status of Maxwell's displacement current. *Eur. J. Phys.*

(1998). doi:10.1088/0143-0807/19/2/009

160. Kawai, H. The Piezoelectricity of Poly (vinylidene Fluoride). *Jpn. J. Appl. Phys.* **8**, 975–976 (1969).

161. Motamedi, A. S., Mirzadeh, H., Hajiesmaeilbaigi, F., Bagheri-Khoulenjani, S. & Shokrgozar, M. A. Piezoelectric electrospun nanocomposite comprising Au NPs/PVDF for nerve tissue engineering. *J. Biomed. Mater. Res. Part A* **105**, 1984–1993 (2017).

162. Yu, Y. *et al.* Biocompatibility and in vivo operation of implantable mesoporous PVDF-based nanogenerators. *Nano energy* **27**, 275–281 (2016).

163. Sobreiro-Almeida, R. *et al.* Human Mesenchymal Stem Cells Growth and Osteogenic Differentiation on Piezoelectric Poly(vinylidene fluoride) Microsphere Substrates. *Int. J. Mol. Sci.* **18**, 2391 (2017).

164. Lee, Y.-S., Wu, S., Arinzeh, T. L. & Bunge, M. B. Transplantation of Schwann Cells Inside PVDF-TrFE Conduits to Bridge Transected Rat Spinal Cord Stumps to Promote Axon Regeneration Across the Gap. *J. Vis. Exp.* (2017). doi:10.3791/56077

165. Sharma, T., Aroom, K., Naik, S., Gill, B. & Zhang, J. X. J. Flexible thin-film PVDF-TrFE based pressure sensor for smart catheter applications. *Ann. Biomed. Eng.* **41**, 744–51 (2013).

166. Martins, P., Lopes, A. C. & Lanceros-Mendez, S. Electroactive phases of poly(vinylidene fluoride): Determination, processing and applications. *Prog. Polym. Sci.* **39**, 683–706 (2014).

167. Weber, N., Lee, Y.-S., Shanmugasundaram, S., Jaffe, M. & Arinzeh, T. L. Characterisation and in vitro cytocompatibility of piezoelectric electrospun scaffolds. *Acta Biomater.* **6**, 3550–3556 (2010).

168. Tseng, H. J., Tian, W. C. & Wu, W. J. P(VDF-TrFE) polymer-based thin films deposited on stainless steel substrates treated using water dissociation for flexible

tactile sensor development. *Sensors (Switzerland)* **13**, 14777–14796 (2013).

169. Hitscherich, P. *et al.* The effect of PVDF-TrFE scaffolds on stem cell derived cardiovascular cells. *Biotechnol. Bioeng.* **113**, 1577–85 (2016).

170. Cheng, X. *et al.* Implantable and self-powered blood pressure monitoring based on a piezoelectric thinfilm: Simulated, in vitro and in vivo studies. *Nano Energy* **22**, 453–460 (2016).

171. Persano, L. *et al.* High performance piezoelectric devices based on aligned arrays of nanofibers of poly(vinylidenefluoride-co-trifluoroethylene). *Nat. Commun.* **4**, 1633 (2013).

172. Chang, C., Tran, V. H., Wang, J., Fuh, Y. K. & Lin, L. Direct-write piezoelectric polymeric nanogenerator with high energy conversion efficiency. *Nano Lett.* (2010). doi:10.1021/nl9040719

173. Pan, C. T. *et al.* Significant piezoelectric and energy harvesting enhancement of poly(vinylidene fluoride)/polypeptide fiber composites prepared through near-field electrospinning. *J. Mater. Chem. A* (2015). doi:10.1039/c5ta00147a

174. Dagdeviren, C. *et al.* Conformal piezoelectric systems for clinical and experimental characterisation of soft tissue biomechanics. *Nat. Mater.* **14**, 728–736 (2015).

175. Dadsetan, M. *et al.* The effects of fixed electrical charge on chondrocyte behavior. *Acta Biomater.* (2011). doi:10.1016/j.actbio.2011.01.012

176. Kitsara, M. *et al.* Permanently hydrophilic, piezoelectric PVDF nanofibrous scaffolds promoting unaided electromechanical stimulation on osteoblasts. *Nanoscale* (2019). doi:10.1039/c8nr10384d

177. Klee, D. *et al.* Surface modification of poly(vinylidenefluoride) to improve the osteoblast adhesion. *Biomaterials* **24**, 3663–3670 (2003).

178. Defteralı, Ç. *et al.* In Vitro Evaluation of Biocompatibility of Uncoated Thermally

Reduced Graphene and Carbon Nanotube-Loaded PVDF Membranes with Adult Neural Stem Cell-Derived Neurons and Glia. *Front. Bioeng. Biotechnol.* (2016). doi:10.3389/fbioe.2016.00094

179. Lee, Y.-S., Collins, G. & Livingston Arinzeh, T. Neurite extension of primary neurons on electrospun piezoelectric scaffolds. *Acta Biomater.* **7**, 3877–3886 (2011).

180. Ribeiro, C. *et al.* Dynamic piezoelectric stimulation enhances osteogenic differentiation of human adipose stem cells. *J. Biomed. Mater. Res. Part A* n/a-n/a (2014). doi:10.1002/jbm.a.35368

181. Parssinen, J. *et al.* Enhancement of adhesion and promotion of osteogenic differentiation of human adipose stem cells by poled electroactive poly(vinylidene fluoride). *J. Biomed. Mater. Res. - Part A* (2015). doi:10.1002/jbm.a.35234

182. Pereira, J. D. A. S. *et al.* Biomaterials from blends of fluoropolymers and corn starch - Implant and structural aspects. *Mater. Sci. Eng. C* (2014). doi:10.1016/j.msec.2013.12.008

183. Ribeiro, C. *et al.* Electroactive poly(vinylidene fluoride)-based structures for advanced applications. *Nat. Protoc.* **13**, 681–704 (2018).

184. Genchi, G. G. *et al.* P(VDF-TrFE)/BaTiO3 Nanoparticle Composite Films Mediate Piezoelectric Stimulation and Promote Differentiation of SH-SY5Y Neuroblastoma Cells. *Adv. Healthc. Mater.* **5**, 1808–20 (2016).

185. Genchi, G. G. *et al.* Ultrasound-activated piezoelectric P(VDF-TrFE)/boron nitride nanotube composite films promote differentiation of human SaOS-2 osteoblast-like cells. *Nanomedicine* **14**, 2421–2432 (2018).

186. Fang, F., Shan, S. C. & Yang, W. Magnetoelectric coupling of Terfenol-D/P(VDF-TrFe)/Terfenol-D laminates mediated by crystallite size of electroactive polymer. *Acta Mech.* **224**, 1169–1174 (2013).

187. Brito-Pereira, R., Ribeiro, C., Lanceros-Mendez, S. & Martins, P. Magnetoelectric

response on Terfenol-D/ P(VDF-TrFE) two-phase composites. *Compos. Part B Eng.* **120**, 97–102 (2017).

188. Cha, S. *et al.* Porous PVDF as effective sonic wave driven nanogenerators. *Nano Lett.* (2011). doi:10.1021/nl202208n

189. Cho, K. Y. *et al.* Enhanced Electrical Properties of PVDF-TrFE Nanocomposite for Actuator Application. *Key Eng. Mater.* (2014). doi:10.4028/www.scientific.net/KEM.605.335

190. Guo, W. *et al.* Self-Powered Electrical Stimulation for Enhancing Neural Differentiation of Mesenchymal Stem Cells on Graphene-Poly(3,4-ethylenedioxythiophene) Hybrid Microfibers. *ACS Nano* (2016). doi:10.1021/acsnano.6b00200

191. Zheng, Q. *et al.* Biodegradable triboelectric nanogenerator as a life-time designed implantable power source. *Sci. Adv.* **2**, e1501478 (2016).

192. Nuccitelli, R. A Role for Endogenous Electric Fields in Wound Healing. *Current Topics in Developmental Biology* (2003). doi:10.1016/S0070-2153(03)58001-2

193. Ladoux, B. & Mège, R.-M. Mechanobiology of collective cell behaviours. *Nat. Rev. Mol. Cell Biol.* **18**, 743–757 (2017).

194. Iskratsch, T., Wolfenson, H. & Sheetz, M. P. Appreciating force and shape — the rise of mechanotransduction in cell biology. *Nat. Rev. Mol. Cell Biol.* **15**, 825–833 (2014).

195. Xia, S. & Kanchanawong, P. Nanoscale mechanobiology of cell adhesions. *Semin. Cell Dev. Biol.* **71**, 53–67 (2017).

196. Turner, C. H. *et al.* Mechanobiology of the skeleton. *Sci. Signal.* **2**, pt3 (2009).

197. Li, Q. *et al.* Structural mechanism of voltage-dependent gating in an isolated voltage-sensing domain. *Nat. Struct. Mol. Biol.* (2014). doi:10.1038/nsmb.2768

198. Wang, J., Tian, L., Chen, N., Ramakrishna, S. & Mo, X. The cellular response of nerve cells on poly-l-lysine coated PLGA-MWCNTs aligned nanofibers under electrical stimulation. *Mater. Sci. Eng. C. Mater. Biol. Appl.* **91**, 715–726 (2018).

199. Mario Cheong, G. L. *et al.* Conductive hydrogels with tailored bioactivity for implantable electrode coatings. *Acta Biomater.* **10**, 1216–26 (2014).

200. Cui, H. *et al.* In vitro studies on regulation of osteogenic activities by electrical stimulus on biodegradable electroactive polyelectrolyte multilayers. *Biomacromolecules* **15**, 3146–57 (2014).

201. Gilmore, K. J. *et al.* Skeletal muscle cell proliferation and differentiation on polypyrrole substrates doped with extracellular matrix components. *Biomaterials* **30**, 5292–304 (2009).

202. Chen, Q.-Q. *et al.* Electrical field stimulation induces cardiac fibroblast proliferation through the calcineurin-NFAT pathway. *Can. J. Physiol. Pharmacol.* **90**, 1611–22 (2012).

203. Seo, G. Y. *et al.* A Novel Synthetic Material, BMM, Accelerates Wound Repair by Stimulating Re-Epithelialization and Fibroblast Activation. *Int. J. Mol. Sci.* **19**, 1164 (2018).

204. Head, B. P., Patel, H. H. & Insel, P. A. Interaction of membrane/lipid rafts with the cytoskeleton: impact on signaling and function: membrane/lipid rafts, mediators of cytoskeletal arrangement and cell signaling. *Biochim. Biophys. Acta* **1838**, 532–45 (2014).

205. Yang, G. *et al.* Regulation of adipose-tissue-derived stromal cell orientation and motility in 2D- and 3D-cultures by direct-current electrical field. *Dev. Growth Differ.* **59**, 70–82 (2017).

206. Greco, F. *et al.* Microwrinkled conducting polymer interface for anisotropic multicellular alignment. *ACS Appl. Mater. Interfaces* **5**, 573–84 (2013).

207. Serena, E. *et al.* Electrical stimulation of human embryonic stem cells: Cardiac differentiation and the generation of reactive oxygen species. *Exp. Cell Res.* **315**, 3611–3619 (2009).

208. Das, S. R. *et al.* Electrical Differentiation of Mesenchymal Stem Cells into Schwann-Cell-Like Phenotypes Using Inkjet-Printed Graphene Circuits. *Adv. Healthc. Mater.* **6**, 1601087 (2017).

209. Wu, Z. *et al.* Mechanosensory hair cells express two molecularly distinct mechanotransduction channels. *Nat. Neurosci.* **20**, 24–33 (2017).

210. Cox, C. D., Wann, K. T. & Martinac, B. Selectivity mechanisms in MscS-like channels. *Channels* **8**, 5–12 (2014).

211. Lacroix, J. J., Botello-Smith, W. M. & Luo, Y. Probing the gating mechanism of the mechanosensitive channel Piezo1 with the small molecule Yoda1. *Nat. Commun.* **9**, 2029 (2018).

212. Zilly, F. E. *et al.* Ca 2+ induces clustering of membrane proteins in the plasma membrane via electrostatic interactions. *EMBO J.* (2011). doi:10.1038/emboj.2011.53

213. Yang, W. P., Onuma, E. K. & Hui, S. W. Response of C3H/10T1/2 fibroblasts to an external steady electric field stimulation. Reorientation, shape change, ConA receptor and intramembranous particle distribution and cytoskeleton reorganisation. *Exp. Cell Res.* **155**, 92–104 (1984).

214. Vacek, T. P. *et al.* Electrical stimulation of cardiomyocytes activates mitochondrial matrix metalloproteinase causing electrical remodeling. *Biochem. Biophys. Res. Commun.* **404**, 762–6 (2011).

215. Titushkin, I. & Cho, M. Regulation of cell cytoskeleton and membrane mechanics by electric field: role of linker proteins. *Biophys. J.* **96**, 717–28 (2009).

216. Liu, L. *et al.* Mechanoresponsive stem cells to target cancer metastases through

biophysical cues. *Sci. Transl. Med.* (2017). doi:10.1126/scitranslmed.aan2966

217. Isaksson, H., Wilson, W., van Donkelaar, C. C., Huiskes, R. & Ito, K. Comparison of biophysical stimuli for mechano-regulation of tissue differentiation during fracture healing. *J. Biomech.* (2006). doi:10.1016/j.jbiomech.2005.01.037

218. Pruitt, B. L., Dunn, A. R., Weis, W. I. & Nelson, W. J. Mechano-Transduction: From Molecules to Tissues. *PLoS Biol.* (2014). doi:10.1371/journal.pbio.1001996

219. Sauer, H. *et al.* DC electrical field-induced c-fos expression and growth stimulation in multicellular prostate cancer spheroids. *Br. J. Cancer* **75**, 1481–8 (1997).

220. Ruffini, G. *et al.* Transcranial current brain stimulation (tCS): models and technologies. *IEEE Trans. Neural Syst. Rehabil. Eng.* **21**, 333–45 (2013).

221. Zhao, H., Steiger, A., Nohner, M. & Ye, H. Specific Intensity Direct Current (DC) Electric Field Improves Neural Stem Cell Migration and Enhances Differentiation towards βIII-Tubulin+ Neurons. *PLoS One* **10**, e0129625 (2015).

222. Wartenberg, M., Hescheler, J. & Sauer, H. Electrical fields enhance growth of cancer spheroids by reactive oxygen species and intracellular Ca2+. *Am. J. Physiol.* **272**, R1677-83 (1997).

223. Yamada, M. *et al.* Electrical Stimulation Modulates Fate Determination of Differentiating Embryonic Stem Cells. *Stem Cells* (2006). doi:10.1634/stemcells.2006-0011

224. Feng, J. F. *et al.* Electrical Guidance of Human Stem Cells in the Rat Brain. *Stem Cell Reports* (2017). doi:10.1016/j.stemcr.2017.05.035

225. Patel, Y. A. & Butera, R. J. Differential fiber-specific block of nerve conduction in mammalian peripheral nerves using kilohertz electrical stimulation. *J. Neurophysiol.* (2015). doi:10.1152/jn.00529.2014

226. Ackermann, D. M., Foldes, E. L., Bhadra, N. & Kilgore, K. L. Nerve conduction

block using combined thermoelectric cooling and high frequency electrical stimulation. *J. Neurosci. Methods* (2010). doi:10.1016/j.jneumeth.2010.07.043

227. Kadow-Romacker, A., Hoffmann, J. E., Duda, G., Wildemann, B. & Schmidmaier, G. Effect of mechanical stimulation on osteoblast- and osteoclast-like cells in vitro. *Cells Tissues Organs* (2009). doi:10.1159/000178022

228. Yao, R. & Wong, J. Y. The Effects of Mechanical Stimulation on Controlling and Maintaining Marrow Stromal Cell Differentiation Into Vascular Smooth Muscle Cells. *J. Biomech. Eng.* (2015). doi:10.1115/1.4029255

229. Zhang, C. *et al.* Effects of mechanical vibration on proliferation and osteogenic differentiation of human periodontal ligament stem cells. *Arch. Oral Biol.* (2012). doi:10.1016/j.archoralbio.2012.04.010

230. Tsimbouri, P. M. *et al.* Publisher Correction: Stimulation of 3D osteogenesis by mesenchymal stem cells using a nanovibrational bioreactor. *Nat. Biomed. Eng.* **1**, 1004–1004 (2017).

231. Karode, N., Fitzhenry, L., Matthews, S., Walsh, P. & Coffey, A. Enhancement of the Mechanical Properties of PEBAX Graphene Nanocomposite Using Supercritical Fluid Assisted Extrusion Polymer Processing Technique. *Mater. Sci. Forum* (2017). doi:10.4028/www.scientific.net/MSF.883.75

232. Avrami, M. Kinetics of phase change. I: General theory. *J. Chem. Phys.* (1939). doi:10.1063/1.1750380

233. Avrami, M. Kinetics of phase change. II Transformation-time relations for random distribution of nuclei. *J. Chem. Phys.* (1940). doi:10.1063/1.1750631

234. Avrami, M. Kinetics of Phase Change. *J. Chem. Phys.* (1939). doi:10.1590/S1516-14392000000300002

235. Avrami, M. Granulation, phase change, and microstructure kinetics of phase change. III. *J. Chem. Phys.* (1941). doi:10.1063/1.1750872

236. Jeziorny, A. Parameters characterizing the kinetics of the non-isothermal crystallization of poly(ethylene terephthalate) determined by d.s.c. *Polymer (Guildf).* (1978). doi:10.1016/0032-3861(78)90060-5

237. Ozawa, T. Kinetics of non-isothermal crystallization. *Polymer (Guildf).* (1971). doi:10.1016/0032-3861(71)90041-3

238. Liu, F. & Yang, G. Effects of anisotropic growth on the deviations from Johnson-Mehl-Avrami kinetics. *Acta Mater.* (2007). doi:10.1016/j.actamat.2006.10.022

239. Lanceros-Méndez, S., Mano, J. F., Costa, A. M. & Schmidt, V. H. FTIR and DSC studies of mechanically deformed β-PVDF films. *J. Macromol. Sci. - Phys.* (2001). doi:10.1081/MB-100106174

240. Fialka, J. & Benes, P. Comparison of Methods for the Measurement of Piezoelectric Coefficients. *IEEE Trans. Instrum. Meas.* **62**, 1047–1057 (2013).

241. Binning, G., Rohrer, H., Gerber, C. & Weibel, E. Surface studies by scanning tunneling microscopy. *Phys. Rev. Lett.* (1982). doi:10.1103/PhysRevLett.49.57

242. Huang, H., Gu, L. & Ozaki, Y. Non-isothermal crystallization and thermal transitions of a biodegradable, partially hydrolyzed poly(vinyl alcohol). *Polymer (Guildf).* (2006). doi:10.1016/j.polymer.2006.03.089

243. Liu, Y., Wang, L., He, Y., Fan, Z. & Li, S. Non-isothermal crystallization kinetics of poly(L-lactide). *Polym. Int.* (2010). doi:10.1002/pi.2894

244. Furukawa, T. Ferroelectric properties of vinylidene fluoride copolymers. *Phase Transitions* (1989). doi:10.1080/01411598908206863

245. Vinogradov, A. & Holloway, F. Electro-mechanical properties of the piezoelectric polymer PVDF. *Ferroelectrics* (1999). doi:10.1080/00150199908230298

246. Martins, P. *et al.* Role of nanoparticle surface charge on the nucleation of the electroactive β-poly(vinylidene fluoride) nanocomposites for sensor and actuator

applications. *J. Phys. Chem. C* (2012). doi:10.1021/jp3038768

247. Wang, Y. J. & Kim, D. Crystallinity, morphology, mechanical properties and conductivity study of in situ formed PVdF/LiClO4/TiO2nanocomposite polymer electrolytes. *Electrochim. Acta* (2007). doi:10.1016/j.electacta.2006.09.070

248. Steinhart, M., Senz, S., Wehrspohn, R. B., Gösele, U. & Wendorff, J. H. Curvature-directed crystallization of poly(vinylidene difluoride) in nanotube walls. *Macromolecules* (2003). doi:10.1021/ma0260039

249. Cao, Y. *et al.* Bridging tendon defects using autologous tenocyte engineered tendon in a hen model. *Plast. Reconstr. Surg.* (2002). doi:10.1097/00006534-200210000-00011

250. Chen, J. M., Willers, C., Xu, J., Wang, A. & Zheng, M.-H. Autologous Tenocyte Therapy Using Porcine-Derived Bioscaffolds for Massive Rotator Cuff Defect in Rabbits. *Tissue Eng.* (2007). doi:10.1089/ten.2006.0266

251. Spanoudes, K., Gaspar, D., Pandit, A. & Zeugolis, D. I. The biophysical, biochemical, and biological toolbox for tenogenic phenotype maintenance in vitro. *Trends Biotechnol.* **32**, 474–482 (2014).

252. Stoll, C. *et al.* Extracellular matrix expression of human tenocytes in three-dimensional air-liquid and PLGA cultures compared with tendon tissue: Implications for tendon tissue engineering. *J. Orthop. Res.* (2010). doi:10.1002/jor.21109

253. Juncosa-Melvin, N., Matlin, K. S., Holdcraft, R. W., Nirmalanandhan, V. S. & Butler, D. L. Mechanical Stimulation Increases Collagen Type I and Collagen Type III Gene Expression of Stem Cell–Collagen Sponge Constructs for Patellar Tendon Repair. *Tissue Eng.* (2007). doi:10.1089/ten.2006.0339

254. Jiang, C., Shao, L., Wang, Q. & Dong, Y. Repetitive mechanical stretching modulates transforming growth factor-β induced collagen synthesis and apoptosis in human patellar tendon fibroblasts. *Biochem. Cell Biol.* (2012). doi:10.1139/o2012-024

255. Kilian, K. A., Bugarija, B., Lahn, B. T. & Mrksich, M. Geometric cues for directing the differentiation of mesenchymal stem cells. *Proc. Natl. Acad. Sci. U. S. A.* **107**, 4872–7 (2010).

256. Nikukar, H. *et al.* Osteogenesis of mesenchymal stem cells by nanoscale mechanotransduction. *ACS Nano* (2013). doi:10.1021/nn400202j

257. Wang, J. H.-C. *et al.* Cyclic mechanical stretching of human tendon fibroblasts increases the production of prostaglandin E2 and levels of cyclooxygenase expression: a novel in vitro model study. *Connect. Tissue Res.* **44**, 128–33 (2003).

258. Zhang, J. & Wang, J. H. C. Production of PGE2 increases in tendons subjected to repetitive mechanical loading and induces differentiation of tendon stem cells into non-tenocytes. *J. Orthop. Res.* (2010). doi:10.1002/jor.20962

259. Love, M. R., Palee, S., Chattipakorn, S. C. & Chattipakorn, N. Effects of electrical stimulation on cell proliferation and apoptosis. *J. Cell. Physiol.* **233**, 1860–1876 (2018).

260. Balint, R., Cassidy, N. J. & Cartmell, S. H. Electrical Stimulation: A Novel Tool for Tissue Engineering. *Tissue Eng. Part B Rev.* **19**, 48–57 (2013).

261. Shao, S. *et al.* Osteoblast function on electrically conductive electrospun PLA/MWCNTs nanofibers. *Biomaterials* (2011). doi:10.1016/j.biomaterials.2011.01.051

262. Ning, C., Zhou, Z., Tan, G., Zhu, Y. & Mao, C. Electroactive polymers for tissue regeneration: Developments and perspectives. *Progress in Polymer Science* (2018). doi:10.1016/j.progpolymsci.2018.01.001

263. Zhang, J., Li, M., Kang, E. T. & Neoh, K. G. Electrical stimulation of adipose-derived mesenchymal stem cells in conductive scaffolds and the roles of voltage-gated ion channels. *Acta Biomater.* **32**, 46–56 (2016).

264. Chiu, C. H., Lei, K. F. & Yeh, W. L. Development of a co-culture device for the

study of human tenocytes in response to the combined stimulation of electric field and platelet rich plasma (PRP). *Biomed. Microdevices* (2017). doi:10.1007/s10544-017-0214-z

265. Basas, Á. *et al.* Effects of a strength protocol combined with electrical stimulation on patellar tendinopathy: 42 months retrospective follow-up on 6 high-level jumping athletes. *Phys. Ther. Sport* **34**, 105–112 (2018).

266. Yanase, K. *et al.* Electrical Stimulation to the Infraspinatus on Hypertrophy and Strength of the Shoulder. *Int. J. Sports Med.* **39**, 828–834 (2018).

267. Yan, Z. *et al.* [Effects of electrical stimulation on the differentiation of mesenchymal stem cells into cardiomyocyte-like cells]. *Sheng Wu Yi Xue Gong Cheng Xue Za Zhi* **30**, 556–61 (2013).

268. Pardo-Pastor, C. *et al.* Piezo2 channel regulates RhoA and actin cytoskeleton to promote cell mechanobiological responses. *Proc. Natl. Acad. Sci. U. S. A.* **115**, 1925–1930 (2018).

269. Islam, A., Mbimba, T., Younesi, M. & Akkus, O. Effects of substrate stiffness on the tenoinduction of human mesenchymal stem cells. *Acta Biomater.* **58**, 244–253 (2017).

270. Barsby, T., Bavin, E. P. & Guest, D. J. Three-Dimensional Culture and Transforming Growth Factor Beta3 Synergistically Promote Tenogenic Differentiation of Equine Embryo-Derived Stem Cells. *Tissue Eng. Part A* (2014). doi:10.1016/j.foreco.2016.02.006

271. Qi, J. *et al.* IL-1β decreases the elastic modulus of human tenocytes. *J. Appl. Physiol.* (2006). doi:10.1152/japplphysiol.01128.2005

272. Tsuzaki, M., Bynum, D., Almekinders, L., Faber, J. & Banes, A. J. Mechanical loading stimulates ecto-ATPase activity in human tendon cells. *J. Cell. Biochem.* (2005). doi:10.1002/jcb.20491

273. Archambault, J., Tsuzaki, M., Herzog, W. & Banes, A. J. Stretch and interleukin-1β induce matrix metalloproteinases in rabbit tendon cells in vitro. *J. Orthop. Res.* (2002). doi:10.1016/S0736-0266(01)00075-4

274. Tsuzaki, M. *et al.* IL-1β induces COX2, MMP-1, -3 and -13, ADAMTS-4, IL-1β and IL-6 in human tendon cells. *J. Orthop. Res.* (2003). doi:10.1016/S0736-0266(02)00141-9

275. Jelinsky, S. A., Archambault, J., Li, L. & Seeherman, H. Tendon-selective genes identified from rat and human musculoskeletal tissues. *J. Orthop. Res.* **28**, n/a-n/a (2009).

276. Delgado Caceres, M., Pfeifer, C. G. & Docheva, D. Understanding Tendons: Lessons from Transgenic Mouse Models. *Stem Cells Dev.* **27**, 1161–1174 (2018).

277. Inaba, S., Akaishi, K., Mori, T. & Hane, K. Analysis of the resonance characteristics of a cantilever vibrated photothermally in a liquid. *J. Appl. Phys.* (1993). doi:10.1063/1.353060

278. Kwak, M. K. & Kim, K. C. Axisymmetric vibration of circular plates in contact with fluid. *J. Sound Vib.* (1991). doi:10.1016/0022-460X(91)90696-H

279. Nikukar, H. *et al.* Osteogenesis of Mesenchymal Stem Cells by Nanoscale Mechanotransduction. *ACS Nano* **7**, 2758–2767 (2013).

280. Wang, T. *et al.* Programmable mechanical stimulation influences tendon homeostasis in a bioreactor system. *Biotechnol. Bioeng.* (2013). doi:10.1002/bit.24809

281. Zhang, J. & Wang, J. H. C. Mechanobiological response of tendon stem cells: Implications of tendon homeostasis and pathogenesis of tendinopathy. *J. Orthop. Res.* (2010). doi:10.1002/jor.21046

282. Aspenberg, P. Stimulation of tendon repair: Mechanical loading, GDFs and platelets. a mini-review. *International Orthopaedics* (2007). doi:10.1007/s00264-007-0398-6

283. Busch, T., Köttgen, M. & Hofherr, A. TRPP2 ion channels: Critical regulators of organ morphogenesis in health and disease. *Cell Calcium* (2017). doi:10.1016/j.ceca.2017.05.005

284. Chachisvilis, M., Zhang, Y.-L. & Frangos, J. A. G protein-coupled receptors sense fluid shear stress in endothelial cells. *Proc. Natl. Acad. Sci.* (2006). doi:10.1073/pnas.0607224103

285. Wu, J., Lewis, A. H. & Grandl, J. Touch, Tension, and Transduction – The Function and Regulation of Piezo Ion Channels. *Trends Biochem. Sci.* **42**, 57–71 (2017).

286. Popov, C. *et al.* Mechanical stimulation of human tendon stem/progenitor cells results in upregulation of matrix proteins, integrins and MMPs, and activation of p38 and ERK1/2 kinases. *BMC Mol. Biol.* **16**, 1–11 (2015).

287. Maksimovic, S. *et al.* Epidermal Merkel cells are mechanosensory cells that tune mammalian touch receptors. *Nature* (2014). doi:10.1038/nature13250

288. Zhang, W., Yan, Z., Jan, L. Y. & Jan, Y. N. Sound response mediated by the TRP channels NOMPC, NANCHUNG, and INACTIVE in chordotonal organs of Drosophila larvae. *Proc. Natl. Acad. Sci.* (2013). doi:10.1073/pnas.1312477110

289. Kim, J. *et al.* A TRPV family ion channel required for hearing in Drosophila. *Nature* (2003). doi:10.1038/nature01733

290. Rayleigh, J. W. S. *The Theory of Sound Vol. II. Macmillan* (1896). doi:10.1017/CBO9781107415324.004

291. Sroka, J., Zimolag, E., Lasota, S. & Korohoda, W. Electrotaxis : Cell Directional Movement in Electric Fields. **1749**, 325–340

292. Banks, T. A., Luckman, P. S. B., Frith, J. E. & Cooper-White, J. J. Effects of electric fields on human mesenchymal stem cell behaviour and morphology using a novel multichannel device. *Integr. Biol. (Camb).* **7**, 693–712 (2015).

293. Guerin, S. *et al.* Control of piezoelectricity in amino acids by supramolecular packing. *Nat. Mater.* (2018). doi:10.1038/NMAT5045

294. Boriek, A. M. & Kumar, A. Regulation of Intracellular Signal Transduction Pathways by Mechanosensitive Ion Channels. in *Mechanosensitive Ion Channels* (2007). doi:10.1007/978-1-4020-6426-5_14

295. Coste, B. *et al.* Piezo1 and Piezo2 are essential components of distinct mechanically activated cation channels. *Science (80-.).* (2010). doi:10.1126/science.1193270

296. Goodier, H. C. J. *et al.* Comparison of transforming growth factor beta expression in healthy and diseased human tendon. *Arthritis Res. Ther.* (2016). doi:10.1186/s13075-016-0947-8

297. Zhuang, H. *et al.* Electrical stimulation induces the level of TGF-β1 mRNA in osteoblastic cells by a mechanism involving calcium/calmodulin pathway. *Biochem. Biophys. Res. Commun.* (1997). doi:10.1006/bbrc.1997.7118

298. Hirata, H., Tatsumi, H., Hayakawa, K. & Sokabe, M. Non-channel mechanosensors working at focal adhesion-stress fiber complex. *Pflügers Arch. - Eur. J. Physiol.* **467**, 141–155 (2015).

299. Prindle, A. *et al.* Ion channels enable electrical communication in bacterial communities. *Nature* (2015). doi:10.1038/nature15709

300. Brohawn, S. G., Campbell, E. B. & MacKinnon, R. Physical mechanism for gating and mechanosensitivity of the human TRAAK K+ channel. *Nature* (2014). doi:10.1038/nature14013

301. Lin, Y. Lo, Moolenaar, H., van Weeren, P. R. & van de Lest, C. H. A. Effect of microcurrent electrical tissue stimulation on equine tenocytes in culture. *Am. J. Vet. Res.* (2006). doi:10.2460/ajvr.67.2.271

302. STROYAN, J. J. PROCESSING AND CHARACTERISATION OF PVDF, PVDF-TrFE, AND PVDF-TrFE-PZT COMPOSITES. *J. Chem. Inf. Model.* (2013).

doi:10.1017/CBO9781107415324.004

303. Dodds, J. S., Meyers, F. N. & Loh, K. J. Piezoelectric characterisation of PVDF-TrFE thin films enhanced with ZnO nanoparticles. *IEEE Sens. J.* (2012). doi:10.1109/JSEN.2011.2182043

304. Chen, H. J. *et al.* Investigation of PVDF-TrFE composite with nanofillers for sensitivity improvement. *Sensors Actuators, A Phys.* (2016). doi:10.1016/j.sna.2016.04.056

305. Simoes, R. D., Rodriguez-Perez, M. A., De Saja, J. A. & Constantino, C. J. L. Thermomechanical characterisation of PVDF and P(VDF-TrFE) blends containing corn starch and natural rubber. *J. Therm. Anal. Calorim.* (2010). doi:10.1007/s10973-009-0285-z

306. Seminara, L., Capurro, M., Cirillo, P., Cannata, G. & Valle, M. Electromechanical characterisation of piezoelectric PVDF polymer films for tactile sensors in robotics applications. *Sensors Actuators, A Phys.* (2011). doi:10.1016/j.sna.2011.05.004

307. Mohamad Hafiz, M. W. *et al.* Effect of Annealing Temperature on the Crystallinity, Morphology and Ferroelectric of Polyvinylidenefluoride-Trifluoroethylene (PVDF-TrFE) Thin Film. *Adv. Mater. Res.* (2013). doi:10.4028/www.scientific.net/AMR.812.60

308. Lu, X., Qu, H. & Skorobogatiy, M. Piezoelectric microstructured fibers via drawing of multimaterial preforms. *Sci. Rep.* (2017). doi:10.1038/s41598-017-01738-9

309. Wong, S. C., Baji, A. & Leng, S. Effect of fiber diameter on tensile properties of electrospun poly(ε-caprolactone). *Polymer (Guildf).* (2008). doi:10.1016/j.polymer.2008.08.022

310. Chen, F. *et al.* Mechanical characterisation of single high-strength electrospun polyimide nanofibres. *J. Phys. D. Appl. Phys.* (2008). doi:10.1088/0022-3727/41/2/025308

311. Baji, A., Mai, Y. W. & Wong, S. C. Effect of fiber size on structural and tensile properties of electrospun polyvinylidene fluoride fibers. *Polym. Eng. Sci.* (2015). doi:10.1002/pen.24020

312. Ico, G. *et al.* Size-dependent piezoelectric and mechanical properties of electrospun P(VDF-TrFE) nanofibers for enhanced energy harvesting. *J. Mater. Chem. A* (2016). doi:10.1039/c5ta10423h

313. O'Hagan, D. Understanding organofluorine chemistry. An introduction to the C-F bond. *Chem. Soc. Rev.* (2008). doi:10.1039/b711844a

314. Wang, J. H.-C. Mechanobiology of tendon. *J. Biomech.* (2006). doi:10.1016/j.jbiomech.2005.05.011

315. Lin, T. W., Cardenas, L. & Soslowsky, L. J. Biomechanics of tendon injury and repair. *J. Biomech.* (2004). doi:10.1016/j.jbiomech.2003.11.005

316. James, R., Kesturu, G., Balian, G. & Chhabra, A. B. Tendon: Biology, Biomechanics, Repair, Growth Factors, and Evolving Treatment Options. *Journal of Hand Surgery* (2008). doi:10.1016/j.jhsa.2007.09.007

317. Wang, J. H. C., Guo, Q. & Li, B. Tendon Biomechanics and Mechanobiology—A Minireview of Basic Concepts and Recent Advancements. *J. Hand Ther.* **25**, 133–141 (2012).

318. Rees, J. D., Wilson, A. M. & Wolman, R. L. Current concepts in the management of tendon disorders. *Rheumatology* (2006). doi:10.1093/rheumatology/kel046

319. Yang, G., Crawford, R. C. & Wang, J. H. C. Proliferation and collagen production of human patellar tendon fibroblasts in response to cyclic uniaxial stretching in serum-free conditions. *J. Biomech.* (2004). doi:10.1016/j.jbiomech.2004.01.005

320. Skutek, M., Van Griensven, M., Zeichen, J., Brauer, N. & Bosch, U. Cyclic mechanical stretching modulates secretion pattern of growth factors in human tendon fibroblasts. *Eur. J. Appl. Physiol.* (2001). doi:10.1007/s004210100502

321. Zeichen, J., Van Griensven, M. & Bosch, U. The proliferative response of isolated human tendon fibroblasts to cyclic biaxial mechanical strain. *Am. J. Sports Med.* (2000). doi:10.1177/03635465000280061901

322. Jagodzinski, M. *et al.* Influence of cyclic mechanical strain and heat of human tendon fibroblasts on HSP-72. *Eur. J. Appl. Physiol.* (2006). doi:10.1007/s00421-005-0071-y

323. Skutek, M., Van Griensven, M., Zeichen, J., Brauer, N. & Bosch, U. Cyclic mechanical stretching of human patellar tendon fibroblasts: Activation of JNK and modulation of apoptosis. *Knee Surgery, Sport. Traumatol. Arthrosc.* (2003). doi:10.1007/s00167-002-0322-y

324. Youngstrom, D. W., Rajpar, I., Kaplan, D. L. & Barrett, J. G. A bioreactor system for in vitro tendon differentiation and tendon tissue engineering. *J. Orthop. Res.* **33**, 911–918 (2015).

325. Bayer, M. L. *et al.* Release of tensile strain on engineered human tendon tissue disturbs cell adhesions, changes matrix architecture, and induces an inflammatory phenotype. *PLoS One* (2014). doi:10.1371/journal.pone.0086078

326. Moffat, K. L. *et al.* Novel Nanofiber-Based Scaffold for Rotator Cuff Repair and Augmentation. *Tissue Eng. Part A* (2008). doi:10.1089/ten.tea.2008.0014

327. Dabiri, B. E., Lee, H. & Parker, K. K. A potential role for integrin signaling in mechanoelectrical feedback. *Progress in Biophysics and Molecular Biology* (2012). doi:10.1016/j.pbiomolbio.2012.07.002

328. Butler, D. L. *et al.* The use of mesenchymal stem cells in collagen-based scaffolds for tissue-engineered repair of tendons. *Nat. Protoc.* (2010). doi:10.1038/nprot.2010.14

329. Schwartz, A. & Thomopoulos, S. The role of mechanobiology in the attachment of tendon to bone. in *Structural Interfaces and Attachments in Biology* (2013). doi:10.1007/978-1-4614-3317-0_11

330. Durant, T. J. S. *et al.* Mesenchymal stem cell response to growth factor treatment and low oxygen tension in 3-dimensional construct environment. *Muscle Ligaments Tendons J.* (2019). doi:10.32098/mltj.01.2014.09

331. Bagnaninchi, P. O. *et al.* Chitosan Microchannel Scaffolds for Tendon Tissue Engineering Characterised Using Optical Coherence Tomography. *Tissue Eng.* (2007). doi:10.1089/ten.2006.0168

332. Bagnaninchi, P. & Yang, Y. Tissue engineering for tendon repair. *Br. J. Sport. ...* (2007). doi:10.1136/bjsm.2006.030643

333. Stanton, A. E., Tong, X., Lee, S. & Yang, F. Biochemical Ligand Density Regulates Yes-Associated Protein Translocation in Stem Cells through Cytoskeletal Tension and Integrins. *ACS Appl. Mater. Interfaces* (2019). doi:10.1021/acsami.8b21270

334. Driscoll, T. P., Cosgrove, B. D., Heo, S. J., Shurden, Z. E. & Mauck, R. L. Cytoskeletal to Nuclear Strain Transfer Regulates YAP Signaling in Mesenchymal Stem Cells. *Biophys. J.* (2015). doi:10.1016/j.bpj.2015.05.010

335. Méjat, A. & Misteli, T. LINC complexes in health and disease. *Nucleus* (2010). doi:10.4161/nucl.1.1.10530

336. Crisp, M. *et al.* Coupling of the nucleus and cytoplasm: Role of the LINC complex. *J. Cell Biol.* (2006). doi:10.1083/jcb.200509124

337. Isermann, P. & Lammerding, J. Nuclear mechanics and mechanotransduction in health and disease. *Current Biology* (2013). doi:10.1016/j.cub.2013.11.009

338. Watkins-Castillo, S. & Andersson, G. United States Bone and Joint Initiative: The Burden of Musculoskeletal Diseases in the United States (BMUS). *The Burden of Musculoskeletal diseases int he United States* (2014).

339. Biewener, A. A. Muscle-tendon stresses and elastic energy storage during locomotion in the horse. *Comp. Biochem. Physiol. - B Biochem. Mol. Biol.* (1998). doi:10.1016/S0305-0491(98)00024-8

340. Yang, G., Rothrauff, B. B. & Tuan, R. S. Tendon and ligament regeneration and repair: Clinical relevance and developmental paradigm. *Birth Defects Research Part C - Embryo Today: Reviews* (2013). doi:10.1002/bdrc.21041

341. Foolen, J., Wunderli, S. L., Loerakker, S. & Snedeker, J. G. Tissue alignment enhances remodeling potential of tendon-derived cells - Lessons from a novel microtissue model of tendon scarring. *Matrix Biol.* (2018). doi:10.1016/j.matbio.2017.06.002

342. Kimura, A., Aoki, M., Fukushima, S., Ishii, S. & Yamakoshi, K. Reconstruction of a defect of the rotator cuff with polytetrafluoroethylene felt graft. Recovery of tensile strength and histocompatibility in an animal model. *J. Bone Joint Surg. Br.* (2003).

343. Rowe, R. W. D. The structure of rat tail tendon. *Connect. Tissue Res.* (1985). doi:10.3109/03008208509089839

344. Chan, H. K. F., Fung, D. T. C. & Ng, G. Y. F. Effects of Low-Voltage Microamperage Stimulation on Tendon Healing in Rats. *J. Orthop. Sport. Phys. Ther.* **37**, 399–403 (2007).

345. West, C. R. & Bowden, A. E. Using tendon inherent electric properties to consistently track induced mechanical strain. *Ann. Biomed. Eng.* (2012). doi:10.1007/s10439-011-0504-1

346. Liu, Z. & Kim, J. Effect of Strain Rate and Loading on the Piezoelectric Properties of Tendon. **8**, 3193 (2006).

347. Subramanian, A., Kanzaki, L. F., Galloway, J. L. & Schilling, T. F. Mechanical force regulates tendon extracellular matrix organisation and tenocyte morphogenesis through TGFbeta signaling. *Elife* **7**, 1–24 (2018).

348. Kannus, P., Józsa, L., Natri, A. & Järvinen, M. Effects of training, immobilization and remobilization on tendons. *Scand. J. Med. Sci. Sports* (2010). doi:10.1111/j.1600-0838.1997.tb00121.x

349. Matsumoto, F., Trudel, G., Uhthoff, H. K. & Backman, D. S. Mechanical effects of immobilization on the Achilles' tendon. *Arch. Phys. Med. Rehabil.* (2003). doi:10.1016/S0003-9993(02)04834-7

350. Kim, B. S. *et al.* The effect of dry needling and treadmill running on inducing pathological changes in rat Achilles tendon. *Connect. Tissue Res.* **8207**, 1–17 (2015).

351. De Castro Pochini, A. *et al.* Overuse of training increases mechanoreceptors in supraspinatus tendon of rats SHR. *J. Orthop. Res.* (2011). doi:10.1002/jor.21320

352. Yuan, T. *et al.* Creating an animal model of tendinopathy by inducing chondrogenic differentiation with kartogenin. *PLoS One* (2016). doi:10.1371/journal.pone.0148557

353. Wada, S. *et al.* Post-operative Tendon Loading with Treadmill Running Delays Tendon-to-Bone Healing: Immunohistochemical Evaluation in a Murine Rotator Cuff Repair Model. *J. Orthop. Res.* (2019). doi:10.1002/jor.24300

354. Zhang, J. & Wang, J. H.-C. The Effects of Mechanical Loading on Tendons - An In Vivo and In Vitro Model Study. *PLoS One* (2013). doi:10.1371/journal.pone.0071740

355. Zhang, J., Pan, T., Liu, Y. & Wang, J. H. C. Mouse treadmill running enhances tendons by expanding the pool of Tendon Stem Cells (TSCs) and TSC-related cellular production of collagen. *J. Orthop. Res.* (2010). doi:10.1002/jor.21123

356. Glazebrook, M. A., Wright, J. R., Langman, M., Stanish, W. D. & Lee, J. M. Histological analysis of Achilles tendons in an overuse rat model. *J. Orthop. Res.* (2008). doi:10.1002/jor.20546

357. Houghton, L., Dawson, B. & Rubenson, J. Achilles tendon mechanical properties after both prolonged continuous running and prolonged intermittent shuttle running in cricket batting. *J. Appl. Biomech.* (2013). doi:10.1123/jab.29.4.453

358. Eliasson, P., Andersson, T. & Aspenberg, P. Achilles tendon healing in rats is improved by intermittent mechanical loading during the inflammatory phase. *J.*

Orthop. Res. (2012). doi:10.1002/jor.21511

359. Xu, S. Y. *et al.* Response of Decorin to different intensity treadmill running. *Mol. Med. Rep.* (2018). doi:10.3892/mmr.2018.8802

360. Xu, S. Y. *et al.* Intensity-dependent effect of treadmill running on rat Achilles tendon. *Exp. Ther. Med.* (2018). doi:10.3892/etm.2018.6084

361. Kuo, C. K. & Tuan, R. S. Mechanoactive Tenogenic Differentiation of Human Mesenchymal Stem Cells. *Tissue Eng. Part A* (2008). doi:10.1089/ten.tea.2006.0415

362. Scott, A. *et al.* Mechanical force modulates scleraxis expression in bioartificial tendons. *J. Musculoskelet. Neuronal Interact.* (2011).

363. Lohberger, B. *et al.* Impact of cyclic mechanical stimulation on the expression of extracellular matrix proteins in human primary rotator cuff fibroblasts. *Knee Surgery, Sport. Traumatol. Arthrosc.* (2016). doi:10.1007/s00167-015-3790-6

364. Sawaguchi, N. *et al.* Effect of cyclic three-dimensional strain on cell proliferation and collagen synthesis of fibroblast-seeded chitosan-hyaluronan hybrid polymer fiber. *J. Orthop. Sci.* (2010). doi:10.1007/s00776-010-1488-7

365. D., D. Running far and fast: An emerging role of tenomodulin. *J. Orthop. Res.* (2017).

366. Zhang, J., Yuan, T. & Wang, J. H.-C. Moderate treadmill running exercise prior to tendon injury enhances wound healing in aging rats. *Oncotarget* (2016). doi:10.18632/oncotarget.7381

367. Cushman, D. & Rho, M. E. Conservative Treatment of Subacute Proximal Hamstring Tendinopathy Using Eccentric Exercises Performed With a Treadmill: A Case Report. *J. Orthop. Sport. Phys. Ther.* (2015). doi:10.2519/jospt.2015.5762

368. Heinemeier, K. M. *et al.* Uphill running improves rat Achilles tendon tissue mechanical properties and alters gene expression without inducing pathological

changes. *J. Appl. Physiol.* (2012). doi:10.1152/japplphysiol.00401.2012

369. Abraham, T., Fong, G. & Scott, A. Second harmonic generation analysis of early Achilles tendinosis in response to in vivo mechanical loading. *BMC Musculoskelet. Disord.* (2011). doi:10.1186/1471-2474-12-26

370. Jafari, L., Vachon, P., Beaudry, F. & Langelier, E. Histopathological, biomechanical, and behavioral pain findings of achilles tendinopathy using an animal model of overuse injury. *Physiol. Rep.* (2015). doi:10.14814/phy2.12265

371. Ng, G. Y. F., Chung, P. Y. M., Wang, J. S. & Cheung, R. T. H. Enforced bipedal downhill running induces Achilles tendinosis in rats. *Connect. Tissue Res.* (2011). doi:10.3109/03008207.2011.562334

372. Mendias, C. L., Gumucio, J. P., Bakhurin, K. I., Lynch, E. B. & Brooks, S. V. Physiological loading of tendons induces scleraxis expression in epitenon fibroblasts. *J. Orthop. Res.* (2012). doi:10.1002/jor.21550

373. Esteves de Lima, J. *et al.* TGFβ and FGF promote tendon progenitor fate and act downstream of muscle contraction to regulate tendon differentiation during chick limb development. *Development* (2016). doi:10.1242/dev.136242

374. Brent, A. E. FGF acts directly on the somitic tendon progenitors through the Ets transcription factors Pea3 and Erm to regulate scleraxis expression. *Development* (2004). doi:10.1242/dev.01275

375. Shukunami, C., Takimoto, A., Oro, M. & Hiraki, Y. Scleraxis positively regulates the expression of tenomodulin, a differentiation marker of tenocytes. *Dev. Biol.* (2006). doi:10.1016/j.ydbio.2006.06.036

376. Hammerman, M., Aspenberg, P. & Eliasson, P. Microtrauma stimulates rat Achilles tendon healing via an early gene expression pattern similar to mechanical loading. *J. Appl. Physiol.* (2013). doi:10.1152/japplphysiol.00741.2013

377. Cheng, N., Hoof, V. A. N. & Hoogmartens, M. J. Generation , Protein Synthesis ,

and Membrane Transport in Rat Skin. *Clin. Orthop. Relat. Researc* (1982).

378. Meng, X. *et al.* PI3K mediated electrotaxis of embryonic and adult neural progenitor cells in the presence of growth factors. *Exp. Neurol.* (2011). doi:10.1016/j.expneurol.2010.11.002

379. Sung, K. M. *et al.* Control of neonatal human dermal fibroblast migration on poly(lactic-co-glycolic acid)-coated surfaces by electrotaxis. *J. Tissue Eng. Regen. Med.* (2015). doi:10.1002/term.1986

380. Li, S. *et al.* Electrical Stimulation Activates Fibroblasts through the Elevation of Intracellular Free Ca 2+ : Potential Mechanism of Pelvic Electrical Stimulation Therapy . *Biomed Res. Int.* (2019). doi:10.1155/2019/7387803

381. Lee, G. S., Kim, M. G. & Kwon, H. J. Electrical stimulation induces direct reprogramming of human dermal fibroblasts into hyaline chondrogenic cells. *Biochem. Biophys. Res. Commun.* (2019). doi:10.1016/j.bbrc.2019.04.027

382. Ni, M. *et al.* Engineered scaffold-free tendon tissue produced by tendon-derived stem cells. *Biomaterials* **34**, 2024–2037 (2013).

383. Xu, S.-Y., Li, S.-F. & Ni, G.-X. Strenuous Treadmill Running Induces a Chondrocyte Phenotype in Rat Achilles Tendons. *Med. Sci. Monit.* (2016). doi:10.12659/msm.897726

384. Carpenter, J. E., Flanagan, C. L., Thomopoulos, S., Yian, E. H. & Soslowsky, L. J. The effects of overuse combined with intrinsic or extrinsic alterations in an animal model of rotator cuff tendinosis. *Am. J. Sports Med.* (1998). doi:10.1177/03635465980260061101

385. Szomor, Z. L., Appleyard, R. C. & Murrell, G. A. C. Overexpression of nitric oxide synthases in tendon overuse. *J. Orthop. Res.* (2006). doi:10.1002/jor.20009

386. Thampatty, B. P. & Wang, J. H. C. Mechanobiology of young and aging tendons: In vivo studies with treadmill running. *J. Orthop. Res.* (2017). doi:10.1002/jor.23761

387. Heinemeier, K. M. *et al.* Effect of unloading followed by reloading on expression of collagen and related growth factors in rat tendon and muscle. *J. Appl. Physiol.* (2009). doi:10.1152/japplphysiol.91092.2008

388. Zhang, J. & Wang, J. H. C. Moderate exercise mitigates the detrimental effects of aging on tendon stem cells. *PLoS One* (2015). doi:10.1371/journal.pone.0130454

389. Dey, D. *et al.* Two tissue-resident progenitor lineages drive distinct phenotypes of heterotopic ossification. *Sci. Transl. Med.* (2016). doi:10.1126/scitranslmed.aaf1090

390. Wood, L. K. & Brooks, S. V. Ten weeks of treadmill running decreases stiffness and increases collagen turnover in tendons of old mice. *J. Orthop. Res.* (2016). doi:10.1002/jor.22824

391. Gimbel, J. A. Long Durations of Immobilization in the Rat Result in Enhanced Mechanical Properties of the Healing Supraspinatus Tendon Insertion Site. *J. Biomech. Eng.* (2007). doi:10.1115/1.2721075

392. Wolfman, N. M. *et al.* Ectopic induction of tendon and ligament in rats by growth and differentiation factors 5, 6, and 7, members of the TGF-β gene family. *J. Clin. Invest.* (1997). doi:10.1172/JCI119537

393. Kishimoto, Y. *et al.* Wnt/β-catenin signaling suppresses expressions of Scx, Mkx, and Tnmd in tendon-derived cells. *PLoS One* (2017). doi:10.1371/journal.pone.0182051

394. Zhou, S., Eid, K. & Glowacki, J. Cooperation between TGF-β and Wnt pathways during chondrocyte and adipocyte differentiation of human marrow stromal cells. *J. Bone Miner. Res.* (2004). doi:10.1359/JBMR.0301239

395. Chen, Y. *et al.* β-Catenin signaling pathway is crucial for bone morphogenetic protein 2 to induce new bone formation. *J. Biol. Chem.* (2007). doi:10.1074/jbc.M602700200

396. Zhang, R. *et al.* Wnt/β-catenin signaling activates bone morphogenetic protein 2

expression in osteoblasts. *Bone* (2013). doi:10.1016/j.bone.2012.09.029

397. Gaur, T. *et al.* Canonical WNT signaling promotes osteogenesis by directly stimulating Runx2 gene expression. *J. Biol. Chem.* (2005). doi:10.1074/jbc.M500608200

398. Kim, J. B. *et al.* Bone regeneration is regulated by Wnt signaling. *J. Bone Miner. Res.* (2007). doi:10.1359/jbmr.070802

399. Minear, S. *et al.* Wnt proteins promote bone regeneration. *Sci. Transl. Med.* (2010). doi:10.1126/scitranslmed.3000231

400. Krishnan, V., Bryant, H. U. & MacDougald, O. A. Regulation of bone mass by Wnt signaling. *Journal of Clinical Investigation* (2006). doi:10.1172/JCI28551

401. Robling, A. G. *et al.* Mechanical stimulation of bone in vivo reduces osteocyte expression of Sost/sclerostin. *J. Biol. Chem.* (2008). doi:10.1074/jbc.M705092200

402. Majidinia, M., Sadeghpour, A. & Yousefi, B. The roles of signaling pathways in bone repair and regeneration. *Journal of cellular physiology* (2018). doi:10.1002/jcp.26042

403. Tu, X. *et al.* Sost downregulation and local Wnt signaling are required for the osteogenic response to mechanical loading. *Bone* (2012). doi:10.1016/j.bone.2011.10.025

404. Brighton, C. T., Wang, W., Seldes, R., Zhang, G. & Pollack, S. R. Signal transduction in electrically stimulated bone cells. *J. Bone Jt. Surg. - Ser. A* (2001). doi:10.2106/00004623-200110000-00009

405. Ashrafi, M., Alonso-Rasgado, T., Baguneid, M. & Bayat, A. The efficacy of electrical stimulation in experimentally induced cutaneous wounds in animals. *Veterinary dermatology* (2016). doi:10.1111/vde.12328

406. Kim, T. H., Cho, H. & Lee, S. M. High-Voltage Pulsed Current Stimulation

Enhances Wound Healing in Diabetic Rats by Restoring the Expression of Collagen, α-Smooth Muscle Actin, and TGF-β1. *Tohoku J. Exp. Med.* (2014). doi:10.1620/tjem.234.1

407.   Wang, Y., Rouabhia, M., Lavertu, D. & Zhang, Z. Pulsed electrical stimulation modulates fibroblasts' behaviour through the Smad signalling pathway. *J. Tissue Eng. Regen. Med.* (2017). doi:10.1002/term.2014

408.   Wang, H., Liu, J., Zeng, J., Zeng, C. & Zhou, Y. Expression of TβR-2, Smad3 and Smad7 in the vaginal anterior wall of postpartum rats with stress urinary incontinence. *Arch. Gynecol. Obstet.* (2015). doi:10.1007/s00404-014-3495-y

409.   Li, Y. *et al.* Effect of integrin β1 in the treatment of stress urinary incontinence by electrical stimulation. *Mol. Med. Rep.* 4727–4734 (2019). doi:10.3892/mmr.2019.10145

410.   Hamadi, A. Regulation of focal adhesion dynamics and disassembly by phosphorylation of FAK at tyrosine 397. *J. Cell Sci.* (2005). doi:10.1242/jcs.02565

411.   Park, M. S., Kim, Y. H. & Lee, J. W. FAK mediates signal crosstalk between type II collagen and TGF-beta 1 cascades in chondrocytic cells. *Matrix Biol.* (2010). doi:10.1016/j.matbio.2009.10.001

412.   Jing, D. *et al.* Pulsed electromagnetic fields partially preserve bone mass, microarchitecture, and strength by promoting bone formation in hindlimb-suspended rats. *J. Bone Miner. Res.* (2014). doi:10.1002/jbmr.2260

413.   Jing, D. *et al.* Moderate-intensity rotating magnetic fields do not affect bone quality and bone remodeling in hindlimb suspended rats. *PLoS One* (2014). doi:10.1371/journal.pone.0102956

414.   Jing, D. *et al.* Pulsed electromagnetic fields improve bone microstructure and strength in ovariectomized rats through a Wnt/Lrp5/β-catenin signaling-associated mechanism. *PLoS One* (2013). doi:10.1371/journal.pone.0079377

415. Lei, T. *et al.* Pulsed electromagnetic fields (PEMF) attenuate changes in vertebral bone mass, architecture and strength in ovariectomized mice. *Bone* (2018). doi:10.1016/j.bone.2017.12.008

416. Kim, M. O., Jung, H., Kim, S. C., Park, J. K. & Seo, Y. K. Electromagnetic fields and nanomagnetic particles increase the osteogenic differentiation of human bone marrow-derived mesenchymal stem cells. *Int. J. Mol. Med.* (2015). doi:10.3892/ijmm.2014.1978

417. Petecchia, L. *et al.* Electro-magnetic field promotes osteogenic differentiation of BM-hMSCs through a selective action on Ca^{2+} -related mechanisms. *Sci. Rep.* (2015). doi:10.1038/srep13856

418. Rouabhia, M., Park, H., Meng, S., Derbali, H. & Zhang, Z. Electrical stimulation promotes wound healing by enhancing dermal fibroblast activity and promoting myofibroblast transdifferentiation. *PLoS One* (2013). doi:10.1371/journal.pone.0071660

419. Cheng, G. *et al.* Sinusoidal electromagnetic field stimulates rat osteoblast differentiation and maturation via activation of NO-cGMP-PKG pathway. *Nitric Oxide - Biol. Chem.* (2011). doi:10.1016/j.niox.2011.05.009

420. Diniz, P., Soejima, K. & Ito, G. Nitric oxide mediates the effects of pulsed electromagnetic field stimulation on the osteoblast proliferation and differentiation. *Nitric Oxide - Biol. Chem.* (2002). doi:10.1016/S1089-8603(02)00004-6

421. Pilla, A. *et al.* Electromagnetic fields as first messenger in biological signaling: Application to calmodulin-dependent signaling in tissue repair. *Biochim. Biophys. Acta - Gen. Subj.* (2011). doi:10.1016/j.bbagen.2011.10.001

422. Hong, J. M., Kang, K. S., Yi, H. G., Kim, S. Y. & Cho, D. W. Electromagnetically controllable osteoclast activity. *Bone* (2014). doi:10.1016/j.bone.2014.02.005

423. Yuan, J., Xin, F. & Jiang, W. Underlying Signaling Pathways and Therapeutic Applications of Pulsed Electromagnetic Fields in Bone Repair. *Cellular Physiology*

and Biochemistry (2018). doi:10.1159/000489206

424.   Pall, M. L. Electromagnetic fields act via activation of voltage-gated calcium channels to produce beneficial or adverse effects. *J. Cell. Mol. Med.* **17**, 958–965 (2013).

Chapter Four

Fabrication and physical characterisation of highly anisotropic fibrous 3D piezoelectric scaffold

The main findings of this chapter have been published in:

4.1 General Introduction

In any tissue, cells rely on cell signalling to process the information on the state of their microenvironment and to respond to the extracellular cues through modulated cell function. Extracellular matrices provide cells with a range of biochemical and biophysical stimuli, including topographical and mechanical cues and bioelectrical signals.

Tendon is a unique tissue that connects muscle to bone and therefore is under continuous mechanical loading (Figure 4-1). This mechanical stress is borne by a highly organised extracellular matrix composed of collagen type I and interestingly, collagen is a piezoelectric material that under mechanical stimulation responds sending bioelectrical signals that might potentially serve to coordinate an adaptive biological response. In this chapter, the roles of mechanical and electrical also topographical cues on tendon cell function were investigated in vitro.
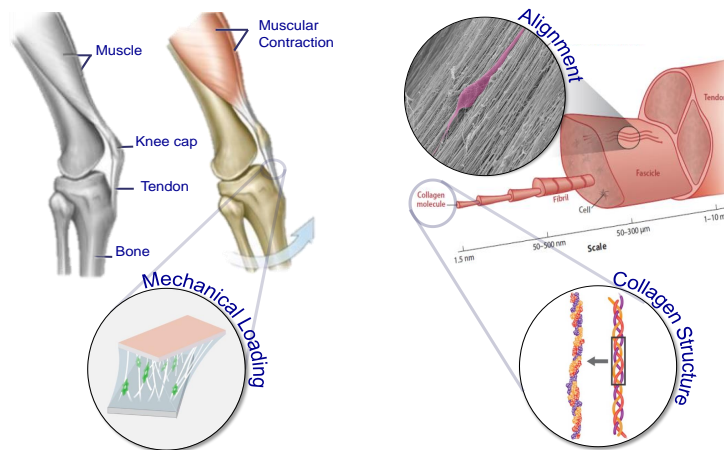
Figure 4-1. The dynamic extracellular tendon microenvironment highly regulates tenocyte function. Observed at different scales: a) macroscopically, the tendon is a tissue that connects muscle with bone and therefore is continuously under mechanical loading. B) at the microscale, this mechanical stress is borne by highly organised ECM that is mainly composed of collagen type I.

In particular, to gain a deeper understanding of the bioelectric regulation of tendon regeneration, there is a need for a dynamic bioreactor system in which the effects of electromechanical stimulation on tenocyte function can be studied. Electrical signalling in

vitro tendon models have been poorly studied to date, and the majority of these studies have focused on the application of exogenous electrical stimulation of tendon cells in 2D culture [35,301]. However, at the time of writing this thesis, there have been no investigations on the role of electromechanical cues on tenocytes morphology and function in a relevant 3D model. Hence, there is a need for a 3D *in vitro* model of tendon healing to study human tenocyte electrophysiology during repair and to provide insight into the regenerative potential of electromechanical stimulation.
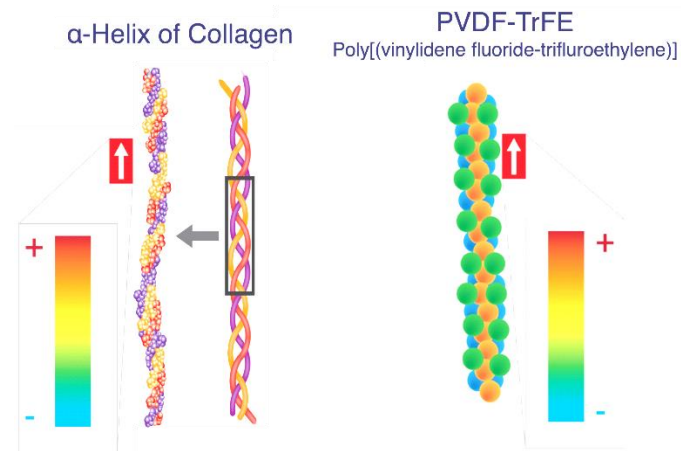
Figure 4-2. Collagen piezoelectric analogue: PVDF-TrFE undergoes electrical polarisation in response to mechanical loading.

Therefore, in this chapter, a new biomimetic scaffold comprised of aligned nanoscale fibres made of PVDF-TrFE is described. The fabrication method chosen was electrospinning due to its ability to mimic the fibrous structure of the native tendon. Furthermore, by altering the collector rotational speed, fibre organisation can be controlled.

Herein, a 3D tissue model of tendon repair that mimics the electrical and morphological properties of tendon tissue was developed through the alignment of electrospun fibres PVDF-TrFE. The piezoelectric output was subsequently quantified under physiologically relevant dynamic mechanical tension to examine the effects of electromechanical modulation on tendon regeneration in vitro. **The goal of this study was to develop a system that models the electromechanical properties of native tendon tissue to dissect the mechanisms by which bioelectric signals might regulate cellular adhesion and function**. It was hypothesised that not only morphological and mechanical features but

electrical gradients play a central role in the functional response and commitment of tendon-derived cells.

4.1.1 Electrospinning

Typically, in the electrospinning process, a polymeric solution is held in a syringe connected to a high voltage power supply through a metallic capillary. When increasing voltage is applied, the surface tension of the polymer is overcome by the electrostatic forces of the following electric field and fibre is ejected from the capillary tip. At this moment the initially rounded shaped drop of polymer in solution elongates and forms a cone shape know as Taylor cone. When the electrical field reaches a level significant enough to break the surface tension forces, a fibre emerges from the tip of the cone and the electrically charged jet is then attracted to a collector. During its flight, the solvent from the polymeric solution is evaporated, and the fibre narrows until is deposited on the collector surface, which is generally grounded or partially charged with an opposite electrical charge to attract the fibres preferentially. Also, the collector cab rotates to organise the fibres in an aligned fashion during collection (see Figure 3)**.** Two types of parameters control the final morphological and chemical properties of the collected fibres, namely solution and working parameters. Solution parameters are those exclusively related to the polymer, including molecular weight, concentration, solvent, conductivity and viscosity. Moreover, working parameters are those related to the electrospinning operation, including flow rate, the distance of the electrode nozzle to the collector, collector rotational speed, applied voltage and nozzle diameter. The ultra-fine fibres found in electrospun mats have a high surface-to-volume ratio and porosity - physical features that mimic the natural extracellular matrix of many tissues.
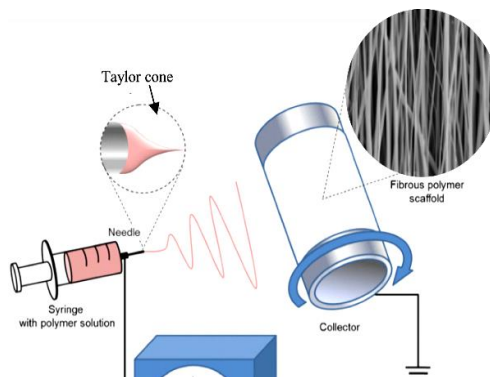
Figure 4-3. Schematic representation of the electrospinning set up used to fabricate scaffolds with aligned fibres.

In this chapter, a tendon graft was fabricated by electrospinning means. It will be shown that by changing the processing parameters, the structure of the scaffolds was modulated to mimic native tendon structure and electrical performance. Also, different protocols to create two types of scaffolds: piezoelectric and non- piezoelectric using different materials PVDF-TrFE and PTFE respectively are discussed. The scaffolds were physically characterised and using a custom-made amplifier; it was shown that piezoelectric scaffolds could generate electrical signals similar or superior to native tendon tissue.

In the second d part of this chapter, it is shown how human tendon-derived cells were cultured on mechanically stimulated scaffolds (piezoelectric and non-piezoelectric) using a mechanical loading reactor. Also, it is shown that cell response is differentially modulated depending on the type of stimulation: mechanical or electromechanical.

4.2 Materials and Methods.

4.2.1 Electrospinning process

P(VDF-TrFE) and PTFE were made into fine fibres by varying the voltage, mandrel rotation speed and the distance between tip and collector with a constant flow rate. Each polymeric solution was placed in an Aladdin programmable syringe pump (AL-1000) (World Precision Instruments) and attached to a 27-gauge stainless steel needle. Aluminium foil was cut in a 10cm x 27/28cm portion and taped around the cylindrical mandrel collector (Linari Engineering S.r.l).

a) P(VDF-TrFE) 75/25 weight % (Solvay Solexis) was dissolved in a 3:2 volume ratio of dimethylformamide (DMF)/acetone (Sigma-Aldrich) at a polymer-solvent concentration of 15-35% w/w. Briefly, 2 ml of solution was placed into a 10 ml plastic syringe (Luer lock). Any excess air remaining in the syringe was removed, and a stopper was placed on the syringe to prevent the sample from drying out. The syringe was placed 6 cm away from the collector, the flow rate was set constant at 1ml/hour, and the collector speed was set at 3700 rpm. Finally, the voltage was switched on and increased up to 24-26kV. The collector was also charged with -6kV. The experiment ran for 2 hours, and lower humidity yielded more favourable results (40-50%).

b) PTFE was electrospun with a 2-step process. First, 240 milligrams of poly(ethylene oxide) (PEO), average M_v □300,000 (Sigma-Aldrich), was weighed out and mixed with 10 ml of PTFE, 60 wt % dispersion in H_2O (Sigma-Aldrich). The syringe was clamped into a polymer blender and mixed gently for 2 hours. After blending, the air from the syringe was removed using centrifugation tube at 1500 RPM for 2 minutes. The solution was removed from the centrifuge and filtered through a syringe filter with 25 mm diameter (Merck Millipore) into a clean syringe at least twice to ensure no precipitates were present. The syringe was placed 10-12cm away from the collector, and the flow rate was pre-set at 1.25ml/hour. The rotator was set at the maximum velocity of 2000 RPM since fibres at higher speed tend to break due to

their poor mechanical integrity. The voltage was set to 11/12 kV. The experiment ran for 4-5 hours, and a higher relative humidity yielded more favourable results (50-60 %). In the second step, PTFE mats were collected and annealed at 185 ℃ for 5 minutes.

4.2.2 Functionalizing electrospun material

Post electrospinning, due to sample chemistry the sample material must be functionalized (adding specific integrin-binding moieties) before use in cell culture as a biomaterial scaffold. The samples were carefully removed from the aluminium foil and placed on a square sample holder. Three functional chemistries were used: Collagen (50µg/ml), Poly-L-lysine (PLL) (10µg/ml) and fibronectin (FN) (20µg/ml) to aid in the promotion of cell attachment.
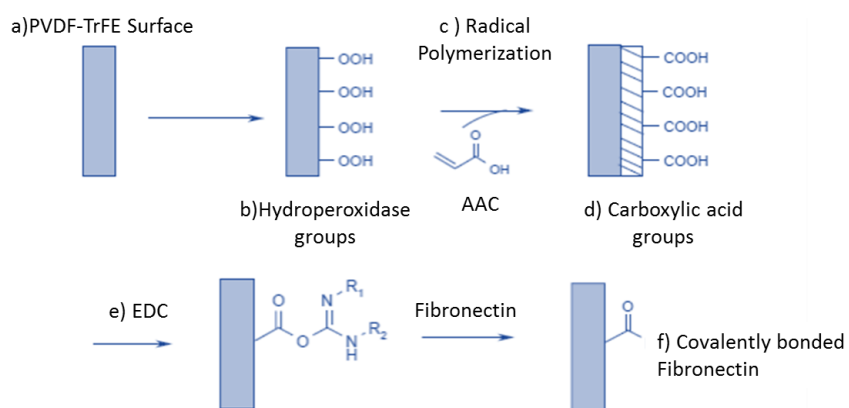
Figure 4-4. The functionalizing process illustrated via a stepwise mechanism. a) First, the square sample holder was placed in an RF (radio frequency) plasma chamber and treated with oxygen plasma for 45 seconds. b) Hydroperoxides produce secondary radicals that initiate the c) polymerisation of Acrylic acid (AAc) process. d) PAAc acts as a spacer on the PVDF surface and offers carboxylic acid groups. e) Carbodiimide compound EDC/NHS was used for crosslinking between primary amine from fibronectin and carboxylic acids. f) Fibronectin was then covalently bound to the PVDF-pAAc surface using N-(3-Dimethylaminopropyl)-N′-ethylcarbodiimide hydrochloride (EDC).

Since the biological activity of proteins on the surface depends upon whether specific active peptide sequences are accessible to the cells, the accessibility of the cell-binding

domain was ensured by the covalent binding of fibronectin to modified surfaces using Poly-Acrylic Acid (PAAc) as a spacer.

4.2.3 Physical Characterisation

The following chapter describes the different techniques utilised to characterise the electrical properties of the piezoelectric scaffolds for cellular electromechanical stimulation. Since the material is well known since its discovery in 1969, a large number of studies on the physical characterisation of the polymer have been already conducted[167,302–307]. A brief description of the most popular techniques to study PVDF-TrFE electrical output will be presented. Finally, the experimental results obtained from the characterisation of PVDF-TrFE using a mechanical loading reactor will be presented. The characterisation described further include the development of a secure and cost-effective method of the charge and open-voltage measurements, d_{33} direct measurements and PFM measurements.

4.2.3.1 Structural characterisation

4.2.3.2 X-ray diffraction (XRD)

XRD is a powerful technique to help to identify the crystalline structure of PVDF-TrFE films. X-ray diffraction patterns from films were collected by using a Philips Xpert PRO automatic diffractometer operating at 40 kV and 40 mA, in theta-theta configuration, secondary monochromator with Cu-K☐ radiation (λ = 1.5418 Å) and a PIXcel solid-state detector (active length in 2θ 3.347º). Data were collected from 5 to 70° 2θ (step size 0.026 and time per step = 347 s) at RT. A fixed divergence and anti-scattering slit giving a constant volume of sample illumination were used. The signal deconvolution was evaluated using the peak-fit option of the WinPLOTR program. The profile fitting procedure (XRFIT calculation) uses pseudo-Voigt functions with a global FWHM (Full width at half maximum and a global eta (proportion of Lorentzian), and a linear background. Each peak is characterised by its position, intensity, FWHM and eta shifts concerning the global parents. The average size of the crystalline domains β (coherently diffracting domains) of the samples was extracted from the broadening of the signal using the Scherrer equation:

$$\beta_{hkl} = k \cdot \lambda / L_{hkl} \cdot \cos\theta$$

Equation 4-1

Where β_{hkl} is the broadening of the diffraction line measured at half the maximum line intensity (FWHM) taking into account instrumental contribution ($\beta_{Inst}=0.1°$), λ is the X-ray wavelength, L_{hkl} is the crystal size, and θ is the diffraction angle. K is the Scherrer shape factor (k=0.9 was used for the calculations).

4.2.3.3 Differential scanning calorimetry (DSC)

The thermal transitions of the PVDF-TrFE scaffolds were determined on a DSC Q200 (TA Instruments). Samples of 8-10 mg were heated from -10ºC to 200ºC at 10ºC min-1. This first scan was used to determine the melting temperature (T_m) and the melting enthalpy (ΔH_m), as well as the Curie temperature (Tc) and the Curie enthalpy (ΔH_c). After this first scan, the samples were quenched in the DSC and a second scan was collected from -10 to 200ºC at 10ºC min-1. For the non-isothermal crystallisation studies, the films were heated at a constant heating rate (30°C /min) from room temperature to 260°C and held there for 2 min to eliminate the residual crystals and memory effects due to thermal history, and then cooled to crystallize at the same cooling rate under nitrogen environment to room temperature. For isothermal crystallisation kinetics, the films were heated at a constant heating rate of 30°C/ min from room temperature to 260°C and held there for 2 min to eliminate the thermal history, then the melt was cooled at the same rate up to 148°C and kept constant at 148°C for 10 min until the sample completely crystallized.

4.2.3.4 Fourier transform infrared (FTIR)

Infrared spectra of PVDF-TrFE scaffolds were recorded on a Nicolet AVATAR370 Fourier transform infrared spectrophotometer (FTIR) operating in the Attenuated Total Reflectance (ATR-FTIR) mode. Spectra were taken with a resolution of 2 cm^{-1} and were averaged over 64 scans. Using the absorption band of α and β phases at 532 cm−1 and 846 cm−1, the fraction of β phases were calculated using the following equation The β-phase content F(β) was calculated by the following equation [1]:

$$F(\beta) = \frac{X_\beta}{X_\alpha + X_\beta} = \frac{A_\beta}{1.26A_\alpha + A_\beta} \qquad \text{Equation 4-2}$$

where A_{EA} is the absorbance value at 841 cm^{-1}, A_α is the absorbance at 764 cm^{-1}, and the factor 1.26 is the ratio of absorption coefficients at 841 cm-1 (K_{841} = 7.7 x 10^4 cm^2 mol^{-1}) to 764 cm^{-1} (K_{764}= 6.1 x 10^4 cm^2 mol^{-1}) at the respective wavenumber.

4.2.3.5 Mechanical properties

Tensile analysis of scaffolds was performed using Zwick/Roell Z010 with 1 kN load cell with a crosshead speed of 500 mm/min and a maximum extension of 500%. Thin scaffolds were cut per ASTM D 882 type specimen. Results are presented as average values of n = 5 replicate experiments with standard deviation.

4.2.3.6 Piezoelectric characterisation

Signal conditioning

Due to the capacitive characteristic of piezoelectric materials and especially the impedance, of PVDF-TrFE scaffolds, amplifiers matching this impedance must be used. It is essential to arrange an **input** that controls the rate of charge leakage appropriately for the application. Merely connecting a piezo film element to the input of an oscilloscope will create a **high-pass filter** that removes any low-frequency content of the original piezo signal, and this can lead to an incorrect evaluation of the material's true electrical potential.
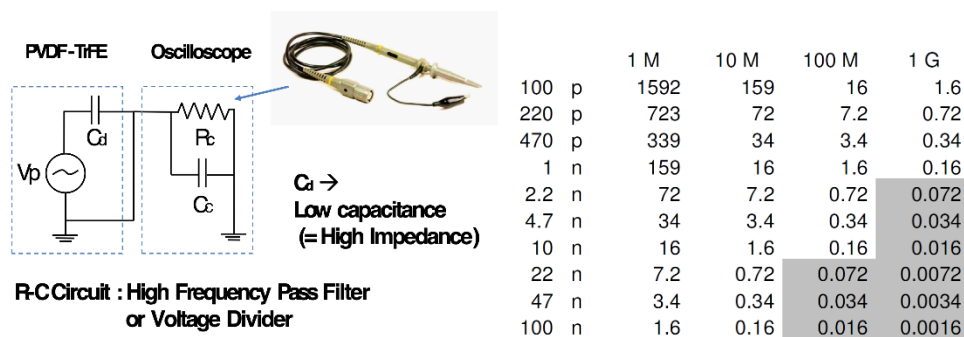
Figure 4-5. a) R-C circuit or voltage divider circuit. b) Table of Input impedance equivalence to piezoelectric capacitance. A charge amplifier with an input impedance in GΩ range can precisely measure capacitances in the nano coulomb range

For applications with piezoelectric transducers, a preamp using charge amplification settings usually are used. This configuration has high input impedance (>1GΩ), and it integrates current signals at the entrance delivering a voltage signal at the output.

The charge amplifier configuration is obtained by using a feedback capacitor (Cf), as illustrated in In this configuration, the feedback resistor (Rf) has the function of limiting the DC output voltage and influences the low cut-off frequency. Vt, Ct and Rt represent respectively voltage, capacitance and resistance.
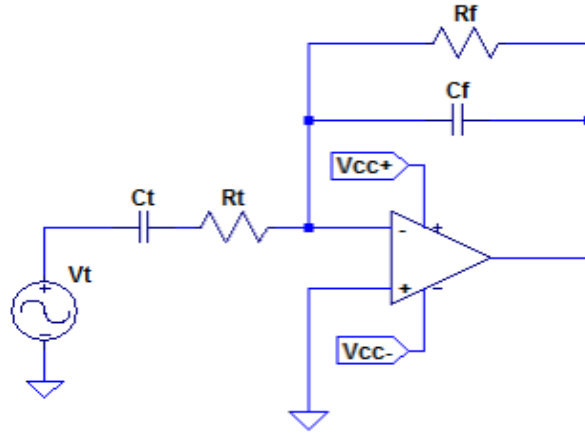
Figure 4-6. Simplified schematic representation of the charge amplifier configuration. The piezoelectric scaffolds and cable are electrically represented by Ct (capacitor) and Rt (resistor). The charge amplifier configuration is defined by Cf (capacitor) and Rf (resistor). Vcc represents DC voltage to power the amplifier.

The circuit transfer equation is given below:

$$\frac{Vout}{Vin}(s) = -\frac{Rf}{1+s*Cf*Rf} * \frac{s*Ct}{1+s*Ct*Rt}$$

Equation 4-3

The gain of the charge amplifier is given largely by feedback capacitor. The simplified circuit gain, as well as the low and high cutoff frequencies, can be expressed by the following equations:

$$Gain = \frac{1}{Cf} \quad fl = \frac{1}{2\pi * Rf * Cf} \quad Fh = \frac{1}{2\pi * Rt * Ct}$$

Equation 4-4

Charge measurements: Development of a custom-made charge amplifier

As the piezoelectric scaffold has a high internal impedance, the voltage measurements can be altered by the cable capacitance, stray capacitance and input impedance of the measurement equipment. Also, the voltage measurement can be influenced by small changes in the sample capacitance, Cp, resulting from mechanical loading. In order to minimise all these effects above, a charge amplifier was employed. The use of a charge amplifier eliminates effects arising from the capacitance of the cables and the measurement equipment from the system.

Due to the sizeable open-circuit gain of the amplifier, the effects of the parasitic capacitance were suppressed, rendering the device sensitivity unaffected by changes in type and length of input cables. Also, as the charge amplifier, only measures charge the effects of impedance changes due to mechanical loading are minimised. In summary, the charge amplifier converts the high-input impedance charge into a usable low impedance voltage output.
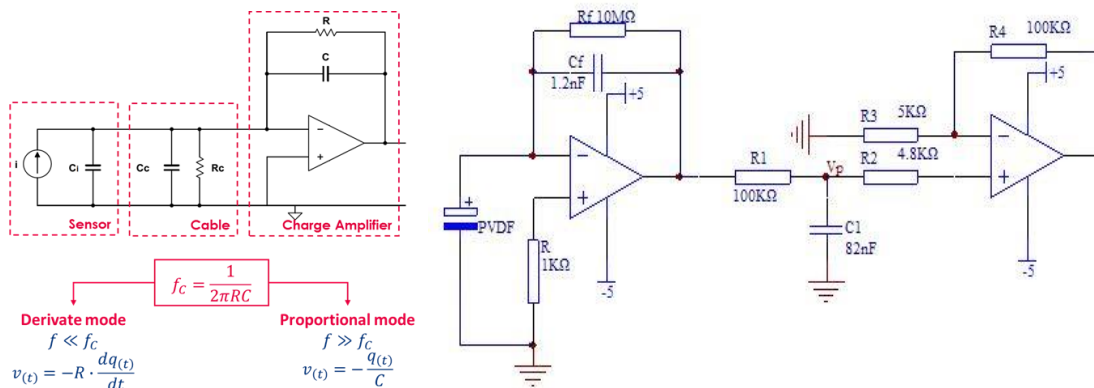
Figure 4-7. Signal conditioning circuitry composed of two parts: 1) charge amplifier, 2) low pass filter to eliminate signals of no interest and 3) a voltage multiplier to increase the sensitivity of the device. The chip used in both steps was BiMOS Operational Amplifier CA3140 (A).

The signal conditioning was based on an operational amplifier (CA3140) that offer an internal impedance in the TΩ range. The voltage gain is defined by the ratio G = 1+R4/R3.

The charge amplifier also has a low-pass filter (LPF) stage to match the signal characteristics and reduce noise.

Piezoscaffolds are not suitable for static measurements as the charges generated decay with a time constant proportional to their internal resistance. Therefore, practically speaking piezoscaffolds can only generate electrical forces when they are under time-varying mechanical strains or stresses. To measure accurately the electrical energy generated in electrospun scaffolds an electronic circuit with high input impedance (more substantial than the internal impedance of the scaffold) and low current leakages was needed. Some examples of the different tried low leakage buffer electronics included: JFET - 4117 (Siliconix, Sprague); Operational amplifiers — LMC660, LF353 (National Semiconductor), OP80 (PMI), and 2201 (Texas Instruments).

Electrode

The piezoelectric voltage coefficient (g) is a measure of the electric field generated due to the piezoelectric conversion of stress or strain. Top/bottom electrodes and interdigitated electrodes (IDEs) were used to measure d_{31} and d_{33} coefficients of piezoscaffolds, respectively. The open-circuit voltage (V_{3j}) generated under deformation (ε_{xx}) is calculated following this equation:

$$V = g_{3j}\, E\, \varepsilon_{xx}.\, Lj \qquad\qquad\qquad \text{Equation 4-5}$$

Where g_{3j} is the piezoelectric voltage constant ($g3j = d3j\, \varepsilon T$, εT denotes the permittivity under a constant strain), E (young modulus) and Lj is the distance between the electrodes. From Equation above, it becomes clear the importance of the inter-electrode gap on piezoelectric materials to achieve a high output voltage from a piezoelectric stimulator.

Voltage output measurements using a custom-built rig.

Unlike the piezoelectric films described in chapter II, a commercial d33 piezometer is not useful here to determine the piezoelectric coefficient of the electrospun scaffolds as these are mechanically compliant and obtaining an accurate and stable d33 readings became extremely difficult. Therefore, in order to analyse the electromechanical behaviour of these scaffolds, a custom made rig was developed to monitor applied strain and induced voltage

using an electrometer (Keithley 6514) with virtual infinite input impedance. The Keithley electrometer was connected to the scaffold with a triaxial cable possessing three inputs (high, low and ground). However, leakage resistance and capacitance can appear between the inputs and affect the measurement precision by introducing an offset ramp. In this case, a plausible solution was to use guarding to eliminate these effects. In this mode, the electrometer drives a current through the conductive sheet surrounding the sample inducing the same potential as the high input terminal. With both ends at the same potential, current leakage is not possible. The electrometer used here can operate in guarded mode or un-guarded mode, as appropriate. Finally, we used LabVIEW from National Instruments to collect the data and a mechanical loading reactor to apply strain to the samples following a sinusoidal signal at different frequencies and fixed strain.

4.2.4 In vitro Characterisation

4.2.4.1 Optimisation of the culture conditions

Human tendon cells, which were isolated from two donors 63 and 66 years old (LOT #TENM012214F and #TEN020415L), were purchased from Zen-Bio (Research Triangle Park, NC). Cells were expressing TBSH4 and surfaces markers were characterised (CD90+/CD29+ ; CD45-/CD31-) . Cells were seeded into T-75 flask collagen type I coated with tendon cell culture medium (Zen-Bio) and incubated overnight at 37 °C with 5% CO_2. After the medium was exchanged, the cells were further incubated for 24 h and used for experiments at P3. Briefly, cells were cultured on scaffolds at a density of 7 500 cells/cm2 and left for 24 hours to attach. Cells were kept in static or dynamic conditions (8 hours/day of 4% deformation at 0.5, 1 and 2 Hz) for 24h, five days or 10 days. Analysis of TNMD and SCX gene expression and TNMD (ab203676, Abcam) protein expression were used to optimise the culture conditions.

4.2.4.2 Protein microarray

The search for genes related to the adhesion, collagen synthesis, inflammation, mechano/voltage-receptors and cell differentiation processes towards the bone, cartilage and tendon were conducted in two stages. First, an array of genes was chosen based on a literature review (PubMed), and in a second stage, an array of genes was obtained from the analysis of functional networks focused on the cell differentiation processes

(http://geneontology.org/, DAVID, EGAN). Finally, after comparing both pools of genes, a total of 88 genes were chosen for this study. A custom 384 (96x4)-well plate RT-qPCR Array containing the 88 selected genes was designed and produced by Qiagen specifically for this study (SA Biosciences, Frederick, MD, USA) (Table 1). The fabricated and validated arrays also included five housekeeping genes, a negative genomic DNA control, and positive reverse transcription and PCR controls.

RNA extraction, purification and custom RT2-qPCR array processing

RNA was extracted using a trizol and chloroform precipitation method and purified using a Qiagen column. RNA quality after purification was assessed using an Agilent 2100 Bioanalyzer and RNA 6000 Pico Kit for low sample quantities (Agilent Technologies, USA) providing data on the integrity of RNA (RNA Integrity Number; RIN) and RNA concentration. RNA concentrations above 20 ng/µl and RIN >9 were used for subsequent conversion into cDNA. Following the manufacturer's instructions, cDNA was synthesised by reverse transcription of RNA using the RT2 First Strand Kit (SA Biosciences). PCR was performed in iQ5 Thermal Cycler (Bio-Rad, Munich, Germany), using diluted cDNA as template (10 µl of cDNA, 10 µl of Genomic DNA Elimination Mixture and 91 µl of RNase free water) and the RT2 SYBR Green qPCR Master Mix (SA Biosciences), according to the manufacturer's guidelines. Each experiment was done in triplicate using the two donors (N=2), and all samples were analysed in technical duplicate for each gene set.

Generation of expression values

Quantification results were normalised against stable housekeeping genes (*TOP1*, *GAPDH*, *HSP90AB1*, *RPLP0* and *TBP*), using the geometric mean of the threshold cycle (Ct) of the genes included in each plate. Expression changes were calculated using the $\Delta\Delta_{Ct}$ method and followed by calculation of regulation fold changes.

Statistical analysis

For statistical comparisons and according to the small sample size, nonparametric tests were used. The Wilcoxon test was used to compare both sample types with their baseline levels.

Correlation between gene expression and IOP was examined using Spearman's correlation test. Gene expression patterns related to surgical success and failure were identified using Correspondence Analysis (COA). Statistical analysis was performed using SPSS 19.0 (SPSS Sciences, Chicago, IL, USA). The level of statistical significance was $p < 0.05$.

4.3 Results

4.3.1 Fabrication of aligned PVDF-TrFE nanofibres piezoelectric scaffolds

The below multiple variables in the electrospinning setup required optimisation in order to fabricate uniform nanofibres.

Time of electrospinning	1h	2.5h
1	24	74
2	35	78
3	23	72
4	35	73
5	27	76
6	20	75
Thickness (µm)	**27 ± 6**	**75 ± 2**

Table 4-1. The averaged thickness of scaffolds after 1 or 2.5 h of electrospinning time.
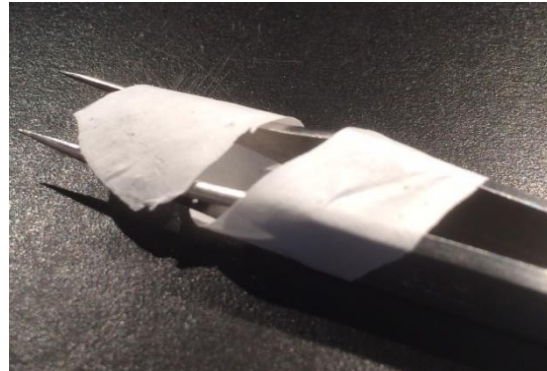
Figure 4-8. Photography image of a scaffold showing the high compliance of the scaffolds.

The quality and morphology of the scaffolds nanofibres were greatly influenced by solution and working parameters; however; one of the most critical parameters appeared to be flow rate and concentration. The optimal averaged fibre diameter of the scaffolds used here was measured as 540 nm ± 120 nm.

In this work, a 30 kV potential difference between collector and nozzle tip (200 um), a flow rate of 1 ml/hr and a collector - tip distance of 6 cm was identified as the working parameters for optimal electrospinning of PVDF-TrFE. Also, a collector disk with 8 mm width and 8 cm diameter was used to concentrate the electrical field while rotating at 3500 rpm (30 m/s linear speed) to draw and align the collected fibres. The advantage of using

293

large linear speeds is 1) it promotes the formation of mesoscopic joints between adjacent fibres (as result of residual no evaporated solvent due to short flight times) to maximise the mechanical properties of the scaffold and 2) it mechanically draws the fibres increasing their mechanical and electrical performance[308–310]. We used DMAc in combination with acetone (50:50 v/v) since the surface morphology of the fibres is slightly rough and due to the high boiling point of DMAc (Tb: 165ºC) it helps for the formation of fibre interconnections as described by Persano *et al.* in similar studies [2].
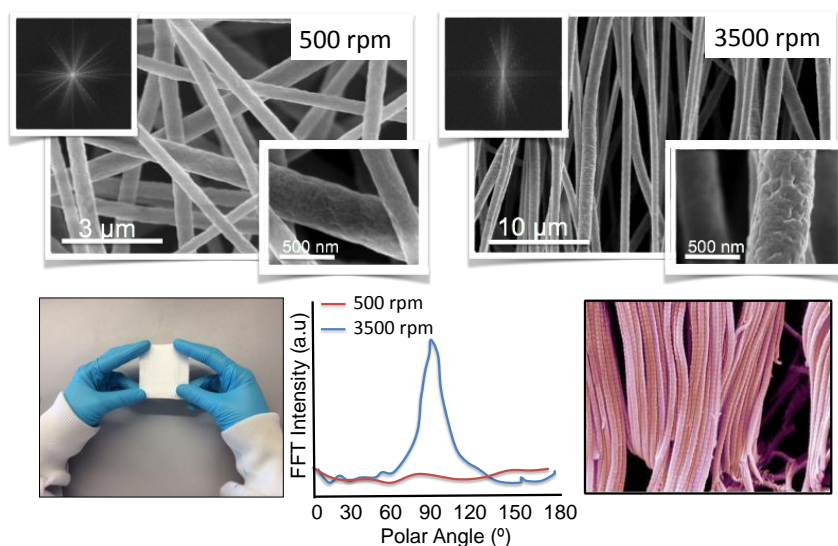
Figure 4-9. Morphology of the scaffolds obtained by electrospinning collected at low (500 rpm) and high (3500 rpm) rotational speeds. Fast Fourier Transform (FFT) spectra show a broad distribution of intensities for low speed (500 rpm) scaffolds. In contrast, FFT spectra for scaffolds fabricated at high rotational speeds (3500 rpm) shows a clear peak demonstrating the highly repetitive and organised structure. Taking as template the native tendon tissue it was observed that at high rpm fibre alignment was significantly increased as shown by FFT intensity.

With the present setup strips of 8 mm width, 25 cm length and thickness between 27 and 75 um depending on the spinning time were obtained. The diameter of the nanofibres produced was around 540 nm with a narrow dispersion (see Figure 4-9).

a)   b)
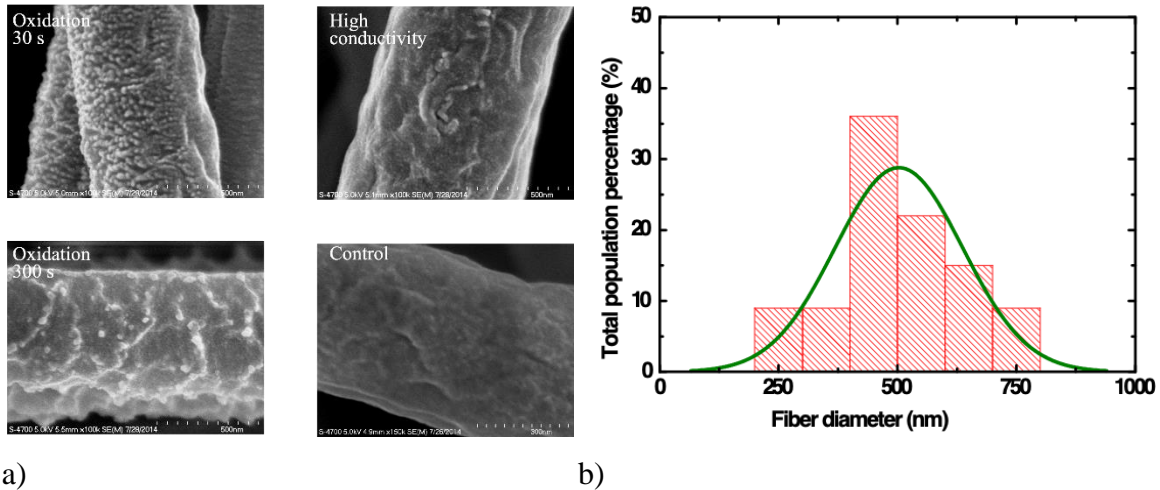
Figure 4-10. SEM images showing a different range of surface morphologies. a) Effect on fibre surface morphology of plasma treatment for 30 or 300 seconds and the effect of increasing conductivity on surface morphology b) Fibre diameter distribution.

The total alignment was calculated using Fast Fourier Transform (ImageJ) of scanning electron images of fibres organised randomly or in an aligned fashion. The alignment was constant along the entirety of the scaffold, and the porosity of the scaffolds was measured to be around 75 %. In general fibre, collection speed resulted in highly aligned scaffolds with higher rigidity. Other processing parameters were also explored including conductivity of the polymeric solution, plasma treatment effect and distance between collector and syringe.

To assess the effect of conductivity salt (NaCl) was incorporated into the solution. The main effect observed was changes of the surface morphology that might alter the mechanical strength of the scaffold (Figure 4-10). It is well recognised that surface roughness can generate defects nucleation and affects the mechanical strength of the material. Therefore, smoother surfaces are always preferred when looking to maximise mechanical properties. Conversely, roughness can increase cell attachment since more area for cellular adhesion is available and cells can sense nanoscale topographies. A shown in Figure 4-10, prolonged exposure times to ion bombardment during plasma treatment results in high levels of nanoscale roughness and oxidation (incorporation of hydroxyl groups into the surface chemistry) that result in a change from hydrophobic to a hydrophilic character.

It is known that the distance between collector and needle might affect the microstructural properties of individual fibres and also to the formation of interconnections between fibres as less time flight is used to reach the surface collector. Therefore, the effect of distance between syringe and collector was evaluated. Conventional electrospinning using long distance (20 cm) between collector and nozzle was used. Also, a systematic comparison of the effect of the distance across a broad range of fibre diameters was studied. In order to control fibre diameter, a range of different polymer concentrations was used. The concentration ranged from 11% to 35% to obtain a library of fibres between 180 and 540 nm. Finally, scaffolds were functionalized to covalently attach fibronectin their surface following the process described in Figure 4-4.
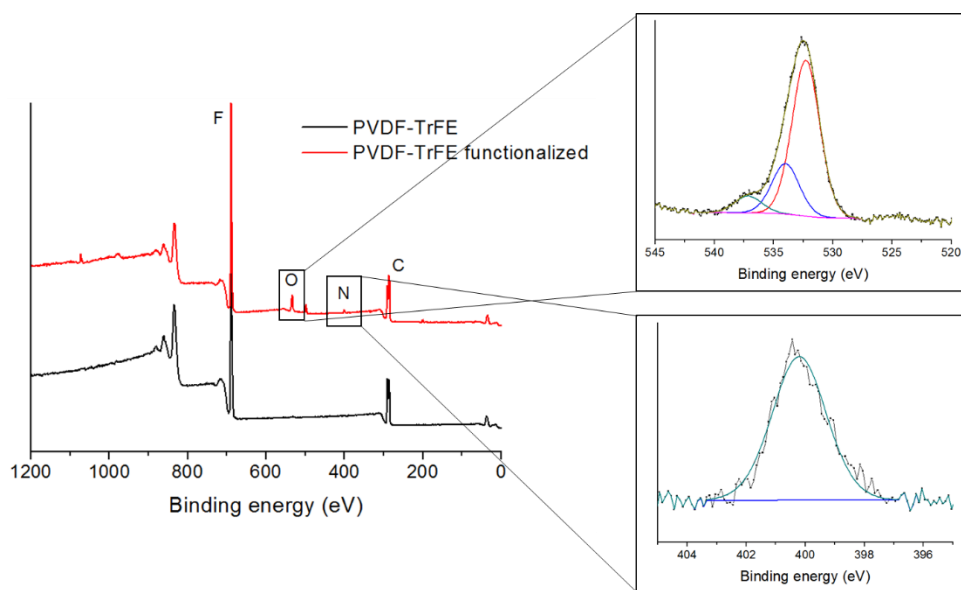
Figure 4-11. Surface chemistry analyses. X-ray Photoelectron Spectroscopy (XPS) spectra are shown for surfaces following fibronectin surface immobilisation (in red) and compared to pristine surfaces without surface functionalization (in black). High-resolution spectra are showing the presence of peaks corresponding to Nitrogen (N1s at 405.5 eV) and Oxygen (O1s at 530.9 eV).
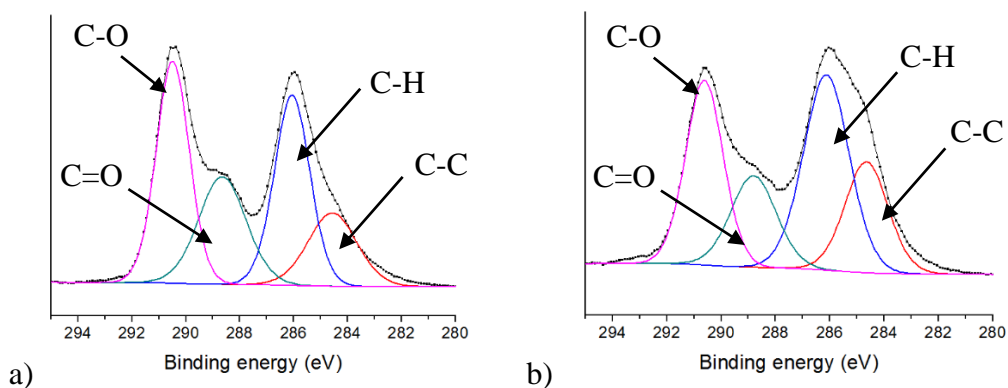
Figure 4-12. Surface chemistry analyses. X-ray Photoelectron Spectroscopy (XPS) high-resolution spectrum for Carbon (C1s) showing typical hydrocarbon contamination with C==, C-C, C-H and C-O components. Carbon signal was deconvoluted for a) pristine and b) functionalized scaffolds showing significant changes in C-C component.

As shown in Figure 10, oxygen (O1s) and nitrogen (N1s) XPS signals were measured after functionalization with fibronectin on PVDF-TrFE and PTFE scaffolds. It is also shown that before functionalization nitrogen and oxygen peaks were not significantly detected. The spectrum of the C1s carbon signal (see Figure 11) at 284.6 V revealed changes in the C-C and C-H bond energy suggesting new covalent bonds have been formed. The other three contributions is related to intra-chain polymer bonds C-F. Finally, the evident Fluor signal present on both spectra suggests that the modification with fibronectin is in the nanoscale range (< 20 nm).

The thermal transition properties of P(VDF-TrFE) scaffolds were evaluated using differential scanning calorimetry (DSC). As it can be observed in Figure 12, PVDF-TrFE scaffolds demonstrated two main transitions: an initial endothermic peak, associated to the Curie temperature and a second endothermic peak that is associated to the melting temperature. Little differences were observed in the thermal transitions of the studied samples, indicating that the concentration of the polymer solution has a negligible effect on the thermal transition of the resulting scaffolds. Accordingly, all the samples showed a T_c and T_m at ~117ºC and ~141ºC, respectively. The observed ΔH_c and the ΔH_m values were ~5 J g^{-1} and ~17 J g^{-1} in all the studied samples. It has to be mentioned that the functionalised scaffold (oxidized for 45 sec and treated at 90ºC for 1h with pAAC) showed a different

behaviour, with a slight endothermic transition at ~90ºC and much lower ΔH_m value (ΔH_m=12.74 J g^{-1}).

ID	Diamet	T_c	ΔH_c	T_m	ΔH_m
1.1	180	118.	4.7	141.	16.5
1.2	240	117.	4.9	141.	15.5
1.3	320	117.	5.2	141.	17.0
1.4	390	117.	5.1	141.	16.7
1.5	430	117.	5.2	141.	17.2
1.6	490	116.	5.4	140.	17.9
1.7	540	117.	5.4	140.	17.1
1.7	540 a*	117.	5.2	140.	17.4
1.7	540 b+	117.	3.4	139.	12.7

*Long distance   +Treatment (fibronectin bonding)
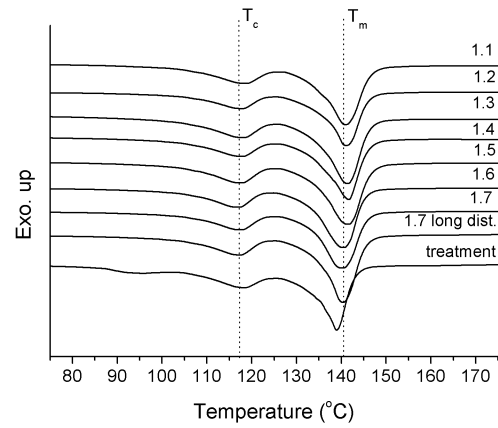
Table 4-2. T_c, ΔH_c, T_m and ΔH_m values of the PVDF-TrFE scaffolds. (a* Long distance and b* functionalised)

Figure 4-13. First DSC scans of PVDF-TrFE scaffolds with different diameters

a)

b)
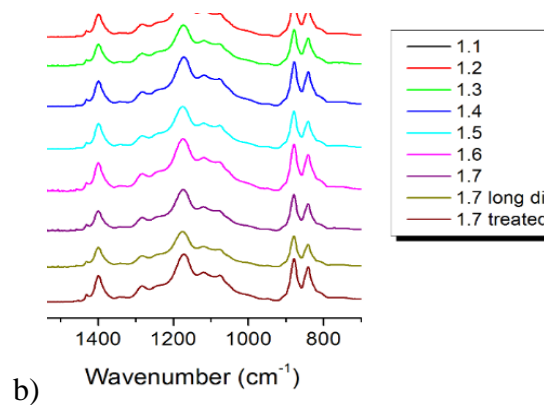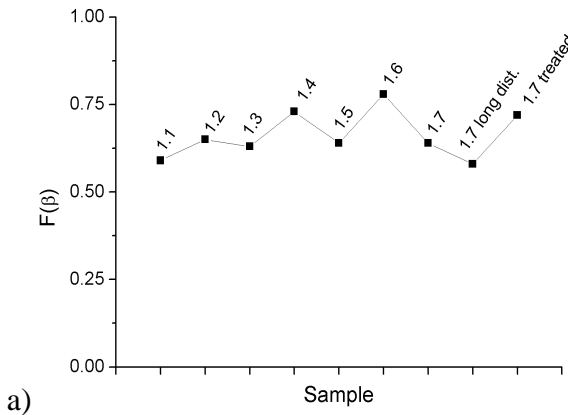
Figure 4-14. Total β-phase content (calculated from equation 4-2 using FTIR spectra) in the function of fibre diameter. b) Typical FTIR spectrum of PVDF-TrFE scaffolds for all the different fibre diameters (from 180 to 540 nm).

Figure 13b shows the typical FTIR spectra of PVDF-TrFE scaffolds. Here, those bands that are exclusively associated with β-phase are discerned (i.e., bands at 840 cm^{-1} and 1279 cm^{-1}). However, bands associated with the α-phase (i.e., bands at 764 cm-1 and 976 cm^{-1}) did not appear in the spectra, suggesting that the β-phase is the predominant crystalline phase in

the PVDF-TrFE scaffolds. A clear trend was not observed between the concentration of the polymer solution and the β-phase content. Scaffolds with 390 nm (1.4), 490 nm (1.6) and 540 nm (1.7) fibre diameter had the highest β-phase content (73%; 78% and 72% respectively). Differently, scaffolds with the lowest fibre diameter (180 nm) or spun using long-distance (between collector and needle) showed at the lowest β-phase content (59% and 58% respectively). These results differ from other studies that suggest a positive linear correlation between increasing β-phase with decreasing fibre diameter[311]. A possible explanation for these findings lies in the idea that further refinement of the fibre diameter might be a pursuit to achieve a better correlation. As shown in different study fibre diameters less than 100 nm showed a more dramatic effect on the crystal structure and β-phase content.[312]
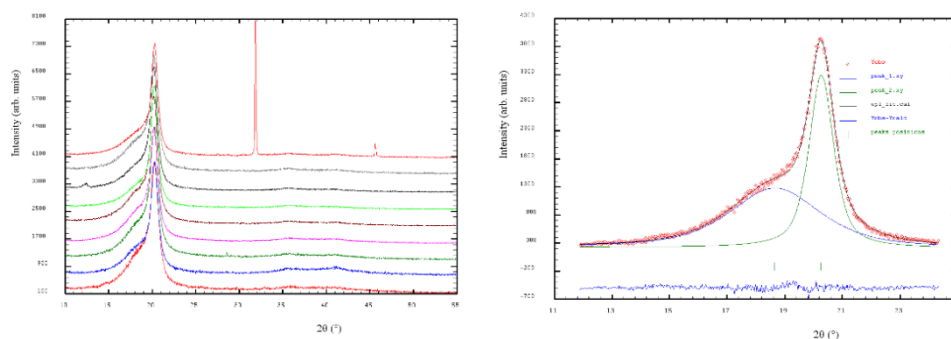
Figure 4-15.a) XRD spectra of the PVDF-TrFE scaffolds b) Deconvolution of the spectra into crystalline phase and amorphous halo.

X-ray diffraction offered information regarding the level of crystallinity and crystal structure. As it can be observed in Figure 14, a well-defined single peak at 2θ=20.26º is observed in the XRD spectra, which is characteristic of the (1 1 0) and (2 0 0) planes of the β-phase. The degree of crystallinity was calculated by deconvolution of XRD spectra into crystalline peaks and amorphous halo.

As observed in Table 2, all the samples showed a similar degree of crystallinity (44-53%) and the average size of the crystalline domain (~10 nm).

Table 4-3. Degree of crystallinity and the average size of the crystalline domain of the PVDF-TrFE scaffolds. a*long distance b*random fibres c* fibronectin functionalisation

Sample	Deg.crystallinity	Crystalline size
180 nm	44	9
240 nm	46	10
320 nm	45	9
390 nm	45	9
430 nm	47	9
490 nm	53	10
540 nm	49	10
540 a* long. dist.	43	9
540 b* random.	40	9
540 c* funct.	47	11

As shown by XRD, FTIR and DSC measurements, conventional long distance electrospinning resulted in less β-phase content. Also, further analyses of alignment and fibre diameter dispersion showed the decreased organisation of fibres and more significant dispersion on fibre distributions. Also, mechanical analyses of long-distance electrospun scaffolds confirmed these results. Long-distance scaffolds showed inferior mechanical performance compared to short distance electrospun scaffolds (see Figure 15).
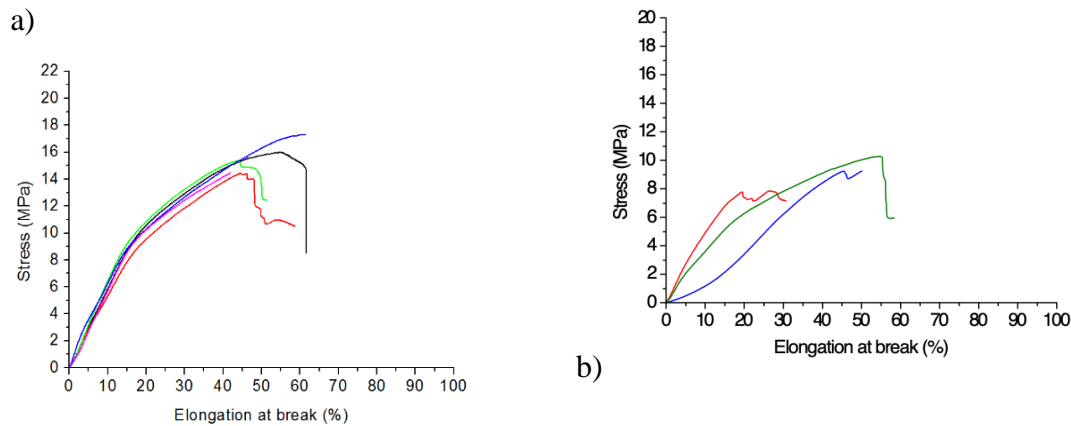
Figure 4-16. Tensile mechanical test spectra for a) Short distance (6 cm) b) long-distance (20 cm) electrospun scaffolds. Results showed that short distance scaffolds have superior elastic modulus, yield stress, elongation and reproducibility of than long-

distance scaffolds.
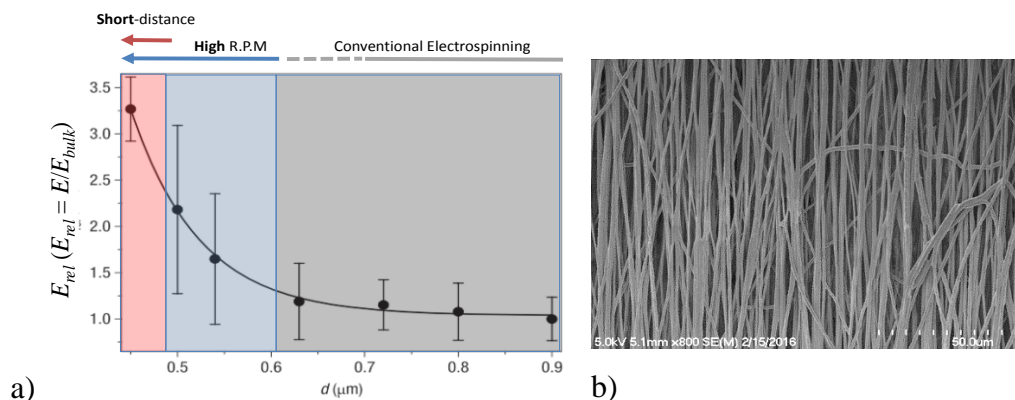
Figure 4-17. a) Diagram showing the relationship between fibre diameter and Young relative modulus (E_{rel}). It is shown that fibre diameter affects the mechanical behaviour of highly aligned scaffolds. b) Scanning electron microscopy (SEM) image representative of highly aligned scaffold comprised of electrospun fibres of PVDF-TrFE.

When comparing the mechanical properties of samples with varying fibre diameter using short distance electrospinning, a three-fold increase in the elasticity modulus was obtained for scaffolds with fibre diameters ranging from 180 nm to 540 nm. However, it is interesting to note that the level of crystallinity did not account for this increase in mechanical properties. Samples with 180 nm fibre diameter showed 44% crystallinity whereas scaffolds with 490 nm showed 53 % crystallinity. Similarly, the overall crystallinity for scaffolds with random fibres with a fibre diameter of 590 nm was 40%. These results suggest that mechanical drawing during fibre collection at high rotational speeds results in enhancement of crystallinity level, in particular, the polar β-phase. It can be hypothesized that the increase in mechanical properties of highly aligned scaffolds with a fibre diameter of 490 nm is a result of a high level of chain extension and orientation along the fibre axis as a result of fibres being drawn by the centripetal forces. It has been shown that stress hardening does not depend on crystallinity but the density of

entanglement of the amorphous part in semi-crystalline polymers (including PVDF-TrFE). In turn, entanglement can be affected by cooling/crystallisation rate and by annealing (cold crystallisation). Therefore, mechanical properties depend ultimately on processing parameters including the distance between needle and syringe, rotational speed and polymer solution concentration.

Mechanical properties are essential to generate higher stresses under fixed strains (resulting in higher electromechanical/piezoelectric signals); however, a growing body of research suggests that higher electromechanical/piezoelectric performance is crystallinity dependent, in particular, the content of β-phase content. The most recognised methods to increase β-phase content is via post-processing processes. Therefore, two post-processing processes, thermal annealing (cold crystallisation) and strain-hardening (cold-drawing) were investigated for controlling further the mechanical properties, crystallinity and β-phase content. Mechanical and structural scaffold properties were evaluated by tensile tests SEM inspection. Crystallinity was evaluated using FTIR and DSC.

In general thermal annealing (over Tc temperature 132ºC for 2h) resulted in highly crystalline samples (>70% as shown in chapter 2). The increase in crystallinity after annealing originates from increased γ-phase (15% on annealed samples compared to 1% on as-spun samples). However, under SEM visualisation, it was noticed that thermal annealing resulted in the loss of fibre organisation and introduced defects on the structure (in the form of cracks) due to thermal expansion coefficient changes between crystalline and amorphous phases. It was obtained that annealing at 90ºC for 1 hour during fibronectin functionalization process was a good compromise. Higher annealing temperatures (i.e.110 to 135) had a negative impact on essential characteristics of the samples (fibre organisation and surface morphology, increased brittleness) for the indented tissue engineering (decreased porosity as fibre start forming more mesoscale and macroscale joints between the fibres as seen in Figure 17 and the total volume of scaffold was reduced by 30%). Interestingly, despite no significant difference in crystallinity level was observed between stretched and the as-spun samples, mechanical properties such as stiffness was significantly improved. As shown in Figure 4-39 the organisation of fibres is dramatically enhanced.

Based on the initial properties of the scaffolds (45 % maximum elongation), we decided to perform drawing at 12% and 20% to induce stress-hardening through plastic deformation of the scaffolds.

a)   b)
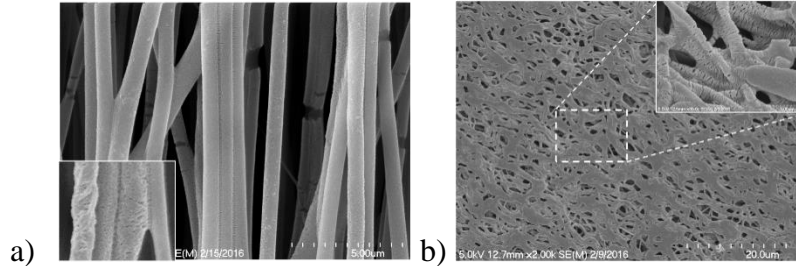
Figure 4-18. SEM images representing negatives structural changes including cracks (a) or reduced porosity (b) when a) annealing at 120ºC or b) 135ºC for 2 hours.

a)   b)
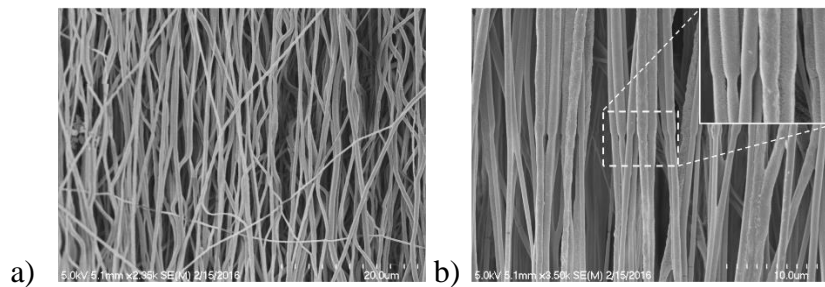
Figure 4-19. Representative SEM images showing effects on fibre organisation when a) using long distance (>20 cm) between needle and syringe during electrospinning. b) Cold-drawing post long distance electrospinning results in narrowed nanofibres and the significant increase in alignment and mechanical properties.

The diameter of fibres was reduced from 540 nm to 490 nm after cold drawing at 20% strain and from 540 to 516 nm after cold drawing at 12 % strain. The reduction in fibre diameter can be calculated from the following equation:

$$V_o = \pi.l_o.d_{o2}/A \hspace{4cm} \text{Equation 4-6}$$

Therefore, considering the volume constant and an elongation of 20%, we obtain that the reduction coefficient was 0.91 and the fibre diameter was $d = (0.91) d_o$ corresponding to 492 nm. For 12% the reduction coefficient was 0.95, resulting in d= 513 nm. Stretching resulted overall in a better alignment of fibres (from 65% to 98%) and a small reduction on

fibre diameter. I was also noticed that cold drawing resulted in typical fibre necking that might have different mechanical behaviour and might act as a stress concentrator. Therefore a minimum of 12 % cold drawing was chosen.

a)

b)
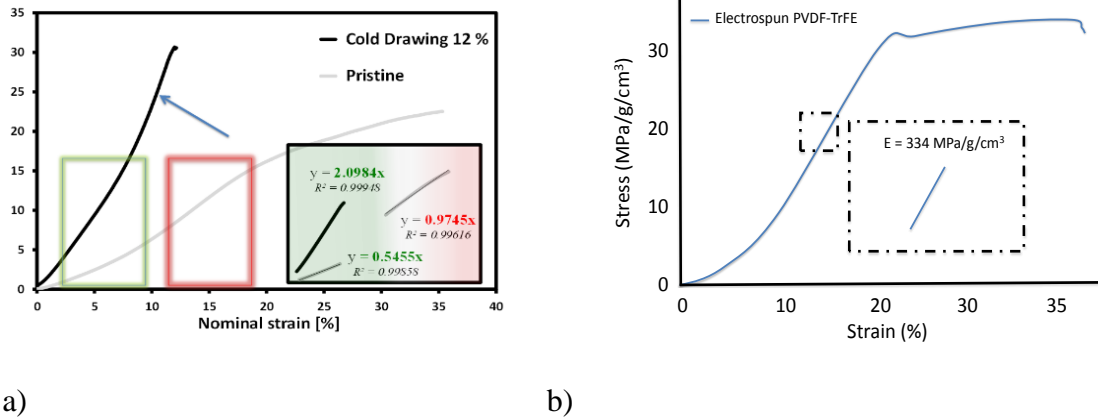
Figure 4-20. Effect of a post-long-distance electrospinning cold drawing (a) or short distance electrospinning (b) on mechanical properties. a) Real strain-stress curves for samples before and after cold drawing at 12% resulting in higher young modulus at elongation break cost. b) Strain-stress curve for typical short distance electrospun scaffold that underwent orientation strengthening.

The elastic modulus was measured after 12% cold drawing and corresponded to 334 MPa /gr/cm^2. However, an increase in the scaffold mechanical strength (30 MPa/g/cm^2) and elasticity was at the cost of toughness that was reduced from 24 J/gr to 15 J/gr (see Figure 4-20).

Above all, the most significant effect of cold drawing was the increase of elastic behaviour and reduction against stress relation/creep. It is well known that a common problem of the electrospun scaffolds is stress relaxation. Under repetitive mechanical loading, electrospun samples tend to readjust their disorganised structure to better comply with the mechanical challenge resulting in changes on stress at fixed cyclic strains (see Figure 4-21). Given the above, cold drawing is an essential step to consider when using electrospun scaffolds under repetitive mechanical loading conditions.
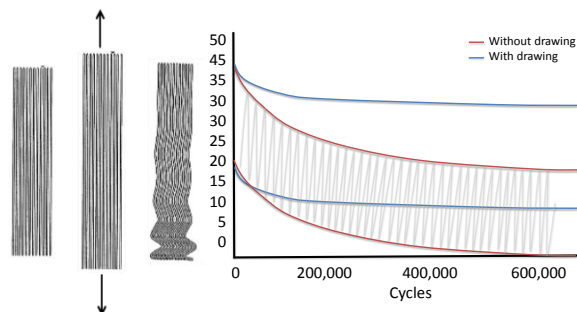
Figure 4-21. Effect of cold drawing in stress relation. a) Schematic of the effect of cyclic loading of electrospun scaffolds. As a result of loading the entangled fibres tend to align increasing the overall length of the scaffold and reducing the experienced stress over the time b) Stress measurement of scaffolds after 600,000 loading cycles (corresponding to the equivalent of applying strain cycles 8 hours/day for 20 days at 1 Hz). Stress relaxation is significantly reduced after cold drawing.

4.3.2   Fabrication of aligned PTFE nanofibres non-piezoelectric scaffolds

This chapter aimed to unravel the difference between mechanical and electromechanically stimulation on the cellular response of human tenocytes. Therefore, to uncouple the effect of mechanical loading, it is necessary to use non-piezoelectric scaffolds. Moreover, it is vital to maintain all the rest of physical variables including fibrous structure, mechanical properties and chemistry constant.

In this thesis project, a copolymer of PVDF, poly (vinylidene fluoride-co-trifluoroethylene) (P(VDF-TrFE)) is compared against a highly non-piezoelectric polymer poly(tetrafluoroethylene) (PTFE) both highly fluorinated polymers (See Figure 4-22 for the chemical structure of both polymers). PVDF-TrFE chemical structure $-(CH_2-CF_2)_n$ lies in between polyethene (PE) $-(CH_2-CH_2)_n-$ and PTFE $-(CF_2-CF_2)_n-$ structures. Further, PTFE is non-piezoelectric due to the presence of a centrosymmetric structure and C-F polar covalent bonds. Unlike PTFE, PVDF-TrFE has a non-centrosymmetric and dipoles generated by the high electronegative difference between Hydrogen and Fluorine atoms. One major of their distinct chemical structures is the change of C-C chain flexibility. PE has a planar zigzag conformation offering high flexibility to the structure.

On the other hand, PTFE offers some stereochemical constraint. In crystal form, the chemical conformation of PTFE always results in a helix whereas in PVDF-TrFE due to the ability of chain rotation it sometimes forms helices from the planar zigzag. To attain piezoelectric behaviour, chain rotation for dipole orientation to achieve inherent dipole moment is essential. Also, the partial charges between the Carbon and Fluorine atoms ($C^{\partial+}$—$F^{\partial-}$) attract, generating the 'strongest bond in organic chemistry' (100kcal mol^{-1} bond strength)[313]. For these reasons PTFE is exceptionally chemically stable and exhibits <u>no piezoelectric effect</u>.

a)   PVDF   TrFE
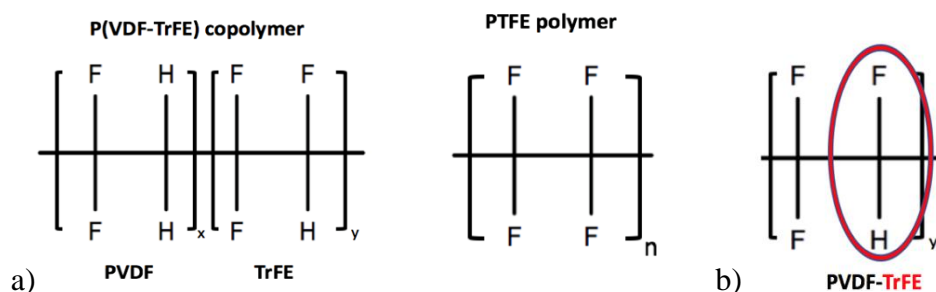
b)   PVDF-TrFE

Figure 4-22 a) Schematic of the molecular structure of P(VDF-TrFE) copolymer and PTFE polymer. Note the structure of PTFE with four polar covalent Carbon—Fluorine bonds making it extremely stable and therefore Non-Piezoelectric. b) Within the P(VDF-TrFE) copolymer, the -TrFE component exhibits a strong dipole across the Hydrogen to Fluorine bond (red circle).

Unfortunately, also for the reasons mentioned above, direct electrospinning of PTFE is not possible. Basically, due to the strong C-F bond (melting point of 327ºC), dissolving PTFE and obtain a conductive polymeric solution using an organic solvent is not possible. PTFE is a high-molecular-weight polymer, and the only practical solvent would be a low molecular weight polymer of itself such as a perfluorinated solvent (PFC) containing only C-F bonds and C-H bonds.

In this study, a two-step process to obtain electrospun PTFE scaffolds was used. First, a stable dispersion (surfactant content 7.2% wt %) of 160 nm PTFE particles (62 wt%, pH 10.5) was electrospun in combination with a fibre forming agent such as polyethene oxide (PEO). Importantly, an average molecular weight of PEO (300,000 MW) showed better

results than higher molecular PEO (1,000,000 MW). An optimisation process of the PTFE:PEO ratio for the generation of electrospun fibres was performed. High-quality and continuous PTFE nanofibres were obtained using a ratio between 0.01 and 0.05 (the viscosity was lower than 10 Poise) and increasing the ratio results in larger fibre diameter being the range 690 to 1720 nm.

Further reduction of diameter can be achieved by incorporating salt into the solution (normally KCl at 1% w/w), but the organisation of fibres is also decreased. In a typical experiment, 260 mg PEO into 10 ml of PVDF-TrFE (60 % w /v) aqueous solution was employed. Prior, electrospinning, the solution was homogenized for 2 hours in a water-saturated atmosphere (> 80% humidity) using a high-viscosity mixer at low speed. After mixing, the solution was centrifuged for 5 min at 100-200 g to eliminate air bubbles and filtered (0.75 -1 µm) to eliminate any precipitate or inhomogeneity and generate a uniform solution. The final solution was then loaded into a 10 ml syringe (Luer Lock®) with a 27G needle and placed into a pump set at 1 ml/hr for electrospinning.

Moreover, lower flow rates were used to decrease fibre diameter. Finally, a distance between needle and syringe was set to 12-15cm cm, and the collector was restricted to a size of 10 cm long to concentrate the electrical field enough to obtain high alignment of the fibres. Also, the collector consisted of a mandrel (8 cm diameter) that rotates at 2000 rpm (max). If the rotation was higher, the fibres would break due to their lack of cohesiveness. Finally, the positive side of the DC power supply was connected to the needle and the negative to the collector. The needle was then charged with 7-10 kV and the collector with -5kV generating a 12-15 kV voltage difference and the experiment run for 4 to 5 hours The most optimal results during electrospinning were obtained at humidity levels not superior to 50-60%. The level of fibre alignment in these conditions was always superior to 90%.

In a second step, the scaffolds were annealed at a temperature beyond the melting point so the PTFE particles can sinter together and PEO will carbonise resulting in smooth PTFE fibres.
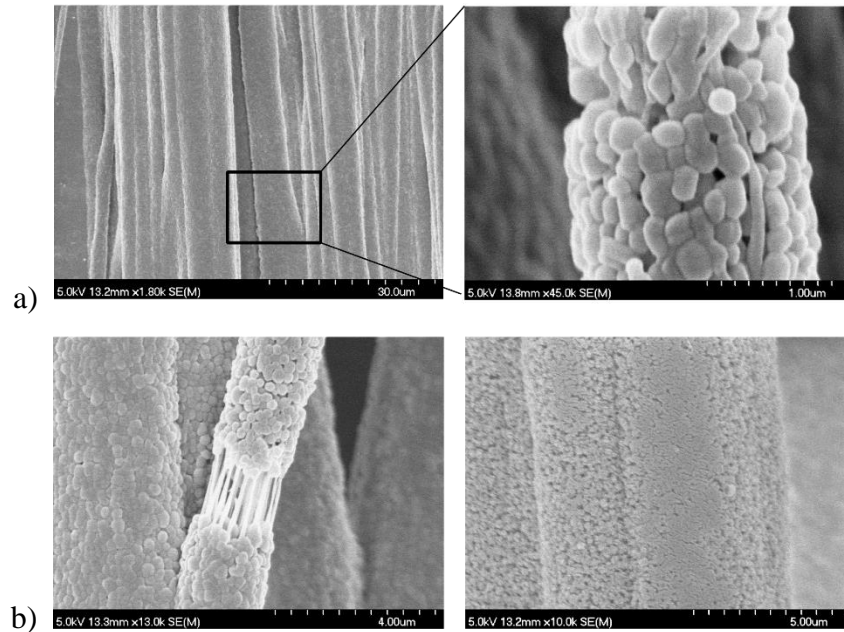
Figure 4-23. SEM images of electrospun PTFE: PEO scaffolds during the optimisation of the annealing temperature for PTFE scaffolds. a) Results obtained at temperatures below 385ºC (i.e. 360ºC). It is noticed that particles warped and fused around the PEO to form pristine PTFE fibres as sintering temperature increases.

In order to obtain robust and uniform fibres, further optimisation of the sintering temperature was performed. It was observed, that to obtain completely fused and smooth continuous fibres, a sintering temperature of 285 ºC was needed. Sintering at temperatures below that point, resulted in insufficient melting and flow of PTFE particles to confirm a uniform fibre (see Figure 4-23). The sintering process was done in two steps, a) during the first step samples were heated at 10ºC/min until 350ºC and maintained at this temperature for 5 min (to minimize effects generation during shrinkage of the fibres) and b) finally samples were subsequently heated to 385ºC at 10 ªC/min and maintained at this temperature for at least 5 min. PTFE particles start melting resulting in shrinkage and PEO decomposes and the result is a significant change in the thickness and length of the scaffold (up to 60 %). A critical action that is required to avoid fibre ruptures during shrinkage is to allow the scaffold to relax and be contracted to counterbalance the posterior shrinkage. Also, hardening of the fibres was carried out by drying the scaffold for 12 to 24 hours at 70ºC. The scaffold was then removed and placed into a device that allowed contraction (up

to 50%) during sintering. Optionally the device had a tubular form to generate tubular shapes instead of a sheet as in Figure 4-24. Finally, the total removal of PEO was confirmed using DSC, and the overall physical and chemical properties of the scaffold was measured using FTIR, XRD and mechanical properties testing.

For facilitating cell, attachment is it is essential that the surface might be partially wettable by water and allow protein adsorption. However, PTFE is highly hydrophobic. For this reason, a necessary step to change the surface energy was used. A method of increasing hydrophilicity is to graft highly hydrophilic groups of acrylic acid on the surface. Briefly, the surfaces were treated with oxygen plasma for at least 45 min. After plasma treatment, the hydrophobicity is increased due to a superimposed nanoscale roughness, but hydro peroxidase groups are formed on the surface. Immediately after plasma treatment, samples were immersed in methanol for 2 min to wet the surface and transfer into an aqueous solution of acrylic acid (20 % w/w) for 20 min at 90°C using under reflux. After the process, a thin nanometric layer of polyacrylic acid is formed. Samples are then kept immersed in a solution with NaCl 0.9 % to preserve the layer.
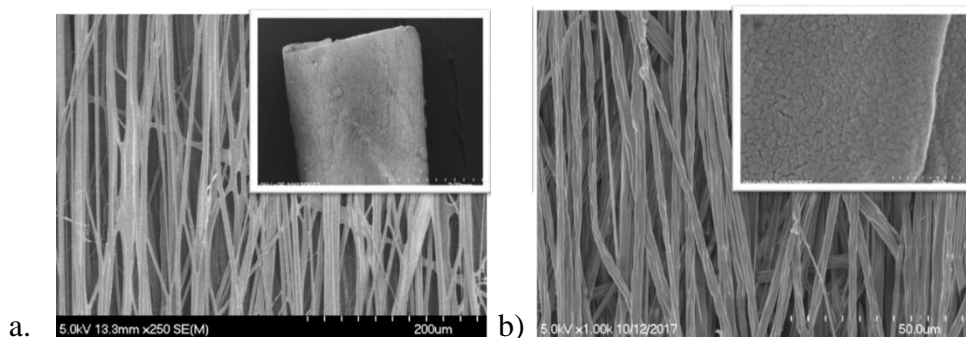
Figure 4-24. a) SEM images showing the structure and conduit formation after sintering using a tubular solid for generating the conduit. b) SEM image showing the structure and surface changes after plasma after 45 min of continuous plasma.
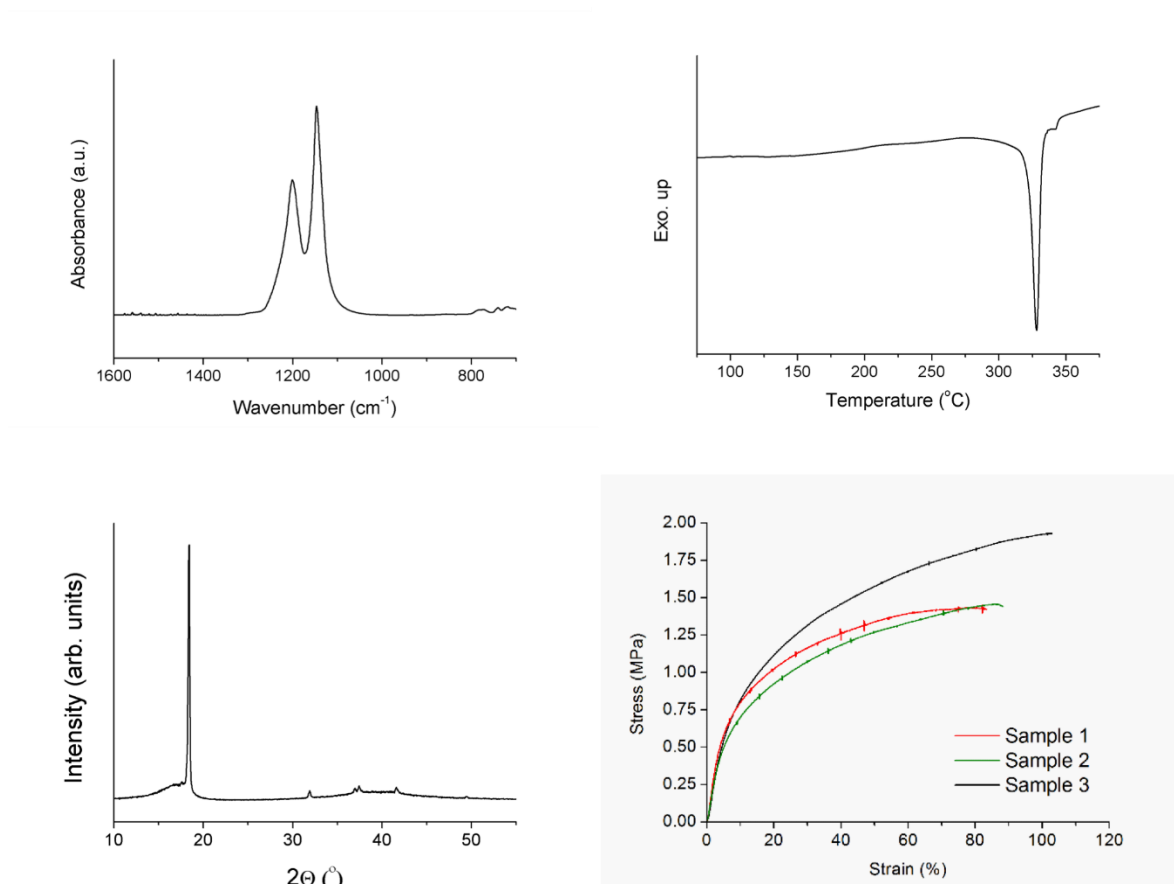
Figure 4-25. Physical properties of electrospun PTFE. a) FTIR spectrum of electrospun PTFE scaffolds showing the bands (1205 and 1145 cm^{-1}) associated with symmetrical and anti-symmetrical stretching modes of the C-F bond in the -CF$_2$- unit. b) DSC curve of PTFE scaffold showing the melting point at T=327ºC. c) X-ray diffraction spectra of PTFE scaffold. It shows the typical peak at 2θ=18.2º, and the amorphous phase appears as a shoulder. d) Tensile test showing the mechanical properties of the scaffold characterised by elongation break superior to 90% and tensile strength ranging from 1.35 to 2 MPa.

As observed in Figure 4-25, DSC measurements showed a clear single peak of a highly crystalline phase (ΔXc= 61.1 %, PTFE). FTIR and XRD measurements further confirmed the PEO removal. After sintering, only peaks at 1201 and 1145 cm^{-1} in the FTIR spectra corresponding to C-F bonds from PTFE were obtained. XRD measurements showed four peaks, a unique dominant peak at 18.2 and peaks at 31.8, 37.1 and 42.2 that correspond to the same fingerprint of pure PTFE powder. Mechanical properties obtained are shown in

Table 4-4, the low mechanical ultimate strength obtained does not correspond to values in the literature it can be attributed to defects presents in the fibres due to PEO decomposition.

Table 4-4. Mechanical properties of PTFE scaffolds.

Elastic Modulus	Tensile Strength	Elongation
14.5 ± 1.7 MPa	1.6 ± 0.3 MPa	91.3 ± 10.4 %

4.3.3 Electromechanical performance of scaffolds.

Tendons have a great ability to respond to mechanical forces by adapting their structure and composition. Cyclic mechanical stretching (progressive rehabilitation) of the tendon is an excellent and recognised method for treating tendon-related injuries and benefits tendon health. Nevertheless, excessive loading can lead to tendon overuse injuries. The Figure 4-26 shows how a specific range of mechanical strain (4 to 6% strain) can trigger an anabolic (A) response in healthy tendon tissue whereas excessive loading (>6% strain) results in a dramatic catabolic reaction (C). Several biomechanical studies have confirmed that tendon is subjected to 3-4 % strain during normal activities[314–317]
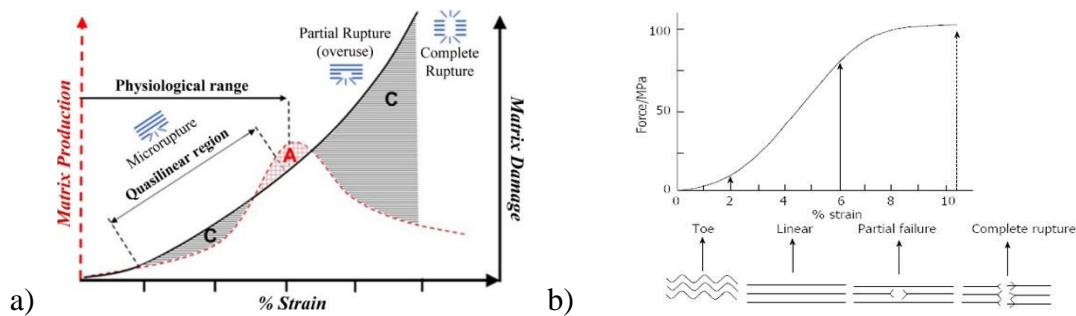
Figure 4-26. a) Matrix production-damage and b) Stress-strain relationships for progressive loading of the tendon. The graphs show four distinct regions namely 1) toe 2) quasilinear/linear 3) partial/micro rupture and 4) complete rupture. It is shown approximate strain and stress for anabolic (4-5%) and catabolic responses (1-3 and >6% strain) [318].

In vitro, it has widely been demonstrated that tendon cells are sensitive to mechanical loading and often leads to increased gene expression, protein synthesis and mitogenesis through activation of mechanotransductive processes[254,257,319–323]. Strain rates (loading

311

frequency) are also important in modulating the cellular response. In physiological conditions, strain rate is around 0.1- 0.5 Hz; however, during intense activity the frequency can be as high as 10 Hz.

Piezoelectric systems can also have frequency-modulated performance (output charge) due to the frequency dependence of the elasto/piezoelectric constants. Therefore, in this study, we have studied the effect of strain rate/frequency (0.5, 1 and 2 Hz) whereas the total amplitude was fixed to a physiologically relevant magnitude of 4% strain.
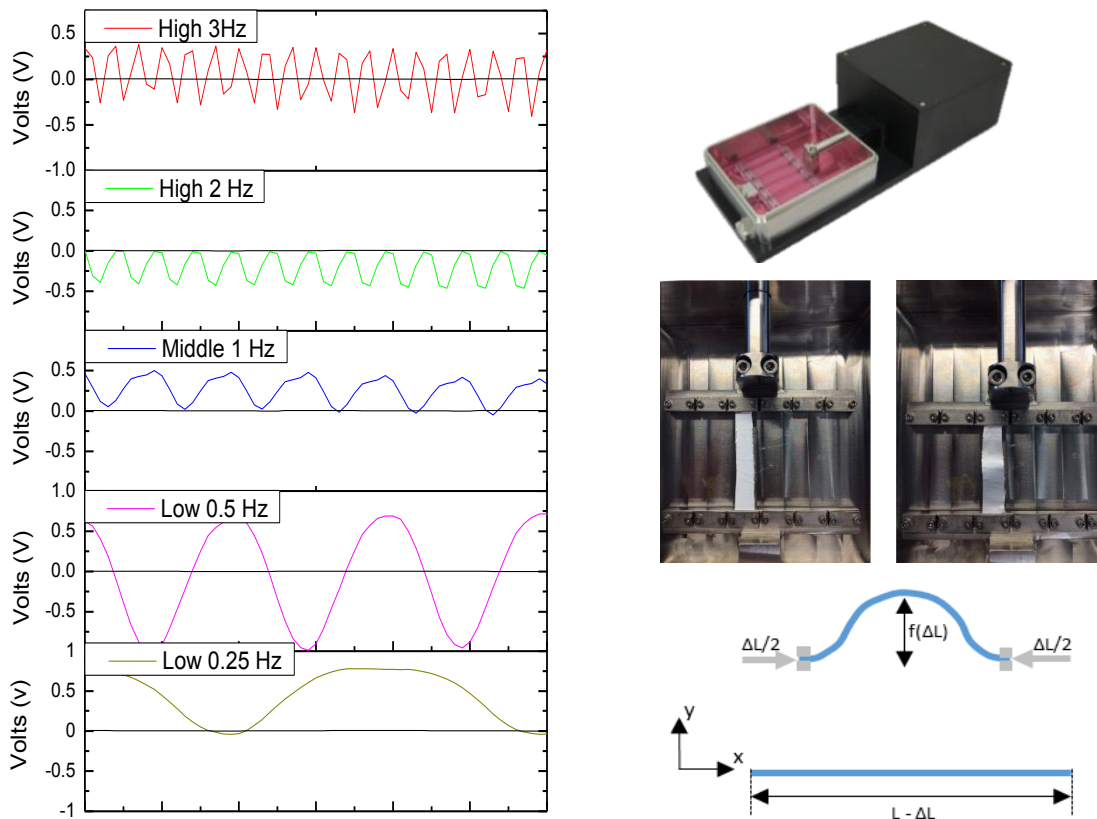
Figure 4-27. a) Voltage measurements as a function of frequency using an electrometer at a constant amplitude of 4% strain. PTFE is shown to have no piezoelectric behavior. (black line). b) Overview of the mechanical loading system used to measure voltage output and for *in vitro* studies.
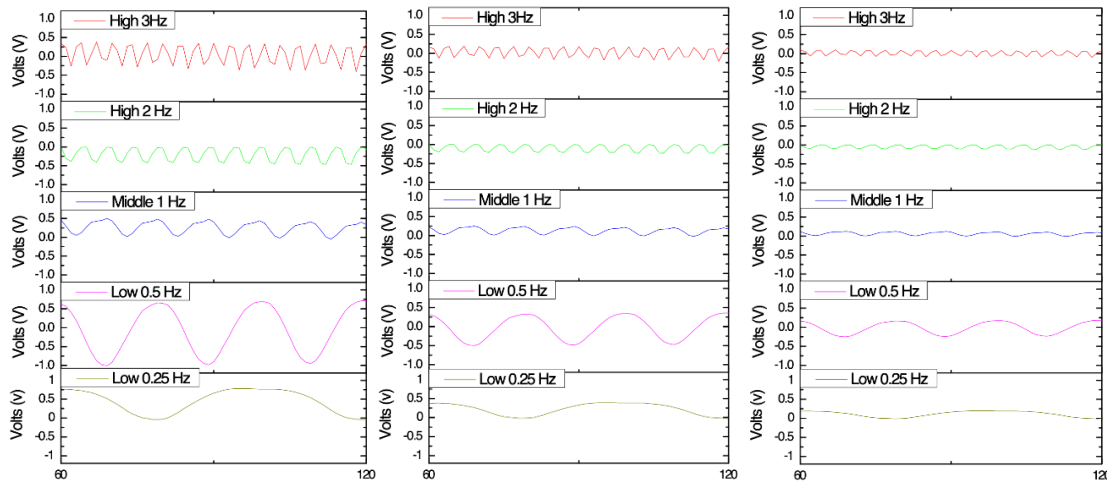
Figure 4-28. a) Voltage measurements as a function of frequency/strain rate and amplitude (2 mm, 1mm, 0.5 mm) using an Electrometer.

It was observed (Figure 4-27) that concerning all the investigated frequencies, the range of voltage output was 0.51 – 1.21 V. Furthermore, stability analysis of up to 500 cycles of continuous dynamic strain did not reveal any significant changes to this output. To demonstrate piezoelectric behavior linear relationship between amplitude and electrical response was also assessed (Figure 4-28).

4.3.4 Optimization of mechanical loading conditions for elicited tendon-derived cell response.

Cells were seeded onto aligned and randomly (non-aligned) scaffolds and alignment of cells by contact guidance was assessed after 1, 3 and 7 days (Figure 4-29).
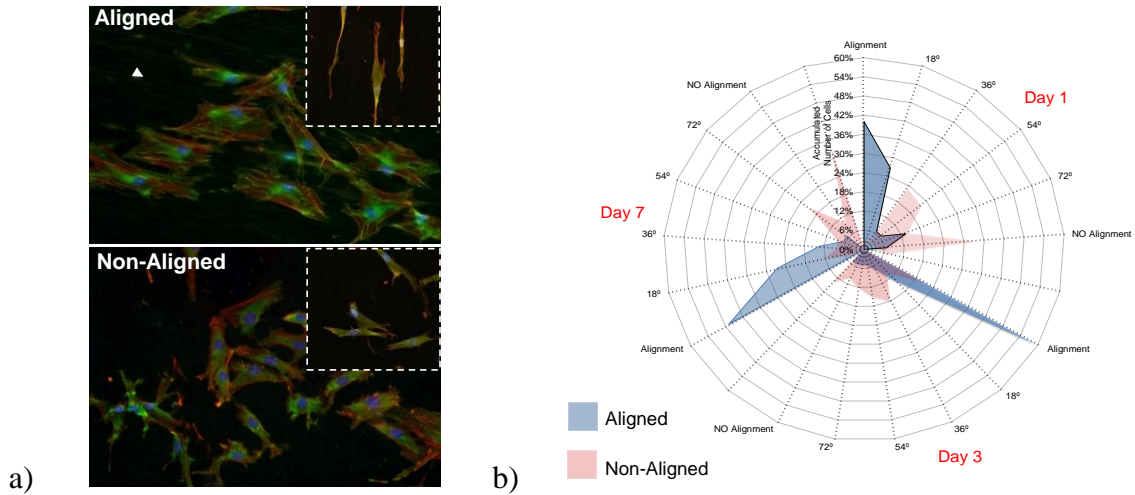
Figure 4-29. Alignment and morphological characterisation of tenocytes on scaffolds showing different fibre organisation (aligned or non-aligned). a) Stained tenocytes for vinculin (red), actin (green) and nucleus (blue) showing different morphologies (elongated or rounded) at day 1 and day 7 (magnification). b) Angle distributions radar chart showing percentage level of alignment of cells. The angle of cell is shown relative to fibre direction (0º and 90º correspond to alignment and no alignment of cells, respectively) at day 1, 3 and 7.

UniMechanoCulture T6 (CellScale®): Axial Mechanical Loading

Material preparation:
PTFE
PVDF-TrFE
12% cold drawing
O_2 Plasma + 90ºC (PAAc) + EDC/NHS + Fn
Mechanical loading conditions:
0 - 4% (2mm) stretch
0 - 0.5,1,2 Hz
Cell culture : (N=6)
7.500 cells/cm^2
24h attachment
2 different human donors (age 63 & 66)
(markers: CD90+/CD29+ ; CD45-/CD31-)
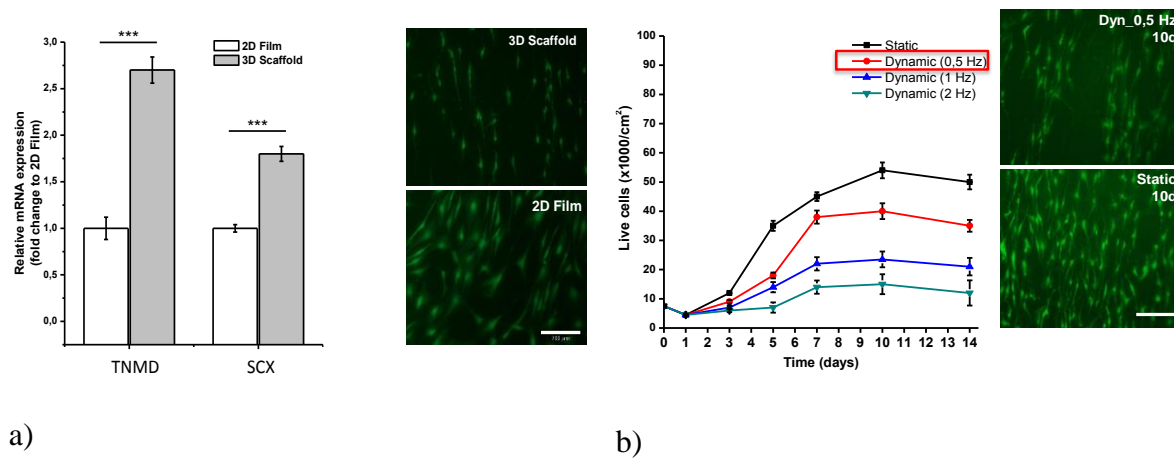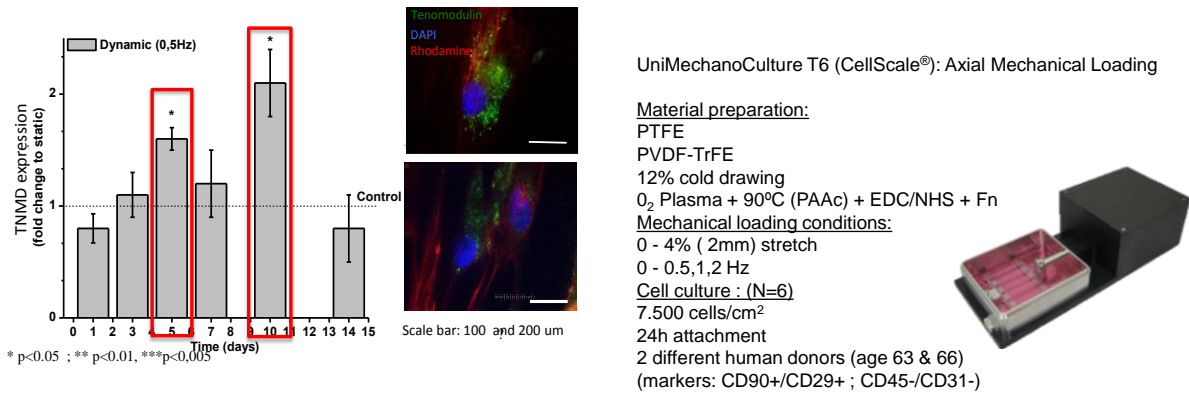
c)   d)

Figure 4-30. Biological *in vitro* characterisation of human tenocytes seeded on scaffolds under static and dynamic conditions. a) Effect of morphological cues on tenocyte function. Cells show a modulated cell response depending on their morphology. b) The proliferation of tenocytes on piezoelectric scaffolds under dynamic stimulation at different strain rates (0.5, 1 and 2Hz compared to static conditions c) Effect of dynamic stimulation of piezoelectric scaffolds on tenocytes. It is shown an increase of TNMD expression at days 5 and 10. d) Cell culture conditions. Dedifferentiated tenocytes restore their phenotype under mechanical stimulation and piezoelectric stimulation induced immediate up-regulation of tendon-related genes.
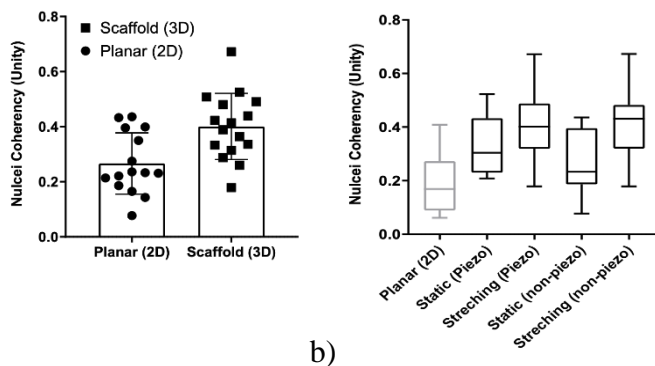
a)   b)

Figure 4-31. a) Comparison between planar and fibrous (aligned fibres) morphologies on nuclei coherency (aspect ratio/deformation) and b) Comparison between static and dynamic (stretched 4%) cultures of tenocytes using piezoelectric and non-piezoelectric scaffolds on nuclei coherency (aspect ratio/deformation).

Tenomodulin expression (TNMD) was used to optimise the stretching loading conditions for maintenance of tenocyte phenotype before in-depth genomic analysis. TNMD is a glycoprotein that regulates tenocyte proliferation and ECM production and SCX, its transcription factor, was initially assessed in vitro under static conditions (see Figure 27 a). It was observed that tenocytes that lost their elongated morphology underwent significant down-regulation in TNMD and SCX expression when cultured on 2D planar films. On the other hand, when tenocytes were cultured on 3D electrospun scaffolds, they maintained a spindle-like morphology (see Figure 4-32), nuclear deformation (see Figure 4-31) and demonstrated increased expression of TNMD and SCX relative to planar 2D films. Thus, through modulated morphology cells exhibited differential function.
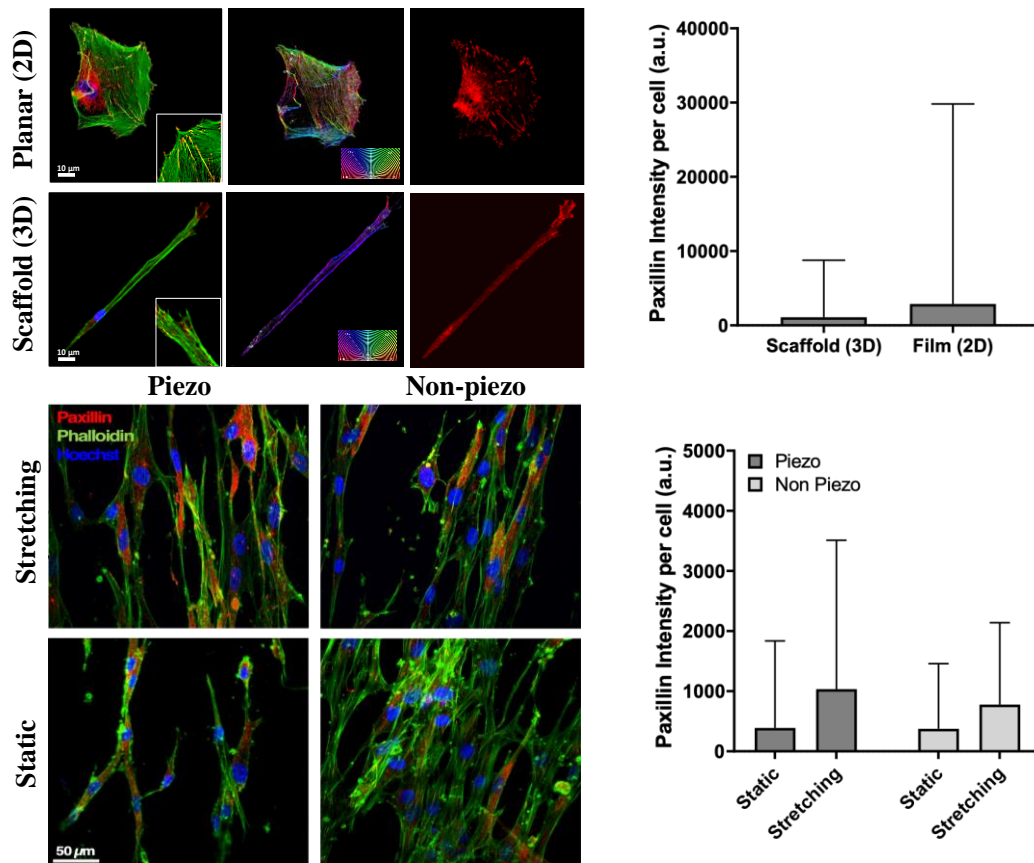
Figure 4-32. Paxillin intensity per cell on a) Static and b) dynamic (stretched 4%) cultures of human tenocytes.

Under continuous mechanical stimulation of scaffolds, it was observed that cell proliferation was reduced and proportional to the loading frequency. A final stimulation

frequency of 0.5 Hz was chosen based on an analysis of cell survival under dynamic conditions (see Figure 27c). Finally, expression of TNMD in tenocyte cells in static or dynamic conditions over time was evaluated. An upregulation of TNMD was indicated in cells under continuous EM stimulation, with highest expression levels obtained at day 5 and day 10. Focal adhesion paxillin was highly expressed when comparing EM and mechanical stimulation.

Following optimisation of mechanical loading condition through analysis of tenocyte morphology, viability and TNMD and SCX expression, genomic analysis of tendon cells cultured on piezoelectric PVDF-TrFE and non-piezoelectric PTFE scaffolds under both static (0Hz) and dynamic conditions (0,5 Hz, 4% strain) were performed in vitro.

4.4 The functional response of tenocytes to electromechanical stimulation via electrospun PVDF-TrFE scaffolds

A custom-made microarray was designed to assess the expression of genes associated with focal adhesion proteins, collagens, receptors (integrins, ion channels and growth factor receptors) and, inflammation and cell differentiation towards the bone, cartilage or tendon. Gene analysis was performed on cells cultured on non-piezoelectric and piezoelectric scaffolds under mechanical stimulation (0.5 Hz, 8 hours/day) at days 1, 5 and 10. Electromechanical stimulation induced a rapid and significant up-regulation of tendon-related genes in tenocytes cultured on PVDF-TrFE scaffolds following one day in culture. Whereas mechanical stimulation alone induced up-regulation of bone-related genes by day 1 in tenocytes cultured on non-non-piezoelectric PTFE scaffolds. However, by day ten bone-related genes were also up-regulated in tenocytes subjected to electromechanical stimulation on PVDF-TrFE scaffolds. These observations indicate possibly trans-differentiation of tenocytes towards an osteogenic/chondrogenic lineage mechanically loaded piezoelectric (PVDF-TrFE) and non-piezoelectric scaffolds (PTFE).
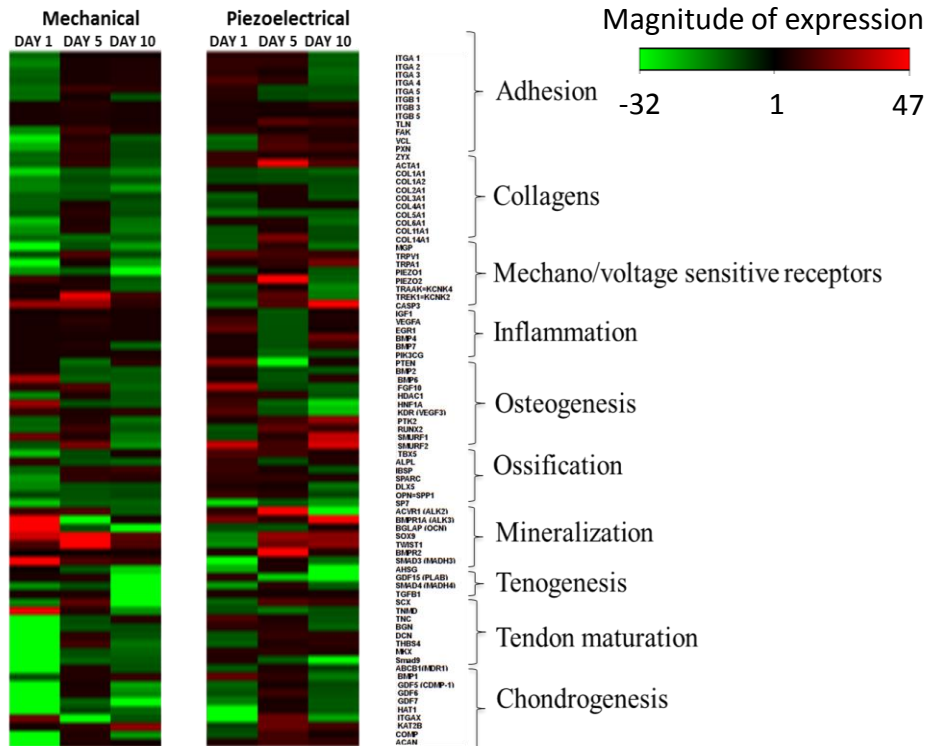
Figure 4-33. Heat map corresponding to the expression of genes associated with cell adhesion, collagen isoform synthesis, mechano/voltage receptors, inflammation, osteogenesis, ossification, mineralisation, tenogenesis, tendon maturation and chondrogenesis in tenocytes under mechanical or piezoelectrical stimulation.

The best-studied mediator of tendon function is Scleraxis (Scx), a helix-loop-helix transcription factor. In mice, genetic loss of scleraxis (Scx) disrupts tenocytes differentiation and leads to loss of Col1a1, Col14a1 and Tnmd in tendons and consequently, tendon formation is impaired. Similarly, transcription factors Mohawk and Egr1 have also been shown to be necessary for Col1a1 transcription in developing and adult mouse tendons.

Analysis of gene expression correlated well with the results observed at the protein level (see Figure 4-33). SCX and MKX were upregulated at days 5 and 10 and are involved in collagen synthesis and fibrillogenesis. Collagens, predominantly Col1a, constitute the bulk of mature mammalian tendon ECM. Collagen I, III and IV were also upregulated at days 5 and ten under electromechanical stimulation (see Figure 4-34).
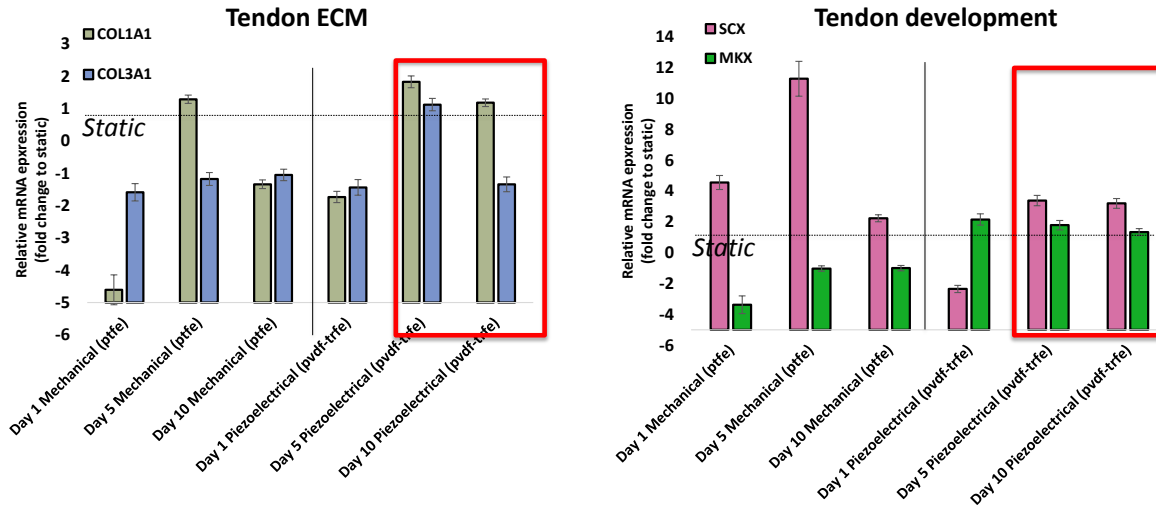
Figure 4-34. Relative expression of genes associated with tendon ECM and development at days 1, 5 and 10 for mechanical and piezoelectrical stimulation.

Analysis of custom made gene array data yielded significant alterations in broad functional signalling pathways in human tenocytes. Canonical signalling pathways with the greatest number of modulated gene expression were associated with piezoelectric stimulation at day 10 (see Figure 4-35) .
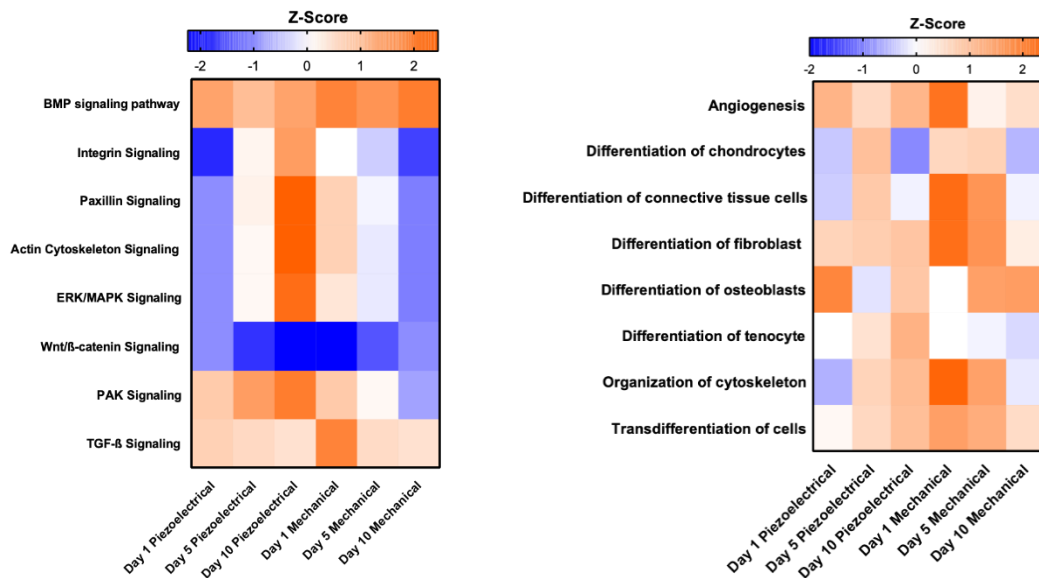
a)
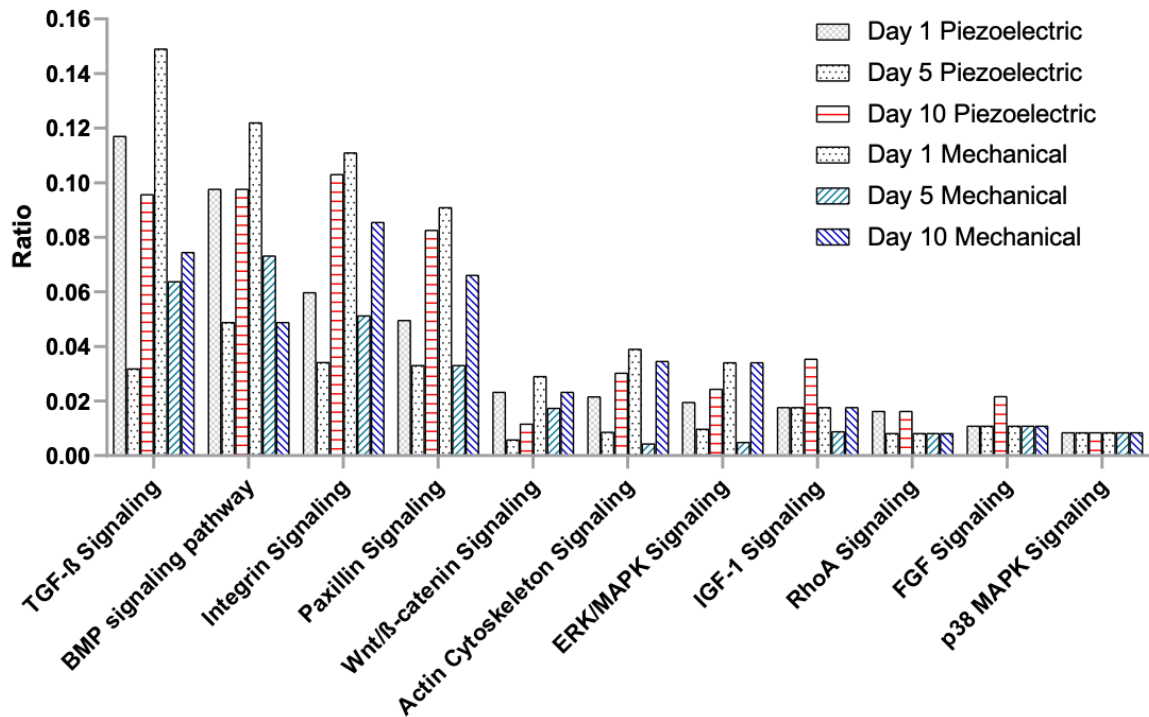
b)

Figure 4-35. a) Signalling pathway analysis of human tenocytes under mechanical and electromechanical stimulation. Tenocytes cultured under piezoelectric stimulation were associated with significant changes in gene expression and function. b) Which could be classed into broad biological pathways. Ingenuity Pathway Analysis (IPA, Ingenuity Systems) identified several canonical signalling pathways related to cell adhesion, which were up-regulated at day 1 and 5 under electromechanical stimulation.

BMP signalling was consistently activated thought both types of stimulation; however, it was significantly more intense for mechanical loading at days 1 and 10. Similarly, higher activation of differentiation of osteoblast and Wnt/β-Catenin signalling pathways were attributed to mechanical activation at day 5 and 10. However, under electromechanical stimulation osteoblast differentiation was deactivated at day 5. Interestingly, differentiation of tenocyte was activated at day 10 for electromechanical stimulation whereas for mechanical stimulation it was deactivated. Further, at this specific time point, different pathways showed significant differential activation. Pathways ERK/MAPK, PAK, Integrin

and actin cytoskeleton signalling pathways were upregulated during electromechanical stimulation and downregulated during mechanical stimulation.

4.4.1 Ion channel signalling

Ingenuity Pathway Analysis (IPA, Ingenuity Systems) was used to determine protein-protein interactions and a functional network with differentially regulated genes associated with cellular differentiation function was obtained. The network included the recently discovered mechanosensitive membrane mechanoreceptors and voltage-gated receptors. Critically, ion channel expression was evaluated, and increased expression of Piezo 1 and 2 under electromechanical stimulation was observed.

Under mechanical stimulation, the regulated expression of genes via mechanosensitive receptors and activation cartilage/bone formation showed a strong correlation. In contrast, under EM stimulation, the regulation of gene expression through piezosensitive receptors was associated with differentiation towards tenocyte. However, piezoelectric control of cell function also resulted in a significant upregulation of important bone transcription factors such as RUNX2 and BMP2 proteins. Therefore, piezoelectric control of gene expression might activate both bone and tendon related signalling pathways.

The main distinct regulatory effect was associated with the differential expression of Piezo 1&2, TRPA1 and KNCK4 ion channels. Under mechanical stimulation, TRPA1 showed strong activation and regulated the expression of transcription factors SOX9, HDAC1 and SP7 that have a recognised role during osteogenesis processes. Alternatively, during EM stimulation the ion channels Piezo 1&2 and KCNK4 were significantly activated along with tendon-related transcription factors SCX and EGR1.
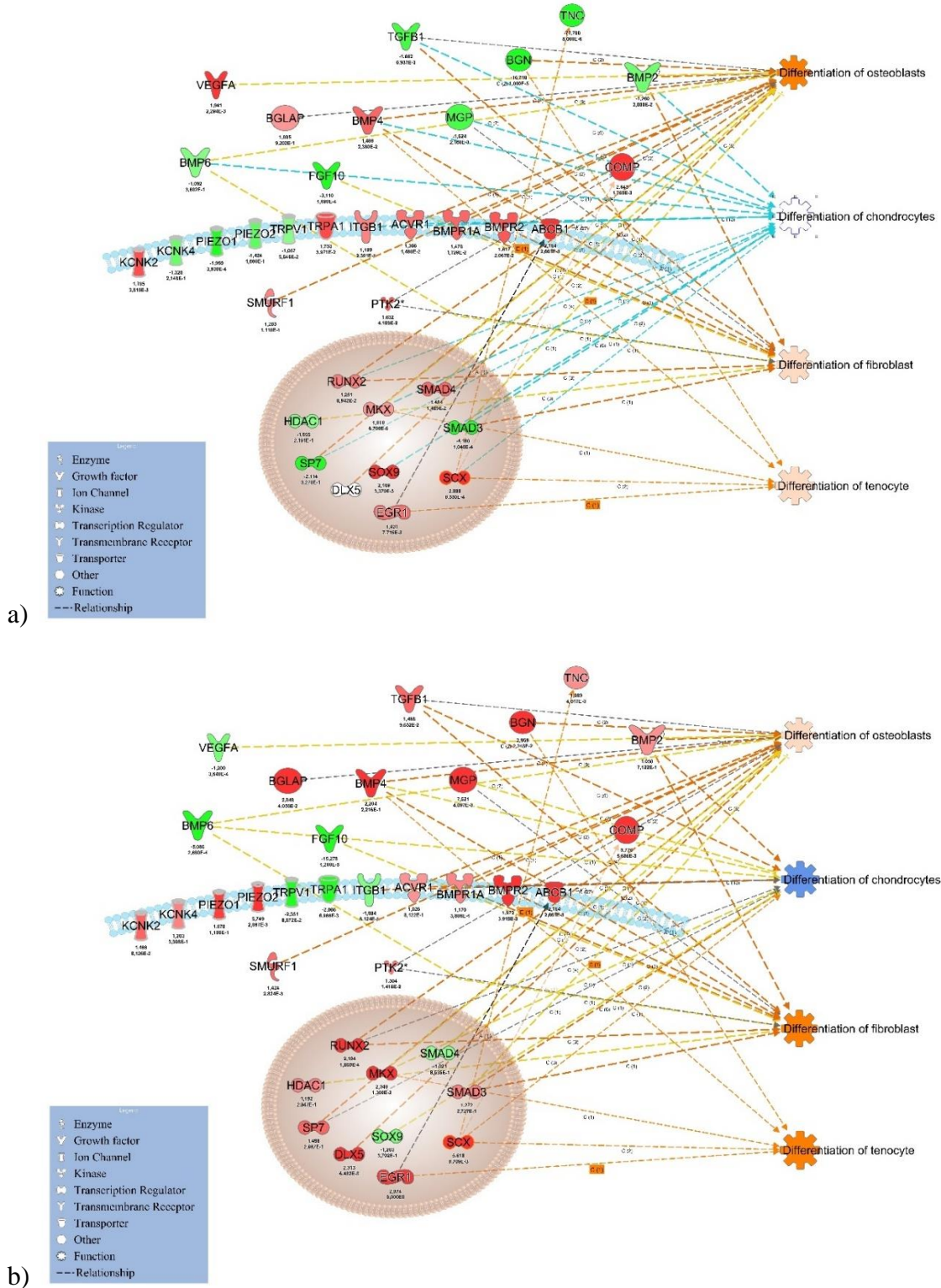
Figure 4-36. a) Mechanical and b) electromechanical (piezo) stimulation for 10 days induced modulated cell function including differentiation. Ingenuity pathway analysis identified a mechanistic network of 37 genes which underwent statistically significant

modulation. Network analysis of the identified genes: recently discovered mechanoreceptors Piezo1 and Piezo 2 indicated a positive correlation with changes in gene expression and increased tenospecific function.

4.4.2 Integrin signalling

Examination of integrin signalling revealed significant changes in gene expression in tenocytes cultured under mechanical and piezoelectric stimulation. Both stimulation types induced genetic modulation of approximately 8% of the genes involved in integrin signalling in human tenocytes.

Tenocytes subjected to mechanical stimulation exhibited down-regulations in integrin signalling pathways (see Figure 4-37), with exceptions observed in cytoskeleton rearrangement. In particular, down-regulation of vinculin (VCL) was prominent with mechanical stimulation as was the gene associated with the linker protein paxillin (PXN). Conversely, up-regulation of VCL and PXN were observed in tenocytes subjected to piezoelectric stimulation, initiating cytoskeleton rearrangement mediated transcription of tendon specific proteins.
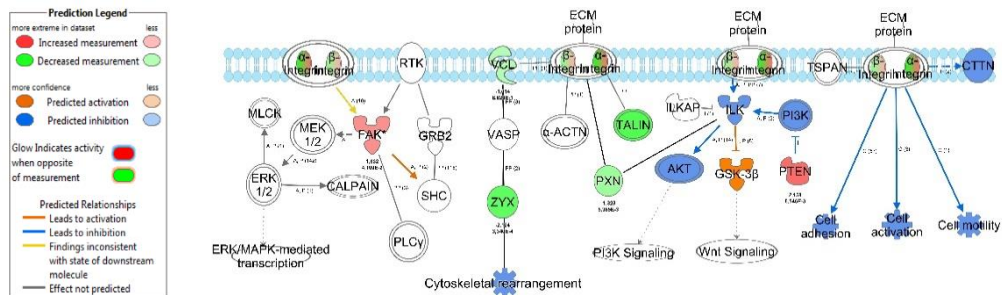
a)
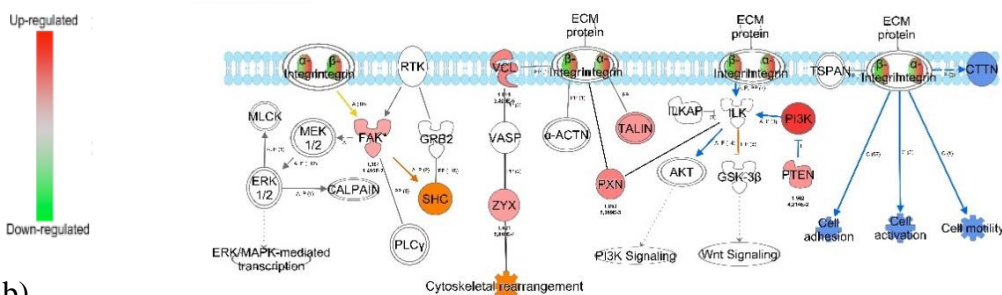
b)

Figure 4-37. Expression of genes involved in integrin signalling pathways were differentially regulated in tenocytes cultured under a) mechanical and b) piezoelectric stimulation at day 10. Red = Up-regulated, green = down-regulated, grey = no change, colourless = not tested, Orange = up-regulated (predicted) and Blue= Down-regulated (predicted).

4.4.3 Wnt/β -Catenin Signalling

Canonical pathway analysis of human tenocytes subjected to mechanical and electromechanical stimulation was correlated to significant modulation in genetic pathways linked to osteospecific transdifferentiation. Both stimulation types were associated with changes in approximately 4% of genes involved in Wnt/β-catenin signalling (see Figure 4-38). Specifically, tenocytes subjected to mechanical stimulation exhibited significant up-regulation in Wnt/β –Catenin, osteoblast differentiation and BMP signalling pathways.
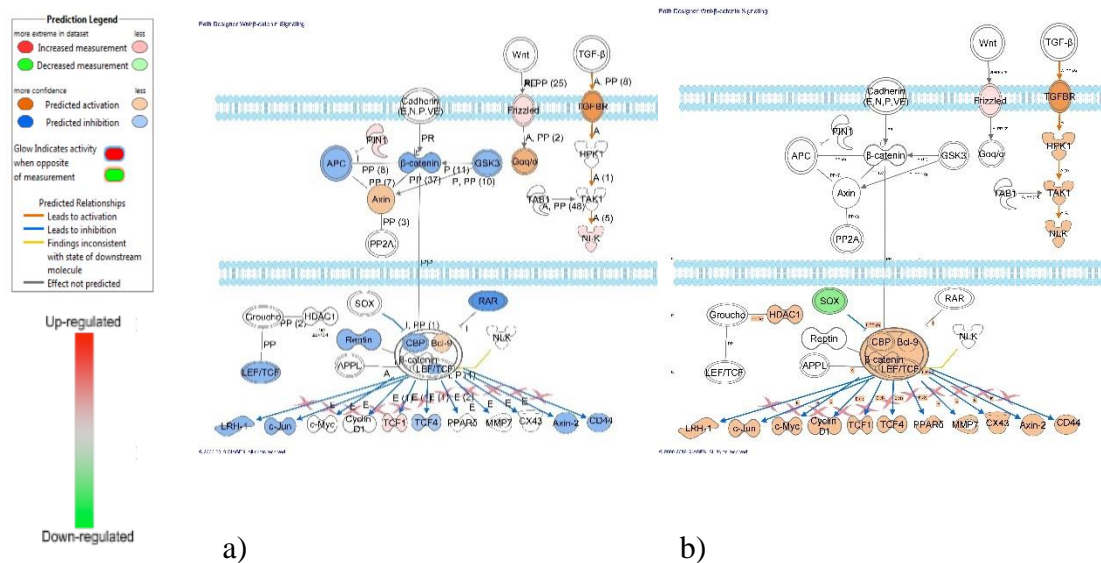
Figure 4-38. Modulation of Wnt/β-Catenin Signalling in human tenocytes under a) mechanical and b) piezoelectric stimulation at day 10. Expression of genes involved in Wnt/β-Catenin Signalling pathways was differentially regulated in tenocytes cultured under mechanical or piezoelectric stimulation. Red = Up-regulated, green = down-regulated, grey = no change, colourless = not tested, Blue= down-regulated (predicted) and Orange: up-regulated (predicted).

4.4.4 TGF-β /BMP Signalling

Canonical pathway analysis of human tenocytes cultured on experimental substrates was correlated to significant modulation in genetic pathways linked to osteospecific transdifferentiation. Both stimulation types were associated with changes in approximately 14% of genes involved in TGF-β /BMP signalling (see Figure 4-39). An in-depth examination of these modulations revealed significant down-regulation in gene expression in human tenocytes. Tenocytes cultured under mechanical (see A and B) and piezoelectric (see Figure 4-39 C and D) stimulation were both associated with increased transforming growth factor- β (TGF- β) expression, and multiple instances of down-regulated signalling molecule expression. An in-depth examination of these modulations revealed significant down-regulation in gene expression in human tenocytes. Tenocytes cultured under mechanical (see Figure 4-39 B) stimulation were both associated with increased transforming growth factor- β (TGF- β) expression, and multiple instances of down-regulated signalling molecule expression.

a)   b)

c)   d)
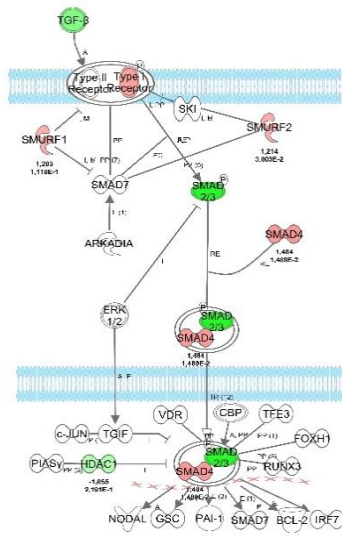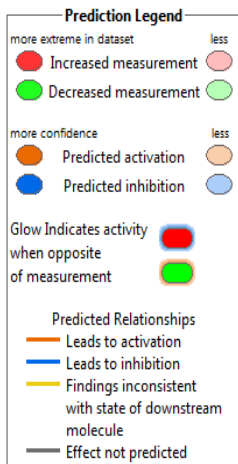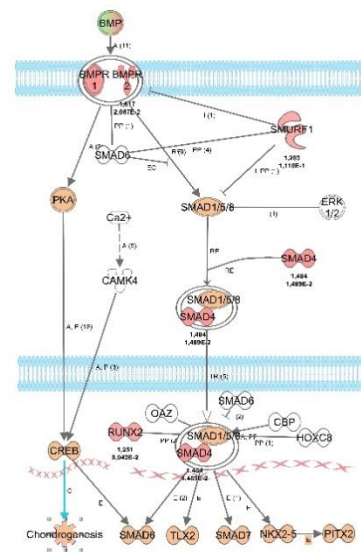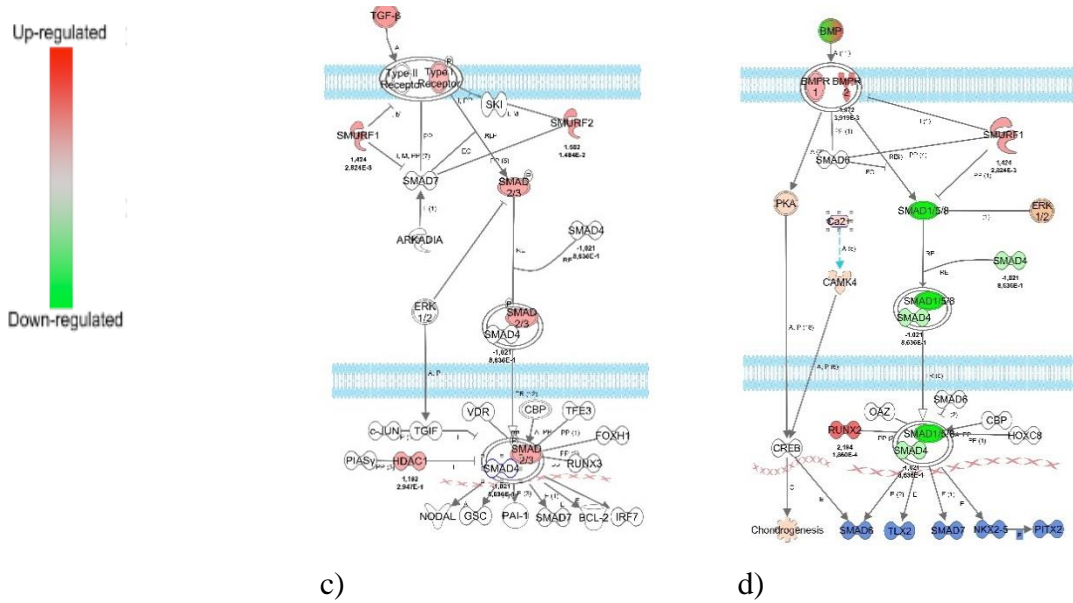
Figure 4-39. Modulation of TGF-β /BMP signalling in human tenocytes under mechanical (a and b, TGF and BMP signalling respectively) and piezoelectric (c and d, TGF and BMP signalling respectively) stimulation at day 10. Expression of genes were differentially regulated in tenocytes cultured under mechancial and piezoelectric stimulation. Red = Up-regulated, green = down-regulated, grey = no change, colourless = not tested.

4.5 Discussion

Aligned nanofibres P(VDF-TrFe) were electrospun onto a rotating collector to produce elastic piezoelectric scaffolds. DSC, tensile and SEM analysis showed that short distance electrospinning yielded high alignment at the micro and molecular level, thereby avoiding the need for post-treatment processes (i.e. electrical poling and mechanical drawing) to enable a high piezoelectric response (i.e. increase in beta phase formation).

Mechanical and electrical forces have been shown to influence biological functions including cellular division, migration and differentiation [3–5] and the interplay between mechanical and electrical forces can modulate cellular response to maintain tenocyte phenotype and function in vitro[139,251,324]. The cell response to electrical and mechanical forces include the activation of cell receptors such as integrins [325–327], transient receptor potential (TRP) ion channels, voltage-gated ion channel and piezo channels[6–8]. It was hypothesized that the use of electrical charges in combination with uniaxial cyclic stretching similar to that observed *in vivo* during physiological tendon function, would support human tendon-derived cells function via activation of mechanical and electro responsive cell receptors. In this chapter uniaxial stretching was used to activate a piezoelectric response of PDVF-TrFE scaffolds at constant frequency/strain rate of 0.5 Hz and strain amplitude of 4%. Human tenocytes cultured on mechanically loaded piezoelectric scaffolds exhibited a positive functional response after 5 and 10 days of electromechanical stimulation relative to mechanically loaded non-piezoelectric scaffolds. Modulation of cellular function through engineered microenvironments (i.e. scaffold with tailored mechanochemical properties) has been well studied for the development of functional tissues[328–332]. Mechanical loading, in particular, has been shown to promote cell cytoskeletal reorganisation and morphological changes *in vitro* [9,10]; however, electrical charges effect on cellular function is poorly understood. In this chapter, gene-level response to tensile loading coupled with electromechanical stimulation at multiple time points (1, 5 and 10 days) was evaluated using a custom-made microarray.

Firstly, it was important to observe how stable the gene expression changes were over time. It was noticed that tenocytes were more active on day 1 and 10 but less active at day 5 (see Figure 43). It is known, that mesenchymal type of is initially very proliferative (day 0-3) but then this proliferation decreases and the cell starts to differentiate and produce matrix (day 3-15). It is hypothesised that, as cell organisation is facilitated by the highly organised scaffold structure in combination with mechanical loading and thus cells take less random morphologies, this specific geometric constriction in chromosomal rearrangements might result in gene expression down-regulation at day 5. Taking these results altogether it might be expected to observe transient gene expression as result of the natural proliferative and differentiation stages of tendon cell cultures in addition to the biophysical stimulation effects provoked by either EM or mechanical forces.

Mechanical loading has been employed extensively to align cells, promote a physiologically relevant elongated morphology and to alter gene expression in vitro[11,12]. In addition to adhesion-related (surface receptors) force-sensing mechanisms, mechanical forces transduced to the nuclear envelope via ECM can regulate tissue growth and direct cell differentiation[333,334]. In this study, although aligned fibres scaffolds promoted cell elongation (relative to non-aligned scaffolds), the nuclear shape was not significantly changed either in static or dynamic conditions (see Figure 4-31). This could be in part due to laminins that support cell nuclei membrane. There is growing evidence that mechanotransductive pathways and gene expression changes can be triggered by cell membrane receptors linked to the nucleus through intermediated filaments (i.e vimentin, nestin or glial fibrillary acidic protein) that help to maintain the shape of the nucleus [335–337].

Membrane receptors and tyrosine kinases (i.e. FAK) are of great importance in mechanotransduction mediated cell signalling as they lead to translation of mechanical signals into biochemical signals resulting in i.e. modulated growth factor synthesis. As shown in Figure 4-30, directly culturing cells on aligned fibrous scaffolds induced changes in cytoskeletal organisation, morphology and adhesion formation that resulted in a functional response and higher expression of tendon markers TNMD and SCX. Tenocytes cultured on planar surfaces (2d films) formed more mature focal adhesions and had well-spread phenotypes (see Figure 4-32a). Conversely, fibrous scaffolds demonstrated a high

degree of contact guidance and resulted in highly polarized (elongated) tenocyte-like morphologies. Nevertheless, focal adhesion formation was perturbed in fibrous scaffolds and they were located parallel to the fibre direction. Focal adhesions were more predominant in piezoelectric scaffolds compared to non-piezoelectric scaffolds that correlated to significant alterations in gene expression (see Figure 4-32b).

Further, under electromechanical (EM) stimulation tenocytes exhibited a modulated cell function. From the obtained pathway analyses results, it was evident that integrin signalling was significantly altered after EM stimulation, supporting the hypothesis that EMS plays a fundamental role in the activation of cell adhesion receptors (integrins and ion channel). Furthermore, these changes were correlated to significant upregulation in tendon-related genetic expression and modulated activation of adhesion-related pathways (see Figure 4-37).

From a classical mechanotransduction point of view, it is recognised that the application of mechanical forces tends to aggregate integrins promoting FA assembly and actin polymerisation through activation of Rho (guanosine triphosphatase) and Rho-associated kinase (ROCK) to produce intracellular tension and modulate the production of specific ECM. In addition to integrin signalling, osteospecific signalling such as Wnt/β-catenin which plays an essential role in osteogenic events was significantly downregulated under electromechanical stimulation control of human tendon derived cells relative to mechanical stimulation. On the other hand, tendon cells undergoing mechanical stimulation showed a more significant transient upregulation of tendon-related genes and, after 10 days of continuous mechanical stimulation, osteospecific pathways (Wnt/β-Catenin and BMP signalling) were significantly activated relative to EM stimulation.

In general, gene expression was observed to be differentially expressed extensively with EM stimulation (10 days), which specifically induced a significant increase in the expression of the transcription factors SMAD 3, MKX, SCX, EGR1, GDF-5 controlling tenogenic differentiation and decrease in SOX 9 (cartilage-related transcription factor) which play an essential role in tendon development [13–16]. It also induced an increase in expression of growth factors TGF-β1 and decrease in BMP6, FGF10[17,18] that are intrinsically involved in the regulation of differentiation of tendon cells. The modulation of

these transcription factors may be linked to the deactivation of Wnt signalling indicating that piezoelectricity can induce epigenetic control of cell identity and function. Interestingly, potent osteogenic growth factors including BMP2 and transcription factors SP7 and RUNX2 were also significantly modulated that indicates how intricate osteogenic and tenogenic pathways are and EM appears to be a potent biophysical key regulator. On the other hand, mechanical loading was associated with increased Wnt signalling activation (relative to EM stimulation) that may encourage cells to undergo dedifferentiation pathways towards osteospecific lineages. Even though Wnt signalling was significantly regulated, the experimental results indicated that TGF- β/BMP pathway was one of the most significantly modulated by mechanical stimulation (non-piezoelectric scaffolds) demonstrating the defining role of mechanical forces for tendon function. TGF- β is one of the most abundant growth factors along with fibroblast growth factors (FGF) in adult tendon tissues, where FGF is known as a potent mitogen and helps in the formation of granulation tissue and TGF- β is involved in the regulation of tendon development mediated by Smads and scar tissue formation. TGF-β expression was effected in tendon cells on all time points. For all samples, initially it showed a high expression on day 1 followed by a temporal decrease at day 5 and again increased at day 10 (transient expression). The BMP family is part of the TGF- β superfamily and stimulates bone formation as well as tendon healing. In particular BMP-2 stimulates osteoblastic differentiation, and BMP-14 (GDF-5) induces the formation and differentiation of tendon tissue and is required for maintenance and homeostasis of mature tendons. Interestingly, under electromechanical stimulation but not in mechanical loading a high activation of TGF- β was correlated with downregulation of Wnt signalling suggesting an again an evident interplay between signalling pathways. It becomes clear that piezoelectrical control of tenocytes function is result of a combination of multiple mechanotransductive pathways.

4.6   Conclusion

Alignment of cells and cytoskeletal rearrangement through activation of cell membrane receptors is a desirable elicited cell response for tenocyte function maintenance. It has been shown that mechanical forces play a determinant role in modulating the function and phenotype of tendon cells. After the application of mechanical forces, an intense tenogenic and osteogenic differentiation processes were initiated trough activation of mechanosensitive receptors including action channel TRPA1 and focal adhesion genes. Furthermore, in this chapter, it has been shown that piezoelectricity reinforces cell adhesion by differentially activating key adhesion receptors such as integrins and focal adhesion kinase (FAK). Importantly, it was shown that piezoelectrical control of cell function was the result of interplay between TGF/BMP signalling and direct osteospecific pathways such as Wnt signalling. Piezoelectricity mediated changes in the morphology and cell adhesion also modulated indirect intracellular signalling including MAPK/ERK and ROCK/RhoA via activation of piezosensitive channels receptors including Piezo 1&2. The experimental results presented in this chapter indicated that tendon derived cells responded to piezoelectricity, and a piezoelectric scaffold may be fabricated capable of promoting tendon to bone tissue repair. Piezoscaffolds may have a potential regenerative capabilities for enhancing tendon healing and for future clinical translation.

4.7 References

1. Lanceros-Méndez, S., Mano, J. F., Costa, A. M. & Schmidt, V. H. FTIR and DSC studies of mechanically deformed β-PVDF films. *J. Macromol. Sci. - Phys.* (2001). doi:10.1081/MB-100106174

2. Persano, L. *et al.* High performance piezoelectric devices based on aligned arrays of nanofibres of poly(vinylidenefluoride-co-trifluoroethylene). *Nat. Commun.* **4**, 1633 (2013).

3. Roman, B. L. & Pekkan, K. Mechanotransduction in embryonic vascular development. *Biomech. Model. Mechanobiol.* (2012). doi:10.1007/s10237-012-0412-9

4. Hamada, H. Role of physical forces in embryonic development. *Seminars in Cell and Developmental Biology* (2015). doi:10.1016/j.semcdb.2015.10.011

5. Hauschild, R. *et al.* Forces Driving Epithelial Spreading in Zebrafish Gastrulation. *Science (80-.).* (2012). doi:10.1126/science.1224143

6. Busch, T., Köttgen, M. & Hofherr, A. TRPP2 ion channels: Critical regulators of organ morphogenesis in health and disease. *Cell Calcium* (2017). doi:10.1016/j.ceca.2017.05.005

7. Wu, J., Lewis, A. H. & Grandl, J. Touch, Tension, and Transduction – The Function and Regulation of Piezo Ion Channels. *Trends in Biochemical Sciences* (2017). doi:10.1016/j.tibs.2016.09.004

8. Biggs, M. J. P. *et al.* The use of nanoscale topography to modulate the dynamics of adhesion formation in primary osteoblasts and ERK/MAPK signalling in STRO-1+ enriched skeletal stem cells. *Biomaterials* (2009). doi:10.1016/j.biomaterials.2009.05.049

9. Halder, G., Dupont, S. & Piccolo, S. Transduction of mechanical and cytoskeletal cues by YAP and TAZ. *Nature Reviews Molecular Cell Biology* (2012).

doi:10.1038/nrm3416

10.   Fu, J. *et al.* Mechanical regulation of cell function with geometrically modulated elastomeric substrates. *Nat. Methods* (2010). doi:10.1038/nmeth.1487

11.   Dartsch, P. C. & Betz, E. Response of cultured endothelial cells to mechanical stimulation. *Basic Res. Cardiol.* (1989). doi:10.1007/BF01907974

12.   Goli-Malekabadi, Z., Tafazzoli-Shadpour, M., Rabbani, M. & Janmaleki, M. Effect of uniaxial stretch on morphology and cytoskeleton of human mesenchymal stem cells: Static vs. dynamic loading Zahra Goli-Malekabadi. *Biomed. Tech.* (2011). doi:10.1515/BMT.2011.109

13.   Docheva, D., Müller, S. A., Majewski, M. & Evans, C. H. Biologics for tendon repair. *Advanced Drug Delivery Reviews* (2015). doi:10.1016/j.addr.2014.11.015

14.   Liu, H. *et al.* Mohawk promotes the tenogenesis of mesenchymal stem cells through activation of the TGFβ signalling pathway. *Stem Cells* (2015). doi:10.1002/stem.1866

15.   Murchison, N. D. *et al.* Regulation of tendon differentiation by scleraxis distinguishes force-transmitting tendons from muscle-anchoring tendons. *Development* (2007). doi:10.1242/dev.001933

16.   Kishimoto, Y. *et al.* Wnt/β-catenin signalling suppresses expressions of Scx, Mkx, and Tnmd in tendon-derived cells. *PLoS One* (2017). doi:10.1371/journal.pone.0182051

17.   Lincoln, J., Alfieri, C. M. & Yutzey, K. E. BMP and FGF regulatory pathways control cell lineage diversification of heart valve precursor cells. *Dev. Biol.* (2006). doi:10.1016/j.ydbio.2005.12.042

18.   Galvin-Burgess, K. E., Travis, E. D., Pierson, K. E. & Vivian, J. L. TGF-β-superfamily signalling regulates embryonic stem cell heterogeneity: Self-renewal as a dynamic and regulated equilibrium. *Stem Cells* (2013). doi:10.1002/stem.1252

Chapter Five

In vivo assessment of a physiologically-activated piezoelectric scaffold to modulate tendon tissue repair and promote functional recovery

Marc A. Fernandez-Yague, Alex Trotier, ArunThirumaran, Aitor Larrañaga, Tofail Syed, Matteo Palma, Abhay Pandit, and Manus J. Biggs Piezoscaffolds: Mediating tendon repair through activation of piezosenstivie receptors (under preparation).

Marc A. Fernandez-Yague, Alex Trotier, Abhay Pandit, and Manus J Biggs. Differential response in the functional recovery of Full-thickness tendon transection animal model after treadmill running (under preparation).

5.1   General Introduction

Musculoskeletal injuries caused by trauma, injury or age-related degeneration affect over 126.6 million individual each year (50% involving tendon injuries) costing an estimated $213 billion in annual treatment with the number of clinical interventions to continue to increase as the world population ages[338]. In particular, a complete tear of the Achilles or rotator cuff tendons is one of the leading causes of activity-related disability. Moreover, one of the most significant unmet clinical challenges in musculoskeletal surgery (with 20 to 90 % repair failure rates just three months post-injury). The Achilles tendon is the largest tendon in the body and connects the muscles of the calf (gastrocnemius and soleus) to the bone of the heel (calcaneus). During its function, the Achilles tendon can withstand loads of up to eight times the body weight and store up to 40% of the deformation energy during gait. This extreme mechanical demand is borne by a highly organised extracellular matrix that is composed of resilient fibrous cords of collagen type I [339]. However, due to a low cellular content and lack of a vascular network, the regenerative capacity of the tendon is limited and generally repaired tendons never match the biomechanical properties of native tendon tissue following injury. Tendon repair is a slow and complicated process that requires appropriate mechanical stimulation to happen.

Normal tendon healing after an injury results in the formation of disordered scar tissue followed by gradual remodelling over time (see Figure 5-1). Briefly, the natural healing of tendon involves three overlapping phases: an inflammatory phase that occurs immediately after injury; a proliferative phase starts within the first week and results in the formation of a scar tissue that bridges the two ends of the ruptured tendon; and finally a remodeling phase which begins around 4 to 6 weeks after injury [140,315].
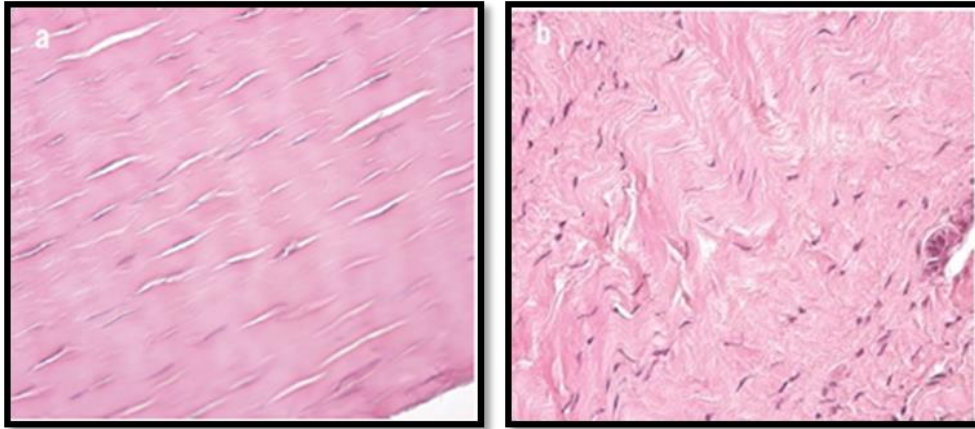
Figure 5-1. H&E pictures of Histological differences between intact and healed tendons after an injury. Tendon structure is lost after healing and is associated with hypercellularity and poor mechanical performance due to immature collagen III overexpression.

During the remodelling phase, there is a gradual increase in collagens organisation and anisotropy, increased collagen cross-linking, and an increased in mechanical properties followed by a decrease in matrix production and cellular infiltration and activity[340] — also, the expression of phenotypic markers of tendon fibroblasts, such as tenomodulin or scleraxis, decreases[341]. Complete tendon repair can require up to two years, driving interest in the regenerative medicine field to develop new treatments that can accelerate the repair process. Current therapies involve (1) direct end-to-end suture repair when possible, (2) tendon grafts (GraftJacket®, TissueMend®, Restore™, CuffPatch®, Permacol™, OrthADAPT ®, Bio-Blanket®) or (3) synthetic polymer support conduits (Gore-Tex® patch WL, Lars® ligament , Leeds–Keio® or Poly-tape®, and Artelon® & Sportmesh™). Repaired tendons using synthetic scaffolds from materials such as Teflon (PTFE) have to date yielded better clinical outcomes compared to biological structures due to their permanent mechanical support. However, synthetic scaffold approaches are also associated with limited long-term tissue compatibility and poor tissue integration[342]. Common clinical complications include inflammatory processes related to a foreign body reaction and adhesion formations, restricting widespread clinical adoption. In summary, current devices using synthetic materials focus primarily on early restoration of function but fail to address the underlying mechanisms of adhesion formation or the poor mechanical properties of healed tissues due to loss of ECM organisation.

Tissue engineering attempts to control ECM organisation and maintain tendon function have involved the use of fibrous scaffolds, typically scaffolds containing aligned nanoscale fibres to recreate the native structured ECM of the tendon[18,343]. Indeed, the biomimetic design is a key tenet of musculoskeletal device technology, and in particular, the development of responsive surfaces that can direct cellular adhesion, differentiation and aid the regeneration of tissue, hold promise in tendon tissue repair strategies. Moreover, the evidence is gathering pace on the complexity of the tendon electromechanical environment (strain, stress, shear, pressure, fluid flow, streaming potentials and electric fields) and electrical stimulation has been used to mimic the naturally occurring electrical currents in tendon to facilitate wound healing[301,344]. While ultimately it may not be possible to separate the effects of each of these factors, it is clear that the extracellular matrix of the tendon as a piezoelectric substance can generate electric potentials which may modulate tendon maintenance and metabolism during regeneration[37,345,346].

The amplitude of electrical potentials generated in the stressed tendon is dependent upon the rate and magnitude of tensile strain, while the direction of loading determines polarity. In many existing therapies, primarily orthopaedic centred approaches, electrical stimulation by direct and alternating electric currents using invasive or semi-invasive methods, pulsing electromagnetic fields and capacitive coupled electric fields, have all been observed to increase regeneration directly[37,345,346]. Thus, new research must focus on understanding the cellular response and modulation of the ECM organisation to subtle dual mechanical and electrical fields and how these influence cell function and tissue regeneration. One approach to investigating this phenomenon is via the incorporation of a piezoelectric component, to provide regenerating tendon with dynamic electrical cues in response to applied mechanical loading.

In this chapter, a novel approach using a piezoelectric nanofibrous scaffold made from electrospun PVDF-TrFE is investigated. Using structural features that more closely mimic the natural tendon, these scaffolds provide a biomimetic morphology and enhanced mechanical properties relative to tubular conduits. Furthermore, as shown in the previous chapter, piezoelectric structures electrical response to physiological mechanical loading aids in the repair of the tendon tissue through the activation of specific regenerative

pathways. Therefore, to assess the effects of electromechanical forces on tendon regeneration *in vivo*, piezoscaffolds were employed as tendon conduits in a rat model of tendon injury. In particular, an adapted protocol of treadmill running following scaffold implantation was used to promote piezoelectrical stimulation of tendon repair.

5.1.1 The development of a treadmill-running protocol to mechanically load tendon.

Muscles and tendons work as a single unit to transmit forces and are co-dependent for their correct function. Mechanical forces are fundamental during embryonic development of tendons and are involved during the repair process after tendon injury. The muscle generated forces regulate tendon ECM organisation and support tendon cell function through TFG-Beta signaling[347]. Several studies have shown that immobilisation of tendon during repair is detrimental and that early mechanical loading of injured tendons is beneficial to healing[348,349]. Treadmill running is a standard method to apply physiological loading to tendons to aid healing, induce functional repair and studies with rodent indicate treadmill regimes influence associated histological changes[350–352]. However, mechanical loading does not exclusively induce tenogenic regeneration, and if applied in excess, can activate osteogenic pathways[353,354]. Previous studies have shown the effect of exercise on tendon wound healing using a moderate rat treadmill running (MTR) model. It was found that MTR accelerated wound healing and increased tenogenic gene expression (COL1α1, SCX and TNMD)[354,355].

On the other hand, other studies have shown that intensive treadmill running (ITR) protocols result in increased bone gene expression[258,356–358]. Moreover, TNMD, COLlα1 and SCX are shown to be mechanosensitive, and their expression levels are positively correlated with the intensity of treadmill running[359,360] or strain during cyclic loading of 3D bioengineered tendons[361–365]. Furthermore, previous studies (see Table 5-1) have clearly shown that moderate exercising has an anabolic result and strengths the tendons[366] but excessive exercise causes dysregulation of collagens and collagen structure (MMPs catabolic effect) and the expression of non-tenocyte related genes/proteins (tendinopathy)[351,352,367,368].

Table 5-1. In vivo biological response to different mechanical loading protocols.

Animal Model	Age/N°	Protocol	Responses
SD rats/Achilles	4 M/12	17 m/min,1 h/day, 6-7 days/week ; 12 weeks	Phenotypic drift, impaired collagen I synthesis and organisation[369]
SD rats/Achilles	2 M/10	17 m/min, 1 h/day, 5 days/week for 12 weeks	Impaired collagen I organisation, intense collagen staining, phenotypic drift[356]
SD rats/Achilles	3–4 M/16	18 m/min, , 1 h/day, 5 days/week for 6 weeks	Higher cell density and cell clusters, impaired collagen organisation [370]
SD female rats/Achilles	3 M/14	17 m/min, 1 h/day for 8 weeks	Collagen bundle disintegration, tenocyte shape change, and increased cellularity[371]
Mice/patellar and Achilles	2.5 M/18	13 m/min, 50 min/day, 5 days/week, 3 weeks	Higher expression of MGF, upregulation of tenocyte-like gene expression, increased expression of collagen type I and tenomodulin[354]
Transgenic ScxGFP	4 M/10	8–14 m/min, 30 min/day, 5 days/week, 6 weeks	Increased expression of scleraxis, tenomodulin, and type I collagen genes. [372]

5.1.2 *In vivo* **mechanotransductive molecular mechanism during tendon repair**

The exact mechanism by which mechanical forces are transduced into intracellular biochemical signalling and promote specific biological functions remains still elusive.

Although, it is clear that the fundamental role of mechanical forces in tendon biology, including changes in cell cytoskeleton organisation, ECM synthesis or gene transcription, the cellular and molecular mechanisms during tendon repair remain unclear. At present, it is known that mechanical parameters and biological responses converge to drive tendon development and that TGF-β–SMAD2/3 and FGF–ERK/MAPK[373] are recognised as the main mechanotransductive pathways for tendon formation and repair. Specifically, SCX activation by FGF/TGF- β acts downstream of mechanical forces to modulate cell commitment and differentiation during tendon development[373–375]. As shown in previous *in vitro* work in this thesis, mechanical loading increased ERK/MAPK phosphorylation and expression levels of tenogenic markers, including EGR1, TGF-B1 and MHK. In similar studies, it was demonstrated that EGR1 transcription increased *in vivo* after just 15 min of mechanical loading in a rat Achilles tendon model of injury [376]. Although much is known about the effect of mechanical stimulation, the cellular and molecular events due to the electrical properties of tendon tissue have been less explored. Studies have shown that direct electrical current induces cell migration (electro or galvanotaxis) and promotes collagen growth factor and protein synthesis, including the collagens[377–380]. Transforming growth factor (TGF-β) is a potent cytokine that reduces the inflammatory response and enhances the healing process of the tendon by promoting cell migration and collagen synthesis. More recent studies have shown that electrical stimulation (in the absence of exogenous growth factors) can affect cell differentiation and induce fibroblast reprogramming into chondrocytes. It was also found that electrical stimulation increased chondrogenic markers (Collagen II, Aggrecan and Sox9) and the secretion levels of TGF-β[381]. In this thesis (see Chapter Three), it has been shown that piezoelectricity reinforces cell adhesion by differentially activating key adhesion receptors such as integrins and focal adhesion kinase (FAK). Importantly, it was shown that piezoelectric control of cell function was the result of an interplay between TGF-β /BMP signalling and direct osteospecific pathways such as Wnt signalling. Piezoelectricity mediated changes in the morphology and cell adhesion also modulated indirect intracellular signalling including MAPK/ERK and ROCK/RhoA via activation of piezosensitive channels receptors including Piezo 1 & 2. *These observations lead to the question, how can physical cues drive the transcription and production of growth factors to promote tendon regeneration and tenocyte differentiation?*

Similarities are shared between mechanotransduction molecular programmes of tendon development, homeostasis and repair. It is also possible to hypothesize that the molecular pathways of tendon repair employ the same mechanotransduction processes that drive tendon cell differentiation during embryonic development (see Figure 5-2)
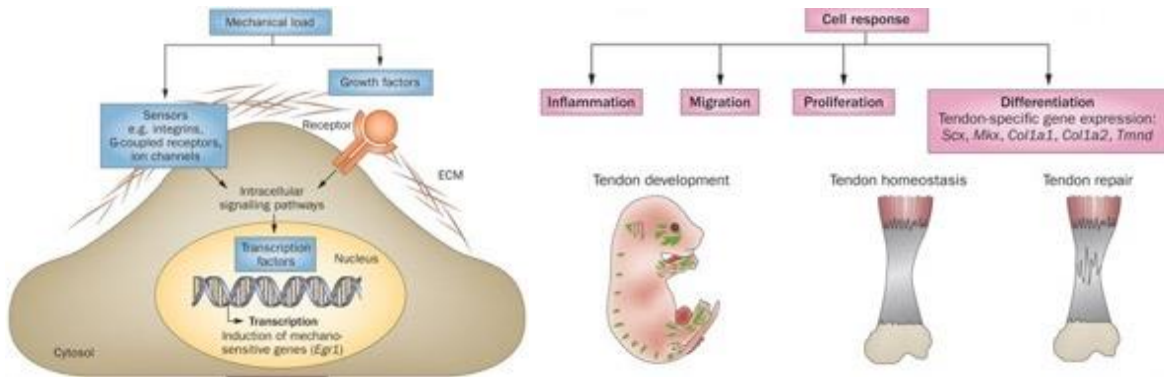
Figure 5-2. Tendon mechanobiology during embryonic development. Specific tendon response to mechanical forces is transduced via the ECM, growth factors, receptors, intracellular pathways and transcription factors.

Thus, this chapter hypothesizes that the delivery of electrical and mechanical cues through physiologically-activated piezoelectric fibrous scaffolds will modulate the tendon repair response and promote functional tendon repair in vivo. Furthermore, biomaterial-mediated electromechanical stimulation will result in changes to the ECM composition and the expression of tendon specific markers, leading to quantifiable differences in the ability of animals to perform natural gait.

Therefore, the objectives that support this hypothesis are:

- To assess whether the protocol of treadmill running induces detrimental histological and structural changes in repaired tendon tissue.
- To assess the influence of electromechanical stimulation on functional recovery in an Achilles injury rat model using gait analyses
- To evaluate the influence of electromechanical on histological structures of repaired tendons in an Achilles injury rat model.

- To evaluate changes in specific ECM protein expression using a custom protein array of an Achilles injury rat model after electromechanical stimulation through an implanted piezoelectric scaffold.

5.1.3 Material and methods

5.1.4 Scaffold fabrication

PVDF-TrFE (piezo) or PTFE (non-piezo) nanofibrous scaffolds were fabricated into tubular scaffolds composed of aligned fibres via an electrospinning process as described in chapter four. Briefly, PVDF-TrFE or PTFE solution was delivered at a flow of 1.0 ml/hr using an 18G Luer-lock needle. A +20 kV potential difference between needle and collector at a distance of 6-10 cm was used, and fibres were collected onto a negatively charged mandrel (-6kV) rotating at 4000 rpm.

The ethics committee approved all the animal procedures and treatments used in this study at the National University of Ireland, Galway. Also, animal care and management followed the Standard Operating Procedures of the Animal Facility of the National University of Ireland, Galway. Animals were allowed to acclimatise for at least seven days before any surgical procedures. Subsequently, animals were acclimated to the treadmill running for one week, and their behaviour was analysed.

A total of 105 Female Lewis rats aged 6-8 (220g) weeks were used in this study. The animals were anaesthetised by isofluorane inhalation (5% induction reducing to 1- 2% for maintenance during procedures). The right leg was shaved and swabbed with iodine to minimise the risk of bacterial contamination. An incision was created through the skin (~1cm) from the myotendinous junction distally to the osteotendinous junction. The incision provided ample exposure to the Achilles tendon. The fascia surrounding the Achilles was transected longitudinally and carefully to avoid creating injury, and the Achilles tendon was exposed. Before implantation and tendon transection, two looped sutured are inserted at the top (muscle) and bottom (bone). After the total tendon length was measured a 3 mm defect in proximal/distal extension (at 3 mm from the calcaneus) was created using a positioning device and an 11 surgical blade, resulting in a 6 mm gap after tissue retraction. The construct was then sutured (4-0 Ethicon) to both ends of the tendon to

bridge the gap using a modified Kessler technique, and the skin was sutured. After a period of 2, 4 and 8 weeks the animals were euthanised and tendon tissue, as well as contralateral tendons, were harvested,

a)   b) c)
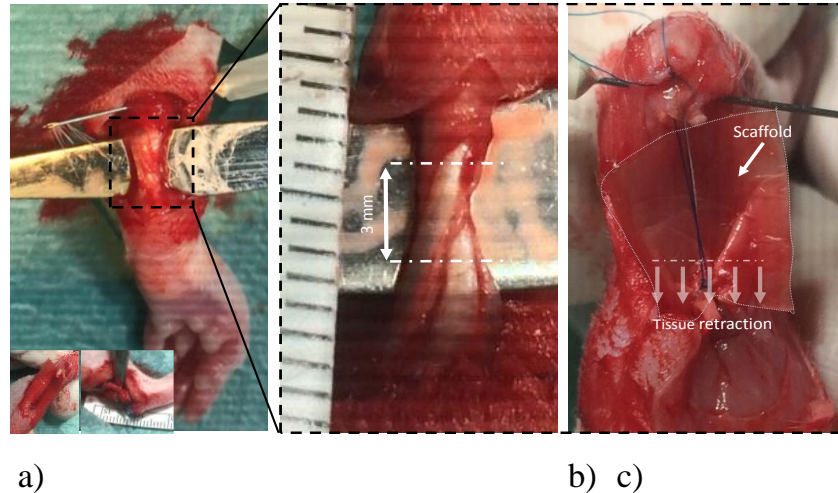
Figure 5-3. Construct implantation. a) Tendon is exposed b) tendons is measured and 3 mm is removed c) After tissue retraction a 6 mm gap is generated and the implant is attached to both free ends using a modified Kessler technique.

Animals were then left to heal for 2 weeks and were gradually exposed to a treadmill running (see Table 5-2) based on published studies where non-adverse effects on the tendon morphology were detected respect to healthy rat Achilles tendon without training. It is reported that beyond these values, tendon would be considered overused and risk of tear would be increased. Briefly, the treadmill running was increased from once a week for 5 min to 30-45 min 5 days a week.

Table 5-2.Running protocol used for the running group of rats (treadmill)

		Duration (min)	Speed (m/min)
	Day 14	5	8-9
	Day 15	10	9-10
Week 2	Day 16	15	9-10
	Day 17	20	9-10
	Day 18	30	9-10
	Day 19	45	9-11
	Day 20	30	9-11
Week 3	Day 21	45	9-12
	Day 22	30	10-14
	Day 23	45	10-14
Week 4		30	10-14
Week 5		45	10-14
Week 6		30	10-14
Week 7		45	10-14
Week 8		30	10-14
Week 9		45	10-14
Week 10-16		30	10-14

5.1.5 Histology

Repaired tendon tissues and contralateral tendons of all groups (n=7) were dissected from the proximal myotendinous junction to the distal osteotendinous junction and processed for histological analysis. The samples were fixed in 10% neutral buffered formalin (24 hours), dehydrated in gradient alcohols, cleared, and embedded in paraffin blocks, as reported previously[382]. Histological sections (6 um thick) were prepared using microtome sectioning (Leica Rotary Microtome). In order to distinguish between scar tissue or new tendon formation, polarisation microscopy and picrosirius red staining were used. Also, for descriptive histology 6 µm, thick sections were stained using Hematoxylin & Eosin stain, Masson-Goldner's stain, Alcian Blue, O-safranin stain, Red picrosirius satin or Herovici's polychrome stain according to the manufacturer's guidelines. Areas of chondrification

within the defect region at 4 or 8 weeks after surgery were measured using Safranin O staining and ImageJ (v1.52i). For each tissue, 3 different frontal-longitudinal sections were analysed (1 section of the middle tendon, 1 section ventral to this middle part and 1 section dorsal to this middle part). For each section 5 consecutive images were captured spanning the entire length of the tissue, omitting the transition zones of original tendon stumps to regenerate tissue. Volume fraction (VV) of tendon cells were used to estimate cell proliferation. A 192-point grid was overlaid on 40X images of H&E stained tissue sections. The number of tendon cells intersecting points of the grid was counted (PP), along with the total number of points on the tissue (PT). The volume fraction of tendon cells (VV) was calculated using the formula below:

$$V_V = P_P / P_T$$ Equation 5-1

5.1.6 Histomorphometry and point-based scoring system.

In order to evaluate the effect of treadmill running on the progression of tendon repair, histomorphometric measurements on stained samples from three animals (5 sections in total per animal) were employed. A point-based scoring system was used, and the following parameters were scored based on the percentage of 1) increase in the number of cells compared to control intact tendon (sham) 2) Increase of calcification compared to intact tendon 3) Increase in the vascularization and innervation compared to intact tendon 4) Increase of fat deposits compared to intact tendon 4) Increase of fiber orientation compared to intact tendon 5) Increase of cell morphology compared to intact tendon.

5.1.7 Micro-CT scan

At 8 weeks after Achilles tenotomy, the right hind legs of each group were collected at sacrifice for micro-computed tomography analyses (µCT 100, Scanco Medical, Bruttisellen, Zurich, Switzerland). Samples were scanned using the following settings: 60 kV, 150 µA with a mean 20 µm slice thickness. The reconstructed scaffold and Achilles tendons were selected for quantification of calcifications volume.

5.1.8 Protein array

Tissue samples were immediately frozen at -80 °C until needed. Samples were then pulverized in a cell crasher for five minutes at least three times until the tissue was completely powdered. Samples were then thawed on ice and incubated in a lysis buffer containing a cocktail of protease (aprotinin, leupeptin, pepstatin and EDTA) and phosphatase inhibitors (Sodium Orthovanadate, beta-Glycerophosphate, Sodium Fluoride and Pyrophosphate)for ten minutes and the lysate was cleared at 15,000 g for 15 minutes. The protein fraction of the centrifuged sample was then extracted, aliquoted and stored at -80 °C until further use.

The protein expression in the newly formed tendon tissues was examined using a custom made array technology as described in chapter three and four to analyse the effect of electromechanical stimulation on ECM production, signalling pathways and activation of receptors.

5.1.9 Functional recovery

An animal treadmill (Exer 3/6, Columbus Instruments) track integrated with a video-based system was used to obtain spatiotemporal parameters of gait. The animal gait was analysed through a clear plastic Lexan at the sides of the system consisting of a cage (50.8 cm x 50.8 cm x 33 cm) with gates placed at each end of the walkway. A digital camera (8 M pixels and 120 frames per seconds) was positioned 30 cm in front of the walkway to capture the sagittal view of the rat from the walkway. The data were analysed and processed with Kinovea software (v0.8.27). For all groups, the system was calibrated using the same scale bar located in the image and modelled the leg motion using pairs of circle markers.

The ankle, knee, hip and MTP joint angles (see Figure 5-4) were measured using the automatic black ink marker feature recognition on the hip, knee, ankle, and 3rd metatarsal head at the four gait stages: initial contact, mid-stance, pre-swing, and mid-swing.

a)   b)
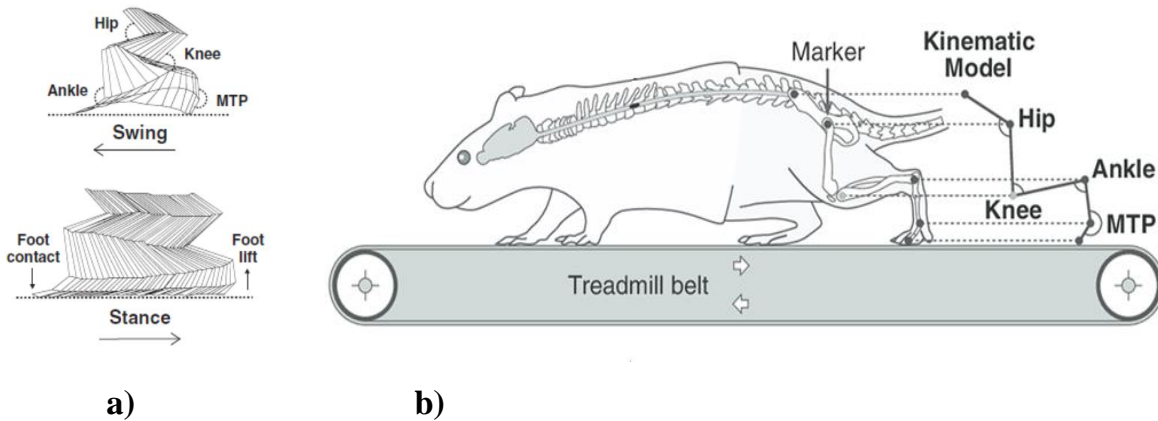
Figure 5-4. a) Schematic representation of the kinematic model extracted from the ilium, hip, ankle, knee, MTP and 3rd toe markers on bare skin. b) Schematic representation of the sagittal view of the walkway corresponding to the horizontal plane recorded during the experiment.

The spatial and temporal gait parameters analyzed were step length, angle and cycle time. The walking speed was calculated by dividing the step length by the cycle time. Each angle joint curve was normalized by cycle time before further analysis. To determine the change on gait angle, the maximum difference in amplitude (Ampl.) between initial contact and end of swing was measured during an entire step and was calculated according to the following formula:

$$\text{Max.}(°) - \text{Min.}(°) = \text{Ampl.}(°)$$ Equation 5-2

$$\text{Functional Recovery} = \text{Ampl.}(°)_{\text{post transection}} / \text{Ampl.}(°)_{\text{prior transection}}$$ Equation 5-3

5.1.10 Statistical Analysis

Minitab (v.17 Minitab Software) was used for statistical analysis. Analysis of variance (ANOVA) and Tukey's posthoc test was used to determine statistical significance between groups. All graphical data are presented as the mean ± standard deviation of the mean. p values of < 0.05 were considered statistically significant.

5.2   Results

5.2.1   The effect of electrospun piezoscaffolds on tendon repair in irreversible tendinopathy (full-thickness Achilles injury) rat model.

Developing a preclinical load-bearing injury model was necessary to investigate the effect of piezoelectric scaffolds during tendon repair. Therefore, a full-thickness transection of the tendon of 3 mm was performed in the rat Achilles tendon, as shown in Figure 5-5 to study tendon repair.

a)   **b)   c)**
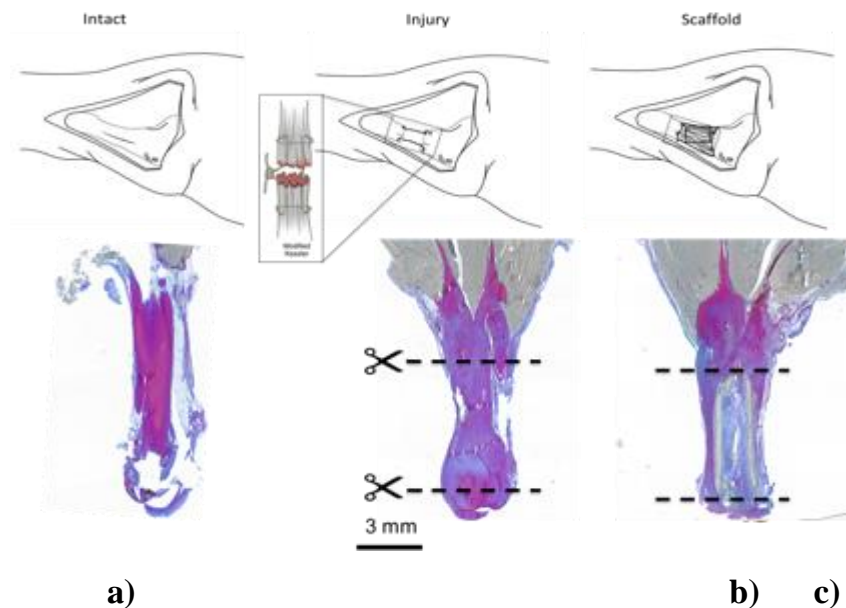
Figure 5-5. Schematic representation and images obtained from histological samples stained with Herovici's stain of a) intact tendon b) injured tendon repaired with sutures and c) injured tendon repaired with PTFE scaffold (non-piezoelectric). Complete closure of the tendon defect was observed in all groups by 2 weeks post-injury.

Under normal conditions, in intact tendons, cells were observed to be elongated and encapsulated in a rich and dense ECM composed of predominantly collagen type I cross-linked by GAGs (see Figure 5-6). However, after an Achilles injury resident and invading, cells adopted a non-elongated, non-aligned morphology as shown in Figure 5-7.
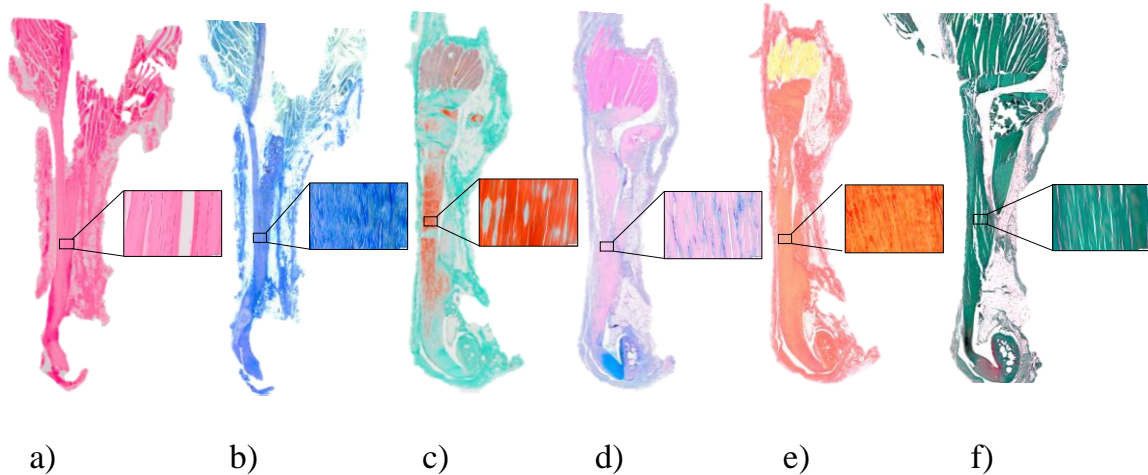
a)   b)   c)   d)   e)   f)

Figure 5-6. Histological images of intact tendon a) H&E staining showing cell organisation and collagen fibre bundles (in blue the cell nuclei, and in pink the extracellular matrix /cytoplasm). b) Herovici staining showing the distribution of collagen III and I. (in blue the young collagen and in red the mature collagen red) c) Masson's Trichrome staining showing the connective tissue (green),cell nuclei (dark brown) and muscle fibres/cytoplasm (red) d) Alcian blue showing mucopolysaccharides (blue),cytoplasm (pale pink) surrounding tenocyte cells (red to pink) e) Picrosirius red showing structured collagen fibre organisation (red) and muscle fibres/cytoplasm (yellow) f) Safranin O-stained sections showing connective tissue (green) and the absence of any ectopic ossification (red) in the mid tendon and cartilage formation (red to orange) at the tendon-bone insertion.

The disruption to tendon cell morphology is illustrated in Figure 5-7, in intact tendons bundles of cells elongate longitudinally along collagen fibres showing a particular phenotype characteristic of tenocytes. Conversely, after 2 weeks post-injury, fibroblastic cells present in the granulation tissue lack the characteristic fusiform phenotype of tenocytic cells.
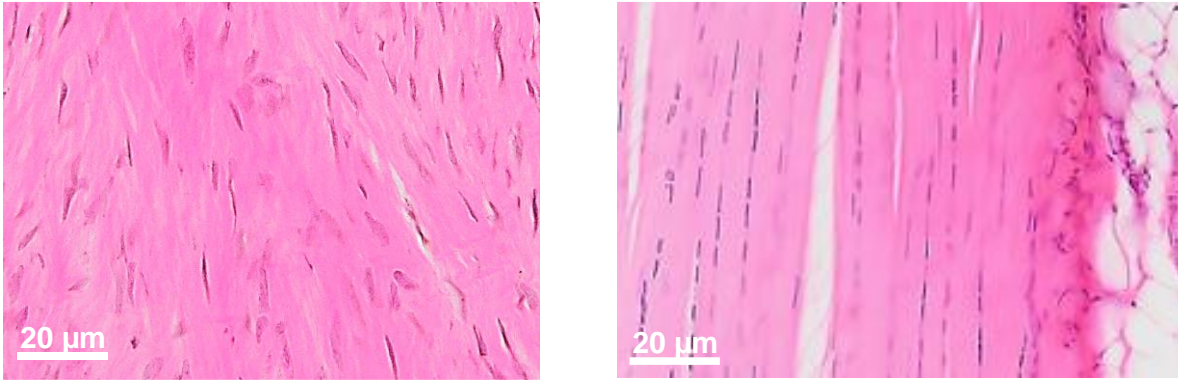
Figure 5-7. H&E images of a) injured tendon sample (1 week) and b) intact tendon sample showing differences in cell morphology. Pink, tissue matrix; purple, cytoplasm; blue, nuclei (Scale bar 20 and 10 μm respectively).

Macroscopically, injured tendon samples presented a significantly thicker mean diameter irrespective of scaffold deployment relative to control non-injured tendons. Table 5-1 shows the morphometric values of the repaired tendons and intact tendons.

Table 5-3. The effect of electromechanical stimulation on tendon diameter after injury in animals undergoing treadmill running (dynamic) or confined to a cage (static)

	2 weeks	four weeks	8 weeks
Intact tendon	1.6 ± 0.2 mm	1.6± 0.2 mm	1.7 ± 0.2 mm
Injury (static)	5.4± 0.5 mm	4.9± 0.4 mm	4.6 ± 0.4 mm
Injury (TR)	5.4± 0.4 mm	4.3± 0.5 mm	3.8 ± 0.8 mm
Non-piezo (static)	5.1± 0.4 mm	4.1± 0.6 mm	3.4 ± 0.7 mm
Non-piezo (TR)	5.1± 0.2 mm	4.0± 0.3 mm	3.3 ± 0.5 mm
Piezo (static)	5.5± 0.6 mm	4.1± 0.6 mm	4.1 ± 0.9 mm
Piezo (TR)	5.2± 0.7 mm	4.1± 0.4 mm	3.9 ± 0.9 mm

The functional recovery of the injured tendons in animal not conditioned via mechanical treadmill exercise (static) was measured using gait analyses of animals walking on a treadmill at a low speed of 9 m/min. Gait analysis was conducted once at pre-surgery and again at 1, 2, 4 and 8 weeks after Achilles tenotomy. The gait analyses tracked the joint side angles of the knee, MTP, hip and ankle.(see figure 5-8)
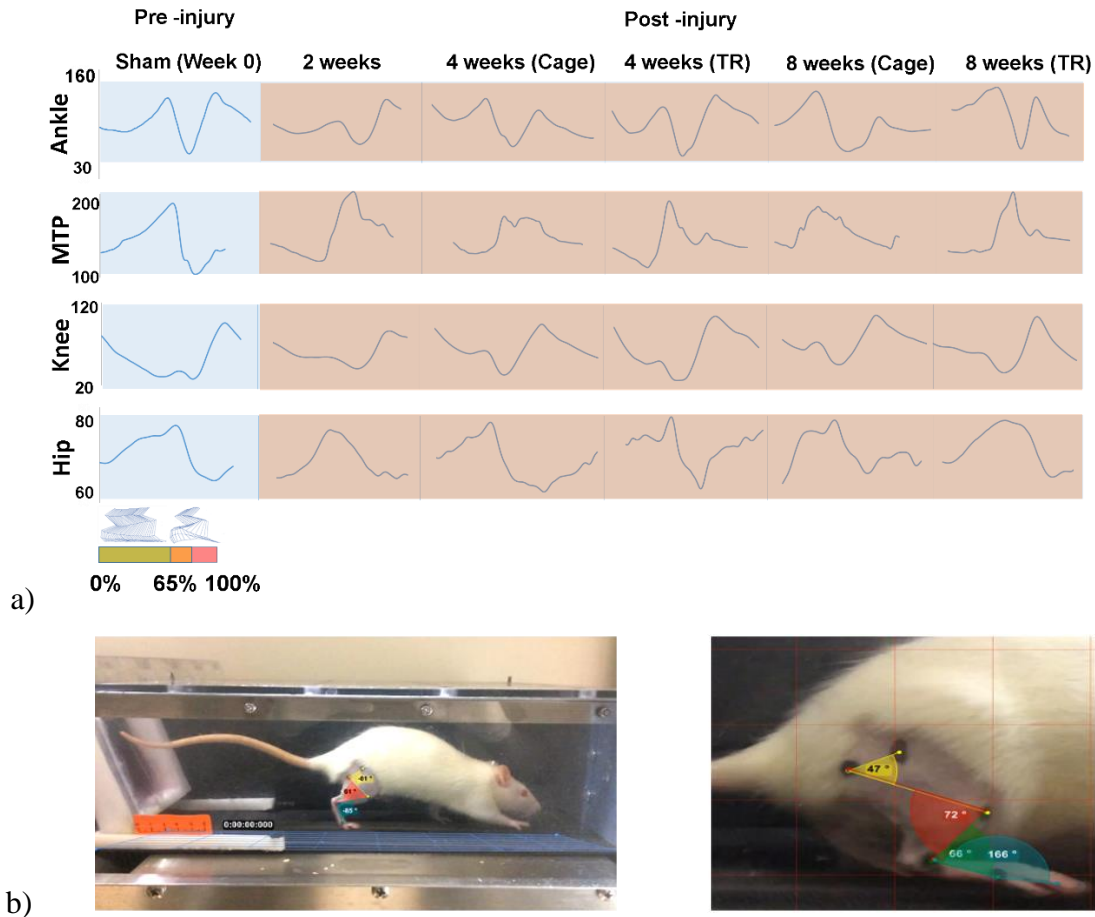
Figure 5-8. a) Gait analysis for injury group: A total of four different joint angles were measured (Ankle, MTP, Knee and Hip) at weeks 2, 4 and 8. Different amplitudes were obtained for animals before and after surgery (injury) at all time points.b) Example of the image analysis used for the measurement of the 4 angles.

The gait of animals not conditioned via mechanical treadmill exercise (static) was quantified using a custom-made system and the data is presented in Table 5-4. Functional recovery analyses over a period of 8 weeks. It was observed that the use of a scaffold promoted a faster recovery of the leg motion in static animals (N=7). Immediately after injury (1 week), animals did not demonstrate gait recovery and they adopted an antalgic gait by decreasing the MTP joint angle, increasing the hip join angle and increasing the time in stance by 20-30%. Conversely, 2 weeks post-injury all animals exposed to control and experimental conditions were able to utilise and load the tendon.

Table 5-4. Functional recovery analyses over a period of 8 weeks. It was observed that the use of a scaffold promoted a faster recovery of the leg motion in static animals (N=7).

	Injury (static)					Non-piezo (static)				Piezo (static)			
	Pre-surgery (°)	1 week (°)	2 weeks (°)	4 weeks (°)	8 weeks (°)	1 week (°)	2 weeks (°)	4 weeks (°)	8 weeks (°)	1 week (°)	2 weeks (°)	4 weeks (°)	8 weeks (°)
MTP	*100±2*	*32±4*	*51±6*	*52±5*	*51±7*	*42±4*	*54±3*	*56±5*	*55±9*	*40±4*	*53±8*	*55±5*	*52±8*
Knee	*80±3*	*49±5*	*54±8*	*53±4*	*63±7*	*55±5*	*55±10*	*55±4*	*55±2*	*45±5*	*54±9*	*56±10*	*54±6*
Hip	*18±2*	*16±2*	*15±5*	*12±4*	*9±4*	*14±2*	*13±5*	*10±1*	*12±5*	*17±3*	*14±7*	*10±3*	*8±6*
Ankle	*70±2*	*41±5*	*56±3*	*57±11*	*58±7*	*48±6*	*57±3*	*53±7*	*51±5*	*43±4*	*68±6*	*55 ±9*	*55±5*

Again, the gait of animals subjected to mechanical treadmill exercise was quantified using the above system, and the data is presented in Table 5-5.It was observed that the patterns of the gait motion were unchanged in experimental groups relative to the control (pre-surgery) gait motion. However, considerable differences in the amplitudes of the joint angle were measured (Table 5-5). First, it was noted that the joint angle amplitudes were at their lowest values one week after surgery compared to the control group (pre-surgery) except for the hip joint angle amplitude that was at its highest. Also, all the recorded joint angle amplitudes for the ankle, MTP and knee joint angles were significantly lower in the repaired groups relative to the control group at weeks 1, 2, 4 and 8 ($p < 0.05$).

Table 5-5. Functional recovery analysis over a period of 8 weeks in animals undergoing treadmill running. Significant differences were observed between the animals undergoing treadmill running relative to animals subjected to static conditions (N=7).

	Injury (TR)			Non-piezo (TR)		Piezo (TR)	
	Pre-surgery (°)	4 weeks (°)	8 weeks (°)	4 weeks (°)	8 weeks (°)	4 weeks (°)	8 weeks (°)
MTP	*100 ±2*	*48±3*	*71±8*	*58±5*	*92±8*	*48±5*	*62±8*
Knee	*80±3*	*58±7*	*67±7*	*62±3*	*72±3*	*60±7*	*64±6*
Hip	*18±2*	*15±5*	*15±5*	*14±2*	*15±3*	*8±2*	*12±8*
Ankle	*70±2*	*55 ±3*	*61±3*	*54±4*	*67±3*	*57±3*	*67±7*

Notably, gait analysis suggested that treadmill running had a consistent significant positive effect in animal motility, in particular on the experimental group which received a non-piezo scaffold (TR) at week 4 ($p<0.05$) for the ankle and at week 8 for ankle, knee and MTP joints ($p<0.01$, see Figure 5-9). It was also noted that after 8 weeks, the recovery of the MTP angle to baseline was complete ($p<0.01$) indicating enhanced functional recovery and tendon repair. A similar trend was observed for the animal group, which received the piezoelectric scaffold undergoing treadmill running, yet this was significant for the knee joint angle only at week 8 ($p<0.05$).

In summary, non-piezoelectric scaffolds induced complete functional recovery at four weeks in animals undergoing treadmill running and partially complete functional recovery for piezoelectric scaffolds group undergoing treadmill running at week 8.
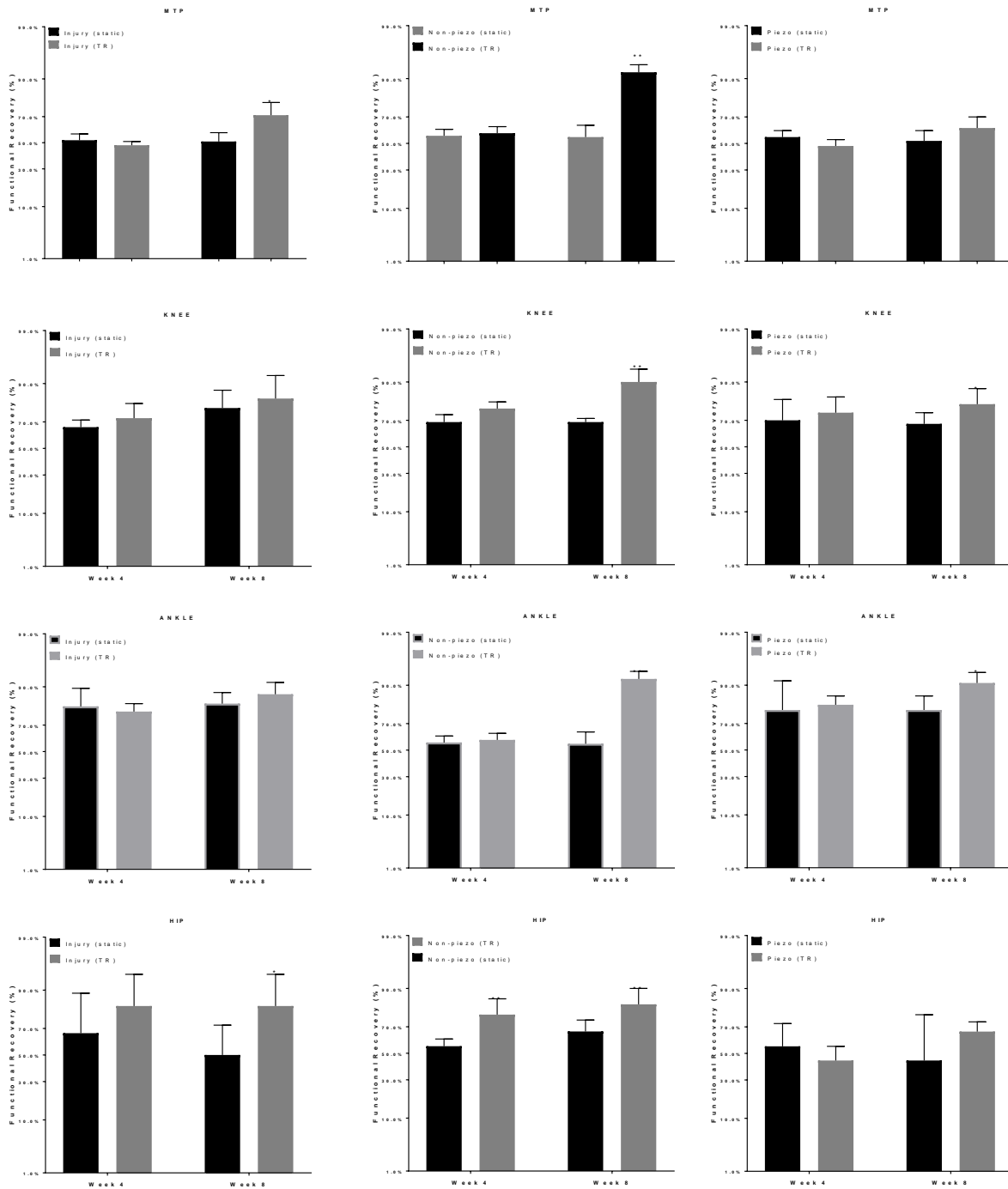
Figure 5-9. Functional recovery analysis following injury in animals treated with non-piezo and piezo scaffolds (static and TR) at weeks 4 and 8 after injury. It was observed that animals treated with a non-piezo scaffold (TR) showed significant functional recovery in the ankle, MTP and knee joints after 4 and 8 weeks. Results are expressed by mean ± standard deviation, * p<005, ** p<0.01.

5.2.2 Tendon regeneration and tissue organisation is enhanced after electromechanical stimulation

After the injury, the tendon stumps were observed to retract, generating a gap that became filled with granulation tissue. The fibrous regenerating tissue was characterised by loose collagen fibre organisarion and an overall heterogeneous texture after 2, 4 and 8 weeks, with increased cellularity and ingrowth of vessels, nerves, fat deposition and calcification (see Figure 5-14). At 1-week post-injury, the newly formed tissue was observed to be composed of disorganised granulation tissue (Figure 5-10) comprised of collagen III (shown in Figure 5-11).
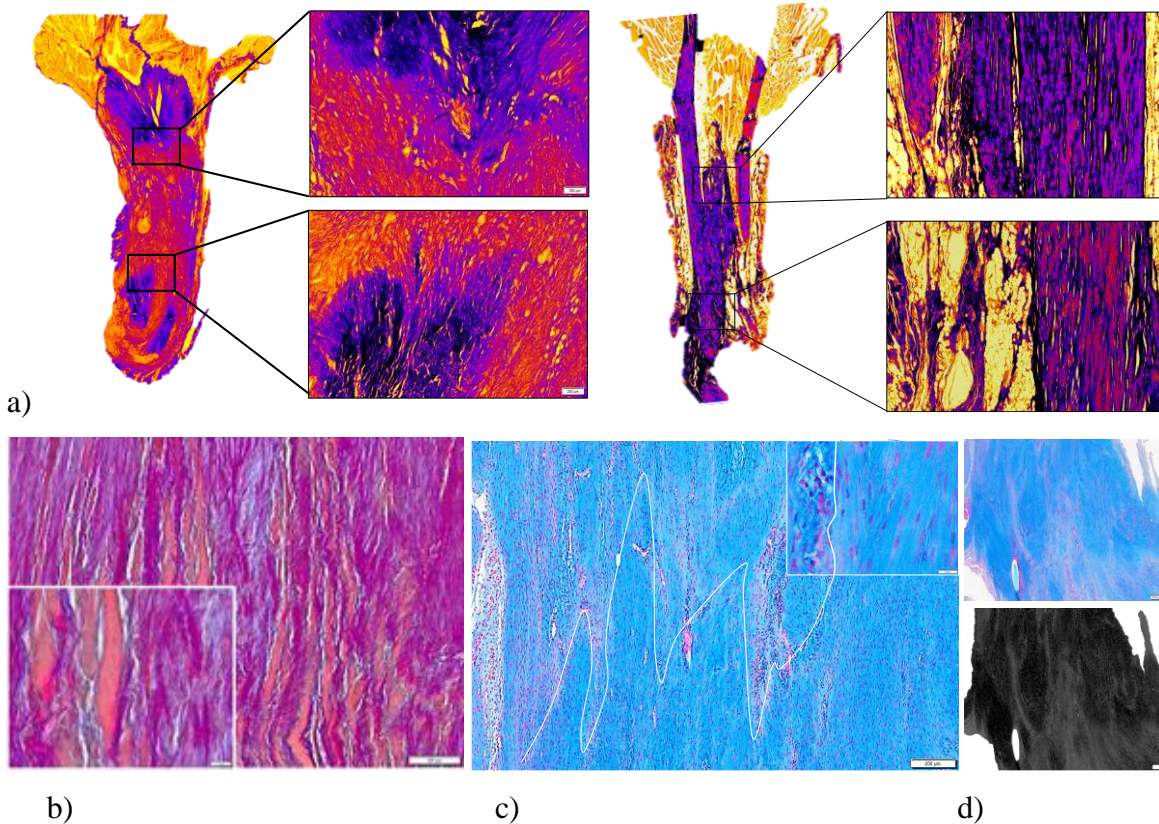
Figure 5-10. a) Picrosiruis red-stained tendon histological sections 1-week post tendon transection modified digitally to enhance the contrast between the different phases (granulation tissue in red and native tendon tissue in purple). Macroscopic and 10x magnifications of areas showing the interface between the native tendon and newly formed granulation tissue. b) Herovici stained sample 2 weeks post tendon transection showing the persistent breakdown of the tendon fibrils at the cut ends c) Alcian blue-stained sample 2

weeks post tendon transection showing a large bundle of fibres of collagen separated due to disruption of organised tissue. d) Alcian blue-stained samples 2 weeks after injury contrasted digitally using grayscale. The tendon end stump is separated from the granulation tissue.
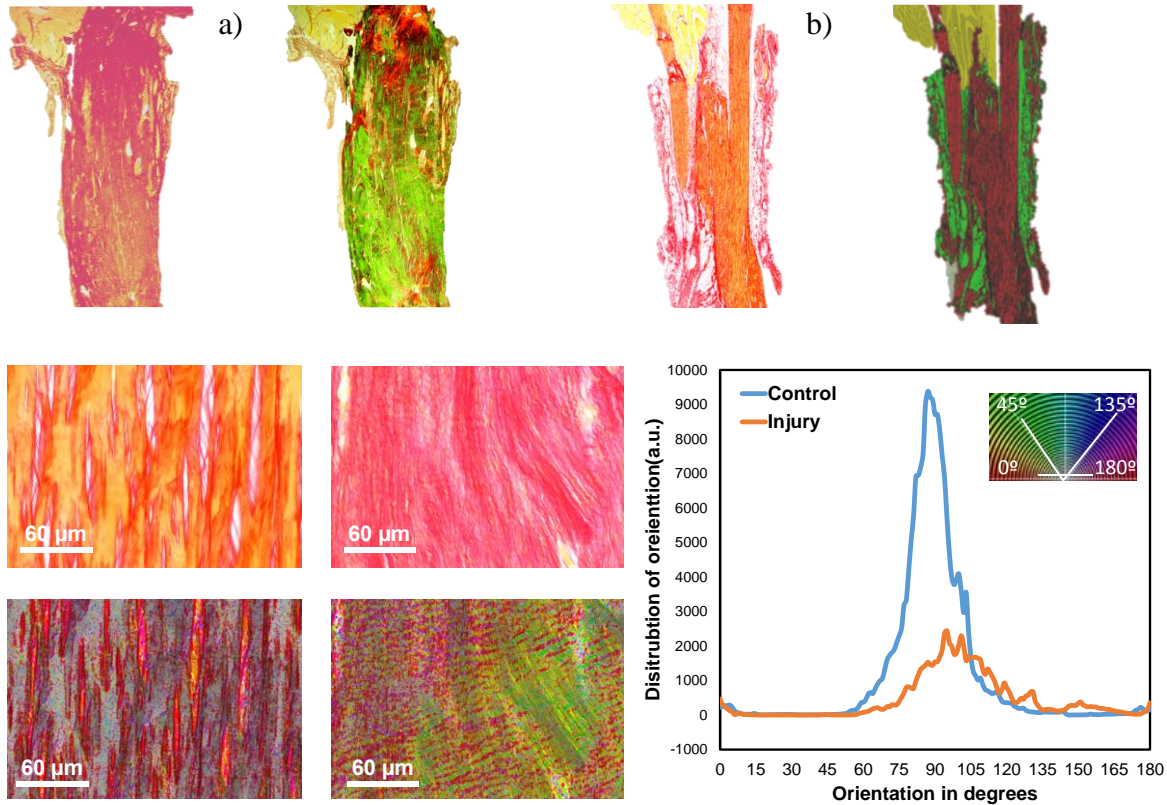
c)

Figure 5-11. a) Picrosirius red-stained tendon histological sections 1-week post tendon transection without (left) and with polarisation (right). b) Picrosirius red-stained histological sections of intact tendon and with polarisation (right) c) The digital analysis shows that the distribution of the orientation of fibres was broad and disorganised. A circular colour map shows the correlation between orientation and colour code. The polarised image demonstrates that the deposited collagen is highly disorganised and shows poor birefringence, characteristic of collagen type III.

A significant ($p<0.05$) decrease in the presence of related cartilage glycosaminoglycans (GAGs) relative to the other experimental and control groups was detected in tendon tissues supported with a non-piezo (TR) scaffold using safranin-O staining intensity

measurements, (see Figure 5-12). Furthermore, using polarized light microscopy of picrosirius red-stained samples (see figure 5-13) it was confirmed that both synthetic scaffolds (piezo and non-piezo) induced significant increases in the maturation and organisation of collagen fibres as indicated by a birefringence derived fibre organisation score (>3) compared to suture (1.5).
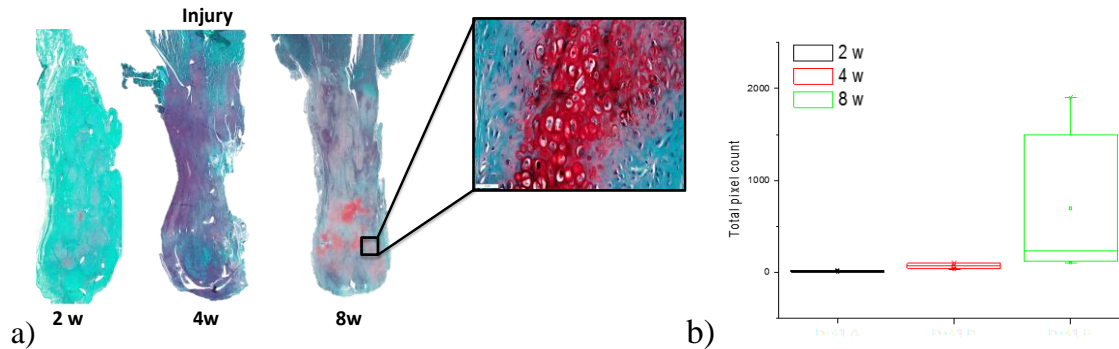
Figure 5-12. a) Control (injury only) Safranin-O stained histological sections at 2, 4 and 8 weeks post-injury. After 8 weeks, calcified areas in the mid-region of the tissue were observable. b) Quantification of the chondrification area for all samples after 2, 4 and 8 weeks post-injury. Histomorphometric analysis indicates a significant increase in chondrification 8 weeks post-injury.

In order to evaluate the degree of tendon repair and the effect of treadmill running on tendon ECM morphology, organisation and biochemistry, histomorphometric measurements on stained histological sections from three animals (5 slides in total per animal) were employed at 8 weeks post-injury. A point-based scoring system was employed to grade tissue repair using parameters based on 1) the cell number relative to intact tendon 2) the tissue calcification relative to intact tendon 3) the tissue vascularization and innervation corresponding to intact tendon 4) the extent of fat deposition relative to intact tendon 4) the fiber orientation relative to intact tendon 5) the cellular morphology relative to that of cells from to intact tendon.

Significant increases in tissue organisation and regeneration scores were observed in tendon tissues derived from animals which were treated with the non-piezoelectric (TR) and piezoelectric (TR) scaffolds following a tendon injury. Here, the non-piezoelectric (TR) and the piezoelectric (TR) groups induced a significantly (p<0.01) higher tissue repair score

(16.5 and 15 respectively) relative to all other experimental and control injury groups (see Table 5-6).

Table 5-6. A scoring system was employed for the histological evaluation of repair at 8 weeks post-injury. Values are expressed in Mean ± SEM of scored points. 0-25 % (4 points); 26-50 % (3 points); 51-75% (2 points) and 76-100% (1 point).

	Parameters						
Group	Cell number	Calcified area	Vessels and nerves	Fat deposits	Fibre orientation	Cell shape (aspect ratio)	Total
Control	4 ± 0	4 ± 0	3.5 ± 0.25	3.5 ± 0.5	3.75 ± 0.25	4 ± 0	**23**
Injury	1 ± 0.25	2 ± 0.5	3.25 ± 0.5	2.5 ± 0.5	1.5 ± 0.5	2.5 ± 0.5	**12.75**
Injury (TR)	1 ± 0.5	2.5 ± 0.25	2.5 ± 0.5	2.5 ± 0.5	2.5 ± 0.5	2.5 ± 0.5	**13.5**
NonPiezo	1 ± 0.75	2.25 ± 0.5	2.5 ± 0.5	2.5 ± 0.5	3.0 ± 0.5	2.5 ± 0.5	**13.5**
NonPiezo (TR)	2 ± 0.5	2.5 ± 0.5	3.25 ± 0.5	2.5 ± 0.5	3.25 ± 0.75	3 ± 0.5	**16.5**
Piezo	1 ± 0.75	1 ± 0.5	2.5 ± 0.5	2.25 ± 0.5	2.0 ± 0.75	2.5 ± 0.5	**12.5**
Piezo (TR)	1.5 ± 1	2.25 ± 0.5	2.5 ± 0.25	2.5 ± 0.5	3.25 ± 1.25	2.5 ± 0.75	**15.0**
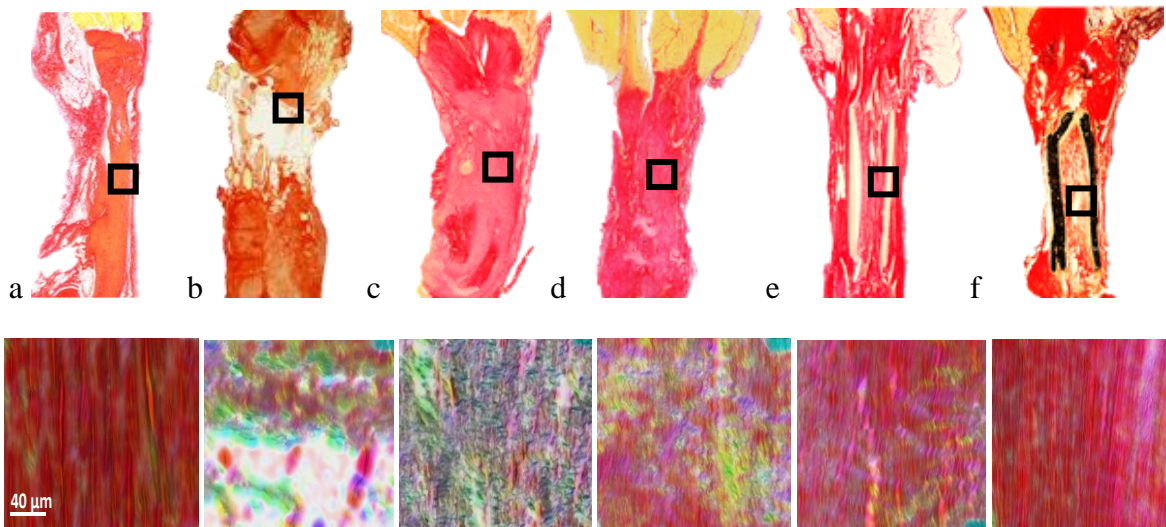
Figure 5-13. a) Picrosirius red staining of intact, suture-repaired and scaffold-repaired tendon tissue: a) intact tendon, b) sutured tendon 24 hours post-injury, c) 1 week post-surgery and d) 8 weeks post-injury; e) scaffold-mediated healed tendon using piezoelectric and f) non-piezoelectric scaffolds 8 weeks post-injury. Orientation distribution analysis

using high-magnification images (box region) indicated that tissue organisation was increased in animals treated with piezo and non-piezo scaffolds.

5.2.3 Electromechanical stimulation decreases endochondral ossification and promotes functional tendon repair.

At two weeks post-injury, the tendon tissue composition was highly heterogeneous, possessing an increased cellular content and noted ingrowth of nerves and blood vessels relative to earlier time-points (see Figure 5-14). At two weeks post-injury irregular voids were present between the large collagen type I fibres which were filled with granulation tissue and cells demonstrating a chondrogenic phenotype. At four weeks post-injury, a condensation of these cells showing a chondrogenic phenotype in both injury and piezo and non-piezo scaffold treated animals was observed. four weeksThis process, initiated by mechanical compression and the hypoxic conditions experienced by resident and infiltrating cells, was pronounced at the bone and tendon insertion areas. Indeed, by eight weeks post-injury endochondrial ossification was prominent in all static (cage) groups. Figure 5-14 shows the distribution of chondrocyte cells and cartilage nodules at the distal and in the mid-regions of the tendon granulation tissue following injury. As newly formed chondrocytes progressed in their maturation, the cartilage nodules were replaced by mineralised bone, as shown in Figure 5-15.

Following the inflammation phase (2 weeks post-injury), tendon structure reorganisation was initiated, and areas of high cell density were observed close to the tendon stumps endings. Cartilage formation first appeared at the distal stump region. By four weeks post-injury, a large number of cartilage nodules (see Figure 5-15) were formed in the region of the granulation tissue close to the distal stump ending. Within this region, the chondrocytes matured into hypertrophic chondrocytes and mineralisation of the tissue was initiated. Several small cartilage nodules were present from four weeks both at the tendon stumps and throughout the granulation tissue. Progressively, cartilage nodules served as template for new bone formation via endochondral ossification (see Figure 5-15 and Figure 5-12), and ectopic bone formation resulted from hypertrophy of chondrocytes and blood vessel infiltration (see Figure 5-16).
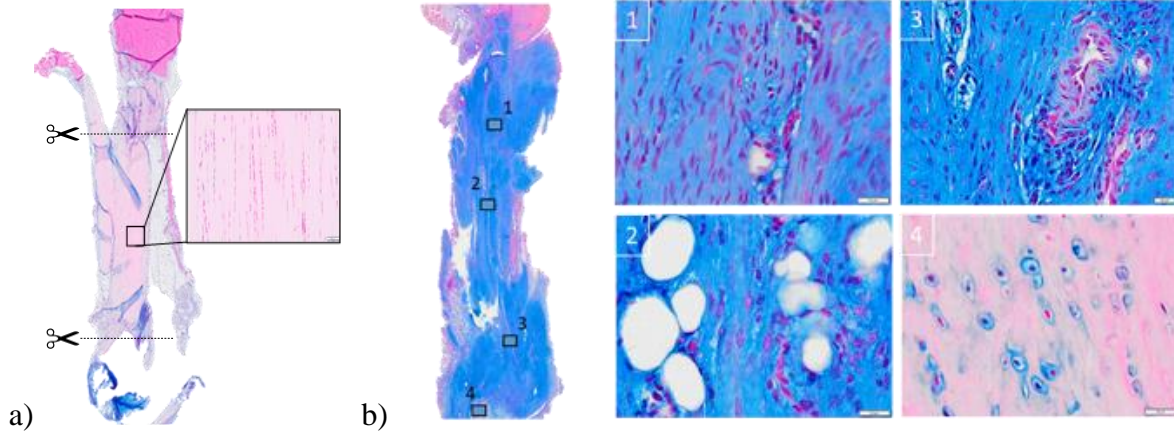
Figure 5-14. Alcian blue stained histological sections of a) intact tendon showing aligned tenocytes and tendon ECM and b) 2 weeks post tendon transection repaired using a suture showing disruption of organized tissue and a significant presence of glycosaminoglycan (GAGs) in the matrix (blue). High-magnification images were subsequently from this section (indicated). 1) Upper region showing cells undergoing phenotype changes 2) Lipid deposition in the mid part of the injury 3) Vessel formation for cartilage formation at the lower region 4) Chondrocyte cells surrounded by their lacunae producing bone-specific matrix.

e)

f)
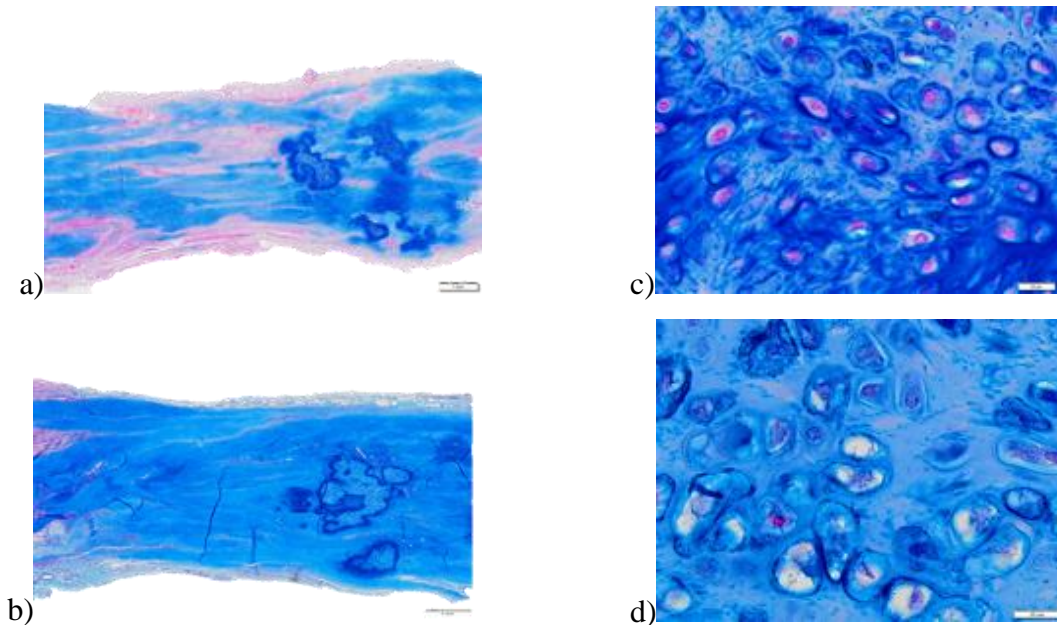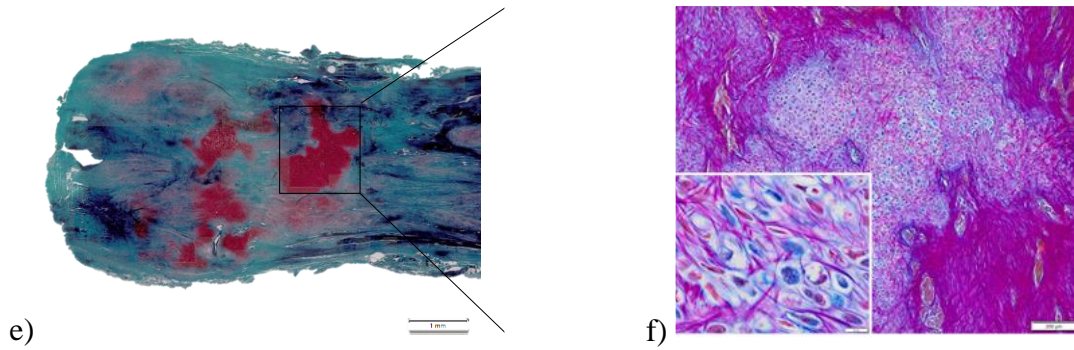
Figure 5-15. Alcian blue stained histological sections of tendon transection after a) four weeks post-injury (cage) and b) 8 weeks post-injury (cage). c) Discrete cartilage nodule formation and d) hypertrophic chondrocytes were observed at the mid granulation region at 8 week post-injury. e) O-safranin stained histological section of 8 weeks post-injury (cage) showing endochondral ossification. f) Herovici staining of 8 weeks post-injury (cage) showing Hypertrophic Chondrocytes encapsulated by their lacunae and separated by ECM characteristic of endochondral ossification.
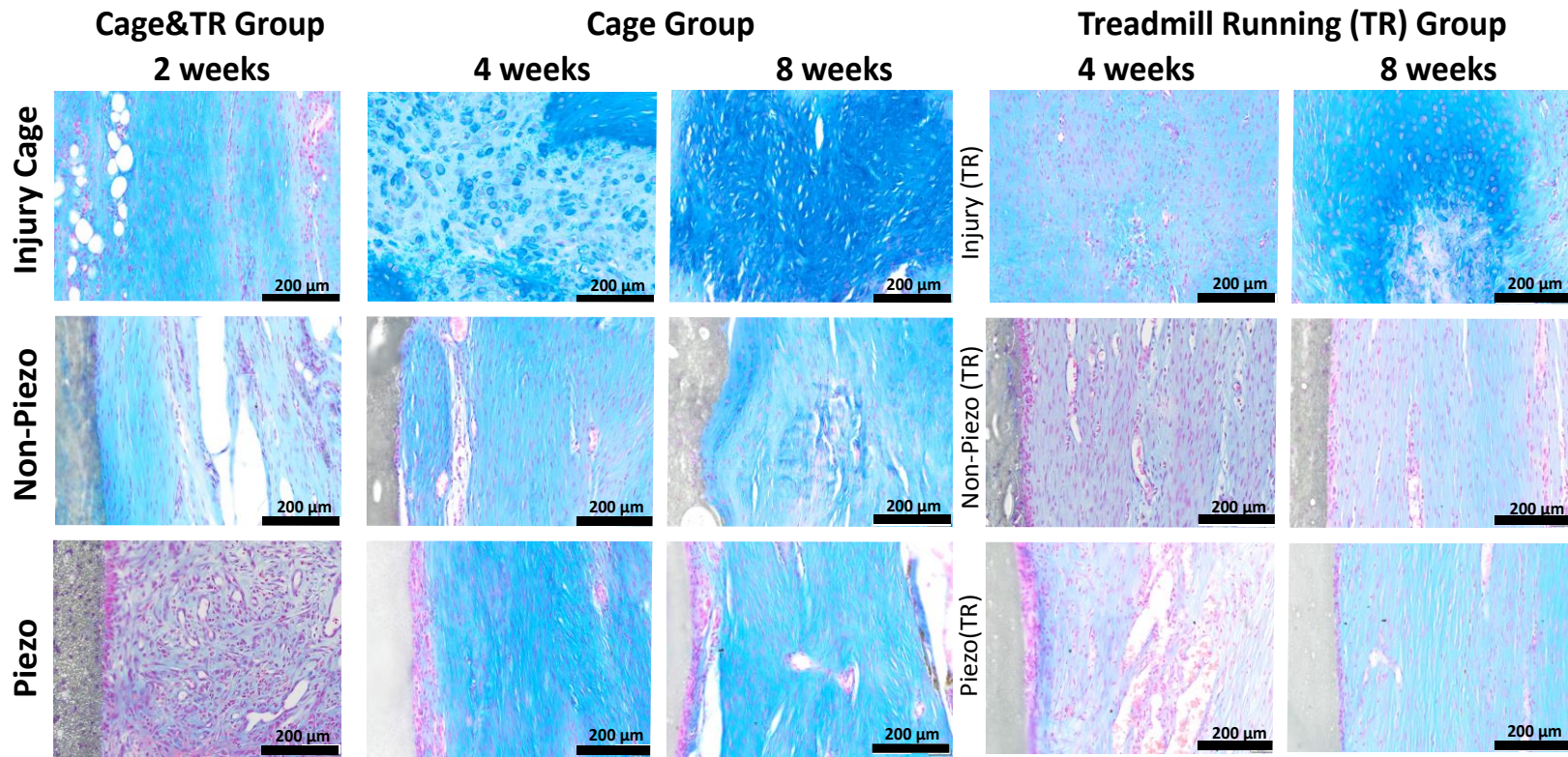
Figure 5-16. Alcian blue-stained representative histological images indicating the role of electromechanical stimulation on proteoglycan deposition in animals subjected to static or treadmill running conditions. Tendon repaired with piezoelectric and non-piezoelectric scaffolds showed less intense proteoglycan (GAG) content. Conversely, transection injuries treated with a suture possessed highly disorganised tissues with increased cell proliferation, increased vasculature and fat deposition, and/or an increased GAG content. Scale bar is 200 μm.
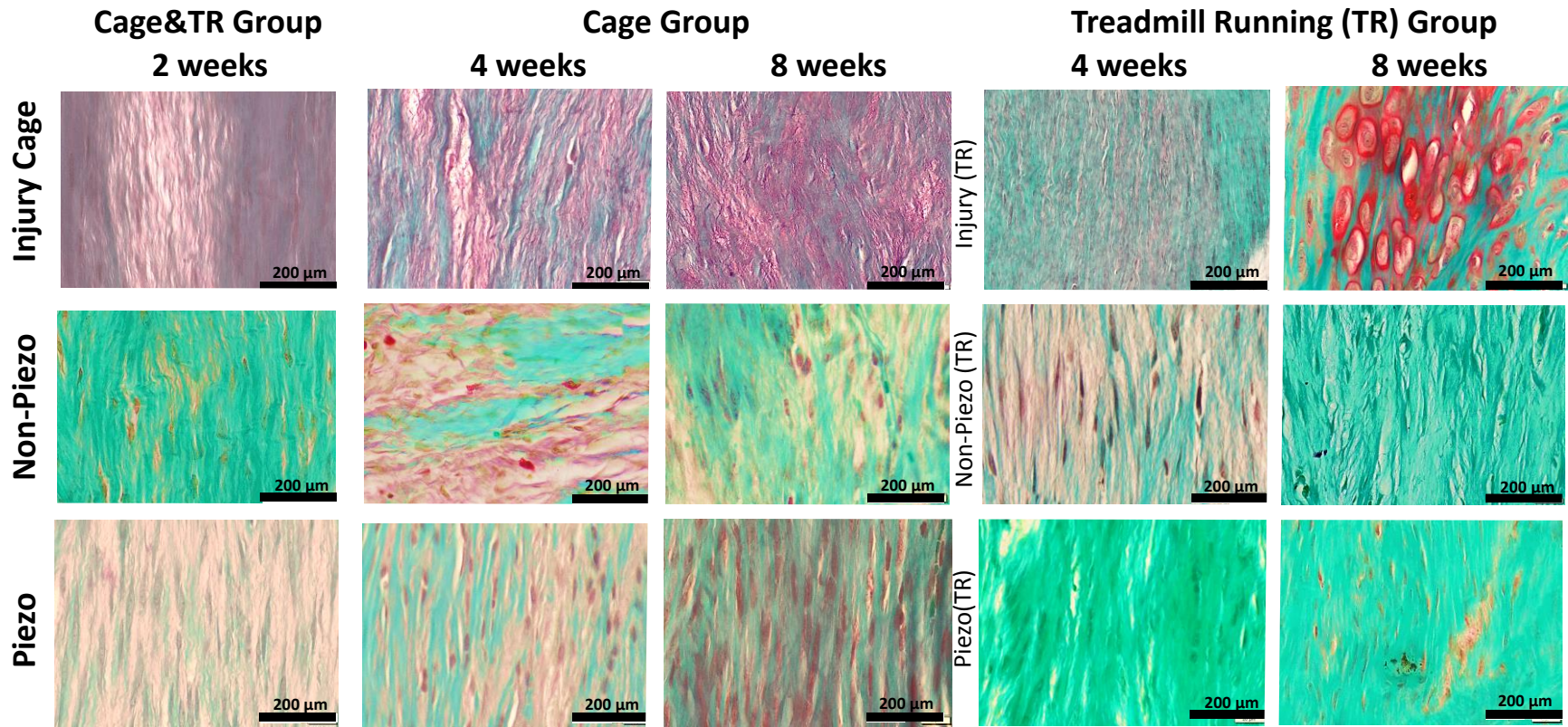
Figure 5-17. Safranin O stained representative histological images indicating the role of electromechanical stimulation on proteoglycan and collagen II deposition and chondrocyte distribution in animals subjected to static or tread-mill running conditions in red. Tendon repaired with non-piezo and piezo scaffolds and subjected to tread-mill running showed less intense proteoglycan (GAG) (red) and collagen II (green) content relative to the cage groups. Injured tendon repaired with a suture possessed a highly disorganised tissues structure with increased GAG and collagen II content and increased chondrocyte presence. Scale bar is 200 μm.
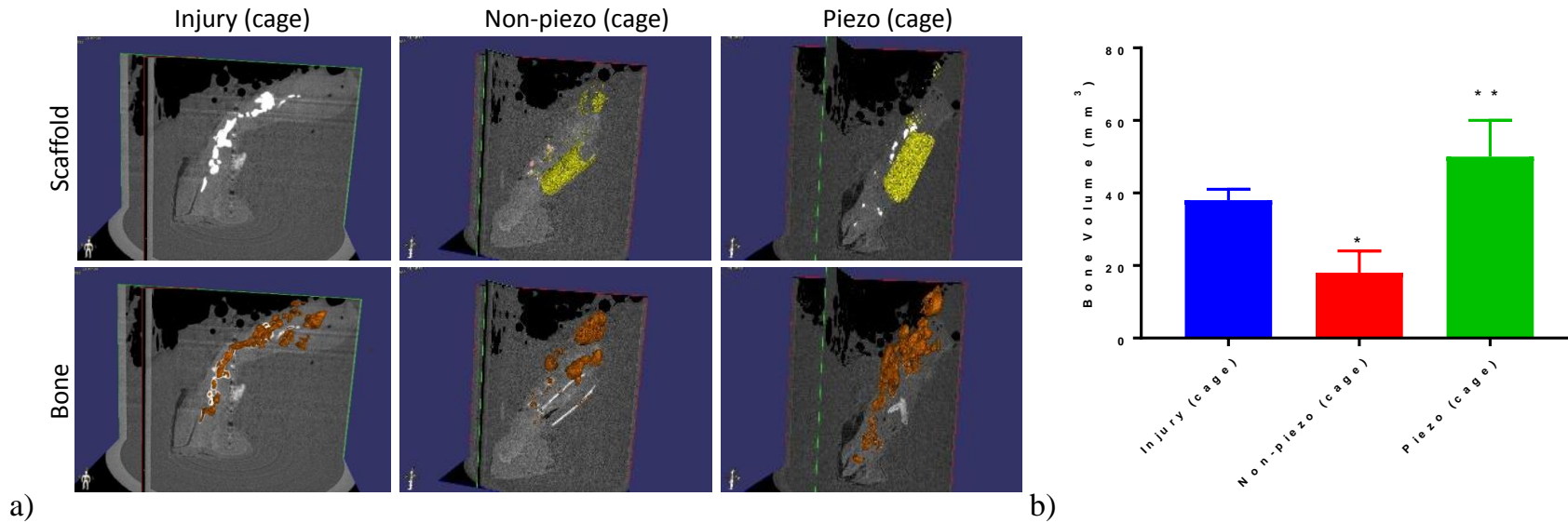
Figure 5-18. a) Representative 3D micro CT reconstructions of injury in tendons treated with suture, non-piezoelectric and piezoelectric scaffolds 8 weeks post tendon transection (cage). Mineralised tissue was observed in the distal part of the tendon corresponding to the bone insertion region. However, in animals treated the piezoelectric scaffolds, a significant amount of mineralised tissue was detected at the peri-implant region. b) Micro CT reveals quantitative differences in ectopic bone volume in tendon injuries treated with piezo and non-piezo scaffolds Analysis performed using one-way ANOVA with post-hoc Tukey HSD (N=3,*p<0.05 Non-piezo vs injury, **p<0.01 piezo vs non-piezo).

To confirm ectopic bone tissue at 8 weeks post-injury, micro CT scanning was employed in animals treated with suture, non-piezo and piezo scaffolds (cage). As shown in Figure 5-18, mineralised tissue at the peri-implant region was observed, with the highest volume of calcified tissue observed in tissues repaired using the piezoelectric scaffolds under static conditions (cage).

5.2.4 Collagen synthesis and tendon-related protein expression are promoted during electromechanical stimulation

It was observed that treadmill running significantly modulated the expression of collagen II in regenerating tendon tissue relative to control non-injured tissues as shown in Figure 5-19. Treadmill exercise resulted in an increase in collagen II expression consistently across all groups by week 4. This trend was halted and even reversed in tendon injuries stabilized using a piezoelectric scaffold 8 weeks post-injury.
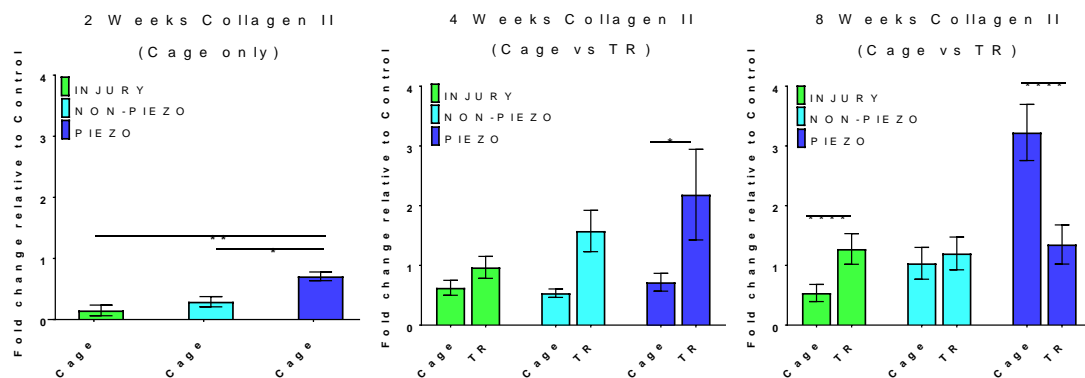
Figure 5-19. Collagen II expression comparison between animals subjected to treadmill running (TR) and cage conditions (Cage). (Results are Mean ± SEM). Analysis performed using one-way ANOVA with post-hoc Tukey HSD ($*p<0.05, **p<0.01, ***p<0.001$).

No significant differences were observed in the expression of collagen II between repair approaches at any time point. However, It was observed that tendon injuries treated with a piezoelectric scaffold exhibited a significant increase in the collagen II content 8 weeks post-injury. This increased in collagen II was not noted in tendon tissues exposed to mechanical loading, however.

During wound healing, early granulation tissue is produced by fibroblasts to act as a temporary scaffold for cell attachment and proliferation. Generally, granulation tissue is mainly comprised of collagen III, and low levels of collagen I. As the healing continues, the ratio of collagen I / collagen III becomes higher but generally never reaches its original values (around 1.4). As shown in Figure 5-20, a significant increase in the ratio of collagen type III to collagen I was observed 4 weeks for all TR groups yet returned to baseline 8 weeks post-injury.

Collagens are the main bulk constituent of tendon tissue. In particular, Collagen type I expression is associated with tissues under tensile loads and is the main protein responsible for the mechanical strength and durability of tendon tissue. An increase in the synthesis of collagen I over collagen III is a good indicator of tendon tissue maturation. During embryonic tendon tissue development, immature disorganised collagen III fibres mature into thick collagen, I fibres with strong birefringence and a highly aligned organisation. Conversely, Collagen II represents almost 80% of the total collagen content in cartilage and is specialised in supporting compressive forces. In tendon, collagen II appears in small amounts in the regions near the bone insertion. Conversely, fibrils of collagen III are always associated with collagen I.
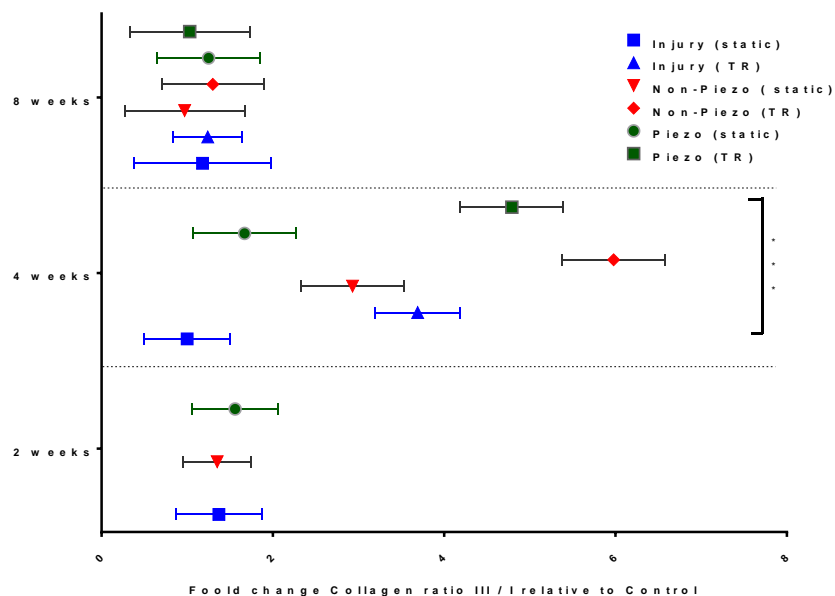
Figure 5-20. Fold change values of collagen III to I ratio relative to contralateral control at weeks 2, 4 and 8 after injury for all the experimental and control groups. The expression of collagen I and III was normalised first by the expression of β-actin and

then by the contralateral control. Analysis performed using one-way ANOVA with posthoc Tukey HSD (*$p<0.05$, **$p<0.01$,*** $p<0.001$).

Among the most important tendon-related markers, SCX, Tenascin-C, Tenomodulin, Collagen I and III and Thrombospondin 4 are the most recognised. The transcription factor scleraxis (Scx) is proposed as the most relevant, as it is highly specific for tendon cells and is considered the master regulator of the tenocyte phenotype. It has been demonstrated that mice lacking SCX showed complete loss of tendon during embryonic development. For this reason, looking at SCX expression is an ideal tool for evaluating phenotypic drift of tenocytes during tendon repair. Conversely, Tenomodulin (TNMD) is a glycoprotein involved in tenocyte proliferation. It was shown (see Figure 5-22 and Figure 5-23) that SCX and TNMD were significantly upregulated after 4 and 8 weeks ($p<0.01$ and $p>0.001$ respectively) of continuous mechanical loading in tendons treated with non-piezo scaffolds in both cage and TR conditions. Whereas SCX and TNMD demonstrated upregulations (>2 fold change) during tendon maturation (after 8 weeks) in tendons treated with piezoelectric scaffolds in both cage and TR conditions.

During maturation, tendon tissue develops mechanical resilient via cross-linking of the organised collagenous network by the incorporation of proteoglycans Biglycan and Decorin. It was observed that Decorin (DCN) was significantly modulated in conjunction with SCX and TNMD at weeks 4 and 8 in treadmill conditioned animals (TR) who received a non-piezoelectric scaffold ($p<0.05$). Despite a similar trend being observed in TR conditioned animals that were treated with a piezoelectric scaffold, the effect was not as significant at either week 4 or 8 ($p>0.05$). The glycoprotein tenascin-C is a marker of embryonic tendon tissue organisation and is normally associated after tendon injury. Tenascin-C was significantly increased at 4 and 8 weeks in the non-piezo (TR) group ($p<0.05$) indicating that tenascin-C may also act as a mechanosensitive protein that modulates tissue organisation (Figure 5-21 & Figure 5-23)
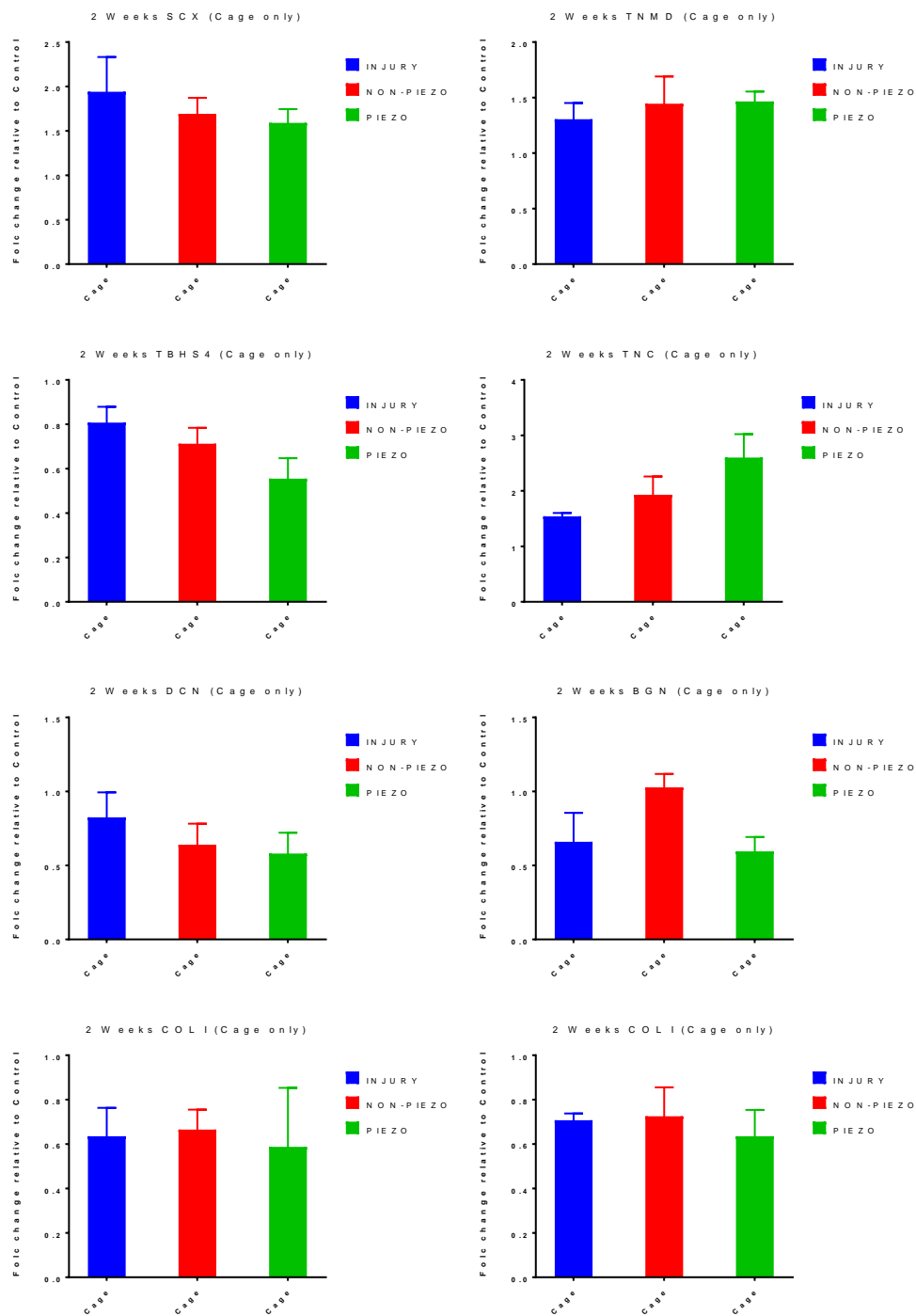
Figure 5-21. Expression of tendon specific proteins at 2 weeks post-injury (cage only). Data represent mean ± SEM (N=4). Analysis performed using one-way ANOVA with post-hoc Tukey HSD (*p<0.05, **p<0.01,***p<0.0001).
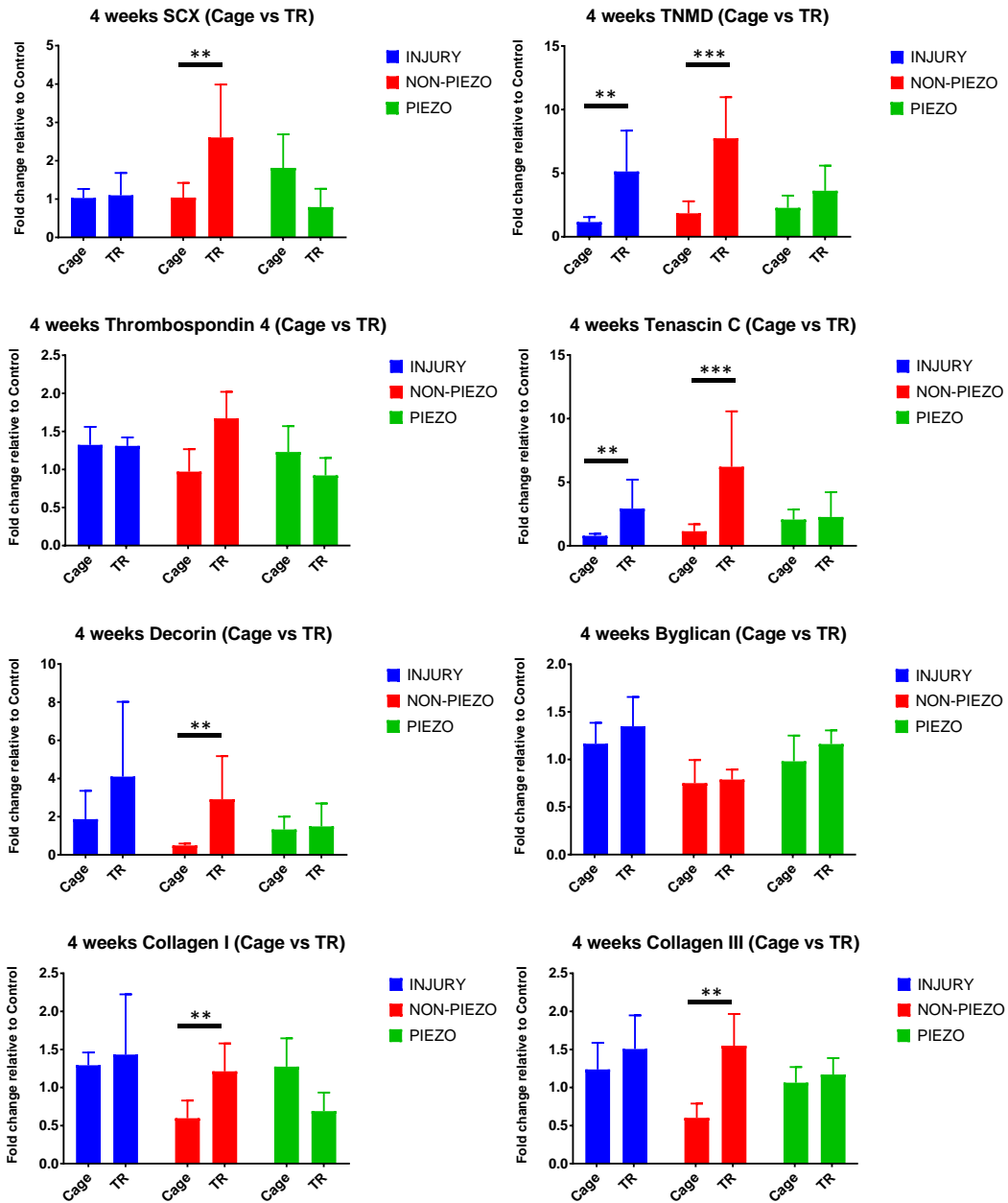
Figure 5-22. Expression of tendon specific protein at four weeks post-injury. Data represent mean ± SEM (N=4). Analysis performed using one-way ANOVA with post-hoc Tukey HSD (*p<0.05, **p<0.01,***p<0.0001).
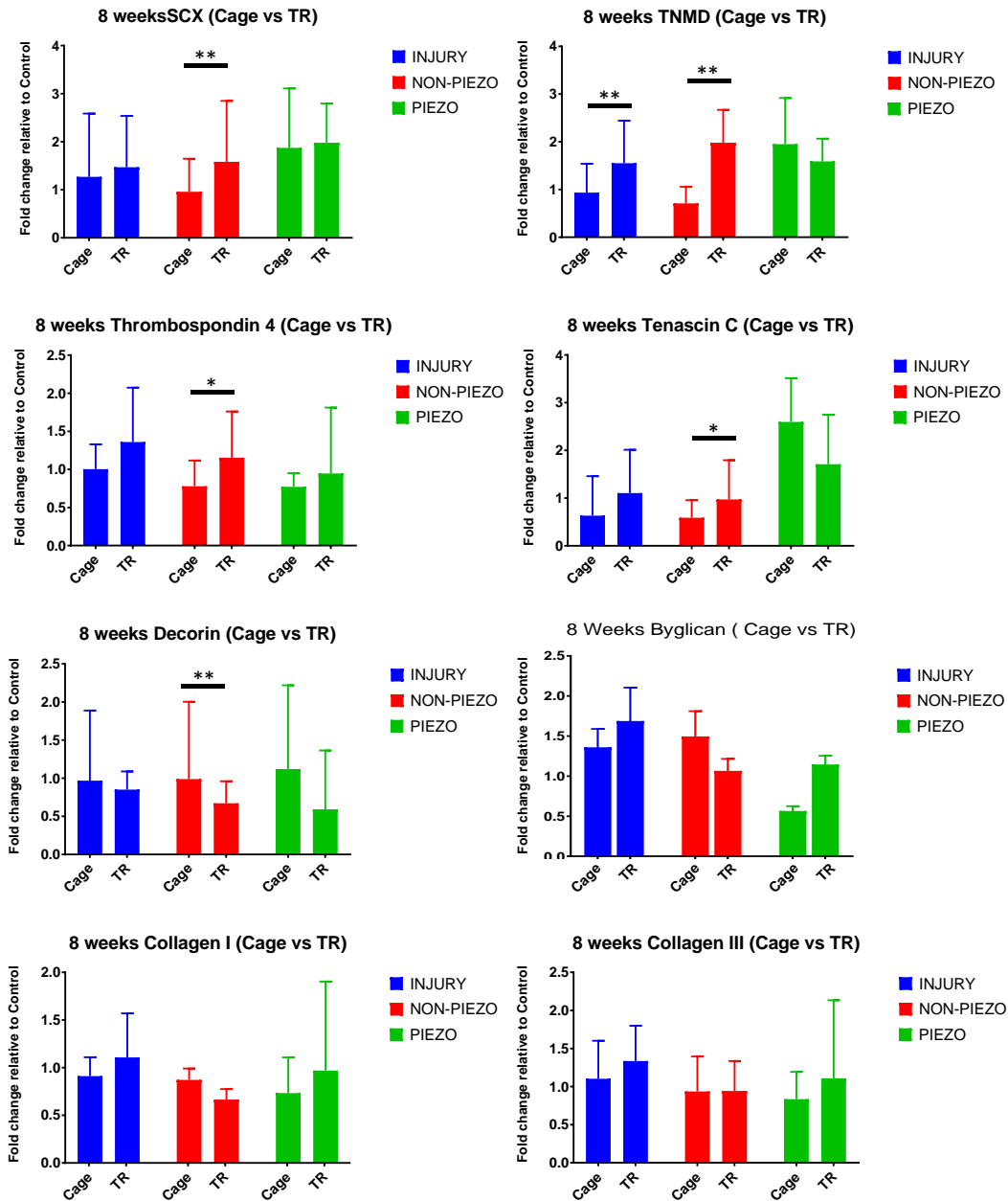
Figure 5-23. Expression of tendon specific proteins at 8 weeks post-injury. Data represent mean ± SEM (N=4). Analysis performed using one-way ANOVA with post-hoc Tukey HSD (*p<0.05. **p<0.01,***p<0.0001.)

5.2.5 Electromechanical stimulation induces activation of tissue development signalling pathways.

Over the last century, it has been recognised that a clear link exists between biomechanical loading and tissue function. Although significant progress has been made

in the field of mechanobiology, the exact mechanism of how cells can sense and respond biochemically to mechanical forces remains elusive. There is an increasing body of research showing that cells utilise diverse molecular machinery for sensing distinct mechanical stimuli with high spatiotemporal resolution. The biological response can range from cytoskeletal reorganisation, modulated ECM adhesion or complete cell reprogramming. At the tissue level, transient mechanical cues result in alterned cellular states and changes in the composition of the interstitial matrix (remodelling) to reach a homeostatic balance between mechanical loading and tissue mechanics.

To explore the tendon response to mechanical loading at the molecular level, two types of different protein families have were assessed as "active sensors" of mechanical stresses to initiate biological responses. The first group is adhesion-related proteins, including integrins (integrin β1, β3 and β5), and signalling proteins (Paxillin). The second group studied were transmembrane ion channel proteins (including KCNK4, TRPV1, TREK1, ANKTM, Piezo1&2 and Ca^{2+} L-type), receptors specifically sensitive to mechanical and electrical stimuli.

Increased expression of the Piezo2 and ANKTM1 (see Figure 5-24) ion channels at weeks 2 and 4 were also observed in tendon tissues isolated from non-piezo (TR) group animals relative to cage animals. The increased expression of these ion channels was positively correlated with the activation of the FGF-ERK/MAPK and FAK pathway (p<0.01). Other significantly modulated molecules were Collagen I and V, Scleraxis, Tenascin-C, Tenomodulin, CD81, BMPR1A, Chondroitin Sulphate (CS), Paxillin and Integrins β1 and β5, that were upregulated at week 4 (non-piezo, TR).

The most significant changes in the functional response of tendon repaired tissue was observed in treadmill-conditioned animals treated with non-piezoelectric or piezoelectric scaffolds. Importantly, electromechanical stimulation for 8 weeks was characterised by an increase on Nestin expression, associated to tendon stem cells. It is know that nestin is highly expressed during tendon postnatal development and plays a pivotal role in tendon tissue differentiation.It was noted that the use of mechanical loading induced by treadmill running during the tendon repair process resulted in significant upregulation in the synthesis of collagen and other tendon-related molecules such as Tenomodulin (TNMD), Tenascin-C (TNC) and Scleraxis (SCX) by week 4. In

371

contrast, static groups (cage) were associated with a down-regulation of tendon-related proteins including SCX, COL I/III, SMAD3, TNC and DCN and upregulation of collagen II. Interestingly, these changes were also associated with a deactivation of integrin beta 1, TRPV1 and Piezo2(see Figure 5-24).
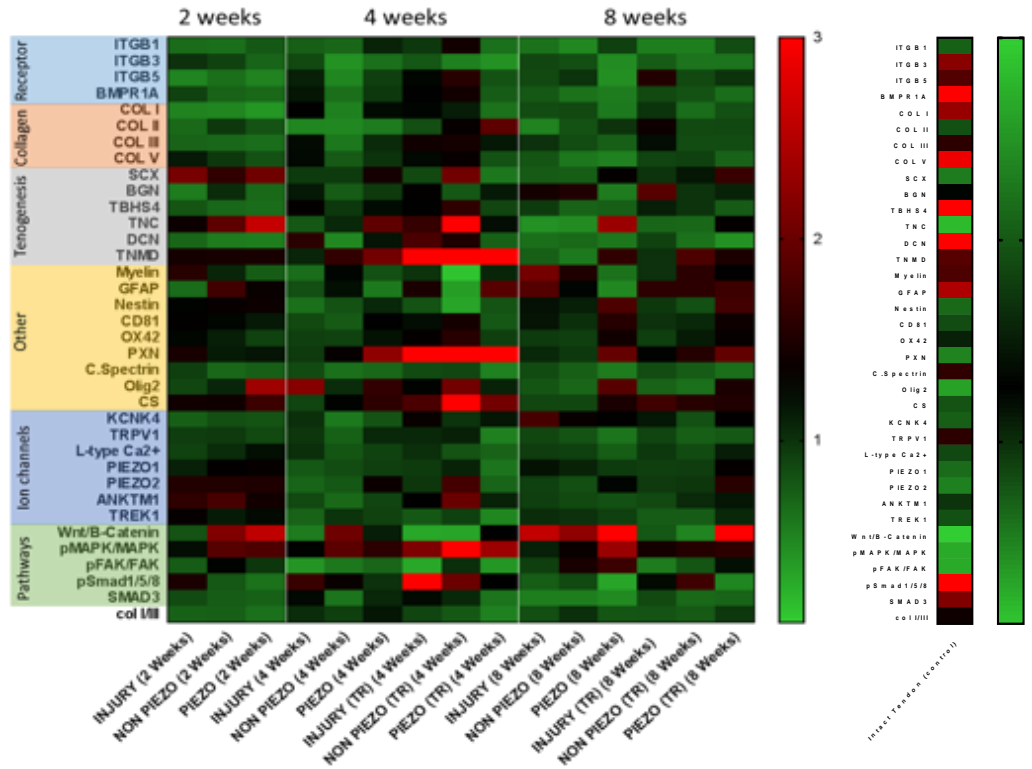
Figure 5-24. The effect of mechanical and electromechanical stimulation on the expression of proteins associated with cellular receptors, pathway functions, ECM production and molecular mechanisms related to tenogenesis. Heat maps of proteins analysed across samples collected from injury, non-piezo and piezo groups at weeks 2, 4 and 8 (static and TR) relative to β-actin. The 35 proteins are represented in rows and classified in different groups according to their function. Data represents mean value of fold change relative first to β-actin and then to control sample (N=4). Intact tendon sample is represented by fold change mean value relative to β-actin of all contralateral samples collected at weeks 2, 4 and 8 for static and TR groups (N=21).

It is largely recognised MAPK/ERK signaling pathway.is activated during exercise and is the link between exercise and adaptive changes in tendon composition. In addition, MAPK/ERK signaling pathway plays a central role in mediating cell division, migration and survival. The activation of the MAPK/ERK pathway was observed in all (TR) groups relative to cage groups at all times except for piezo (TR) at week 8 (p<0.01) that

showed significant dysregulation. The upregulation of FAK signaling was significant only for non-piezo (TR) at week 4 and downregulated at week 8 (p<0.01) (see Figure 5-25).
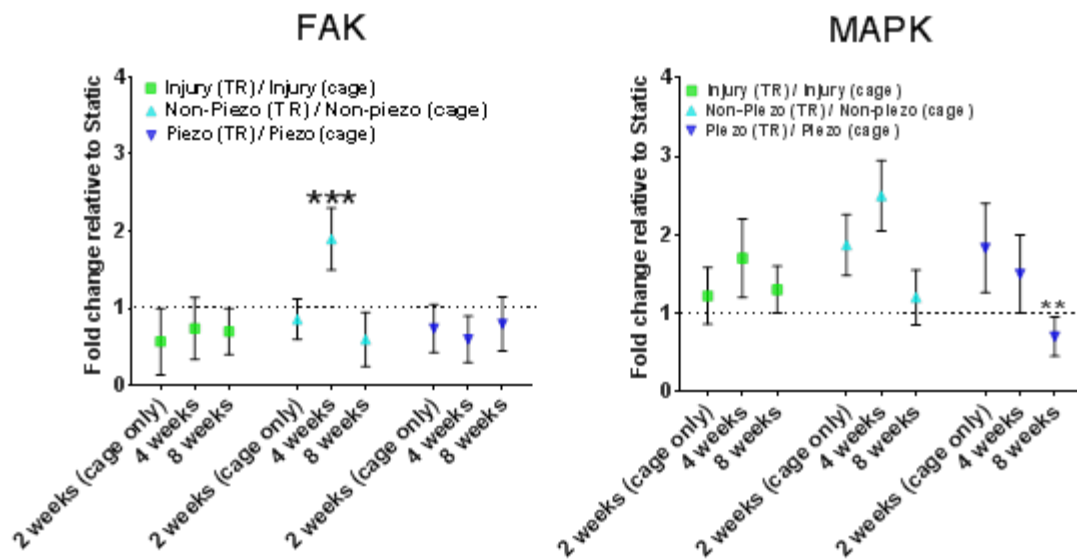
Figure 5-25. Protein Microarray data showing fold change in MAPK and FAK expression in tissues derived from TR animals relative to tissues derived from cage animals for each experimental group at weeks 4 and 8. Significance is shown between samples and week 2 (cage only). Analysis performed using one-way ANOVA (N=4) with posthoc Tukey HSD (*p<0.05. **p<0.01).

The activation of the Smad-dependent pathway (TGF-β/BMP) was observed in (TR) groups at weeks 4 and 8 compared to their corresponding static group (p<0.05) as shown in Figure 5-26. The upregulation of Smad3 and activation of TGF/BMP signalling pathways are involved in the homeostasis of the native tendon and during normal (healthy tendon) structural adaptation, collagen I to collagen III ratio was 1.4 and the main upregulated proteins were integrins β3 and 5, BMPR1A, Collagen I and V, Thrombospondin 4, Decorin and Tenomodulin.
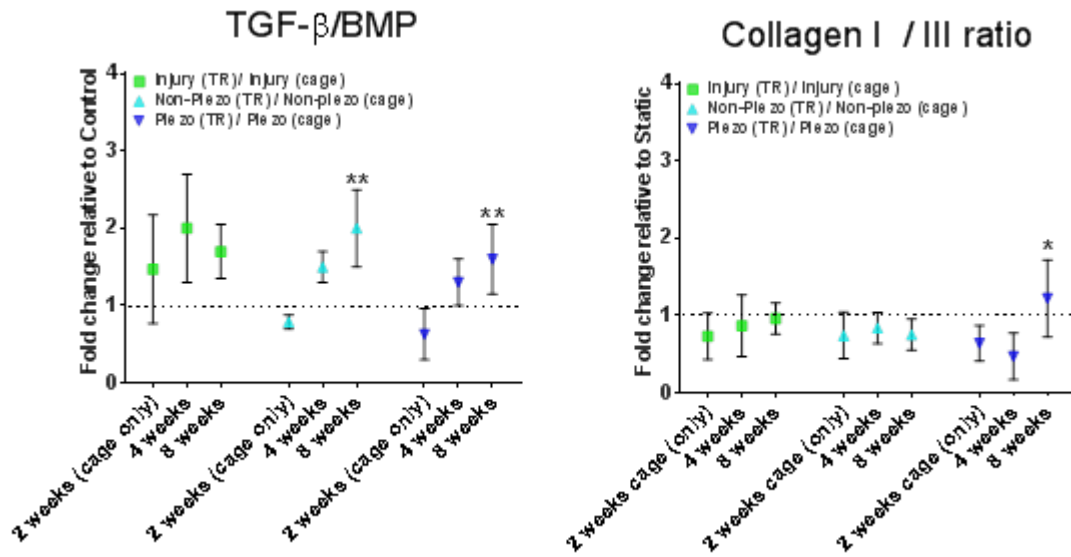
Figure 5-26. Protein. Microarray data showing fold changes in TGF-β/BMP and Collagen I/III ratio expression in tissues derived from TR animals relative to tissues derived from cage animals for each group at weeks 4 and 8. Significance is shown between samples and week 2 (cage only). Analysis performed using one-way ANOVA (N=4) with post-hoc Tukey HSD (*$p<0.05$. **$p<0.01$).

The molecular pathways associated with the ectopic formation of bone after injury was also studied, and significant upregulation in Wnt/β-catenin signaling was observed in caged animals treated with both piezoelectric and non-piezoelectric scaffolds at week 4 ($p<0.01$). In addition, it was observed that piezoelectrical scaffolds under static and dynamic (TR) conditions induced a transient activation of Wnt/β-catenin at week 2 ($p<0.01$) and 8 ($p<0.01$) compared to the non-piezo (static) group that showed prolonged Wnt/β-catenin activation at weeks 2, 4 and 8 ($p<0.01$) (see Figure 5-27).

In summary, mechanical loading of tendon tissues *in vivo* resulted in upregulation of mechanotransductive pathways and collagen synthesis, and ectopic bone formation was correlated with prolonged activation of Wnt/β-catenin and scaffolds under static conditions. Interestingly, when piezoelectric scaffolds were dynamically stimulated, ectopic bone formation was reduced and associated with transient modulation of Wnt/β-catenin and smad3 (see Figure 5-27).
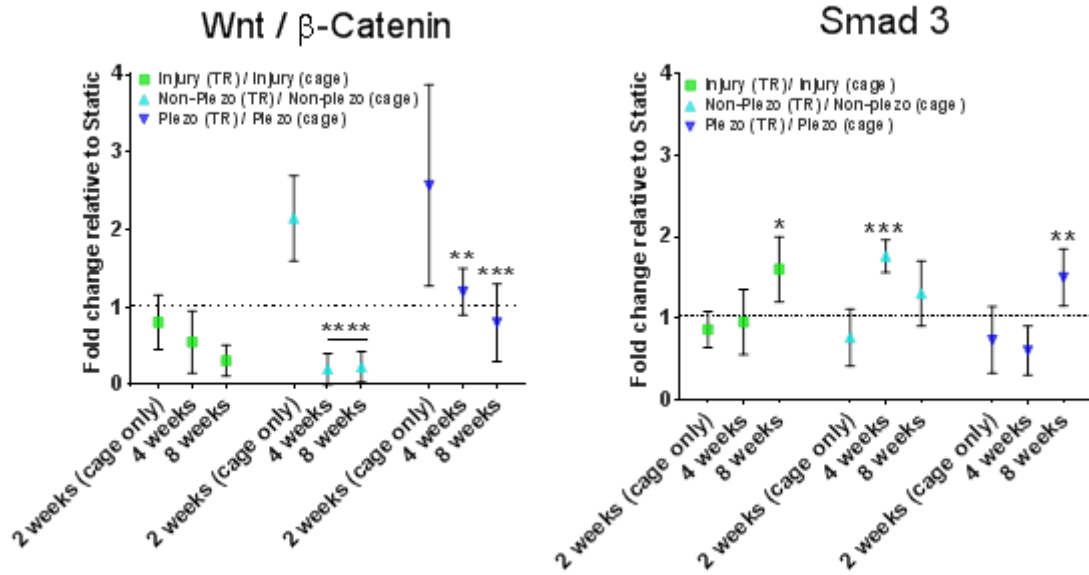
Figure 5-27. Protein. Microarray data showing fold changes in Smad3 and Wnt expression in tissues derived from TR animals relative to tissues derived from cage animals for each group at weeks 4 and 8. Significance is shown between samples and week 2 (cage only). Analysis performed using one-way ANOVA (N=4) with post-hoc Tukey HSD (*$p<0.05$. **$p<0.01$,***$<p.001$, ****$p<0.0001$).

A significant upregulation in integrin β1 expression was observed at week 4 for the animals treated with suture repair (injury) and subjected to treadmill exercise (TR) relative to animals treated with suture repair (cage) ($p<0.05$) and for animals treated with a non-piezo scaffold (TR) relative to non-piezo (cage) ($p<0.0001$). Similarly, at week 4 the activation of integrin β5 was also noted in animals treated with a non-piezo scaffold (TR) relative to animals treated with a non-piezo scaffold (cage) ($p<0.05$). Significant upregulations in the expression of integrin β5 were also observed at week 8 post-injury (TR) relative to injury (cage) ($p<0.01$) and for piezo (TR) relative to piezo (cage) ($p<0.01$).
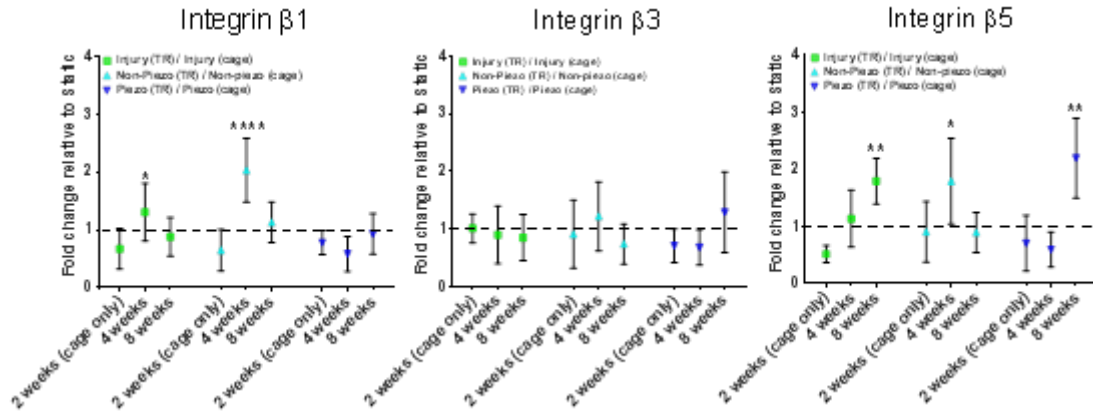
Figure 5-28. Protein. Microarray data are showing fold changes in integrins β1, β3 and β5 expression in tissues derived from TR animals relative to tissues derived from cage animals for each group at weeks 4 and 8. Significance is shown per condition (injury, non-piezo or piezo) between samples at week 4 and 8 vs samples at week 2 (cage only). Analysis performed using one-way ANOVA (N=4) with post-hoc Tukey HSD (*p<0.05. **p<0.01,***<p.001, ****p<0.0001).

It was observed a significant upregulation of Piezo 2 (p<0.001),TRPA1 (p<0.01), KCNK4 (p<0.001) and TRPV1 (p<0.05) at week 4 for non-piezo (TR) relative to non-piezo (cage). Similarly, at week 4 it was also noted deactivation of piezo 2 (p<0.0001) and KCNK2 (p<0.05) for piezo (TR) relative to piezo (cage). Finally, deactivation of Piezo2 (p<0.05) and KCNK2 (p<0.05)was observed after 8 weeks fro injury (TR) relative to injury (cage) .
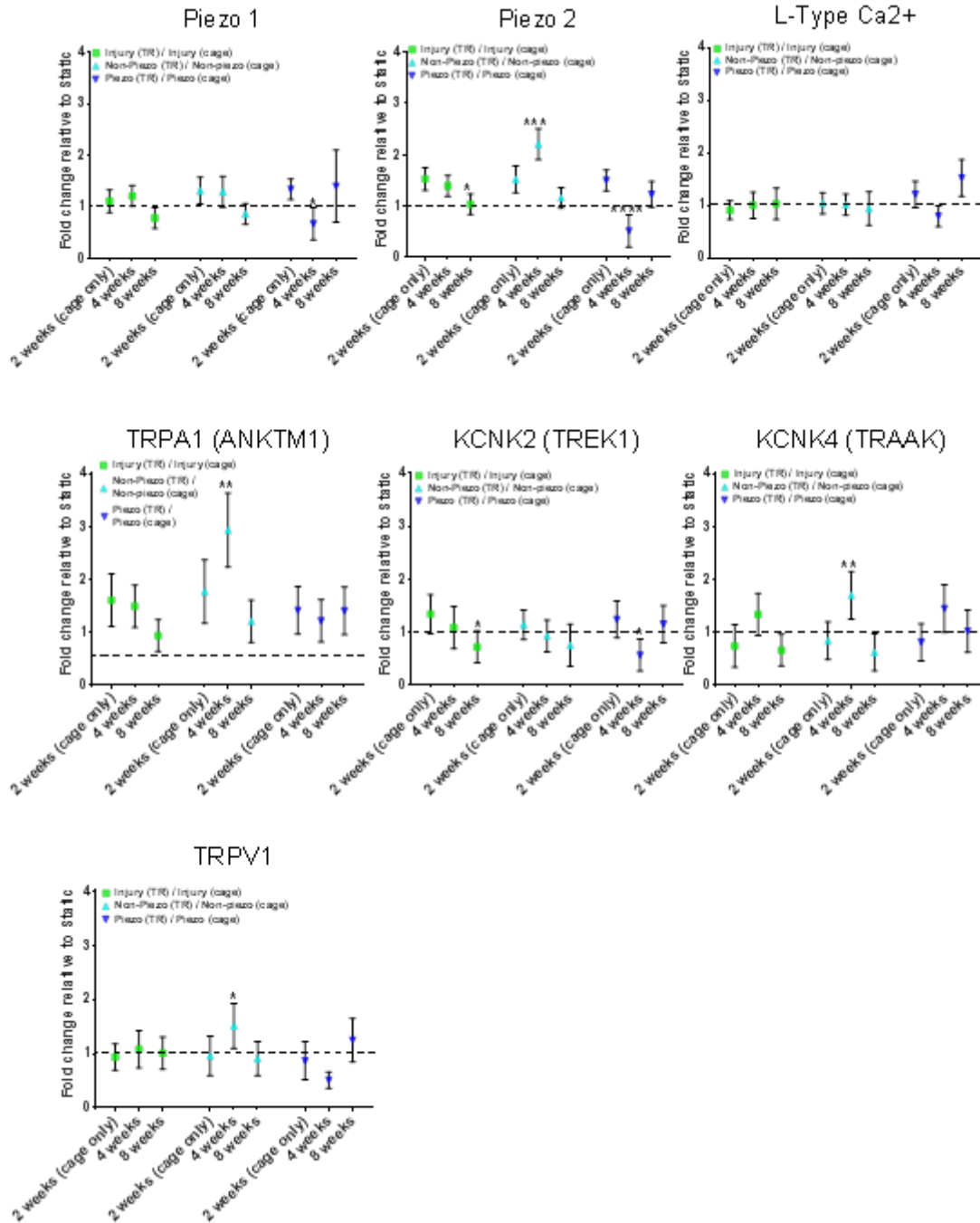
Figure 5-29. Protein. Microarray data are showing fold changes in Piezo1,Piezo2, TREK1, TRAAK, ANKTM1 and L-type Ca^{2+} ion channels expression in tissues derived from TR animals relative to tissues derived from cage animals for each group at weeks 4 and 8. Significance is shown per condition (injury, non-piezo or piezo) between samples at week 4 and 8 vs samples at week 2 (cage only). Analysis performed using one-way ANOVA (N=4) with post-hoc Tukey HSD (*p<0.05. **p<0.01,***<p.001, ****p<0.0001).

5.3   Discussion

Tendon is a highly specialised and mechanosensitive tissue, capable of modulating its structure and composition when it is mechanically loaded. Although the mechanical properties of tendon tissues are well-characterised, an often overlooked characteristic of tendon is its piezoelectric behaviour under dynamic physiological conditions. The electrical response to a changing mechanical environment is believed to play a fundamental role in the initiation of cell signalling cascades and during the tissue remodelling process. In this study, piezoelectric scaffolds were explored to synthetically replicate the natural piezoelectric characteristic of tendon and assess whether piezoelectric scaffolds can be utilised to enhance regeneration in a tendinopathy animal model. Finally, different pathways of mechanotransduction were studied to unravel the mechanistic effect of piezoelectricity on intracellular signalling processes during tendon repair.

It is well known that mechanical loading has a beneficial effect on tendon repair, and therapeutic loading levels have been identified in various tendons tissues for improved clinical outcomes. In particular, studies have shown that a moderate loading regime (i.e 30-50 min/day, 5 days/week, 9 -11m/min = 1350-2250 m/week) of the tendon can result in enhanced tendon repair. Conversely, if the mechanical forces become too intense (60 min/day 5 days week, 13-18m/min = 3900-5400 m/week), tendinopathy is promoted. Tendon responses to overuse/intense treadmill running regimes during healing has been shown to increase cartilage formation or ossification with higher expression levels of Collagen II, Sox-9, Aggrecan, Osterix or Runx-2 and characteristic histological changes include intense collagen staining, lipid deposition, loss of fibre organisation, calcification, vascularity and increased number of dedifferentiated tenocyte cells (phenotypic drift)[351,352,356,370,383–385]. Conversely, following moderate exercise, the rate of synthesis of collagen I/III and levels of growth factors (i.e. TGF-β) have been observed to increase in vivo[20,53,54]. The effect of moderate exercise conditioning on wound healing has also been studied in a rat model of moderate treadmill running[366]. Here it was observed that rats pre-conditioned with moderate exercise before the injury were able to heal tendon wounds more rapidly than non-pre-conditioned animals. In this model, collagen I/III synthesis and organisation was promoted as well as tendon cell function (increase in Tenomodulin and Collagen I) compared to the "static" model (non-running rats). In these non-conditioned animals, tendon tissue was characterised by osteochondral formation (increase in Runx2 and Collagen II).

A recent study using moderate treadmill running (30 min/day, 13 m/min, 5 days/week) on mice for 10 weeks showed that the detrimental ageing effects could be modified using mechanical loading. Here glycation products and calcification typical of ageing tendons decreased by more than 60% [386]. The study demonstrates that there is an optimal range of mechanical stimulation to induce faster healing, and a moderate mechanical loading is generally beneficial for tendon formation.

It has also been shown that moderate treadmill running can increase the expression of stem cell markers (Nestin and Nanog), tenocyte gene expression (TNMD and SCX) and decreases lipid deposition, proteoglycan accumulation, calcification and expression of non-tenocyte markers [366,388]. Conversely, studies suggest that chondro specific differentiation and chondrogenesis can be mediated by SCX expressing tendon cells. Histologically, endochondral ossification involves four stages: inflammation, chondrogenesis, osteogenesis and maturation. First, during inflammation, immune cells invade the injury site and infiltrate. After, endothelial cells from the surrounding epitenon undergo endothelial to mesenchymal transition and acquire stem cell-like phenotype. During inflammatory processes post-injury, cells from the epitenon and muscle start proliferating and invade the injury site along with immune cells that clear space from broken-down collagen fibres disrupting the highly organised structure. A recent study demonstrated that Scx^+ tendon-derived and interstitial muscle-derived $Mkx1^+$ progenitor cells mediate chondrogenesis by differentiation into chondrocytes[389].

In this study, the chosen moderate treadmill running protocol (as previously reported) was treadmill running 5 days a week for 30 to 60 min at speed between 9 to 11 m/min[355,358,386,390]. The results in our model are consistent with the literature and demonstrated a robust positive effect of treadmill running on the functional recovery in a rat tendon injury model. The rat Achilles tendon repaired using sutures and subjected to treadmill running showed a faster recovery compared to animals in cages, as shown in the recovery of MTP joint displacements during animal gait. However, the most significant benefits were found when scaffolds and treadmill were used synergistically to repair the physically injured tendon. When using non-piezoelectric scaffolds and treadmill running, the repair was enhanced in as little as four weeks, and the effect was more evident after 8 weeks.

Similarly, piezoelectric scaffolds and treadmill running showed an incremental functional recovery after 4 and 8 weeks. In similar studies, Zhang et al. examined the effects of exercise on tissue healing using a rat model and moderate treadmill running (MTR) and found that MTR accelerated the healing process by promoting the organisation of collagen fibres and decreasing senescent cells when compared to the cage group. Also, MTR increased stem cell markers nestin and tendon-related markers, including tenomodulin, the collagen I to collagen III ratio and downregulated osteochondral related markers including collagen II and Runx-2[354,366,388].

It was observed that collagen II expression was initially increased in animals undergoing treadmill running, but after 8 weeks, the treadmill running group exhibited lower levels of collagen II expression that can be translated into reduced ectopic bone formation[354]. Interestingly, the most significant modulation of collagen II expression was obtained via electromechanical stimulation (treatment with a piezoelectric scaffold combined with treadmill running). Similarly, the synthesis of collagen I and III was increased in the dual MTR/scaffold groups. It was noted that the collagen III to collagen I ratio was increased for both groups four weeks post-injury, indicative of the proliferative stage of wound healing. However, the ratio levels returned to baseline after 8 weeks, a condition characteristic of the early remodelling phase.

To quantify the differences obtained in histological tendon regeneration a modified tendon healing scoring was used. The results demonstrated that the experimental conditions which promoted the most rapid healing response were the non-piezoelectric scaffold/MTR followed by the piezoelectric/MTR scaffold group. The obtained histological tendon regeneration scores for all the MTR groups was significantly higher than that of all cage groups. Similarly, tendon related markers Tenomodulin, Scleraxis, Thrombospondin 4 and Tenascin-C were significantly upregulated in the non-piezo MTR group at week 4 and 8. Moreover, the rest of the TR groups also followed this trend, but differences in scores did not reach significant levels.

Finally, measurements of cartilage and bone formation using histomorphometric analysis suggested a reduction of ectopic bone formation in animals undergoing treadmill running. These results are consistent with similar studies conducted in rats[391] and mice[353], which concluded that increasing exercise activity delays ectopic bone

formation in a tendon injury model. Unfortunately, these studies did not investigate systematically the mechanism underlying the role of exercise in reducing tendon calcification; they showed that bone formation is related to the activation of the Wnt/β-catenin signalling pathway[392–397]. Although many studies have sought to elucidate the effects of mechanical stimulation on tendon regeneration, in this chapter, the pathways involved in tendon repair in response to piezoelectric and mechanical stimulation after tendon injury were investigated.

It was shown that the maximum of functional recovery at week 4 in the non-piezo MTR group was accompanied by an activation of the FGF-MAPK/ERK and TGF-β/BMP signalling pathways. Conversely, the electromechanical stimulation as induced in the piezoelectric MTR group induced significant modulation of the FAK and Wnt/β-catenin signalling pathways. Furthermore, cage groups also showed significant activation of the Wnt/β-catenin signalling pathway relative to the control group. According to a growing body of research, Wnt/β-catenin signalling plays a pivotal role in tissue regeneration and development[398–400] and a growing number of studies suggest a direct 'link between mechanical stress and activation of the Wnt pathway in regeneration[401–403]. Even though it is commonly believed that activation of bone formation related signalling pathways might be not desired during tendon healing, it becomes central for the tendon to bone insertion. In our studies, it was shown that the higher levels of activation of this pathway were obtained when using piezoelectric scaffolds in static conditions and were decreased in the mechanically stimulated tendon. These results suggest that electrical charges might promote the activation of this pathway and bone formation. Hence, transient activation of this pathway might enhance tendon to bone healing; however, a prolonged activation might become detrimental for the functional tendon repair. Similarly, a recent study has shown that activation of Wnt/β-catenin signalling suppresses the expression of tenogenic-related genes SCX and TNMD and reduces the expression of smad3, suggesting that Wnt/β-catenin is a repressor for tenogenic gene expressions[393]. Again, dynamic electrical stimulation (ES) might results in moderate or transient activation Wnt/β-catenin as shown by the decrease when using mechanically stimulated piezoelectric scaffolds.

ES has been extensively applied in clinics with relative success; however, the therapeutic mechanism is poorly understood. The beneficial effect of ES on collagen synthesis and activation of TGF-beta signalling has mainly been demonstrated in the

remodelling process of different tissues including bone, skin and ligament[404–407]. Collagens provide strength to the injured tendon tissue, which biomechanical properties are constantly probed by the resident tendon cells that regulate the collagen metabolism through integrin/TGF-β signalling. Integrins link the actin cytoskeleton to the surrounding ECM and have a regulatory function on different critical signalling pathways, including TGF-Beta. In particular, studies have shown that inhibiting integrin β1 by an antibody dysregulates completely TGF-β and MAPK signalling[408] pathways that are essential for functional tendon repair. In a recent study, electrical stimulation was utilised to increase the levels of integrin β1, TGF-β1, Collagen II, Aggrecan and Sox9 for promoting chondrogenic stem cell differentiation and subsequent condensation of chondrocytes without exogenous biochemical factors. In this study, the regulatory effect of electrical stimulation was negated by blocking TGF-β signalling by SB-431542[107]. The conclusions obtained from these studies suggest that the activation of TGF-β signalling and upregulation of collagen synthesis by electrical stimulation might be dependent on integrin β1 accumulation. It has been shown that electrical stimulation can improve TGF-β-mediated collagen synthesis only when sufficient integrin β1 expression levels are achieved [409].The primary downstream regulator of β1 integrin accumulation is focal adhesion kinase (FAK) activation characterised by FAK autophosphorylation in the tyrosine residue 397 site[410]. Therefore it is suggested that FAK and TGF-β can act synergistically to achieve increased collagen synthesis[411]. In this chapter, it was observed that the highest levels of Col I, SCX and TNMD via β1 aggregation and tyrosine kinase activitity (FAK) followed by TGF-β significant activation under mechanical stimulation (non-piezo scaffolds under TR) and in less degree under electromechanical stimulation.

Conversely, electrical stimulation (ES) relative to mechanical stimulation showed higher activation level of the Wnt signalling cascade independent of integrin synthesis. However, activation of Wnt signalling was reversed after 8 weeks of continuous stimulation. Noteworthy, β-catenin stabilises in the cytoplasm prior to Wnt signalling pathway activation to regulate cell proliferation and fate determination. An increasing number of *in vitro* and *in vivo* studies have demonstrated the potent regulatory effect of ES-mediated Wnt signalling control of MSC osteogenic differentiation. For instance, *in vitro* electrical stimulation of bone cells (during both proliferative and differentiation phase) has been shown to increase gene and protein expression of canonical Wnt/β-

catenin signalling pathway including Wnt1, LPR6 and β-catenin [412,413]. In bone tissue, electrical stimulation could prevent mass and structure loss (analysed by MicroCT) via activation Wnt/β-catenin signalling pathway [414412,415]. These studies suggest that electrical stimulation enhances the differentiation of progenitor cells through activation of Wnt signalling. Also, electrical stimulation increases cytoplasm calcium activity and accelerates differentiation processes via regulation of expression of ion channels. For instance, electrically mediated MSCs osteogenesis resulted in elevated levels of expression of voltage-gated ion channels (L-type calcium) together with Runx2, ALP and collagen I [416,417]. Moreover, electrical stimulation has been shown to exert an anti-inflammatory and pro-angiogenic effect by modulating the release of the cytokines interleukin-1β and FGF [418] through activation of Ca^{2+}/nitric oxide/PKG pathway [419–421]. Interestingly, different electrical stimulation conditions can selectively influence cell activity and determine different cell fates. A recent study showed that high levels of electrical stimulation (45Hz) increased MSC osteogenesis and enhanced the level of expression of RUNX2, ALP and Ca^{2+}. In contrast, low-level electrical stimulation (7Hz) promoted osteoclast MSC differentiation via MAPK signalling pathway activation[422]. In summary, evidence is increasingly gathering and suggests a balanced cross-talk between Ca^{2+}, TGF-β/BMP, Wnt/β-catenin and FGF/MAPK-ERK under electrical stimulation that controls cell dedifferentiation and functional tendon tissue repair processes [423,424].

5.4 Conclusion

Scaffold-mediated tendon repair reduced ectopic bone formation and enhanced mature tendon tissue formation. Furthermore, enhanced tendon tissue regeneration was obtained with the use of non-piezoelectric scaffolds in mechanically stimulated animals relative to piezoelectric scaffolds. In contrast, piezoelectric scaffolds promoted bone formation in caged animals, but this bone formation was decreased in response to mechanical stimulation. In conclusion, functional tendon tissue repair and remodelling can be modulated by mechanical and electrical stresses. However, how cells can sense and transduce these signals remains elusive. In this chapter, the effects of electromechanical stimulation on the activation of the two (identified in our in vitro studies) mechanical and electrical sensitive receptors were investigated (ion channels and adhesion proteins). The results showed that functional tendon repair (characterised by upregulation of SCX, TNMD and Collagen I) was promoted by mechanical stimulation that initiates TGF-β/BMP signalling via integrin β1/FAK activation and FGF/MAPK-ERK pathway via TRP-(i.e ANKTM1) and Piezo (i.e Piezo 2) ion channels upregulation. Conversely, electrically mediated activation of Wnt/β-catenin via integrin β5 activation resulted in ectopic bone formation, the deactivation of Piezo (i.e Piezo 2) ,TRP (i.e TRPV1) ion channels and FAK and a reduction of integrin β1 expression.

5.5   References

1.   Snedeker, J. G. & Foolen, J. Tendon injury and repair – A perspective on the basic mechanisms of tendon disease and future clinical therapy. *Acta Biomaterialia* **63**, 18–36 (2017).

2.   Walden, G. *et al.* A Clinical, Biological, and Biomaterials Perspective into Tendon Injuries and Regeneration. *Tissue Eng. Part B Rev.* (2017). doi:10.1089/ten.teb.2016.0181

3.   Docheva, D., Müller, S. A., Majewski, M. & Evans, C. H. Biologics for tendon repair. *Advanced Drug Delivery Reviews* (2015). doi:10.1016/j.addr.2014.11.015

4.   Kartus, J., Movin, T. & Karlsson, J. Donor-site morbidity and anterior knee problems after anterior cruciate ligament reconstruction using autografts. *Arthroscopy* (2001). doi:10.1053/jars.2001.28979

5.   Yasuda, K., Tsujino, J., Ohkoshi, Y., Tanabe, Y. & Kaneda, K. Graft Site Morbidity with Autogenous Semitendinosus and Gracilis Tendons. *Am. J. Sports Med.* (1995). doi:10.1177/036354659502300613

6.   Kartus, J., Movin, T. & Karlsson, J. Donor-site morbidity after anterior cruciate ligament reconstruction using autografts clinical, radiographic, histological, and ultrastructural aspects. in *Anterior Knee Pain and Patellar Instability* (2006). doi:10.1007/1-84628-143-1_19

7.   Seo, J. G. *et al.* Ankle morbidity after autogenous Achilles tendon harvesting for anterior cruciate ligament reconstruction. *Knee Surgery, Sport. Traumatol. Arthrosc.* (2009). doi:10.1007/s00167-009-0729-9

8.   Kuo, C. K., Marturano, J. E. & Tuan, R. S. Novel strategies in tendon and ligament tissue engineering: Advanced biomaterials and regeneration motifs. *BMC Sports Sci. Med. Rehabil.* **2**, 20 (2010).

9.   Lomas, A. J. *et al.* The past, present and future in scaffold-based tendon treatments. *Advanced Drug Delivery Reviews* **84**, 257–277 (2015).

10.   Liu, Y., Ramanath, H. S. & Wang, D. A. Tendon tissue engineering using scaffold enhancing strategies. *Trends in Biotechnology* **26**, 201–209 (2008).

11.   Mammoto, T. & Ingber, D. E. Mechanical control of tissue and organ development. *Development* (2010). doi:10.1242/dev.024166

12.   Obregón, R., Ramón-Azcón, J. & Ahadian, S. Bioreactors in Tissue Engineering. in *Tissue Engineering for Artificial Organs: Regenerative Medicine, Smart*

Diagnostics and Personalized Medicine (2016). doi:10.1002/9783527689934.ch6

13. Plonsey, R., Barr, R. C., Plonsey, R. & Barr, R. C. Electrical Stimulation of Excitable Tissue. in *Bioelectricity* (2000). doi:10.1007/978-1-4757-3152-1_7

14. Rajabi, A. H., Jaffe, M. & Arinzeh, T. L. Piezoelectric materials for tissue regeneration: A review. *Acta Biomater.* **24**, 12–23 (2015).

15. Tandon, N. *et al.* Electrical stimulation systems for cardiac tissue engineering. *Nat. Protoc.* (2009). doi:10.1038/nprot.2008.183

16. Chen, J., Xu, J., Wang, A. & Zheng, M. Scaffolds for tendon and ligament repair: Review of the efficacy of commercial products. *Expert Review of Medical Devices* **6**, 61–73 (2009).

17. Longo, U. G., Lamberti, A., Maffulli, N. & Denaro, V. Tendon augmentation grafts: A systematic review. *Br. Med. Bull.* (2010). doi:10.1093/bmb/ldp051

18. Yin, Z. *et al.* The regulation of tendon stem cell differentiation by the alignment of nanofibers. *Biomaterials* **31**, 2163–2175 (2010).

19. Kew, S. J. *et al.* Regeneration and repair of tendon and ligament tissue using collagen fibre biomaterials. *Acta Biomaterialia* (2011). doi:10.1016/j.actbio.2011.06.002

20. Font Tellado, S., Balmayor, E. R. & Van Griensven, M. Strategies to engineer tendon/ligament-to-bone interface: Biomaterials, cells and growth factors. *Advanced Drug Delivery Reviews* (2015). doi:10.1016/j.addr.2015.03.004

21. Cross, L. M., Thakur, A., Jalili, N. A., Detamore, M. & Gaharwar, A. K. Nanoengineered biomaterials for repair and regeneration of orthopedic tissue interfaces. *Acta Biomaterialia* (2016). doi:10.1016/j.actbio.2016.06.023

22. Pesqueira, T. *et al.* Engineering magnetically responsive tropoelastin spongy-like hydrogels for soft tissue regeneration. *J. Mater. Chem. B* (2018). doi:10.1039/c7tb02035j

23. Pesqueira, T., Costa-Almeida, R. & Gomes, M. E. Magnetotherapy: The quest for tendon regeneration. *J. Cell. Physiol.* (2018). doi:10.1002/jcp.26637

24. Silva, E. D. *et al.* Multifunctional magnetic-responsive hydrogels to engineer tendon-to-bone interface. *Nanomedicine Nanotechnology, Biol. Med.* (2018). doi:10.1016/j.nano.2017.06.002

25. Gonçalves, A. I., Rodrigues, M. T. & Gomes, M. E. Tissue-engineered magnetic cell sheet patches for advanced strategies in tendon regeneration. *Acta Biomater.* (2017). doi:10.1016/j.actbio.2017.09.014

26. Holzapfel, B. M. *et al.* How smart do biomaterials need to be? A translational science and clinical point of view. *Advanced Drug Delivery Reviews* (2013). doi:10.1016/j.addr.2012.07.009

27. J.E. Commission, ETN nanomedicine: roadmaps in nanomedicine towards 2020, Expert Report 2009, 2009, p. 56.

28. Schneider, M., Angele, P., Järvinen, T. A. H. & Docheva, D. Rescue plan for Achilles : Therapeutics steering the fate and functions of stem cells in tendon wound healing. *Adv. Drug Deliv. Rev.* **129**, 352–375 (2018).

29. Yin, W. *et al.* Biomaterials Functional replication of the tendon tissue microenvironment by a bioimprinted substrate and the support of tenocytic differentiation of mesenchymal stem cells. **33**, 7686–7698 (2012).

30. Brian, J. *et al.* The piezoelectric tensor of collagen fibrils determined at the nanoscale. (2017).

31. Manuscript, A. LAW ": A CRITICAL REVIEW. **31**, 733–741 (2010).

32. Manuscript, A. Nanoscale. (2018). doi:10.1039/C8NR01634H

33. Jacob, J., More, N., Kalia, K. & Kapusetti, G. Piezoelectric smart biomaterials for bone and cartilage tissue engineering. *Inflamm. Regen.* **38**, 2 (2018).

34. Vivekananthan, V. *et al.* Energy , Environmental , and Catalysis Applications Biocompatible collagen-nanofibrils : An approach for sustainable energy harvesting and battery-free humidity sensor applications Biocompatible collagen-nanofibrils : An approach for sustainable energy ha. (2018). doi:10.1021/acsami.8b02915

35. Michlovitz, S. L. Is there a role for ultrasound and electrical stimulation following injury to tendon and nerve? *J. Hand Ther.* (2005). doi:10.1197/j.jht.2005.02.013

36. Khan, S. I. & Burne, J. A. Inhibitory mechanisms following electrical stimulation of tendon and cutaneous afferents in the lower limb. *Brain Res.* (2010). doi:10.1016/j.brainres.2009.10.020

37. Williams, W. S. & Breger, L. Piezoelectricity in tendon and bone. *J. Biomech.* (1975). doi:10.1016/0021-9290(75)90076-7

38. Long, S. B., Campbell, E. B. & MacKinnon, R. Voltage sensor of Kv1.2: Structural basis of electromechanical coupling. *Science (80-.).* (2005). doi:10.1126/science.1116270

39. Pfeiffer, E. R., Tangney, J. R., Omens, J. H. & McCulloch, A. D. Biomechanics

of Cardiac Electromechanical Coupling and Mechanoelectric Feedback. *J. Biomech. Eng.* (2014). doi:10.1115/1.4026221

40. Alcaino, C., Farrugia, G. & Beyder, A. Mechanosensitive Piezo Channels in the Gastrointestinal Tract. *Curr. Top. Membr.* **79**, 219–244 (2017).

41. Michael Lavagnino1, Michelle E. Wall2, Dianne Little3, Albert J. Banes2,4, Farshid Guilak3,4,5, and S. P. A. Tendon Mechanobiology: Current Knowledge and Future Research Opportunities. *J Orthop Res.* **33**, 813–822 (2015).

42. Yoshimoto, Y., Takimoto, A., Watanabe, H., Hiraki, Y. & Kondoh, G. Scleraxis is required for maturation of tissue domains for proper integration of the musculoskeletal system. *Nat. Publ. Gr.* 1–16 (2017). doi:10.1038/srep45010

43. Chen, X. *et al.* promote the commitment of human ES cells derived MSCs to tenocytes. 1–9 (2012). doi:10.1038/srep00977

44. Wu, F. & Nerlich, M. Tendons basic biology Tendon injuries: basic science and new repair proposals. *Efort Open Rev.* (2017). doi:10.1302/2058-5241.2.160075

45. Bayer, M. L. *et al.* The initiation of embryonic-like collagen fibrillogenesis by adult human tendon fibroblasts when cultured under tension. *Biomaterials* (2010). doi:10.1016/j.biomaterials.2010.02.062

46. Zhang, G. *et al.* Development of tendon structure and function: regulation of collagen fibrillogenesis. *J. Musculoskelet. Neuronal Interact.* (2005).

47. Kostrominova, T. Y. & Brooks, S. V. Age-related changes in structure and extracellular matrix protein expression levels in rat tendons. *Age (Omaha).* (2013). doi:10.1007/s11357-013-9514-2

48. Brumitt, J. & Cuddeford, T. CURRENT CONCEPTS OF MUSCLE AND TENDON ADAPTATION TO STRENGTH AND CONDITIONING. *Int. J. Sports Phys. Ther.* (2015).

49. Robinson, K. A. *et al.* Decorin and biglycan are necessary for maintaining collagen fibril structure, fiber realignment, and mechanical properties of mature tendons. *Matrix Biol.* (2017). doi:10.1016/j.matbio.2017.08.004

50. Shetye, S. S. *et al.* Collagen V haploinsufficiency results in deficient mechanical and structural recovery of injured mouse patellar tendons. *J. Orthop. Res.* (2017).

51. Spiess, K. & Zorn, T. M. T. Collagen types I, III, and V constitute the thick collagen fibrils of the mouse decidua. *Microsc. Res. Tech.* (2007). doi:10.1002/jemt.20381

52. Hulmes, D. J., Wess, T. J., Prockop, D. J. & Fratzl, P. Radial packing, order, and

disorder in collagen fibrils. *Biophys. J.* (1995). doi:10.1016/S0006-3495(95)80391-7

53. Ireland, D. *et al.* Multiple changes in gene expression in chronic human Achilles tendinopathy. *Matrix Biol.* (2001). doi:10.1016/S0945-053X(01)00128-7

54. Deshmukh, S., Dive, A., Moharil, R. & Munde, P. Enigmatic insight into collagen. *J. Oral Maxillofac. Pathol.* (2016). doi:10.4103/0973-029x.185932

55. Anderson, J. C. & Eriksson, C. Piezoelectric properties of dry and wet bone. *Nature* **227**, 491–492 (1970).

56. Denning, D. *et al.* Electromechanical properties of dried tendon and isoelectrically focused collagen hydrogels. *Acta Biomater.* **8**, 3073–3079 (2012).

57. Denning, D., Paukshto, M. V., Habelitz, S. & Rodriguez, B. J. Piezoelectric properties of aligned collagen membranes. *J. Biomed. Mater. Res. - Part B Appl. Biomater.* **102**, 284–292 (2014).

58. Bassett, C. A. L. Biologic significance of piezoelectricity. *Calcif. Tissue Res.* **1**, 252–272 (1967).

59. Vasquez-Sancho, F., Abdollahi, A., Damjanovic, D. & Catalan, G. Flexoelectricity in Bones. *Adv. Mater.* **30**, 1–5 (2018).

60. Yao, L., Bestwick, C. S., Bestwick, L. A., Maffulli, N. & Aspden, R. M. Phenotypic Drift in Human Tenocyte Culture. *Tissue Eng.* (2006). doi:10.1089/ten.2006.12.ft-90

61. Zhu, J. *et al.* The regulation of phenotype of cultured tenocytes by microgrooved surface structure. *Biomaterials* **31**, 6952–6958 (2010).

62. Shukunami, C. *et al.* Scleraxis is a transcriptional activator that regulates the expression of Tenomodulin, a marker of mature tenocytes and ligamentocytes. *Sci. Rep.* (2018). doi:10.1038/s41598-018-21194-3

63. Berthet, E. *et al.* Smad3 binds Scleraxis and Mohawk and regulates tendon matrix organisation. *J. Orthop. Res.* (2013). doi:10.1002/jor.22382

64. Tan, S. L. *et al.* The effect of growth differentiation factor-5 (GDF-5) on the proliferation and tenogenic differentiation potential of human mesenchymal stem cells in vitro. *J. Univ. Malaya Med. Cent.* (2013).

65. Killian, M. L. & Thomopoulos, S. Scleraxis is required for the development of a functional tendon enthesis. *FASEB J.* (2016). doi:10.1096/fj.14-258236

66. Brown, D., Wagner, D., Li, X., Richardson, J. A. & Olson, E. N. Dual role of the basic helix-loop-helix transcription factor scleraxis in mesoderm formation and

chondrogenesis during mouse embryogenesis. *Development* (1999).

67. Sharma, P. & Maffulli, N. Biology of tendon injury: Healing, modeling and remodeling. *Journal of Musculoskeletal Neuronal Interactions* (2006).

68. Nourissat, G., Berenbaum, F. & Duprez, D. Tendon injury: from biology to tendon repair. *Nat. Rev. Rheumatol.* **11**, 223–233 (2015).

69. Bi, Y. *et al.* Identification of tendon stem/progenitor cells and the role of the extracellular matrix in their niche. *Nat. Med.* **13**, 1219–1227 (2007).

70. Lui, P. P. Y. Identity of tendon stem cells - how much do we know? *Journal of Cellular and Molecular Medicine* (2013). doi:10.1111/jcmm.12007

71. Yin, Z. *et al.* Single-cell analysis reveals a nestin+ tendon stem/progenitor cell population with strong tenogenic potentiality. *Sci. Adv.* **2**, 1–15 (2016).

72. Ruprecht, V. *et al.* How cells respond to environmental cues – insights from bio-functionalized substrates. *J. Cell Sci.* (2017). doi:10.1242/jcs.196162

73. Gupta, M. *et al.* Micropillar substrates: A tool for studying cell mechanobiology. *Methods Cell Biol.* (2015). doi:10.1016/bs.mcb.2014.10.009

74. Kshitiz *et al.* Control of stem cell fate and function by engineering physical microenvironments. *Integrative Biology (United Kingdom)* (2012). doi:10.1039/c2ib20080e

75. Guilak, F. *et al.* Control of Stem Cell Fate by Physical Interactions with the Extracellular Matrix. *Cell Stem Cell* (2009). doi:10.1016/j.stem.2009.06.016

76. Frantz, C., Stewart, K. M. & Weaver, V. M. The extracellular matrix at a glance. *J. Cell Sci.* (2010). doi:10.1242/jcs.023820

77. Fehrer, C. *et al.* Reduced oxygen tension attenuates differentiation capacity of human mesenchymal stem cells and prolongs their lifespan. *Aging Cell* (2007). doi:10.1111/j.1474-9726.2007.00336.x

78. Li, P. *et al.* Role of the ERK1/2 signaling pathway in osteogenesis of rat tendon-derived stem cells in normoxic and hypoxic cultures. *Int. J. Med. Sci.* (2016). doi:10.7150/ijms.16045

79. Reinwald, Y. & El Haj, A. J. Hydrostatic pressure in combination with topographical cues affects the fate of bone marrow-derived human mesenchymal stem cells for bone tissue regeneration. *J. Biomed. Mater. Res. - Part A* (2018). doi:10.1002/jbm.a.36267

80. Docheva, D., Müller, S. A., Majewski, M. & Evans, C. H. Biologics for tendon repair. *Adv. Drug Deliv. Rev.* **84**, 222–239 (2015).

81. Khan, K. M. & Scott, A. Mechanotherapy: How physical therapists' prescription of exercise promotes tissue repair. *British Journal of Sports Medicine* (2009). doi:10.1136/bjsm.2008.054239

82. Wang, Z. *et al.* Functional regeneration of tendons using scaffolds with physical anisotropy engineered via microarchitectural manipulation. *Sci. Adv.* (2018). doi:10.1126/sciadv.aat4537

83. Biggs, M. J. P. *et al.* Interactions with nanoscale topography: Adhesion quantification and signal transduction in cells of osteogenic and multipotent lineage. *J. Biomed. Mater. Res. - Part A* (2009). doi:10.1002/jbm.a.32196

84. Levin, M. Bioelectric mechanisms in regeneration: Unique aspects and future perspectives. *Semin. Cell Dev. Biol.* (2009). doi:10.1016/j.semcdb.2009.04.013

85. Tseng, A. S. & Levin, M. Transducing Bioelectric Signals into Epigenetic Pathways During Tadpole Tail Regeneration. *Anatomical Record* (2012). doi:10.1002/ar.22495

86. Sundelacruz, S., Li, C., Choi, Y. J., Levin, M. & Kaplan, D. L. Bioelectric modulation of wound healing in a 3D invitro model of tissue-engineered bone. *Biomaterials* (2013). doi:10.1016/j.biomaterials.2013.05.040

87. Engler, A. J., Sen, S., Sweeney, H. L. & Discher, D. E. Matrix elasticity directs stem cell lineage specification. *Cell* (2006). doi:10.1016/j.cell.2006.06.044

88. Mamidi, A. *et al.* Mechanosignalling via integrins directs fate decisions of pancreatic progenitors. *Nature* (2018). doi:10.1038/s41586-018-0762-2

89. Biggs, M. J. P. *et al.* The Functional Response of Mesenchymal Stem Cells to Electron-Beam Patterned Elastomeric Surfaces Presenting Micrometer to Nanoscale Heterogeneous Rigidity. *Adv. Mater.* **29**, 1702119 (2017).

90. Wang, N., Tytell, J. D. & Ingber, D. E. Mechanotransduction at a distance: Mechanically coupling the extracellular matrix with the nucleus. *Nat. Rev. Mol. Cell Biol.* **10**, 75–82 (2009).

91. Lin, X., Shi, Y., Cao, Y. & Liu, W. Recent progress in stem cell differentiation directed by material and mechanical cues. *Biomed. Mater.* (2016). doi:10.1088/1748-6041/11/1/014109

92. Hao, J. *et al.* Mechanobiology of mesenchymal stem cells: Perspective into mechanical induction of MSC fate. *Acta Biomaterialia* (2015). doi:10.1016/j.actbio.2015.04.008

93. Molloy, T., Wang, Y. & Murrell, G. A. C. The roles of growth factors in tendon

and ligament healing. *Sports Medicine* (2003). doi:10.2165/00007256-200333050-00004

94. Caliari, S. R. & Harley, B. A. C. The effect of anisotropic collagen-GAG scaffolds and growth factor supplementation on tendon cell recruitment, alignment, and metabolic activity. *Biomaterials* (2011). doi:10.1016/j.biomaterials.2011.04.021

95. Kjær, M. *et al.* From mechanical loading to collagen synthesis, structural changes and function in human tendon. *Scandinavian Journal of Medicine and Science in Sports* (2009). doi:10.1111/j.1600-0838.2009.00986.x

96. Zhao, M. *et al.* Electrical signals control wound healing through phosphatidylinositol-3-OH kinase-γ and PTEN. *Nature* (2006). doi:10.1038/nature04925

97. Ciombor, D. M. & Aaron, R. K. The role of electrical stimulation in bone repair. *Foot and Ankle Clinics* (2005). doi:10.1016/j.fcl.2005.06.006

98. Tandon, B., Blaker, J. J. & Cartmell, S. H. Piezoelectric materials as stimulatory biomedical materials and scaffolds for bone repair. *Acta Biomaterialia* (2018). doi:10.1016/j.actbio.2018.04.026

99. Mollon, B., Da Silva, V., Busse, J. W., Einhorn, T. A. & Bhandari, M. Electrical stimulation for long-bone fracture-healing: A meta-analysis of randomized controlled trials. *Journal of Bone and Joint Surgery - Series A* (2008). doi:10.2106/JBJS.H.00111

100. Yuan, X., Arkonac, D. E., Chao, P. H. G. & Vunjak-Novakovic, G. Electrical stimulation enhances cell migration and integrative repair in the meniscus. *Sci. Rep.* (2015). doi:10.1038/srep03674

101. Kloth, L. C. Electrical stimulation for wound healing: A review of evidence from in vitro studies, animal experiments, and clinical trials. *International Journal of Lower Extremity Wounds* (2005). doi:10.1177/1534734605275733

102. Fukada, E. & Yasuda, I. On the Piezoelectric Effect of Bone. *J. Phys. Soc. Japan* (1957). doi:10.1143/JPSJ.12.1158

103. Brighton, C. T., Jensen, L., Pollack, S. R., Tolin, B. S. & Clark, C. C. Proliferative and synthetic response of bovine growth plate chondrocytes to various capacitively coupled electrical fields. *J. Orthop. Res.* (1989). doi:10.1002/jor.1100070519

104. Armstrong, P. F., Brighton, C. T. & Star, A. M. Capacitively coupled electrical

stimulation of bovine growth plate chondrocytes grown in pellet form. *J. Orthop. Res.* (1988). doi:10.1002/jor.1100060214

105. Wang, W., Wang, Z., Zhang, G., Clark, C. C. & Brighton, C. T. Up-regulation of chondrocyte matrix genes and products by electric fields. in *Clinical Orthopaedics and Related Research* (2004). doi:10.1097/01.blo.0000143837.53434.5c

106. Walther, M., Mayer, F., Kafka, W. & Schütze, N. Effects of weak, low-frequency pulsed electromagnetic fields (BEMER type) on gene expression of human mesenchymal stem cells and chondrocytes: An in vitro study. *Electromagn. Biol. Med.* (2007). doi:10.1080/15368370701580814

107. Kwon, H. J., Lee, G. S. & Chun, H. Electrical stimulation drives chondrogenesis of mesenchymal stem cells in the absence of exogenous growth factors. *Sci. Rep.* **6**, 1–13 (2016).

108. Mathews, J. & Levin, M. The body electric 2.0: recent advances in developmental bioelectricity for regenerative and synthetic bioengineering. *Current Opinion in Biotechnology* (2018). doi:10.1016/j.copbio.2018.03.008

109. McLaughlin, K. A. & Levin, M. Bioelectric signaling in regeneration: Mechanisms of ionic controls of growth and form. *Dev. Biol.* **433**, 177–189 (2018).

110. Tseng, A. & Levin, M. Cracking the bioelectric code: Probing endogenous ionic controls of pattern formation. *Commun. Integr. Biol.* (2013). doi:10.4161/cib.22595

111. Pai, V. P. *et al.* HCN2 Rescues brain defects by enforcing endogenous voltage pre-patterns. *Nat. Commun.* **9**, 998 (2018).

112. Levin, M. Molecular bioelectricity: how endogenous voltage potentials control cell behavior and instruct pattern regulation in vivo. *Mol. Biol. Cell* **25**, 3835–50 (2014).

113. Pietak, A. & Levin, M. Exploring Instructive Physiological Signaling with the Bioelectric Tissue Simulation Engine. *Front. Bioeng. Biotechnol.* **4**, (2016).

114. Zhao, M. Electrical fields in wound healing-An overriding signal that directs cell migration. *Seminars in Cell and Developmental Biology* (2009). doi:10.1016/j.semcdb.2008.12.009

115. Huang, Y., Li, Y., Chen, J., Zhou, H. & Tan, S. Electrical Stimulation Elicits Neural Stem Cells Activation: New Perspectives in CNS Repair. *Front. Hum.*

Neurosci. (2015). doi:10.3389/fnhum.2015.00586

116. Martinac, B. The ion channels to cytoskeleton connection as potential mechanism of mechanosensitivity. *Biochim. Biophys. Acta - Biomembr.* **1838**, 682–691 (2014).

117. Everaerts, W., Nilius, B. & Owsianik, G. The vanilloid transient receptor potential channel TRPV4: From structure to disease. *Progress in Biophysics and Molecular Biology* (2010). doi:10.1016/j.pbiomolbio.2009.10.002

118. Moran, M. M., McAlexander, M. A., Bíró, T. & Szallasi, A. Transient receptor potential channels as therapeutic targets. *Nature Reviews Drug Discovery* (2011). doi:10.1038/nrd3456

119. Earley, S. & Brayden, J. E. Transient Receptor Potential Channels in the Vasculature. *Physiol. Rev.* (2015). doi:10.1152/physrev.00026.2014

120. Liedtke, W. B. *TRPV Channels' Function in Osmo- and Mechanotransduction. TRP Ion Channel Function in Sensory Transduction and Cellular SignalingCascades* (2007).

121. Okumura, R. *et al.* The odontoblast as a sensory receptor cell? The expression of TRPV1 (VR-1) channels. *Arch. Histol. Cytol.* (2006). doi:10.1679/aohc.68.251

122. Qi, Y. *et al.* Uniaxial cyclic stretch stimulates TRPV4 to induce realignment of human embryonic stem cell-derived cardiomyocytes. *J. Mol. Cell. Cardiol.* (2015). doi:10.1016/j.yjmcc.2015.08.005

123. Goswami, R. *et al.* TRPV4 calcium-permeable channel is a novel regulator of oxidized LDL-induced macrophage foam cell formation. *Free Radic. Biol. Med.* (2017). doi:10.1016/j.freeradbiomed.2017.06.004

124. Suzuki, T. *et al.* TRPV4 (transient receptor potential vanilloid 4), a mechanosensor for bone is required for the maintenance of bone mineral density of mandible exposed to occlusal force. *J. Bone Miner. Res.* (2010).

125. Saotome, K. *et al.* Structure of the mechanically activated ion channel Piezo1. *Nature* (2018). doi:10.1038/nature25453

126. etem, ebru *et al.* The increased expression of Piezo1 and Piezo2 ion channels in human and mouse bladder carcinoma. *Adv. Clin. Exp. Med.* (2018). doi:10.17219/acem/71080

127. Gao, Q., Cooper, P. R., Walmsley, A. D. & Scheven, B. A. Role of Piezo Channels in Ultrasound-stimulated Dental Stem Cells. *J. Endod.* (2017). doi:10.1016/j.joen.2017.02.022

128. Song, Y. *et al.* The Mechanosensitive Ion Channel Piezo Inhibits Axon Regeneration. *Neuron* (2019). doi:10.1016/j.neuron.2019.01.050

129. He, L., Si, G., Huang, J., Samuel, A. D. T. & Perrimon, N. Mechanical regulation of stem-cell differentiation by the stretch-activated Piezo channel. *Nature* **555**, 103–106 (2018).

130. Lavagnino, M., Arnoczky, S. P., Egerbacher, M., Gardner, K. L. & Burns, M. E. Isolated fibrillar damage in tendons stimulates local collagenase mRNA expression and protein synthesis. *J. Biomech.* (2006). doi:10.1016/j.jbiomech.2005.08.008

131. Maeda, T. *et al.* Conversion of mechanical force into TGF-β-mediated biochemical signals. *Curr. Biol.* (2011). doi:10.1016/j.cub.2011.04.007

132. Chen, Y., Ju, L., Rushdi, M., Ge, C. & Zhu, C. Receptor-mediated cell mechanosensing. *Mol. Biol. Cell* (2017). doi:10.1091/mbc.e17-04-0228

133. Elosegui-Artola, A., Trepat, X. & Roca-Cusachs, P. Control of Mechanotransduction by Molecular Clutch Dynamics. *Trends Cell Biol.* (2018). doi:10.1016/j.tcb.2018.01.008

134. Massia, S. P. & Hubbell, J. A. An RGD spacing of 440 nm is sufficient for integrin αvβ3-mediated fibroblast spreading and 140 nm for focal contact and stress fiber formation. *J. Cell Biol.* (1991). doi:10.1083/jcb.114.5.1089

135. Oria, R. *et al.* Force loading explains spatial sensing of ligands by cells. *Nature* (2017). doi:10.1038/nature24662

136. Salmeron-Sanchez, M. *et al.* Molecular clutch drives cell response to surface viscosity. *Proc. Natl. Acad. Sci.* (2018). doi:10.1073/pnas.1710653115

137. Fernandez-Yague, M. A. *et al.* Biomimetic approaches in bone tissue engineering: Integrating biological and physicomechanical strategies. *Advanced Drug Delivery Reviews* **84**, 1–29 (2015).

138. Galloway, M. T., Lalley, A. L. & Shearn, J. T. The role of mechanical loading in tendon development, maintenance, injury, and repair. *Journal of Bone and Joint Surgery - Series A* (2013). doi:10.2106/JBJS.L.01004

139. Wang, T. *et al.* Bioreactor Design for Tendon/Ligament Engineering. *Tissue Eng. Part B Rev.* **19**, 133–146 (2013).

140. Thomopoulos, S., Parks, W. C., Rifkin, D. B. & Derwin, K. A. Mechanisms of tendon injury and repair. in *Journal of Orthopaedic Research* (2015). doi:10.1002/jor.22806

141. Screen, H. R. C., Berk, D. E., Kadler, K. E., Ramirez, F. & Young, M. F. Tendon functional extracellular matrix. in *Journal of Orthopaedic Research* (2015). doi:10.1002/jor.22818

142. Xu, B. *et al.* RhoA/ROCK, cytoskeletal dynamics, and focal adhesion kinase are required for mechanical stretch-induced tenogenic differentiation of human mesenchymal stem cells. *J. Cell. Physiol.* **227**, 2722–2729 (2012).

143. Mackley, J. R., Ando, J., Herzyk, P. & Winder, S. J. Phenotypic responses to mechanical stress in fibroblasts from tendon, cornea and skin. *Biochem. J.* (2006). doi:10.1042/bj20060057

144. Fong, K. D. *et al.* Microarray analysis of mechanical shear effects on flexor tendon cells. *Plast. Reconstr. Surg.* (2005). doi:10.1097/01.prs.0000182345.86453.4f

145. Deng, D. *et al.* Engineering human neo-tendon tissue in vitro with human dermal fibroblasts under static mechanical strain. *Biomaterials* (2009). doi:10.1016/j.biomaterials.2009.08.054

146. Maharam, E. *et al.* Rho/Rock signal transduction pathway is required for MSC tenogenic differentiation. *Bone Res.* **3**, (2015).

147. Lin, J. *et al.* Acta Biomaterialia Cell-material interactions in tendon tissue engineering. *Acta Biomater.* 1–11 (2018). doi:10.1016/j.actbio.2018.01.012

148. Robertson, B. D. & Sawicki, G. S. Unconstrained muscle-tendon workloops indicate resonance tuning as a mechanism for elastic limb behavior during terrestrial locomotion. *Proc. Natl. Acad. Sci.* (2015). doi:10.1073/pnas.1500702112

149. Lau, E. *et al.* Effect of low-magnitude, high-frequency vibration on osteogenic differentiation of rat mesenchymal stromal cells. *J. Orthop. Res.* (2011). doi:10.1002/jor.21334

150. Curtis, A. S. G. *et al.* Cell interactions at the nanoscale: Piezoelectric stimulation. *IEEE Trans. Nanobioscience* (2013). doi:10.1109/TNB.2013.2257837

151. Tsimbouri, P. M. *et al.* Stimulation of 3D osteogenesis by mesenchymal stem cells using a nanovibrational bioreactor. *Nat. Biomed. Eng.* (2017). doi:10.1038/s41551-017-0127-4

152. Miller, S. L. The mechanism of synthesis of amino acids by electric discharges. *BBA - Biochim. Biophys. Acta* (1957). doi:10.1016/0006-3002(57)90366-9

153. Pietak, A. & Levin, M. Bioelectrical control of positional information in

development and regeneration: A review of conceptual and computational advances. *Progress in Biophysics and Molecular Biology* (2018). doi:10.1016/j.pbiomolbio.2018.03.008

154. Akai, M., Oda, H., Shirasaki, Y. & Tateishi, T. Electrical stimulation of ligament healing. An experimental study of the patellar ligament of rabbits. *Clin.Orthop.Relat Res.* (1988).

155. Sirohi, J. & Chopra, I. Fundamental understanding of piezoelectric strain sensors. *J. Intell. Mater. Syst. Struct.* (2000). doi:10.1106/8BFB-GC8P-XQ47-YCQ0

156. Ramadan, K. S., Sameoto, D. & Evoy, S. A review of piezoelectric polymers as functional materials for electromechanical transducers. *Smart Mater. Struct.* **23**, 033001 (2014).

157. Maxwell, J. C. A treatise on electricity and magnetism, Vol. II. *Journal of the Franklin Institute* (1954). doi:10.1017/CBO9780511709333

158. Wang, Z. L. On Maxwell's displacement current for energy and sensors: the origin of nanogenerators. *Mater. Today* **20**, 74–82 (2017).

159. Roche, J. The present status of Maxwell's displacement current. *Eur. J. Phys.* (1998). doi:10.1088/0143-0807/19/2/009

160. Kawai, H. The Piezoelectricity of Poly (vinylidene Fluoride). *Jpn. J. Appl. Phys.* **8**, 975–976 (1969).

161. Motamedi, A. S., Mirzadeh, H., Hajiesmaeilbaigi, F., Bagheri-Khoulenjani, S. & Shokrgozar, M. A. Piezoelectric electrospun nanocomposite comprising Au NPs/PVDF for nerve tissue engineering. *J. Biomed. Mater. Res. Part A* **105**, 1984–1993 (2017).

162. Yu, Y. *et al.* Biocompatibility and in vivo operation of implantable mesoporous PVDF-based nanogenerators. *Nano energy* **27**, 275–281 (2016).

163. Sobreiro-Almeida, R. *et al.* Human Mesenchymal Stem Cells Growth and Osteogenic Differentiation on Piezoelectric Poly(vinylidene fluoride) Microsphere Substrates. *Int. J. Mol. Sci.* **18**, 2391 (2017).

164. Lee, Y.-S., Wu, S., Arinzeh, T. L. & Bunge, M. B. Transplantation of Schwann Cells Inside PVDF-TrFE Conduits to Bridge Transected Rat Spinal Cord Stumps to Promote Axon Regeneration Across the Gap. *J. Vis. Exp.* (2017). doi:10.3791/56077

165. Sharma, T., Aroom, K., Naik, S., Gill, B. & Zhang, J. X. J. Flexible thin-film PVDF-TrFE based pressure sensor for smart catheter applications. *Ann. Biomed.*

Eng. **41**, 744–51 (2013).

166. Martins, P., Lopes, A. C. & Lanceros-Mendez, S. Electroactive phases of poly(vinylidene fluoride): Determination, processing and applications. *Prog. Polym. Sci.* **39**, 683–706 (2014).

167. Weber, N., Lee, Y.-S., Shanmugasundaram, S., Jaffe, M. & Arinzeh, T. L. Characterisation and in vitro cytocompatibility of piezoelectric electrospun scaffolds. *Acta Biomater.* **6**, 3550–3556 (2010).

168. Tseng, H. J., Tian, W. C. & Wu, W. J. P(VDF-TrFE) polymer-based thin films deposited on stainless steel substrates treated using water dissociation for flexible tactile sensor development. *Sensors (Switzerland)* **13**, 14777–14796 (2013).

169. Hitscherich, P. *et al.* The effect of PVDF-TrFE scaffolds on stem cell derived cardiovascular cells. *Biotechnol. Bioeng.* **113**, 1577–85 (2016).

170. Cheng, X. *et al.* Implantable and self-powered blood pressure monitoring based on a piezoelectric thinfilm: Simulated, in vitro and in vivo studies. *Nano Energy* **22**, 453–460 (2016).

171. Persano, L. *et al.* High performance piezoelectric devices based on aligned arrays of nanofibers of poly(vinylidenefluoride-co-trifluoroethylene). *Nat. Commun.* **4**, 1633 (2013).

172. Chang, C., Tran, V. H., Wang, J., Fuh, Y. K. & Lin, L. Direct-write piezoelectric polymeric nanogenerator with high energy conversion efficiency. *Nano Lett.* (2010). doi:10.1021/nl9040719

173. Pan, C. T. *et al.* Significant piezoelectric and energy harvesting enhancement of poly(vinylidene fluoride)/polypeptide fiber composites prepared through near-field electrospinning. *J. Mater. Chem. A* (2015). doi:10.1039/c5ta00147a

174. Dagdeviren, C. *et al.* Conformal piezoelectric systems for clinical and experimental characterisation of soft tissue biomechanics. *Nat. Mater.* **14**, 728–736 (2015).

175. Dadsetan, M. *et al.* The effects of fixed electrical charge on chondrocyte behavior. *Acta Biomater.* (2011). doi:10.1016/j.actbio.2011.01.012

176. Kitsara, M. *et al.* Permanently hydrophilic, piezoelectric PVDF nanofibrous scaffolds promoting unaided electromechanical stimulation on osteoblasts. *Nanoscale* (2019). doi:10.1039/c8nr10384d

177. Klee, D. *et al.* Surface modification of poly(vinylidenefluoride) to improve the osteoblast adhesion. *Biomaterials* **24**, 3663–3670 (2003).

178. Defteralı, Ç. *et al.* In Vitro Evaluation of Biocompatibility of Uncoated Thermally Reduced Graphene and Carbon Nanotube-Loaded PVDF Membranes with Adult Neural Stem Cell-Derived Neurons and Glia. *Front. Bioeng. Biotechnol.* (2016). doi:10.3389/fbioe.2016.00094

179. Lee, Y.-S., Collins, G. & Livingston Arinzeh, T. Neurite extension of primary neurons on electrospun piezoelectric scaffolds. *Acta Biomater.* **7**, 3877–3886 (2011).

180. Ribeiro, C. *et al.* Dynamic piezoelectric stimulation enhances osteogenic differentiation of human adipose stem cells. *J. Biomed. Mater. Res. Part A* n/a-n/a (2014). doi:10.1002/jbm.a.35368

181. Parssinen, J. *et al.* Enhancement of adhesion and promotion of osteogenic differentiation of human adipose stem cells by poled electroactive poly(vinylidene fluoride). *J. Biomed. Mater. Res. - Part A* (2015). doi:10.1002/jbm.a.35234

182. Pereira, J. D. A. S. *et al.* Biomaterials from blends of fluoropolymers and corn starch - Implant and structural aspects. *Mater. Sci. Eng. C* (2014). doi:10.1016/j.msec.2013.12.008

183. Ribeiro, C. *et al.* Electroactive poly(vinylidene fluoride)-based structures for advanced applications. *Nat. Protoc.* **13**, 681–704 (2018).

184. Genchi, G. G. *et al.* P(VDF-TrFE)/BaTiO3 Nanoparticle Composite Films Mediate Piezoelectric Stimulation and Promote Differentiation of SH-SY5Y Neuroblastoma Cells. *Adv. Healthc. Mater.* **5**, 1808–20 (2016).

185. Genchi, G. G. *et al.* Ultrasound-activated piezoelectric P(VDF-TrFE)/boron nitride nanotube composite films promote differentiation of human SaOS-2 osteoblast-like cells. *Nanomedicine* **14**, 2421–2432 (2018).

186. Fang, F., Shan, S. C. & Yang, W. Magnetoelectric coupling of Terfenol-D/P(VDF-TrFe)/Terfenol-D laminates mediated by crystallite size of electroactive polymer. *Acta Mech.* **224**, 1169–1174 (2013).

187. Brito-Pereira, R., Ribeiro, C., Lanceros-Mendez, S. & Martins, P. Magnetoelectric response on Terfenol-D/ P(VDF-TrFE) two-phase composites. *Compos. Part B Eng.* **120**, 97–102 (2017).

188. Cha, S. *et al.* Porous PVDF as effective sonic wave driven nanogenerators. *Nano Lett.* (2011). doi:10.1021/nl202208n

189. Cho, K. Y. *et al.* Enhanced Electrical Properties of PVDF-TrFE Nanocomposite

for Actuator Application. *Key Eng. Mater.* (2014). doi:10.4028/www.scientific.net/KEM.605.335

190. Guo, W. *et al.* Self-Powered Electrical Stimulation for Enhancing Neural Differentiation of Mesenchymal Stem Cells on Graphene-Poly(3,4-ethylenedioxythiophene) Hybrid Microfibers. *ACS Nano* (2016). doi:10.1021/acsnano.6b00200

191. Zheng, Q. *et al.* Biodegradable triboelectric nanogenerator as a life-time designed implantable power source. *Sci. Adv.* **2**, e1501478 (2016).

192. Nuccitelli, R. A Role for Endogenous Electric Fields in Wound Healing. *Current Topics in Developmental Biology* (2003). doi:10.1016/S0070-2153(03)58001-2

193. Ladoux, B. & Mège, R.-M. Mechanobiology of collective cell behaviours. *Nat. Rev. Mol. Cell Biol.* **18**, 743–757 (2017).

194. Iskratsch, T., Wolfenson, H. & Sheetz, M. P. Appreciating force and shape — the rise of mechanotransduction in cell biology. *Nat. Rev. Mol. Cell Biol.* **15**, 825–833 (2014).

195. Xia, S. & Kanchanawong, P. Nanoscale mechanobiology of cell adhesions. *Semin. Cell Dev. Biol.* **71**, 53–67 (2017).

196. Turner, C. H. *et al.* Mechanobiology of the skeleton. *Sci. Signal.* **2**, pt3 (2009).

197. Li, Q. *et al.* Structural mechanism of voltage-dependent gating in an isolated voltage-sensing domain. *Nat. Struct. Mol. Biol.* (2014). doi:10.1038/nsmb.2768

198. Wang, J., Tian, L., Chen, N., Ramakrishna, S. & Mo, X. The cellular response of nerve cells on poly-l-lysine coated PLGA-MWCNTs aligned nanofibers under electrical stimulation. *Mater. Sci. Eng. C. Mater. Biol. Appl.* **91**, 715–726 (2018).

199. Mario Cheong, G. L. *et al.* Conductive hydrogels with tailored bioactivity for implantable electrode coatings. *Acta Biomater.* **10**, 1216–26 (2014).

200. Cui, H. *et al.* In vitro studies on regulation of osteogenic activities by electrical stimulus on biodegradable electroactive polyelectrolyte multilayers. *Biomacromolecules* **15**, 3146–57 (2014).

201. Gilmore, K. J. *et al.* Skeletal muscle cell proliferation and differentiation on polypyrrole substrates doped with extracellular matrix components. *Biomaterials* **30**, 5292–304 (2009).

202. Chen, Q.-Q. *et al.* Electrical field stimulation induces cardiac fibroblast proliferation through the calcineurin-NFAT pathway. *Can. J. Physiol. Pharmacol.* **90**, 1611–22 (2012).

203. Seo, G. Y. *et al.* A Novel Synthetic Material, BMM, Accelerates Wound Repair by Stimulating Re-Epithelialization and Fibroblast Activation. *Int. J. Mol. Sci.* **19**, 1164 (2018).

204. Head, B. P., Patel, H. H. & Insel, P. A. Interaction of membrane/lipid rafts with the cytoskeleton: impact on signaling and function: membrane/lipid rafts, mediators of cytoskeletal arrangement and cell signaling. *Biochim. Biophys. Acta* **1838**, 532–45 (2014).

205. Yang, G. *et al.* Regulation of adipose-tissue-derived stromal cell orientation and motility in 2D- and 3D-cultures by direct-current electrical field. *Dev. Growth Differ.* **59**, 70–82 (2017).

206. Greco, F. *et al.* Microwrinkled conducting polymer interface for anisotropic multicellular alignment. *ACS Appl. Mater. Interfaces* **5**, 573–84 (2013).

207. Serena, E. *et al.* Electrical stimulation of human embryonic stem cells: Cardiac differentiation and the generation of reactive oxygen species. *Exp. Cell Res.* **315**, 3611–3619 (2009).

208. Das, S. R. *et al.* Electrical Differentiation of Mesenchymal Stem Cells into Schwann-Cell-Like Phenotypes Using Inkjet-Printed Graphene Circuits. *Adv. Healthc. Mater.* **6**, 1601087 (2017).

209. Wu, Z. *et al.* Mechanosensory hair cells express two molecularly distinct mechanotransduction channels. *Nat. Neurosci.* **20**, 24–33 (2017).

210. Cox, C. D., Wann, K. T. & Martinac, B. Selectivity mechanisms in MscS-like channels. *Channels* **8**, 5–12 (2014).

211. Lacroix, J. J., Botello-Smith, W. M. & Luo, Y. Probing the gating mechanism of the mechanosensitive channel Piezo1 with the small molecule Yoda1. *Nat. Commun.* **9**, 2029 (2018).

212. Zilly, F. E. *et al.* Ca 2+ induces clustering of membrane proteins in the plasma membrane via electrostatic interactions. *EMBO J.* (2011). doi:10.1038/emboj.2011.53

213. Yang, W. P., Onuma, E. K. & Hui, S. W. Response of C3H/10T1/2 fibroblasts to an external steady electric field stimulation. Reorientation, shape change, ConA receptor and intramembranous particle distribution and cytoskeleton reorganisation. *Exp. Cell Res.* **155**, 92–104 (1984).

214. Vacek, T. P. *et al.* Electrical stimulation of cardiomyocytes activates mitochondrial matrix metalloproteinase causing electrical remodeling. *Biochem.*

Biophys. Res. Commun. **404**, 762–6 (2011).

215. Titushkin, I. & Cho, M. Regulation of cell cytoskeleton and membrane mechanics by electric field: role of linker proteins. *Biophys. J.* **96**, 717–28 (2009).

216. Liu, L. *et al.* Mechanoresponsive stem cells to target cancer metastases through biophysical cues. *Sci. Transl. Med.* (2017). doi:10.1126/scitranslmed.aan2966

217. Isaksson, H., Wilson, W., van Donkelaar, C. C., Huiskes, R. & Ito, K. Comparison of biophysical stimuli for mechano-regulation of tissue differentiation during fracture healing. *J. Biomech.* (2006). doi:10.1016/j.jbiomech.2005.01.037

218. Pruitt, B. L., Dunn, A. R., Weis, W. I. & Nelson, W. J. Mechano-Transduction: From Molecules to Tissues. *PLoS Biol.* (2014). doi:10.1371/journal.pbio.1001996

219. Sauer, H. *et al.* DC electrical field-induced c-fos expression and growth stimulation in multicellular prostate cancer spheroids. *Br. J. Cancer* **75**, 1481–8 (1997).

220. Ruffini, G. *et al.* Transcranial current brain stimulation (tCS): models and technologies. *IEEE Trans. Neural Syst. Rehabil. Eng.* **21**, 333–45 (2013).

221. Zhao, H., Steiger, A., Nohner, M. & Ye, H. Specific Intensity Direct Current (DC) Electric Field Improves Neural Stem Cell Migration and Enhances Differentiation towards βIII-Tubulin+ Neurons. *PLoS One* **10**, e0129625 (2015).

222. Wartenberg, M., Hescheler, J. & Sauer, H. Electrical fields enhance growth of cancer spheroids by reactive oxygen species and intracellular Ca2+. *Am. J. Physiol.* **272**, R1677-83 (1997).

223. Yamada, M. *et al.* Electrical Stimulation Modulates Fate Determination of Differentiating Embryonic Stem Cells. *Stem Cells* (2006). doi:10.1634/stemcells.2006-0011

224. Feng, J. F. *et al.* Electrical Guidance of Human Stem Cells in the Rat Brain. *Stem Cell Reports* (2017). doi:10.1016/j.stemcr.2017.05.035

225. Patel, Y. A. & Butera, R. J. Differential fiber-specific block of nerve conduction in mammalian peripheral nerves using kilohertz electrical stimulation. *J. Neurophysiol.* (2015). doi:10.1152/jn.00529.2014

226. Ackermann, D. M., Foldes, E. L., Bhadra, N. & Kilgore, K. L. Nerve conduction block using combined thermoelectric cooling and high frequency electrical

stimulation. *J. Neurosci. Methods* (2010). doi:10.1016/j.jneumeth.2010.07.043

227. Kadow-Romacker, A., Hoffmann, J. E., Duda, G., Wildemann, B. & Schmidmaier, G. Effect of mechanical stimulation on osteoblast- and osteoclast-like cells in vitro. *Cells Tissues Organs* (2009). doi:10.1159/000178022

228. Yao, R. & Wong, J. Y. The Effects of Mechanical Stimulation on Controlling and Maintaining Marrow Stromal Cell Differentiation Into Vascular Smooth Muscle Cells. *J. Biomech. Eng.* (2015). doi:10.1115/1.4029255

229. Zhang, C. *et al.* Effects of mechanical vibration on proliferation and osteogenic differentiation of human periodontal ligament stem cells. *Arch. Oral Biol.* (2012). doi:10.1016/j.archoralbio.2012.04.010

230. Tsimbouri, P. M. *et al.* Publisher Correction: Stimulation of 3D osteogenesis by mesenchymal stem cells using a nanovibrational bioreactor. *Nat. Biomed. Eng.* **1**, 1004–1004 (2017).

231. Karode, N., Fitzhenry, L., Matthews, S., Walsh, P. & Coffey, A. Enhancement of the Mechanical Properties of PEBAX Graphene Nanocomposite Using Supercritical Fluid Assisted Extrusion Polymer Processing Technique. *Mater. Sci. Forum* (2017). doi:10.4028/www.scientific.net/MSF.883.75

232. Avrami, M. Kinetics of phase change. I: General theory. *J. Chem. Phys.* (1939). doi:10.1063/1.1750380

233. Avrami, M. Kinetics of phase change. II Transformation-time relations for random distribution of nuclei. *J. Chem. Phys.* (1940). doi:10.1063/1.1750631

234. Avrami, M. Kinetics of Phase Change. *J. Chem. Phys.* (1939). doi:10.1590/S1516-14392000000300002

235. Avrami, M. Granulation, phase change, and microstructure kinetics of phase change. III. *J. Chem. Phys.* (1941). doi:10.1063/1.1750872

236. Jeziorny, A. Parameters characterizing the kinetics of the non-isothermal crystallization of poly(ethylene terephthalate) determined by d.s.c. *Polymer (Guildf).* (1978). doi:10.1016/0032-3861(78)90060-5

237. Ozawa, T. Kinetics of non-isothermal crystallization. *Polymer (Guildf).* (1971). doi:10.1016/0032-3861(71)90041-3

238. Liu, F. & Yang, G. Effects of anisotropic growth on the deviations from Johnson-Mehl-Avrami kinetics. *Acta Mater.* (2007). doi:10.1016/j.actamat.2006.10.022

239. Lanceros-Méndez, S., Mano, J. F., Costa, A. M. & Schmidt, V. H. FTIR and DSC studies of mechanically deformed β-PVDF films. *J. Macromol. Sci. - Phys.*

(2001). doi:10.1081/MB-100106174

240. Fialka, J. & Benes, P. Comparison of Methods for the Measurement of Piezoelectric Coefficients. *IEEE Trans. Instrum. Meas.* **62**, 1047–1057 (2013).

241. Binning, G., Rohrer, H., Gerber, C. & Weibel, E. Surface studies by scanning tunneling microscopy. *Phys. Rev. Lett.* (1982). doi:10.1103/PhysRevLett.49.57

242. Huang, H., Gu, L. & Ozaki, Y. Non-isothermal crystallization and thermal transitions of a biodegradable, partially hydrolyzed poly(vinyl alcohol). *Polymer (Guildf).* (2006). doi:10.1016/j.polymer.2006.03.089

243. Liu, Y., Wang, L., He, Y., Fan, Z. & Li, S. Non-isothermal crystallization kinetics of poly(L-lactide). *Polym. Int.* (2010). doi:10.1002/pi.2894

244. Furukawa, T. Ferroelectric properties of vinylidene fluoride copolymers. *Phase Transitions* (1989). doi:10.1080/01411598908206863

245. Vinogradov, A. & Holloway, F. Electro-mechanical properties of the piezoelectric polymer PVDF. *Ferroelectrics* (1999). doi:10.1080/00150199908230298

246. Martins, P. *et al.* Role of nanoparticle surface charge on the nucleation of the electroactive β-poly(vinylidene fluoride) nanocomposites for sensor and actuator applications. *J. Phys. Chem. C* (2012). doi:10.1021/jp3038768

247. Wang, Y. J. & Kim, D. Crystallinity, morphology, mechanical properties and conductivity study of in situ formed PVdF/LiClO4/TiO2nanocomposite polymer electrolytes. *Electrochim. Acta* (2007). doi:10.1016/j.electacta.2006.09.070

248. Steinhart, M., Senz, S., Wehrspohn, R. B., Gösele, U. & Wendorff, J. H. Curvature-directed crystallization of poly(vinylidene difluoride) in nanotube walls. *Macromolecules* (2003). doi:10.1021/ma0260039

249. Cao, Y. *et al.* Bridging tendon defects using autologous tenocyte engineered tendon in a hen model. *Plast. Reconstr. Surg.* (2002). doi:10.1097/00006534-200210000-00011

250. Chen, J. M., Willers, C., Xu, J., Wang, A. & Zheng, M.-H. Autologous Tenocyte Therapy Using Porcine-Derived Bioscaffolds for Massive Rotator Cuff Defect in Rabbits. *Tissue Eng.* (2007). doi:10.1089/ten.2006.0266

251. Spanoudes, K., Gaspar, D., Pandit, A. & Zeugolis, D. I. The biophysical, biochemical, and biological toolbox for tenogenic phenotype maintenance in vitro. *Trends Biotechnol.* **32**, 474–482 (2014).

252. Stoll, C. *et al.* Extracellular matrix expression of human tenocytes in three-

dimensional air-liquid and PLGA cultures compared with tendon tissue: Implications for tendon tissue engineering. *J. Orthop. Res.* (2010). doi:10.1002/jor.21109

253. Juncosa-Melvin, N., Matlin, K. S., Holdcraft, R. W., Nirmalanandhan, V. S. & Butler, D. L. Mechanical Stimulation Increases Collagen Type I and Collagen Type III Gene Expression of Stem Cell–Collagen Sponge Constructs for Patellar Tendon Repair. *Tissue Eng.* (2007). doi:10.1089/ten.2006.0339

254. Jiang, C., Shao, L., Wang, Q. & Dong, Y. Repetitive mechanical stretching modulates transforming growth factor-β induced collagen synthesis and apoptosis in human patellar tendon fibroblasts. *Biochem. Cell Biol.* (2012). doi:10.1139/o2012-024

255. Kilian, K. A., Bugarija, B., Lahn, B. T. & Mrksich, M. Geometric cues for directing the differentiation of mesenchymal stem cells. *Proc. Natl. Acad. Sci. U. S. A.* **107**, 4872–7 (2010).

256. Nikukar, H. *et al.* Osteogenesis of mesenchymal stem cells by nanoscale mechanotransduction. *ACS Nano* (2013). doi:10.1021/nn400202j

257. Wang, J. H.-C. *et al.* Cyclic mechanical stretching of human tendon fibroblasts increases the production of prostaglandin E2 and levels of cyclooxygenase expression: a novel in vitro model study. *Connect. Tissue Res.* **44**, 128–33 (2003).

258. Zhang, J. & Wang, J. H. C. Production of PGE2 increases in tendons subjected to repetitive mechanical loading and induces differentiation of tendon stem cells into non-tenocytes. *J. Orthop. Res.* (2010). doi:10.1002/jor.20962

259. Love, M. R., Palee, S., Chattipakorn, S. C. & Chattipakorn, N. Effects of electrical stimulation on cell proliferation and apoptosis. *J. Cell. Physiol.* **233**, 1860–1876 (2018).

260. Balint, R., Cassidy, N. J. & Cartmell, S. H. Electrical Stimulation: A Novel Tool for Tissue Engineering. *Tissue Eng. Part B Rev.* **19**, 48–57 (2013).

261. Shao, S. *et al.* Osteoblast function on electrically conductive electrospun PLA/MWCNTs nanofibers. *Biomaterials* (2011). doi:10.1016/j.biomaterials.2011.01.051

262. Ning, C., Zhou, Z., Tan, G., Zhu, Y. & Mao, C. Electroactive polymers for tissue regeneration: Developments and perspectives. *Progress in Polymer Science* (2018). doi:10.1016/j.progpolymsci.2018.01.001

263. Zhang, J., Li, M., Kang, E. T. & Neoh, K. G. Electrical stimulation of adipose-derived mesenchymal stem cells in conductive scaffolds and the roles of voltage-gated ion channels. *Acta Biomater.* **32**, 46–56 (2016).

264. Chiu, C. H., Lei, K. F. & Yeh, W. L. Development of a co-culture device for the study of human tenocytes in response to the combined stimulation of electric field and platelet rich plasma (PRP). *Biomed. Microdevices* (2017). doi:10.1007/s10544-017-0214-z

265. Basas, Á. *et al.* Effects of a strength protocol combined with electrical stimulation on patellar tendinopathy: 42 months retrospective follow-up on 6 high-level jumping athletes. *Phys. Ther. Sport* **34**, 105–112 (2018).

266. Yanase, K. *et al.* Electrical Stimulation to the Infraspinatus on Hypertrophy and Strength of the Shoulder. *Int. J. Sports Med.* **39**, 828–834 (2018).

267. Yan, Z. *et al.* [Effects of electrical stimulation on the differentiation of mesenchymal stem cells into cardiomyocyte-like cells]. *Sheng Wu Yi Xue Gong Cheng Xue Za Zhi* **30**, 556–61 (2013).

268. Pardo-Pastor, C. *et al.* Piezo2 channel regulates RhoA and actin cytoskeleton to promote cell mechanobiological responses. *Proc. Natl. Acad. Sci. U. S. A.* **115**, 1925–1930 (2018).

269. Islam, A., Mbimba, T., Younesi, M. & Akkus, O. Effects of substrate stiffness on the tenoinduction of human mesenchymal stem cells. *Acta Biomater.* **58**, 244–253 (2017).

270. Barsby, T., Bavin, E. P. & Guest, D. J. Three-Dimensional Culture and Transforming Growth Factor Beta3 Synergistically Promote Tenogenic Differentiation of Equine Embryo-Derived Stem Cells. *Tissue Eng. Part A* (2014). doi:10.1016/j.foreco.2016.02.006

271. Qi, J. *et al.* IL-1β decreases the elastic modulus of human tenocytes. *J. Appl. Physiol.* (2006). doi:10.1152/japplphysiol.01128.2005

272. Tsuzaki, M., Bynum, D., Almekinders, L., Faber, J. & Banes, A. J. Mechanical loading stimulates ecto-ATPase activity in human tendon cells. *J. Cell. Biochem.* (2005). doi:10.1002/jcb.20491

273. Archambault, J., Tsuzaki, M., Herzog, W. & Banes, A. J. Stretch and interleukin-1β induce matrix metalloproteinases in rabbit tendon cells in vitro. *J. Orthop. Res.* (2002). doi:10.1016/S0736-0266(01)00075-4

274. Tsuzaki, M. *et al.* IL-1β induces COX2, MMP-1, -3 and -13, ADAMTS-4, IL-1β

and IL-6 in human tendon cells. *J. Orthop. Res.* (2003). doi:10.1016/S0736-0266(02)00141-9

275. Jelinsky, S. A., Archambault, J., Li, L. & Seeherman, H. Tendon-selective genes identified from rat and human musculoskeletal tissues. *J. Orthop. Res.* **28**, n/a-n/a (2009).

276. Delgado Caceres, M., Pfeifer, C. G. & Docheva, D. Understanding Tendons: Lessons from Transgenic Mouse Models. *Stem Cells Dev.* **27**, 1161–1174 (2018).

277. Inaba, S., Akaishi, K., Mori, T. & Hane, K. Analysis of the resonance characteristics of a cantilever vibrated photothermally in a liquid. *J. Appl. Phys.* (1993). doi:10.1063/1.353060

278. Kwak, M. K. & Kim, K. C. Axisymmetric vibration of circular plates in contact with fluid. *J. Sound Vib.* (1991). doi:10.1016/0022-460X(91)90696-H

279. Nikukar, H. *et al.* Osteogenesis of Mesenchymal Stem Cells by Nanoscale Mechanotransduction. *ACS Nano* **7**, 2758–2767 (2013).

280. Wang, T. *et al.* Programmable mechanical stimulation influences tendon homeostasis in a bioreactor system. *Biotechnol. Bioeng.* (2013). doi:10.1002/bit.24809

281. Zhang, J. & Wang, J. H. C. Mechanobiological response of tendon stem cells: Implications of tendon homeostasis and pathogenesis of tendinopathy. *J. Orthop. Res.* (2010). doi:10.1002/jor.21046

282. Aspenberg, P. Stimulation of tendon repair: Mechanical loading, GDFs and platelets. a mini-review. *International Orthopaedics* (2007). doi:10.1007/s00264-007-0398-6

283. Busch, T., Köttgen, M. & Hofherr, A. TRPP2 ion channels: Critical regulators of organ morphogenesis in health and disease. *Cell Calcium* (2017). doi:10.1016/j.ceca.2017.05.005

284. Chachisvilis, M., Zhang, Y.-L. & Frangos, J. A. G protein-coupled receptors sense fluid shear stress in endothelial cells. *Proc. Natl. Acad. Sci.* (2006). doi:10.1073/pnas.0607224103

285. Wu, J., Lewis, A. H. & Grandl, J. Touch, Tension, and Transduction – The Function and Regulation of Piezo Ion Channels. *Trends Biochem. Sci.* **42**, 57–71 (2017).

286. Popov, C. *et al.* Mechanical stimulation of human tendon stem/progenitor cells results in upregulation of matrix proteins, integrins and MMPs, and activation of

p38 and ERK1/2 kinases. *BMC Mol. Biol.* **16**, 1–11 (2015).

287. Maksimovic, S. *et al.* Epidermal Merkel cells are mechanosensory cells that tune mammalian touch receptors. *Nature* (2014). doi:10.1038/nature13250

288. Zhang, W., Yan, Z., Jan, L. Y. & Jan, Y. N. Sound response mediated by the TRP channels NOMPC, NANCHUNG, and INACTIVE in chordotonal organs of Drosophila larvae. *Proc. Natl. Acad. Sci.* (2013). doi:10.1073/pnas.1312477110

289. Kim, J. *et al.* A TRPV family ion channel required for hearing in Drosophila. *Nature* (2003). doi:10.1038/nature01733

290. Rayleigh, J. W. S. *The Theory of Sound Vol. II. Macmillan* (1896). doi:10.1017/CBO9781107415324.004

291. Sroka, J., Zimolag, E., Lasota, S. & Korohoda, W. Electrotaxis : Cell Directional Movement in Electric Fields. **1749**, 325–340

292. Banks, T. A., Luckman, P. S. B., Frith, J. E. & Cooper-White, J. J. Effects of electric fields on human mesenchymal stem cell behaviour and morphology using a novel multichannel device. *Integr. Biol. (Camb).* **7**, 693–712 (2015).

293. Guerin, S. *et al.* Control of piezoelectricity in amino acids by supramolecular packing. *Nat. Mater.* (2018). doi:10.1038/NMAT5045

294. Boriek, A. M. & Kumar, A. Regulation of Intracellular Signal Transduction Pathways by Mechanosensitive Ion Channels. in *Mechanosensitive Ion Channels* (2007). doi:10.1007/978-1-4020-6426-5_14

295. Coste, B. *et al.* Piezo1 and Piezo2 are essential components of distinct mechanically activated cation channels. *Science (80-.).* (2010). doi:10.1126/science.1193270

296. Goodier, H. C. J. *et al.* Comparison of transforming growth factor beta expression in healthy and diseased human tendon. *Arthritis Res. Ther.* (2016). doi:10.1186/s13075-016-0947-8

297. Zhuang, H. *et al.* Electrical stimulation induces the level of TGF-β1 mRNA in osteoblastic cells by a mechanism involving calcium/calmodulin pathway. *Biochem. Biophys. Res. Commun.* (1997). doi:10.1006/bbrc.1997.7118

298. Hirata, H., Tatsumi, H., Hayakawa, K. & Sokabe, M. Non-channel mechanosensors working at focal adhesion-stress fiber complex. *Pflügers Arch. - Eur. J. Physiol.* **467**, 141–155 (2015).

299. Prindle, A. *et al.* Ion channels enable electrical communication in bacterial communities. *Nature* (2015). doi:10.1038/nature15709

300. Brohawn, S. G., Campbell, E. B. & MacKinnon, R. Physical mechanism for gating and mechanosensitivity of the human TRAAK K+ channel. *Nature* (2014). doi:10.1038/nature14013

301. Lin, Y. Lo, Moolenaar, H., van Weeren, P. R. & van de Lest, C. H. A. Effect of microcurrent electrical tissue stimulation on equine tenocytes in culture. *Am. J. Vet. Res.* (2006). doi:10.2460/ajvr.67.2.271

302. STROYAN, J. J. PROCESSING AND CHARACTERISATION OF PVDF, PVDF-TrFE, AND PVDF-TrFE-PZT COMPOSITES. *J. Chem. Inf. Model.* (2013). doi:10.1017/CBO9781107415324.004

303. Dodds, J. S., Meyers, F. N. & Loh, K. J. Piezoelectric characterisation of PVDF-TrFE thin films enhanced with ZnO nanoparticles. *IEEE Sens. J.* (2012). doi:10.1109/JSEN.2011.2182043

304. Chen, H. J. *et al.* Investigation of PVDF-TrFE composite with nanofillers for sensitivity improvement. *Sensors Actuators, A Phys.* (2016). doi:10.1016/j.sna.2016.04.056

305. Simoes, R. D., Rodriguez-Perez, M. A., De Saja, J. A. & Constantino, C. J. L. Thermomechanical characterisation of PVDF and P(VDF-TrFE) blends containing corn starch and natural rubber. *J. Therm. Anal. Calorim.* (2010). doi:10.1007/s10973-009-0285-z

306. Seminara, L., Capurro, M., Cirillo, P., Cannata, G. & Valle, M. Electromechanical characterisation of piezoelectric PVDF polymer films for tactile sensors in robotics applications. *Sensors Actuators, A Phys.* (2011). doi:10.1016/j.sna.2011.05.004

307. Mohamad Hafiz, M. W. *et al.* Effect of Annealing Temperature on the Crystallinity, Morphology and Ferroelectric of Polyvinylidenefluoride-Trifluoroethylene (PVDF-TrFE) Thin Film. *Adv. Mater. Res.* (2013). doi:10.4028/www.scientific.net/AMR.812.60

308. Lu, X., Qu, H. & Skorobogatiy, M. Piezoelectric microstructured fibers via drawing of multimaterial preforms. *Sci. Rep.* (2017). doi:10.1038/s41598-017-01738-9

309. Wong, S. C., Baji, A. & Leng, S. Effect of fiber diameter on tensile properties of electrospun poly(ε-caprolactone). *Polymer (Guildf).* (2008). doi:10.1016/j.polymer.2008.08.022

310. Chen, F. *et al.* Mechanical characterisation of single high-strength electrospun

polyimide nanofibres. *J. Phys. D. Appl. Phys.* (2008). doi:10.1088/0022-3727/41/2/025308

311. Baji, A., Mai, Y. W. & Wong, S. C. Effect of fiber size on structural and tensile properties of electrospun polyvinylidene fluoride fibers. *Polym. Eng. Sci.* (2015). doi:10.1002/pen.24020

312. Ico, G. *et al.* Size-dependent piezoelectric and mechanical properties of electrospun P(VDF-TrFE) nanofibers for enhanced energy harvesting. *J. Mater. Chem. A* (2016). doi:10.1039/c5ta10423h

313. O'Hagan, D. Understanding organofluorine chemistry. An introduction to the C-F bond. *Chem. Soc. Rev.* (2008). doi:10.1039/b711844a

314. Wang, J. H.-C. Mechanobiology of tendon. *J. Biomech.* (2006). doi:10.1016/j.jbiomech.2005.05.011

315. Lin, T. W., Cardenas, L. & Soslowsky, L. J. Biomechanics of tendon injury and repair. *J. Biomech.* (2004). doi:10.1016/j.jbiomech.2003.11.005

316. James, R., Kesturu, G., Balian, G. & Chhabra, A. B. Tendon: Biology, Biomechanics, Repair, Growth Factors, and Evolving Treatment Options. *Journal of Hand Surgery* (2008). doi:10.1016/j.jhsa.2007.09.007

317. Wang, J. H. C., Guo, Q. & Li, B. Tendon Biomechanics and Mechanobiology— A Minireview of Basic Concepts and Recent Advancements. *J. Hand Ther.* **25**, 133–141 (2012).

318. Rees, J. D., Wilson, A. M. & Wolman, R. L. Current concepts in the management of tendon disorders. *Rheumatology* (2006). doi:10.1093/rheumatology/kel046

319. Yang, G., Crawford, R. C. & Wang, J. H. C. Proliferation and collagen production of human patellar tendon fibroblasts in response to cyclic uniaxial stretching in serum-free conditions. *J. Biomech.* (2004). doi:10.1016/j.jbiomech.2004.01.005

320. Skutek, M., Van Griensven, M., Zeichen, J., Brauer, N. & Bosch, U. Cyclic mechanical stretching modulates secretion pattern of growth factors in human tendon fibroblasts. *Eur. J. Appl. Physiol.* (2001). doi:10.1007/s004210100502

321. Zeichen, J., Van Griensven, M. & Bosch, U. The proliferative response of isolated human tendon fibroblasts to cyclic biaxial mechanical strain. *Am. J. Sports Med.* (2000). doi:10.1177/03635465000280061901

322. Jagodzinski, M. *et al.* Influence of cyclic mechanical strain and heat of human tendon fibroblasts on HSP-72. *Eur. J. Appl. Physiol.* (2006). doi:10.1007/s00421-

005-0071-y

323. Skutek, M., Van Griensven, M., Zeichen, J., Brauer, N. & Bosch, U. Cyclic mechanical stretching of human patellar tendon fibroblasts: Activation of JNK and modulation of apoptosis. *Knee Surgery, Sport. Traumatol. Arthrosc.* (2003). doi:10.1007/s00167-002-0322-y

324. Youngstrom, D. W., Rajpar, I., Kaplan, D. L. & Barrett, J. G. A bioreactor system for in vitro tendon differentiation and tendon tissue engineering. *J. Orthop. Res.* **33**, 911–918 (2015).

325. Bayer, M. L. *et al.* Release of tensile strain on engineered human tendon tissue disturbs cell adhesions, changes matrix architecture, and induces an inflammatory phenotype. *PLoS One* (2014). doi:10.1371/journal.pone.0086078

326. Moffat, K. L. *et al.* Novel Nanofiber-Based Scaffold for Rotator Cuff Repair and Augmentation. *Tissue Eng. Part A* (2008). doi:10.1089/ten.tea.2008.0014

327. Dabiri, B. E., Lee, H. & Parker, K. K. A potential role for integrin signaling in mechanoelectrical feedback. *Progress in Biophysics and Molecular Biology* (2012). doi:10.1016/j.pbiomolbio.2012.07.002

328. Butler, D. L. *et al.* The use of mesenchymal stem cells in collagen-based scaffolds for tissue-engineered repair of tendons. *Nat. Protoc.* (2010). doi:10.1038/nprot.2010.14

329. Schwartz, A. & Thomopoulos, S. The role of mechanobiology in the attachment of tendon to bone. in *Structural Interfaces and Attachments in Biology* (2013). doi:10.1007/978-1-4614-3317-0_11

330. Durant, T. J. S. *et al.* Mesenchymal stem cell response to growth factor treatment and low oxygen tension in 3-dimensional construct environment. *Muscle Ligaments Tendons J.* (2019). doi:10.32098/mltj.01.2014.09

331. Bagnaninchi, P. O. *et al.* Chitosan Microchannel Scaffolds for Tendon Tissue Engineering Characterised Using Optical Coherence Tomography. *Tissue Eng.* (2007). doi:10.1089/ten.2006.0168

332. Bagnaninchi, P. & Yang, Y. Tissue engineering for tendon repair. *Br. J. Sport. ...* (2007). doi:10.1136/bjsm.2006.030643

333. Stanton, A. E., Tong, X., Lee, S. & Yang, F. Biochemical Ligand Density Regulates Yes-Associated Protein Translocation in Stem Cells through Cytoskeletal Tension and Integrins. *ACS Appl. Mater. Interfaces* (2019). doi:10.1021/acsami.8b21270

334. Driscoll, T. P., Cosgrove, B. D., Heo, S. J., Shurden, Z. E. & Mauck, R. L. Cytoskeletal to Nuclear Strain Transfer Regulates YAP Signaling in Mesenchymal Stem Cells. *Biophys. J.* (2015). doi:10.1016/j.bpj.2015.05.010

335. Méjat, A. & Misteli, T. LINC complexes in health and disease. *Nucleus* (2010). doi:10.4161/nucl.1.1.10530

336. Crisp, M. *et al.* Coupling of the nucleus and cytoplasm: Role of the LINC complex. *J. Cell Biol.* (2006). doi:10.1083/jcb.200509124

337. Isermann, P. & Lammerding, J. Nuclear mechanics and mechanotransduction in health and disease. *Current Biology* (2013). doi:10.1016/j.cub.2013.11.009

338. Watkins-Castillo, S. & Andersson, G. United States Bone and Joint Initiative: The Burden of Musculoskeletal Diseases in the United States (BMUS). *The Burden of Musculoskeletal diseases int he United States* (2014).

339. Biewener, A. A. Muscle-tendon stresses and elastic energy storage during locomotion in the horse. *Comp. Biochem. Physiol. - B Biochem. Mol. Biol.* (1998). doi:10.1016/S0305-0491(98)00024-8

340. Yang, G., Rothrauff, B. B. & Tuan, R. S. Tendon and ligament regeneration and repair: Clinical relevance and developmental paradigm. *Birth Defects Research Part C - Embryo Today: Reviews* (2013). doi:10.1002/bdrc.21041

341. Foolen, J., Wunderli, S. L., Loerakker, S. & Snedeker, J. G. Tissue alignment enhances remodeling potential of tendon-derived cells - Lessons from a novel microtissue model of tendon scarring. *Matrix Biol.* (2018). doi:10.1016/j.matbio.2017.06.002

342. Kimura, A., Aoki, M., Fukushima, S., Ishii, S. & Yamakoshi, K. Reconstruction of a defect of the rotator cuff with polytetrafluoroethylene felt graft. Recovery of tensile strength and histocompatibility in an animal model. *J. Bone Joint Surg. Br.* (2003).

343. Rowe, R. W. D. The structure of rat tail tendon. *Connect. Tissue Res.* (1985). doi:10.3109/03008208509089839

344. Chan, H. K. F., Fung, D. T. C. & Ng, G. Y. F. Effects of Low-Voltage Microamperage Stimulation on Tendon Healing in Rats. *J. Orthop. Sport. Phys. Ther.* **37**, 399–403 (2007).

345. West, C. R. & Bowden, A. E. Using tendon inherent electric properties to consistently track induced mechanical strain. *Ann. Biomed. Eng.* (2012). doi:10.1007/s10439-011-0504-1

346. Liu, Z. & Kim, J. Effect of Strain Rate and Loading on the Piezoelectric Properties of Tendon. **8**, 3193 (2006).

347. Subramanian, A., Kanzaki, L. F., Galloway, J. L. & Schilling, T. F. Mechanical force regulates tendon extracellular matrix organisation and tenocyte morphogenesis through TGFbeta signaling. *Elife* **7**, 1–24 (2018).

348. Kannus, P., Józsa, L., Natri, A. & Järvinen, M. Effects of training, immobilization and remobilization on tendons. *Scand. J. Med. Sci. Sports* (2010). doi:10.1111/j.1600-0838.1997.tb00121.x

349. Matsumoto, F., Trudel, G., Uhthoff, H. K. & Backman, D. S. Mechanical effects of immobilization on the Achilles' tendon. *Arch. Phys. Med. Rehabil.* (2003). doi:10.1016/S0003-9993(02)04834-7

350. Kim, B. S. *et al.* The effect of dry needling and treadmill running on inducing pathological changes in rat Achilles tendon. *Connect. Tissue Res.* **8207**, 1–17 (2015).

351. De Castro Pochini, A. *et al.* Overuse of training increases mechanoreceptors in supraspinatus tendon of rats SHR. *J. Orthop. Res.* (2011). doi:10.1002/jor.21320

352. Yuan, T. *et al.* Creating an animal model of tendinopathy by inducing chondrogenic differentiation with kartogenin. *PLoS One* (2016). doi:10.1371/journal.pone.0148557

353. Wada, S. *et al.* Post-operative Tendon Loading with Treadmill Running Delays Tendon-to-Bone Healing: Immunohistochemical Evaluation in a Murine Rotator Cuff Repair Model. *J. Orthop. Res.* (2019). doi:10.1002/jor.24300

354. Zhang, J. & Wang, J. H.-C. The Effects of Mechanical Loading on Tendons - An In Vivo and In Vitro Model Study. *PLoS One* (2013). doi:10.1371/journal.pone.0071740

355. Zhang, J., Pan, T., Liu, Y. & Wang, J. H. C. Mouse treadmill running enhances tendons by expanding the pool of Tendon Stem Cells (TSCs) and TSC-related cellular production of collagen. *J. Orthop. Res.* (2010). doi:10.1002/jor.21123

356. Glazebrook, M. A., Wright, J. R., Langman, M., Stanish, W. D. & Lee, J. M. Histological analysis of Achilles tendons in an overuse rat model. *J. Orthop. Res.* (2008). doi:10.1002/jor.20546

357. Houghton, L., Dawson, B. & Rubenson, J. Achilles tendon mechanical properties after both prolonged continuous running and prolonged intermittent shuttle running in cricket batting. *J. Appl. Biomech.* (2013). doi:10.1123/jab.29.4.453

358. Eliasson, P., Andersson, T. & Aspenberg, P. Achilles tendon healing in rats is improved by intermittent mechanical loading during the inflammatory phase. *J. Orthop. Res.* (2012). doi:10.1002/jor.21511

359. Xu, S. Y. *et al.* Response of Decorin to different intensity treadmill running. *Mol. Med. Rep.* (2018). doi:10.3892/mmr.2018.8802

360. Xu, S. Y. *et al.* Intensity-dependent effect of treadmill running on rat Achilles tendon. *Exp. Ther. Med.* (2018). doi:10.3892/etm.2018.6084

361. Kuo, C. K. & Tuan, R. S. Mechanoactive Tenogenic Differentiation of Human Mesenchymal Stem Cells. *Tissue Eng. Part A* (2008). doi:10.1089/ten.tea.2006.0415

362. Scott, A. *et al.* Mechanical force modulates scleraxis expression in bioartificial tendons. *J. Musculoskelet. Neuronal Interact.* (2011).

363. Lohberger, B. *et al.* Impact of cyclic mechanical stimulation on the expression of extracellular matrix proteins in human primary rotator cuff fibroblasts. *Knee Surgery, Sport. Traumatol. Arthrosc.* (2016). doi:10.1007/s00167-015-3790-6

364. Sawaguchi, N. *et al.* Effect of cyclic three-dimensional strain on cell proliferation and collagen synthesis of fibroblast-seeded chitosan-hyaluronan hybrid polymer fiber. *J. Orthop. Sci.* (2010). doi:10.1007/s00776-010-1488-7

365. D., D. Running far and fast: An emerging role of tenomodulin. *J. Orthop. Res.* (2017).

366. Zhang, J., Yuan, T. & Wang, J. H.-C. Moderate treadmill running exercise prior to tendon injury enhances wound healing in aging rats. *Oncotarget* (2016). doi:10.18632/oncotarget.7381

367. Cushman, D. & Rho, M. E. Conservative Treatment of Subacute Proximal Hamstring Tendinopathy Using Eccentric Exercises Performed With a Treadmill: A Case Report. *J. Orthop. Sport. Phys. Ther.* (2015). doi:10.2519/jospt.2015.5762

368. Heinemeier, K. M. *et al.* Uphill running improves rat Achilles tendon tissue mechanical properties and alters gene expression without inducing pathological changes. *J. Appl. Physiol.* (2012). doi:10.1152/japplphysiol.00401.2012

369. Abraham, T., Fong, G. & Scott, A. Second harmonic generation analysis of early Achilles tendinosis in response to in vivo mechanical loading. *BMC Musculoskelet. Disord.* (2011). doi:10.1186/1471-2474-12-26

370. Jafari, L., Vachon, P., Beaudry, F. & Langelier, E. Histopathological,

biomechanical, and behavioral pain findings of achilles tendinopathy using an animal model of overuse injury. *Physiol. Rep.* (2015). doi:10.14814/phy2.12265

371. Ng, G. Y. F., Chung, P. Y. M., Wang, J. S. & Cheung, R. T. H. Enforced bipedal downhill running induces Achilles tendinosis in rats. *Connect. Tissue Res.* (2011). doi:10.3109/03008207.2011.562334

372. Mendias, C. L., Gumucio, J. P., Bakhurin, K. I., Lynch, E. B. & Brooks, S. V. Physiological loading of tendons induces scleraxis expression in epitenon fibroblasts. *J. Orthop. Res.* (2012). doi:10.1002/jor.21550

373. Esteves de Lima, J. *et al.* TGFβ and FGF promote tendon progenitor fate and act downstream of muscle contraction to regulate tendon differentiation during chick limb development. *Development* (2016). doi:10.1242/dev.136242

374. Brent, A. E. FGF acts directly on the somitic tendon progenitors through the Ets transcription factors Pea3 and Erm to regulate scleraxis expression. *Development* (2004). doi:10.1242/dev.01275

375. Shukunami, C., Takimoto, A., Oro, M. & Hiraki, Y. Scleraxis positively regulates the expression of tenomodulin, a differentiation marker of tenocytes. *Dev. Biol.* (2006). doi:10.1016/j.ydbio.2006.06.036

376. Hammerman, M., Aspenberg, P. & Eliasson, P. Microtrauma stimulates rat Achilles tendon healing via an early gene expression pattern similar to mechanical loading. *J. Appl. Physiol.* (2013). doi:10.1152/japplphysiol.00741.2013

377. Cheng, N., Hoof, V. A. N. & Hoogmartens, M. J. Generation , Protein Synthesis , and Membrane Transport in Rat Skin. *Clin. Orthop. Relat. Researc* (1982).

378. Meng, X. *et al.* PI3K mediated electrotaxis of embryonic and adult neural progenitor cells in the presence of growth factors. *Exp. Neurol.* (2011). doi:10.1016/j.expneurol.2010.11.002

379. Sung, K. M. *et al.* Control of neonatal human dermal fibroblast migration on poly(lactic-co-glycolic acid)-coated surfaces by electrotaxis. *J. Tissue Eng. Regen. Med.* (2015). doi:10.1002/term.1986

380. Li, S. *et al.* Electrical Stimulation Activates Fibroblasts through the Elevation of Intracellular Free Ca 2+ : Potential Mechanism of Pelvic Electrical Stimulation Therapy . *Biomed Res. Int.* (2019). doi:10.1155/2019/7387803

381. Lee, G. S., Kim, M. G. & Kwon, H. J. Electrical stimulation induces direct reprogramming of human dermal fibroblasts into hyaline chondrogenic cells.

Biochem. Biophys. Res. Commun. (2019). doi:10.1016/j.bbrc.2019.04.027

382. Ni, M. *et al.* Engineered scaffold-free tendon tissue produced by tendon-derived stem cells. *Biomaterials* **34**, 2024–2037 (2013).

383. Xu, S.-Y., Li, S.-F. & Ni, G.-X. Strenuous Treadmill Running Induces a Chondrocyte Phenotype in Rat Achilles Tendons. *Med. Sci. Monit.* (2016). doi:10.12659/msm.897726

384. Carpenter, J. E., Flanagan, C. L., Thomopoulos, S., Yian, E. H. & Soslowsky, L. J. The effects of overuse combined with intrinsic or extrinsic alterations in an animal model of rotator cuff tendinosis. *Am. J. Sports Med.* (1998). doi:10.1177/03635465980260061101

385. Szomor, Z. L., Appleyard, R. C. & Murrell, G. A. C. Overexpression of nitric oxide synthases in tendon overuse. *J. Orthop. Res.* (2006). doi:10.1002/jor.20009

386. Thampatty, B. P. & Wang, J. H. C. Mechanobiology of young and aging tendons: In vivo studies with treadmill running. *J. Orthop. Res.* (2017). doi:10.1002/jor.23761

387. Heinemeier, K. M. *et al.* Effect of unloading followed by reloading on expression of collagen and related growth factors in rat tendon and muscle. *J. Appl. Physiol.* (2009). doi:10.1152/japplphysiol.91092.2008

388. Zhang, J. & Wang, J. H. C. Moderate exercise mitigates the detrimental effects of aging on tendon stem cells. *PLoS One* (2015). doi:10.1371/journal.pone.0130454

389. Dey, D. *et al.* Two tissue-resident progenitor lineages drive distinct phenotypes of heterotopic ossification. *Sci. Transl. Med.* (2016). doi:10.1126/scitranslmed.aaf1090

390. Wood, L. K. & Brooks, S. V. Ten weeks of treadmill running decreases stiffness and increases collagen turnover in tendons of old mice. *J. Orthop. Res.* (2016). doi:10.1002/jor.22824

391. Gimbel, J. A. Long Durations of Immobilization in the Rat Result in Enhanced Mechanical Properties of the Healing Supraspinatus Tendon Insertion Site. *J. Biomech. Eng.* (2007). doi:10.1115/1.2721075

392. Wolfman, N. M. *et al.* Ectopic induction of tendon and ligament in rats by growth and differentiation factors 5, 6, and 7, members of the TGF-β gene family. *J. Clin. Invest.* (1997). doi:10.1172/JCI119537

393. Kishimoto, Y. *et al.* Wnt/β-catenin signaling suppresses expressions of Scx, Mkx, and Tnmd in tendon-derived cells. *PLoS One* (2017).

doi:10.1371/journal.pone.0182051

394. Zhou, S., Eid, K. & Glowacki, J. Cooperation between TGF-β and Wnt pathways during chondrocyte and adipocyte differentiation of human marrow stromal cells. *J. Bone Miner. Res.* (2004). doi:10.1359/JBMR.0301239

395. Chen, Y. *et al.* β-Catenin signaling pathway is crucial for bone morphogenetic protein 2 to induce new bone formation. *J. Biol. Chem.* (2007). doi:10.1074/jbc.M602700200

396. Zhang, R. *et al.* Wnt/β-catenin signaling activates bone morphogenetic protein 2 expression in osteoblasts. *Bone* (2013). doi:10.1016/j.bone.2012.09.029

397. Gaur, T. *et al.* Canonical WNT signaling promotes osteogenesis by directly stimulating Runx2 gene expression. *J. Biol. Chem.* (2005). doi:10.1074/jbc.M500608200

398. Kim, J. B. *et al.* Bone regeneration is regulated by Wnt signaling. *J. Bone Miner. Res.* (2007). doi:10.1359/jbmr.070802

399. Minear, S. *et al.* Wnt proteins promote bone regeneration. *Sci. Transl. Med.* (2010). doi:10.1126/scitranslmed.3000231

400. Krishnan, V., Bryant, H. U. & MacDougald, O. A. Regulation of bone mass by Wnt signaling. *Journal of Clinical Investigation* (2006). doi:10.1172/JCI28551

401. Robling, A. G. *et al.* Mechanical stimulation of bone in vivo reduces osteocyte expression of Sost/sclerostin. *J. Biol. Chem.* (2008). doi:10.1074/jbc.M705092200

402. Majidinia, M., Sadeghpour, A. & Yousefi, B. The roles of signaling pathways in bone repair and regeneration. *Journal of cellular physiology* (2018). doi:10.1002/jcp.26042

403. Tu, X. *et al.* Sost downregulation and local Wnt signaling are required for the osteogenic response to mechanical loading. *Bone* (2012). doi:10.1016/j.bone.2011.10.025

404. Brighton, C. T., Wang, W., Seldes, R., Zhang, G. & Pollack, S. R. Signal transduction in electrically stimulated bone cells. *J. Bone Jt. Surg. - Ser. A* (2001). doi:10.2106/00004623-200110000-00009

405. Ashrafi, M., Alonso-Rasgado, T., Baguneid, M. & Bayat, A. The efficacy of electrical stimulation in experimentally induced cutaneous wounds in animals. *Veterinary dermatology* (2016). doi:10.1111/vde.12328

406. Kim, T. H., Cho, H. & Lee, S. M. High-Voltage Pulsed Current Stimulation

Enhances Wound Healing in Diabetic Rats by Restoring the Expression of Collagen, α-Smooth Muscle Actin, and TGF-β1. *Tohoku J. Exp. Med.* (2014). doi:10.1620/tjem.234.1

407. Wang, Y., Rouabhia, M., Lavertu, D. & Zhang, Z. Pulsed electrical stimulation modulates fibroblasts' behaviour through the Smad signalling pathway. *J. Tissue Eng. Regen. Med.* (2017). doi:10.1002/term.2014

408. Wang, H., Liu, J., Zeng, J., Zeng, C. & Zhou, Y. Expression of TβR-2, Smad3 and Smad7 in the vaginal anterior wall of postpartum rats with stress urinary incontinence. *Arch. Gynecol. Obstet.* (2015). doi:10.1007/s00404-014-3495-y

409. Li, Y. *et al.* Effect of integrin β1 in the treatment of stress urinary incontinence by electrical stimulation. *Mol. Med. Rep.* 4727–4734 (2019). doi:10.3892/mmr.2019.10145

410. Hamadi, A. Regulation of focal adhesion dynamics and disassembly by phosphorylation of FAK at tyrosine 397. *J. Cell Sci.* (2005). doi:10.1242/jcs.02565

411. Park, M. S., Kim, Y. H. & Lee, J. W. FAK mediates signal crosstalk between type II collagen and TGF-beta 1 cascades in chondrocytic cells. *Matrix Biol.* (2010). doi:10.1016/j.matbio.2009.10.001

412. Jing, D. *et al.* Pulsed electromagnetic fields partially preserve bone mass, microarchitecture, and strength by promoting bone formation in hindlimb-suspended rats. *J. Bone Miner. Res.* (2014). doi:10.1002/jbmr.2260

413. Jing, D. *et al.* Moderate-intensity rotating magnetic fields do not affect bone quality and bone remodeling in hindlimb suspended rats. *PLoS One* (2014). doi:10.1371/journal.pone.0102956

414. Jing, D. *et al.* Pulsed electromagnetic fields improve bone microstructure and strength in ovariectomized rats through a Wnt/Lrp5/β-catenin signaling-associated mechanism. *PLoS One* (2013). doi:10.1371/journal.pone.0079377

415. Lei, T. *et al.* Pulsed electromagnetic fields (PEMF) attenuate changes in vertebral bone mass, architecture and strength in ovariectomized mice. *Bone* (2018). doi:10.1016/j.bone.2017.12.008

416. Kim, M. O., Jung, H., Kim, S. C., Park, J. K. & Seo, Y. K. Electromagnetic fields and nanomagnetic particles increase the osteogenic differentiation of human bone marrow-derived mesenchymal stem cells. *Int. J. Mol. Med.* (2015). doi:10.3892/ijmm.2014.1978

417. Petecchia, L. *et al.* Electro-magnetic field promotes osteogenic differentiation of BM-hMSCs through a selective action on Ca^{2+} -related mechanisms. *Sci. Rep.* (2015). doi:10.1038/srep13856

418. Rouabhia, M., Park, H., Meng, S., Derbali, H. & Zhang, Z. Electrical stimulation promotes wound healing by enhancing dermal fibroblast activity and promoting myofibroblast transdifferentiation. *PLoS One* (2013). doi:10.1371/journal.pone.0071660

419. Cheng, G. *et al.* Sinusoidal electromagnetic field stimulates rat osteoblast differentiation and maturation via activation of NO-cGMP-PKG pathway. *Nitric Oxide - Biol. Chem.* (2011). doi:10.1016/j.niox.2011.05.009

420. Diniz, P., Soejima, K. & Ito, G. Nitric oxide mediates the effects of pulsed electromagnetic field stimulation on the osteoblast proliferation and differentiation. *Nitric Oxide - Biol. Chem.* (2002). doi:10.1016/S1089-8603(02)00004-6

421. Pilla, A. *et al.* Electromagnetic fields as first messenger in biological signaling: Application to calmodulin-dependent signaling in tissue repair. *Biochim. Biophys. Acta - Gen. Subj.* (2011). doi:10.1016/j.bbagen.2011.10.001

422. Hong, J. M., Kang, K. S., Yi, H. G., Kim, S. Y. & Cho, D. W. Electromagnetically controllable osteoclast activity. *Bone* (2014). doi:10.1016/j.bone.2014.02.005

423. Yuan, J., Xin, F. & Jiang, W. Underlying Signaling Pathways and Therapeutic Applications of Pulsed Electromagnetic Fields in Bone Repair. *Cellular Physiology and Biochemistry* (2018). doi:10.1159/000489206

424. Pall, M. L. Electromagnetic fields act via activation of voltage-gated calcium channels to produce beneficial or adverse effects. *J. Cell. Mol. Med.* **17**, 958–965 (2013).

Chapter Six

Future directions and conclusions

6.1   General Introduction

Biomimetic design of materials capable of adapting their functional response to the dynamic characteristics of their specific surroundings is a key tenet for tissue engineering applications. Since the discovery of piezoelectricity in biological tissues and individual proteins, the question of whether or not piezoelectricity is important in modulating regeneration or cell function has been raised. Thanks to advancements in engineering we can now fabricate biomaterials with tunable piezoelectric properties. In the past decade, various piezoelectric materials have been employed to control cell function and for different tissue engineering applications, particularly in bone repair and neural tissue engineering. Among the well-studied piezoelectric polymers polyhydroxybutyrate (PHB) and poly-L-lactide (PLLA), polyvinyledene fluoride (PVDF) and its copolymers including PVDF-trFE which displays the highest piezoelectric response and have received considerable attention for the development of biomedical devices. Despite extensive research have been carried demonstrating the ability of piezoelectric systems to modulate cell function and hold great potential for tissue engineering application, the molecular mechanism remains elusive. With that in mind, two different possible biomedical applications have been proposed for piezoelectric systems (i) a piezoelectric system for tendon tissue engineering applications have been developed to unravel the effect of piezoelectricity in cellular processes such as differentiation and (ii) a piezoelectric scaffold has been optimized for in vivo tendon repair applications. The overall goal of the project was on mediating tendon repair through the activation of piezo sensitive receptors and it involved a number of different sequential phases.

1.- Phase I: Development, fabrication and physical characterisation of piezoelectric films for in vitro tissue engineering applications

2.- Phase II: Optimization of tendon derived cells culture conditions and use of a nanovibrational bioreactor to induce phenotypic drift on tendon cells and unravel the effect of piezoelectricity using protein microarray technology.

3.- Phase III : Use of mechanical loading and fibrous piezoelectric scaffolds to explore the potential of piezoscaffolds for tendon repair (in vitro)

4.- Phase IV: Evaluate the regenerative potential of piezoscaffolds in a full-thickness rat Achilles model.

6.2 Summary

6.2.1 Phase I

The objective of this study was to develop a novel PVDF-TrFE/BNNT nanocomposite that is suitable for tendon cell culture and displays a superior piezoelectric performance relative to pristine films. It was shown that nanocomposites enhance the adhesion of tendon cells, significantly negating the common anti-adhesive properties of PVDF-TrFE. Analysis of physical characterisation of the nanocomposites demonstrated that nanocomposites display superior electrical, mechanical and piezoelectric behaviour relative to pristine samples.

6.2.2 Phase II

The objective of this study was to evaluate the ability of previously developed 2D piezoelectric membranes under vibrational stimulation to maintain tendon cell function during *in vitro* cell culture expansion relative to pristine samples.

It was shown that tendon cells cultured on non-piezoelectric films underwent phenotypic drift under vibrational stimulation at high frequencies following the same pathways (BMP and Wnt signalling) as previously described in our model of MSC osteogenesis stimulated at high frequencies. Interestingly, this effect was significantly reversed when using mechanical stimulation at lower frequencies or piezoelectric membranes. Using protein and gene array studies, we showed that the primary signalling pathways associated (BMP and Wnt signalling) to dedifferentiation (at 1500 Hz) was shown to be reversible when using electromechanical stimulation (at 1500 Hz). The highest levels of SCX and tendon related markers TBHS4, DCN and BGN were obtained as a result of continuous electromechanical stimulation at 1500 Hz for 10 days. However, SCX was downregulated when using Rho/Rock inhibitors, suggesting that adhesion-related pathways are responsible for the modulation of tendon function during electromechanical stimulation. Further, FAK and MAPK were significantly modulated under electromechanical stimulation supporting the statement that electromechanical stimulation reinforces cell adhesion that in turn promotes the maintenance of tendon cell phenotype.

6.2.3 Phase III

The objective of this study was to develop a 3D piezoelectric system based on aligned fibres of PVDF-TrFE and evaluate its ability to enhance tendon function *in vitro* under physiologically relevant mechanical loading conditions (4% strain, 0.5 Hz , 8h/day).

It was shown that piezoelectric control of cell function was the result of the interplay between TGF/BMP signalling and direct osteospecific pathways such as Wnt signalling. Piezoelectricity mediated changes in the morphology and cell adhesion also modulated indirect intracellular signalling including MAPK/ERK and Rock/RhoA via activation of piezosensitive channels receptors including Piezo 1&2. The experimental results presented in this chapter indicated that tendon-derived cells responded to piezoelectricity, and a piezoelectric scaffold may be fabricated capable of promoting tendon to bone tissue repair. Piezoscaffolds may have potential regenerative capabilities for enhancing tendon healing and for future clinical translation

6.2.4 Phase IV

The final phase of the project was to evaluate the regenerative ability of piezoelectric scaffolds in an *in vivo* animal model. The objective was to promote tendon regeneration and to inhibit the ossification that generally occurs after acute tendon injuries. Two materials were examined, piezoelectric and non-piezoelectric scaffolds, along with the conventional golden standard in the clinic that is the use of suture material alone. In order to activate the piezoelectricity, an adopted protocol based on early exercise using mild treadmill running was used. The effect of piezoelectricity on tendon repair was assessed at weeks 2, 4 and 8. The groups examined were :

1. Suture alone (injury_static) without undergoing treadmill running
2. Suture alone (injury_dynamic) undergoing treadmill running for 8 weeks
3. Piezoelectric scaffolds (Piezo_static) without undergoing treadmill running
4. Piezoelectric scaffolds (Piezo_dynamic) undergoing treadmill running for 8 weeks
5. Non-piezoelectric scaffolds (Non-Piezo_static) without undergoing treadmill running
6. Non-piezoelectric scaffolds (Non-Piezo_dynamic) undergoing treadmill running for 8 weeks

It was shown that that functional tendon repair follows the activation of TGF-β/BMP and FGF/MAPK-ERK pathways together with TRP-like and Piezo 2 ion channels and integrins β1. Conversely, activation of Wnt/β-catenin via integrin β5 upregulation resulted in ectopic bone formation, the deactivation of Piezo2 and TRPV1 ion channels and a reduction in integrin β1 expression.

6.3 Limitations

6.3.1 Phase I

Ferroelectric hysteresis loop measurements (P-E) of polymeric piezoelectric thick samples (> 5 um thickness) is very complex, and it involves the use of commercial Radiant Precision LC Ferroelectric tester with special voltage source. In this study, we could not evaluate the macroscopic P-E hysteresis loop of the samples since high voltages to reverse the polarity of the dipoles would be required, and equipment was not available. Instead, we used switching spectroscopy piezoresponse force microscopy (SS-PFM), d_{33} meter and dielectric measurements to characterise the piezoelectric performance of the samples.

6.3.2 Phase II

Human tenocyte viability depends significantly on the use of suitable media, reagents, and sterile fibronectin coated membranes. Especially, when coating did not achieve the minimum ligand density required, limited differentiation occurred, and cell growth was deficient. Also ,working with human-derived tendon cells is a limitation since their availability is very low and generally obtained from patients over 60 years old .Unfortunetly, in this work we could not perform a systematic comparison between young and old patients. Alternatively, we worked with a minimum of 6 donors including one young patient of 18 years old.

One major limitation of this or any study on tendon tissue engineering is understanding the fundamental molecular mechanisms behind tenogenic differentiation of tendon derived cells biology, including tendon stem cells. However, to date and despite enormous efforts made in this area, the markers specific for tenocytes or tendon stem cells are poorly defined and, moreover, there is a tremendous need to a proper stem cell tenogenic differentiation assay. Specifically, tendon stem cells are heterogeneous so

defining a single biomarker for their definition is likely imprecise, and instead looking a panel of co-expressed markers seems more realistic. In this work, we look at a panel of co-expressed markers, but a more extensive panel would be required in future looking also to stemness, proliferation and self-renewal markers. For tenocytes, the most well-studied marker is Scleraxis (SCX); however, this marker is also upregulated during injury by other fibroblastic cells.

Another limitation is the use of laboratory standard approaches to culture tendon cells as these cells are susceptible to atmospheric levels of oxygen. Generally, the highly specialized environment where tendon cells reside provides tendon cells with hypoxic conditions (between 2-6%). In this study, the experiments were performed under normoxic conditions.

6.3.3   Phase III

Tenocytes are histologically arranged in rows within large amounts of ECM. Therefore, there is currently a lack of definition on what tenocyte cytoplasm and focal adhesion look like in three dimensions (i.e. fine processes or in sheet form). In addition, this has not been defined in immature or injured tendons (characterised by high cellular content) or adult intact tendons (characterised by low cellular content). More importantly, when tendon cells are derived from the tendon specimen either by enzymatic digestion or grown in culture tissue plastics, we are not sure of what exact population is derived. Therefore the term of tendon-derived cell rather than tenocytes is used along instead in this thesis.

Even though there is a definite advantage of using 3D scaffolds such as electrospun scaffolds, still the infiltration of these cells is limited and talking about complete 3D structure would be inexact.

6.3.4   Phase IV

In this work, there are several limitations in our animal model. Especially, longer time points to assess chronic inflammation, and tendon remodelling would be required. This is due to the potential slow regeneration response. Reporting a quick and short-term gait recovery is not enough (i.e. 8-week period is not sufficient). The recovery should be shown over time. In some therapies, there might be initial short-term effect, and that

would not be enough to show maintained return of the function. In addition, moving to larger animals with more anatomically resemblance to human such a pig or sheep is mandatory. Study on rats is a useful first step, but it is not clinically relevant as the load on rat tendon is much lower than in the case of humans. Additionally, this animal model is not highly relevant to human subjects as regenerative properties of this species are much better than humans. Therefore, rats can be used in exploratory studies but are not the best choice at later stages. Another limitation found in this study is the control group choice. The ideal scaffold that should be used for benchmarking is decellularized tissue allografts;however, the use of these tissues becomes extremely challenging in small rodent animal models. One of the opportunities that should also be considered is focusing on chronic tendon defects. This would be most clinically relevant as most of the tendon injuries develop due to degeneration rather than mechanical injury. This model could be achieved by partially damaging the relevant tendon and rather than suturing it immediately; the surgery takes place after a period of time (the induced damage should not constrain the animal in performing its everyday activities).

6.4 Future directions

A number of future projects are proposed based on the further modification of the piezoelectric systems for enhanced cytocompatibility and extensive biological characterisation to further unravel the molecular mechanisms to understand how cells sense and integrate piezoelectrical cues.

The first project proposed would consist of the study of the effect of piezoelectricity activated by the nano-vibrational system on focal adhesion formation and paxillin signalling.

6.4.1 Focal adhesion studies: Paxillin, FAK and integrin signalling.

Based on our genomic studies, several pathways associated with cell adhesion have been modulated by piezoelectric signals. Paxillin is a main component of focal adhesions (FAs) and plays an essential role in the transduction of extracellular signals into intracellular responses, triggered by the engagement of integrins with the extracellular matrix (ECM). As a scaffolding protein, paxillin contributes to the recruitment of specific kinases and phosphatases, cofactors, oncoproteins, and structural proteins, involved in intracellular signalling cascades. The activation of these pathways ultimately leads to the reorganisation of the actin cytoskeleton and the

assembly/disassembly of focal adhesions (FAs) required for cell attachment, spreading, and migration .Paxillin is not only recruited at nascent FAs at the cell front for the assembly of adhesion complexes but also required for the disassembly of FAs at the rear end of the cell during cell movement and migration . Hence, paxillin may exert positive or negative effects on cell migration. Although paxillin is mainly localized at FAs, it is also present at cytoplasmic and nuclear locations, where it may affect gene transcription, thus acting as a direct link from the plasma membrane and the cytoskeleton to the nucleus. In spite of its inclusion in protein complexes with cytoskeletal proteins and enzymes, paxillin does not exhibit enzyme activity but provides docking sites for other proteins to facilitate the assembly of multiprotein complexes. Nevertheless, paxillin recruitment to the leading edge of membrane protrusions is an early event in the formation of focal adhesions , although FAK incorporation to these complexes precedes that of paxillin. In fact, the inhibition of FAK/paxillin interaction results in the absence of FAK from focal adhesions, a decrease in the phosphorylation of several adhesion proteins and the consequent alteration of cell migration and invasion. Upon the activation of integrin receptors, FAK phosphorylation of Tyr31 and Tyr118, as well as ERK phosphorylation of serines have been shown to regulate paxillin disassembly from adhesion complexes and to promote cell movement.
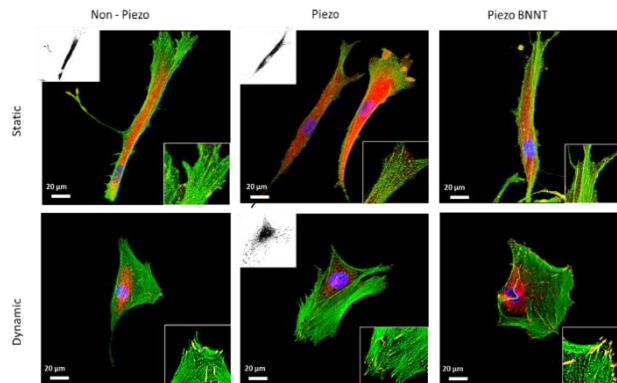
Figure 6-1. Representative image of paxillin expression and cytoskeleton reorganisation during stimulation for 5 days.

An increase in cell area and reduction in circularity is seen. Cell shape has previously been noted to be dependent on the nature of the surface. For example, stiffer surfaces show greater cell spreading as well as cell shape's being a key regulator in cellular processes, such as lineage commitment, growth, and apoptosis. Here it is seen that

increasing piezoelectricity, leads to a monophasic change in the cell shape to a bigger and more rounded morphology, with a concomitant reduction in cytoskeletal tension, which is mediated by α5β1 and α5β3 integrins.

6.4.2 Calcium dynamics on tendon-derived cells
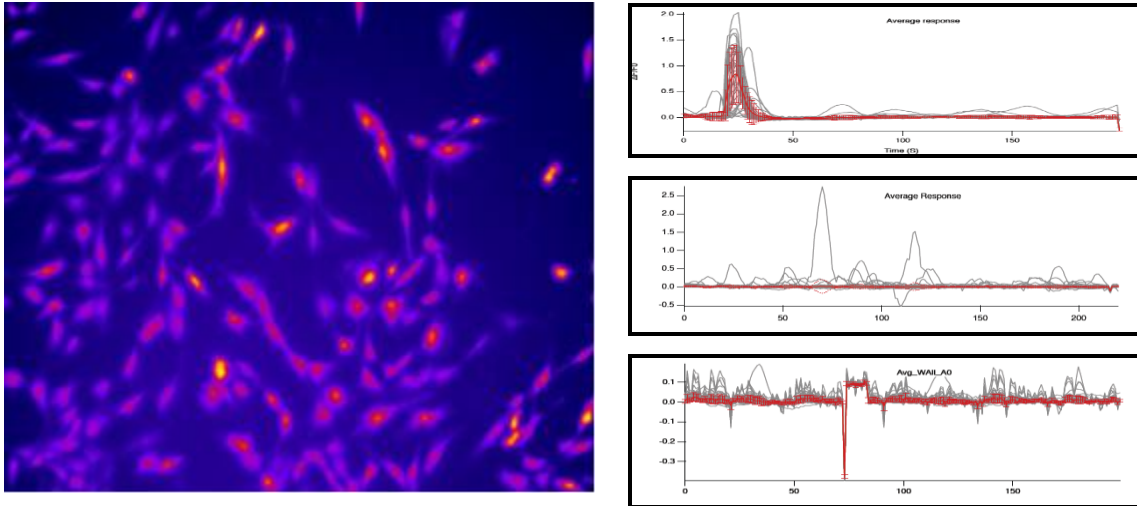
Figure 6-2. Representative image of calcium dynamics. Calcium signals of a) healthy tendon cells b) ATP stimulated tendon cells and c) electrically stimulated cells at 1000 Hz

We have observed that tendon cells are susceptible to stimulation of purinergic receptors with ATP. To demonstrate that tendon cells are sensitive to high-frequency, low amplitude (1 mV) electrical stimulation, we have assessed the calcium dynamics under 1kHz biphasic electrical stimulation (1 mV). It was observed that the response of cells electrically stimulated inhibited calcium spiking.

Future work should centre on calcium dynamics changes upon electromechanical stimulation using piezoelectric membranes and with the use of either enhancer or inhibitors of ion channels and focal adhesions.

6.4.3 A new application for piezoelectric bioreactors : Maturation of iPSCs cardiomyocytes

Pluripotent cells are an ideal cell source for any application. It is possible to genetically modified adult fibroblast to express four factors (Yamanaka factors). Subsequently, it is possible to induce differentiation following a secure 2D culture protocol.

Briefly, a GSK3 inhibitor is used to enhance differentiation via Wnt signalling activation first in RPMI/B27- as insulin inhibits cardiomyocyte differentiation (directs it to a neuroectoderm fate). At this point, we obtain mesoderm progenitor cells so we block Wnt Signalling with inhibitors of Wnt ligand production (IWPs) to initiate specific cardiomyocyte differentiation. Finally , we add insulin when cells are already committed to the cardiac fate

The function of iPSC derived cardiomyocytes is assessed to show consistent calcium transients, regular beat rate and ability to be paced at different frequencies using microelectrode arrays. We obtained results using fibrous piezoelectric scaffolds with different fibre organisation (random and aligned).
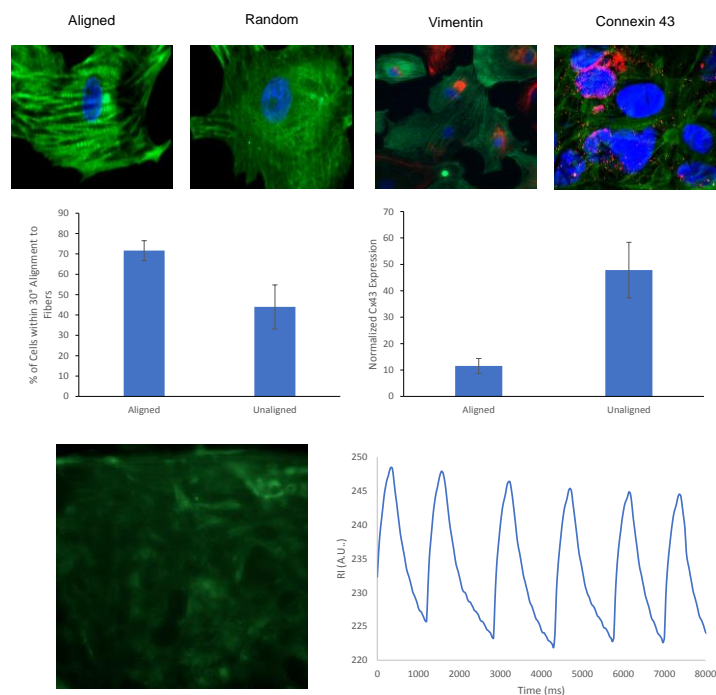
Figure 6-3. Representative image of calcium dynamics of electrically stimulated tendon cells

Future work should include new applications for piezoelectric scaffolds, especially in the field of stimulating electrically excitable cells and also for sensing applications. Maturation of human-induced pluripotent stem cell-derived cardiomyocytes (hiPSC-CMs) remains an unsolved problem that limits their clinical application, and further experimental research is needed in order to unlock their full potential. The main objective of the future project is exploring how biomimetic physicomechanical cues influence hiPSCs-CMs function and maturation. To investigate that, the following objectives are proposed 1) fabricate a 3D scaffold by electrospinning and 3D printing

means to recreate the biophysical and structural properties of the tissue and 2) use electromechanical stimulation to accelerate hiPSC-CMs maturation by recapitulating the intrinsic cardiac properties and explore how these mimetic biophysical cues interplay and influence the CMs behaviour.

6.4.4 Biodegradable piezoelectric scaffolds with enhanced biocompatibility and piezoelectric performance for energy harvesting.

One approach to scavenge the energy from the environment is utilizing piezoelectric materials to perform the energy harvesting process.

In this thesis was shown that a highly piezoelectric system was obtained based on the development of nanocomposite PVDF-TrFE / BNNT membrane activated by vibrational waves. The maximum sensitivity of the membrane was as high as 0,18 mV/nm for nanocomposites compared to 0,03 mV/nm for pristine membranes. A finite element method (COMSOL Multiphysics 5.2) was used to analyze the resonant frequencies of the film that corresponded to around 700 and 1500 Hz. The modelling parameters such as pre-stress and fluid interaction needed to be incorporated to obtain an excellent fidelity between the model and the experimental work. After defining a pre-stress and incorporating the fluid-membrane interactions, the model represented accurately the experimental observations.

Importantly, PVDF-based electro-active polymers can release toxic residues into the body or to cells environment during their decomposition processes. Therefore, eco-friendly piezoelectric polymers are more indicated for in vivo applications of piezoelectric scaffolds including bioenergy harvesting.. Interestingly, new materials based on the specific arrangement of amino acids crystal including (γ) glycine (178 pm/V) have shown to have superior performance than PVDF (39 pm/V) and even comparable to ceramic piezoelectrics such barium titanate or lead zirconate titanate. Moreover, The highest predicted piezoelectric voltage constant for β-glycine crystals is $8 \, V \, mN^{-1}$, which is an order of magnitude larger than the voltage generated by any currently used ceramic or polymeric piezoelectric material.

Possible synthetic alternatives are being proposed for future works studies based on biodegradable synthetic polymers such as PLLA or biopolymers including chitin or amino acids displaying excellent theoretical electrical outputs.

6.4.4.1 Natural crystal-forms for bioelectrets

Fibrous molecules: α-Helical crystalline form in which (CONH) peptide dipoles align in the axial direction forming a large dipole moment (intrinsic tensile piezoelectricity)

Oriented films: β-sheet crystalline form in which hydrogen bonds between extended molecules align in parallel (non-intrinsic shear piezoelectricity, most common in biopolymers).

Examples:

- Fibrous molecules
- Keratin
- Chitin
- Cellulose
- Amylose
- Oriented films
- Collagen
- DNA

6.4.4.2 Natural polypeptides for biodegradable piezoelectric polymers

Synthetic single amino acid residues in helical form producing piezoelectricity by internal rotation of peptide bonds (CONH) under shear forces.

- Poly-γ-methy-(L)-glutamate (PMLG)
- Poly-γ-benzyl-L-glutamate (PBLG): Highly oriented film (8 kV/m)

Table 6-1. Properties of differently processed polypeptides

Polymer	Molecular conformation	Oriented	Elongation ratio	d14 (pC/N)
Poly-L-alanine	α	Roll	1.5	-1
PM(L)G	α	Stretch	2	-2
PM(L)G	β	Roll	2	-0.5
PM(D)G	α	Stretch	2	1.5
PB(L)G	α	Electric field		-4
PB(L)G	α	Roll	2	1
PB(L)Aspartate	w	Roll	2	-3

6.4.4.3 Optically active biodegradable piezoelectric material

- Poly-β-hydroxybutyrate (PHB): Elongated 4x
- PLLA: Elongatated
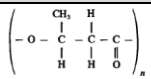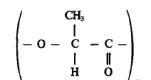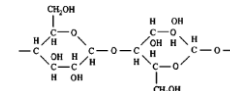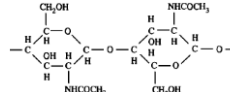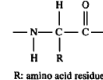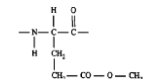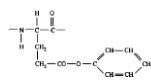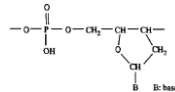
Name	Chemistry	d (pC/N)	e (mC/m²)	$\varepsilon_r = \varepsilon/\varepsilon_0$	c (GN/m²)	g (Vm/N)	ρ (g/cm³)	Young Modulus (GPa)
PHB		0.1-1	0.2	1.9	2	0.05	1.3	1.8
PLLA		3.3-10	18	3.5	2	0.1-0.2	1.43	5.5
Cellulose		0.15	-	-	-	-	1.5	-
Chitin		1.5	-	-	-	-	-	-
Proteins (COL)		1.5-3	-	-	-	-	-	-
PMLG		3	11	3	3.9	0.04	1.38	2.77
PBLG		3.5	13	3	3.9	0.04	1.39	3.64
DNA		0.01	-	-	-	-	-	-
PVDF-TrFE (ctrl)		*-15-33*	*10-30*	*10.7*	*3.69*	*0.1-0.3*	*1.78*	*1*

Table 6-2. Dielectric,elastic and piezoelectric properties of different materials

6.4.4.4 Model and comparison of voltage and electrical energy output

PVDF-TrFE   0.1 GΩ / 1 V / 10 nW
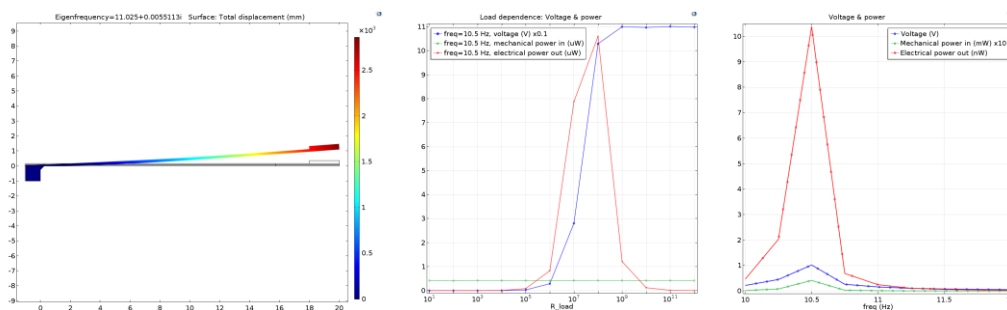
Figure 6-4. a) Geometry b) Power as function of electrical load (fixed frequency) c) Power as function of electrical load (fixed electrical load).

This model analyzes a simple "seismic" energy harvester that is designed to generate electrical energy from local variations in acceleration that occur, for example, when a wireless sensor is mounted on a vibrating tissue. The energy harvester analyzed in this model consists of a piezoelectric bimorph (2 piezoelectric films sandwiching a PLA support cantilever) clamped at one end to the vibrating tissue with a proof mass mounted on its other end.

Figure 6-4. a) Geometry b) Power as function of electrical load (fixed frequency) c) Power as function of electrical load (fixed electrical load).shows device geometry. The bimorph has a ground electrode embedded within it (coincident with the neutral plane of the beam) and two electrodes on the exterior surfaces of the cantilever beam. This configuration ensures that same voltage is induced on the exterior electrodes, even though the stress above and below the neutral layer is of opposite sign. Since the clamp is mounted to a piece of vibrating machinery the device is analyzed in a vibrating reference frame (modelled in COMSOL by the application of a sinusoidal body load). The model performs two analyses of the mechanical part of the energy harvester system. First, the power output is analyzed as a function of vibration frequency (see figure 1 c), with a fixed electrical load. Then the power output as a function of electrical load is explored (see figure 1b).

6.4.4.5 The treatment recommended for stretched (4x) PLLA or PBLG .

Piezoelectric PLLA or PBLG material used for the fabrication of energy harvesting just produce electrical outputs when shear stress is applied. However, is material is rotated it can produce voltage while non-rotated film can't. The relationship between the different geometrical parameters, input stress/strain and electrical output to roughly estimate shear-piezoelectric constants in vibration is shown in figure 2.
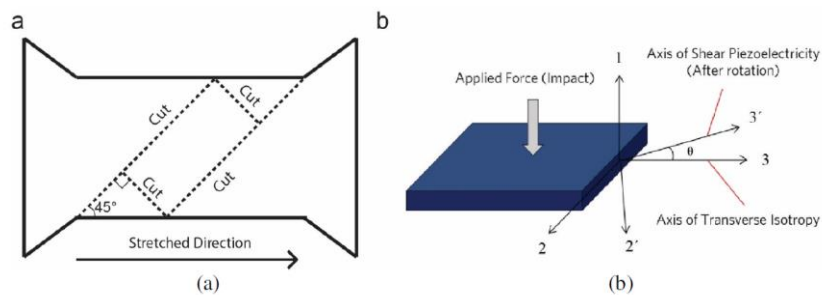
Figure 2. a) Simplified schematic of cutting the processed PLLA or PBLG to transform it into a piezoelectric material. It is important to note that a cutting angle of 45 degrees is utilised for the optimal signal output according to the model derived below. b) Schematic illustrating the direction of the applied force to the treated films. The axis illustrated in this image is used to derive the model below. Axis 3 is the stretched direction of the film as shown in a).

PLLA (non-treated)	PLLA (treated)	PBLG (treated)

0V / 0 nW	0.2 V / 0.4 nW	0.1 V / 0.1 nW
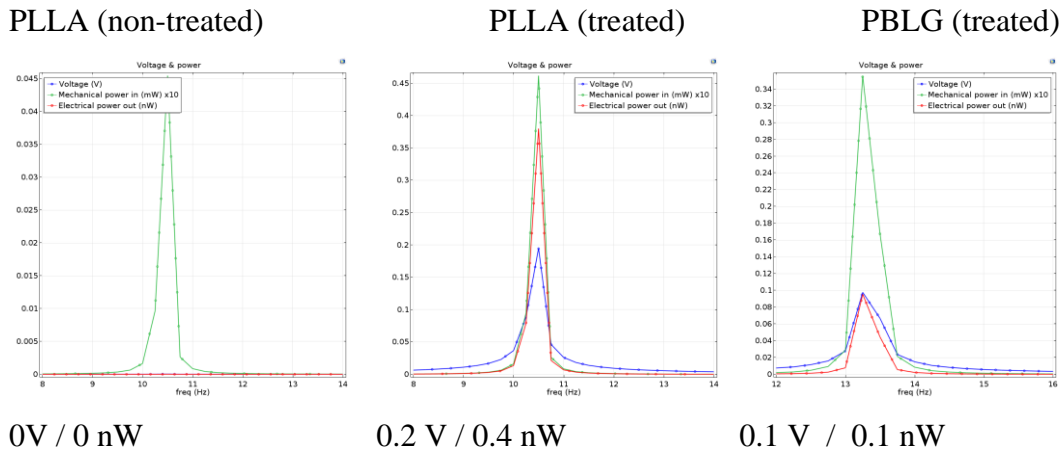
Figure 6-5**.** Input mechanical power (fixed), electrical power harvested and peak voltage for 3 different materials (PLLA, PLLA treated and PBLG treated).

The electrical load is 01 GΩ and the response of the systems shows a peak around 10-15 Hz (dependent on system design).

Based on this preliminary research PLLA is chosen as an ideal biodegradable piezoelectric candidate material. PVDF-based systems are normally used for energy harvesting applications; however, PVDF loses its performance when processed at temperatures above 75ºC and is not biodegradable. PLLA, a biodegradable polymer, synthesized by lactic acid (sugar and starch) via ring-opening polymerization can be processed up to 140 ºC PLLA (for drawing the material) and still exhibits excellent piezoelectric performance when is processed. Previous studies have shown that it can generate 10 uW power output under vibration.

6.5   Conclusions

In conclusion, a piezoelectric based bioreactor has been created as a responsive platform to induce tendon cell phenotype maintenance. This system is capable of providing cells with electrical and mechanical cues simultaneously, with the ability to provide either just mechanical or both. When just intense mechanical stimulation was selected, the system was able to initiate osteogenic differentiation pathways on tendon cells leading them to dedifferentiate. Interestingly, this effect was reversed when electrical cues were also provided. The combination of both signals had an effect on the sensitivity and function of ion channels and, as shown by inhibitory studies, more pronounced on focal adhesions than in ion channels.

Consequently, piezoelectric scaffolds for tendon repair applications were developed. In a full-thickness Achilles rat tendon, the ability of the piezoelectric scaffolds for mediating tendon repair and promote functionality was investigated. Following optimization of the scaffold in vitro, an optimal treadmill running protocol was obtained for early loading of the tendons post transection. A resultant change in the functional recovery and protein expression of tendon-related proteins was measured following treatment with piezoelectric scaffolds. Assessment of GAG and collagen II revealed a significant change between treatments and demonstrated a functional regenerative effect of mechanical stimulation. Tissue electrical stimulation by piezoelectric scaffolds resulted in increased ectopic bone formation.

Thus, it can be seen that electrical signals provided through piezoelectric scaffolds activated by physiological body motion-induced mechanical forces that can modify tendon repair *in vivo*. As shown in our *in vitro* and *in vivo* experiments, this is likely to happen by the activation of adhesion-related pathways such as FAK and MAPK via integrin clustering.

Appendices

7.1 Gene array design

Table 7-1Regulated genes obtained (piezoelectric vs non-piezoelectric).

Symbol	Entrez Gene Name
ABCB1	ATP binding cassette subfamily B member 1
ACAN	aggrecan
ACTA1	actin, alpha 1, skeletal muscle
ACVR1	activin A receptor type 1
AHSG	alpha 2-HS glycoprotein
ALPL	alkaline phosphatase, liver/bone/kidney
BGLAP	bone gamma-carboxyglutamate protein
BGN	biglycan
BMP1	bone morphogenetic protein 1
BMP2	bone morphogenetic protein 2
BMP4	bone morphogenetic protein 4
BMP6	bone morphogenetic protein 6
BMP7	bone morphogenetic protein 7
BMPR1A	bone morphogenetic protein receptor type 1A
BMPR2	bone morphogenetic protein receptor type 2
CASP3	caspase 3
COL11A1	collagen type XI alpha 1 chain
COL14A1	collagen type XIV alpha 1 chain
COL1A1	collagen type I alpha 1 chain
COL1A2	collagen type I alpha 2 chain
COL2A1	collagen type II alpha 1 chain
COL3A1	collagen type III alpha 1 chain
COL4A1	collagen type IV alpha 1 chain
COL5A1	collagen type V alpha 1 chain
COL6A1	collagen type VI alpha 1 chain
COMP	cartilage oligomeric matrix protein
DCN	decorin
DLX5	distal-less homeobox 5
EGR1	early growth response 1
FGF10	fibroblast growth factor 10
GDF15	growth differentiation factor 15
GDF5	growth differentiation factor 5
GDF6	growth differentiation factor 6
GDF7	growth differentiation factor 7
HAT1	histone acetyltransferase 1
HDAC1	histone deacetylase 1
HNF1A	HNF1 homeobox A
IBSP	integrin binding sialoprotein
IGF1	insulin like growth factor 1
ITGA1	integrin subunit alpha 1
ITGA2	integrin subunit alpha 2
ITGA3	integrin subunit alpha 3
ITGA4	integrin subunit alpha 4
ITGA5	integrin subunit alpha 5
ITGAX	integrin subunit alpha X
ITGB1	integrin subunit beta 1
ITGB3	integrin subunit beta 3
ITGB5	integrin subunit beta 5
KAT2B	lysine acetyltransferase 2B
KCNK2	potassium two pore domain channel subfamily K member 2
KCNK4	potassium two pore domain channel subfamily K member 4
KDR	kinase insert domain receptor
MGP	matrix Gla protein
MKX	mohawk homeobox

PIEZO1	piezo type mechanosensitive ion channel component 1
PIEZO2	piezo type mechanosensitive ion channel component 2
PIK3CG	phosphatidylinositol-4,5-bisphosphate 3-kinase catalytic subunit
PTEN	phosphatase and tensin homolog
PTK2	protein tyrosine kinase 2
PTK2	protein tyrosine kinase 2
PXN	paxillin
RUNX2	runt related transcription factor 2
SCX	scleraxis bHLH transcription factor
SMAD3	SMAD family member 3
SMAD4	SMAD family member 4
SMAD9	SMAD family member 9
SMURF1	SMAD specific E3 ubiquitin protein ligase 1
SMURF2	SMAD specific E3 ubiquitin protein ligase 2
SOX9	SRY-box 9
SP7	Sp7 transcription factor
SPARC	secreted protein acidic and cysteine rich
SPP1	secreted phosphoprotein 1
TBX5	T-box 5
TGFB1	transforming growth factor beta 1
THBS4	thrombospondin 4
TLN1	talin 1
TNC	tenascin C
TNMD	tenomodulin
TRPA1	transient receptor potential cation channel subfamily A member 1
TRPV1	transient receptor potential cation channel subfamily V member 1
TWIST1	twist family bHLH transcription factor 1
VCL	vinculin
VEGFA	vascular endothelial growth factor A
ZYX	zyxin
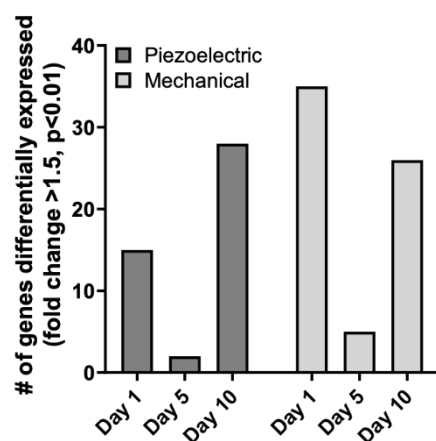
Comparison of genes differentially expressed for mechanical (A) and piezoelectric stimulation (B) at days 1, 5 and 10 respectively.

7.2   In vitro characterisation of tendon cells on electrospun scaffolds

7.2.1   Nuclear deformations

a)   b)
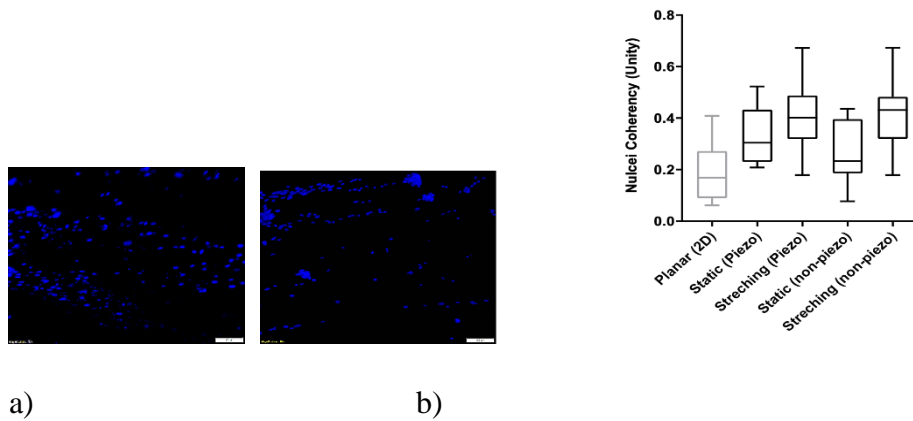
Figure 7-1. -7-2. a) Static and b) dynamic (stretched 4%) cultures of tenocytes using piezoelectric scaffolds.

7.2.2 Paxillin expression and adhesion area
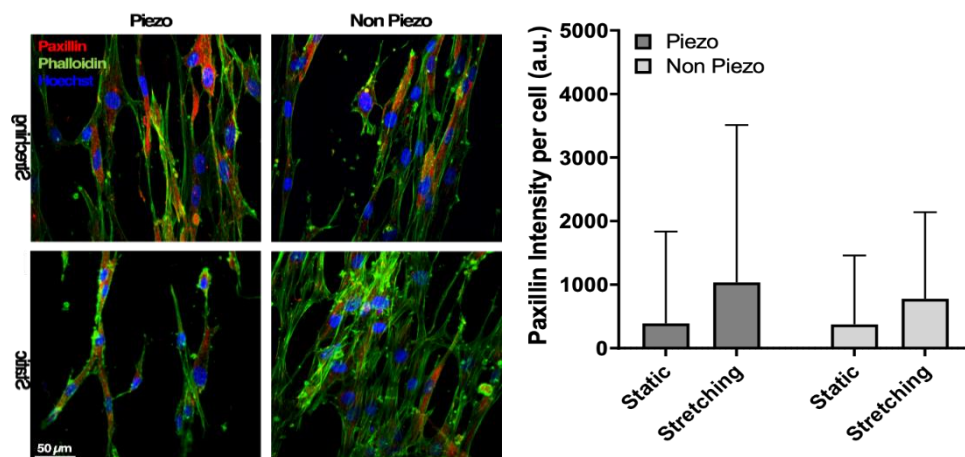
Figure 7-3. Paxillin intensity per cell on a) Static and b) dynamic (stretched 4%) cultures of human tenocytes.
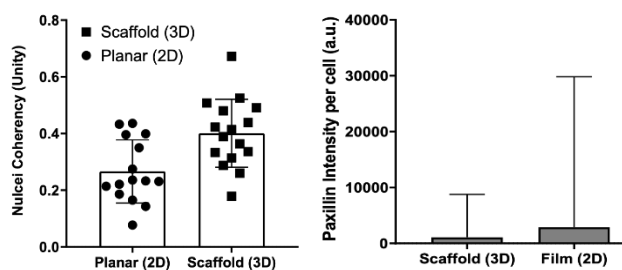
Figure 7-4. Paxillin intensity per cell on a) Plana and b) Scaffold

7.2.3   Calcium imaging.
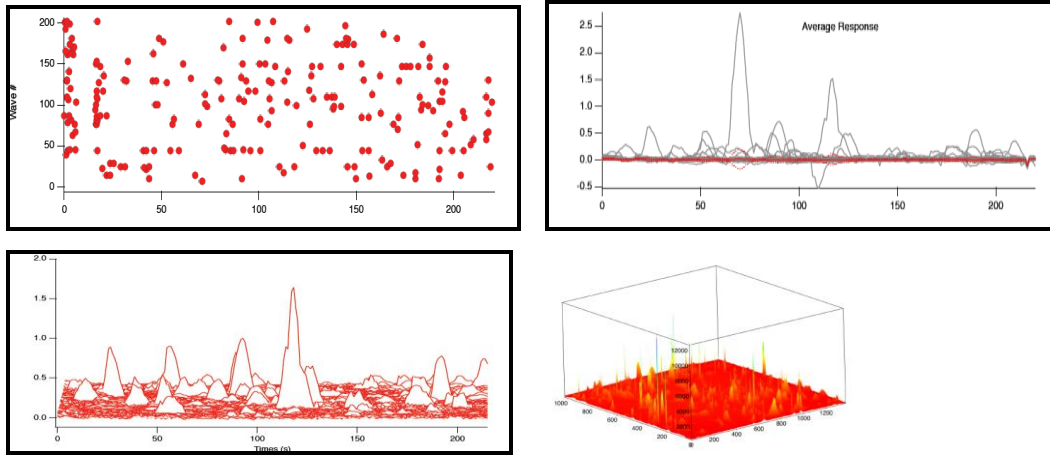
Figure 7-5. Representative image of calcium dynamics of non stimulated tendon cells
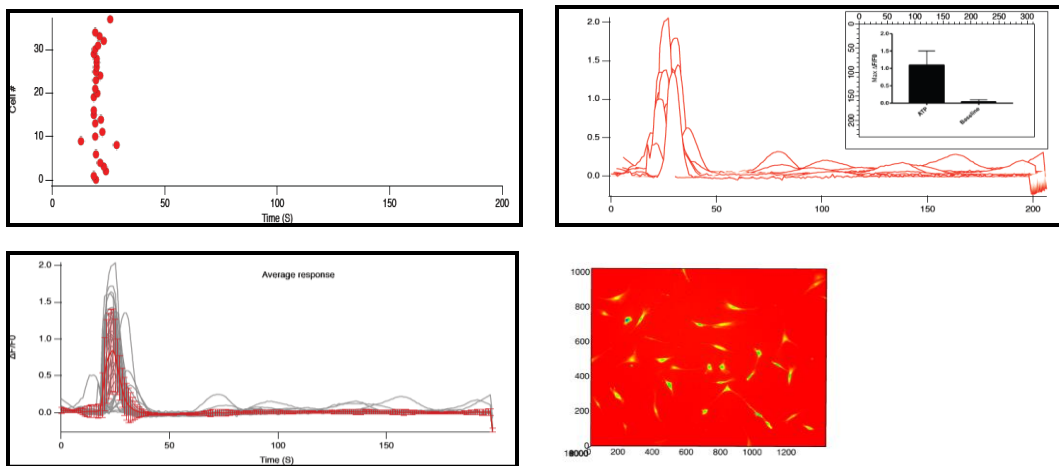
Figure 7-6. Representative image of calcium dynamics of ATP stimulated tendon cells
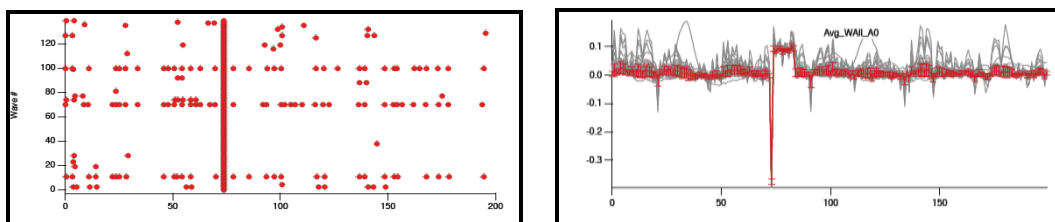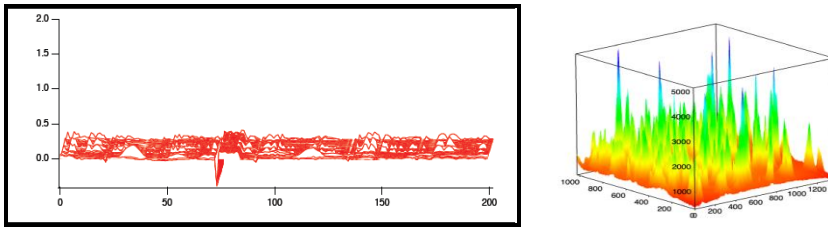
Figure 7-7. Representative image of calcium dynamics of piezoelectrically stimulated tendon cells

7.2.4 Induced pluripotent stem cells
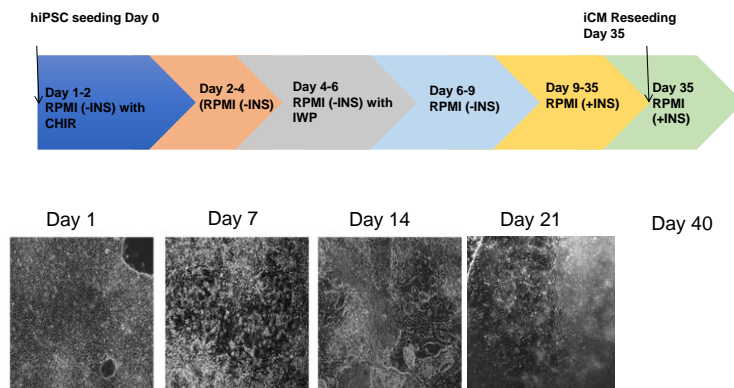
Figure 7-8.. Representative image of calcium dynamics of electrically stimulated stimulated tendon cells

441
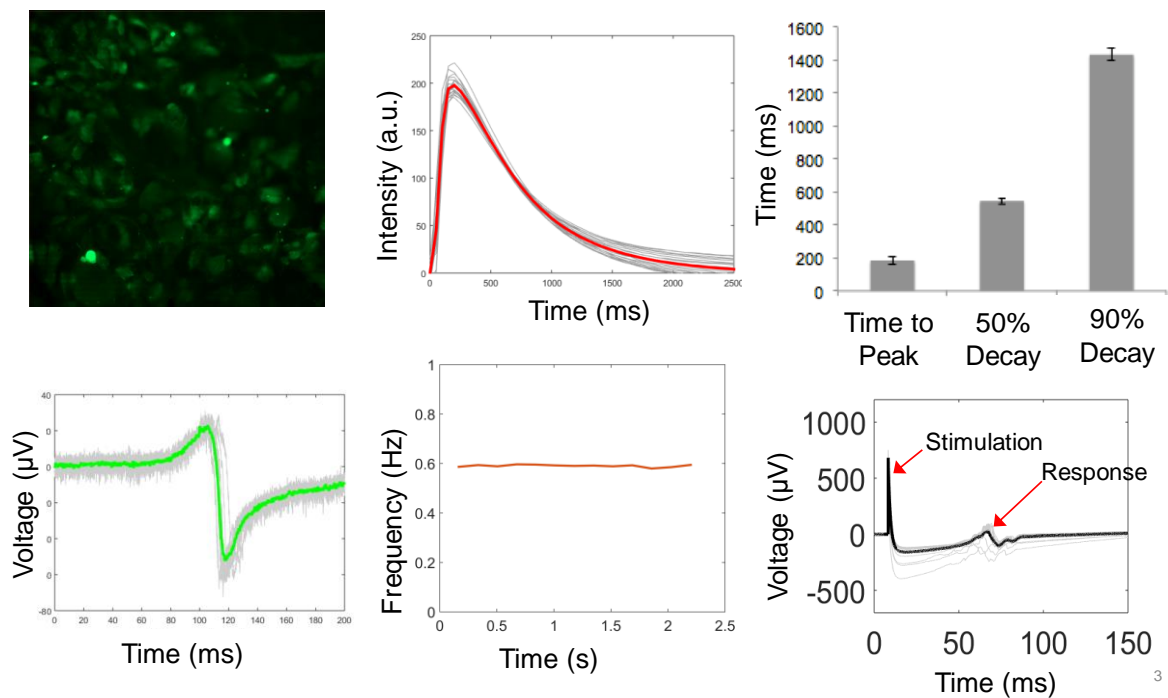
Figure 7-9.. Representative image of calcium dynamics of electrically stimulated stimulated tendon cells

7.3 Protocols

7.3.1 Thawing liquid nitrogen frozen cells

1. Find the location of cells on inventory prior to opening a liquid nitrogen container.

2. Wearing protective gloves and face shield, remove box that contains cells and locate and remove vial containing your cells. Remove cells from inventory.

3. Gently add 10 ml of prewarmed media into 15 ml falcon tube.

4. Warm cells tube in the palm of hands or in water-bath for 90 sec . Make sure lid of vial does not go below the level of water. When have thawed add them to the 15 ml falcon tube.

5. Centrifuge at 250g for 5 minutes. Remove and discard media.

6. Re-suspend cells in 10 ml of pre-warmed media. Transfer the contents to a cell culture flask.

7. Place tissue culture flask in incubator at 37°C and 5% CO_2. Change media every two to three days (depending on cell type).

7.3.2 Changing media

1. Remove media from flask. Note: when pipetting, do not let liquid get up to the cotton at the top of the pipette as this will break the pipette boy.

2. Place waste media in waste container.

3. Pipette in new pre-warmed media (T25: 3-5 mL media, T75: 8-10 mL media, T175: 25-30 mL media).

4. Return flask to incubator.

7.3.3 Splitting cells

1. When cells are 80% confluent they need to be split.

2. Remove waste media and place in waste container.

3. Add 10 ml of pre-warmed Hanks balanced salt solution (HBSS). Gently agitate the flask.

4. Remove the HBSS and discard into waste container.

5. Add Trypsin-EDTA such that the surface of the flask is completely covered (typically 3-5 ml).

6. Place in incubatory. After 5 minutes check under light microscope if cells have detached. If not, gently tap flask to detach remaining cells.

7. Add pre-warmed media to bring total volume up to 10 ml. Transfer to 15 ml falcon tube and centrifuge at 250g for 5 minutes.

8. Remove supernatant, being careful not to disturb the cell pellet.

9. Re-suspend cell pellet in 5-10 ml media (depending on desired concentration).

10. Remove 50 □l from cell suspension and add 50 □l trypan blue.

11. Use haemocytometer to count live cells (exclusion of blue) and dead cells (blue) on grid.

12. Average cell number on either side of haemocytometer, and multiply by two (to account for dilution by trypan blue) and 10,000 to calculate cell density per ml.

13. Cells may be further diluted to be seeded at required density.

7.3.4 Freezing cells

1. Repeat steps 1-8, appendix J.

2. Re-suspend cells in freezing media and count as previous (steps 10-12, appendix I). Freezing media constitutes 45 ml FBS, 5 ml DMSO. Typically 500,000 to 1,000,000 cells are frozen down per vial. This is dependent on the cell type.

3. Place vials in Mr. Frosty™ freezing container and place in -80°C freezer. After 24 Hour

7.3.5 Alamarblue® metabolic activity assay

1. Remove media from cells in culture.

2. Add HBSS into the required number of wells in a sterile 24/96 well plate.

3. Prepare alamarBlue® working solution in Hanks' balanced salt solution (ratio 1:9 respectively). Add into well plate. Ensure to have control wells without cells containing (a.) alamarBlue® working solution and (b.) HBSS alone.

4. Incubate for two hours at 37 °C.

5. After incubating for two hours, transfer 200 μl of the dye into a clear 96 well, flat bottomed plate.

6. Measure the absorbance at 550 nm and 595 nm (0.5 seconds per well).

7. Subtract the absorbance values of HBSS only from the absorbance values of the alamarBlue® in media. This gives the absorbance of alamarBlue® in media only. Denote these values AOLW; absorbance of oxidized form at lower wavelength, and AOHW ; absorbance of oxidized form at higher wavelength.

8. To calculate the percent of reduced alamarBlue®

%reduction = (ALW (AHW R0)) 100

9. To calculate the relative % difference in metabolic activity: Metabolic activity relative to control =

7.3.6 PicoGreen® proliferaton assay

1. Remove the media and gently rinse the cells with HBSS. Add 250μl of DNase free water. Freeze-thaw cells three times (-80°C for 15 minutes minimum and thaw at room temperature until it is completely defrosted). If a collagen scaffold/hydrogel has been used, transfer the construct to an eppendorf tube and digest it by 1mL of proteinase K at a concentration of 1mg/mL at 56°C overnight. Use the digestion product directly or freeze it at -20°C.

2. Prepare 1X TE buffer (initial solution at 20X), 2μg/mL DNA stock solution

(100μg/mL DNA standard) and 50ng/mL DNA stock solution (2μg/mL DNA stock

solution). Note: Prepare the standard curve with DNase free water.

3. Prepare a standard curve using the volumes in table U-1 below.

4. Transfer 100μl of each sample in the 96 well plate.

5. Make up the diluted PicoGreen® solution: 5.376mL 1X TE + 27μL concentrated

PicoGreen® solution.

6. Add 100μl diluted PicoGreen® solution to each sample in the 96 well plate.

7. Incubate at room temperature in the dark (cover with foil) for two to five minutes.

8. Read the plate for fluorescence (excitation: ~480nm; emission: ~520nm).

9. Plot the standard curve and determine the concentration of DNA as a function of the

7.3.7 Rhodamine phalloidin staining

1. Remove media from cells and gently wash with HBSS.

2. Add the appropriate volume of 4% paraformaldehyde (PFA) in PBS.

3. Incubate at room temperature for 15 minutes.

4. Remove 4% PFA (dispose of in an appropriate manner) and wash three times with

PBS.

5. Add 0.1% Triton-X and leave at room temperature for five minutes.

6. Remove 0.1% Triton-X and wash with PBS three times.

7. Add rhodamine phalloidin solution (diluted 1:100 in PBS) and leave at room

temperature for 30 minutes. Note: protect from light.

8. Remove rhodamine phalloidin solution and wash three times with PBS.

9. Add DAPI solution (diluted 1:1000 in PBS) for 30 minutes at room temperature.

10. Remove DAPI solution and wash three times with PBS.

11. Add Vectashield® mounting media and place coverslip over slide. Seal slide with nail polish and proceed to image

7.3.8 RNA isolation

1. Add 1 ml of TRI Reagent® to wells containing scaffolds/cells.

2. Homogenize samples containing scaffold using a tissue rupture, being careful not to contaminate any adjacent wells. Make sure scaffolds have been completely homogenized. Using a 1 ml pipette tip, aspirate the solution.

3. Store homogenate for five minutes at room temperature to dissociate nucleoprotein complexes. Remove the TRI Reagent® solution to a sterile 1.5 ml eppendorf.

4. Add 200 µl of chloroform per 1 ml of TRI Reagent®. Shake vigorously for 15 seconds by inversion. Incubate for 15 minutes at room temperature.

5. Centrifuge at 12,000 g for 15 minutes at 4 °C. Following the centrifugation, three phases will appear; -a lower red phenol-chloroform phase, an interphase, and an aqueous phase (translucent). The mRNA is located within the aqueous phase.

6. Remove the clear upper aqueous phase (~ 650 µl) to a sterile eppendorf. Be careful not to touch the interface. Leave a little of the upper phase to avoid contact with the interface.

7. Slowly add an equal volume of 70% ethanol and mix by inversion.

8. Add 700 µl sample from previous step to RNeasy™ column.

9. Centrifuge at 8,000 g for 15 seconds and discard the collected solution.

10. Repeat step 10 and 11 for remaining sample.

11. Add 350 µl of RW1 buffer to centre of column, centrifuge at 8,000 g for 15 seconds. Discard the collected solution.

12. Transfer column to new 1.5 ml eppendorf. Add 500 µl RPE to centre of column,

centrifuge at 8,000 g for 15 seconds. Discard the collected solution.

13. Add 500 μl of RPE buffer to centre of column, centrifuge at 8,000 g for 15 seconds.

Discard the collected solution and centrifuge for a further two minutes at 8,000 g.

14. Transfer column to a new 1.5 ml eppendorf. Add 30 μl RNase-free water onto the

column, incubate at room temperature for one minute and centrifuge for one minute at

8,000 g.

15. Add a further 30 μl RNase-free water onto the column, incubate at room

temperature

for one minute and centrifuge at 8,000 g for one minute. Split the collected sample

into three for storage purposes.

16. Determine the concentration using the NanoDrop™ and freeze at -80 °C.

17. Dilute RNA 1:50 or 1:100 in water RNase Free. Measure the absorbance at 260 nm.

(Calibrate the spectrometer with water).The purity is determined from the ratio

between A260 and A280. The ratio A260/A280 should be above 1.8 to indicate pure

RNA.

7.3.9   Synthesis of cDNA

1. Add up to 1 μg of RNA and 0.5 μg random primers in a pre-chilled tube and bring

volume up to 5 μl with nuclease-free water.

2. Denature the target RNA and primers by incubation at 70 °C for 5 minutes. Chill on

ice for 5 minutes.

3. Prepare reverse transcription mix as per table Z-1 below. Begin by adding the biggest

volume. Add the reverse transcriptase last.

Table Z-1: Recipe for reverse transcriptase mix. Volumes are shown for one sample and

must be scaled up depending on number of samples.

Component Volume per Reaction (μl)

Nuclease free H2O	5.6
ImProm-II™ 5 X Reaction Buffer	4
MgCl2, 25 mM	2.4
dNTP mix (10mM each dNTP)	1
Recombinant Rnasin ribonuclease inhibitor	1
ImProm-II ™ reverse transcriptase	1
Final volume reaction mix	15

4. Gently vortex to mix.

5. Add 15 μl to each tube containing RNA and random primers. Gently vortex to mix.

6. Run samples on program outlined in table Z-2 below.

Table Z-2: PCR machine program for reverse transcription of RNA to cDNA.

Step	Temperature	Time
Annealing	25 °C	5 minutes
Extension	42 °C	60 minutes
Heat inactivation of reverse transcriptase	70 °C	15 minutes
End	4 °C	Indefinitely

7. When program has finished proceed with PCR or store cDNA at -20°C.

7.3.10 RT-PCR

1. Dilute cDNA template so as to obtain a final concentration of 20ng per well.

2. Make sure that the cDNA concentration does not exceed 100ng/reaction and 10% of the final volume.

3. Add the components listed in Table AA-1 below to prepare master mix.

Table AA-1: Recipe for one RT-PCR reaction. Must be scaled up for multiple samples.

Component	Volume per Reaction (μl)
2 X Quantifast SYBR™ Green PCR Master mix	12.5

Forward primer, pmol 0.25

Reverse primer, pmol 0.25

Template cDNA 1.49

Nuclease free water 10.51

Final volume 25

4. For a triplicate reaction, add cDNA template in triplicate and also add a negative

control by replacing cDNA with nuclease free water.

5. Mix the master mix by pipetting and add to each well to obtain final volume of 25 μl.

6. Add the plastic cover provided by supplier on the PCR plate.

7. Centrifuge 1 minute at 1400 rpm. Place the plate in the machine.

8. Open the step one software and enter the details to map the plate on the software.

9. Choose Sybr™ Green filter for each well.

10. Choose the endogenous control from the plate and enter in the software.

11. Set up the steps in accordance to the gene and melting temperature (Tm) of the

primers. A general program is detailed in Table AA-2 below.

Annealing/Extension 60 °C 20 seconds 1

Final denaturation 95 °C 15 seconds

7.3.11 Scaffold implantation in a Sprague Dawley rat model

1. At time 0, rats will be weighed and a health check conducted

2. Anaestheize using isofluorane inhalation (5% induction reducing to 1-2% for
maintenance).

3. Maintain the animals under anaesthetic with a maintenance dose of 1-2% isofluorane
and room air inhaled through a mask.

4. Shave the leg of the rats and swab the area of implantation with 4% chlorohexidine
or 10% iodine to control bacterial contamination and minimize any potential risk of
infection.

5. Create an incision through the skin (~1cm) on the side of the right knee.Open the fascia above the tendon carefully, avoiding creating injury. Clean wound area once patellar tendon is exposed. The Achilles tendon will removed and create a defect of 6 mm in length. One of the constructs will be inserted into the empty site and aligned parallel to the direction of loading. Fibrin glue and sutures will also be applied in order to ensure the construct remains in place. The wound area will be closed in layers

6.   The health of the animals will be monitored daily immediately following surgery and a comprehensive analysis will be conducted and recorded weekly. This analysis will consist of functional evaluation of the tendon to ensure that it has not ruptured and to compare the relative efficacies of the various constructs.

7.   At each time point, the animals will be euthanized and the samples explanted for analysis. Post-operatively, place animals on a heating pad or in an incubator until able to regulate their own temperature and fully recovered from anaesthesia.

8. If any signs of infection are observed in an animal, administer antibiotic therapy (Baytril - enrofloxacin) daily for three to four days. Monitor the infection and ensure that it clears up.

9.. Mark each individual animal with an individual tail mark. House animals in two's or three's.

7.3.12 Treadmill running

The treadmill, model Eco 3/6 from Columbus Instruments, will be bought and located in in BRU Biomedical Sciences Building. It has the capability of exercising up to three rats or six mice simultaneously in individual lanes. The user can adjust the running speed from ~7 to 70 m/min with a resolution of 0.1 m/min, and the running surface can be inclined from 0° to 25° above horizontal in 5° increments.

A stimulus can be created using the electrical shock grids, and grids can be enabled or disabled individually for each lane. The intensity and repetition rate of the stimulus is user controlled. All data collection and analysis must be done manually. During the pilot study we will determine the electric stimulation (in terms of number of shocks) that a rat will need to induce running for a minimum time (between 15 to 35 min). Both the number of shocks and touches of the grid we will be recorded for each group. As result of the pilot study we will establish a threshold for the number of times that a rat

touches the grid to stop the session/experiment and a maximum number of electrical shocks that can be expected for each session (i.e. 10). In this way all rats for a particular time point will receive a similar number of shocks and none of them will receive significantly more shocks than animals in other groups.

1.   All rats will be acclimated to the treadmill for 1 week before the implantation. The rats will be trained between 11:00 am and 1:00 pm, approximately 5 hours after dark cycle started. They will be placed and left undisturbed for 15 min in their lanes and then they will be running for warming up for 5 min at 8 m/min followed by 35 min at 15-20 m/min.

2.   After 2 weeks of implantation, all the rats will be placed in the treadmill at least for 5 min/day once or twice per week. This will be done to reduce the handling stress on day of sacrifice in rats that are left free in cage (subgroup).

3.   The rats on the treadmill subgroup will be on the treadmill 5 days/week for 16 weeks. During the weeks 5,9 and 13 rats will undergo just treadmill 2days/week in order to rest. All training sessions will consist of 15 min acclimation (animals left on their lanes undisturbed), 5 minute warm-up at 8-10 m/min and then slowly ramp up the speed until a given training intensity (see table 10). The acceleration might never be bigger than 1 m/min2. The rats will rest of exercise the week 5, 9 and 13 where they will just undergo treadmill twice a week.

4.   If at any point during the experiment a rat becomes exhausted, the shock grid for that lane will be turned off and the rat allow to rest.

7.3.13 Sacrifice animals by CO2 asphyxiation.

4. Shave dorsum of rat.

5. Prepare labeled tubes with formalin for each sample. In addition, prepare labelled empty tubes and place on ice.

6. Make an incision into the skin and proceed to cut around the four injection sites (if they can be identified).

7. Remove patch of skin and identify the four implants.

8. Cut out the implants and split each sample in two. Place one sample in formalin and place the other sample on ice. Note: Be sure to have tubes label clearly and accurately.

9. Store tissue in formalin at 4°C for 24 hours. Place tissue which had been on ice in freezer at -80°C.

7.3.14 X-ray

For the 16 week time point the animals will have the same procedure as procedure 3 followed by x-ray imaging immediately afterwards while the animals are still under anaesthetic.

The X-ray photographs of whole animals will be captured with a non-invasive Kodak-FX in vivo imaging system (Kodak, Inc.) to evaluate ectopic bone formation.

7.3.15 Histological staining

Hematoxylin & eosin staining protocol

1. Stain in hematoxylin for eight minutes.

2. Wash in running tap water for eight minutes.

3. Differentiate in 1% acid alcohol for 30 seconds.

4. Note: prepare the 1% acid alcohol fresh and be strict with the 30 seconds time).

5. Wash slides in running H_2O for five minutes.

6. Blue in 0.2 % ammonia H_2O or saturated lithium carbonate for 30 seconds to one minute.

7. Wash in running tap water for five minutes.

8. Rinse in 95% EtOH – dip ten times.

9. Counterstain in eosin solution for 30 seconds – 1 minute.

10. Dehydrate:

i. 95% ethanol for 5 minutes

ii. 100% ethanol for 5 minutes twice

iii. Xylene for 5 minutes twice.

11. Mount immediately in DPX solution with coverslips. Leave overnight to hard-set.

Herovici's polychrome staining protocol

Herovici's polychrome staining visualises collagen fibres.

•   Young collagen and reticulin – blue (Collagen type III)

•   Mature collagen – red (Collagen type I)

•   Cytoplasm – yellow

•   Muscle tissue - green

•   Nuclei – black

Solutions required:

•   1% Aqueous acid fuchsin: 100 mg acid fuchsin (Sigma-Aldrich, Cat. No. 857408 or F8129) dissolve in 10 ml deionized water

•   0.1% Van Gieson stain (Note 1): 495 ml picric acid (saturated; 1.3% in H20, Sigma-Aldrich P6744-1GA). 5 ml 1% aqueous acid fuchsin (this would actually be a 0.01% solution)

      90mL picric acid + 10mL 1% acid fuchsin (aqueous)!!!

•   1% Acetic acid: 1 ml glacial acetic acid + 99 ml deionized water

•   0.05% Methyl blue stain 50 mg methyl blue (Sigma-Aldrich, Cat. No. M5528). 100 ml 1% acetic acid.

•   Polychrome Solution (Note 2): 50 ml 0.1% van Gieson stain + 25 ml 0.05% methyl blue

Procedure

1.   Deparaffinise slides and hydrate to water (Notes 3 and 4).

2.   Stain nuclei with the acid resistant nuclear stain (optional – Weigert's Iron Hematoxylin – see Masson Goldner Trichrome Staining protocol)

3.   Place slides in the polychrome solution for 5 min at room temperature.

4.   Remove slides and immediately place in 1% acetic acid for 2 min.

5.   Rinse in 100% ethanol for 5 min (Note 5).

6.   Dehydrate and clear beginning at 100% alcohol:

(a)   100% ethanol – 1 min.

(b)   100% ethanol – 1 min.

(c)   Xylene – 3 min.

(d)   Xylene – 3 min.

6.   Coverslip using non-aqueous mountant (Note 6).

Notes

1.   0.05% Van Gieson acid fuchsin solution (Sigma-Aldrich) can be substituted for laboratory-prepared 0.1% van Gieson stain without detriment to the final staining.

2.   Herovici's original method used a 1:1 mix of van Gieson stain and methyl blue and included the addition of 10 ml glycerol and 0.5 ml saturated lithium carbonate solution. We have found that a 2:1 ratio gave more consistent staining by helping to keep the picric acid saturation. We found no benefit in the addition of glycerol to the solution, while the addition of saturated lithium carbonate notably reduced methyl blue staining and increased staining variability.

3.   We have tested 10% neutral buffered formalin and Bouin's solution for fixation of tissue and found both to be comparable with Bouin's solution, giving a slight increase in stain intensity.

4.   Any excess water should be removed from the slides before immersion in the polychrome solution to maintain dye saturation.

5.   Water and other aqueous solutions will desaturate the stain and wash the stain out of the tissue sections. Slides should remain in 100% ethanol until ready for coverslipping.

6.   Examples of non-aqueous mountant we have used include Surgipath MM24 (Leica Microsystems), Shandon-mount (Thermofisher) and DPX (Sigma-Aldrich).

Collagen fibers are visualised by Herovici's polychrome staining

Masson – Goldner Trichrome Staining Protocol

Description: Collagen fibers will be stained green (blue), nuclei will be stained brown-black, the cytoplasm is stained red and erythrocytes will be stained in orange. Times need to be adjusted for different types of tissues.

Reagents needed:

- Weigert's Iron-Haematoxylin

    o Weigert A – Haematoxylin solution (X906.1, Carl Roth)

    o Weigert B - Ferric chloride solution (X907, Carl Roth)

    o Freshly prepare a 1:1 mixture of solution A and B (solution is stable up to 8 days at RT)

- 0.5% HCl-EtOH (70% ETOH + 0.5-1% HCl (6ml HCl 32% in 200ml 70% EtOH)

- 1% Acetic Acid (you can collect the slides here, nothing happens in 1% Acetic acid)

- Goldner I solution (Ponceau – Acidfuchsin)

- Goldner II solution (Phosphotungstic acid - Orange G)

Goldner III solution (Light green SF yellowish) (instead of Light green solution it is possible to use a 0.1 - 0.2% solution of Anilinblue for counterstaining)

- Graded alcohols and Xylene for Rehydration and Dehydration

Stain slides in a humidity chamber, drop staining solutions on slides, don't pour solutions back in original bottles! Make sure slides do not dry out.

Weigert's Haematoxylin can also be prepared as follows:

Weigert A: 1g Haematoxylin 100ml 96% EtOH

Weigert B: 2.8g $FeCl_3.6H_2O$ (31232-M, Sigma) in 100mL Aqua dest. 1ml Hydrochloric acid (concentrated grade). 95ml Aqua dest.

Fastgreen: 0,2g Fastgreen SF yellowish 100ml Aqua dest. 200µl Acetic acid

Dewaxing (= Rehydration)

- Xylene I 10 min

- Xylene II 10 min

- EtOH 100% I 5 min

- EtOH 100% II 5 min

- EtOH 96% 5 min

- EtOH 70% 5 min

(EtOH 50% is not good for tissue preservation and should be avoided)

- Weigert's Iron-Haematoxylin max 3 min

- Stop reaction in 1% Acetic Acid

- 0.5% HCl-EtOH 5 sec (dip 1-2x) · for de-staining of connective tissue

- Bluing: running tap water 5-15 min (colour change: brown-blue · blue)

- Goldner I solution 5-10 min

- Stop reaction in 1% Acetic Acid

- Goldner II solution 1-3 min (up to 1h for tendon tissue) until connective tissue is de-stained (check under microscope)

- Stop reaction in 1% Acetic Acid

- Goldner III 2-5 min (up to 10 min) check under microscope!

- Stop reaction in 1% Acetic Acid

Dehydration

- EtOH 70% <30 sec (Fast green will be washed out!)

- EtOH 96% 30 sec - 1 min

- EtOH 100% I 30 sec - 1 min

- EtOH 100% II   30 sec - 1 min

- Xylene I   2 min

- Xylene II   2 min – until mounting

- Mounting with DPX

<u>Alcian Blue Staining Protocol</u>

Description: Alcian blue stains acid mucosubstances and acetic mucins. Excessive amounts of non-sulfated acidic mucosubstances are seen in mesotheliomas, certain amounts occur normally in blood vessel walls but increase in early lesions of atherosclerosis. Strongly acidic mucosubstances will be stained blue, nuclei will be stained pink to red, and cytoplasm will be stained pale pink.

Fixation: formalin fixed, paraffin embedded tissue sections.

Solutions and Reagents:

3% Acetic Acid Solution:

     Glacial acetic acid ----------------- 3 ml

     Distilled water --------------------- 97 ml

Alcian Blue Solution (pH 2.5):

     Alcian blue, 8GX -------------------- 1 g

     Acetic acid, 3% solution ----------- 100 ml

     Mix well and adjust pH to 2.5 using acetic acid.

0.1% Nuclear Fast Red Solution:

     Nuclear fast red ------------------- 0.1 g

     Aluminum sulfate------------------ 5 g

     Distilled water ---------------------100 ml

     Dissolve aluminum sulfate in water. Add nuclear fast red and slowly heat to boil and cool. Filter and add a grain of thymol as a preservative.

Procedure:

1.   Deparaffinize slides and hydrate to distilled water.

2.   Stain in alcian blue solution for 30 minutes.

3.   Wash in running tap water for 2 minutes.

4.   Rinse in distilled water

5.   Counterstain in nuclear fast red solution for 5 minutes.

6.   Wash in running tap water for 1 minute.

7.   Dehydrate and through 95% alcohol, 2 changes of absolute alcohol, 3 minutes each.

8.   Clear in xylene or xylene substitute.

9.   Mount with resinous mounting medium.

Results:

   Strongly acidic sulfated mucosubstances -------------- blue

   Nuclei --- pink to red

   Cytoplasm --- pale pink

Positive Controls:

   Small intestine, appendix, or colon.

Safranin O Staining Protocol for Cartilage

Description: This method is used for the detection of cartilage, mucin, and mast cell granules on formalin-fixed, paraffin-embedded tissue sections, and may be used for frozen sections as well. The cartilage and mucin will be stained orange to red, and the nuclei will be stained black. The background is stained bluish green.

Fixation: Formalin fixed, paraffin embedded sections.

Solutions and Reagents:

Weigert's Iron Hematoxylin Solution:

   Stock Solution A:

   Hematoxylin ---------------------------- 1 g

459

95% Alcohol ---------------------------- 100 ml

Stock Solution B:

29% Ferric chloride in water ----------- 4 ml

Distilled water ------------------------- 95 ml

Hydrochloric acid, concentrated ---- 1ml

Weigert's Iron Hematoxylin Working Solution:

Mix equal parts of stock solution A and B. This working solution is stable for about 4 weeks.

0.05% Fast Green (FCF) Solution:

Fast green, FCF, C.I. 42053 ------------- 0.5 g

Distilled water --------------------------- 1000 ml

1% Acetic Acid Solution:

Acetic acid, glacial ------------------------ 1 ml

Distilled water ----------------------------- 99 ml

0.1% Safranin O Solution:

Safranin O, C.I. 50240 -------------------- 0.1 g

Distilled water ---------------------------- 100 ml

Procedure:

1. Deparaffinize and hydrate slides to distilled water.

2. Stain with Weigert's iron hematoxylin working solution for 10 minutes.

3. Wash in running tap water for 10 minutes.

4. Stain with fast green (FCF) solution for 5 minutes.

5. Rinse quickly with 1% acetic acid solution for no more than 10 −15 seconds.

6. Stain in 0.1% safranin O solution for 5 minutes.

7.   Dehydrate and clear with 95% ethyl alcohol, absolute ethyl alcohol, and xylene, using 2 changes each, 2 minutes each.

8.   Mount using resinous medium.

Results:

   Nuclei --- black

   Cytoplasm --------------------------------------- bluish green

   Cartilage, mucin, mast cell granules ----------- orange to red

7.3.16 Stereology

<u>Taking images</u>

1. Place stained slide under bright field light at 1.25X and identify the tissue.

2. Switch to the 10X magnification and identify the implant site as best you can (it may be partially or fully degraded).

3. Switch to 40X magnification and take three pictures at random in the vicinity of the implant.

<u>Blood vessel density</u>

1. Choose a cycloid grid in the command box.

2. Calibrate all images for this measurement. A microscope slide with markings of known dimensions has been captured in Image Pro® previously, with images at every objective and saved on the computer.

3. Open the calibration folder. Select the appropriate objective lens folder, and open an image.

4. Scroll down 'measurements' toolbar, and select 'calibration wizard'.

5. In the pop-up menu, select 'set calibration'. Choose the objective lens, and measure

the size of the circle on the open image.

6. In the next command, enter the actual measurement of the circle (given in the name of the image). Save this calibration, in your working folder. This file must be re-opened every time ImagePro® is re-opened.

8. Open the calibration file. Go to 'measurements' and 'set system'.

9. Apply a cycloid grid of radius 20 μm, spacing 40 μm and set margins to 20 μm.

10. Overlay the grid.

11. As the length of the cycloid grid is twice its height, each arc is 40 μm. Therefore, multiply the number of arcs by 40 to calculate the length of test line.

12. Count the number of intersections between blood vessels and the cycloid grid.

13. Use the following formula to calculate surface density of blood vessels:

SV = 2 x I/LT

SV = surface density

I = number of intersections

LT= total length of test line

Volume of inflammatory or specific cells

1. Open image and select 'grid mask' command.

2. Choose a line grid with 40 x 40 pixel spacing and margins of 20 pixels. Click 'apply'.

3. Make sure cells/objects of interest are not bigger than the area enclosed by four grid points.

4. Record both the number of inflammatory cells that hit grid points and also the number of grid points that hit the tissue of interest.

5. Calculate the volume fraction of inflammatory cells using the following formula:

VV = PI/PT

VV = volume fraction of inflammatory cells

PI = number of grid points which hit inflammatory cells

PT = number of grid points which hit the tissue of interest quantify inflammatory volume fraction.

7.3.17 Fiber orientation

To estimate the local orientation of the collagen fibers, we used OrientationJ, which is an ImageJ plug-in developed inhouse based on structure tensors. Structure tensors are matrix representatives of partial derivatives and are commonly used in the field of image processing (R. Rezakhaniha et al., Experimental Investigation of Collagen Waviness and Orientation in the Arterial Adventitia, Biomechanics and Modeling in Mechanobiology, vol. 11, 2012.) OrientationJ evaluates the local orientation and isotropic properties (coherency and energy) of every pixel of the image. Using OrientationJ plug-in for ImageJ, we obtained the histogram of local angles for all individual images of collagen fibers.

7.3.18 Immunostaining

1. Prepare the following solutions:

Antigen retrieval buffers

I. Tris-EDTA buffer (10 mM Tris-Base, 1 mM EDTA ,0 .05% Tween20, pH 9.0)

□ Tris Base 1.21 g

□ EDTA 0.37 g

□ ddH2O 1000 ml

□ Tween- 20 0.5 ml

II. Citrate buffer (10mM Citric acid, .05% Tween-20, pH 6.0)

□ Citric acid (anhydrous) 1.92 g

□ ddH2O 1000 ml

□ Tween-20 0.5 ml

Blocking buffers

Goat block

□ 1% BSA (stabilizer) 0.5 g or 1.67 ml

□ 0.1% Triton x100 50 μl

□ 0.1% cold-water fish skin gelatin 50 μl

☐ 0.05% Tween-20 25 µl

☐ Add PBS up to 50 ml

2. Immerse the slides in a staining dish and cover with the appropriate buffer (if both buffers are to be used, use the tris-EDTA buffer first, allow to cool down, wash once with PBS and then repeat with the citrate buffer).

3. Half fill the pressure cooker with water and place the staining dish in the pressure cooker.

4. Cook in the microwave for approximately eight minutes.

5. Allow the staining dish to stand at room temperature for approximately 15 minutes. Following this place on ice for 15 minutes or until cool.

6. Was three times with PBS.

7. Incubate for 30 minutes in 1% TritonX-100 in PBS (skip this step if the antigen is on the

membrane).

8. Wash three times with PBS.

9. Use PapPen™ to draw circles around tissue sections on each slide.

10. Block the tissue for 30 minutes at room temperature. Note: Use serum from the species

in which the secondary antibody is raised i.e if secondary antibody is raised in goat, use

got serum in blocking buffer.

11. Wash three times with PBS.

12. Wash three times with 0.05% PBS-Tween.

13. Incubate overnight at 4°C with primary antibody at appropriate dilution. Ensure that the

slide will not dry out by using a humidity chamber.

14. Wash three times with 0.05% PBS-Tween.

15. Incubate secondary antibody at appropriate dilution for 30 minutes at room temperature

in the dark.

16. Wash three times with PBS.

17. Incubate in DAPI solution at room temperature for 10-15 minutes in the dark.

18. Wash three times with PBS.

19. Mount the slides with Prolong Gold Anti-fade solution. Put the slides at 4°C overnight

in the dark and seal the edges of the glass coverslips the next day.

7.3.19 Protein extraction from tissue

1. Retrieve protein samples from -80°C storage and keep on icebox.

2. Pulverize the tissue using liquid nitrogen and a cellcrasher. Place approximately 1 gram of tissue into eppendorf suitable for TissueLyserLT beadmill (Qiagen) with 1 ml lysis buffer (RIPA buffer) and one stainless steel bead. The TissueLyser LT functions by vertically oscillating the rupture chamber at a high speed to move the stainless steel bead up and down rapidly within the eppendorf to rupture and homogenise the associated tissue.

3. Place eppendorfs into the pre-cooled bead mill chamber and begin rupture for one minute. Check samples to see if complete homogenisation has taken place. Otherwise repeat rupture until complete homogenisation occurs, taking care to keep the eppendorfs cool.

4. Spin samples in a centrifuge at 10,000 rpm for 5 minutes at 4°C. Remove supernatant and quantify total protein content using BCA protein assay.

7.3.20 Conjugation with AF555

Materials

-Boric acid 250 uM

-Alexa Fluor 555 or alternative CF 555 succinimidyl ester (SCJ4600022 sigma-aldrich) (1 mg for 20

samples)

-Filters 3kDa (ref= 2740169 – 96EA) (1 per sample)

-PBS pH 7.4

Methods

1.- Measure protein concentration in nanodrop and reach 0,65-0,75 mg/ml using normal BCA not

micro BCA assay (you can dilute 1:5 or 1:10 the samples). In nanodrop should be around A280 =

0,8 for all the samples.

7.3.21 Sample tagging

a) In 500 ml add 7,5 g of boric acid and adjust to pH=8,5 with NaOH 1-5M (very important ! it

takes time)

b) Resuspend 1 mg of Alexafluor® 555(ref= A20009) with 100 ul DMSO

In an amber tube = 50 ul of boric acid 250 uM

+ 50 ul sample

+ 4 ul of Alexa fluor 555

3.- Leave incubate for 1 hour at RT in dark room

4.- After 1-hour incubation, wash the samples with centrifugal filter units, Amicen ®,ultra 0,5, 3 kDa

-3 times for 10 min at 14 000 RCF at 4 ºC .

-Each time, add around 400 ul of PBS pH 7.4 to the remaining sample in the column.

5.- Final step. Invert filter and recover the tagged sample using 500 RCF at 4ºC for 5 min.

6.- Store sample at 4ºC in the dark.

7.- Quantify all the samples with the nanodrop at "280 nm" and "555" nm.

Process the data and get the following information :

- Substitution rate of the dye (make sure to vortex the samples !!)

- Quantity in ul of the sample that it is needed to use on 100 ul of TBS-T to perform

the titration. (Do several measurements)

7.3.22 Incubating printed slides for protein microarray applications*

Materials

1.- Preparation of 10 X TBS: This is a modified low salt version of TBS.

 1X = 20 mM Tris (NOT Trizma), 100 mM NaCl, 1 mM CaCl2 and 1 mM MgCl2, pH to 7.2 with c.HCl.

- 200 mM Tris 24.22 g (Sigma)

- 1 M NaCl 58.44 g (Sigma)

- 10 mM MgCl2 0.9521 g

- 10 mM CaCl2 1.4702 g

2.- Prepare 2xTBS:

3.- Use 1 TBS to prepare TBS-T : Add 0.5 mL Tween-20 to the 1X solution (0.05% Tween-20 =

TBS-T)

Protocol: The following protocol should be carried out in the dark at all times!

1.- Take ice for the tagged samples (Take samples from fridge)

2.- Take slides from the fridge and leave to stabilize for 30 min prior to use to avoid water condensation.

Remove the slide box intact in the bag with desiccant from the fridge at least 30 min before

incubation to allow the slides to come to room temperature.

3. Draw a map of your samples (Use the same order for pippeting!):

- A titration curve should be initially carried out to determine optimum sample concentration in terms of signal to noise ratio and feature overload. Samples are diluted into a final volume of 70 uL with TBS-T.

- Include two quality control wells and experimental controls (i.e. inhibition) in the experimental design.

- Take metal holder from the first drawer. Pick the gasket in the shelf Check the rubber of the 8-well gasket before aliquoting sample into thegasket wells (70 uL per well).

5. Sandwich the printed microarray slide on top of the gasket slide with aliquoted samples. Assemble gasket holder steel assembly immediately. Make sure screw is finger tight and not over tight.

6. Incubate slide for 1 hour at the desired temperature with gentle rocking/rotation (i.e. in hybridisation oven at 4 rpm).

7. Remove gasket and slide from steel assembly and separate gasket and slide under incubation solution. This is done by opening the slide gasket into a container full of TBS-T to avoid cross contamination by encouraging immediate dilution.

- To use less TBS-T use tilting!

- Open computer to go faster but not the screen.

8. Wash microarray slides in TBS-T x3 or 4 for 2 min (depending on your sample optimisation) in a

Coplin jar.

9. Wash in TBS x1 in a Coplin jar.

10. Dry by centrifugation (1,500 rpm, 5 min, 10 °C).

11. Place dried microarray slides into slide holders for microarray scanner and scan immediately.

7.3.23 Washing Agilent gaskets after use*

1. Place 8-well gasket in a 50 mL tube with approximately 35 mL 0.1% SDS solution.

2. Rotate for 30 minutes to 1 hour. DO NOT LEAVE LONGER.

3. Remove the SDS and wash (3 times, 5 min each) with dH2O with gentle shaking or rotation.

4. Centrifuge dry and store on the bench in a slide container until next use.

5. 8-well gaskets should be carefully checked for damage to the rubber of the wells. If any defects are

noted, the gasket should be discarded.

• * Please note that these are lab standard protocol.

• * Please do not make any individual changes as we must be able to compare data.

• * Please adhere to initial training techniques.

7.3.24 Array Software

1.- Open software

2- Turn on the laser

3.- Check channels (Green channel) and put to 90% and maximum resolution (5 um).

7.3.25 Calcium imaging

Materials and reagents
Fura-2 AM (ab120873)
ATP/Ionomycin, free acid (ab120370)
HBSS (10x)

Protocol

1. Mix Fura-2 AM 50 µg lyophilized by adding 50 µL of DMSO and vortex for 1 min. Store at -20 oC wrapped in foil for light protection.

2. <u>Mix HBSS-1x solution:</u>

Mix 100 mLs of the 10X HBSS solution with 800 mLs of distilled H20. Add 0.14 g of anhydrous CaCl2 (FW 111, 1.3 mM), 1g of d-glucose (FW 180.2, 5.5 mM) and 0.35 g NaHCO3 (FW 84.01, 4.2 mM). Bring to 1000 mL volume with distilled H20, pH to 7.4 and store for ~1 week at 4 oC.

4. <u>Mix 50 mM KCl:</u>

NaCl (FW 58.44)   5.0843 g (87 mM)

KCl (FW 74.56)   3.728 g (50 mM)

MgCl2 (FW 203.3)   0.2033 g (1 mM)

CaCl2 (1 M Stock from certified volumetric stock)   5 ml (5 mM)

HEPES (FW 238.3)   2.833 g (~12 mM)

Glucose (FW 180.16) 1.8016 g (10 mM)

1 liter volume, pH 7.35, ~290-310 mOsm. Store 4 oC.

5. Replating: One to two days prior to experimentation, replate cells to collagen coated coverslips (see protocol below, round, glass, sterilized with ethanol, dried) placed in 35 mm tissue culture dishes. The 35 mm dishes are placed in 150 mm Petri dishes to be used as a microincubator and carrier between incubator and experiments.

6. When replating, place cells in center of round glass coverslips to settle and to ensure that imaging is optimized. Empirically determine the density of cells and how to replate in order to have cells stick to glass through the washes and the perfusion of solutions.

7. On day of experiment: Take the HBSS and 50 mM K solutions out of the refrigerator, turn on equipment, perform calibration curve, check that cells are well adhered to glass.

8. Take 2 x 50 ml Falcon tubes, label as HBSS and HBSS+BSA. Pour HBSS from the HBSS container into the 50 ml tube labeled as HBSS.

9. Mix HBSS+BSA: Measure out ~45 mg of BSA (Fatty acid free) and add to the empty tube labeled HBSS + BSA. Transfer ~45 ml of HBSS and mix gently so as not to create a lot of bubbles, but to mix the BSA completely, let settle. This should be a 1 mg/mL mixture of BSA and HBSS.

10. Mix Fura-2 + HBSS+BSA: Thaw the Fura-2 AM 50 µl DMSO and mix with room lights turned off. Only load 2 of the 35 mm dishes at a time, as the timing for imaging will not work well for timing of the post-Fura wash. Pipette 4-10 µL/35 mm dish of cells of this Fura-2/HBSS/BSA mixture into a 15 mL Falcon tube (lower concentration of Fura-2 AM in the cells for imaging will reduce the intracellular buffering capacity). Add 4 mL of HBSS+BSA into the 15 mL tube with Fura-2. Get two dishes of coverslips from the incubator, place on the bench, then vortex the 15 mL tube on high for 1 min. Set in rack with the 2 x 50 mL tubes of HBSS and HBSS+BSA (loosen/remove lids to all Falcon tubes). Have a waste container nearby and sterile pipette tips open and ready.

11. Load Fura: Remove 2 of the 35 mm dishes from the incubator. With 1 mL sterile pipette tips, remove all media from one 35 mm dish of cells and eject into a waste container. With the same tip, bring up 1 mL of HBSS and gently add to the cells, being careful to place along the side and gently to not cause disruption of plated cells. Pull up the same 1 mL of HBSS and eject into the waste container, bringing up the next 1 mL of HBSS with the same tip and placing gently on the cells. Remove solution again, and discard tip. With a new sterile pipette tip, pipette up 1 mL of HBSS+BSA and wash gently, removing to waste. With the same pipette tip, repeat 2 more times to wash the cells 3x with HBSS + BSA. With the same tip, immediately add 1 mL of the Fura +HBSS+BSA that was vortexed for 1 min. Add the second 1 mL of Fura-2 AM to the cells and label the lid of the coverslip dish with the time. Repeat for the second dish.

12. Typically, load for 45 min, but this might need to be varied as well as the 4-10 µL of Fura-2 AM in 2 mL of HBSS+BSA. Replace both dishes in CO2/37 oC incubator for the 45 min loading time.

13. Wash: Remove both dishes and gently, with a new sterile tip, pull 1 mL of the Fura-HBSS+BSA mix to waste, and then the second 1 mL. With a new pipette tip, wash the cells 3-4x with 1 mL of HBSS (not HBSS+BSA) each time gently, and placing the wash in the waste. After the 4th wash, leave on 1 mL of HBSS and add a second mL of HBSS. Label the time and replace in the incubator for 30 min-45 min.

14. Get the first coverslip of cells about 25 min into the wash and set up on the imaging rig in the chamber. Perform the imaging experiment in 7-15 min maximum, and then get the next dish from the incubator. All experiments should be completed in the dark.

15. Constantly perfuse the cells with HBSS on the recording chamber for resting Ca2+ measurements and to stimulate use a stimulant of some sort, either the test solution, or 50 mM KCl solution, or electrical stimulation. To stimulate use a range of high K+ solutions (matched monovalents): 20 mM, 40 mM and 60 mM KCl solutions as well, each time replacing NaCl with equivalent amounts of KCl.

16. To obtain a positive control for imaging, use 20 µM working concentration ATP/ionomycin (ab120370, 5 mg free acid mixed to 20 mM in DMSO) by placing the appropriate volume into the volume of the chamber while perfusing.

17. To continue through the day, we recommend beginning the next 2 coverslips of cells loading about the same time as washing the first sets, keeping track of loading/washing and knowing how long it takes to switch coverslips and do the imaging experiments.

7.4 Thesis outputs

7.4.1 Journal publications and conference proceedings

7.4.1.1 Researh Articles: 10

1. **Marc A. Fernandez-Yague,** Anup Poudel, Tofail Syed A. M., Manus J. P. Biggs. Boron Nitride Nanotube Addition Enhances the Crystallinity and Cytocompatibility of PVDF-TrFE Frontiers in Chemistry; 2019;7; 364.

2. **M.A. Fernandez-Yague***, Gemma Mestres*, D.Pastorino, E.Montufar, M.Manzanares, M.P.Ginebra. "In vivo comparative study of the anti-inflammatory effects of CPC foam with drug delivery and Mg CPC". (under review) (2018). Materials Science and Engineering: C *These authors contributed equally* **(IF: 5.1)**

3. **M.A. Fernandez-Yague**, R.A.Perez, M.J Biggs, FJ.Gil, M.Pegueroles "Enhanced osteoconductivity on electrically charged Ti c.p implants treated by physicochemical surface modifications methods". Nanomedicine (Lond) (2018) (under review). **(IF: 6.5)**

4. C Vallejo-Giraldo, K Krukiewicz, I Calaresu, J Zhu, M Palma, **MA Fernandez**, Benjamin G, N Peixoto, Nazar Farid, G O'Connor, L Ballerini, A Pandit, and M Biggs Attenuated Glial Reactivity on Topographically Functionalized Poly(3,4-Ethylenedioxythiophene):P-Toluene Sulfonate (PEDOT:PTS) Neuroelectrodes Fabricated by Microimprint Lithography Small May 2018 **(IF: 8.3)**

5. Larrañaga A, Isa ILM, Patil V, Thamboo S, Lomora M, **MA Fernández-Yague**, Sarasua JR, Palivan CG, Pandit A. Antioxidant functionalized polymer capsules to prevent oxidative stress. Acta Biomater. Feb 2018; **(IF:6.3)**

6. Manus J. P. Biggs, **MA. Fernandez-Yague**, Dilip Thomas, Ryan Cooper, Matteo Palma, Jinyu Liao, Teresa Fazio, Carl Dahlberg, Helen Wheadon, Anuradha Pallipurat, Abhay Pandit, Jeffrey Kysar and Shalom J. Wind The Functional Response of Mesenchymal Stem Cells to Electron-Beam Patterned Elastomeric Surfaces Presenting Micron to Nanoscale Heterogeneous Rigidity. Advanced Materials (2017) **(IF:21.9)**

7.   Aitor Larrañaga, Jose Ramon Sarasua, Florent Pompanon, Nicolas Gruffat, Teodoro Palomares, Ana Isabel Alonso-Varona, Aitor Larrañaga Varga, **MA Fernandez-Yague**, Manus Jonathan Paul Biggs. Effects of isothermal crystallisation on the mechanical properties of an elastomeric medium chain length polyhydroxyalkanoate. European Polymer Journal (2016) **(IF:3.5)**

8.   Vallejo-Giraldo C, Pugliese E, Larrañaga A, **Fernandez-Yague MA**, Britton JJ, Trotier A, Tadayyon G, Kelly A, Rago, I, Sarasua JR, Dowd E, Quinlan LR(1,)(5), Pandit A(1,)(2), Biggs MJ Polyhydroxyalkanoate/carbon nanotube nanocomposites: flexible electrically conducting elastomers for neural applications. Nanomedicine (Lond) (2016) **(IF:5.9)**

9.   **MA. Fernandez-Yague**, Aitor Larrañaga, Olga Gladkovskaya, Alanna Stanley, Ghazal Tadayyon, Yina Guo, Jose-Ramon, Sarasua, Tofail A.M Syed, DimitriosI Zeugolis, Abhay Pandit and Manus J.P Biggs.   Effects of Polydopamine Functionalization on Boron Nitride Nanotube Dispersion and Cytocompatibility. Bioconjugate Chemistry (2015) **(IF:4.51)**

10.   P Mokarian-Tabari, C. Vallejo-Giraldo, **MA Fernandez-Yague**, C. Cummins, M.A. Morris, M.J.P Biggs. 'Nanoscale Neuroelectrode Modification via Sub-20 nm Si Nanowires through Self-assembly of Block Copolymers.' Journal of Materials Science: Materials in Medicine. (2014) **(IF: 2,4)**

7.4.2 Review Papers: 2

1.   **Marc A. Fernandez-Yague**, Abhay Pandit, Manus J. Biggs, Piezoelectric control of tendon regeneration, JPhys Materials, 2019, (under review)

2.   **MA. Fernandez-Yague**, Sunny Akogwu Abbah, Laoise McNamara, Dimitrios I. Zeugolis, Abhay Pandit, Manus J. Biggs. Biomimetic Approaches in Bone Tissue Engineering: Integrating Biological and Physicomechanical Strategies. Advanced drug delivey reviews. (2015) **(IF: 12,7)**

7.4.3 Book Chapters: 1

1.   **MA. Fernandez-Yague**, C. Vallejo-Giraldo, C. Cummins, M.A. Morris, M.J.P Biggs. Biological activity on piezoelectric PVDF. <u>Electrically Active Materials for Medical Devices</u>. (2015)

7.4.3.1 Research Presentations: 27

1.   **Marc A. Fernandez-Yague**, Abhay Pandit and Manus J.P Biggs. "Mechanically loaded Piezoelectric scaffolds to define the cell microenvironment." Podium presentation at <u>the 26th annual meeting of European Orthopaedic Research Society </u>(EORS2018), Galway, Ireland, October 2018

2.   **Marc A. Fernandez-Yague**, Abhay Pandit and Manus J.P Biggs "Piezoelectric scaffolds for tendon repair". Podium presentation at the <u>Signal Transduction by Engineered Extracellular Matrices Gordon Research Conference</u> (GRC2018), Andover, US, July 2018

3.   **Marc A. Fernandez-Yague**, Abhay Pandit and Manus J.P Biggs "Piezoelectric scaffolds: tendon repair through electromechanical stimulation". Podium presentation at <u>the 8th World Congress of Biomechanics</u> (WCB2018), Dublin, Ireland, July 2018

4.   **Marc A. Fernandez-Yague**, Abhay Pandit and Manus J.P Biggs "Cellular Responses to Electron-Beam Modified Elastomeric Surfaces Presenting Micron to Nanoscale Heterogeneous Rigidity". Podium presentation at <u>the 8th World Congress of Biomechanics</u> (WCB2018), Dublin, Ireland, July 2018

5.   **Marc A. Fernandez-Yague**, Abhay Pandit and Manus J.P Biggs "Piezoelectric scaffolds for tendon repair through electromechanical stimulation". Podium presentation at<u> Bioengineering in Ireland conference </u>(BINI2018), Dublin, Ireland, January 2018

6.   **Marc A. Fernandez-Yague**, Abhay Pandit and Manus J.P Biggs "Piezoelectric nanoscaffolds: the differential expression and possible function of mechanosensitive genes in human tendon cells". Podium presentation at the 5th annual meeting of <u>Matrix Biology Ireland</u> (MBI2017) Dublin, Ireland, December 2017

7.   **Marc A. Fernandez-Yague**, Mattew Dalby, Abhay Pandit and Manus J.P Biggs "Piezoelectric nanoscaffolds: the effect of piezoelectricy on biological processes." Podium presentation at <u>the 28th annual meeting</u> of the <u>European Society of Biomaterials</u> (ESB2017). Athens, Greece, September 2017.

8.   **Marc A Fernandez-Yague**, Dimitrios Zeugolis, <u>Tofail Syed</u>, Abhay Pandit, Manus JP Biggs PVDF-TrFE /BNNT: Piezoelectric system for mediating tendon repair through activation of voltage and stretch sensitive transmembrane receptors Poster Presentation at the <u>Second International Workshop Modern Nanotechnologies</u> (IWMN2016) Rusia, August 2016.

9.   **Marc A. Fernandez-Yague**, Dimitrios Zeugolis, Abhay Pandit and Manus J.P Biggs "Piezoelectric nanoscaffolds: mediating tendon regeneration through activation of piezoresponsive receptors."Podium presentation at the <u>European Chapter Meeting of the Tissue Engineering and Regenerative Medicine International Society</u> (TERMIS2016) Upsala, Sweden, July 2016.

10.   **Marc A. Fernandez-Yague**, Dimitrios Zeugolis, Abhay Pandit and Manus J.P Biggs Piezoelectric nanoscaffolds: mediating tendon regeneration through activation of piezoresponsive receptors. Podium presentation at the <u>10th World Biomaterials Congress (WBC2016)</u>. Montreal, Canada, May 2016.

11.   **Marc A. Fernandez-Yague**, Dimitrios Zeugolis, Abhay Pandit and Manus J.P Biggs "Piezoelectric nanoscaffolds for tendon regeneration". Podium presentation at <u>the 24th annual meeting of European Orthopaedic Research Society (EORS2016)</u>,

12.   **Marc A. Fernandez-Yague**, Dimitrios Zeugolis, Abhay Pandit and Manus J.P Biggs   "Piezoelectric nanoscaffolds: mediating tendon regeneration through activation of piezoresponsive receptors." Podium presentation at the <u>22th Bioengineeering in Ireland anual meeting</u> (BINI2016) Dublin Ireland , January 2016

13.   **Marc A. Fernandez-Yague**, Gemma Orpella-Aceret, Ghazal Tadayyon, Matteo Palma, Tofail Syed, Dimitrios Zeugolis, Abhay Pandit and Manus J.P Biggs " The Role of Electrical Stimulation in Tendon Maintenance and Repair: Electrospun PVDF-TrFE/Boron Nitride Nanotubes as Bioactive Scaffold for Promoting Tendon Regeneration." Podium presentation at the <u>27th European Conference on Biomaterials (ESB2015)</u> Krakow, Poland Setembre 2015

14.   Catalina Vallejo-Giraldo, **Marc A. Fernandez-Yague**, Abhay Pandit, Eilís Dowd, Manus J. P. Biggs Topographical and Biochemical "Functionalized PEDOT films as Coating Strategies for Improved Neuroelectrode Functionality". Podium presentation at the <u>27th European Conference on Biomaterials </u>(ESB2015) Krakow, Poland Setembre 2015

15.   Gemma Orpella, **Marc A. Fernandez-Yague**, Matteo Palma, Dimitrios Zeugolis, Abhay Pandit and Manus J.P Biggs. Electrospun Piezoelectric P(VDF-TrFE) Scaffolds and the Effect of Electrical Stimulation for Tendon Tissue Regeneration. Poster presentation at the the <u>27th European Conference on Biomaterials (ESB20</u>15). Krakow, Poland Setembre 2015

16.   **Marc A. Fernandez-Yague**, Aitor Larrañaga, Olga Gladkovskaya, Alanna Stanley,Ghazal Tadayyon, Yina Guo , Jose-Ramon Sarasua, Tofail, Syed, Dimitrios Zeugolis, Abhay Pandit, Manus J. Biggs. "Piezoresponse (PFM) and Transmission Electron Microscopy (TEM) study of Boron Nitride Nanotubes (BNNT)." Podium presentation at the <u>39th Annual Symposium of the Microscopy Society of Ireland (MSI2015) </u>Limerick, Ireland, August 2015

17.   **Marc A. Fernandez-Yague**, Gemma Orpella-Aceret, Matteo Palma, Tofail Syed, Dimitrios Zeugolis, Abhay Pandit and Manus J.P Biggs "Piezoelectric Meshes of P(VDF-TrFE)/MWCNT for Cellular Electric Stimulation." Poster presention at 5th Postgraduate Research Day Galway, Ireland, August 2015

18.   **Marc A. Fernandez-Yague**, Gemma Orpella-Aceret, Matteo Palma, Tofail Syed, Abhay Pandit and Manus J.P Biggs "Composite PVDF-TrFE/BNNT used as bioactive scaffold for promoting bone regeneration." Poster presention at the Advanced Functional Polymers for Medicine (AFPM2015) conference, Galway, Ireland, March 2015

19.   **Marc A. Fernandez-Yague**, Gemma Orpella-Aceret, Matteo Palma, Tofail Syed, Abhay Pandit and Manus J.P Biggs" Cellular electric stimulation mediated by poled piezoelectric meshes of P(VDF-TrFE)/MWCNT for bone regeneration in vitro." Poster presention at the 21st Annual Conference of the Bioengineering Section of the Royal Academy of Medicine in Ireland (BINI2015), Dublin, Ireland, January 2015

20.   **Marc A. Fernandez-Yague**, Gemma Orpella-Aceret, Abhay Pandit and Manus J.P Biggs Effect of "Electrical Stimulation through Electrospun Piezoelectric Scaffolds on the Distribution of Focal Adhesion in Human Dermal Fibroblasts." Podium presentation at the 2nd Matrix Biology Ireland Meeting (MBI2014) Galway, Ireland, November 2014

21.   Cecile Comte, **Marc A. Fernandez-Yague**, Abhay Pandit and Manus J.P. Biggs "Preparation of mineralized piezoelectric meshes and DNA quantification in human osteoblasts." Podium presention at the 26th Symposium and Annual Meeting of International Society for Ceramics in Medicine (BIOCERAMICS26) Barcelona, Spain, November 2014

22.   **M. Fernandez**, M.Pegueroles, M.C. Manzanares-Cespedes, M. Herrero-Climent, F.J. Gil "Bone osseointegration influence of physicochemical and bioactive surface treatments on titanium dental implant: an in vivo study with minipigs." Podium presention at the 26th Symposium and Annual Meeting of International Society for Ceramics in Medicine (BIOCERAMICS 26) Barcelona, Spain November 2014

23.   R. Schieber, **M. Fernández-Yagüe**, M. Hans, M. Díaz-Ricart, G. Escolar, F. Javier Gil, F. Mücklich, M. Pegueroles. Endothelization and thrombogenicity response of CoCr alloy nano depth patterns for cardiovascular stents Podium presention at the 26th European Society of Biomaterials (ESB2014) Liverpool, UK August 2014

24.   Parvaneh Mokarian-Tabari, Catalina Vallejo-Giraldo, **M. Fernandez-Yague**, Cian Cummins, Michael A. Morris and Manus J.P.Biggs. Title: 6 Nanoscale Neuroelectrode Modification Through Self-Assembly of Block Copolymers. Podium presention at the 26th European Society of Biomaterials (ESB2014) Liverpool, UK, August 2014

25.   D.Pastorino, **M. Fernandez**, G. Mestres, E.B. Montufar, M.C. Manzanares-Cespedes, C. Canal, M.P. Ginebra. "Multi-aspect evaluation of antibiotic-loaded injectable calcium phosphates in an acute osteomyelitis rabbit model". Podium presention at the 26th Symposium and Annual Meeting of International Society for Ceramics in Medicine (BIOCERAMICS 26) Barcelona, Spain, November 2014

26.   Cecile Comte, **Marc A. Fernandez-Yague**, Abhay Pandit and Manus J.P. Biggs "Fabrication of piezoelectric PVDF-TrFE nanocomposite scaffolds for bone-tissue engineering." Podium presentation at the Royal Acacdemy of Medicine in Ireland (RAMI2014). Dublin, Ireland, June 2014

27.   Parvaneh Mokarian-Tabari, Catalina Vallejo-Giraldo, **M. Fernandez-Yague**, Cian Cummins, Michael A. Morris and Manus J.P.Biggs. "Fabrication of "intelligent nanosurfaces" for controlled cell-substrate interaction. Poster preseantion at The physics of soft and biological matter (IOP) Cambridge, UK, june 2014

7.4.4 Teaching Experience: 2

2017-2018   **Associate Lecturer**, National University of Ireland, Galway

− Taught, designed and developed coursework for fourth year biomedical engineering undergraduate and master students

1.- Tissue Engineering BME 405

2.- Advanced Tissue Engineering BME 502

7.4.5 Research Stays: 5

2017   University of Glasgow (UK). Prof. Matthew Dalby Research Group

2016   University College Dublin (IRL). Dr. Brain Rodriguez Group

2015   Queen Mary Univesity of London (UK). Dr. Matteo Palma Research Group

2014   University of Limerick (IRL). Pr. Tofail Syed Group

7.4.6 Awards: 2

2016   WBC 2016 Trainee Award World Biomaterials Congress 2016 "Piezoelectric nanoscaffolds: mediating tendon regeneration through activation of piezoresponsive receptors."

2014   PhD Scholarship - FP7-PEOPLE (618861)

Piezoscaff. Osteoinductive ferroelectric polymers for bone tissue engineering

7.4.7 Grants

2018 Enterprise Ireland Grant. Commercial Case Feasibility Support "Electrospun PTFE scaffold for tissue repair applications". 14.800 E.